ISBN 978-2-87355-028-8

Proceedings of the International Meteor Conference

Giron, France

18–21 September, 2014

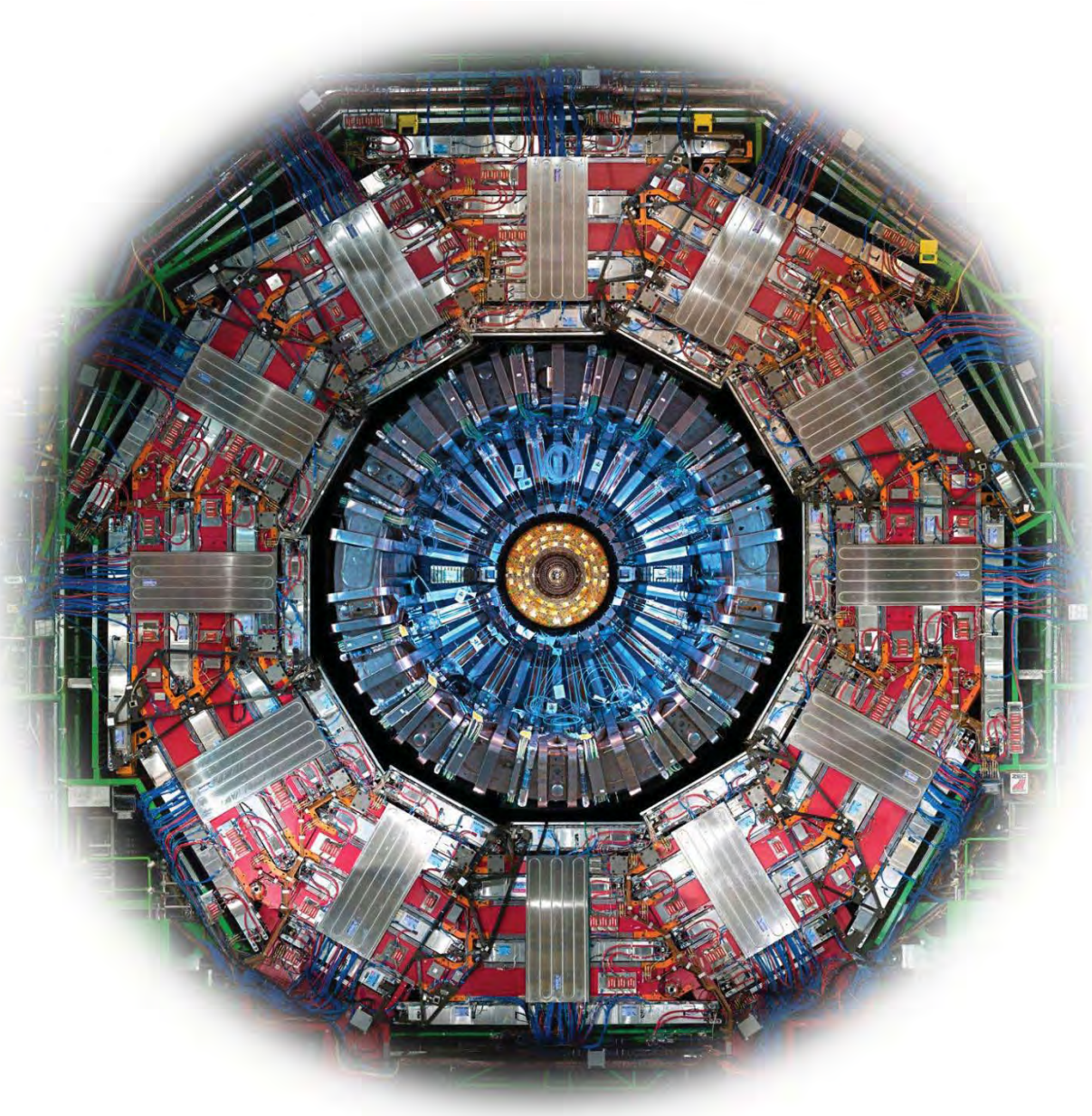

Published by the International Meteor Organization

Edited by Jean-Louis Rault and Paul Roggemans

Proceedings of the International Meteor Conference

Giron, France

18–21 September, 2014

Published by the International Meteor Organization

Edited by Jean-Louis Rault and Paul Roggemans

Proceedings of the International Meteor Conference

Giron, France, 18–21 September 2014

International Meteor Organization

ISBN 978-2-87355-028-8
EAN 9782873550288

Copyright notices
© 2014 The International Meteor Organization.
The copyright of papers submitted to the IMC Proceedings remains with the authors.

It is the aim of the IMO to increase the spread of scientific information, not to restrict it. When material is submitted to the IMO for publication, this is taken as indicating that the author(s) grant(s) permission for the IMO to publish this material any number of times, in any format(s), without payment. This permission is taken as covering rights to reproduce both the content of the material and its form and appearance, including images and typesetting. Formats may include paper and electronically readable storage media. Other than these conditions, all rights remain with the author(s). When material is submitted for publication, this is also taken as indicating that the author(s) claim(s) the right to grant the permissions described above. The reader is granted permission to make unaltered copies of any part of the document for personal use, as well as for non-commercial and unpaid sharing of the information with third parties, provided the source and publisher are mentioned. For any other type of copying or distribution, prior written permission from the publisher is mandatory.

Editing and printing
Front cover picture: The CMS Detector at CERN.
Publisher: The International Meteor Organization
Printed: l'Observatoire de Paris and IMCCE, Paris, France
Design IMC logo: Amélie Rault
Typesetting: MS Word template prepared by Vincent Perlerin.
Editors: Jean-Louis Rault, Paul Roggemans
Proofreaders : Megan Argo, Richard Fleet, Bob Lunsford, Tony Markham, Aswin Sekhar, Vincent Perlerin.
Bibliographic records: all papers are listed with the SAO/NASA Astrophysics Data System (ADS) – http://adsabs.harvard.edu with publication *code 2014pim4.conf*.

Distribution
Further copies of this publication may be ordered from the International Meteor Organization, through the IMO website (http://www.imo.net).
Legal address: International Meteor Organization, Mattheessensstraat 60, 2540 Hove, Belgium.

Contents

The IMO is very grateful to the local organizing team and to the main organizer François Colas for all the efforts made, especially for solving the nightmare scenario with the bankruptcy of one of the main accommodation hosts. No efforts, no costs were avoided to accommodate as many participants as possible and to make the very best possible of this IMC. Great thanks also to the fabulous manager of the main IMC host “La Fauconnière” for his unlimited support and help from the early morning till late at night. To all of those who made this IMC possible: thank you, we’ll remember this conference with pleasure.

Editors' notes

Jean-Louis Rault and Paul Roggemans

The Proceedings you have in front of you contain 54 papers related to scientific studies presented during the 33rd International Meteor Conference (IMC) held in Giron, France, from 18 to 21 September 2014. A special effort was made this year to publish these Proceedings soon, just after the end of the conference, in order to disseminate the information and knowledge and to get the papers listed by the SAO/NASA Astrophysics Data System as soon as possible.

First of all, the authors were kindly but firmly requested to deliver their papers before or just after the conference. A warm thank you to all of those who accepted this challenge! A conference without Proceedings would be rather meaningless as all the interesting lectures and posters would be soon forgotten and remain without any use. Who wants to spend this effort, time and money to attend a conference only for the entertainment aspect? The IMCs would not exist for long if the scientific content had not been preserved in Proceedings. Of course the production of these Proceedings requires a considerable effort. Lectures and posters in general are just an overview of the topic they cover. A paper is the best alternative for a more in-depth description and most conference participants are eager to consult these papers as soon as possible. To achieve this goal, big efforts were made since the 1986 IMC to encourage everybody to submit a paper within a reasonable time and to produce Proceedings within a few months of each conference. This worked well until the 1996 IMC but started to falter in the later 1990s with increasing delays in appearance, which soon resulted in ever less complete Proceedings. The larger the time lapse between the conference and the release of its Proceedings, the less the authors were motivated to share their conference materials. With delays larger than one year and coverage of less than 50% of the IMC presentations, this publication failed in its purpose and became no more than an archive item. This was of no help to motivate authors to prepare their paper; nobody likes to write papers that go straight into some archive.

What had been possible, from the end of the 1980s until the mid-1990s became suddenly impossible. Some editors didn't bother to collect papers, contributions that were not submitted spontaneously remained ignored, and up to 90% of the time spent editing Proceedings was dead time, with submitted papers collecting dust for many months. This lack of commitment had a rather discouraging effect for authors to make any effort at all to write a paper. The usefulness of such incomplete and delayed IMC Proceedings could be questioned, and when the Proceedings would fail to get produced it would be only a matter of time until the usefulness of the IMC itself would be questioned. Of course the many delays with various publications also did no good to the reputation of the IMO, all this in spite of the huge advantages offered by internet and e-mail facilities since the late 1990s.

When after the 2011 IMC in Sibiu the Proceedings were also at risk, Marc Gyssens and Paul Roggemans decided to make an effort to restore the reputation of the IMC Proceedings. A lot of time was invested to communicate with all authors to convince them to make the effort to submit a paper. This proved to be rather difficult as very little credibility was left for the IMC Proceedings. For some authors it was really a matter of a very last chance for the editors to prove they could manage to produce Proceedings within a more reasonable time. As nothing had been done before or during the IMC to collect papers, together with the disappointments of authors because of previous Proceedings, the collection of papers was a very slow and time consuming effort. Finally, for the first time in 15 years, all presentations (except one) were covered and printed in time for distribution at the next IMC. This generated confidence again and a lot of goodwill among authors to submit sooner, better elaborated papers. While the Sibiu Proceedings included 44 papers in 148 pages, the 2012 La Palma Proceedings counted 59 papers and 236 pages. A remarkable change in mentality had occurred: for the 2013 Poznan Proceedings, the quality of the papers increased considerably, making the collection of the papers and the editing work much easier. Would it be possible to have Proceedings within a few months after the conference?

LaTeX has been used for years by the IMO to produce the IMC Proceedings. LaTeX is perfectly suited to editing science papers which include a lot of tables, mathematical equations, curves and various symbols. However, LaTeX tools require particular skills from the editors and are really not user-friendly, and the great majority of authors is not familiar with such tools and prefers to use other text editors. In fact only 10% of the 162 papers of the past 3 Proceedings were delivered as LaTeX. Most authors used recent versions of Microsoft Word, LibreOffice or Open Office software which nowadays allow the editing of scientific papers in decent quality. Another problem with LaTeX is that the few people who master LaTeX within the IMO don't have sufficient time and still cause a lot of 'dead time' in any editing process. Microsoft Word being the first choice of almost 90% of all authors, the editors of the present Proceedings have chosen to use Microsoft Word for its ease of use and for its WYSIWYG[1] interface.

Using MS Word instead of LaTeX saves a lot of work as the papers submitted in Word must no longer be transformed into LaTeX code which was a labor intensive job. Moreover the editing work is no longer affected by the critical lack of

[1] WYSIWYG: "**W**hat **Y**ou **S**ee **I**s **W**hat **Y**ou **G**et"

time of the few LaTeX adepts. As a result the editing procedure can be shortened by more than half a year, which means that the Proceedings can indeed be produced within a few months of the conference.

Since the 2012 La Palma Proceedings, authors have been encouraged to submit their paper before or at latest during the conference. In fact there is no logic to prepare a lecture or poster before a conference and do the paper some months later. That is an inefficient way of working and only leads to further delay and postponing. Investing sufficient time into a lecture while writing the related paper, improves the quality of the lecture. Moreover the early availability of IMC papers enables some quality control by the SOC, which may improve the quality of the IMC program. At some past IMCs poorly-prepared presentations were given, with almost pure improvisation that had no end or beginning, a pity to lose the time when more lecture time is solicited than is available.

The choice of MS Word had one drawback: having no preliminary experience with MS Word to edit IMC Proceedings, the editors had to start from scratch. As editors we were very well aware of the challenge. The experiment with MS Word as text editor would confront us with plenty of software issues to solve. We were lucky to receive plenty of support from Vincent Perlerin to bring these Proceedings to a good end. Vincent produced a Word template for the IMC Proceedings and his constant advice was a great help for the editors during the painstaking work to prepare the final document. This experiment with MS Word as editor indeed required time and effort to learn and to gain experience with Word. Some bugs and complications with Word documents produced with different systems and versions required time to be solved. During the editing procedure the template was fine-tuned as we gained more experience. Never before have so many IMC authors delivered their papers so early. Step by step, the bad habits of postponing that characterized IMO publications for many years, have disappeared. We experienced a lot of goodwill among authors to make the effort to submit early, which is a dramatic change compared to the situation four years ago. Let's hope the IMC Proceedings will appear within few months after the conference from now on.

With this early delivery of the 2014 Giron Proceedings we hope we can reward all the efforts made by the authors. We hope that with this historically-early availability we have proven that publishing early is easily possible thanks to the goodwill of everybody involved. The 54 papers involved 145 different authors and co-authors, an impressive number of people. We are in particularly grateful to Vincent Perlerin for providing us with the Word template and for his most valuable advice whenever we asked him. We also thank the proofreaders for their tedious effort to proofread these proceedings in a final week of quality control; Megan Argo, Richard Fleet, Bob Lunsford, Tony Markham, Vincent Perlerin and Aswin Sekhar. A great thank-you also to the printing works of the "Observatoire de Paris" who produced these Proceedings in time and at a reasonable price.

Enjoy reading all these papers which highlight the dynamism of the professional and amateur meteor community!

22 November 2014

Program of the 33rd International Meteor Conference

Giron , 18–21 September, 2014

Thursday, 18 September, 2014

14:00 – 19:00	Arrival and registration IMC participants in Giron at "La Fauconnière".
19:00 – 20:00	Welcome speeches by local authorities.
	• Opening of the 33rd IMC by Cis Verbeeck;
	• Welcome speech and announcements;
	• Welcome drink at "La Fauconnière" .
20:00 – 21:00	Cold buffet in "La Fauconnière" (available until midnight for late arriving participants).
21:00 – 23:00	Workshop: "Planning of the new IMO website".

Friday, 19 September, 2014

07:30 – 08:30	Breakfast at Fauconnière/Hotel Kyriad.
	Session 1 Meteor networks (video and others) (Chair: *Jürgen Rendtel*).
09:00 – 09:30	*Detlef Koschny*. "CILBO – lessons learned from the operation of a double-station meteor camera setup".
09:30 – 09:50	*Esther Drolshage*. "Meteor velocity distribution from CILBO double station video camera data".
09:50 – 10:10	*Theresa Ott.* "Meteoroid flux determination using image intensified video camera data from the CILBO double station".
10:10 – 10:20	*Felix Bettonvil*. "High-resolution velocity determination on meteors".
10:20 – 10:40	*François Colas.* "FRIPON and 'Vigie Ciel' networks".
10:40 – 10:50	*Yoan Audureau*. "New acquision and detection sofware".
10:50 – 11:00	*Min-Kyung Kwon.* "Astrometry with fish eye lens and orbit determination".
11:00 – 11:30	Coffee break & Poster Session.
	Session 1 (continued) Meteor networks (video and others) (Chair: *Thomas Weiland*).
11:30 – 11:50	*Pete Gural*. "Offbeat and Wacky Projects using a Video Meteor Camera".
11:50 – 12:00	*Auriane Egal*. "Low dispersion meteor velocity measurements with CABERNET".
12:00 – 12:15	*Juraj Toth*. "Expeditions during 2014 with AMOS Cameras".
12:15 – 12:25	*Felix Bettonvil*. "The Benelux CAMS network".
12:25 – 12:35	*Denis Vida*. "CMN_ADAPT and CMN_binViewer software".
12:35 – 12:45	*Ana Georgescu*. "ROAN – from analog to digital solutions".
13:00 – 14:00	Lunch – (Restaurant Fauconnière).
	Session 2 Meteor shower observations (Chair: *Jérémie Vaubaillon*).
14:00 – 14:30	*Sirko Molau*. "Obtaining population indices from video observations of meteors".
14:30 – 14:40	*Roman Piffl*. "Double station meteor train from brightest Lyrid in EDMOND database".
14:40 – 14:55	*Damir Šegon*. "A Possibe New Shower On Eridanus-Orion Border".
14:55 – 15:10	*Mariusz Wiśniewski*. "Camelopardalids expedition".
15:10 – 15:20	*Bill Ward*. "Camelopardalids 2014. A radio view".
15:20 – 15:40	*Przemysław Żołądek*. "Future plans of the Polish Fireball Network".
15:40 – 16:00	*Thomas Weiland*. "Geminids 2012 – a spectacular show from Oman".
16:00 – 16:30	Coffee break & Poster Session.

Session 2 (continued) Meteor Shower observations
(Chair: *Detlef Koschny*).

16:30 – 16:50 *Jürgen Rendtel*. "Daytime meteor showers".

16:50 – 17:00 *Regina Rudawska*. "Independent identification of meteor showers in EDMOND database".

17:00 – 17:15 *Anna Kartashova*. "Meteor observations in Russia".

17:15 – 17:35 *Kristina Veljković & Ilija Ivanović*. "Software for analysis of visual meteor data".

17:35 – 18:00 *Oleg Ugolnikov*. "Perseids and Sporadic Meteor Dust in the Earth's Atmosphere by All-sky Polarization Measurements of the Twilight Background".

Poster session and introduction of all poster authors

01. *Željko Andreić, Damir Šegon and Denis Vida*. "A statistical walk through the IAU MDC database".

02. *Peter Dolinský, Ivan Dorotovič and Marian Vidovenec*. "Report on Radio Observation of Meteors (Iža, Slovakia)".

03. *Abderrahmane Ibhi*. "Tighert: A New Eucrite Meteorite Fall from Morocco".

04. *Alexandra Terentjeva and Elena Bakanas*. "Meteorite-producing fragment on the orbit of Apophis".

05. *Maria Hajdukova Jr., Regina Rudawska, Leonard Kornos and Juraj Toth*. "April ρ Cygnids".

06. *Regina Rudawska, Juraj Tóth, Dušan Kalmančok and Pavol Zigo*. "Slovak Video Meteor Network – Meteor Spectra".

07. *Tudor Georgescu, Mirel Birlan, Cezar Leseanu, Octavian Ghita and Cosmin Banica*. "Evolution – ROAN 2014".

08. *Mike Hankey and Vincent Perlerin*. "Meteor Terminology poster translated into different languages".

09. *Roman Piffl*. "Open Meteor Data".

10. *Peter Zimnikoval*. "Activity and Observability of Meteor Showers throughout the Year".

11. *Vasily Dmitriev, Valery Lupovka, and Maria Gritsevich*. "Determination of meteoroid orbits using numerical integration of equation of motion".

12. *Jean-Jacques Maintoux and Tioga Gulan*. "RETRAM : A network of passive radars to detect and track meteors to help in fireball recovery".

13. *Victor Stefan Roman and Catalin Buiu*. "Automatic detection of meteors using artificial neural networks".

14. *Daria Kuznetsova, Maria Gritsevich and Vladimir Vinnikov*. "Košice meteoroid investigation: from observational data to analytic model".

15. *Jim Wray and Dave Samuels*. "The Performance of New Low Cost 1/3" Security Cameras for Meteor Surveillance".

16. *Sirko Molau*. "Obtaining population indices from video observations of meteors".

17. *N. Rambaux, D. Galayko, J.F. Mariscal, M-A Breton., J. Vaubaillon. M. Birlan, F. Colas, T. Fouchet*. "Detection of spectral UV from meteors by a nanosatellite".

18. *Alexander Golubaev, Ivan Bryukhanov, Anastasia Tabolich, Valentin Tabolich, Anastasia Kulakovskaya, Dmitry Akulich and Ivan Sergey*. "Observations of Leonids, Draconids, α-Monocerotids, ε-Perseids and meteors of comet C/2012 S1 (ISON)".

19:00 – 20:00 Dinner.

20:00 – 20:45 26th IMO General Assembly.

Reception offered by the IMO Council (wine – juice – water).
Informal socializing (Bar).

Saturday, 20 September 2014

07:30 – 08:30	Breakfast at Fauconnière, Hotel Kyriad.
	Session 3 Meteoroid streams, structure and evolution (Chair: *Jean-Louis Rault*).
09:00 – 09:20	*Jérémie Vaubaillon*. "Update on recent-past and near-future meteor shower outbursts on Earth and on Mars".
09:20 – 09:30	*Berenice Reffet*. "A new meteor detection algorithm for shuttered photography".
09:30 – 09:45	*Maria Hajdukova*. "The prediction of meteor showers from all potential parent comets".
09:45 – 10:00	*Rachel Soja*. "Interplanetary Meteoroid Environment for eXploration".
10:00 – 10:15	*Meryem Guennoun*. "Meteor observations from double station in Morocco".
10:15 – 10:25	*Regina Rudawska*. "DON QUIXOTE -- a possible parent body of a meteor shower".
10:25 – 10:55	Coffee break & Poster Session.
	Session 4 Fireball events & various (Chair: *Ana Georgescu*).
10:55 – 11:10	*Mike Hankey and Vincent Perlerin*. "IMO Fireball Reports".
11:10 – 11:20	*Vasily Dmitriev*. "New meteorite recovered in northern Russia based on observations made by the Finnish Fireball Network".
11:20 – 11:30	*Chris Peterson*. "Early Education Opportunities in Metoritics".
11:30 – 11:45	*Zeljko Andreic*. "A statistical walk through the IAU MDC database".
11:50 – 12:35	Lunch.
13:00	Departure for excursion to CERN.
14:00 – 17:00	Guided visit at CERN.
17:00 – 17:30	CERN Shop and Lavatories.
18:30	Return at Giron.
18:30 – 19:00	Closing reception.
19:00 – 20:00	Closing dinner.
20:00-..:..	Last night of the IMC in the bar, free entertainment and informal chat.

Sunday, 21 September 2014

09:00 – 10:00	Breakfast at Fauconnière/Hotel Kyriad.
	Session 5 Radio and radar observations (Chair: *Cis Verbeeck*).
10:00 – 10:15	*Jean-Louis Rault*. "Radio observation for Fripon Network".
10:15 – 10:30	*Giancarlo Tomezzoli*. "EARS, MARS Combined Meteor Radio Observations – 2014".
10:30 – 10:45	*Chris Steyaert*. "The Global Radio CAMs".
10:45 – 11:00	*Stijn Calders*. "Automatic detection of meteors in the BRAMS data".
11:00 – 11:20	*Tom Roelandts*. "Meteor Detection for BRAMS Using Only the Time Signal".
11:20 – 11:40	*Antonio Martinez Picar*. "Modeling and calibration of BRAMS antenna systems".
11:40 – 11:55	*Geert Barentsen*. "Conference summary".
11:55 – 12:05	Conference closing by IMO President Cis Verbeeck.
12:30 – 13:30	Lunch.
	Departure of participants.

CILBO - Lessons learned from a double-station meteor camera setup in the Canary Islands

Detlef Koschny[1], Jonathan Mc Auliffe[2], Esther Drolshagen[3], Felix Bettonvil[4], Javier Licandro[5], Cornelis van der Luijt[1], Theresa Ott[3], Hans Smit[1], Hakan Svedhem[1], Olivier Witasse[1], Joe Zender[1]

[1] **European Space Agency, ESTEC, Noordwijk, The Netherlands**
Detlef.Koschny@esa.int, Cornelis.van.der.Luijt@esa.int, Hans.Smit@esa.int, Hakan.Svedhem@esa.int, Olivier.Witasse@esa.int, Joe.Zender@esa.int

[2] **European Space Agency, ESAC, Villanueva de la Canada, Spain**
Jonathan.McAuliffe@esa.int

[3] **Univ. Oldenburg, Oldenburg, Germany**
Esther.Drolshagen@uni-oldenburg.de, Theresa.Ott@uni-oldenburg.de

[4] **Astronomical Institute Utrecht, Utrecht, The Netherlands**
f.c.m.bettonvil@astro-uu.nl

[5] **Instituto de Astrofisica de Canarias, La Laguna, Tenerife/Spain**
jlicandr@iac.es

We have been operating a double-station meteor camera setup and have collected more than 12 months of simultaneous observations until mid-2014. First science is being produced. In this paper we report on the lessons learned and provide information on what went well and what did not. The intention is to help other teams considering setting up similar systems to avoid the same issues.

1 Introduction

CILBO stands for **C**anary **I**slands **L**ong-**B**aseline **O**bservatory. We use two automated stations hosting an image-intensified video camera observing the same volume in the atmosphere during the night, one located on Tenerife, one on La Palma, in the Canary Islands, Spain. The complete setup is robotic, i.e. the system switches itself on when it is dark and the weather conditions are appropriate. Meteor data is saved automatically and sent via ftp to a central server. From there it is downloaded for data analysis. An additional camera on Tenerife is equipped with an objective grating. It records spectra of the brightest meteors.

The two main scientific goals of the system are:

(a) To study physical and chemical properties of meteoroids, and, taking into account the modifications of the meteoroid properties during their flight in the solar system, to constrain the physical and chemical properties of their parent body.

(b) To study the variability of the background dust flux in the Earth environment during a complete year.

The use of image intensifiers allows the system to record fainter meteors than non-intensified systems, bridging the gap to radar observations.

In this paper, we briefly describe the setup to provide the context. We present some observational statistics to demonstrate the performance of the system. Finally we produced a (most likely not complete) list of points relevant for setting up other similar systems, so-called 'lessons learned'. We strongly encourage everybody who wants to set up a similar system to not only read through our lessons learned, but also apply them.

2 The Setup

This section gives a brief overview of the setup. For a much more detailed description please refer to Koschny et al. (2013).

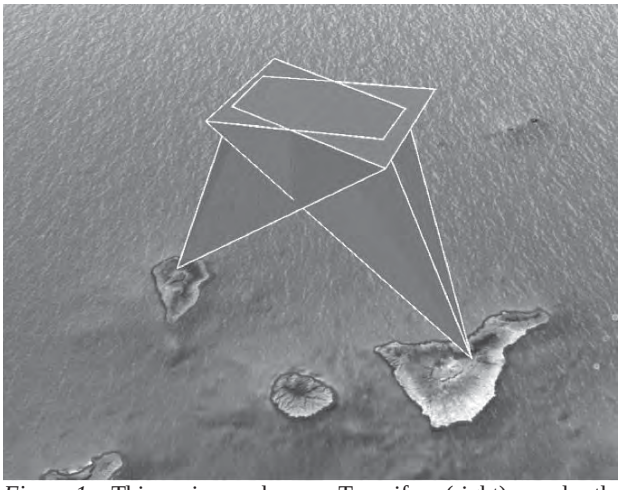

Figure 1 – This view shows Tenerife (right) and the corresponding field of view of ICC7 and La Palma (left) with the field of view of ICC9. The cones for the field of view are cut off at 100 km height.

Figure 1 shows a sketch of the system produced with Google Earth. The cones indicate the field of view of the two cameras. One is located on Tenerife (ICC7) and one on La Palma (ICC9). Note that ICC stands for 'Intensified

CCD Camera'. The fields intersect at a point half way between the islands in a height of 100 km. The top cut of the field of views is done at 100 km and shows the overlapping area in this reference height. *Table 1* is taken from Koschny et al. (2013) but corrects an inadvertent swap of longitude and latitude in this reference.

The additional camera with the objective grating is called ICC8. It is located on Tenerife and tilted such that it can record spectra of meteors observed by ICC7.

Table 1 – Geographical positions of the two observing stations and the aim point.

Island	Station code	Latitude	Longitude	Elevation
Tenerife (ICC7/ICC 8)	CILBO-T	28°18'04" N 28.3011° N	16°30'43" W -16.5119°	2395 m
La Palma (ICC9)	CILBO-L	28°45'36" N 28.7600° N	17°52'57" W -17.8824°	2327m
Aim point		28°32'00" N 28.5333° N	17°10'00" W -17.1667°	100000m

The complete setup is automated. Commercial motorized roofs house cover a small hut poured from concrete. A steel pier has mounting facilities for up to four commercial tripod heads. The cameras are custom-built video systems using image intensifiers. While they increase the sensitivity of the camera systems to about a limiting stellar magnitude of 7.0, they also mean that the camera can be damaged when the Moon enters the field of view.

The detection of meteors is done with the software MetRec (Molau, 1999). A custom-written scheduling software launches MetRec in the evening and sends the data of the night to a central server in the morning. This scheduling software also checks that the system is only operational when the weather conditions are ok.

The computer for ICC7 on Tenerife is located in the basement of the Optical Ground Station (the building housing ESA's 1-m telescope). The computer for ICC9 on La Palma is located in the nearby building of the Automated Transit Circle. A weatherproof box mounted directly at the housing protects the local control electronics, i.e. the roof controller and a watchdog system.

3 Operations up to now

ICC7/8 have been operational since 13 September 2011, ICC9 since 13 December 2011. Due to an unknown error the Moon went through the field of view of ICC9 in March 2012 and left a permanent visible dark track. We switched off ICC9. Due to travel and weather constraints, we managed to bring ICC9 back online only in January 2013. Since then, both cameras have been operating continuously with only small interruptions.

Table 2 gives some relevant statistical information on operating time and meteor numbers. We consider the time until May 2013 the commissioning period and provide the statistics only for the time frame of one year starting from 1 June 2013. In total, ICC7 has obtained data from more than 45000 meteors so far, ICC9 almost 40000.

Figure 2 shows a histogram plot of the meteor number per night, for the two stations.

Table 2 – Operating nights and hours of ICC7 and ICC9, as well as observed meteor numbers in the time frame 1 June 2013 to 31 May 2014.

	ICC7	ICC9	Simultaneous
Number of meteors	12491	15913	6663
Observing nights	287	299	
Observing hours	2245.0	2106.6	1799.5

4 System availability and reasons for downtimes

Table 2 shows that within one year, both cameras have been operated individually for more than 2100 hours. Assuming an average nighttime availability of 8 hours per night we estimate a maximum possible dark time of 8 h * 365.25 = 2922 h. Then the availability are for ICC7: 76.8 %; for ICC9: 72.1 %; for the complete system with both cameras simultaneously: 61.6 %.

The following items were reasons for the unavailability of the cameras:

(a) The Moon. A large part of the unavailability of the complete system is due to the Moon. The way the system is set up is that when the Moon gets closer to the center of the field of view than 30 degrees, the system shuts off and closes the roof to protect the intensifier from moonlight. ICC7 points northwest and is affected in times before the Moon sets. ICC9 points southeast and is affected in times after the Moon rises. Thus in times between quarter and full moon, first ICC9 is switched off, then ICC7.

(b) *Adverse weather conditions*. We use a Boltwood cloud sensor that can detect cloud cover by measuring the temperature of the night sky in the thermal infrared. We have set it such that it closes the roof at a sky temperature of 40 K below ambient temperature. We still have the occasional night (about 3 or 4 per year) where scattered clouds go through the field of view, but all in all we are very satisfied with the operations of the sensor. We also close the roof if the humidity is larger than 70 % or wind speeds larger than 50 km/h.

(c) *Intensifier damage*. The main technical problem which we had was that for an unknown reason ICC9 did not switch off when the Moon went through the field of view on 5 March 2012. An attempt to exchange the camera in spring 2012 failed due to severe weather conditions for a whole week. We then took the camera

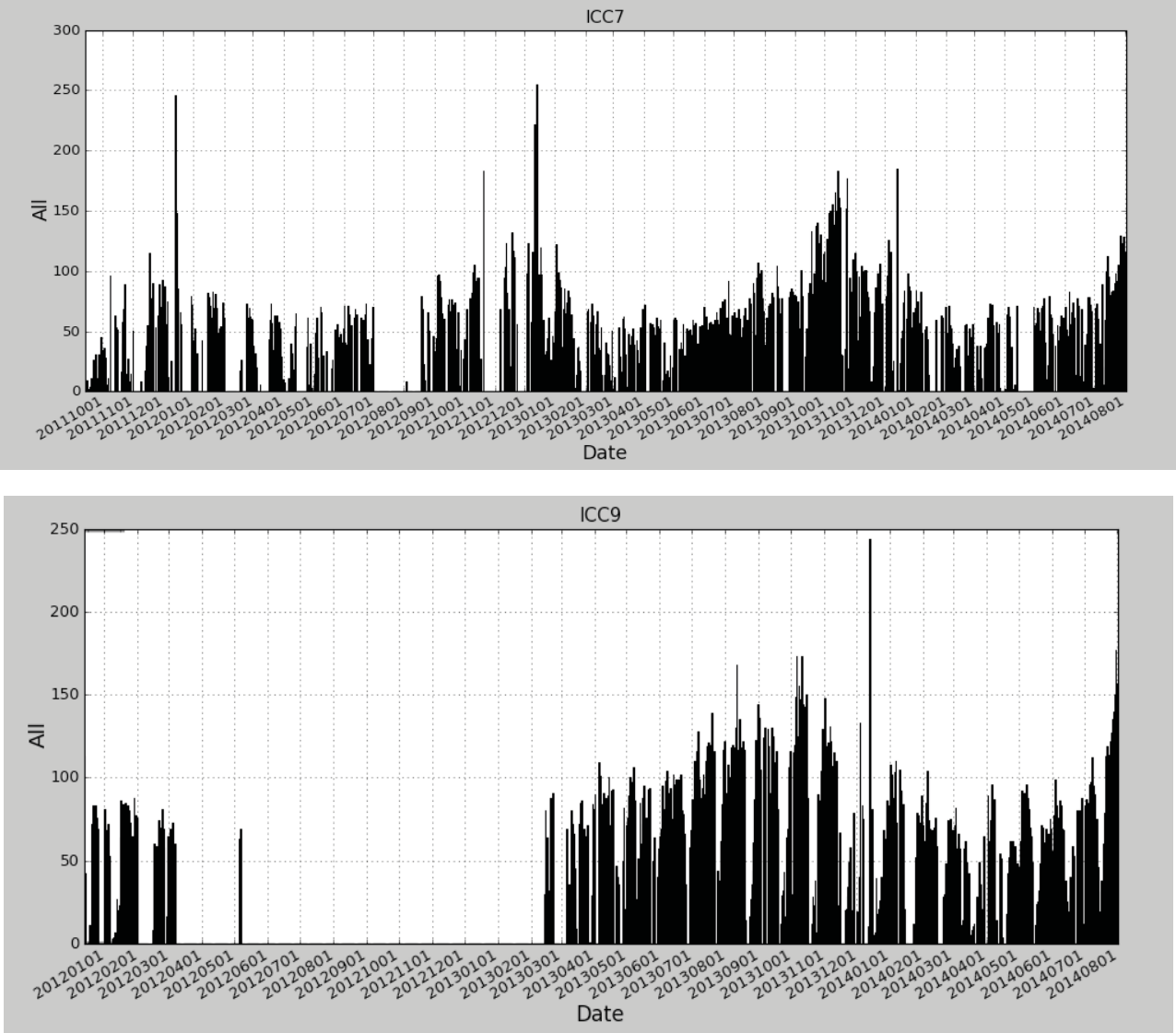

Figure 2 – The number of meteors per night as a function of time. These plots give a top-level overview of the availability of the systems. It also shows a systematic variation of the total meteor numbers per night due to the camera unavailability because of the Moon too close to the field of view. Some streams like the Geminids are apparent, as well as an increase in meteor numbers in spring and summer with respect to fall and winter.

back to ESA after the visit of our station during the IMC 2012. We shipped the repaired camera to La Palma but our local support staff did not feel qualified to install it. One of us (JL) installed the camera in January 2013. While the camera was then operating, the aperture was set to minimum and we lost a few more nights until the camera was fully back in operation on 14 February 2013.

(d) *Pressed emergency button*. The camera stations are small and the wall height is only about 1 m. In principle it is possible to step into the station when the roof is open. The motor to close the roof is fairly strong. Even though there is a current limiter that senses if the motor meets resistance and then cuts off the motor current, we have added an emergency stop button to the station. We had two occasions on Tenerife where a pressed emergency stop button was the reason that the roof did not open; in one other occasion the roof did not close. We were initially told that there is no need to put a fence around the station, so one can just walk up to it. We suspect passing visitors to have pressed the button 'for fun'. On La Palma, we have not (yet) observed this issue. Note that in the case of the 'stuck open' case we were lucky - the whole mountain was within clouds and local personnel were able to close the roof before the sun could do any damage.

(e) *Power failure*. We have experienced several power failures (3-4 per year) on La Palma. The computer is setup such that it boots upon power up. In principle all software is installed as Windows services and should start running. This normally works well. Occasionally, however, in particular the time synchronization did not start properly. Only one power failure has occurred on Tenerife. Other than the only hour-long failures on La Palma, this one lasted for several days. We had relied on un-interrupted power supply services from the Optical Ground Station. Apparently this had not worked, for reasons beyond our control.

Other issues which are worth mentioning:

(f) *Time synchronization stopped*. So far the time synchronization has stopped working twice for ICC7.

We use the freeware program 'timememo.exe' for synchronizing via NTP (Network Time Protocol) our PC time with some timeserver. Timememo.exe is installed as a service on our computer and should in principle always be running. For unknown reasons, however, it stopped working twice since the beginning of operations for ICC7. Every morning, a log file is written into the data directory of the night. We have failed to verify, on a daily basis, the existence of this file.

We have checked at what dates the log file is missing. By comparing the logged difference of the PC time with the correct UTC time upon restart of the software, we know the drift of the PC clock in the non-synchronized time period. It is now straight-forward to correct the recorded times of ICC7 by applying a linear interpolation of the time difference. For ICC9, we have not yet seen any issues.

(g) *Time server issues.* We have found time periods where apparently the timeserver (swisstime.ch) had provided a wrong time. Checking this issue via the Internet, we found notes that this has been done on purpose. Because of an overload of the 'swisstime' timeserver, the service provider had decided to purposely make wrong time information available in short periods of time in the order of seconds. Polling the timeserver every few tens of seconds to minutes, one would not notice this time error. As a result, we have reduced the time interval when we poll the server to 1 min rather than 15 s.

From the list of issues which we have encountered and from the positive experiences of what has actually worked well, we draw a number of 'lessons learned' which we will share in the next section.

5 Lessons learned

(a) *The robotic roof.* We are using an electric roll-off roof from the company Pier-Tech in the US[1]. It comes with its own dedicated controller and includes a 'Boltwood' cloud sensor from the company Cyanogen. ESA lab technicians have added some electronics to this controller. In particular they have added a watchdog that checks the communication between the computer and the roof. If there is no communication for a certain time period, the roof will close automatically independent on the weather conditions. This functionality constitutes a 'hardware override' to all automation implemented in software. It has the advantage that even if the control computer fails, the system will get itself into a safe state. This additional electronics has demonstrated its usefulness a couple of times already and is definitely worth the effort. But, all in all, the existing roof controller has been proven to be quite satisfactory.

(b) *Robotic roof - the emergency shutdown button.* We have added a manual emergency stop button for the roof. The roof motor is quite strong (e.g. to overcome problems of ice blocking the mechanics). If a person were stuck in the roof it could result in injuries. We have therefore added an easily visible emergency stop button. We had three occasions where for unknown reasons this button was pressed and the roof did not move any more. It could be that animals had jumped onto the button, or it could be that by-passers pressed it on purpose. The lesson here is to put a fence around your observatory to avoid unwanted people or animals to get close.

(c) *Boltwood cloud sensor.* We are using the so-called cloud sensor as a general weather sensor. It provides information not only on cloud cover, but also on humidity and rough wind speeds. It has worked extremely well and only failed once on ICC7 when it fell off its mast. We assume that the constant load from the wind has weakened the mechanical connection of the sensor to its mast. The lesson learned is to only use self-locking screws and double-redundant mechanical connections. The environmental conditions at 2800 m altitude can be very severe.

(d) *Our scheduling software – and: testing.* Our self-written scheduling software has worked well so far - but only after it had been beta-tested in a real-sky environment. Even though we have performed many module-level tests, a number of critical issues have only been discovered during a test when the complete setup had been installed in the backyard of the first author for 6 months, see *Figure 3*. The lesson learned is that testing is very important – a seemingly obvious statement, which is still often ignored.

(e) *Camera hardware.* Here we propose the same concept as in the previous bullet: Test, test, test. We have used camera hardware which, on component level, we had used before for many years. The actual cameras used for the Canary Islands were first operated for a few weeks in the real-sky test environment. The lesson: Only use equipment you are familiar with.

Figure 3 – The CILBO hut is the small hut on the left, next to the first author's private observatory with IAU code B12. CILBO was used in this configuration for a 6-month real-sky system test. The control computer was located in the hut of B12. A simple plastic pipe was used as a cable duct.

(f) *Manpower support.* While we have set up a robotic observatory, it is still useful to have personnel available

[1] http://www.pier-tech.com

on-site for emergency maintenance. We had one occasion where the emergency button had been pressed and prevented the roof to close. This could have resulted in the 'roof open' position in damage to the image intensifier if the sun had shone into the system. We were lucky and it was cloudy on that morning. In addition, we managed to send observatory staff to manually close the roof within a few hours. However, we did realize that we did not have all telephone numbers to reach the right people. Our lesson learned is: Always prepare an emergency procedure – know whom you need to call, and have some backup in case the contact person is on leave.

(g) *Time synchronization:* As described in the previous section we had two occasions where the time synchronization had stopped working. While this can be recovered by subsequent processing it is annoying and makes the data analysis less straightforward. This issue could have been avoided, had we checked the existence of the log file from the time synchronization software in a timely manner, i.e. once per day. This can be implemented by a software script, which sends out an email notification if the log file is not there. Lesson learned: Perform timely checks (once per day) of the completeness of your data.

(h) *The Moon.* Our scheduling software computes the apparent distance of the Moon to the center of the camera field of view. If the Moon is closer than a certain value (currently 30 degrees) the camera will be switched off to avoid damage to the intensifier. It turns out that the increase in background brightness will result in a large number of false detections, often several hundred per night. We have decided to accept these false detections and delete them manually. However, one should be aware of this and take the Moon's influence into account.

(i) *Mounting stability.* In particular for ICC7, we see slight changes in the pointing position of the camera. Sometimes during the course of one night, but also during several nights, the actual position of the stars had moved by up to two pixels (about 2') with respect to the expected position as displayed by the meteor detection software. This shift is observed only in the up-down direction of the camera. We assume that it is linked to a change in the pointing due to the load by cables on the back of the camera, or by thermal effects. ICC7 is mounted to the pier together with ICC8, thus the holder has to hold twice the mass compared to ICC9. MetRec is correcting its internal reference star file during the night. This means that re-computing the meteor coordinates with the reference star file of the night will give better results than using the normal reference star file obtained at just one epoch. Unfortunately MetRec does not automatically use the latest reference star file for computing the positions. Lessons learned: For cameras with pixel scales of 1' or less, the mounting stability can be an issue. In particular if one is interested in the best possible astrometric accuracy, one should use the reference star file generated during the observing night. It is suggested that MetRec should use this file for the computation of the meteor position.

(j) *Timeliness of data checking and log files.* We are generating a number of log files and a graphical overview of the observations of the night, see *Figure 4*. This overview has proven extremely useful. With just one glance one can get a feeling for the conditions during the night. The system sends an email to some key people every morning after the end of an observing night. We know that if we do not receive an email something went wrong; if we do receive an email, opening the graphical summary gives us a quick idea of what happened during the night.

And, as mentioned before: We have been able to follow and correct the missing time synchronization via the log files of the application 'timememo.exe'. We generate log files for all our applications. These have proven to be essential for error tracking and correcting.

Lesson learned: Log files are important. A graphical overview arriving every morning in the users email inbox is extremely helpful. Do not forget to check these emails. As a result of item (g) we will include some kind of flag to show whether the time synchronization log file was written or not.

(k) *Person in the loop* - All data is being checked, following the standard IMO visual network procedures, by a human operator. While this is a time-consuming task, it was seen that it is important. False detections may accidentally lead to reasonable trajectory solutions which would not be real.

6 Summary

In this paper we present lessons learned from setting up and operating a double-station meteor camera setup in the Canary Islands. Our main lessons learned are: Test, test, test. Keep logfiles, ensure your time synchronization works. Check your data in a timely manner.

We have been operating our setup, after a commissioning phase of 1.5 years, since May 2013. First science is being produced (see Drolshagen et al. and Ott et al., this issue). We showed that the setup works and could be reproduced if necessary.

We have chosen the approach of using a comparatively large hut with a roll-off roof to house our cameras. In principle one could simplify the weather protection by using covers for individual cameras. Our system has the advantage that it is easy to add additional camera systems.

Acknowledgments

We thank the Instituto de Astrofisica de Canarias for providing space for our systems and assisting in the setup and maintenance. We thank the ESA SSO lab facilities and machine shop for providing extensive support in the construction of the equipment. The hardware for the setup was supported by the research budget of ESA's Science Support Office.

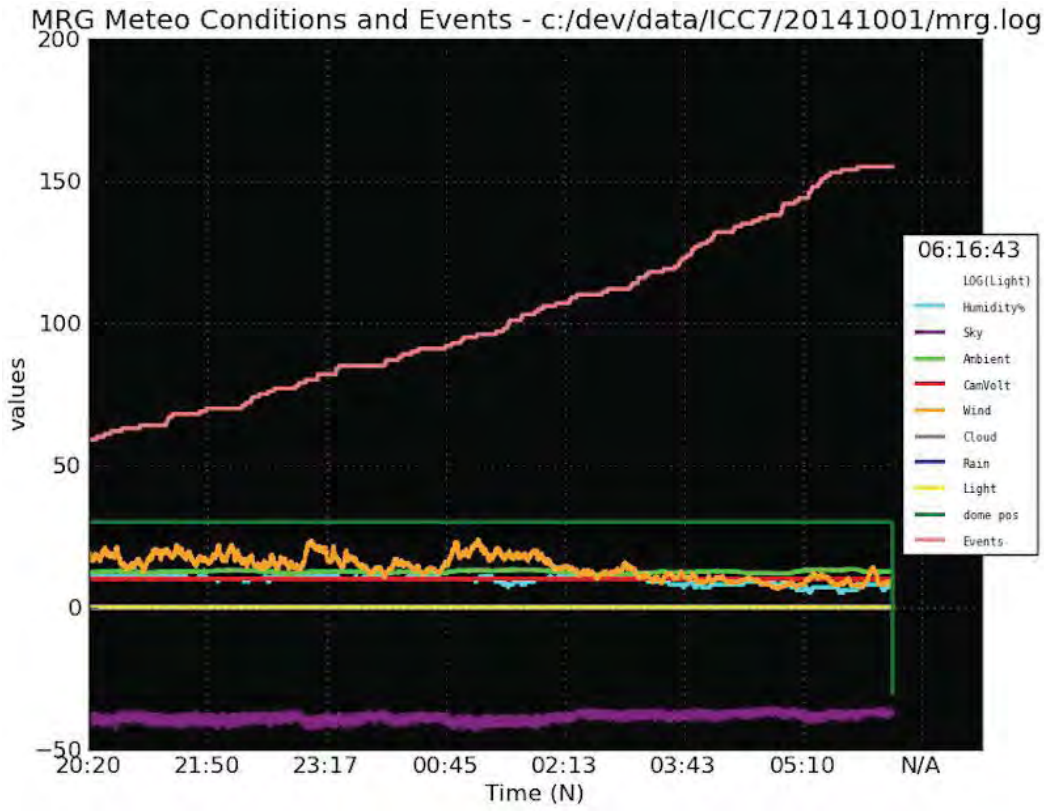

Figure 4 – Screenshot of the log of one night of observation for ICC7. The different lines denote the weather conditions, the position of the roof, and the cumulative number of detections. This graph gives a quick overview of the observation night.

References

Drolshagen E., Ott T., Koschny D., Drolshagen G., Poppe B. (2014). "Meteor velocity distribution from CILBO double station video camera data". In Rault J.-L., and Roggemans P., editors, *Proceedings of the International Meteor Conference*, Giron, France, 18–21 September 2014. IMO, pages 16–22.

Koschny D., Bettonvil F., Licandro J., v. d. Luijt C., Mc Auliffe J., Smit H., Svedhem H., de Wit F., Witasse O., Zender J. (2013). "A double-station meteor camera setup in the Canary Islands – CILBO". *Geosci. Instrum. Method. Data Syst*., **2**, 339–348.

Molau S. (1999). "The Meteor Detection Software MetRec". In Arlt R., Knoefel A., editors, *Proceedings of the International Meteor Conference*, Stara Lesna, Slovakia, 20–23 August 1998. IMO, pages 9–16.

Ott T., Drolshagen E., Koschny D., Drolshagen G., Poppe B. (2014). "Meteoroid flux determination using image intensified video camera data from the CILBO double station". In Rault J.-L., and Roggemans P., editors, *Proceedings of the International Meteor Conference*, Giron, France, 18–21 September 2014. IMO, pages 23–29.

Meteor velocity distribution from CILBO double station video camera data

Esther Drolshagen[1], Theresa Ott[1], Detlef Koschny[2], Gerhard Drolshagen[2], Bjoern Poppe[1]

[1] **University of Oldenburg, Oldenburg, Germany**
Esther.Drolshagen@uni-oldenburg.de, Theresa.Ott@uni-oldenburg.de,
Bjoern.Poppe@uni-oldenburg.de

[2] **European Space Agency, ESTEC, Noordwijk, The Netherlands**
Detlef.Koschny@esa.int, Gerhard.Drolshagen@esa.int

This paper is based on data from the double-station meteor camera setup on the Canary Islands - CILBO. The data has been collected from July 2011 until August 2014. The CILBO meteor data of one year (1 June 2013 – 31 May 2014) were used to analyze the velocity distribution of sporadic meteors and to compare the distribution to a reference distribution for near-Earth space. The velocity distribution for 1 AU outside the influence of Earth derived from the Harvard Radio Meteor Project (HRMP) was used as a reference. This HRMP distribution was converted to an altitude of 100 km by considering the gravitational attraction of Earth. The new, theoretical velocity distribution for a fixed meteoroid mass ranges from 11 - 71 km/s and peaks at 12.5 km/s. This represents the predicted velocity distribution. The velocity distribution of the meteors detected simultaneously by both cameras of the CILBO system was examined. The meteors are sorted by their stream association and especially the velocity distribution of the sporadics is studied closely. The derived sporadic velocity distribution has a maximum at 64 km/s. This drastic difference to the theoretical curve confirms that fast meteors are usually greatly over-represented in optical and radar measurements of meteors. The majority of the fast sporadics are apparently caused by the Apex contribution in the early morning hours. This paper presents first results of the ongoing analysis of the meteor velocity distribution.

1 Introduction

For this paper data is used from the CILBO (Canary Island Long-Baseline Observatory) setup on the Canary Islands. CILBO has been active since July 2011. The evaluations presented in this paper were done using the data collected in one year (1 June 2013 – 31 May 2014). During this year the system collected data for 6663 meteors which were simultaneously observed by both cameras.

The CILBO System consists of two automated stations with image-intensified video cameras named ICC (Intensified CCD camera). Each of them reach a limiting stellar magnitude of about +7.0. One camera is located on Tenerife (ICC7) and one on La Palma (ICC9), in the Canary Islands. They are pointed at the same spot in the sky at 100 km height, therefore the covered observation volumes overlap. Meteors that were observed in this overlap can be registered by both cameras making it possible to determine the trajectory of the observed meteor. Because the meteor observation is done with video cameras, a meteor is visible on a number of single frames. *Figure 1* shows the setup of the system generated with Google Earth. The system automatically checks the weather conditions during the night and only records when they allow observation. The data is saved every night and sent to a central server via ftp.

One additional camera belongs to the setup, ICC8 on Tenerife. This camera has an objective grating and records the spectrum of the brighter meteors. The meteor identification is carried out by the software MetRec (Molau, 1999). For a more detailed description of the CILBO setup see Koschny et al. (2013). Furthermore, if you want to know more about the data set and about 'lessons learnt' see Koschny et al. (2014).

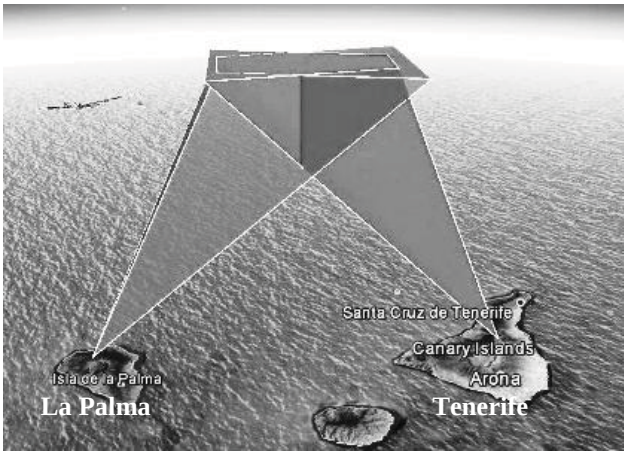

Figure 1 – Sketch of the CILBO system with the field of view of both cameras up to a height of 100 km. Additionally, the overlapping volume that is covered by both cameras is visible. La Palma with the ICC9 is on the left and Tenerife with the ICC7 is on the right.

In this paper the analysis of the CILBO data of one year is presented. Also, the theoretical velocity distribution based on the guidelines provided by the Space Environment Standard of the European Cooperation for Space Standardization (ECSS, 2008) is explained. The velocity distribution of the collected data and the bias towards higher velocities is examined.

All meteors which were simultaneously observed are separated into shower meteors and sporadics. Sporadics are meteors which do not belong to a (known) meteor stream. The velocity distributions of the Southern Taurids and the Perseids are presented. The calculated shower velocities were found to match the literature values. The sporadic velocity distribution is relatively even distributed at the slow velocities and has a peak at 64 $/s$. The majority of fast sporadics were caused by the Apex contribution in the early morning hours.

2 The ECSS distribution

The Space Environment Standard of the European Cooperation for Space Standardization (ECSS, 2008) contains the velocity distribution for the sporadic meteoroid flux at 1 AU in free space. A. D. Taylor calculated these values using parts of the data which were observed by the Harvard Radio Meteor Project (HRMP) from 1968 to 1969 (Taylor, 1995). The initial velocity distribution for meteoroids in free space, v_∞ , contains the amount of meteoroids found for certain velocities in 1 km/s bins. The standard provides a procedure to re-calculate the distribution for other heights since the velocities near Earth change due to Earth's gravitation. The normalized distribution for meteoroids in free space are plotted as the solid line in *Figure 2*. For this work the distribution at the standard altitude of 100 km will be computed. Therefore the free space values must be adapted to the reduced distance. Due to gravity, the velocity distribution of meteoroids changes in dependence of their distance to Earth. The new velocity v can be calculated using (1) and (2).

$$\boldsymbol{v^2 = v_{esc}^2 + v_\infty^2} \qquad (1)$$

$$\boldsymbol{v_{esc} = \sqrt{2 \cdot \frac{\mu}{r + H}}} \qquad (2)$$

Utilizing the velocity in free space v_∞ and the escape velocity v_{esc}. v_{esc} depends on the distance between the meteoroid and the Earth's center $r + H$. r is the mean Earth's radius ($r = 6371$ km) and H is the altitude above Earth's surface. In addition it depends on the constant $\mu = 3.986 \cdot 10^5\ km^3/s^2$, which is the product of the Earth's mass with the constant of gravitation.

The reference altitude of 100 km above Earth's surface, corresponds to a distance of $r + H = 6371$ km + 100 km = 6471 km. The corresponding meteoroid flux values were adjusted according to the velocity shift. This is done using the G factor, which shows by which a particle flux far away from Earth, is changed near to Earth. G can be computed using (3). With this factor the new shifted values $n'(v)$ of meteoroids per velocity bin can be determined from the primary values $n(v)$, using equations (3) and (4).

$$G = \frac{v^2}{v^2 - v_{esc}^2} \qquad (3)$$

$$n' = G \cdot n \qquad (4)$$

The new velocity distribution has to be re-binned and re-normalized because the shifted velocity values result in new weights for the new bins.

The velocity distributions for a distance of 100 km (dashed line) and for meteoroids in free space (solid line) were plotted in Figure 2. The integral of both curves was normalized to 1. The maximum of the meteoroid velocity distribution at 100 km is found at 12.5 km/s. The average velocities of the distributions are determined and listed in *Table 1*. The near Earth line is steeper than the velocity distribution in free space. This is a result of the acceleration of the meteoroids by the Earth gravitation. There are no meteoroids expected to be slower than 11.1 km/s which is the escape velocity v_{esc} in 100 km height. Through the process of calculating the new distribution, all contributions from the old velocities, which are smaller than v_{esc}, are collected in the first couple of bins for velocities larger than v_{esc} of the new distribution. This causes the steep increase of the curve. The physical description of this phenomenon is that, the closer the meteoroids come to the Earth, the stronger they are attracted by the Earth's gravity. Even the meteoroids with very small velocities are accelerated in the Earth's gravitation field.

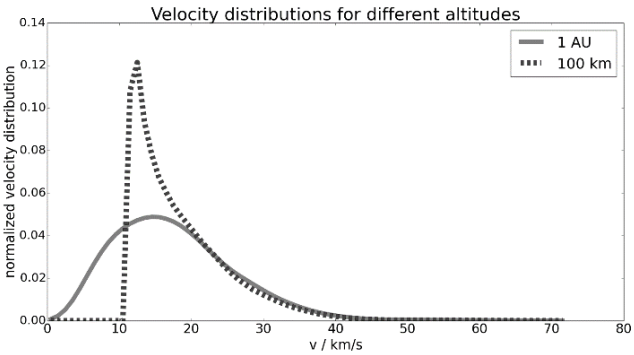

Figure 2 – Velocity distribution at 100 km above the Earth's surface (dashed line) and at 1 AU in free space (solid line).

Table 1 – Average meteoroid velocities for different altitudes above the Earth's surface.

H	$v_{avg}[km/s]$
100 km	18.47
1 AU	17.66

3 The CILBO velocity distribution

In the analyzed year (1 June 2013 – 31 May 2014) there were 6663 meteors observed simultaneously by both cameras. The information about the velocities of the double-station meteors were taken from *.daf (detailed altitude file) files which were created by a software called MOTS (Meteor Orbit and Trajectory software) (Koschny and Diaz del Rio, 2002). Furthermore, a control program has eliminated all faulty *.daf files. This are those with unphysical entries, i.e. negative velocity values or altitudes and are not used in the following. The result is 6132 double-station meteors detected simultaneously

between the 1 June 2013 and the 31 May 2014. Furthermore, MOTS provides *.kml files for all double station meteors, which can be read by Google Earth, showing the trajectory of a meteor. In *Figure 3* some exemplary meteor trajectories are shown, generated with Google Earth. For this picture the data of 9 double-station meteors recorded on the 13 December 2011 and analyzed by MOTS are utilized.

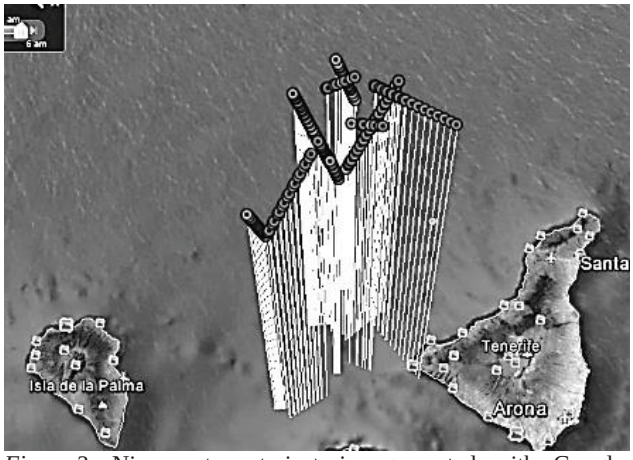

Figure 3 – Nine meteor trajectories generated with Google Earth from the *.kml files. The different dots were derived from meteor information of frames detected by ICC7/ICC9.

For every double-station meteor a *.daf file is generated and named hhmmss.daf (hour, minute, second of the meteor detection). It contains information about all single frames of both cameras at which the meteor is recorded. This includes, amongst others, the time of detection and the position of the meteor which is needed to calculate the meteor's velocity. In *Figure 5* an exemplary *.daf file of a meteor observed on the 6 August 2013 at $03^h03^m09^s$ is shown. The meteor is observed by ICC7 on 17 frames and by ICC9 on 19 frames. For each recorded video frame the file contains information about the meteor as seen by one station. The first column is the consecutive number and the second lists the image time in decimal seconds. In the third column of the table the apparent brightness in magnitudes is noted and the following entries are the relative x and y positions of the meteor in the field of view. The sixth column contains the calculated altitude of the meteor above the Earth's surface and the following the respective error estimate. The latitude and longitude of the point under the meteor are also listed. Furthermore, the distance to the camera in meters with an error estimate is shown in the columns 11 respectively 12. The last two entries present the velocity, as determined for that video frame and the former one, and its error estimate.

With the information of the *.daf files an average velocity is calculated, to reduce the effect of errors in the velocity calculations. The uncertainties are obvious in the last column of *Figure 5* which shows the apparent meteor velocities between two frames. To determine the average velocity, the time interval between the time of the second and the penultimate frame is computed. This way, the majority of the meteor trajectory is utilized. Using the first and the last frame at which a meteor is detected would result in higher uncertainties because in the first frame the meteor is in the process of appearing and in the last frame it is in the process of disappearing. If only 3 frames are available for a recorded meteor, the first and last frames are used to obtain the velocity. Furthermore, the information about the meteor position in longitude and latitude is extracted for those frames from the table. With this it is possible to determine an average velocity. It is calculated for both stations. The mean value of those velocities is utilized in the following. This is done for each double-station meteor. The resulting velocity distribution for all simultaneously detected meteors in the one year is plotted in *Figure 4*. The distribution shows two maxima, one at about 30 km/s and one at about 60 km/s. This differs largely from the theoretical distribution of the former section, which peaks at 12.5 km/s. This measurement bias towards higher velocities will be explained in section 5.

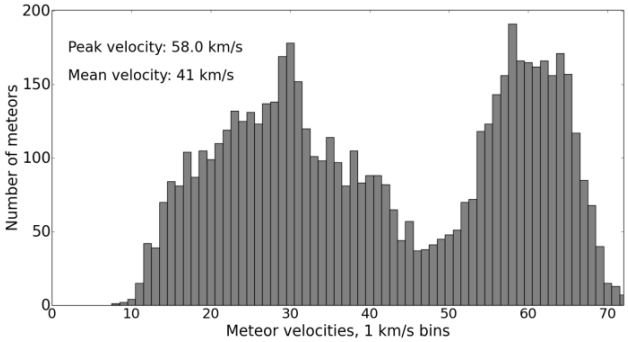

Figure 4 – Velocity distribution of all meteors detected simultaneously by both cameras in the analyzed year in 1 km/s bins.

4 Showers

For further examinations the meteors are sorted by their stream association (sporadic or shower). For this the classification by MetRec for the single station observations is used. Hereafter the Southern Taurids and the Perseids are examined. In the analyzed year 235 Southern Taurids and 149 Perseids were simultaneously detected. *Figure 6* and *Figure 7* show the number of detected Southern Taurids as a function of their velocity. For *Figure 6* only the meteors classified by both cameras as a Southern Taurid were utilized. For *Figure 7*, all meteors which were categorized either by both cameras or only by ICC7 or only by ICC9 as a Southern Taurid were taken. *Figure 8* and *Figure 9* show the same for all meteors related to the Perseids. The known velocities of the showers were extracted from the International Meteor Organization Handbook for Visual Observers (Rendtel, 2014). According to this the Southern Taurids (STA) and the Perseids (PER) have a velocity in free space (v_∞) relative to Earth of:

$$v_{\infty,STA} = 27\ km/s\,, \qquad v_{\infty,PER} = 59\ km/s$$

Figure 6 to Figure 9 also show the peak velocity. The peak velocity is the velocity with the maximum number of observed meteors, derived using the CILBO data. Additionally, the mean velocities of the velocity distributions are calculated.

```
Station 1 - ICC7 - Tenerife
LogFile: 20130805.log
AppearanceDate: 06.08.2013
AppearanceTime: 03:03:09
INFFilename: 030309.inf
FrameCount: 17

!                    Position         Altitude in m            SubPoint        Cam. dist in m  Velocity in km/s
!###   Time  Bright   x      y        h        h            pos   lon/deg  lat/deg     dist   dist     v       v
000  09.31    3.3  0.992  0.898  109052.2  ----.-    56.8   -16.940   28.784   126653.1  ----.-   --.---  --.---
001  09.35    1.5  0.976  0.872  107474.7  ----.-     4.2   -16.950   28.772   125110.9  ----.-   56.028  --.---
002  09.39    0.4  0.960  0.845  105905.7  ----.-    29.8   -16.960   28.760   123599.8  ----.-   58.601  --.---
003  09.43   -0.2  0.943  0.815  104238.1  ----.-    14.3   -16.971   28.748   122019.7  ----.-   62.296  --.---
004  09.47   -0.7  0.926  0.785  102612.9  ----.-     3.8   -16.982   28.735   120507.2  ----.-   57.770  --.---
005  09.51   -1.0  0.909  0.757  101085.0  ----.-    40.8   -16.992   28.724   119110.7  ----.-   57.112  --.---
006  09.55   -1.0  0.892  0.727   99535.8  ----.-    21.8   -17.002   28.712   117721.0  ----.-   55.098  --.---
007  09.59   -0.7  0.873  0.693   97833.7  ----.-    15.9   -17.013   28.699   116224.4  ----.-   63.660  --.---
008  09.63   -0.6  0.853  0.659   96135.5  ----.-     4.7   -17.024   28.686   114765.7  ----.-   60.431  --.---
009  09.67   -0.4  0.834  0.626   94543.8  ----.-    15.1   -17.035   28.674   113430.5  ----.-   59.566  --.---
010  09.71    0.3  0.820  0.602   93404.0  ----.-    14.5   -17.042   28.666   112496.5  ----.-   40.583  --.---

Station 2 - ICC9 - La Palma
LogFile: 20130805.log
AppearanceDate: 06.08.2013
AppearanceTime: 03:03:09
INFFilename: 030309.inf
FrameCount: 19

!                    Position         Altitude in m            SubPoint        Cam. dist in m  Velocity in km/s
!###   Time  Bright   x      y        h        h            pos   lon/deg  lat/deg     dist   dist     v       v
000  09.21    5.1  0.015  0.330  112019.4  ----.-    20.6   -16.920   28.806   145051.9  ----.-   --.---  --.---
001  09.25    4.1  0.031  0.319  110350.9  ----.-    34.2   -16.931   28.794   143045.7  ----.-   60.719  --.---
002  09.29    2.9  0.048  0.308  108636.7  ----.-    13.4   -16.942   28.781   140998.4  ----.-   62.399  --.---
003  09.33    2.1  0.064  0.298  107073.5  ----.-    22.3   -16.952   28.769   139142.9  ----.-   56.922  --.---
004  09.37    1.4  0.082  0.286  105355.2  ----.-    20.7   -16.964   28.756   137118.8  ----.-   62.583  --.---
005  09.41    1.1  0.099  0.274  103764.4  ----.-    12.0   -16.974   28.744   135258.2  ----.-   57.956  --.---
006  09.45    0.6  0.117  0.263  102153.0  ----.-    34.6   -16.985   28.732   133387.8  ----.-   58.726  --.---
007  09.49    0.3  0.136  0.251  100492.4  ----.-    64.9   -16.995   28.719   131476.6  ----.-   60.531  --.---
008  09.53    0.5  0.153  0.239   99031.5  ----.-    22.9   -17.005   28.708   129807.7  ----.-   53.271  --.---
009  09.57    0.8  0.173  0.225   97359.1  ----.-    14.7   -17.016   28.696   127915.4  ----.-   60.997  --.---
010  09.61    1.0  0.194  0.211   95665.5  ----.-    22.2   -17.027   28.683   126018.2  ----.-   61.788  --.---
011  09.65    1.3  0.214  0.198   94103.3  ----.-    16.0   -17.037   28.671   124285.0  ----.-   57.011  --.---
012  09.69    3.4  0.229  0.188   92958.2  ----.-    30.5   -17.045   28.662   123022.9  ----.-   41.799  --.---
```

Figure 5 – Exemplary *.daf file of a meteor observed simultaneously by both cameras on 06 August 2013 at $03^h03^m09^s$.

Figure 6 and *Figure 8* (both stations categorize the meteor as the same stream = bs) yield the following observed peak and mean velocities for the showers:

$$v_{STA,peak,bs} = 29\ km/s, \quad v_{PER,peak,bs} = 58\ km/s$$

$$v_{STA,mean,bs} = 28\ km/s, \quad v_{PER,mean,bs} = 56\ km/s$$

Furthermore, for the velocity distributions of *Figure 7* and *Figure 9* (one or two single-station classification = ss) the peak and mean velocities are computed:

$$v_{STA,peak,ss} = 30\ km/s, \quad v_{PER,peak,ss} = 58\ km/s$$

$$v_{STA,mean,ss} = 29\ km/s, \quad v_{PER,mean,ss} = 55\ km/s$$

These results are quite consistent with the literature values. It has to be taken into account that the meteors near the Earth are accelerated by Earth's gravitation. Additionally, the shower classification is done using the single-station data. This results in higher uncertainties.

To study this in more detail, compare *Figure 6* and *Figure 7*. Both graphs show a similar peak velocity, in agreement with the literature values. However, *Figure 7* (one or two single-station classification) has a higher scattering than *Figure 6* (both cameras categorize the meteor as the same). This shows that most meteors classified as a Southern Taurid by both cameras are quite certain a part of this stream. It also shows, however, that some of the meteors categorized as a Southern Taurid only by one camera are in fact not related to this shower. It follows that the type classification done by MetRec works for the analyzed data, since the peak velocities match the IMO velocities, but is not absolutely reliable, which is reflected by the higher scattering in *Figure 7*.

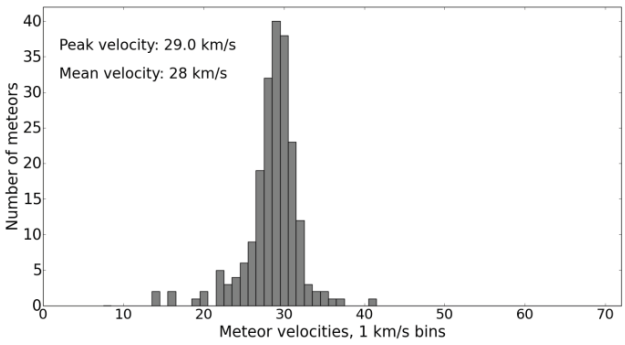

Figure 6 – Velocity distribution of the Southern Taurids detected in one year and classified by both cameras as a Southern Taurid.

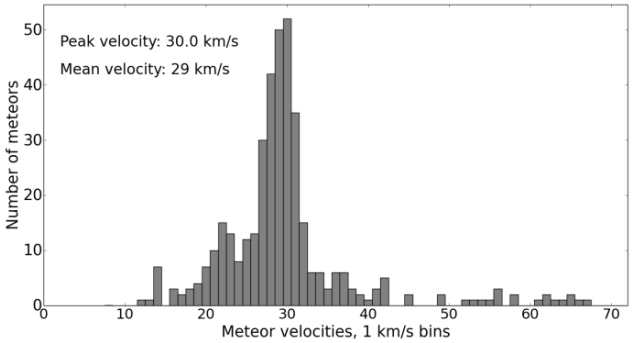

Figure 7 – Velocity distribution of the Southern Taurids detected in one year and classified by at least one of the cameras as a Southern Taurid.

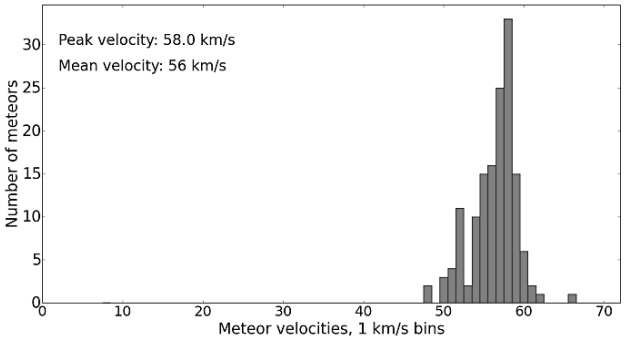

Figure 8 – Velocity distribution of the Perseids detected in one year and classified by both cameras as a Perseid.

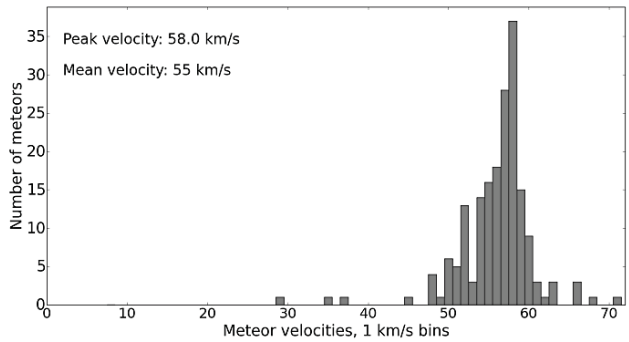

Figure 9 – Velocity distribution of the Perseids detected in one year and classified by at least one of the cameras as a Perseid.

5 Comparison of theory vs. CILBO data

In *Figure 10* the number of detected sporadics as function of their velocity is shown. Only those meteors were utilized which were categorized as sporadics for both camera observations. In *Figure 11* the normalized theoretical velocity distribution for 100 km altitude is shown as a dashed line. Normalizing the sporadic velocity distribution of the CILBO data to one yields the solid line presented in *Figure 11*. The two graphs in this figure are very different. The theoretical line has a high peak at slow velocities around 12.5 km/s. The measured velocities display a more uniform distribution with a minor peak at 64 km/s. This divergence can be attributed to a measuring bias towards higher velocities. The higher the meteor's velocity the brighter the meteor. Due to this the fast meteors can be detected more easily and meteors from smaller and more abundant meteoroids can be detected. Whereas, a lot of slow, faint meteors remain undiscovered.

This relation can be examined if only meteoroids with large masses are analyzed since the brightness of meteors is also proportional to the size of the corresponding meteoroid. The larger the meteoroid, the brighter the meteor. Consequently it is possible to detect large meteoroids even if they are slow. This means that the bias towards high velocities can be minimized if only large meteoroids are analyzed, due to the high detection probability of heavier meteoroids irrespective of their velocity. With the information of the *.daf files the masses of the meteoroids are determined utilizing the mass formula by Verniani (1973):

$$M = 10^{\frac{-m+64.09-10\cdot\log(v)}{2.5}} \qquad (3)$$

Whereas, M is the meteoroid mass outside the Earth's atmosphere, m is the absolute magnitude of the meteor at maximum light and v is the velocity. For a more detailed description see Ott et al. (2014).

We analyzed the velocity distribution, if only meteoroids with a mass ≥ 0.5 g are selected which amount to 469 meteors. For these heavier meteoroids the velocity distribution is computed and plotted in *Figure 12*. This graph has its maxima at slower velocities and a steep slope to even smaller and higher velocities. This velocity distribution agrees better with the theoretical expectation than the one calculated for all meteors. *Figure 12* does not show the bias towards higher velocities. This is consistent with the expectations.

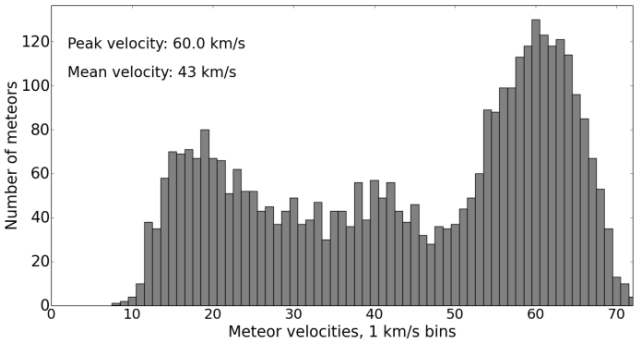

Figure 10 – Velocity distribution of all sporadic meteors detected in one year.

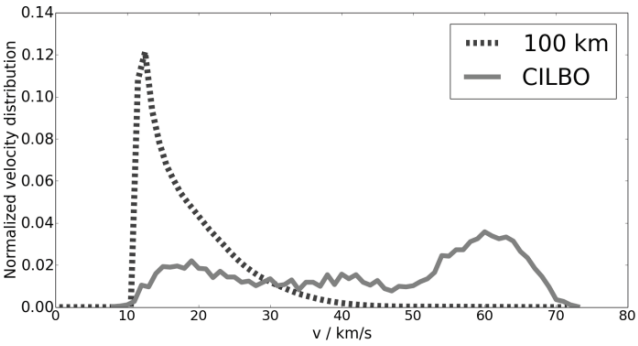

Figure 11 – Normalized theoretical velocity distribution in 100 km above the Earth's surface (dashed line) and the normalized sporadic velocity distribution calculated for one year of CILBO data (solid line).

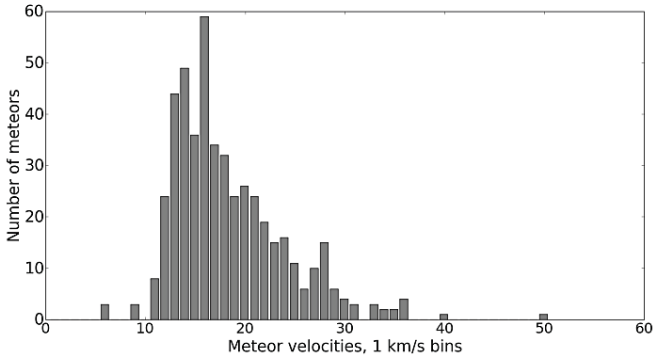

Figure 12 – Velocity distribution of all meteors detected by both cameras in one year with corresponding meteoroid masses ≥ 0.5g.

6 The Apex contribution

Figure 10 shows the velocity distribution of all sporadic meteors detected in one year. The maximum number of meteors were determined to have a velocity of about 64 km/s. Since the sporadics cannot be assigned to showers with certain velocities which might be in the 60 km/s category, other reasons for this distinct look must be assumed.

The reason for the high peak around 64 km/s seems to be Earth's rotation in combination with Earth's orbit around the Sun (compare *Figure 13*). At the beginning of the night the observer is located on the back of the Earth with respect to the Earth's direction of movement (A). Consequently, the meteoroids that become visible meteors have to "catch up" with the Earth. Therefore, they reach the Earth's atmosphere with a relatively small velocity. Their lower velocity yields a fainter trail due to less energy and the strong dependence of the meteor brightness on velocity. By contrast, in the early morning hours the observer is located in the front (B). Hence, the meteoroids have a higher velocity with respect to the Earth than the ones in the early evening hours. As a result they cause brighter meteors. Another consequence is that meteors flying from the East to the West move on average faster with respect to the Earth than those from West to East. This is due to the fact that the perceived meteor speed on Earth does not take the speed of the inertial systems, with the observer in the center, into account. This is called the Apex contribution.

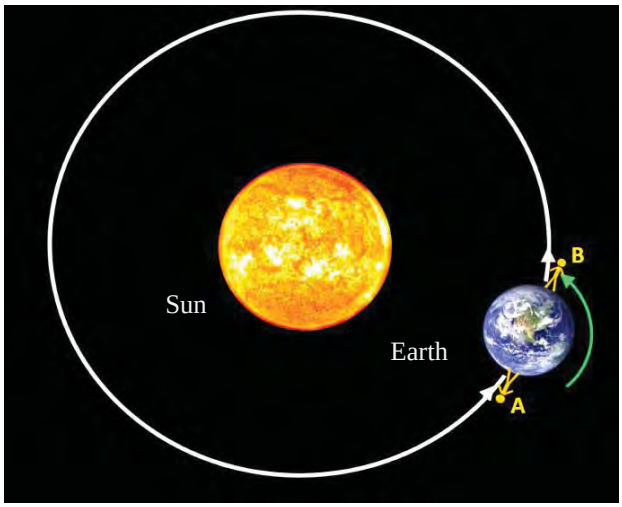

Figure 13 – The Earth orbiting the sun and the Earth's self-rotation. Early evening observations (A) and early morning observations (B).

7 Conclusion and future work

The CILBO data offers a lot of information about the velocities of meteors. The one year double-station data yield information on more than 6000 meteors with usable simultaneous observations.

The shower velocities match the IMO values. An error analysis has to be considered as well as the examination of more showers. Furthermore, the type classification by MetRec works well for the provided data, but is not perfect.

The velocity distribution of the sporadics shows a bias towards higher velocities. This is due to the fact, that the faster the meteor the brighter. Additionally, the larger the meteoroid the brighter the resulting meteor. The velocity distribution of heavier meteoroids is consistent with the theory and has a maximum at 16 km/s. In the future the true velocity distribution of the unbiased measurements should be determined.

Furthermore the sporadic velocity distribution has a peak velocity at about 64 km/s. This peak is a result of the Apex contribution in the early morning hours, when the observer is located in the front of the Earth with respect to the Earth's direction of movement.

References

ECSS (2008). European Cooperation for Space Standardization Space Engineering, Space Environment, ECSS-E-ST-10-04C. Noordwijk, Netherlands: ESA Requirements and Standards Division.

Koschny D., and Diaz del Rio J. (2002). "Meteor Orbit and Trajectory Software (MOTS) - Determining the Position of a Meteor with Respect to the Earth Using Data Collected with the Software MetRec". *WGN, the Journal of the IMO*, **30**, 87–101.

Koschny D., Bettonvil F., Licandro J., van der Luijt C., Mc Auliffe J., Smit H., Svedhem H., de Wit F., Witasse O., and Zender, J. (2013). "A double-station meteor camera setup in the Canary Islands – CILBO". *Geoscientific Instrumentation Methods and Data Systems*, **2**. 339–348.

Koschny D., Mc Auliffe J., Bettonvil F., Drolshagen E., Licandro J., van der Luijt C., Ott T., Smit H., Svedhem H., Witasse O., and Zender, J. (2014). "CILBO - Lessons learnt from a double-station meteor camera setup in the Canary Islands". In Rault J.-L., and Roggemans P., editors, *Proceedings of the International Meteor Conference*, Giron, France, 18–21 September 2014. IMO, pages 10–15.

Molau S. (1999). "The Meteor Detection Software MetRec". In, Baggaley W. J. and Porubcan V., *Proceedings of the International Conference Meteoroids 1998*, 17–21, 1998, Tatranska Lomnica, Slovakia., pages 131–134.

Ott T., Drolshagen E., Koschny D., Drolshagen G., and Poppe B. (2014). "Meteoroid flux determination using imae intensified video camera data from the CILBO double station". In Rault J.-L., and Roggemans P., editors, *Proceedings of the International Meteor Conference*, Giron, France, 18–21 September 2014. IMO, pages 23–29.

Rendtel J. (editor). (2014). Meteor Shower Workbook 2014. IMO.

Taylor A. D. (1995). "The Harvard Radio Meteor Project meteor velocity distribution reappraised". *Icarus*, **116**, 154–158.

Verniani F. (1973). "An Analysis of the Physical Parameters of 5759 Faint Radio Meteors". *Journal of Geophysical Research*, **78**, 8429–8462.

The author, Esther Drolshagen during her lecture. (credit Bernd Klemt).

Meteoroid flux determination using image intensified video camera data from the CILBO double station

Theresa Ott[1], Esther Drolshagen[1], Detlef Koschny[2], Gerhard Drolshagen[2], Bjoern Poppe[1]

[1] **University of Oldenburg, Oldenburg, Germany**
Theresa.Ott@uni-oldenburg.de, Esther.Drolshagen@uni-oldenburg.de,
Bjoern.Poppe@uni-oldenburg.de

[2] **European Space Agency, ESTEC, Noordwijk, The Netherlands**
Detlef.Koschny@esa.int, Gerhard.Drolshagen@esa.int

The double-station meteor camera setup on the Canary Islands, called CILBO, has been active since July 2011. This paper is based on the meteor data of one year (1.6.2013 – 31.5.2014). As a first step the statistical distribution of all observed meteors from both cameras was analyzed. Parameters under investigation include: the number of meteors observed by either one or both cameras as a function of the months, magnitude and direction. In a second step the absolute magnitude was calculated. It was found that ICC9 (La Palma) detects about 15% more meteors than ICC7 (Tenerife). A difference in the camera setting will be ruled out as a reason but different pointing directions are taken into consideration. ICC7 looks to the north-west and ICC9 looks to the south-east. A suggestion was that ICC9 sees more of the meteors originating from the Apex contribution in the early morning hours. An equation by Verniani (1973) has been used to convert brightness and velocity to the mass of the incident particle. This paper presents first results of the meteor flux analysis and compares the CILBO flux to well-known reference models (Grün et al., 1985) and (Halliday et al., 1996). It was found that the measured CILBO data yield a flux which fits the reference model from Grün et al. quite well.

1 Introduction

The CILBO (**C**anary **I**sland **L**ong-**B**aseline **O**bservatory) setup on the Canary Island has been active since July 2011. For this paper the collected data of one year, between 1 June 2013 and 31 May 2014, is used. In this year ICC7 collected 18398 meteors and ICC9 21158. Of these, 6663 meteors were detected simultaneously by both cameras.

The two camera stations are fully automated. One is located on Tenerife and one on La Palma on the Canary Islands. Each station hosts an image-intensified video camera, ICC (Intensified CCD Camera). The ICCs reach a limiting stellar magnitude of about +7.0. The camera on Tenerife is called ICC7, the one on La Palma ICC9. They are pointed at the same point in the sky in 100 km altitude, resulting in an overlap volume of the two observation volumes which is covered by both cameras. Due to this, it is possible to calculate the trajectory of the meteors observed simultaneously by both cameras in the overlap volume. *Figure 1* shows a sketch of the CILBO setup generated using Google Earth.

If the weather permits it, the system switches on. Every night the data is collected and transferred via ftp to a central server. The meteors are being observed using video data, therefore a meteor is visible on a varying number of single frames. The software *MetRec* (Molau, 1999) accesses the video data of the single stations and examines them in order to find meteors. For more information about the CILBO setup see Koschny et al. (2013) Furthermore, for a more detailed description of the data set and how to avoid mistakes using similar setups see Koschny et al. (2014).

For this paper the CILBO data of one year is presented. First, the magnitude distribution was examined. It has been found that ICC9 sees about 15% more meteors than ICC7. Differences in the settings will be analyzed more closely and ruled out as a reason for this discrepancy. A suggestion was that ICC9, looking to the East, sees more of meteors originating from the Apex contribution in the early morning hours. The mass distribution of the one year data set is presented, as well as the derived flux.

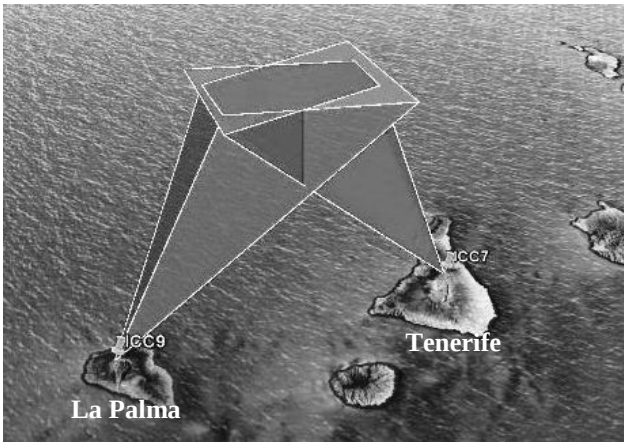

Figure 1 – Sketch of the CILBO system. The field of view of both cameras with an overlap volume covered by both cameras up to a height of 100 km. On the right is the ICC7 on Tenerife and on the left the ICC9 on La Palma.

2 The magnitude distribution

Every night a *.log file is generated by *MetRec* for both stations. This file lists information of each detected meteor. It includes, amongst others, the brightness of the meteor, its angular velocity and its type (shower or sporadic). The single-station data yield a magnitude value

calculated by *MetRec* for every meteor. In *Figure 2* the number of detected meteors in one year over their magnitude is plotted. The striped bars are the meteors collected only by ICC7 (Tenerife). The dotted bars are the meteors detected only by ICC9 (La Palma). The grey bars are the meteors observed by both cameras simultaneously. The utilized magnitudes are the mean values between the magnitudes determined by ICC7 and by ICC9. This first analysis of the data indicates that ICC9 sees more and fainter meteors than ICC7. The maximum of the ICC7 meteor distribution is at a magnitude of +3.5, the maximum of the ICC9 distribution is at +4.0 mag. This suggests that ICC9 is more sensitive than ICC7. This discrepancy will be examined in the following sections.

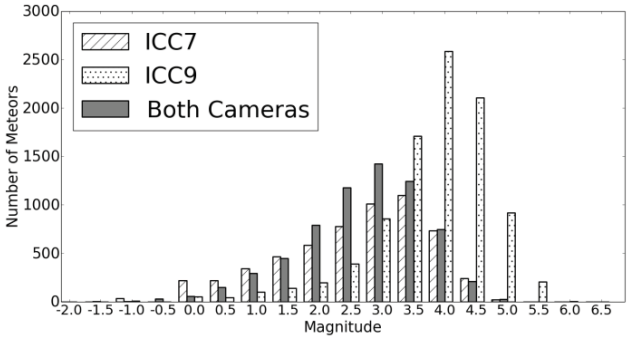

Figure 2 – Magnitude distribution of the CILBO data for one year. White, striped bars: Meteors detected only by ICC7. White, dotted bars: Meteors detected only by ICC9. Grey bars: Meteors detected simultaneously by both cameras.

3 The limiting magnitude

To analyze this difference in detection probability the *.log files have to be examined more closely. Every night *MetRec* determines the limiting magnitude by comparing the detected magnitude of reference stars with their real magnitude. In each *.log file the photometric equation, the color index correction, and the nominal limiting magnitude of the corresponding night are listed. The equations were extracted from the files and an average of the analyzed year is determined. These averaged equations are listed in *Table 1*. This yields a limiting magnitude of +6.64 for ICC7 and +6.29 for ICC9. According to this the ICC7 should detect fainter meteors.

Table 1 – The average photometric equation, color index correction and limiting magnitude of the cameras for data of one year.

	ICC7	ICC9
Photometric equation	$-2.39 \cdot log(pixelsum) + 9.45$	$-2.31 \cdot log(pixelsum) + 9.02$
Color index correction	$-0.33 \cdot (B-V) + 0.25$	$-0.3 \cdot (B-V) + 0.19$
Nominal lim. magnitude	$6.64\ mag$	$6.29\ mag$

4 The absolute magnitude

The absolute magnitude is the magnitude a meteor would have, if it would be in 100 km height in the observer's zenith. The information needed to calculate the absolute magnitude is taken from *.daf files (detailed altitude file) generated by the software *MOTS* (Meteor Orbit and Trajectory Software), see Koschny and Diaz del Rio (2002). An exemplary *.daf file is presented in *Figure 6*. The figure shows the information about one meteor observed simultaneously by both cameras on 07.08.2013 at $01^h44^m06^s$. It was recorded by both cameras on 19 frames. Information about the double-station meteor as seen by one station is listed for each frame on which the meteor was detected. *Figure 6* includes the consecutive number of the frame in the first column. The second column shows the time when the image was taken, in decimal seconds. In the third column of *Figure 6* the apparent magnitudes are listed. The next entries present the relative x and y positions of the meteor with respect to the center of the field of view. The height of the meteor above the Earth's surface with an error estimate is registered in the columns six and seven. The point directly under the meteor is specified in longitude and latitude. These values are also listed. In the columns 11 and 12 the meteor's distance to the camera in meters with an error estimate are presented. The velocity of the meteor, calculated for that video frame and the former one, with an error estimate are entered into the last two columns.

Another program has checked all *.daf files and deleted every file with unphysical entries, for example files that include negative values of velocity or altitudes. In the analyzed year 6663 simultaneously observed meteors were recorded. The control program declared 6132 of them as usable.

The brightness values are extracted from the *.daf file (Column 3 in *Figure 6*). The brightest values of ICC7 and ICC9 are determined separately and named m_{obs} (observed magnitude). Additionally, the corresponding distance between meteor and camera d is obtained. In the case of multiple frames with the same, smallest magnitude value, the one corresponding to the shortest distance to the camera is taken. From the obtained magnitude data, the difference between the camera's magnitudes as well as a mean value are calculated. The plot in *Figure 3* shows the magnitude difference $(m_{ICC7} - m_{ICC9})$ over the mean magnitude.

In the next step the apparent magnitude is corrected to the absolute magnitude. For that the following equation is utilized.

$$m_{100} = m_{obs} + 2.5 \cdot \log_{10}\left(\frac{(100km)^2}{d^2}\right) \qquad (1)$$

With m_{obs} as the observed magnitude, d as the distance to the camera extracted from the *.daf files and m_{100} is the absolute magnitude. Additionally, it is necessary to correct the magnitude to account for atmospheric extinction k. Because of the already quite large

uncertainty in the brightness values a *k*-value for a zenith angle of 50° may be used. A table from Green (1992) yields an extinction value of $k = 0.25$. This corrected magnitude is calculated for both stations. The magnitude difference between the two station's corrected magnitudes $(m_{corr,ICC7} - m_{corr,ICC9})$ as well as the mean magnitude is derived. In *Figure 4* the magnitude difference is plotted over the mean magnitude of the absolute magnitude values. To compare the apparent and absolute magnitude *Figure 3* and *Figure 4* were evaluated. In both pictures the average magnitude difference is given and yields a first impression of the correction quality. The average apparent magnitude difference is $\Delta m_{app} = -0.44$ mag and the average absolute magnitude is $\Delta m_{abs} = -0.50$ mag. The standard deviation is 1.09, respectively 1.11. A further look at the graphs reveals that the corrected values are shifted to the left. This effect has been expected since most detected meteors were further away from the camera than 100 km. Therefore, a correction would reveal that they appear fainter than at 100 km. Due to the fact that the magnitude difference is computed using $m_{ICC7} - m_{ICC9}$ and that the mean difference value is negative, it can be assumed that the camera on La Palma, ICC9, categorizes the same meteor fainter than ICC7 does. The difference in the magnitude determination is shown later to be an effect of the settings of the detection software.

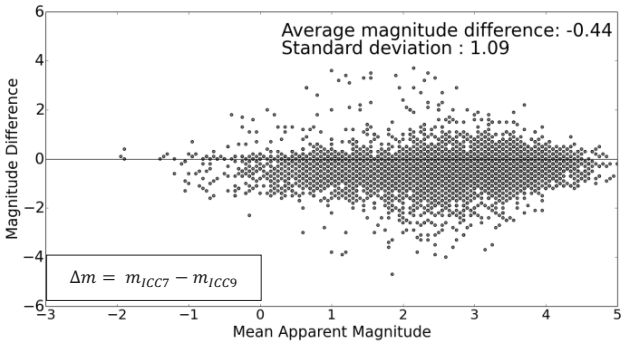

Figure 3 – Magnitude difference over the mean magnitude derived from the apparent magnitude values.

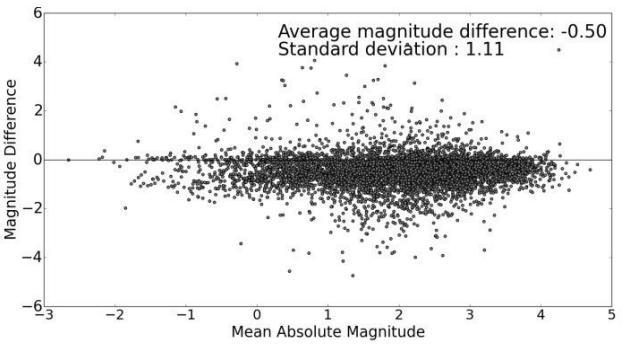

Figure 4 – Magnitude difference over the mean magnitude derived from the absolute magnitude values.

In *Figure 5* the plots from Section 2 are redone with a correction for the magnitude of ICC9. To accomplish that the difference of 0.44 mag is subtracted from the magnitude values of ICC9 to modify the brightness categorization. It is obvious that the magnitudes of ICC9 are now shifted to brighter values. Evidently, ICC9 does not detect fainter meteors than ICC7. Nonetheless ICC9 detected about 15% more meteors than ICC7 in the analyzed year.

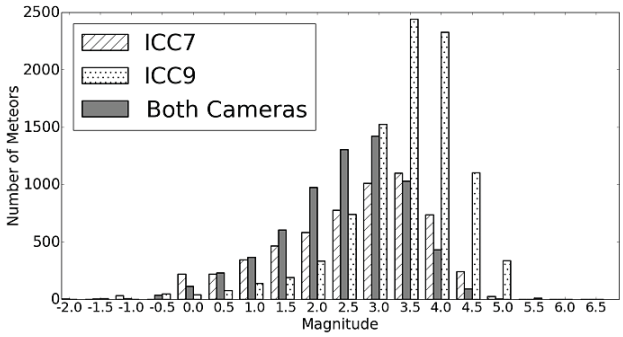

Figure 5 – Number of meteors as a function of their magnitude, whereas the ICC9 magnitude values are corrected by 0.44 mag. White, striped bars: Meteors detected only by ICC7. White, dotted bars: Meteors detected only by ICC9. Grey bars: Meteors detected simultaneously by both cameras.

5 Active times

It has to be taken into account that the cameras were not active the same amount of time. They are located on different islands and can only detect under good weather and sky conditions. The weather conditions may vary on the two islands. Furthermore, the cameras are pointed to the same position in the sky from different observation sites. Due to this they cover two different sides of the sky and the influence of the moonlight is not the same for the two cameras.

To diminish the effect of different active times on the number of recorded meteors an hourly rate is computed. For that the number of detected meteors is divided by the active time of the camera and converted to meteors per hour. The active times were determined by calculating the time between turning the camera on at the beginning of the night and off at the end. Off-times due to poor weather conditions were also taken into consideration. The hourly rate was determined for every night of the analyzed year and a monthly average was calculated. The distribution of the average hourly rate of every month for ICC7 and ICC9 is shown in *Figure 7*. The error bars are the standard deviation from the daily hourly rates in one month. It is evident that the rates of ICC9 are higher than those of ICC7. On average ICC9 detects 2 meteors more per hour than ICC7 does.

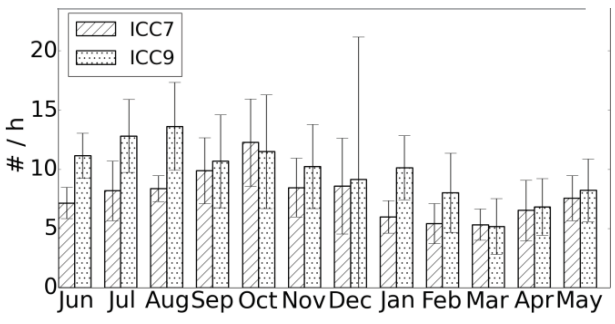

Figure 6 – Monthly average of the hourly rates of ICC7 (striped) and ICC9 (dotted) with error bars.

```
Station 1 - ICC7 - Tenerife
LogFile: 20130806.log
AppearanceDate: 07.08.2013
AppearanceTime: 01:44:06
INFFilename: 014406.inf
FrameCount: 19

!                    Position        Altitude in m          SubPoint        Cam. dist in m  Velocity in km/s
!###   Time  Bright   x      y       h       h  pos   lon/deg  lat/deg     dist    dist     v       v
 000  06.08    4.6  0.259  0.455  96245.1  ----.-    4.6   -17.192   28.385  115803.2  ----.-  --.---  --.---
 001  06.12    4.3  0.266  0.445  95481.0  ----.-    4.9   -17.192   28.389  115209.7  ----.-  21.675  --.---
 002  06.16    4.0  0.275  0.433  94614.0  ----.-   10.1   -17.192   28.394  114539.1  ----.-  25.856  --.---
 003  06.20    3.7  0.282  0.421  93793.7  ----.-    9.1   -17.192   28.398  113910.1  ----.-  23.269  --.---
 004  06.24    3.5  0.291  0.409  92903.3  ----.-    9.5   -17.192   28.403  113231.2  ----.-  26.556  --.---
 005  06.28    3.4  0.300  0.397  92054.8  ----.-    7.4   -17.191   28.407  112589.6  ----.-  25.307  --.---
 006  06.32    3.4  0.307  0.386  91264.3  ----.-    4.9   -17.191   28.412  111997.6  ----.-  22.427  --.---
 007  06.36    3.5  0.317  0.372  90357.4  ----.-   11.9   -17.191   28.416  111321.8  ----.-  27.054  --.---
 008  06.40    3.7  0.325  0.360  89518.4  ----.-    1.3   -17.191   28.421  110703.1  ----.-  23.804  --.---
 009  06.44    3.3  0.333  0.348  88720.8  ----.-    0.9   -17.191   28.425  110119.7  ----.-  23.793  --.---
 010  06.48    3.4  0.342  0.336  87900.0  ----.-   14.4   -17.190   28.429  109524.4  ----.-  23.292  --.---
 011  06.52    3.8  0.350  0.324  87116.5  ----.-    8.0   -17.190   28.433  108960.9  ----.-  23.378  --.---
 012  06.56    4.7  0.359  0.312  86308.5  ----.-   23.9   -17.190   28.438  108384.9  ----.-  22.931  --.---

Station 2 - ICC9 - La Palma
LogFile: 20130806.log
AppearanceDate: 07.08.2013
AppearanceTime: 01:44:06
INFFilename: 014406.inf
FrameCount: 19

!                    Position        Altitude in m          SubPoint        Cam. dist in m  Velocity in km/s
!###   Time  Bright   x      y       h       h  pos   lon/deg  lat/deg     dist    dist     v       v
 000  06.02    5.4  0.753  0.286  96780.4  ----.-    8.4   -17.192   28.383  123888.3  ----.-  --.---  --.---
 001  06.06    5.0  0.747  0.276  95845.2  ----.-   27.8   -17.192   28.388  122995.8  ----.-  25.894  --.---
 002  06.10    4.5  0.741  0.268  94970.6  ----.-   23.5   -17.192   28.392  122163.9  ----.-  26.082  --.---
 003  06.14    4.4  0.736  0.260  94223.0  ----.-    6.3   -17.192   28.396  121453.7  ----.-  22.295  --.---
 004  06.18    4.3  0.730  0.250  93327.5  ----.-   28.0   -17.192   28.401  120607.0  ----.-  25.404  --.---
 005  06.22    4.2  0.724  0.242  92484.9  ----.-   19.2   -17.191   28.405  119813.1  ----.-  25.128  --.---
 006  06.26    4.4  0.718  0.233  91637.7  ----.-   22.9   -17.191   28.410  119017.1  ----.-  24.037  --.---
 007  06.30    4.5  0.712  0.223  90779.4  ----.-   12.6   -17.191   28.414  118214.2  ----.-  25.601  --.---
 008  06.34    4.2  0.706  0.214  89952.7  ----.-   11.7   -17.191   28.418  117442.8  ----.-  23.456  --.---
 009  06.38    4.4  0.700  0.205  89138.2  ----.-    7.0   -17.191   28.423  116685.8  ----.-  24.298  --.---
 010  06.42    4.3  0.694  0.196  88336.2  ----.-    5.4   -17.191   28.427  115942.6  ----.-  22.756  --.---
 011  06.46    4.8  0.687  0.186  87425.2  ----.-   17.3   -17.190   28.432  115103.5  ----.-  27.177  --.---
 012  06.50    5.7  0.682  0.178  86760.7  ----.-    4.9   -17.190   28.435  114490.6  ----.-  18.858  --.---
```

Figure 7 – Exemplary *.daf file of a meteor observed simultaneously by both cameras on the 07.08.2013 at 01:44:06.

6 Corrected settings

After noticing the difference in the detection probability of ICC7 and ICC9 the detection software settings were examined. This revealed a difference in the configurations. ICC7 detected a meteor if it is recognizable on at least two frames. ICC9 needed three frames to register a meteor detection. This discrepancy has been corrected. Since June 2014 both cameras only detect a meteor if it is visible on at least three frames. Furthermore, a new reference star file was created using the tool RefStars from the *MetRec* software suite. This file sets up the relation between pixel value and magnitude. To find out if this was the reason for the higher detection rate of ICC9 the plots of Sections 2 and 5 are redone for June, July and half of August 2014 (compare *Figure 8* and *Figure 9*). In these months the configurations were adjusted. Unfortunately, there was a problem with the time synchronizing of the computers corresponding to the cameras. Therefore, there is no simultaneous meteor data yet.

Figure 8 shows the number of meteors over the magnitude. It is obvious that the brightness distribution is now the same for ICC7 and ICC9, although no magnitude correction was done. This is consistent with the assumption that the apparent sensitivity difference was the effect of the settings of the detection software. However, ICC9 still detects more meteors than ICC7. To compare this number difference *Figure 9* has been created. In this figure the average monthly hourly rate of the months with corrected settings is plotted. Nonetheless, on average ICC9 registered about 1.5 meteors more per hour than ICC7. It has to be taken into account that only data of three months was examined. To get significant results it is necessary to analyze more data

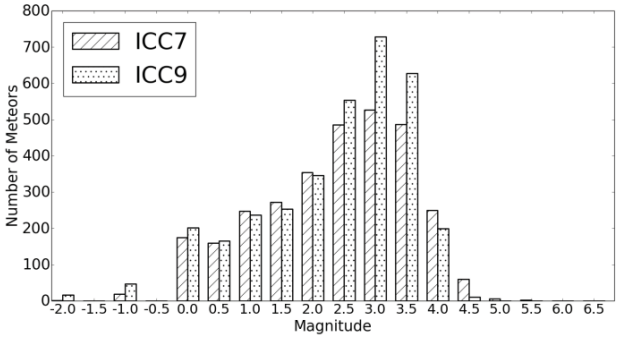

Figure 8 – Magnitude distribution of data form June, July and August 2014. The number of meteors observed by ICC7 is shown as striped bars. Those detected by ICC9 as dotted bars.

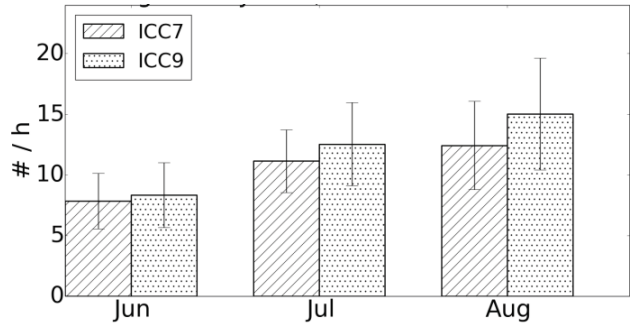

Figure 9 – Monthly average of the hourly rates of the three month data with corrected settings. ICC7: striped bars. ICC9: dotted bars.

with the new, corrected settings. However, the fact that ICC9 detects more meteors than ICC7 seems to be not an effect of the different settings and has to be analyzed more closely.

7 The viewing directions

It is now obvious that ICC9 detects more meteors than ICC7 over the same time period. Sensitivity differences between the cameras were found to not be a significant factor in the previous section. Furthermore, this difference cannot be traced back to longer observation times due to different weather conditions at one station because the hourly rates of the observing times were considered. Still, different detection settings cannot be ruled out as a reason until new data is analyzed.

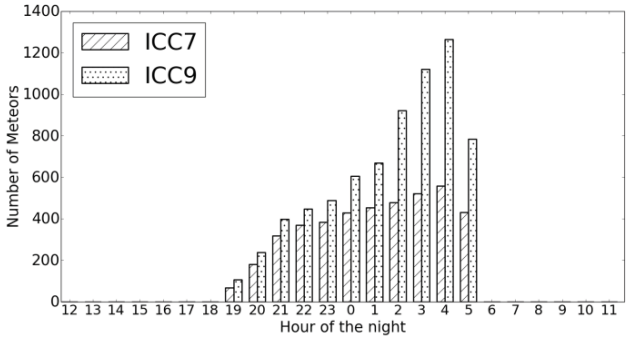

Figure 10 – Number of detected single-station meteors throughout the night. Meteors observed by ICC7 are shown as striped bars, those detected by ICC9 are presented as dotted bars.

If no further factors can be found for the discrepancy, it seems to be a result of the different viewing directions of the cameras (compare *Figure 1*). ICC7 is located on Tenerife and looks at the sky above La Palma. Accordingly, ICC7 looks to North-West. ICC9 is located on La Palma and looks to South-East.

In *Figure 10* the number of detected single-station meteors of one year is plotted over the hour of the night. It can be seen that ICC9 detects more meteors than ICC7, especially during the early morning hours.

The fact that ICC9 sees more meteors than ICC7 can correspondingly be explained by its viewing direction. ICC9 is located on La Palma and looks to the East. In the East a lot of meteors can be detected in the early morning hours. This is due to the Apex contribution in the early morning hours, when the observer sees all the fast meteors orbiting the Sun in the opposite direction as the Earth. Therefore ICC7, looking to the West, detects a lot less meteors in those morning hours, than ICC9 does looking to the East.

8 The mass distribution

To calculate the mass of meteoroids corresponding to the recorded meteors a formula by Franco Verniani (1973) was used. His formula is the result of an analysis of about 6000 meteors recorded under the Harvard Radio Meteor Project. For his data Verniani found pre atmospheric meteoroid masses in the rage of 10^{-6} – 10^{-2}gram, whereas most of the meteoroid masses were found to be in an interval of $4 \cdot 10^{-6}$ – $4 \cdot 10^{-3}$gram. Furthermore, he computed a mean mass value of about 10^{-4} gram. From Verniani (1973) the following equation was extracted:

$$m = 63.71 - 10 \cdot \log(v) - 2.5 \cdot \log(M)$$
$$-2.5 \cdot \log(\cos(Z_R)) \qquad (2)$$

m is the absolute magnitude of the meteor at maximum light, v is the velocity, M is the meteoroid mass outside the Earth's atmosphere and Z_R is the zenith angle. For the CILBO data a mean zenith angle of $Z_R = 45°$ is assumed. The process of deriving the velocity is explained in Drolshagen et al. (2014) and the utilized absolute magnitude was averaged for both cameras. Solved for the mass the equation results in:

$$M = 10^{\frac{-m+64.09-10\cdot\log(v)}{2.5}} \qquad (3)$$

It has to be taken into account that Verniani's formula utilizes CGS-units. Due to this the velocity has to be stated in cm/s and the resulting mass is derived in grams. Furthermore, it has to be noted, that Verniani used the radio method for meteor detection. Therefore, he was able to detect fainter and consequently smaller meteors than those found by the video observing method. For example, about 50% of all his meteors had a magnitude between +8 and +9 whereas the CILBO system detected none in that magnitude interval.

In *Figure 11* the mass distribution resulting from the CILBO data of one year is shown. In this graph the axes are logarithmic. The masses are binned in 0.01 g bins and cumulatively plotted. It is obvious that most of the meteoroids are very small. 1769 meteors were created by meteoroids that fall into the first bin and have a mass under 0.01 g. This agrees with the expectations of very small meteoroids.

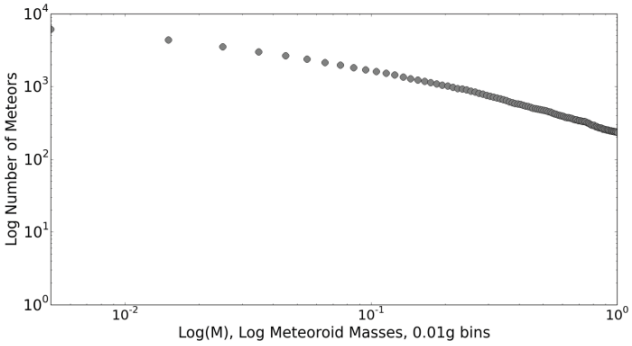

Figure 11 – Mass distribution of the CILBO data of one year calculated using Verniani's mass formula.

9 The flux

To determine the flux the area covered by both cameras in 100 km is needed (cross section of both fields of view at 100 km height). In *Figure 12* a top view of the area

covered by both cameras can be seen. The figure corresponds to a height of 100 km.

The areas of the field of view A in 100 km altitude of the cameras are:

$$A_{ICC7} = 3562.78\,\mathrm{km}^2, \qquad A_{ICC9} = 3878.91\,\mathrm{km}^2$$

And the shared field of view of the cameras is:

$$A_{Overlap} = 2943.71\,\mathrm{km}^2$$

To determine the flux of the double station observations the data of one year is utilized. With the calculated area covered by both cameras, the mass distribution, and the effective observing time $T = 1799.51$ h (the time when both cameras were simultaneously active in the analyzed year) it is possible to determine the flux F. The flux is the cumulative number of meteors per second and m^2 from meteoroids with masses equal to or bigger than M. In *Figure 13* the calculated flux is plotted. For this graph all double station meteors observed in one year are utilized. Furthermore, the theoretical flux curves derived from the models by Grün et al. (1985) and Halliday et al. (1996) are presented. The solid line shows the flux by Grün et al. and the dashed curve the flux by Halliday et al. The dots are the flux values resulting from the CILBO data. It is apparent that until a mass of about 1 g is reached the slope of the CILBO values is similar to the one calculated by Halliday et al. The flux for meteoroids smaller than 1 g is similar to predictions from the Grün et al. model. The decrease for higher masses does not match any of the curves. To compare the three models one has to keep in mind that Verniani has used radio observations for his studies. Due to this the mass formula might not be compatible with the utilized video measurements. Furthermore, it has to be taken into account that Grün's theory is a result of micro lunar crater data, infrared measurements of dust in space and in situ experiments and Halliday et al. have utilized only fireballs for their studies. Nevertheless, our flux values are in the same order as the ones calculated by Grün et al. and Halliday et al. and fit especially the Grün et al. model well.

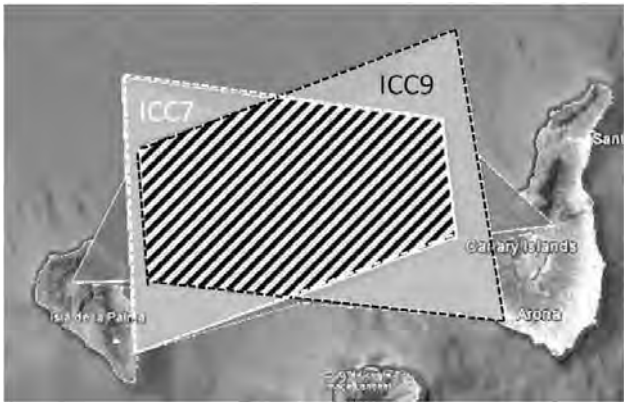

Figure 12 – Sketch of the area covered by both cameras (striped area). The cross section of the field of views at a height of 100 km above the Earth's surface is presented.

A closer look at *Figure 13* reveals a flux value for a meteoroid with a mass of 1 g or bigger of 10^{-14} $Meteoroids/\mathrm{m}^2 \cdot s$. That means that at any given moment such a meteoroid can be found in a cube with edge length of 1000 km.

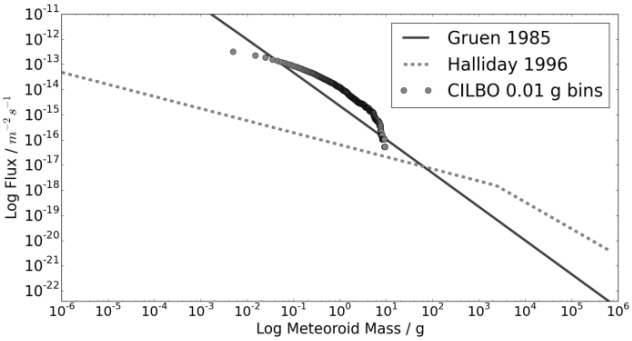

Figure 13 – Meteoroid flux: Number of meteoroids per m^2 and second with meteoroid masses equal to or bigger than M. Dots: The CILBO data flux, solid line: The flux according to Grün et al., dotted line: The flux derived by Halliday et al.

10 Conclusion and future work

The CILBO data collected in one year yield more than 6000 usable simultaneous meteor observations. The double-station data offers a lot of information about the magnitude, the direction and the flux of those meteors.

ICC9 detects about 15% more meteors than ICC7 in the analyzed year. Even after matching all settings the camera on La Palma records on average 1.5 meteors per hour more than the one on Tenerife. The viewing direction is probably one of the reason for the higher number of meteors detected by ICC9, looking towards East, than by ICC7 looking to the West. In the East a lot of meteors can be detected in the early morning hours. This is due to the Apex contribution of the early mornings, when the observer sees all the fast meteors orbiting the Sun in the opposite direction as the Earth. Nevertheless more systematic errors have to be uncovered.

The calculated masses were in the expected size category since a lot of the meteoroids which caused the meteors are smaller than 0.1 g. Despite that, the mass model should be adjusted from radar to video observations.

The computed flux from the CILBO data fits the Grün model well. At any given moment an exemplary meteoroid with a mass equal to or bigger than 1 g would be found in a cube with an edge length of 1000 km. However, the discrepancy of the in situ model or fireball model to actual video computations should be determined.

References

Drolshagen E., Ott T., Koschny D., Drolshagen G., and Poppe B. (2014). "Meteor velocity distribution from CILBO double station video camera data". In Rault J.-L., and Roggemans P., editors, *Proceedings of the International Meteor Conference*, Giron, France, 18–21 September 2014. IMO, pages 16–22.

Green D. (1992). "Magnitude Corrections for Atmospheric Extinction". *International Comet Quarterly*, **14**, 55–59.

Grün E., Zook H., Fechtig H., and Giese R. (1985). "Collisional Balance of the Meteoritic Complex". *Icarus*, **62**, 244–272.

Halliday I., Griffin A., and Blackwell A. (1996). "Detailed data for 259 fireballs from the Canadian camera network and inferences concerning the influx of large meteoroids". *Meteoritics and Planetary Science*, **31**, 185–217.

Koschny D., and Diaz del Rio J. (2002). "Meteor Orbit and Trajectory Software (MOTS) - Determining the Position of a Meteor with Respect to the Earth Using Data Collected with the Software MetRec". *WGN, the Journal of the IMO*, **30**, 87–101.

Koschny D., Bettonvil F., Licandro J., van der Luijt C., Mc Auliffe J., Smit H., Svedhem H., de Wit F., Witasse O., and Zender, J. (2013). "A double-station meteor camera setup in the Canary Islands – CILBO". *Geoscientific Instrumentation Methods and Data Systems*, **2**. 339–348.

Koschny D., Mc Auliffe J., Bettonvil F., Drolshagen E., Licandro J., van der Luijt C., Ott T., Smit H., Svedhem H., Witasse O., and Zender, J. (2014). "CILBO - Lessons learnt from a double-station meteor camera setup in the Canary Islands". In Rault J.-L., and Roggemans P., editors, *Proceedings of the International Meteor Conference*, Giron, France, 18–21 September 2014. IMO, pages 10–22.

Molau S. (1999). "The Meteor Detection Software MetRec". In, Baggaley W. J. and Porubcan V., *Proceedings of the International Conference Meteoroids 1998*, 17–21, 1998, Tatranska Lomnica, Slovakia, pages 131–134.

Verniani F. (1973). "An Analysis of the Physical Parameters of 5759 Faint Radio Meteors". *Journal of Geophysical Research*, **78**, 8429–8462.

The author, Theresa Ott, during her lecture. (credit Bernd Klemt.)

High resolution photographic imaging

Felix Bettonvil[1,2,3]

[1] **Sterrewacht Leiden, Universiteit Leiden, Niels Bohrweg 2, 2333 CA Leiden, The Netherlands**

[2] **NOVA Optical and Infrared Instrumentation Division at ASTRON, Oude Hoogeveensedijk 4, 7991 PD Dwingeloo, The Netherlands**

[3] **KNVWS Meteor Section, The Netherlands**

F.C.M.Bettonvil@strw.leidenuniv.nl

A high-resolution camera is described, based on DSLR technology and long focal length lens together with a 200 cycles/sec optical shutter, with the aim to collect higher accuracy orbital elements. The paper describes the design considerations, test setup, and analyses and discusses the first results.

1 Introduction

Trajectories in the atmosphere and an estimate of the velocity are required for the determination of meteor orbits. In optical imaging the velocity is traditionally measured with a rotating shutter (Millman, 1936; Kohoutek, 1959) in front of the lens or in between the lens and film or detector. The accuracy of this modulation, as well as the modulation speed and astrometric accuracy of the exposure determine how well the velocity of the meteor can be estimated.

In (Bettonvil, 2008) an alternative method for modulation was proposed, which does not rely on rotating choppers but instead on a Liquid Crystal (LC) optical shutter, which periodically switches between dark state and transparent, which was successfully applied to an All-sky camera (Bettonvil, 2014). Recent developments of this technology have now made available even faster LCs, which allow for modulation frequencies up to 200 Hz and even more[1]. This opens the way to observations with higher resolution, which should enable determination of orbits with higher accuracy, allowing for more strict D-criteria (Galligan, 2001), as the parameter velocity is a sensitive parameter in the determination of the orbit. Obtaining orbits with higher accuracy is highly interesting as it allows detection of fine structures in meteoroid streams at a more detailed level.

This paper, i) describes the details of a high-resolution camera based on the LC shutter technology, ii) presents the first results obtained with this system and iii) discusses them.

2 Design

The basis of the system is one of the fast Liquid Crystal optical shutters, as manufactured by LC-Tec, Borlänge, Sweden[1]. From the various types they produce, the X-FOS(G2) type was chosen, having open/closing times of 50µs/1.6ms, and with ~130EUR/pcs at reasonable cost/performance ratio. The switching behavior allows for modulation frequencies up to several hundreds cycles/sec. The modulation signal is achieved through a standard crystal based function generator, typically specified at frequency accuracies at 10^{-6} and stabilities at 10^{-6} level, which is more than sufficient for our needs.

Figure 1 – Setup of the high-resolution camera: Canon EOS 1100D with Nikkor 50mm F/2 lens and in between (not visible, LC-TEC X-FOS(G2) optical shutter. The function generator for shutter control is visible below the tripod (in blue), as well as an exposure controller.

An improved plate scale is achieved by increasing the focal length of the system. Here a wide range of lenses was analyzed and an optimum searched for orbit accuracy and sensitivity/yield. The parameter chosen to be

[1] http://www.lc-tec.com/optical-shutter

optimized is the multiple of both, as both the aim is to increase accuracy, but on the same time not decreasing yield to negligible numbers, which in the extreme case would result in no statistical relevance. Finally, a 50mm F/2 was chosen as best for the first tests, giving a Field of View of 25 x 17 deg^2.

The design is similar to that of the All-sky camera (Bettonvil, 2014), the shutter is built between camera and lens. For the test a Canon EOS, 1100D was used, equipped with a 12.2 MPxl sensor. *Figure 1* gives an overview of the entire camera setup.

3 Test setup and results

A first test was scheduled during the Perseids meteor shower, in August 2014 from Bosnia. Despite the non-perfect conditions (i.e. full moon), this major shower should anyhow result in a number of recordings.

In order to optimally capture the meteor trails, the camera was oriented such that the long axis of the detector was always reasonable well aligned with the radiant. This was done manually by realigning the camera around the third axis of the tripod periodically according to a pre-computed table. This ensured that the meteor in theory would travel over a maximum of pixels.

Figure 2 – Example of Perseid as captured with the camera on August 11, 2014, 20.33 UT: Perseid +1 in Dra/UMa, crop 14° x 14°, Canon 1100D + Nikkor 50mm/F2.8, 200 cycl/sec, ISO6400, T=15s, Međeđa, Bosnia & Herzegovina. The entire trail contains 82 breaks.

For the first test, single station observations were performed, meaning that in theory no orbit could be determined. Nevertheless an estimate could be made based on assumptions on the typical height of (Perseid) meteors. In first order this should give sufficient insight in how well the velocity could be estimated and its impact on the orbital elements.

Camera sensitivity was chosen at ISO 6400 (max for EOS 1100D, diaphragm set to F/2.8 to enhance image quality, and exposure times 15s. Various modulation frequencies were tested (50-100-200 cycl/sec.).

During 9 nights, 13000 exposures were made, which delivered a modulated airplane and 10 meteor trails. The nicest example is reproduced in *Figure 2*.

4 Reduction

Aim of this first test was to analyze which accuracy can be achieved for the orbit. As for this test, as mentioned in the previous section, no double station was available, an assumption was made, as illustrated in *Figure 3*. First, astrometry was done of the real station 'A'. Then we assumed that from a fictive station 'B' the meteor was seen through both zenith and radiant, together forming a (vertical) plane. This plane and the plane through station 'A' and the meteor, then were intersected, with the exact location of station 'B' still a variable. The station location was moved around until the meteor appeared on a proper height (in our case the begin- and end height being 103 respectively 94km).

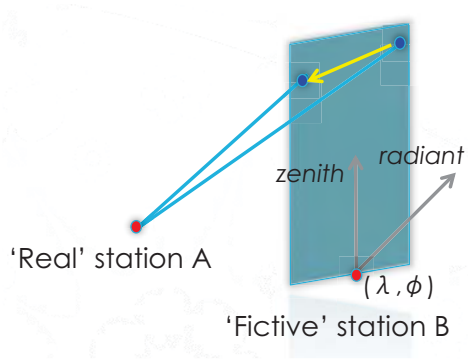

Figure 3 – Principle of estimation of the atmospheric trajectory. For explanation see text.

In this paper we focus entirely on analysis of the meteor of *Figure 2*. The trail shows 82 breaks and spans ~1500 detector pixels, lasting for ~0.3sec. Evidently, only the last part of the trail is captured.

Astrometry of the image was done with help of the online astrometry tool astrometry.net[2]. Due to the only small optical distortion apparent in the image, this gave acceptable results for this test. The obtained plate relation between (x,y) pixel values and (R.A., declination) sky coordinates was double checked with SAO Image DS9.

A rough indication of the brightness of the meteor was done by comparing the break with maximum brightness with a star showing equal counts, and neglecting any spectral difference. Based on this approximation a meteor brightness of ~M_v = +1 was found.

For estimation of the velocity several measurement methods were tested:

1) manual measurement of the start of all breaks (blue curve in *Figure 3*)

[2] http://astrometry.net/

2) Centroiding of all breaks (green curve in *Figure 3*)
3) Fast Fourier Transform of the entire trail.

For all methods, the pixel coordinates of all breaks were obtained from the image, transformed into (R.A., declination) coordinates and then into (h, Az) coordinates. Through all (h,Az) directions a plane is then constructed and intersected with the other plane from the fictive station. The intersection line represents the atmospheric trajectory. The 3D velocities are finally obtained by deriving the points of minimum distance between the direction vector of each break and the atmospheric intersection line.

Method 1 and 2 show that there is not much difference between them, with similar break-to-break variations. A fit through all data points also indicates that no clear evidence of deceleration can be found. With break #1 the beginning of the trail and break #82 the end, the small change in velocity even points the other way around. In the remainder of this paper I assume therefore no deceleration is present, and focus because of this on deriving the *average* velocity.

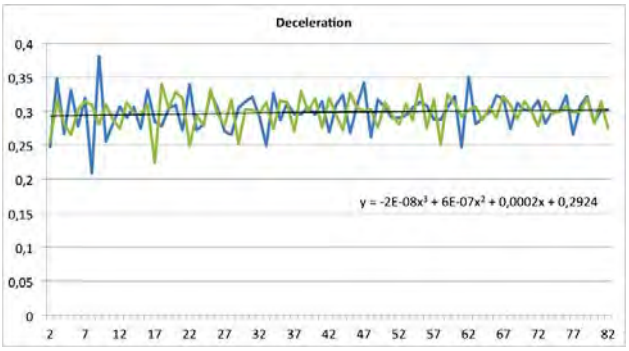

Figure 4 – Measurement of centroids along trails (manual measurement – blue; centroiding – green). The black line represents a fit through all data.

In case of method 1 and 2, for deriving the average velocity, from all measurement points the typical velocity measurement error was estimated, being in the order of 5%. Then three successive points on both beginning and end of the trajectory were identified, of which all three have minimal deviation from the average velocity. These points are regarded as a good representation of the average velocity. The average velocity follows then from the total span of breaks between the two points, divided by the time span, and the accuracy from the average measurement accuracy of all 82 data points. *Table 1* gives the results. No other filtering is applied, e.g. RANSAC as described in (Egal, 2014).

The third method is based on transformation of the trajectory from time domain into frequency domain with the help of the Fast Fourier Transform as introduced in (Bettonvil, 2008). The dominant frequency represents the apparent velocity, which then is converted into a 3D velocity. The estimate for the accuracy is obtained from the deviation of the fit of a Gaussian through the frequency peak (Bettonvil, 2008).

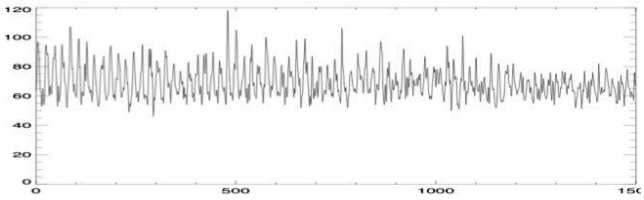

Figure 5 – Intensity profile through the center of the entire meteor trail.

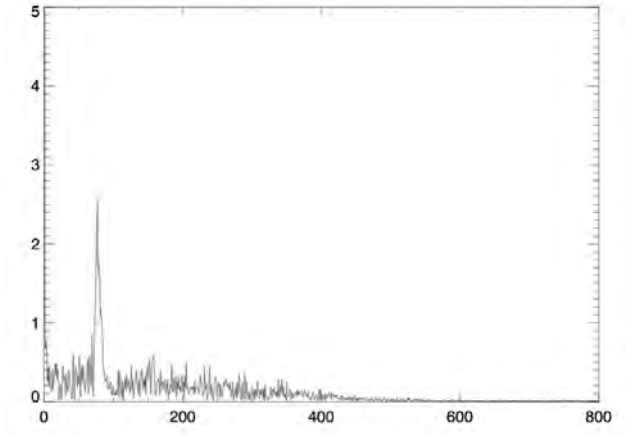

Figure 6 – FFT of the intensity profile of *Figure 5*.

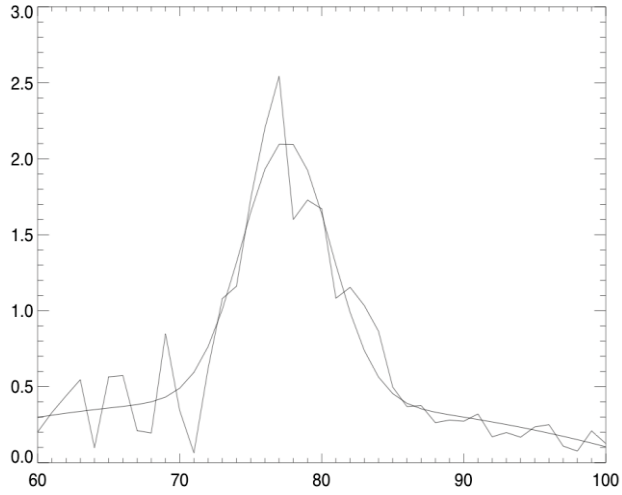

Figure 7 – Detail of Figure 6, with Gaussion fit through the peak.

Table 1 – Derived velocities for all applied methods.

Method	Velocity
Spatial measurement (Method 1, 2)	59,63 ± 0,04 km/s (± 0,06%)
FFT (Method 3)	59,61 ± 0,04 km/s (± 0,06%)

5 Discussion

All methods for the determination of the velocity are in good agreement with each other. In order to get insight in the effect of the velocity on the orbit, the heliocentric orbit elements and associated errors were calculated, solely based on the estimated error in the velocity. No other errors were taken into consideration. *Table 2* lists the results. The semi major axis for this (fictive) example

is 23.3 +/- 2AU. *Figure 8* illustrates how the obtained accuracy fits within the entire sample of IAU orbits.

Table 2 – Orbital elements for the Perseid meteor as analyzed.

Orbit:				
Astr. longitude of ascending node	(OMEGA)	[deg]:	138.901	+/- 0.000
Inclination	(i)	[deg]:	118.906	+/- 0.023
Argument of perihelion	(omega)	[deg]:	158.985	+/- 0.044
Semi major axis	(a)	[AU]:	23.2836	+/- 2.0413
Distance sun ~ perihelion	(q)	[AU]:	0.9805	+/- 0.0001
Distance sun ~ aphelion	(Q)	[AU]:	45.5868	+/- 4.0824

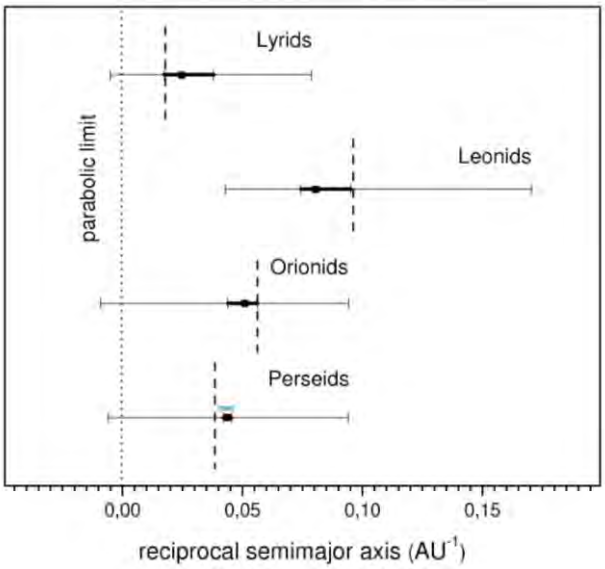

Figure 8 – Reciprocal semi major axis, inserted in a plot from Hydukova of all orbits of th IAU database (from Hydukova Jr, 2011).

6 Conclusions

The first test with the high-resolution camera showed that indeed high accuracy can be obtained, with several analysis methods being in good agreement. No deceleration could be measured from the analyzed meteor.

After this successful initial test, the aim is now to obtain a larger data sample, involving more than one shower. These observations will be done on the basis of double station work, allowing for proper orbit calculations.

Based on these results, another optimization can be done, to verify if a higher accuracy can be achieved by narrowing the field of view even more.

From the technical point of view, to further improvements are planned: 1) observing in RAW format (initial tests were carried out on jpg format; 2) motorizing the third axis of the camera mount, maintaining a proper alignment of the shower meteors and the detection field accurately.

References

Bettonvil F. C. M. (2014). "Remote and automatic small-scale observatories: experience with an all-sky fireball patrol camera". In, Ramsay S. K., McLean I. S., and Takami H., editors, *Proceedings SPIE*, Ground-based and Airborne Instrumentation for Astronomy V, **9147**, id. 91473U, 9 pages.

Bettonvil F. (2008). "Determination of the Velocity of Meteors Based on Sinodial Modulation and Frequency Analysis". *Earth, Moon, and Planets*, **102**, 205–208.

Egal A., Vaubaillon J., Colas F., Atreya P. (2014). "Low dispersion meteor velocity measurements with CABERNET". In Rault J.-L., and Roggemans P., editors, *Proceedings of the International Meteor Conference*, Giron, France, 18–21 September 2014. IMO, pages 49–51.

Galligan D. P. (2001). "Performance of the D-criteria in recovery of meteoroid stream orbits in a radar data set". *Monthly Notices of the Royal Astronomical Society*, **327**, 623–628.

Hajdukova M. Jr. (2011). "The orbital dispersion in the long-period meteor streams". *Contrib. Astron. Obs. Skalnaté Pleso*, **41**, 15–22.

Kohoutek L. (1959). "On the precision of the photographic determination of the geocentric meteor velocity". *Bulletin of the Astronomical Institute of Czechoslovakia*, **10**, 120–132.

Millman P. M. (1936). "Meteor News - A Brilliant Fireball; Meteor Photographs taken with a Rotating Shutter; Effect of Observing Conditions on Meteor Rates". *Journal of the Royal Astronomical Society of Canada*, **30**, 101–104.

The FRIPON and Vigie-Ciel networks

François Colas[1], Brigitte Zanda[2], Sylvain Bouley[3], Jérémie Vaubaillon[1], Pierre Vernazza[4], Jérôme Gattacceca[5], Chiara Marmo[3], Yoan Audureau[3], Min Kyung Kwon[1], Lucie Maquet[1], Jean-Louis Rault[6], Mirel Birlan[1], Auriane Egal[1], Monica Rotaru[7], Cyril Birnbaum[7], François Cochard[8], Olivier Thizy[8]

[1] **IMCCE, Observatoire de Paris, 77 av. Denfert-Rochereau, 75014 Paris, France**
colas@imcce.fr, vaubaill@imcce.fr, Mirel.Birlan@imcce.fr, mkwon@imcce.fr, lucie.maquet@imcce.fr

[2] **IMPMC, MNHN - UPMC, 61 rue Buffon, 75005 Paris, France.**
zanda@mnhn.fr

[3] **GEOPS (Géosciences Paris Sud), Université Paris Sud, 91405 Orsay Cedex, France**
sylvain.bouley@gmail.com, chiara.marmo@u-psud.fr

[4] **LAM (Laboratoire d'Astrophysique de Marseille) UMR 7326, F-13388 Marseille, France**
pierre.vernazza@lam.fr

[5] **CEREGE, Aix - Marseille Université CNRS, Aix en Provence, France**
gattacceca@cerege.fr

[6] **IMO Radio Commission, 16, rue de la Vallée, Epinay sur Orge, France**
f6agr@orange.fr

[7] **UNIVERSCIENCE, 30 Avenue Corentin Cariou, 75019 Paris, France**
urator@hotmail.fr, Cyril.birbaum@universcience.fr

[8] **SHELYAK Instrument 73 rue de Chartreuse 38420 Le Versoud, France**
francois.cochard@shelyak.com, olivier.thizy@shelyak.com

FRIPON (Fireball Recovery and interplanetary Observation Network) is a French fireball network recently founded by ANR (Agence Nationale de la Recherche). His aim is to connect meteoritical science with asteroidal and cometary sciences in order to better understand the solar system formation and evolution. The main idea is to cover all the French territory in order to collect a large number of meteorites (one or two per year) with an accurate orbit computation allowing us to pinpoint the parent bodies of the meteorites. About 100 allsky cameras will be installed in 2015 to create a dense network with an average distance of 100 km between two stations. In order to maximize the accuracy of orbit determination, we will mix our optical data with radar data from the GRAVES beacon received by 25 stations (Rault, 2014). As the network installation and the creation of the research teams for meteorites need many persons, at least much more than our small team of professionals, we will develop in parallel a participative science network for amateurs called Vigie-Ciel. As FRIPON is an open project, anybody will be able to buy a “FRIPON like" camera to be within the network, using our FreeTure detection software (Audureau, 2014; Kwon, 2014). Vigie-Ciel will also be used by observers using other types of cameras and by teams of meteorite researchers. Finally we will use the public affinity with meteors and meteorites to develop scientific activities to popularize science.

1 Scientific goals

The aim of the FRIPON project (Fireball Recovery and interplanetary Observation Network) is to answer questions that arise about the relationship between meteorites and asteroids. It is easy to study a meteorite in a laboratory but we have no idea where it came from because for most of them the orbit is unknown. On the other hand, we have currently more than 700000 orbits of asteroids with little or no physical information. However these parameters are crucial for understanding the origin and evolution of the solar system. In recent years, the planet migration theory has shown that it is possible to find very primitive objects in the main asteroid belt, and that these things may hit the Earth due to the Yarkovsky non-gravitational forces. It is therefore essential to know the orbits of the meteorites found on the ground to connect their dynamic history and composition. This knowledge also works in both directions, namely it will allow us to have an idea about the origin of meteorites, but also about the material that makes up asteroids.

2 The FRIPON and Vigie-Ciel projects

To make the connection between asteroids and meteorites, we need accurate orbit parameters for each recovered meteorite. For this purpose, we plan to install a dense video camera network on the entire French territory. A network with a 100 km spacing between the stations will allow to compute an impact location better than one kilometer (Brown, 2011; Oberts, 2004). We will also install radio receivers using the military radar GRAVES (designed for searching space debris) that will

allow us to minimize velocity measurement errors and therefore to obtain better orbital elements, especially for the semi-axis. One of the originalities of our project is that it is linked to a social network called Vigie-Ciel that will form the basis of our organization. We will use public interest in meteorites and asteroids to provide outreach. Our network will be based on regional laboratories which will be responsible for four or five cameras and a radar receiver. The cameras will be installed in all structures disseminating science, such as museums, planetariums, amateur observatories, etc. The data of the cameras will be accessible via the network. The information collected by the Paris Observatory will allow to decide the triggering of a field search mission.

Another originality of the project is that we associate the know-how of two old laboratories of astronomy and celestial mechanics, IMCCE and the National Museum of Natural History. Associating asteroids and meteorites is also the way to connect two laboratories! At the end of the project, we will have very little altered meteorites for the national collection of the museum but also a unique database combining the best available information on these objects. After 10 years, we hope to have about ten to twenty meteorites with statistically rare items. We will also have hundreds of orbits of quality. We will answer the question about the origin of meteorites and may be based on specimens, discover information about the early solar system.

3 FRIPON compared to other networks

France is isolated, especially when compared to networks in Northern, Eastern and Southern Europe (*Figure 1*). Moreover, if we remove the professional observatories dedicated to meteors, then we only have the European Fireball Network, composed of 40 fish eye cameras covering Germany, Belgium, the Czech Republic and Slovakia and the SPanish Meteor Network (SPMN). These networks use mainly analogic video cameras. We will use modern digital cameras offering a better resolution and higher frame rates. We based our reflections on the successful ASGARD All-Sky Camera Network in Canada[1] (Brown, 2011).

The national meteorite collection was started over 200 years ago and is one of the largest in the world, holding the main masses (or significant samples) of 520 of witnessed falls, leaving only the collections of the British Museum (Natural History) in London (620) and of the Smithsonian Institution in Washington (530) with a larger number of meteorites. To these 520 “falls”, over 1000 “finds” are added - the latter being meteorites found a significant amount of time after their fall, often weathered from being exposed to terrestrial alteration, which makes them scientifically less valuable. Out of the 520 falls within the Museum collection, 59 fell in France. Most of the additional 6 known to have fallen in France date from the 18th century and before and there are no known samples left.

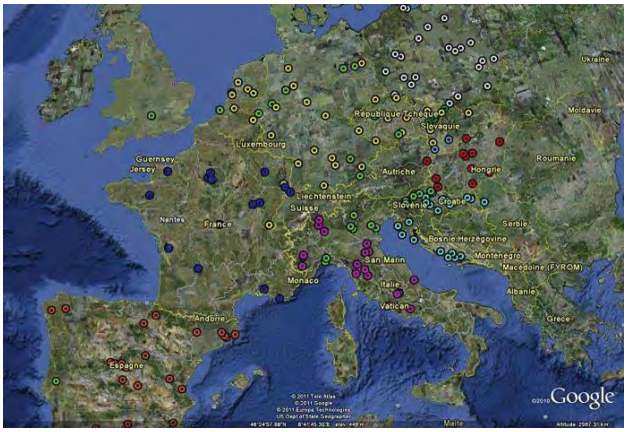

Figure 1 – Observation networks in Europe. The only fish eye observatories are shown by orange (Spain), red (Slovakia) and light blue dots (Czech Republic). All other cameras are small field, not nearly as efficient for the detection of fireballs.

The small number of meteorites known, their scientific interest and financial value (acquired within the last 20 years) makes the national Meteorite Collection unique amongst those preserved at the *Muséum national d’Histoire naturelle* because, despite its patrimonial character, it is being used for outreach and teaching and is, at the same time, the irreplaceable support of the Cosmo-chemistry research of the national and international communities, meaning that a small fraction of samples will be allocated to perform “destructive” analysis or to be included in sample preparations for in situ analysis: over 1300 polished thin and thick sections are thus available for loans. Expending our national collection means to search ourselves newly fallen meteorites in order to bypass the growing private market.

The largest part of the meteorite collections come from unknown falls, so they have undergone significant alteration that prevents comparison with asteroids. Our response time is essential, especially if we find meteorites as fragile as the Orgueil one. Our goal is to start the search for the next day of the fall and to continue for a week. We must also take into account the soil conditions which can quickly get rid of meteorites.

Note that the conservation in the public collections of rare objects is an essential goal. We can compare for example the case of the meteorites Alais (Ales) and Pride, weighing 6 kg and 14 kg respectively, with falls recorded in 1806 and 1864. These meteorites are the only ones to have precisely the same composition as the Sun (except for the most volatile items such as H and He) and are therefore objects of reference for the chemical composition of the solar system. The meteorites of this type have, unfortunately, also the property of being particularly vulnerable. 1864 corresponds to a time when the extraterrestrial origin of meteorites was well established, including the public which had a great interest in science. This led to a great mobilization, many samples reached the Museum. Today, Orgueil is probably the most distributed meteorite of the collection (average 15% of requests for destructive analysis). Despite having the same characteristics, Alais cannot enjoy the same

[1] http://meteor.uwo.ca/research/allsky/overview.html

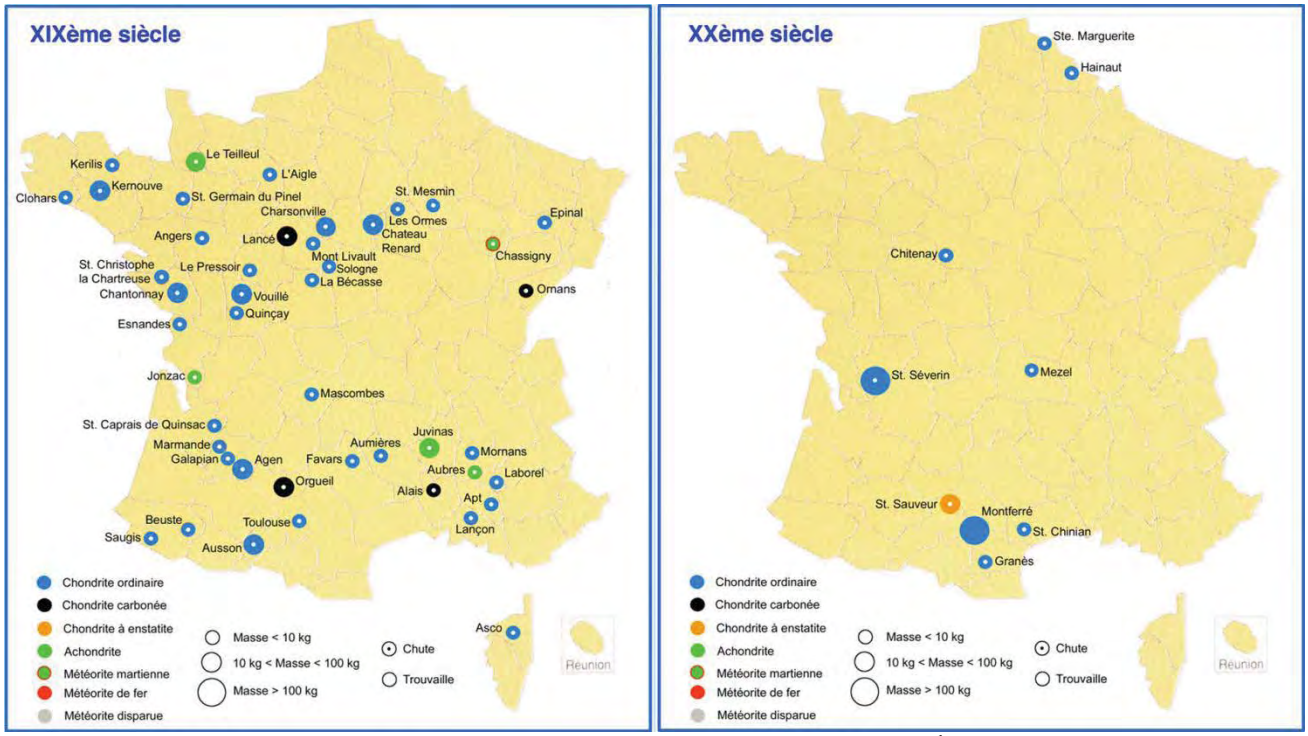

Figure 2 – Comparison of the discoveries in France. There were 64 falls in France during the 19th century, compared to 18 for the UK, 31 for Italy, 32 for Germany and 23 for Spain. Note also that 70% of the French meteorites have been found during the 19th century. This is probably due to the fact that France is (with England) the country where the origin of meteorites was early recognized as extraterrestrial. In the 19th century, the French population was mainly rural but was also aware of science. Our goal is at least to reach the same efficiency!

privileges, only 20 g reached the Museum, mainly due to an unorganized search campaign.

The statistics of *Figure 2* show that in the 19th century about one meteorite was found every two years against one every ten years for the 20th century. Literature (Halliday, 1996) shows that the average fall rate should be about 10 per year for a territory like France. So during the 19th century we found 6% of the meteorites and only 1% for 20th century! So it is possible to perform better especially with our camera network, when we replace farmers by electronic eyes! To conclude, although France is not the best place to search for meteorites (weather, land, etc.); it seems realistic to recover at least one or two meteorites per year.

4 Technical specifications

Camera

We made extended searches and tests to find the best technical solution for the all sky optical cameras. Our requests were to use at least 30 fps devices in order to get many points to measure the fireball. Of course it is better to use the biggest and the fastest camera possible, but for economic reasons, we choose one megapixel cameras presenting an affordable price. The GigE Vision protocol was chosen, as it allows cables as long as 100 m, and because it can deliver power to the camera via the "Power over Ethernet" (PoE) protocol. We focused our efforts on cameras based on the Sony chip ICX445 (1348×976 pixels, 5 x 4 mm). Finally, we choose the DMK 23G445 from the company Imaging Source. This camera can provide exposures as long as 30s, allowing astrometrical calibration frames and it is also able to use a 10µs exposure time for daytime observations. It uses a CS mount.

Lens

As we used a 1/3 inch sensor, we have to use a 1 to 1,5mm focal length. The question was between a long focal length to be more sensitive and to reduce the pixel size on the sky, or a shorter one to get the full sky. The problem was to find a lens covering the whole CCD spectrum, as many "old" design lenses were not computed to use the near infrared spectrum of the CCD. The quality of the lens is important to observe very bright objects: on saturated images, a bad lens can corrupt large CCD areas. Finally we choose the Focusave 1.25mm, f/d = 2.0 (*Figure 3*). The fwhm at zenith is 1.5 pixel and 1.8 at the horizon (*Figure 4*). We have the full sky with this lens; we did not find longer focal lengths with this quality. We choose that lens for its optical quality. The whole set with the camera will be less sensitive, but this is not so important as the goal of the operation is to observe very bright events.

Camera housing

Camera housing is important to protect the camera against weather conditions, to cool it and to avoid mist on the dome (*Figure 5*). Power over Ethernet was choose mainly because it allows using the same cable for data and for power supply, it simplifies the mechanical design but on the other hand, the camera produces as much as 10 watt of heat that must be evacuated. If not the camera will heat too much and will deliver high dark frames incompatible for our use.

Figure 3 – CS mount 1.25mm F/2.0 lens for the FRIPON.

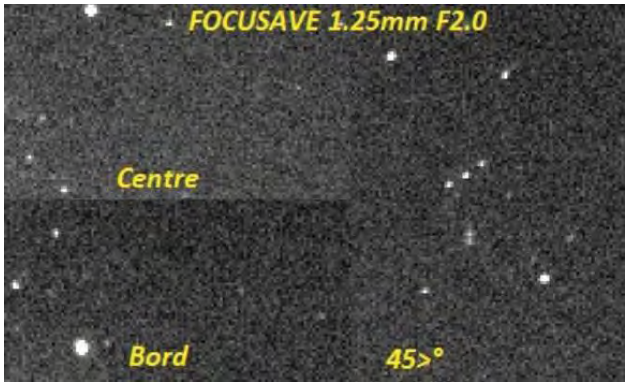

Figure 4 – Test on night sky at zenith (Centre) and horizon (Bord).

So we paid attention to design a passive-cooling system. We performed thermal tests from –20°C to +50°C, we measured a ΔT of 8°C between the temperature outside and inside the camera.

Figure 5 – FRIPON housing with passive-cooling. The main body is semi-transparent to show the camera. The overall dimensions are 150 x 70 mm and the weight is less than 1kg.

Spectroscopic observations

In order to combine all the science from asteroid/comet with meteorites, spectroscopic observations can be made from Earth at possible parent bodies with a telescope and for meteors with dedicated instruments. In fact it will be a kind of Grail to get one meteorite with the best data gathered by the best laboratory on Earth with spectroscopic and dynamical data obtained in space. More than the study of one single object, it will help for all other objects with partial knowledge. As obtaining spectra with a fish eye lens is quite impossible, we have to use small field spectroscopes in just a few locations. Fireballs brighter than magnitude -11 are easily visible from a few hundred kilometers by using a high altitude observatory. As these events occur far from the observatory, they are low on the horizon, so it is possible to use small field spectroscopes only at a low elevation to limit their number. It is typically possible to use only 8 low cost spectroscopes each with one video camera and one prism. In France, it could be possible to use Pic du Midi for the South of France and the North of Spain, Puy de Dôme for almost all France and Aiguille du Midi near Mont Blanc for the East of France and Central Europe.

5 Vigie-Ciel the collaborative network

FRIPON extended network

The FRIPON network (100 cameras over France) is founded by the ANR (Agence Nationale pour la Recherche), but since the entire project is based on open source software and hardware, it will be possible for any person or institution to copy our set-up and to install their own cameras. If the hardware is identical (GigE Vision interface for the camera and a Linux dedicated control computer) it will be possible to integrate FRIPON VPN and to be a real FRIPON partner. In fact, our 100 km spacing is mandatory for astrometric measurements, however weather conditions can be different at locations separated by only a dozens of kilometers, so more observing locations are really valuable.

Vigie Ciel "Camera"

If a person doesn't want to use the FRIPON software (Audureau, 2014), it is possible to participate in the collaborative project Vigie-Ciel. A web service will be proposed for storing any data coming from the public, even small field cameras. Detection can be manual or by using another software like UFOCapture.

Vigie Ciel "Meteorite search"

One of the goals of FRIPON is to be able to go on the strewn field within 24 hours with a large team in order to get the freshest matter. In other words we have to form a team of 50 experienced persons in one day! As this is impossible, we will train persons before the fall and maintain the motivation by organizing meetings and repetitions on the terrain.

Figure 6 – Simulation of a search at "La Ferme des Etoiles" (August 2014).

6 Schedule

FRIPON started in January 2014 for a duration of 3.5 year (ANR grant). The first half of the year was dedicated to the definition of the hardware and to consult literature for the software. The second half of the year was used to prepare contracts with companies chosen to define and to build the hardware. Meanwhile we are testing the reduction pipe line with a few cameras located in the Paris area. 2015 will be used to install the whole optical network and to finalize the software pipe line (acquisition, detection, astrometry, computing orbits and strewn field) (Kwon, 2014). The optical network will be fully operational before the end of 2015. During the same year, we will start to install the radio network. 2016 will be used to mix optical and radar data as well as to process the meteor radar observations, the seismic and the infra-sound data.

7 Conclusion

FRIPON is not really innovative as most of the techniques are known for a long time, but many things are specific:

- Size of the network (640 000Km^2);
- Number of cameras (100);
- Density;
- Daytime operation;
- Mega pixel digital cameras;
- Systematic combination with radar data;
- Systematic spectroscopic observations;
- Systematic measurement of Cosmic Rays;
- Exposition time (CRE);
- Systematic measurement of isotopic elements;
- Formation of a collaborative science network;
- Open project.

This last point is perhaps one of the most important as no detection software at that time is free of charge. Moreover, all the code will be also released for personal modifications. This is important to allow installing new cameras types in the future. We also try to keep the budget reasonable to permit everybody to copy the tools for personal use. To popularize our extended network, it will be possible to use the FreeTure software in a sharing mode (Audureau, 2014). In this mode, 5 to 10% of the time could be used to make long time exposure and therefore nice deep images usable to monitor dark sky, the remaining time could be used for FRIPON with a high acquisition rate.

Acknowledgments

Thanks to ANR (Agence Nationale de la Recherche) for funding the FRIPON network and ANRU (Agence Nationale de la Rénovation Urbaine) for funding the science collaborative network “Vigie-Ciel”. We also want to thank the “Ferme des Etoiles” for allowing us to organize a test search in the field and generally all the FRIPON network people (regional leaders, responsibles for cameras, etc.) which represent 150 persons.

References.

Audureau Y., Marmo C., Bouley S., Kwon M.-K., Colas F., Vaubaillon J., Birlan M., Zanda B., Vernazza P., Caminade S., Gatteccaca J. (2014). “FreeTure, A Free software to capTure meteors for FRIPON”. In Rault J.-L., and Roggemans P., editors, *Proceedings of the International Meteor Conference*, Giron, France, 18–21 September 2014. IMO, pages 39–41.

Brown P., McCausland P. J. A., Fries M., Silber E., Edwards W. N., Wong D. K., Weryk R. J., Fries J., Krzeminski Z. (2011). “The fall of the Grimsby meteorite—I: Fireball dynamics and orbit from radar, video, and infrasound records". *Meteoritics & Planetary Science*, **46**, 339–363.

Halliday I., Griffin A. A., Blackwell A. T. (1996). “Detailed data for 259 fireballs from the Canadian camera network and inferences concerning the influx of large meteoroids”. *Meteoritics & Planetary Science*, **31**, 185–217.

Kwon M.-K., Colas F., Vaubaillon J., Birlan M., Zanda B., Marmo C., Bouley S., Audureau Y., Vernazza P., Gattacceca J. (2014). “Astrometry with fish eye lens and orbit determination”. In Rault J.-L., and Roggemans P., editors, *Proceedings of the International Meteor Conference*, Giron, France, 18–21 September 2014. IMO, pages 42–43.

Oberst J., Heinlein D., Köhler U., Spurný P. (2004). “The multiple meteorite fall of Neuschwanstein: Circumstances of the event and meteorite search campaigns”. *Meteoritics & Planetary Science*, **39**, 1627–1641.

Rault J-L, Colas F, Vaubaillon J. (2014). “Radio set-up design for the FRIPON project”. In Rault J.-L., and Roggemans P., editors, *Proceedings of the International Meteor Conference*, Giron, France, 18–21 September 2014. IMO, pages 185–186.

FreeTure
A Free software to capTure meteors for FRIPON

Yoan Audureau[1], Chiara Marmo[1], Sylvain Bouley[1], Min-Kyung Kwon[2], François Colas[2], Jérémie Vaubaillon[2], Mirel Birlan[2], Brigitte Zanda[3], Pierre Vernazza[4], Stephane Caminade[5], Jérôme Gattecceca[6]

[1] **Université Paris-Sud, Laboratoire GEOPS, UMR8148, Orsay, F-91405, France**
yoan.audureau@u-psud.fr, chiara.marmo@u-psud.fr

[2] **IMCCE, Observatoire de Paris, France**

[3] **MNHN, Paris, France**

[4] **LAM, Université Aix Marseille, Marseille, France**

[5] **Université Paris Sud, IAS, UMR8617, Orsay, France**

[6] **Université Aix Marseille, CEREGE, Aix-en-Provence, France**

The Fireball Recovery and Interplanetary Observation Network (FRIPON) is a French project started in 2014 which will monitor the sky, using 100 all-sky cameras to detect meteors and to retrieve related meteorites on the ground. There are several detection software all around. Some of them are proprietary. Also, some of them are hardware dependent. We present here the open source software for meteor detection to be installed on the FRIPON network's stations. The software will run on Linux with gigabit Ethernet cameras and we plan to make it cross platform. This paper is focused on the meteor detection method used for the pipeline development and the present capabilities.

1 Introduction

The French FRIPON project aims to detect fireballs and to retrieve related meteorites on the ground. It also aims to detect standard meteors and to build a database of computed orbits to find related parent bodies. To do that, more than 100 stations will cover the complete surface of France. Each one will be equipped with an all-sky GigE camera and a computer. On each local computer, a software will be used to control the camera and to detect meteor events. A lot of software exist to do that, but some are proprietary (e.g. UFOCapture[1]) and the others are hardware dependent or not cross platform (Molau, 98). FRIPON needs a new meteor detection software because of its number of stations and it should have the possibility to easily modify or to develop some features. With a free, open source and a cross platform software, FRIPON can be easily extended by installations on amateur or professional stations. Thus, the public could start contributing to the project by sharing their information about a detected event or by adding new features to the software for maintaining or improving it. Anyone could for example add the support of a new camera, add new detection algorithms or build a GUI.

2 Initial features

The software is developed in *C++* using *Boost*[2] and *OpenCV*[3] libraries to easily make it cross platform on Linux and Windows operating systems. The following features were required:

- Continuous real time meteor detection, day and night.
- Input frames grabbed from a GigE camera or from a pre-recorded video.
- Output files in time sequences or stacked frames.
- Output *FITS* files (among others) without any destructive compression for scientific analysis.
- Open Source.

Table 1 – Meteor detection software.

	Open source	Platform	Output
UFO Capture[1]	no	windows	.csv, xml, avi, jpg. …
MetRec (Molau 98)	yes	Msdos, w95, w98	.bmp …
ASGARD[4]	no	Linux (debian)	.tar (.png), .txt, avi …
MeteorScan (Gural96)	no	Mac, windows	.tiff …
FRIPON (fripon.org)	yes	Linux, windows	.avi,, jpg, fits 2D, fits 3D

[1] UFOCapture, http://sonotaco.com/e_index.html.
[2] Boost: http://www.boost.org/
[3] OpenCV: http://opencv.org/

3 General software structure

We describe here the general layout of the software. Four parallel processes run at the same time: Acquisition, Stack acquisition, Detection and Recording. Their parameters may be set in a configuration file included in the package. The first thread is used to manage acquisition from a GigE camera, video or images. Under Linux, an open source library named *Aravis*[4] is used to control the camera. Under Windows, constructor's libraries are used. The acquisition thread grabs a frame and stores it in a shared buffer. Its size depends of how many frames we want to record for a detected event and it determines the memory footprint of the process. The buffer is shared with another thread used to stack frames and also with the detection thread. The last frame stored in the shared buffer and the previous one are both used by the detection process. Detected events have their own buffer shared with a recording thread to save events on the hard disk in a different file format. *Figure 1* summarizes the general structure of the program.

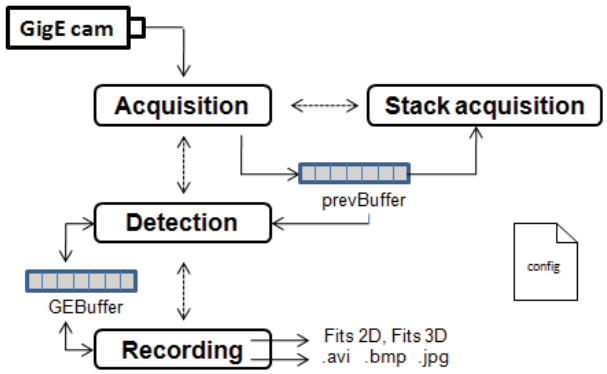

Figure 1 – Software's outline.

4 Detection method

The algorithm used for the meteor detection is quite simple and is more or less based on the detection method used by the ASGARD software (Weryk, 2013). The detection thread receives a notification to indicate that a new frame has been grabbed. The detection process starts to operate two main steps to locate probable events on the current frame and two others to try to build them in time.

The first step starts to filter the current frame to select some pixels which will be used to feed the detection process. To do that, two successive frames are subtracted for removing stationary features and a threshold is defined.

The second step aims to build a list of local event objects. A local event (LE) refers to a group of regions of interest (ROI) which intersect each other. If a pixel exceeds the threshold value, a region of interest (ROI) of 10 x10 pixels around its location is defined and extracted. The ROI is kept if there are more than *n* pixels inside which also exceed the threshold value. In that case, the region of interest is colored in black in the frame to avoid treating the same event many times. The extracted region is compared to the element of the list of local events. If it intersects a ROI of an existing LE, it is added in the same LE. Otherwise a new LE is created and the ROI is added in it. To quickly know if a new ROI intersects an existing ROI in a LE, a colored map is produced. Each LE has its own RGB color on this map, which only exists for the current frame. At the position of the new ROI, the color is extracted. If there is at least one pixel inside with another color than black, this ROI is linked to the LE which has the same color in the LE list.

Once the list of local events is known, the detection on the current frame is done. But the local events must still be linked with global event objects. A global event is a group of local events from different frames. It always exists, contrary to the local event list which only exists during a frame analysis. It is used to link local events which intersect each other not in space but in time. That means that they belong to the same event. If a new local event intersects none of the last local events of a global event, it is added into a new global event. We also check during the link operation if the new potential local event location seems to follow the general global event moving direction. This is done to check if the construction of a global event moves in one direction in function of time.

Finally, the existence of global events stored in a list is managed. Each global event stores the number of frames passed since its creation and the number of frames without any new local event has been linked. A limit which can be defined for an event duration is also used to avoid to record too long events like planes. With these three sets of information, a detected event which is stored in the computer memory is finally saved on the hard disk or removed.

5 Running the software

The software is quite simple to run. There is just need to write a command line with the name of the program to be written together with some arguments according to the chosen mode. Currently, there are three modes.

1) List detected GigE cameras
2) Make a single capture
3) Run detection

The first one is used to list detected GigE cameras with some other information about the devices. The second allows to test a camera by making a single capture and by setting some options like the exposure time, the gain and the acquisition format. Finally, the last mode is the detection mode to start to detect meteors. For the second mode, parameters are directly given as arguments in the command line. For the third mode, parameters may be set in a configuration file.

[4] ARAVIS: https://wiki.gnome.org/Projects/Aravis

6 Results

With our detection software, some first bad and good results have been recorded, like the following plane (*Figure 2*) and meteors (*Figure 3 and 4*).

As planes are longer events than meteors, their recording can be avoided by a definable limit for an event duration.

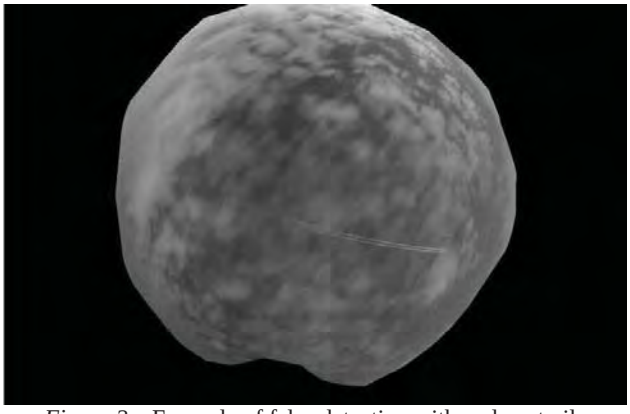

Figure 2 – Example of false detection with a plane trail.

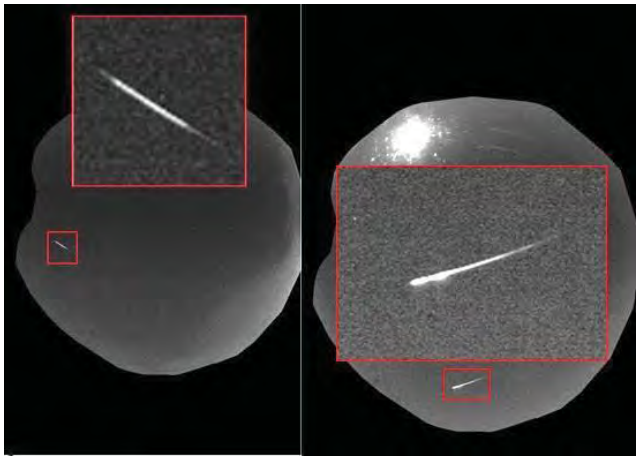

Figure 3 – Meteor examples.

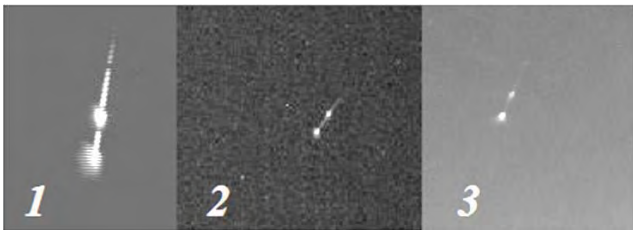

Figure 4 – The same meteor detected by three stations. 1) Stephan Jouin with UFO Capture, 2) Orsay with our software, 3) Observatoire de Paris by regular captures with long exposure.

7 Conclusion and future work

Currently, the main features required are operational and the software can run every night to start detecting meteors events. In the future, we plan to add an algorithm for the daytime detection and to make some comparisons with other meteor detection software to check the efficiency of ours. Finally the Windows version of the software still needs to be packaged.

References

Molau S. (1998). "The Meteor Detection Software MetRec". In, Baggaley W. J., Porubčan V., editors, *Proceedings of the International Conference Meteoroids 1998*, Tatranska Lomnica, Slovakia, August 17–21, 1998. Pages 131–134.

Gural. P. (1997). "An operational autonomous meteor detector". *WGN, Journal of the IMO*, **25**, 136–140.

Weryk R. J., Campbell-Brown M. D., Wiegert P. A., Brown P. G., Krzeminski Z., and Musci R. (2013). "The Canadian Automated Meteor Observatory (CAMO): System overview". *Icarus*, **225**, 614–622.

Astrometry with fish eye lens and orbit determination

Min-Kyung Kwon[1], François Colas[1], Jérémie Vaubaillon[1], Mirel Birlan[1], Brigitte Zanda[2], Chiara Marmo[3], Sylvain Bouley[3], Yoan Audureau[3], Pierre Vernazza[4], Jérôme Gattacceca[5]

[1] **Observatoire de Paris, IMCCE, Paris, France**
mkwon@imcce.fr, colas@imcce.fr, vaubaill@imcce.fr, birlan@imcce.fr

[2] **Museum National d'Histoire Naturelle, Paris, France**
zanda@mnhn.fr

[3] **Université Paris Sud, GEOPS, Orsay, France**
chiara.marmo@u-psud.fr, sylvain.bouley@gmail.com, yoan.audureau@u-psud.fr

[4] **Institut Pythéas, Observatoire des Sciences de l'Univers, LAM, Marseille, France**
pierre.vernazza@lam.fr

[5] **Institut Pythéas Observatoire des Sciences de l'Univers, CEREGE, Aix-en-Provence, France**
gattacceca@cerege.fr

This paper describes a meteor astrometry method for fish-eye lenses and its preliminary results. This work has been done within the framework of the project FRIPON.

1 Introduction

FRIPON (Fireball Recovery and Inter Planetary Observation Network) is a network with 100 cameras which goal is to monitor the French skies in order to find meteorites just after their fall, to track the origin of meteorites and to share this adventure with the public via the "Vigie-Ciel" project. An automated image processing software is currently being developed for FRIPON cameras. This paper is about a new approach of astrometry with fish eye lens.

2 FRIPON pipeline

We can distinguish two parts in the pipeline: the meteor detection part and the trajectory calculation part. Once we made sure that the detection is a meteor, the next step is to compute its trajectory through the atmosphere and its strewn field and orbit. We can split this part of the pipeline into 5 interdependent modules, i.e. astrometry, photometry, trajectory in the atmosphere, orbit and strewn field.

3 Astrometry with fish eye lens

The precision of our trajectories will mainly depend on the accuracy of the astrometry. The very large field of view of our cameras (180°) induces strong distortion that challenges the astrometry process, especially near the horizon. Fortunately, we will have a network of 100 cameras at distant of ~100 km from each other, for which we allow a loss of 10° to 15 ° above the horizon. Several astrometry methods are known. For fish-eye lenses, the methods of Ceplecha (1987) and Borovička et al. (1995) are the best known. We first tried already existing automated solutions like the astrometry software SCAMP[1]. SCAMP software is configurable with standard projections. After several trials with all possible standard projections, we finally had to conclude that it will be difficult to adapt the software for very large fields of view but we did not exclude that solution. We also had a look at documentations provided by opticians[2] and we found out that the mapping function of a fish-eye lens can be expressed as:

$$R = k_1 \times \sin(\frac{i}{k_2})$$

R is the radial distance (between the center of the field and the image point), k_1, k_2 are two parameters that are specific to the lens and i is incident angle of the beam (*Figure 1*).

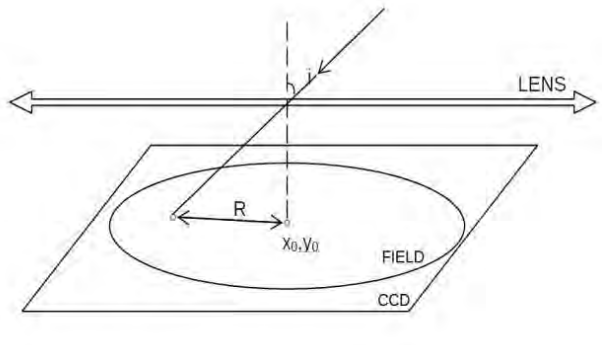

Figure 1 – Illustration of the radial distance.

We thought that it would be an interesting way to explore and we started our own camera calibration on an optical bench. This gave us a first guess of the distortion parameters. For this model, the parameters to optimize are k_1, k_2, x_0 and y_0 (the center of the field, that differs from the center of the CCD plate), θ (the rotation of the field, because our reference is not perfectly aligned on the

[1] www.astromatic.net/software/scamp (Bertin, 2014).

[2] www.pierretoscani.com/echo_fisheyes (Toscani, 2014).

North) *and* α, ε (the tilt angles, because the camera is not on a perfect horizontal plane).

4 Preliminary results

At the moment, by only optimizing k_1,k_2 and x_0, y_0, we get a fit with an accuracy of 0,4 pixel (*Figure 2*). We hope that by correcting the rotation of the field and the tilt angles, we will reach 0.1 pixel (around 1 arcmin).

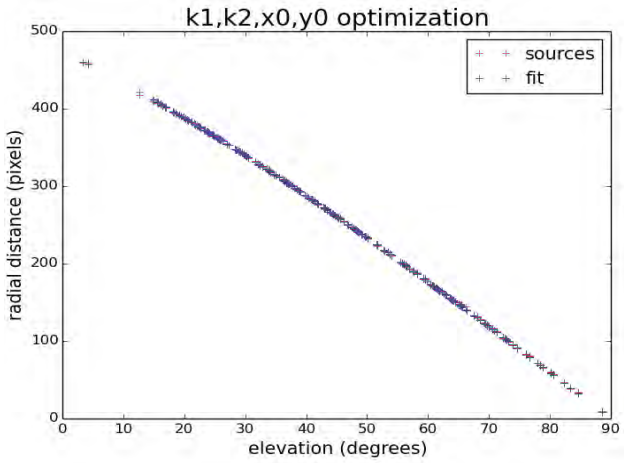

Figure 2 – Extracted sources and fitted function.

5 Future improvements

We are currently working on the optimization of the last two parameters: rotation of the field and tilt angles. Once these optimizations are validated, a graphical interface will be developed to make it user-friendly, even for users not familiar with astrometry. The rest of the pipeline is also to be developed.

6 Conclusion

The preliminary results seem promising and we will keep improving them until we get close to the arcmin of accuracy on the astrometry process. Nevertheless, the accuracy we have now is acceptable for a start. We are now planning to start the development of the other modules of the pipeline so that we can have a functional prototype of the whole pipeline by the beginning of 2015.

Acknowledgments

FRIPON project is supported by ANR (Agence Nationale de la Recherche). Thanks to Emmanuel Bertin, Mark Calabretta, Juraj Toth and Jiri Borovicka for discussions and advices about astrometry.

References

Ceplecha Z. (1987). “Geometric, dynamic, orbital and photometric data on meteoroids from photographic fireball networks”. *Bulletin of the Astronomical Institutes of Czechoslovakia*, **38**, 222–234.

Borovička J., Spurný P., and Keclíková J. (1995). “A new positional astrometric method for all-sky cameras”. *Astronomy and Astrophysics Supplement*, **112**, 173–178.

The author Min-Kyung Kwon during her lecture. (credit Axel Haas.)

Offbeat and wacky projects using a video meteor camera

Peter S. Gural

Gural Software Development, Sterling, Virginia, USA
peter.s.gural@leidos.com

The proliferation of low cost video cameras for nightly meteor collection has almost exclusively been deployed for either moderate or all-sky fields of view. This presentation reviews various concepts using the latest off-the-shelf cameras typically used by meteorists, for some unconventional experiments in meteor detection, spectroscopy, high space-time resolution imaging, as well as non-meteor related projects.

1 Introduction

The relatively easy access to low light sensitive video cameras at very reasonable cost has made doing meteor astronomy reachable by most amateur enthusiasts. But the question arises as to why just do standard moderate field of view (FOV) collection with typically thirty degree sky coverage or alternatively, all-sky imaging with poorer limiting magnitude and resolution. The good news is that these systems are increasingly being deployed as part of distributed camera networks and are providing valuable monitoring and reliable radiant/orbit data year round. However, can we go to the next level and try to address questions beyond just meteor stream association and activity levels, which are within the abilities of amateur meteorists and also fall within their funding constraints. Thus, included herein are a series of project suggestions in both meteor and non-meteor related subject areas, some serious while others perhaps a bit offbeat and wacky, that may appeal to the more adventurous and those with an experimental nature. The goal is to stimulate the creative nature of our diverse community of amateur researchers that make up the IMO.

The discussion will start with a review of low to moderate cost video cameras and frame grabbers available circa 2014. The meteor related projects include daylight meteor detection, robotic meteor tracking, atypical low resolution spectroscopy, telescopic video meteor orbits, faint sporadic imaging, high temporal resolution light curves, and meteoroid impact characterization on the Moon. Non-meteor related projects that could utilize these same camera systems include a directional cosmic ray detector, massive compact halo object (MACHO) detection, and ornithology (bird) migration monitoring.

2 Video cameras and frame grabbers

The variety of choices in low to moderate cost video cameras and frame grabbers for analog NTSC and PAL formats has grown considerably due to the growing popularity of night-time video security surveillance systems. These surveillance cameras have the same features which are found to be desirable for meteor collection. That is, less reliance on image intensifiers and their associated operational concerns and export restrictions, good low light sensitivity in the monochrome camera versions, plus frame rate image capture permitting position estimates of multiple track segments during a meteor's inflight propagation. The summary of camera systems is listed in *Table 1* and is not to be considered all inclusive. High definition and digital cameras are not listed but it is expected their price point will continue dropping making those viable candidates as well.

The most notable change in the past year has been the release of the Effio line of Sony cameras. These cameras employ two chips on a small form factor board that often is embedded within a box-like camera housing that is very lightweight. One chip is used for onboard image processing and is where the Effio name for the cameras originates. Effio-E is the basic model and is adequate for meteor work. Effio-P and Effio-S are higher end image processing chips that have additional processing features like masking, wide dynamic range, stabilizer, and "sense-up" (time integration) that are not necessary to pay for in order to do meteor astronomy. The second more critical chip on the board is the sensor, and this has come in Effio-E variants that include Sony's Super HAD, Exview HAD, or Exview HAD-II in order of enhanced light level sensitivity. These are often color chips in the Effio line that revert to monochrome under low light conditions. One needs to be very cautious about purchasing an Effio-E to ensure the most sensitive chip Exview HAD-II is the embedded sensor. The Effio image processor chip also allegedly produces a digital output in additional to the standard NTSC or PAL analog, but this has not been investigated or tested as of this writing.

To record the analog image sequence onto a computer, one needs to employ a frame grabber or digitizer device. Again many variants can be found and *Table 2* shows a sampling from very low cost to higher quality systems that yield fewer dropped frames. Note that the original EasyCap dongle has been cloned and sold as cheap knock-off variants under the same name EasyCap that many users have experienced problems with. The authentic version is now called Ezcap.tv and originates out of the UK. Also note the Orion capture dongle produces only de-interlaced video so one loses the 2x

sampling rate of an interlaced video sequence if using that device.

Table 1 – Low light cameras on the market circa 2014 used by the meteor community.

Camera	Sensor	Price US$
Watec 902H2 Ultimate	1/2" Exview HAD-II monochrome	342
Mintron 12V6HC	1/2" Exview HAD monochrome	425
Mallincam Jr. Pro	1/2" Exview HAD monochrome	700
Orion Star Shoot	1/2" Mintron 72S85HN-EX Color	500
Effio-E box with OSD	1/3" Exview HAD-II	65
Effio-E board only	1/3" Exview HAD-II	39

Table 2 – Digitizers available on the market circa 2014.

Frame Grabber / Digitizer	# channels/ interface	Price US$
Ezcap.tv	1 channel / USB dongle	32
Orion Video Capture	1 channel / USB dongle / de-interlaced only	50
Dazzle	1 channel / USB	62
ADVC-55	1 channel / USB	175
Sensoray 2255	4 channels / USB	472
Sensoray 812	8 channels / PCI 1x	199
Sensoray 817	16 channels / PCI 1x	1058

The bottom line is that for about US$130 including power supply and cables, one can acquire a good quality single channel video meteor camera. So what can a user do with that outside of standard meteor collection in moderate FOVs or all-sky fireball imaging?

3 Daylight meteor detection

There has been a desire by the optical meteor community to try and capture daylight meteors for fainter trails than just extremely bright fireballs. The issue preventing this has been the bright blue daylight sky that has a broad and continuous intensity profile from 450-650 nm and beyond due to scattered sunlight. Meteor intensity however is centered about a series of narrow emission lines arising from the excitation of both constituent materials such as Ca, Fe, Na, Mg as well as atmospheric O and N. One possible way to enhance the signal-to-noise of meteors relative to the bright sky background, is to place a colored pass band filter in front of the lens, that only passes wavelengths below 430 nm that would try to detect Ca and Fe emission lines. This is a region where the sky spectrum falls off but video cameras are still usually sensitive down to 380 nm. A second approach would be to use an extremely narrow band interference filter centered around any of the common meteor emission lines with the provision that the filter be placed in the optical path where there is little divergence of the light rays. This is necessary because with interference filters, off-axis incidence of the light rays causes the filter's band center to shift, thus missing the narrow-bandwidth meteor emission line. Thus an interference filter cannot simply be placed in front of the lens due to the usually greater than 5 degree off-axis incidence angle of the light. Instead it might potentially be placed between the lens and CCD chip where the light rays are more nearly parallel. Ideally, an optical train where the lens and an additional optical element forms parallel rays, passes through the filter, and is then followed by a focusing element onto the CCD is desired.

4 Meteor acquisition and tracking

In November 2000, the author and George Varros met at Point of Rocks, Maryland, USA to exchange video equipment prior to a Leonid meteor campaign. An ongoing two hour discussion resulted in the origination of the idea of a real-time meteor tracker where a wide field meteor camera would cue the pointing of a narrow field camera before the meteor faded out. George went off to his garage and in two weeks built a two-axis rocker box with stepper motors that could point a camera within one-quarter second of a meteor's first appearance, covering a seventy degree FOV. This evolved into a far more rapid response system using expensive (US$15000) galvanometers and mirrors that responded in 10 milliseconds covering a forty degree FOV with 50 mm clear aperture (Gural et al., 2004). This concept of zoomed imaging of meteors by pointing a single system (or steering the light) rather than deploying many narrow field instruments, can now be revisited a decade later using far less expensive technology.

The model aircraft radio control community commonly uses lightweight servo-motor based pan and tilt systems for recording their flights. These devices are very agile covering any direction of hemispherical pointing in a fraction of a second. They are also inexpensive costing less than US$150. The company RobotGeek sells a two-axis pan-tilt kit with servos that interfaces easily to a computer using Arduino controllers. A more expensive alternative is to explore the video conferencing pan-tilt systems some of which are highly agile and responsive. The goal would be to have an all-sky cueing camera that upon detection of a bright (i.e. long duration) meteor, that directs a narrow field camera to point and potentially track a meteor for high accuracy astrometry. If paired with other equivalent systems at different sites, then high quality trajectories and orbits become possible in all-sky coverage, with only two cameras deployed per site. A key issue in moving forward on a design is the responsiveness of the servo platform with camera mounted so that it slews and captures the meteor before it fades from view.

5 Low wavelength resolution meteor spectroscopy

Meteor spectroscopy typically involves the use of high dispersion gratings to resolve individual emission lines for determining temperature and abundance ratios. However, the meteor spectra yield is low due to the narrow FOV of such systems. An example is the deployment of multiple grating cameras called CAMSS (Jenniskens et al., 2013) to maximize spectral sky coverage between 30 and 55 degrees elevation. But amateurs may contribute in this arena by studying more general questions such as if a particular meteoroid stream is Fe deficient or Na enhanced. To do so only requires very low resolution spectroscopy covering broad bands of wavelength. One approach is to look at the colors of meteors in the respective red, green, and blue (RGB) sensors of a color camera. The new Sony Effio line of cameras is supposed to contain sensitive color chips that may provide broadband color information for brighter meteors (caution: these cameras may revert automatically to monochrome under low light conditions).

An approach that may be more realistic is to use the five Johnson-Cousins standard astronomical filters for UBVRI, one of each on a separate low light sensitive monochrome camera. If all pointed to the same patch of sky, then a fainter meteor than typically obtained by a grating camera could be captured in each of the bands and the relative strength of Ca and Fe in the B-band could be compared to Mg and forbidden O in the V-Band, Na in the R-Band, and atmospheric N and O in the I-Band. One might even consider a color index for meteors similar to one used for stars to categorize each stream. To take this further, since the Johnson-Cousins color filters may still be too broad in each wavelength band, one may consider using narrower band pass alternatives that focus more on each major contributing element species in meteors. In essence a way of choosing selective band passes without employing a grating, and thus obtaining relative line strengths between elements for various shower streams and sporadic meteors.

6 All-sky meteor spectroscopy

The use of a grating is often employed in meteor spectroscopy which is typically manufactured as a parallel set of ruled lines or grooves in a substrate. This limits the directionality of the grating dispersion to just one direction so meteors are effectively “seen” by the sensor off to one side in a narrow field of regard. Consider however, if the grooves were ruled in circles, then the dispersion direction would be radially directed inwards from all aspects (azimuths). Thus one could set up a monochrome imaging camera above such a reflection grating, not unlike the old all-sky meteor camera configurations that used a camera looking down on a mirrored dome or hubcap. Meteors from all aspects could be seen using a single camera. The elevation of the meteor above the horizon will dictate whether the meteor is observed as the first or second order spectrum.

A very inexpensive way to manufacture such a grating is to burn all ones or random one/zero bits on writable computer disk storage media. The write pattern is standardized and is comprised of a spiral series of pits with nominal inter-ring spacing of 1.60 microns for CDs, 0.74 microns for DVDs, 0.40 microns for HD-DVD, and 0.32 microns for Blu-Ray. Note that the 1379 lines/mm gratings used in CAMSS have 0.73 micron spacing. So the DVD spacing provides the same level of dispersion used in CAMSS for resolving critical emission lines in meteors. With the spiral (near circular) pit pattern, a low cost, all-aspect type grating can be coupled to a single camera to provide large area sky coverage. One needs to investigate the efficiency, dispersion pattern, and practicality of using a curved grating. Note that it is visible on DVDs that have NOT been written to, that there is a rainbow dispersion of white light reflected off its surface. It may be that the information (timing track?) embedded on the DVD surface may be sufficient to operate as a reflection grating as is, without having to burn pits into the media.

7 Telescopic video meteor orbits

It comes as a surprise that telescopic meteor work still lies in the domain of visual observers, especially when video camera systems can record trajectories far more accurately and reliably than human observers. The excellent performance of video systems for moderate to wide field of view meteor astronomy has been borne out in the past decade. So why not apply video to telescopic meteor studies done by amateurs? This would begin to cover a mass range of meteors with a greater relative proportion of sporadics for which high accuracy orbits are desired.

Part of the reluctance is two-fold. One issue is that automated detection software is not as well optimized for just one to three frames with very long streaks per frame, although the software suite MeteorScan has a separate detection algorithm for just this scenario. The second and perhaps greater issue is the angular velocity loss a meteor incurs as it rapidly sweeps across the focal plane. Take the Mighty-Mini 200mm f/2.5 system for occultation timing which is based on an Orion 80mm short focal length spotting scope (Degenhardt and Gural, 2009). It has a limiting magnitude stellar of +10.5 for a single frame at 30 fps. However, the faintest typical 40 km/sec meteor that can be seen above the sensor noise when using that system is only +6.8. This is because a meteor dwells in any given 12 arc-second pixel for only a small fraction of the 1/60 second interleave integration time. This is otherwise known as “trailing loss” or “angular velocity loss”. It can be mitigated to some extent with faster lenses and experiments with various optics configurations by the Croatian Meteor Network has indicated that a fast Canon 90mm f/1.0 lens can reach +8.0 or better meteor limiting magnitude without the use of an intensifier. Other low cost f/1.0 surplus lenses are currently under investigation by that same group to trade off focal length, limiting magnitude, and cost.

Assuming that a deep meteor limiting magnitude system can be assembled cheaply, there are some interesting features associated with deploying telescopic video. For two station meteor orbit estimation, the very narrow FOV produces a tiny cone angle in space making it far more difficult to find the camera attitude (geometric pointing) for the two widely separated sites to have the proper volume overlap. However, the small angular resolution of the focal plane pixels when using telescopic FOVs, allows the physical separation between observing sites to be reduced dramatically. Reliable short baseline triangulation has been suggested as possible (Gural 2012; Degenhardt and Gural, 2009) with as little as 5 km separation, but a study should be done to verify the best spacing. With a short baseline between telescopic sites, the attitude (pointing) optimization is far simpler. The two systems can aim to almost exactly the same star field with a simple calculation to determine the small pointing offset for 88 km altitude maximal coverage overlap. Also the near parallel alignment of the telescope viewing cones extend the volume coverage both closer (lower to the ground) and further away (above 90 km) along the mutual line of sight.

8 Faint sporadic detector

One way to mitigate the angular velocity loss in a telescopic FOV is to have the system "follow" the meteor. That is by slewing the sensing system to minimize the effective blurring motion of the meteor across the focal plane. This could be accomplished in one of a number ways and this list is by no means exhaustive. One approach is to simply mount the telescopic camera system on a rocker box and oscillate back and forth with an offset drive cam or direct servo motor. The servo motor would yield a more uniform angular velocity for most of the sensor's travel cycle. A second approach is to rotate an angled camera so it traces out a cone (circle on the sky). A third approach tries to avoid the cable entanglement issue with the second method, by having a fixed telescopic camera stare at a rotating angled mirror that again effectively sweeps out a circle on the sky. A fourth more expensive approach mimics the early days of asteroid hunting called drift scan, wherein a fixed pointed sensor uses a CCD that shifts each row at a user desired rate thereby getting integration gain on moving objects. A fifth approach would be to try matched filter detection techniques (computationally expensive) on a fixed mounted telescopic camera to buy an extra 0.5 to 1.0 in limiting magnitude.

What would be the purpose of such an instrument? To probe into the very faint end of magnitude +9 and +10 sporadics. But there is a catch as these concepts only detect meteors in a narrow speed range and limited direction. But the sporadic flux goes up dramatically at these magnitudes so the geometric constraints may be offset by the sheer number of available events. Also the interesting case would be to explore the slow sporadic population which are often missed in video systems. The second issue is doing astrometry with a moving sensor and backing out the actual speed and direction of the meteor. A very challenging geometric problem.

9 Millisecond resolution meteor light curves

One interesting advantage to interleaved video (which may disappear with the advent of digital progressive scan cameras) is that the meteor tracks can be centroided on the even and odd "fields" and effectively sampled at twice the full frame rate. For a 30 fps NTSC camera, the integration time per field is 1/60 second alternating between even and odd rows. This yields a 15 millisecond temporal resolution in meteor light curves and measurements feeding trajectory analysis.

However, it is often evident that a meteor presents a streak in just one field of the image sequence. That is the meteor spans more than a single pixel. Thus for a vertically oriented meteor on the focal plane, one could extract the meteor intensity on a per row basis and obtain effectively a higher temporal resolution light curve (for horizontal meteors the extraction would be done by column). For moderate FOV cameras this may yield from 4 to 8 millisecond resolution depending on the meteor's speed. With telescopic meteors, the effective resolution is approximately ten times higher than field level time spacing, so one could achieve close to millisecond resolution light curves.

Applying such analysis, it may be possible to view oscillations in the light curve from tumbling meteors, but there should be caution applied since some oscillations could be due to camera focal plane characteristics (less than 100% fill factor for example). This would require new analysis software to automatically extract the higher temporal information. Note that the higher spatial resolution and interleave can also assist in more finely estimating interleave breaks (for example the switch from even to odd fields) and thus provide better apparent angular velocity estimates than simple centroiding of the extremely long streak in telescopic meteors.

10 Lunar meteoroid impact characterization

The NASA/Marshall Meteoroids Environment Office has been monitoring the unlit portion of the near side of the Moon for several years and has accumulated 321 boulder sized impacts through June 2014. These hypervelocity impacts create light flashes typically near magnitude +5 with a duration of a few tens of milliseconds spanning only one or two frames at standard video rates. The interleave integration time of NTSC and PAL is too long to resolve the light curve adequately so high speed video of at least 300 fps would be desirable to better characterize the phenomena. To do so would require more light gathering power than is currently used, such as a one meter telescope coupled to a high frame rate camera. In addition, it would be interesting to obtain spectra of an impact flash but this is an even harder challenge due the faint nature of the flash and further loss

in SNR due to dispersion of the spectrograph. Nevertheless, either aspect would be a worthwhile endeavor for an amateur with the right equipment and time to monitor the Moon for the few hours around first and last quarter each lunation cycle.

11 Directional cosmic ray detector

These next set of projects do not involve meteor research, but would use the typical video meteor camera setup as a starting point. A low-cost directional cosmic ray detector is a concept originally put forward by Damir Segon of the Croatian Meteor Network. It recognizes the fact that the low light cameras in use by amateur meteorists are sensitive to the secondary high energy particle shower that reaches the ground when a cosmic ray interacts with the Earth's atmosphere at tens of kilometers altitude. They typically show up as various length streaks on the focal plane image, sometimes jagged, that do not possess the point spread function blurring due to the normal lens optical train degradation. The streak length depends on the entry angle to the focal plane surface. It is proposed that a directional capability for detecting these tracks can be built by placing two imaging chips (board cameras or lens-less box cameras) face-to-face in a totally dark enclosure and let software monitor the two imagers for coincidental bright pixel traces. The relative spatial offset in row and column plus the face separation between the two focal planes, can be used to determine the angle of arrival. The high energy secondary particles being detected will easily pass through the electronics behind the focal planes. Lead shielding around the perimeter would help reduce off-axial false alarms in any given camera, but the coincidence in time processing will mostly mitigate this effect.

12 MACHO detection

Massive compact halo objects, or MACHOs, are postulated to be Jupiter sized planets that have been ejected from their originating star system and wandering through our galaxy. Their angular extent is sufficient to eclipse a distant star for a brief period time. Robert Hawkes proposed using an intensified video meteor camera that could easily see 400 stars in a single FOV, as a 400 channel photometer to try an detect an occultation (Parker et al., 2004). With the sensitivity of today's non-intensified cameras the same experiment can be tried using a pair of cameras at least one meter apart. The two camera setup is to ensure a time coincident event occurs on the same star and the occultation is not a false alarm from atmospheric scintillation or intervening flying wildlife. One recommendation is to use a dense star field, open cluster, or large globular cluster to maximize the number of star "channels" and increase the odds of an occultation.

13 Bird migration

There is also an interest in the ornithology field about bird migration and calibrating bird populations seen in radar returns. Initial experiments in even dark skies with no Moon or nearby city lights shows that birds present a brighter signature than the background sky. This is likely due to their heat signature in the near IR being picked up by today's Exview HAD II sensors. As in meteor work, ornithologists are interested in speed and altitude. But since the altitudes are at most a few hundred meters, the camera separation baseline can be much smaller, Designing a system for wide area coverage and the corresponding data reduction software, would be most welcome by the bird watching community.

14 Summary

In summary, there are many meteor related projects outside of the normal moderate and all-sky collection systems in common use today. Any thoughts on further exploration of any one of these or alternative ideas on a better approach are most welcome by the author. The author would like to thank Damir Segon and his Croatian Meteor Network team, Dr. Robert Hawkes, Dr. Peter Jenniskens, Dr. Robert Suggs, Dr. Alan Hildebrand, Dr. Peter Brown, and Dr. Margaret Campbell-Brown for many stimulating discussions over the years that have led to the formation of this project compendium.

References

Degenhardt S. and Gural P. (2009). "A telescopic meteor observed during the Metis campaign". *WGN, Journal of the IMO*, **37**, 33–36.

Gural P., Jenniskens P. and Varros G. (2004). "Results from the AIM-IT Meteor Tracking System". Meteoroids 2004 Conference Proceedings, *Earth, Moon, and Planets*, **95**, 541–552.

Gural P. (2012). "A new method of meteor trajectory determination applied to multiple unsynchronized video cameras". *Meteoritics and Planetary Science*, **47**, 1405–1418.

Parker R., Hawkes R, and Gural P. (2004). "Short exposure astronomical techniques for occultation detection". *Quarterly Journal of the Royal Astronomical Society of Canada*, **98**, 120–127.

Jenniskens P. Gural P., and Berdeu A. (2013). "CAMSS: A spectroscopic survey of meteoroid elemental abundances". In Jopek T. J., Rietmeijer F. J. M., Watanabe J., and Williams I. P., editors, *Proceedings of the Meteoroids 2013 Conference*, Poznań, Poland, 26–30 August 2013. A.M. University Press, pages 117–124.

Low dispersion meteor velocity measurements with CABERNET

Auriane Egal[1], Jérémie Vaubaillon[1], François Colas[1], Prakash Atreya[2]

[1] **IMCCE, 77 av. Denfert Rochereau, 75014 Paris, France**
aegal@imcce.fr, vaubaill@imcce.fr

[2] **Arecibo Observatory, HC03 Box 53995, Arecibo, 00612, Puerto Rico**

We present here a method to determine the meteor velocities in a more robust way than what is usually done, working with the images provided by the CABERNET project. Thanks to an electronic shutter coupled to the cameras, meteors look like a succession of centroids in the photographic records. We are able to determine the position of the meteor in the image across the time, as well as its apparent velocity, by plotting the light curve along the track of the meteor. To minimize the measurement errors in the centroid's position, we use the RANSAC algorithm to fit the apparent velocity. Thanks to this fit, the position that the meteor would have at a time t + δt is computed. Following an astrometric reduction process, we finally obtain two sets of values (t, α, δ) and (t + δt, α, δ). By projecting these positions at time t and t + δt on the 3-D trajectory, we compute a 3-D velocity that is not as sensitive to the measurement errors as other methods and which shows a lower data dispersion.

1 Introduction

Currently, the lack of high-accuracy orbits for many meteors showers significantly hampers the research of their parent bodies and the determination of the age of the showers. This limitation is due to the difficulty of precisely measuring the velocity and changes of velocity induced by the atmosphere. In order to link a meteor with its parent body, it is then necessary to focus on the reconstruction in the heliocentric frame. The CAmera for BEtter Resolution NETwork (CABERNET), was developed to measure accurate orbits of meteors, in order to study the dynamics of meteoroid streams and to reliably determine their parent body. The minimum requirement for the project was to improve the accuracy of meteoroid orbits measurements at least by a factor of ten. This network provides 40 x 27° images of the sky from three stations (Atreya et al.,2006). An electronic shutter interrupts the signal at a tunable frequency. Meteors then look like a succession of dashes, which is useful to accurately determine the position and the velocity of the object (see *Figure 1*).

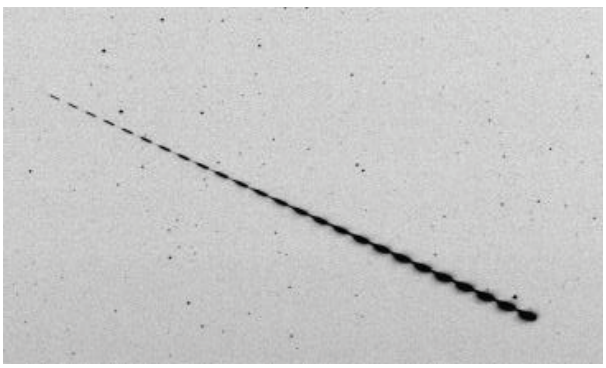

Figure 1 – Meteor detected by the Guzet station, (13/12/2010).

We present here a way to determine the meteoroid velocity from digital photographic records provided by the CABERNET cameras. It mainly relies on the determination of the apparent velocity in the image, helped by the use of the RANSAC algorithm. By limiting the influence of noise on the velocity determination, this method allows us to determine the 3-D velocity of meteors more robustly and more accurately than before.

2 Commonly used method to compute the 3-D velocities of meteors

The standard way to determine the 3-D velocity of meteors starts by measuring the location *(x,y)* of the meteor in the image. In most cases the barycenter of the meteor is identified in this step. Following an astrometric reduction process, which provides us with the sky coordinates, we use a method to reconstruct the 3-D trajectory of the meteor (such as the intersect plane method, Ceplecha, 1987). From this trajectory and time information, we are then able to deduce the 3-D velocity of the meteor and the velocity changes. Indeed, knowing the 3D location of the meteor (X_{3D}) through the time t, we can compute the 3-D velocity:

$$V_{3D} = \frac{\Delta X_{3D}}{\Delta t} \quad (1)$$

However, this approach can be limited due to image contamination by the noise, which hinders the position determination of the meteor. An error at this step can have an important impact on the subsequent computation of velocity. Through having the advantage of working with photographic records, and hence the possibility of analyzing the whole meteor at once, we developed a more robust method to compute the 3-D velocity.

3 New method

The main idea of this method is to use the apparent velocity of meteors in our images to compute more precisely the 3-D velocity of the objects afterwards. To do that, we first need to accurately determine the position of the meteor in the image over time. As we see from

Figure 1, a meteor in our images looks like a succession of dashes (at each time stamp t), whose centroids are determined by extracting the light curve along the trail. After smoothing the light curve using the Savitsky-Golay algorithm (Savitsky et al.,1964), the centroid's location are determined relative to the position of the light curve's maximum. However, this method was not robust enough due to the noise of the light curve, which caused several numbers of false maxima detection and then aberrant values for the apparent velocity. To overcome this, we decided to apply the RANSAC algorithm to remove the aberrant values of the apparent velocity caused by the false maxima detections. The RANdom SAmple Consensus (RANSAC) is a way to determine a mathematical model (here linear), from a set of data which contains outliers. It first chooses a random subset of the original data (values of apparent velocity) of size n defined by the user. A model is then fitted to this subset and we search in all the data which values follow it satisfactorily (distance criteria). We iterate the process until we find the best result, i.e. the more accurate model (minimal distances between the inliers and the fit) for a higher set of points. The RANSAC algorithm is an iterative method which provides a correct result with a defined probability. That is why it is necessary to iterate the whole algorithm k times to be sure to obtain the optimal solution with a sufficient high probability of success (99% or more). This number k can be computed each time we choose a new subset (Fischler et al., 1981), and it determines the end of the iteration process. To summarize, if we consider enough values of the apparent velocity (which decreases linearly with time), we are able to exclude the aberrant values thanks to the RANSAC algorithm with a probability of success higher than 99 %. Thanks to the fit of the apparent velocity, we can compute the apparent position (in the image) the meteor would have a short time δt (here 1 ms) after the position (x, y) measured at t. We then obtain two sets of values, (x, y, t) and (x', y', $t + \delta t$). After projecting them on the 3-D trajectory (Ceplecha, 1987) to get (X_{3D}, t) and (X'_{3D}, $t+\delta t$), we can finally compute the 3-D velocity

$$V_{3D} = \frac{X_{3D} - X'_{3D}}{\delta t} \qquad (2)$$

This makes the determination of the velocity more robust against errors in the measurement of the apparent meteor position. Indeed, in the standard method, a velocity value is dependent on the measurement error of two centroid positions. However with our method, thanks to the RANSAC algorithm, the errors made in the centroids position determination are minimized in the fit of the apparent velocity. With our method, the 3-D velocity is less sensitive to the measurement errors.

4 Results

In *Figures 2 and 3*, we show an example of results obtained with the standard method and with the method presented here, for a double station meteor. We mainly see the great improvement in the quality of the results. In the first case, there is a significant dispersion (about 1/5 of the velocity 6 km/s^{-1} / 30 km/s^{-1}), and in consequence the deceleration is hard to measure. With our method, the dispersion represents 1/300 of the signal (0,1 km.s^{-1} / 30 km.s^{-1}) and the deceleration is easily measurable (1,83 km.s^{-2}).

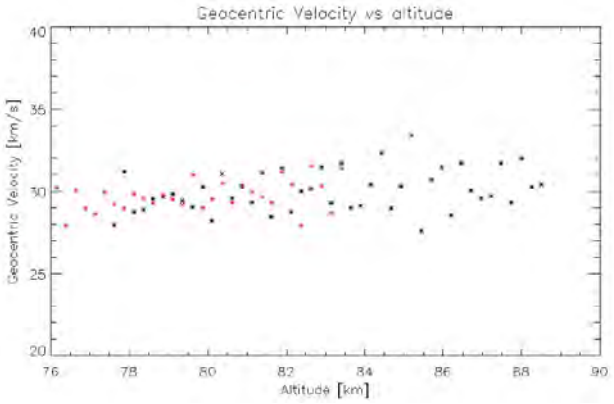

Figure 2 – Determination of the 3-D velocity with standard method. The result is very noisy, and it is extremely hard to recognize the change in velocity.

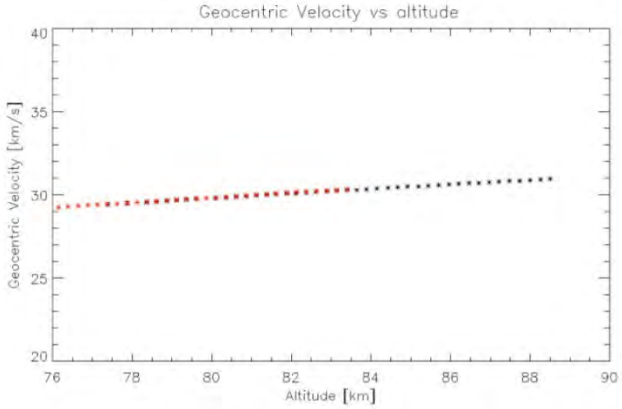

Figure 3 – Determination of the 3-D velocity with our method. The spread is much smaller and the change in velocity is measurable.

The method presented in this work results in a much more robust determination of the velocity, in a lower data dispersion and allows us to measure changes of the 3-D velocity. This process can be fully automated to speed up the data reduction, and we estimate a benefit of one or two orders of magnitude on the velocity accuracy. However, some improvements are still necessary to fully exploit the potential of the CABERNET project.

5 Conclusion

We have developed a method to accurately compute the 3-D velocity of meteors from CABERNET measurements, based on the work of Atreya et al. (2006), and modified for our needs. The computation of the apparent velocity allows us to better define the 3-D velocity in a robust way, thanks to the RANSAC algorithm. Many improvements still remain to be included in order to further improve the accuracy this promising method can provide.

Acknowledgements

The CABERNET project is supported by IMCCE, Observatoire de Paris, the City of Paris and PNP. We are grateful to R. Arlt (at IMC2010), J. Borovička (Ondrejov observatory) and Geert Barentsen for their personal communications, which have greatly helped us during this work.

References

Atreya P., Vaubaillon J., Colas F., Bouley S., Gaillard B. (2012). "CCD modification to obtain high-precision orbits of meteoroids". *Monthly Notices of the Royal Astronomical Society*, **423**, 2840–2844.

Ceplecha Z. (1987). "Geometric, dynamic, orbital and photometric data on meteoroids from photographic fireball networks". *Bulletin of the Astronomical Institutes of Czechoslovakia*, **38**, 222–234.

Fischler M. A., Bolles R. C. (1981). "Random sample consensus : A paradigm for model fitting with applications to image analysis and automated cartography". *Communications of the ACM*, **24**, 381–395.

Bouley S., Vaubaillon J., Colas F. (2012). "Rapport scientifique du projet: Sous le ciel de Paris: des météores", *Technical report*, IMCCE.

Savitzky A., Golay M. J. E. (1964). "Smoothing and differentiation of data by simplified least squares procedures". *Analytical Chemistry*, **36**, 1627–1639.

The IMC brings people together, and jokes means fun. From left to right, Megan Argo, Antonio Martinez Picar, Eva Buzhorova and Nagatoshi Nogami. (credit Axel Haas.)

Expeditions during 2014 with AMOS cameras

Juraj Tóth, Pavol Zigo, Leonard Kornoš, Jozef Világi

Faculty of Mathematics, Physics and Informatics, Comenius University in Bratislava, Slovakia
toth@fmph.uniba.sk

Slovak Video Meteor Network (SVMN) is a project of the Comenius University in Bratislava for continuous monitoring of meteor activity over Slovakia and surrounding countries. The network is based on AMOS (All-sky Meteor Orbit System) Cameras, which astrometric precision was calibrated using several commonly observed fireballs within the European Fireball Network. We cooperate with other national video networks and amateur observers and submit all data to the EDMOND video meteor database. The extension of the AMOS Cameras to the Canary Islands and Chile to cover the Southern hemisphere is planned. We present preliminary results from the expedition on the Canary Islands (April 2014) and from Canada (Camelopardalids, May 2014).

1 Overview of the AMOS system

The system AMOS (Automatic Meteor Orbit System) consists of a fish-eye lens, an image intensifier, a projected lens and a digital video camera (Zigo et al., 2013). The field of view of the AMOS is 180° × 140° and the output digital resolution 1280 × 960 pixels with a video frame rate of 15 per second (the new version uses digital cameras with 1600 x 1200 pixels and 20 frames per second). The limiting sensitivity is comparable to the human eye (mag. +5,5 stellar objects, mag. +4 for moving objects). The operation of the cameras is semi-automatic and needs electric power (110-220/24 V) and an internet connection. The whole system is protected by an outer and inner housing and is monitored by sensors for temperature (inside, outside), rain and illumination of the sky (*Figure 1*). Moonlight does not cause any problems for the observations, other than by brightening the sky background. The system is designed for meteor observation (Tóth et al., 2011a), but could also be used for meteorological, geophysical, aviation or satellite observations. The inner part of the camera is portable (weight ~6.5 kg, size 50 × 25 cm) and suitable for surface expeditions or on board research aircraft (Vaubaillon et al., 2013; Koten et al., 2014).

2 Observations

The first prototype has been working at the AGO Modra Observatory since 2007. The AMOS cameras systematically monitor meteor activity in the Slovak Video Meteor Network (SVMN) at four locations at present, AGO Modra, Arborétum T. Mlyňany, Kysucké Nové Mesto Observatory and Važec stations separated by distances of 80 – 150 km from each other. More stations are planned to be built in central and eastern Slovakia. Each AMOS camera records about 10000 meteors per year plus about 50 transient luminous events (sprites, elves) under Central European sky conditions.

The standard astrometric error is 0.03 – 0.05 degree corresponding to several tens to a few hundred meters in the determined atmospheric trajectory of the meteors. The internal precision of the AMOS cameras is even better, especially when the precise all-sky reduction described in (Ceplecha, 1987; Borovička, 1995) is used with our own trajectory software MT v.085.

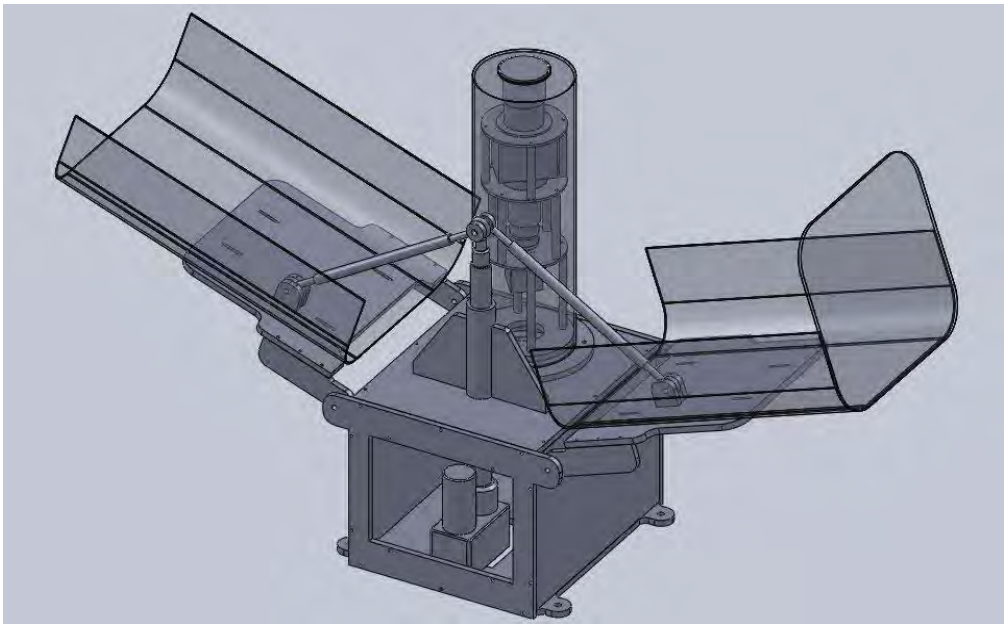

Figure 1 – AMOS camera with opened outer housing.

Figure 2 – Observing team at OT: J.Tóth, J. Világi, L. Kornoš and P. Zigo.

The current version of the orbital dataset of video meteors recorded by SVMN (2009-2013) stations contains about 3000 orbits. The results from the observational expedition on Tenerife and La Palma (Canary Islands 2014) demonstrated that AMOS cameras at high altitudes and dark sites are over 4 times more efficient than networks of the same cameras at Central Europe weather and sky conditions (*Table 1*).

Table 1 – Number of observed meteors by the AMOS cameras at the Canary Islands (La Palma, Tenerife) observatories and in the Slovak Video Meteor Network (SVMN) April 2 – 8, 2014.

2014 April	LaPalma AMOS4	Tenerife AMOS5	Slovakia AGO	Slovakia ARBO	Slovakia KNM	Slovakia VAZEC
2	48	50	26	7	9	6
3	49	50	2	1	6	15
4	46	60	4	2	4	-
5	55	68	-	-	-	-
6	38	56	15	-	6	13
7	45	48	11	-	5	16
8	29	38	-	-	-	-
Σ	310	370	68	10	30	50
	100%	119%	22%	3%	10%	16%

Canary Islands, April 2014

The objectives of the one week observing expedition at the Canary Islands observatories of IAC, *Obsevatorio del Teide (OT)* (*Figure 2*) and *Observatorio del Roque de los Muchachos (ORM)* were:

- To test the Canary Island observatory sites for future permanent AMOS stations;
- To test the efficiency of the AMOS cameras in excellent observing conditions;
- To confirm the potential/predicted meteor shower of asteroidal origin related to the orbits of the Příbram and Neuschwanstein meteorites (Spurný et al, 2003; Tóth et al., 2011b; Koten et al., 2014).

We observed on 7 nights (λ_O = 12°.8 – 19°.1) using two AMOS all-sky intensified digital video cameras. On the first and last nights we observed at the same site (OT) whereas during the 5 nights from April 3–7 we performed double - station observations between ORM and OT, separated by 144.8 km from each other. In total, the cameras recorded 680 meteors of which 516 meteors were recorded during double-station observations (*Figure 3*).

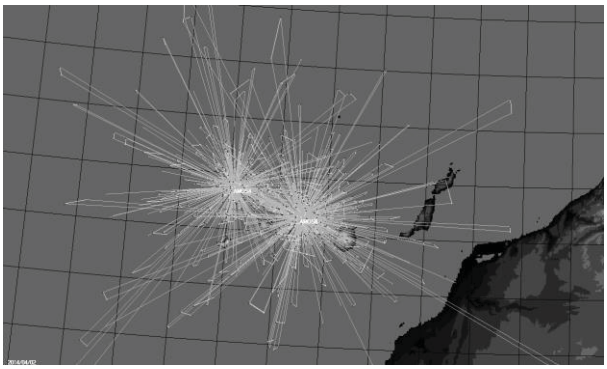

Figure 3 – Meteors observed by AMOS cameras from La Palma and Tenerife.

Only about 20% of these meteors were simultaneously recorded. The magnitude range of the recorded meteors was from –3 to +4 with the peak between 0 – (+2) magnitudes. Overall meteor activity was weak for both, sporadic and shower meteors, typical for that time of year. The ratio of sporadic and shower meteors was about 1:1. We detected activity from 11 meteor showers, one of these being an established shower (027 KSE) and the other 10 being from the working list. The average sporadic activity reached about 3/HR and average shower activity was as follows:

(049 LVI), (509 KVI) ~ 0.3 HR
(043 ZSE), (136 SLE), (131 DAL), (517 ALO) ~ 0.2 HR
(124 SVI), (123 NVI) ~0.1 HR
(027 KSE) ~ 0.1 HR
(272 ACO), (448 AAL) ~ 0.1 HR

We were mostly interested in the ACO shower, which has similar characteristics to our modeled potential meteor stream with the orbit of the Příbram and Neuschwanstein

meteorites (Tóth et al., 2011). We identified 15 single station meteors from both cameras, that had angular velocities and whose paths projected backward to the radiant area of the ACO shower (*Figure 4*), of which 5 had orbits close to the orbit of the Příbram meteorite. However, further investigations will be needed for more conclusive results.

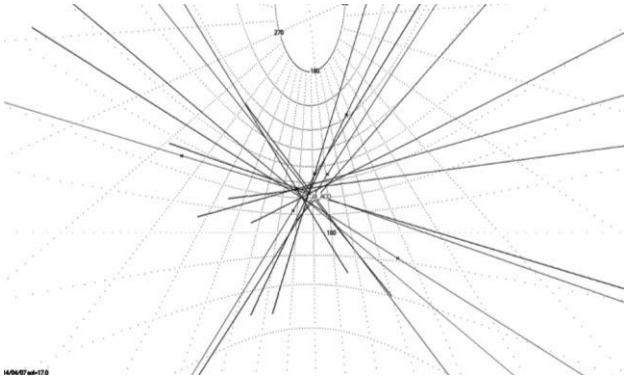

Figure 4 – Radiant positions of 15 ACO meteors.

Canada, May 2014 (CAM) – small outburst

The predicted activity of the new meteor shower – Camelopardalids only delivered a low level meteor outburst. Nevertheless, we set up the AMOS cameras for a double station experiment in Saskatchewan, Canada and obtained 5 orbits for this special meteor shower (*Figure 5*) to demonstrate the capability of the cameras. Double-station meteors were captured simultaneously from locations separated by 100 km in cloudy lightning skies. According to our visual observations, the activity of the Camelopardalids was stable at a ZHR of 20 – 30 in the time interval 5^h-9^h UT, May 24, 2014.

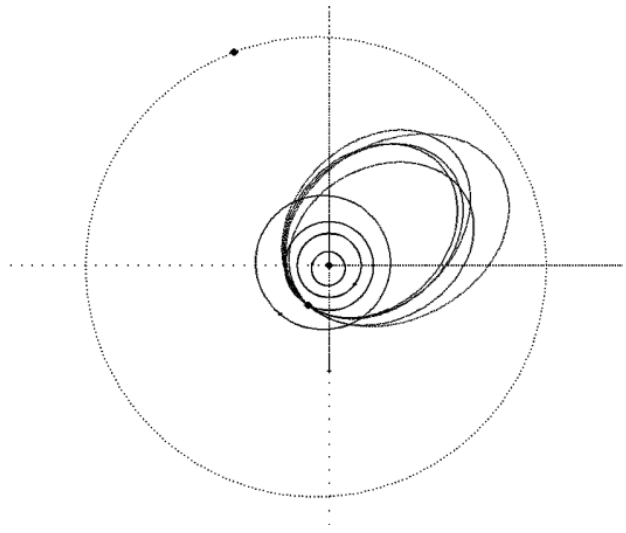

Figure 5 – Orbits (raw data) of Camelopardalid meteors simultaneously detected by AMOS-Cameras (May 24, 2014) from Grass land Park, Saskatchewan, Canada.

3 Conclusion

Both observational expeditions with the AMOS cameras were successful, even though the results are not conclusive in the case of a possible Příbram meteor stream and the amount of data collected was far below expectations for the Camelopardalid meteor outburst.

Acknowledgment

Registered patent in SR PUV 78-2013. PCT. This work was supported by grant APVV-0516-10, APVV-0517-12 and VEGA 1/0225/14.

References

Borovička J., Spurný P., Keclíková J. (1995). "A new positional astrometric method for all-sky cameras". *Astron. Astrophys. Suppl. Ser*., **112**, 173–178.

Ceplecha Z. (1987). "Geometric, dynamic, orbital and photometric data on meteoroids from photographic fireball networks". *Bulletin of the Astronomical Institutes of Czechoslovakia*, **38**, 222–234.

Koten P., Vaubaillon J., Tóth J., Margonis A., Ďuriš F. (2014). "Three Peaks of 2011 Draconid Activity Including that Connected with Pre-1900 Material". *Earth, Moon, and Planets*, **112**, 15–31.

Koten P., Vaubaillon J., Čapek D., Vojáček V., Spurný P., Štork R., Colas F. (2014). "Search for faint meteors on the orbits of Príbram and Neuschwanstein meteorites". *Icarus*, **239**, 244–252.

Spurný P., Oberst J., Heinlein D. (2003). "Photographic observations of Neuschwanstein, a second meteorite from the orbit of the Príbram chondrite". *Nature*, **423**, 151–153.

Tóth J., Kornoš L., Vereš P., Šilha J., Kalmančok D., Zigo Z., Világi J. (2011a). "All-Sky Video Orbits of Lyrids 2009". *Publ.. Astron. Soc. Japan*, **63**, 311–314.

Tóth J., Vereš P., Kornoš L. (2011b). "Tidal disruption of NEAs - a case of Příbram meteorite". *Monthly Notices of the Royal Astronomical Society*, **415**, 1527–1533.

Vaubaillon J., Koten P., Rudawska R., Bouley S., Maquet L., Colas F., Toth J., Zender J., McAuliffe J., Pautet D., Jenniskens P., Gerding M., Borovicka J., Koschny D., Leroy A., Lecacheux J., Gritsevich M., and Duris F. (2013). "Overview of the 2011 Draconids airborne observation campaign". In Gyssens M. and Roggemans P., editors, *Proceedings of the International Meteor Conference*, La Palma, Canary Islands, Spain, 20–23 September 2012. IMO, pages 61–64.

Zigo P., Tóth J., Kalmančok D. (2013). "All-Sky Meteor Orbit System (AMOS)". In Gyssens M. and Roggemans P., editors, *Proceedings of the International Meteor Conference*, La Palma, Canary Islands, Spain, 20–23 September 2012. IMO, pages 18–20.

CAMS BeNeLux

Felix Bettonvil[1,2,3], Carl Johannink[4], Martin Breukers[4]

[1] **Sterrewacht Leiden, Universiteit Leiden, Niels Bohrweg 2, 2333 CA Leiden, the Netherlands**

[2] **NOVA Optical and Infrared Instrumentation Division at ASTRON, Oude Hoogeveensedijk 4, 7991 PD Dwingeloo, the Netherlands**

[3] **KNVWS Meteor Section, the Netherlands**
F.C.M.Bettonvil@strw.leidenuniv.nl

[4] **Dutch Meteor Society, the Netherlands**
c.johannink@t-online.de, breukers@wxs.nl

This paper gives an overview of the current status of the BeNeLux CAMS video meteor network as operated in the Netherlands and Belgium, and part of the NASA funded automated meteor video surveillance project CAMS.

1 Introduction

For meteor detection, one can chose nowadays from an increasing number of video systems. Examples are Metrec (Molau, 2014), UFOCapture[1] or CAMS (Jenniskens, 2011). Rather than being individual instrumental camera projects all of these also succeed in forming substantial networks, administering data, and delivering results in a consistent way. A tracer for their success is that the number of video stations is rapidly growing.

While each system has naturally its own pros and cons, in this paper we focus only on the CAMS system. CAMS stands for *Cameras for All sky Meteor Surveillance* and was developed as NASA sponsored project by Gural and Jenniskens (Jenniskens, 2011) to create a double station network in California/US for the detection of (cometary) meteor streams in order to validate the IAU Working List of Meteor Showers[2] (Kanuchova, 2013). For this reason, CAMS is aimed at delivering heliocentric orbits, and in addition light curves.

In 2011, CAMS was introduced in the Netherlands as part of the NASA Draconid outburst observing campaign in nearby Kühlungsborn (Vaubaillon, 2014), after which trials were carried out from 2 Dutch stations on the Orionids 2011 with 2x4 cameras. The ~100 double station meteors recorded (Johannink, 2013) was considered to be an outstanding success. In March 2012, camera operators Jobse and Neels started regular observations from two stations. One month later the network had already expanded to four stations (operated by Johannink and Breukers). This can be seen as the start of CAMS BeNeLux (BeNeLux being the union of the three neighboring states Belgium, the Netherlands and Luxembourg). With networks in the US and most recently in New Zealand, CAMS BeNeLux acts as the Northern European counterpart within CAMS.

In this paper we are reporting on the status of CAMS BeNeLux and also invite enthusiastic new camera operators to join.

2 CAMS hardware

Although a number of excellent detailed papers have been published about CAMS and its hardware (Jenniskens, 2011; Gural, 2011), we here briefly summarize the technics behind CAMS, all standardized:

- CAMS uses a standard sensitive Watec 902H2 video surveillance camera. No image intensifier is applied.
- It uses a 12mm F1.2 C-mount lens, giving approx. 20x30˚ FoV.
- Image acquisition of the analogue video output is done through a EZCAP USB framegrabber dongle.
- An old (but at least dual core) PC is sufficient for data collection.
- CAMS developed its own software, including a version for single station cameras, called *single-CAMS*, which is available for free. It recognizes meteors in real time, archives them, and enables astrometry. After each observing night all relevant data is to be made available manually by emailing three txt files for further processing.
- CAMS can be easily operated remotely.

The most expensive part in the system is the camera, due to its sensitivity. Recent market investigations have identified newer and cheaper versions (Samuels, 2014), bringing the price down considerably.

Recently the CAMS data format has encouraged others to write additional software, in this particular case a user-friendly image viewer, also freely available (Vida, 2014).

Two examples of recently realized stations of the BeNeLux CAMS network are shown in *Figure 1* and *Figure 2*.

[1] http://sonotaco.com/e_index.html
[2] IAU Working List of Meteor Showers, http://www.astro.amu.edu.pl/~jopek/MDC2007/Roje/roje_lista.php?corobic_roje=0&sort_roje=0

Figure 1 – Station Wildert. The cameras are typically mounted in weatherproof video surveillance casings, these being cheap and make realization of a new station an easy exercise.

Figure 2 – Station Heesch.

3 CAMS BeNeLux status

As of October 2014, the CAMS BeNeLux network consists of 32 cameras, with 3 others being installed, and another ~10 being planned. The current set of 32 cameras is operated from 14 stations, as is illustrated in *Figure 3*. Together they capture meteors over a large fraction of the Netherlands (*Figure 4*). The center and south of the Netherlands is well-covered and further expansion of the network is expected in the North of the Netherlands, Belgium, Luxembourg and Germany. Not visible in *Figure 4* are 2 camera fields that already extend into Germany and into another field west of the Belgian coast over the North Sea.

Figure 3 – Current distribution of stations over Belgium and the Netherlands.

Figure 4 – Covered atmospheric volume with CAMS BeNeLux.

4 Project organization

No network works well for a longer period without proper coordination. The CAMS BeNeLux coordination is primarily done by Carl Johannink. All observers send their results to the coordinator in principle on the same day, and these are then administered and processed soon afterwards (usually also the same day), after which the data products (i.e. orbits) are known. There is also a standby-coordinator (Martin Breukers) who takes over in case Johannink is absent. In this way a fast processing time can be guaranteed as well as a quick response to the observers. Giving fast and proper feedback to the observers is seen as a key element in keeping the network and their operators motivated. In addition, once a year a workshop is organized in which CAMS progress, technical details and questions, as raised by the operators, are discussed.

Through being part of NASA's CAMS project, all data is regularly sent to Jenniskens for further analysis and

publication. The target is that after ~ 1 year all data is made public.

5 CAMS BeNeLux data

Based on the local weather conditions each operator decides for himself/herself whether or not to operate the camera. Typically, each station is in operation on approx half of all nights and captures 5-20 meteors per (quiet) night. During an entire clear night the network is able to register over a hundred double station orbits. On a monthly basis the total number of double station meteors reaches ~1000 or more. *Figure 5* illustrates the monthly yield from the startup of the network up to August 2014. *Figure 6* gives as an idea what can be done with the data: e.g. the radiant distribution around Geminid maximum in 2013. (Preliminary) results are regularly published, as was done for both the η-Aquariids and the Camelopardalids (Johannink (2013), resp. Jenniskens (2014)).

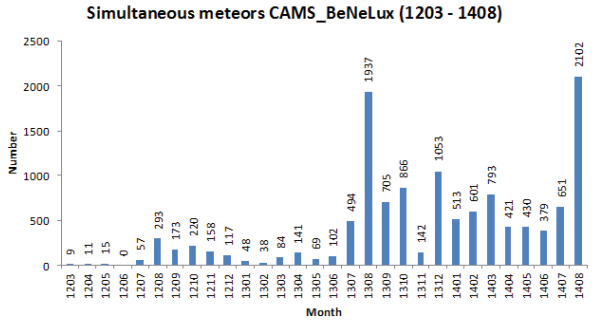

Figure 5 – Monthly distribution of double station meteors, as obtained by CAMS BeNeLux. As the number of stations is constantly increasing, the number of calculated orbits correspondingly increases.

6 Fireball information

Despite the fact that CAMS is not designed as a fireball patrol means, the large number of stations and its coverage enable that any bright fireball event is generally captured by one or more CAMS cameras too. *Figure 7* shows a recent fireball as an example. CAMS is also able to determine fireball orbits, especially when based on the fainter beginning or end of the trail, and for this reason provides additional data alongside the more conventional and less sensitive All-Sky fireball patrol cameras based on fisheye lenses (Bettonvil, 2014). CAMS provides results of similar accuracy.

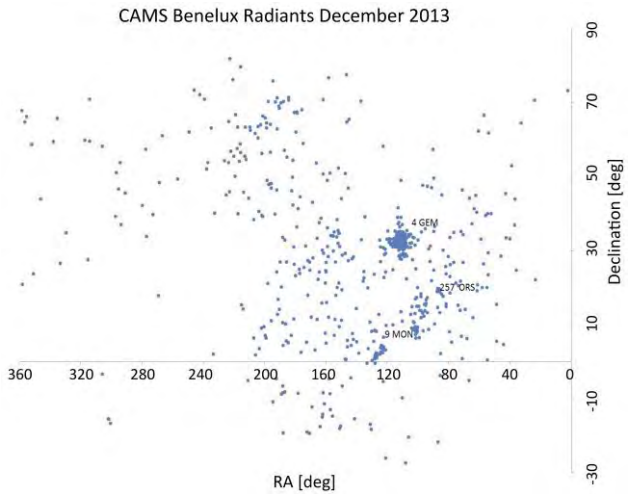

Figure 6 – Radiant distribution in December 2013.

7 Conclusions

With 32 cameras CAMS BeNeLux has grown into a major video network in just 2.5 years. Administration and processing run rather well and provide a wealth of information. We learned a number of things from the rapid network expansion:

- Setting up a CAMS station is easy to do.
- Operating a CAMS station is easily done too, remote access included.
- It delivers very useful information in the form of orbital data and light curves.
- CAMS BeNeLux has excellent coordination, that being one of the keys to its success.
- Data is processed rapidly, with fast feedback to the observers and distribution of intermediate results.
- Being part of NASA's CAMS it offers a paved way to scientific results.

New members would be very welcome.

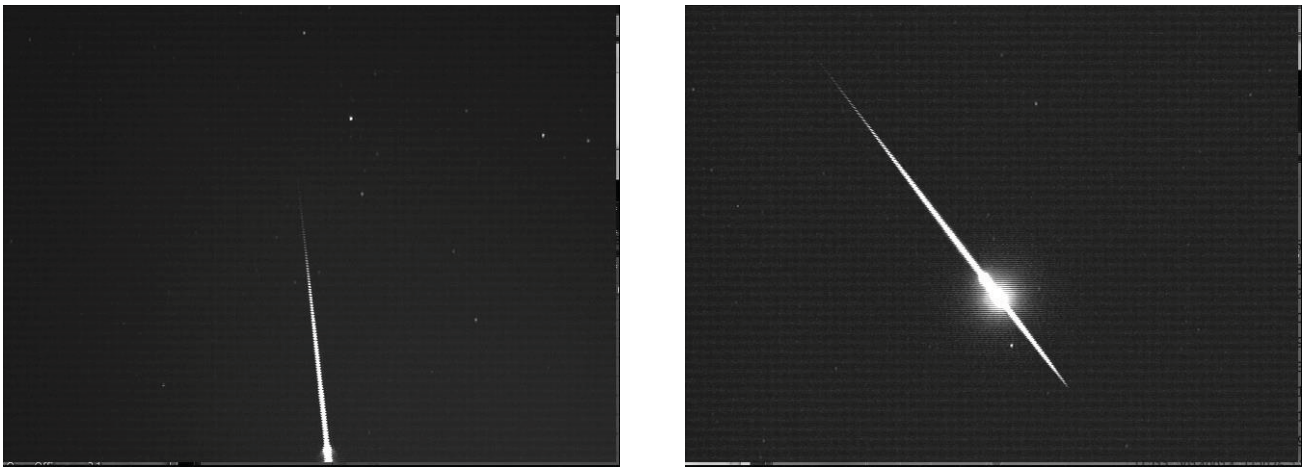

Figure 7 – 2014 September 14 at 23h17m04s UT fireball as captured by the CAMS BeNeLux stations Ermelo and Gronau. CAMS gave as result for the radiant $\alpha = 307.3° \pm 0.4°$, $\delta = +32.7° \pm 0.4°$, $V_g = 18.0 \pm 0.1$ km/s.

References

Bettonvil F. C. M. (2014). "Remote and automatic small-scale observatories: experience with an all-sky fireball patrol camera". In, Ramsay S. K., McLean I. S., and Takami H., editors, *Proceedings SPIE*, Ground-based and Airborne Instrumentation for Astronomy V, **9147**, id. 91473U, 9 pages.

Gural P. S. (2011). "The California All-sky Meteor Surveillance (CAMS) System". In Asher D. J., Christou A. A., Atreya P., and Barentsen G., editors, *Proceedings of the International Meteor Conference*, Armagh, Northern Ireland, 16–19 September 2010. IMO, pages 28–31.

Jenniskens P., Gural P. S., Dynneson L., Grigsby B. J., Newman K. E., Borden M., Koop M., and Holman D. (2011). "CAMS: Cameras for Allsky Meteor Surveillance to establish minor meteor showers". *Icarus*, **216**, 40–61.

Jenniskens J. (2014). "Camelopardalids (IAU#451) from comet 209P/LINEAR". *WGN, Journal of the IMO*, **42**, 98–105.

Johannink C. (2013). "Results for a CAMS double-station video observation Meterik – Gronau". *WGN, Journal of the IMO*, **41**, 14–21.

Johannink C. (2013). "η Aquariids outburst 2013 observed by CAMS". *WGN, Journal of the IMO*, **41**, 199–200.

Molau S., Barentsen G. (2014). "Status and history of the IMO Video Meteor Network". In Jopek T. J., Rietmeijer F. J. M., Watanabe J., and Williams I. P., editors, *Meteoroids 2013, Proceedings of the Astronomical Conference*, held at A. M. University, Poznań, Poland, 26–30 August 2013, A.M. University Press, 297–305.

Samuels D., Wray J., Gural P. S., Jenniskens J. (2014). "Performance of New Low-cost 1/3" Security Cameras for Meteor Surveillance". In Rault J.-L., and Roggemans P., editors, *Proceedings of the International Meteor Conference*, Giron, France, 18–21 September 2014. IMO, pages 66–73.

Vaubaillon J., Koten P., Rudawska R., Bouley S., Maquet L., Colas F., Toth J., Zender J., McAuliffe J., Pautet D., Jenniskens P., Gerding M., Borovicka J., Koschny D., Leroy A., Lecacheux J., Gritsevich M., and Duris F. (2013). "Overview of the 2011 Draconids airborne observation campaign". In Gyssens M. and Roggemans P., editors, *Proceedings of the International Meteor Conference*, La Palma, Canary Islands, Spain, 20–23 September 2012. IMO, pages 61–64.

Vida D., Šegon D., Gural P. S., Martinović G., and Skokić I. (2014). "CMN_ADAPT and CMN_binViewer software". In Rault J.-L., and Roggemans P., editors, *Proceedings of the International Meteor Conference*, Giron, France, 18–21 September 2014. IMO, pages 59–63.

The CAMS team at Halley Observatory in Heesch, 9 November 2014. From l. to r. Luc Gobin, Robert Haas, Hans Betlem, Marc Bouw, Erwin van Ballegoy, Carl Johannink, Klaas Jobse, Piet Neel, Adriana Roggemans, Paul Roggemans, Paul Lindsey, Franky Dubois, Steve Rau, Martin Breukers (hidden), ?, Mark Neijts en Felix Bettonvil. (credit Casper ter Kuile.)

CMN_ADAPT and CMN_binViewer software

Denis Vida[1], Damir Šegon[2], Peter S. Gural[3], Goran Martinović[4], Ivica Skokić[5]

[1] **Astronomical Society "Anonymus", B. Radića 34, 31550 Valpovo, Croatia**
Faculty of Electrical Engineering, J.J. Strossmayer University of Osijek,
Kneza Trpimira 2b, 31000 Osijek, Croatia
denis.vida@gmail.com

[2] **Astronomical Society Istra Pula, Park Monte Zaro 2, 52100 Pula, Croatia**
damir.segon@pu.htnet.hr

[3] **351 Samantha Drive, Sterling, Virginia 20164, USA**
peter.s.gural@leidos.com

[4] **Faculty of Electrical Engineering, J.J. Strossmayer University of Osijek,**
Kneza Trpimira 2b, 31000 Osijek, Croatia
goran.martinovic@etfos.hr

[5] **Astronomical Society "Anonymus", B. Radića 34, 31550 Valpovo, Croatia**
ivica.skokic@gmail.com

As the main focus of the Croatian Meteor Network (CMN) shifted from data collection to data analysis, primarily to the discovery of new meteor showers, it became clear that the current data processing pipeline was slow and outdated. In this paper new software for fully automatic data acquisition and processing is presented. Furthermore, a new tool for viewing the data acquired with the CAMS capture and compression software is described and a link is given for free download from the CMN webpage.

1 Introduction

Since late 2009, when the first procedures for automatic CMN data processing were written (Vida et al., 2011), a constant further development of such tools has been ongoing. Although the process of meteor detection, data calibration (astrometry and photometry) and orbit pairing was mostly a matter of running a few automated scripts, data processing was far from real-time. It is evident from the CMN publications of orbit catalogs (Šegon et al., 2012a; Korlević et al., 2013; Croatian Meteor Network, 2013) that in some cases data had still not been fully processed several years after their initial capture. As the main focus of the network shifted from mere data acquisition to data analysis in 2012 and 2013 (Šegon et al., 2014), it became clear that the existing procedures would no longer be sufficient. CMN staff would not have sufficient time to carry out both activities in parallel. Thus it has been decided to develop a new tool that will provide a fully automatic way of data acquisition and processing.

In the second part of the paper a new tool is presented for viewing the files acquired by the CAMS capture, compression and detection software (Jenniskens et al., 2011), and by Skypatrol.

2 Old data processing pipeline summary

Data acquisition

Since the beginning of the Network, Skypatrol software has been used for data acquisition, mostly because of its low minimum system requirements. In the years of the Network's expansion, acquiring a PC with a top-line configuration to be available only for the purpose of meteor capturing proved very difficult. Thus Skypatrol presented a good alternative to other more demanding solutions. With the further development of computer technology and the wider availability of faster computer configurations, CMN could afford more advanced capturing solutions. Replacing Skypatrol was a high-priority task as it had certain drawbacks. After each image had been captured there was a 6 second pause taken up by for internal processing procedures and for the writing of the data to disk. This meant that 10% of all meteors would be missed. For some bright multi-station fireballs it was found that although several stations captured it properly, there would often be one station the fireball happened to coincide with the "6 second time hole". Furthermore, there was no automatic way to start and to stop the capturing process. Automatic scripts which moved the mouse pointer and clicked the start and stop buttons were not very reliable because the Skypatrol window was often minimized and and it could not be automatically restored as the software randomly changed the name of the window. Among other drawbacks, it also could not capture more than two concurrent events.

Meteor detection and image calibration

Meteor detection was done using MTP_MeteorDetector software (Gural et al., 2009) which was run by a script that allowed large volumes of data to be processed at the same time. The detection procedure was very time-consuming, often requiring more than 24 hours of processor time for a few months of data from only one station. The data collected had to be further filtered to remove unwanted detections and to be calibrated with the CMN_AutoCheckFit software in order to perform astrometry and photometry procedures. In cases where

the PC at the station had no internet connection, an additional step of time synchronization needed to be carried out via the CMN_dTcommander software. This compared common events between two stations and calculated the most probable time difference between them for each day.

Orbit estimation

UFOorbit software[1] was used for orbit estimation. It provided an easy to use user interface and a fair visualization of meteor orbits. However, following further research, some of its limitations became apparent. The most obvious one is the assumption of a constant meteor velocity after entering the atmosphere, i.e. it does not take the deceleration of a meteor into account during the orbit calculation.

All orbits obtained by UFOorbit will be compared with orbits computed by the CAMS software application FTP_Coincidence on the same data set in the near future.

3 New Data Processing Pipeline - CMN_ADAPT

CMN_ADAPT (Automatic Data Acquisition and Processing Tool) was developed with all the data handling needs of the Croatian Meteor Network in mind. It provides a fully automatic solution for data capture, meteor detection, astrometry, photometry and data transfer to the central server, allowing for fully processed data to be ready for orbit estimation less than 6 hours after sunrise. Although the full functionality requires an internet connection and a decent computer configuration, these requirements can be considered one of today's standards. A complete compatibility with the previous processing procedures is retained, enabling a seamless use of any old data such as these obtained with CMN_ADAPT software.

Figure 1 – CMN_ADAPT initial setup window.

Initial setup

A special consideration has been given to the ease of setting up the software, as it is sometimes difficult to educate new station operators only via e-mail or by phone. The software is distributed to individual station's computer via a compressed archive. The operator then extracts this to an appropriate location and then runs the CMN_ADAPT.exe file. The station operator is asked for only two pieces of information: station code and the availability of internet connectivity (*Figure 1*). If the internet connection is available, a configuration file containing all parameters for the specific station is downloaded from the central server and the set up is now complete. If the internet connection is not available, the station operator needs to choose the appropriate configuration file that will have been specifically configured for that particular station and included within the delivered software archive.

During the initial setup some camera parameters such as brightness and contrast can also be adjusted. A configuration window opens and the camera operator can easily adjust the settings to achieve a proper look of the live feed from the camera itself. This step also serves as the last check of a proper hardware setup.

Pre-capturing maintenance

Each time that the software is started, a request is sent to the central server to check for a new software version. If it is available, the software is automatically updated. Before starting a new capturing session, any raw data older than a week is deleted. This prevents accumulation of raw data on the local computer as it would otherwise fill the hard disk in just a few weeks. After the cleanup, the start time and duration of capturing is calculated with regard to the location of the station and the current date.

Capturing and meteor detection

It has been decided to fully replace Skypatrol with a more modern meteor capturing solution. Having considered all available solutions, FTP_CaptureAndDetect by Peter Gural was chosen as the most suitable, as it retains several features from Skypatrol and it has an easily convertible data format, similar to one used by CMN. It also uses video capture via a frame grabber interface that is compatible with all capturing devices currently used by CMN. FTP_CaptureAndDetect is initiated at the calculated start time and the duration of capture is passed to it. Parallel with the capturing thread, the meteor detection thread runs and detects meteors in the captured images. These detections are written to a FTP_detectinfo file.

CMN procedures

When the capturing and detection process has completed, a script to create thumbnails of each captured image is run to provide an easy way to see all events during the night on a single view. It is also necessary to convert the CAMS standard detection information format to the CMN format, in order to apply CMN procedures on the data. For this task a script named CAMS2CMN by Ivica Skokić is implemented in the CMN_ADAPT. Following the conversion, all existing CMN standard procedures are applied on the data. First, detections are filtered using the MTP_filter software in order to eliminate birds, bats, planes and other unwanted detections. Astrometry is performed by running the AutoCheckFit software and photometry is also performed. To make the data compatible again with CAMS standard procedures, the

[1] http://sonotaco.com/soft/UO2/UO21Manual_EN.pdf (SonotaCo, 2008).

final CMN file, which contains meteor parameters, is converted back into the CAMS standard detection information format.

Archiving and transfer

All files containing detection and astrometrical data are archived to a compressed ZIP file and uploaded to the central server. Such files are often only a few megabytes in size. An archive of compressed raw image files which contain only detected meteors is kept locally and not transferred to the central server as these archives can reach several hundreds of megabytes in size. These files are submitted by the station operators via portable hard drives or DVDs.

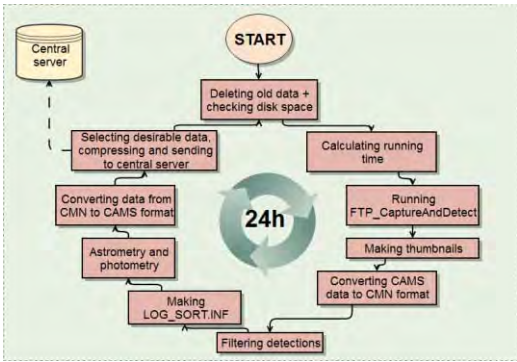

Figure 2 – CMN_ADAPT flowchart.

Orbit estimation

The multi-track coincidence and the orbits procedure is carried out by Peter Gural via the FTP_Coincidence software. The data is downloaded from the CMN central server to his personal computer, the procedure is performed and the processed data is uploaded back to the server. From this point onwards the analysis can be carried out on the orbit data. The possibility of using UFOorbit for orbit estimation is also available, as all output data from the CMN_ADAPT software is fully compatible with it.

4 E-mail alerts and thumbnails

In order to provide some supervision on the current status of the network and an early warning system for fireballs, a daily e-mail report is sent to several CMN members at 22^h00^m local time each day. This task is performed by a script running on the CMN central server. The report contains a list of stations which failed to upload the data that day and a list of detected fireballs. Thumbnail images generated by CMN_ADAPT are added as an attachment. Station operators are immediately contacted to resolve issues at those stations that failed to upload the data so that the issues can be resolved or at least diagnosed via the remote desktop software. Listed fireballs are checked on the thumbnail images, and the thumbnail images themselves are thoroughly examined. If the detected event is determined to be a possible meteorite-dropping fireball, further steps are performed for its analysis.

5 CMN_binViewer software

The use of the new capturing software has highlighted the need for a more advanced solution for viewing captured data. It was decided therefore to develop a new tool for viewing both CAMS standard and Skypatrol standard data. Its goal is to provide an all-around capability for easy data viewing, sorting, saving individual frames and images, making an animation, applying dark and flat frames and correcting image levels. As there are currently numerous networks working with CAMS standard software, CMN_binViewer is given as freeware on the CMN website[2].

Filters

The main advantage of the CMN_binViewer is its filters, special procedures applied to individual images that reveal meteor characteristics which would otherwise be invisible. There are 7 individual filters: Maxpixel image, Colorized image, Detection only, Average frame image, Odd field image, Even field image and Video.

The *Maxpixel image filter* displays the image composed of pixels which had the highest value during the recording period of 256 frames. On the Maxpixel image every recorded meteor should be seen, and thus it is set as the first and the default filter (*Figure 3*).

To get a general idea about the meteor's velocity, without needing to look at the video, the *Colorized filter* is used. It colors intermittent fields with cyan and red color. This is done by deinterlacing the image by odd field duplication. The resulting image is put into the red image channel, and the deinterlaced image by an even field duplication is put into the green and the blue channels. When all channels are viewed simultaneously, the image shows the desired effect. Fast meteors have nicely separated cyan-red detection points, while slow meteors often have detections very close to each other, thus odd field image and even field image are almost indistinguishable from each other. This results in an almost colorless white meteor on the final colorized image.

In Captured mode, the *Detection only filter* subtracts the Average pixel image from the Maxpixel image, and this results in an image which shows only the detection, without background. The resulting image is usually darker than the Maxpixel. This filter is used when the background is very bright, e.g. during Full Moon, to make faint meteors easier to see. In Detected mode, the image is constructed from individual frames of a detection, so that only the particular detection is visible, in cases when there are several detections on a single image.

The *Average pixel image* (Avgpixel in the GUI) depicts the average value of all pixels during the recording period of 256 frames. It shows background features such as background sky brightness, CCD sensor imperfections (hot pixels), stars, the Moon, objects obscuring the field of view, etc. It is used make visible the background conditions when the meteor was recorded.

[2] http:// cmn.rgn.hr/downloads/downloads.html#binviewer

Odd field image depicts the deinterlaced Maxpixel image by odd row duplication. The method consists of copying odd image rows (from top to bottom) to even rows. This filter is often used to see individual detections of a faster fireball in order to reveal the true nature of the fireball. For brighter events, phenomena such as wakes, trains and trails can be visible between the frames. *Even field image* depicts the deinterlaced Maxpixel image by even row duplication.

Video filter is used for viewing the video of a certain file or a detection. Image modifiers (deinterlacing, levels, dark frame and flat frame) are not applied during a video preview as they require a lot of processor time for each frame of the video. During the video preview the current frame number will be shown at the end of the timestamp (and change rapidly according to the FPS entry). When the viewer is showing a static image, the frame number will simply read "FFF".

Modes

In *Captured mode*, every image in a certain folder is shown in the file list box, whether it has a detection (i.e. meteor) or not. This provides a useful way to check through all images from a certain night. In this mode all filters are available for use. *Video filter* will show a movie from the first to the last frame (0 – 255 for CAMS). The temporal range can be narrowed by specifying a new range for the Start Frame and the End Frame entries. When a GIF animation is generated in this mode, it will also produce an animation 255 frames long. To create an animation showing only the detection, the *Detected mode* is used.

In *Detected mode*, only images with detections are shown. All filters are disabled other than *Detection only filter* which shows the specific event (*Figure 4*). The *Video filter* is also available in this mode, but it will show a movie only from the start to the end of a certain event. This can be used to quickly go through all recorded meteors and see their video clips.

Image calibration and adjustments

CMN_binViewer offers the option of applying two calibration images: *dark frame* and *flat frame*. It can deinterlace the image by blending the odd and even fields. It can also apply levels adjustment. These options are used to enhance the final image. In several filters and in the Detection mode some of these features are disabled, as they would interfere with normal operation. When available, all options can be used to produce a combined effect.

Saving images and animations

It is possible to save an image in BMP or JPG formats while it is being shown on the screen often useful to have a short animation of a certain meteor that can be easily viewed across many platforms. The GIF format has been chosen because of the small final size of an animation, and the compatibility with many current web browsers. This provides easy sharing and viewing of the animations.

6 Conclusion

To fulfill the current needs of the Croatian Meteor Network, two software solutions have been developed. CMN_ADAPT provides an automatic and care-free solution for data capturing, processing and transfer. In addition to the CMN_ADAPT, a server-side script generates a daily e-mail report to alert CMN station operators about camera issues and fireballs. The CMN_binViewer software, developed to view CAMS standard and Skypatrol standard data, provides an easy way to view and manage captured data. CMN_binViewer is freeware and is available to all meteor enthusiasts who are using the mentioned capture software solutions. A detailed user manual is provided with the software to help future users utilize all integrated features.

References

Croatian Meteor Network (2013). "Letter – The CMN catalogue of orbits for 2010". *WGN, Journal of the IMO*, **41**, 69.

Gural P. and Šegon D. (2009). "A new meteor detection processing approach for observations collected by the Croatian Meteor Network (CMN)". *WGN, Journal of the IMO*, **37**, 28–32.

Jenniskens P., Gural P. S., Dynneson L., Grigsby B J., Newman K. E., Borden M., Koop M., and Holman D. (2011). "CAMS: Cameras for Allsky Meteor Surveillance to establish minor meteor showers". *Icarus*, **216**, 40–61.

Korlević K., Šegon D., Andreić Ž., Novoselnik F., Vida D., and Skokić I. (2013). "Croatian Meteor Network catalogues of orbits for 2008 and 2009". *WGN, Journal of the IMO*, **41**, 48–51.

Šegon D., Andreić Ž., Korlević K., Novoselnik F., and Vida D. (2012a). "Croatian Meteor Network catalogue of orbits for 2007". *WGN, Journal of the IMO*, **40**, 94–97.

Šegon D., Gural P., Andreić Ž., Skokić I., Korlević K., Vida D. and Novoselnik F. (2014). "A Parent Body Search Across Several Video Meteor Data Bases". In Jopek T. J., Rietmeijer F. J. M., Watanabe J., and Williams I. P., editors, *Proceedings of the Meteoroids 2013 Conference*, Poznań, Poland, 26–30 August 2013. A.M. University Press, pages 251–262.

Vida D. and Novoselnik F. (2011). "Croatian Meteor Network: data reduction and analysis". In Asher D. J., Christou A. A., Atreya P., and Barentsen G., editors, *Proceedings of the International Meteor Conference*, Armagh, Northern Ireland, 16–19 September 2010. IMO, pages 96–100.

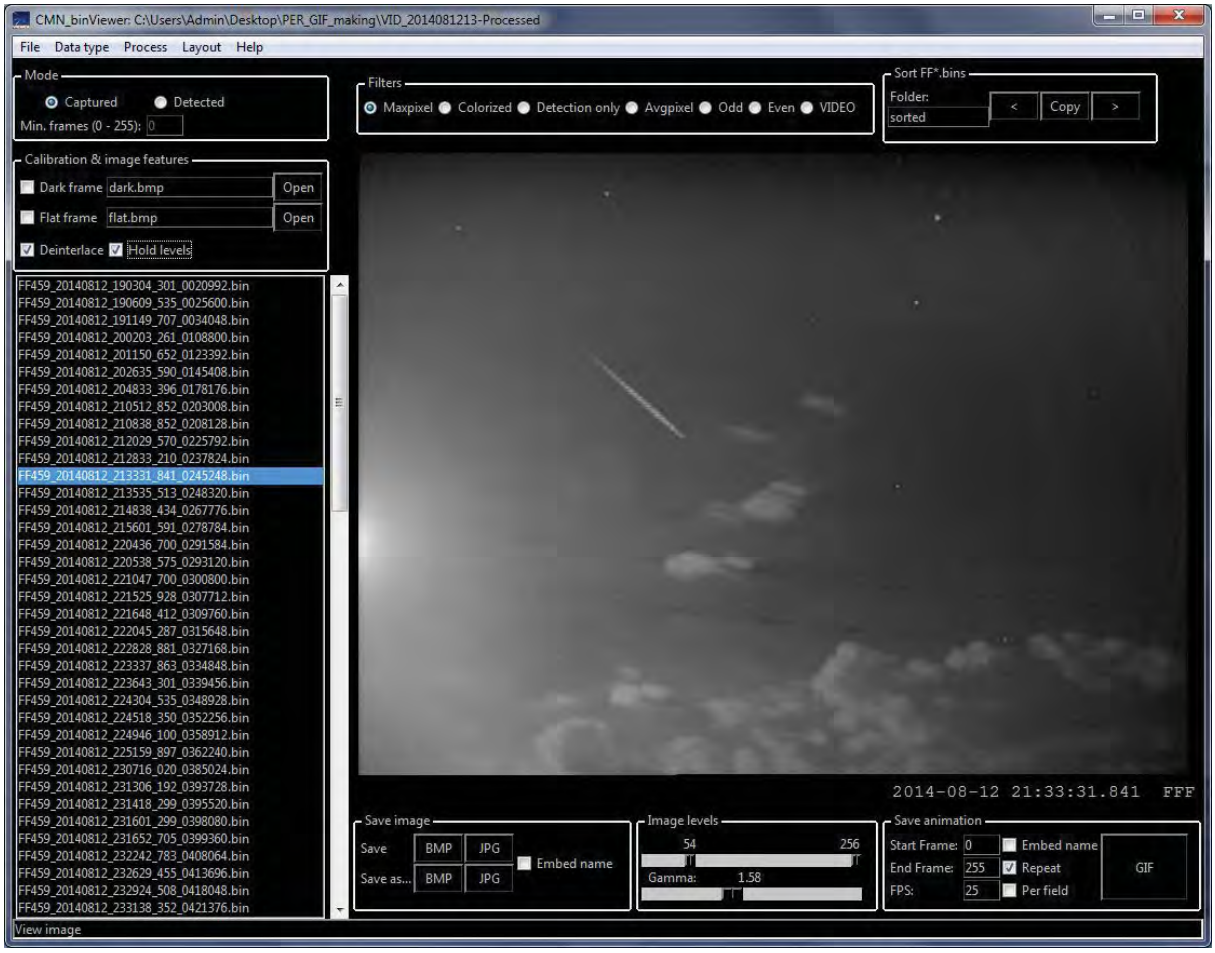

Figure 3 – CMN_binViewer Maxpixel image filter in Captured mode.

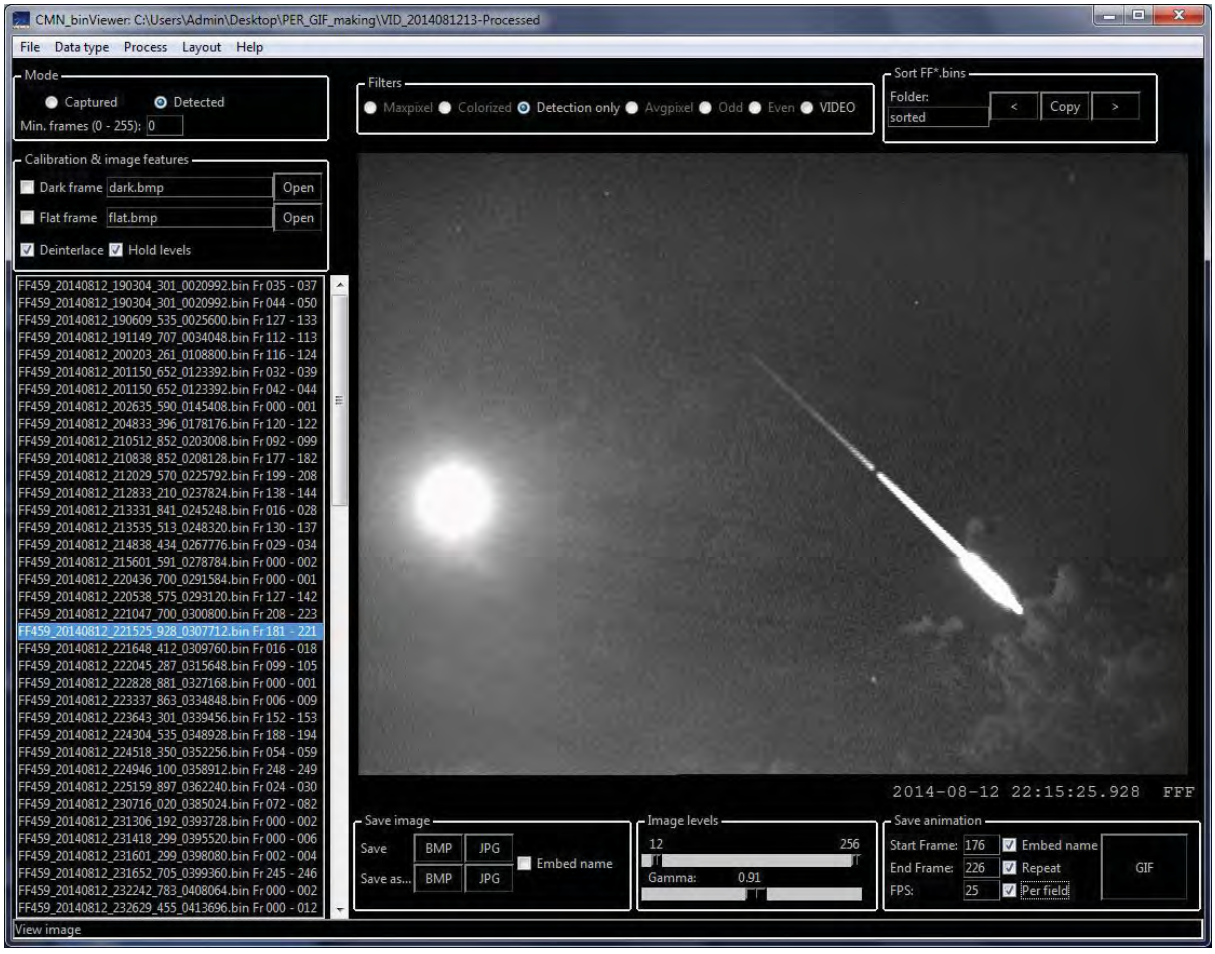

Figure 4 – Detection only filter in Detected mode, ready for saving GIF animation.

Slovak video meteor network – meteor spectra

Regina Rudawska, Juraj Tóth, Dušan Kalmančok and Pavol Zigo

Faculty of Mathematics, Physics and Informatics, Comenius University, Mlynska dolina, Bratislava, Slovakia
reginka@amu.edu.pl, juraj.toth@fmph.uniba.sk

With the updated All-Sky Meteor Orbit System (AMOS) (called AMOS-Spec) we aim to measure the main element abundances of meteors. Here we report the best eight cases.

1 Introduction

Following the great success of the All-Sky Meteor Orbit System (AMOS) (Toth et al., 2011; Zigo et al., 2013), we upgraded the system by adding an AMOS-Spec camera to record meteor spectra. The long-term AMOS-Spec program aims to measure the main element abundances of meteors detected by AMOS. Meteor spectroscopy has received much attention in recent years due to its ability to indirectly measure the main element composition of small bodies of the Solar System, which offers important scientific benefits. Meteor spectra are emission lines containing, mostly, emission features belonging to meteoroid vapors, as well as some lines of atmospheric origin. Here we report results from a sample of meteor spectra collected by the AMOS-Spec camera from November 2013 to May 2014.

2 Observations and results

AMOS-Spec system

Installed at Modra Observatory in Slovakia, the AMOS-Spec system is based on the original AMOS camera. It is equipped with a 30 mm f/3.5 lens (FOV 140° x 100°) and a 500 grooves/mm grating. The limiting magnitude of a meteor for our system (with optimal geometry of meteor flight in front of the camera, and optimal meteor velocity) is around magnitude -2.

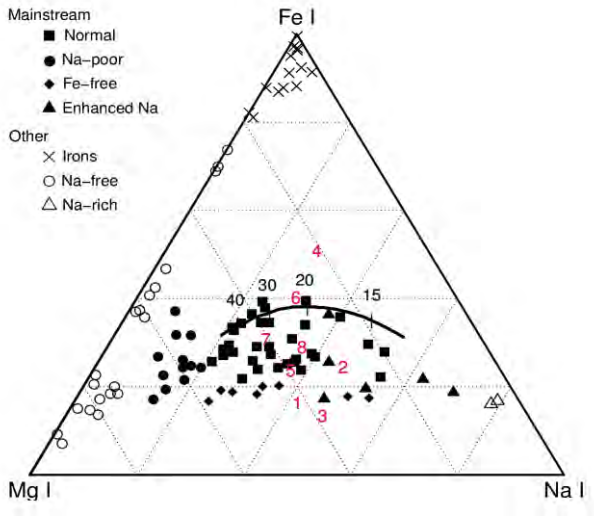

Figure 1 – The measured relative intensities of the Mg I, Na I, and Fe I multiplets. Our data (red) are compared to those derived by Borovicka et al. (2005), defining several classes of meteors.

Data reduction

Since the start of the operation of the AMOS-Spec camera, we have collected over 500 meteors. So far we have captured 45 meteor spectra of variable quality. The collected data has been reduced and the first stage of spectral analysis has been conducted. The spectral events were corrected for dark current, flat-fielded, and multiplied by the cameras spectral response curve. The wavelength scale for each spectrum was determined by means of known lines (Fe, Mg, and Na) in the calibration spectrum, with a spectral resolution of 2.5 nm/pix. If an event was recorded simultaneously by more than one station, we were able to determine a heliocentric orbit for that meteor. Here we report the best eight cases (*Figure 1*).

3 Summary

Spectroscopic analysis is the most powerful scientific tool for studying celestial bodies. Its power in the meteor field is that it allows us to study the chemical composition and other properties of meteoroids and of their parent bodies. Nowadays, routine spectroscopic observations of meteors are mostly carried out during meteor shower campaigns. However, a regular yearlong survey is needed to take full advantage of meteor spectroscopy. It is for this reason that the AMOS-Spec program has been created, to help us to fill this gap.

Acknowledgment

The work is supported by the Slovak grant APVV-0517-12, APVV-0516-10 and VEGA 1/0225/14.

References

Borovička J., Koten P., Spurný P., Boček J., Štork R. (2005). “A survey of meteor spectra and orbits: evidence for three populations of Na-free meteoroids”. *Icarus*, **174**, 15–30.

Tóth J., Kornoš L., Vereš P., Šilha J., Kalmančok D., Zigo P., Világi J., (2011). “All-sky video orbits of Lyrids 2009”. *Publications of the Astronomical Society of Japan*, **63**, 331–334.

Zigo P., Tóth J., Kalmančok D. (2013). “All-sky Meteor Orbit System (AMOS)”. In Gyssens M., and Roggemans P., editors, *Proceedings of the International Meteor Conference*, La Palma, 20–23 September 2012. IMO, pages 18–20.

From left to right Dominique Richard, Christian Paillart, Regina Rudawska and Bernhard Kieffer. (Credit Dominique Richard.)

Here some participants made a mini group picture in front of the frontcover picture of these Proceedings. From left to right Roman Piffl, Paul Sutherland, Alexander Schneider, Geert Barentsen, Bernd Klemt, Jürgen Rendtel, Manuela Rendtel, Axel Haas, Sirko Molau, Detlef Koschny, Roland Winkler, Bill Ward and Gerhard Drolshagen. (Credit Axel Haas.)

Performance of new low-cost 1/3" security cameras for meteor surveillance

Dave Samuels[1,4], James Wray[2,4], Peter S. Gural[3,4], Peter Jenniskens[4]

[1] **Single-CAMS station Brentwood, CA, USA**
dave@davesamuels.com

[2] **Single-CAMS station Foresthill, CA, USA**
jwray@scitech.co

[3] **Single-CAMS North Atlantic Network, VA, USA**

[4] **SETI Institute, Mountain View, CA, USA**

It has been almost 5 years since the CAMS (Cameras for All-sky Meteor Surveillance) system specifications were designed for video meteor surveillance. CAMS has been based on a relatively expensive black-and-white Watec WAT-902H2 Ultimate camera, which uses a 1/2" sensor. In this paper, we investigate the ability of new, lower cost color cameras based on smaller 1/3" sensors to be able to perform adequately for CAMS. We did not expect them to equal or outperform the sensitivity for the same field of view of the Watec 1/2" camera, but the goal was to see if they could perform within the tolerances of the sensitivity requirements for the CAMS project. Their lower cost brings deployment of meteor surveillance cameras within reach of amateur astronomers and makes it possible to deploy many more cameras to increase yield. The lens focal length is matched to the elevation angle of the camera to maintain an image scale and spatial resolution close to that of the standard CAMS camera and lens combination, crucial for obtaining sufficiently accurate orbital elements. An all-sky array based on 16 such cameras, to be operated from a single computer, was built and the performance of individual cameras was tested.

1 Introduction

The Cameras for All-sky Meteor Surveillance project (CAMS) is a NASA sponsored project using video surveillance of the night sky to map the visible meteor showers throughout the year (Jenniskens et al., 2011; Gural 2011). The primary CAMS network in California consists of three 20-camera array boxes positioned at Fremont Peak, Lick Observatory, and Sunnyvale, CA, with data gathered and processed at the SETI Institute. In 2011, software was developed, by Pete Gural, for amateur astronomers to add one or more cameras to this network in a project called *single-CAMS*. Since then, the single-CAMS software has been enhanced to support 2, 4, and 16 cameras from a single computer. Several single-CAMS local networks have been established in Northern California, the Belgium/Netherlands/Luxembourg area (BeNeLux), the Washington DC area, Northern Florida, Croatia, and now also in New Zealand[1].

The de facto standard for video meteor surveillance – and workhorse for this science - has been the Watec 902H2 Ultimate black and white security camera based on its very sensitive 1/2"-inch sensor. This camera is based on the Sony EXview HAD 1/2" architecture. It has several favorable properties: (1) The sensitivity is measured to 0.0001 lux (effectively being able to record stars down to magnitude +5.4 with an f/1.2 12-mm lens); (2) Is a compact camera suitable for flies-eye type all-sky configurations; (3) Uses BNC connectors to achieve a reliable connection to the camera; (4) It is easily configurable. The biggest drawback for amateur astronomers is that the standard camera/lens configuration is expensive. The Watec Wat902H2 Ultimate camera sells for around $US390 (Note that all prices quoted in this paper are internet-derived prices per October 2014 and are prone to changing) and the recommended Pentax 12mm f/1.2 lens (mfr #C61215KP) will typically cost around $US95, plus shipping (internet pricing October, 2014). The expense of the equipment is often a deterrent in setting up new sites or expanding a site to multiple cameras.

In the 5 years since the camera specifications for the CAMS project were made, lower cost color security cameras have come on the market that are based on later model 1/3" sensors. They boast high sensitivity, which we attempt to test in this paper. These new color cameras have a Night Mode. There are several aspects to the Night Mode of these cameras. One major one is that they increase the sensitivity by switching from color mode to black and white mode. The firmware driving the cameras also supports Sens-Up technology. Sens-Up, and the other Night Mode related features degrade the performance for CAMS and they should be disabled.

These new cameras may not be as good as the Watec, but are possibly sensitive enough to perform well enough to be used for the CAMS project. We found a few cameras available for under US$60.00. We also found some f/1.2 near-IR corrected lenses available for US$8.00.

In this paper, we examine whether or not these new cameras might be suitable to expand the data gathering ability of the CAMS project and enable more amateur

[1] http://cams.seti.org.

astronomers to participate in single-CAMS networks. Another question that should be answered is whether these smaller sensors can cover the sky using a 16 camera array?

2 Camera models and properties

Testing was performed from several sites in the Northern California single-CAMS network. The two main test sites were Foresthill, CA and Brentwood, CA. These sites are 132 km apart. The pointing of the cameras was adjusted several times to test the ability to capture low-light meteors at various elevation angles and distances from the camera. For the first few months, the Brentwood station used the standard Watec configuration and the Foresthill site used the 1/3" cameras. Eventually, the Brentwood station switched to using one EXview and one Super HAD II to complete the tests.

Three tiers of elevation angles were used to provide all-sky coverage at this distance. All lenses were tested at each elevation tier.

The sensitivity of security cameras is often specified in lux. However, there is no real standard for advertising lux ratings, so you can't really trust the advertised lux sensitivity without testing unless more detail , such as the focal ratio and gain, is available. In this paper we try to show the usefulness of these cameras regardless of lux levels.

Sony "Effio-E" System

Before we delve into the different cameras, we need to clear up some confusion regarding the firmware utilized with these cameras.

The word "Effio" translates to "Enhanced Features and Fine Image Processor". You can think of it as the operating system for a camera. The Effio system's signal processor has useful security features such as high color reproduction, high S/N ratio, and high resolution. The Effio system also provides the on-screen display menu (OSD). The Effio series cameras also have higher night time sensitivity by changing the camera from color mode to black and white mode. In addition, features, such as Sens-Up and other night mode functions are also part of the Effio system. Many advertisements of Effio series security cameras can boast of lower lux levels due to these Sens-Up and night mode settings. In effect, Sens-Up switches the camera to 1/15 sec exposure time up to 4 second exposure integrations to attain the increased sensitivity. Some of the other features with the Effio-P, S, and E series cameras are Wide Dynamic Range, Privacy Masking, Motion Detection, Image Stabilization, Exposure control for IR lighting, Adaptive Tone Reproduction (ATR), 2D & 3D NR, and Highlight Compensation (HLC). While all of these features are useful in security cameras, only the privacy masking feature is potentially useful with CAMS. However, this feature has not been tested. One of the features of the EXview OSD was a way of making dark frames so that hot pixels could be masked by the in-camera image processor. This will be a useful feature as the camera ages.

The Effio-E System is the entry level Effio system that has a simple, 2-chip structure consisting of an analog IC and a signal processing IC and supports a wide range of sensors. They are provided in compact chip packages (helps in miniaturization) and they consume 1/2 the power of previous systems. The Effio-S and Effio-P Systems provide additional features that are not used for CAMS.

The New 1/3" Cameras

Several new low-light camera models are now on the market. Here, we will discuss the Sony EXview HAD II 960H 700TVL based cameras and the Sony Super HAD II 960H 700TVL based cameras. 20 cameras were used in this test, the camera models tested being: 2 x EQ700; 17 x PSCB-100H; and 1 x LN-300-6H672.

Figure 1 – EverFocus Ultra Series Super Low Light Box Camera" (mfr # EQ700).

Figure 2 – LN-300-9H672 OSD Menu buttons for configuring the camera settings and PSCB-100H Effio-E OSD Menu.

Table 1 – Vendor's advertised specs for the EverFocus EQ700.

Sensor	EQ700 1/3" EXview 960H 700TVL
Resolution	700 TVL
Minimum Illumination	0.0001 lux 30 IRE Normal shutter f/1.2/AGC
S/N Ratio	> 50 dB (AGC OFF)
Pixels	976 x 494 NTSC (976 x 582 PAL)

The sensor types tested have a specified lux rating of 0.003 lux at 30 IRE with a normal shutter and f/1.2 lens and AGC settings (compared to 0.000033 lux for the Watec Wat902H2 Ultimate at high gain setting with an f/0.8 lens – no IRE provided). The lux for the Watec in AGC was not specified. In contrast with the Watec camera, these new cameras provide all configuration settings with an OSD (On-Screen Display) menu using the OSD buttons on the back of the camera. There are pros and cons to this. Ideally, we'd like to see the ability

to control the camera settings via software, but the settings on these cameras are not controlled by software.

Initially, two EXview HAD II type cameras were purchased by JW, the "EverFocus Ultra Series Super Low Light Box Camera" (mfr # EQ700), from B&H, for about US$120 each in May, 2014 (*Figure 1*). We tested these two EQ700 cameras for a few months using various lens configurations.

Later, sixteen Effio-E cameras with the Sony Super HAD II 960H 700TVL sensor (the PSCB-100H) were purchased by JW cameras from AliExpress for US$43 on sale (*Figure 3*). The price at time of writing is US$47. We tested those cameras with various lens configurations and camera settings. *Figure 2* shows the OSD menu for this camera.

Figure 3 – PSCB-100H Super HAD II camera.

The specs for the PSCB-100H camera are as follows:

Table 2 – Vendor's advertised specs for the PCSB-100H-960H.

Sensor	1/3" Super HAD II 960H 700TVL High Sensitivity CCD
Resolution	700 TVL
Minimum Illumination	0.003 lux 30 IRE Normal shutter f/1.2/AGC
S/N Ratio	> 50 dB (AGC OFF)
Pixels	976 x 494 NTSC (976 x 582 PAL)
Size	130 (L) x 60 (H) x 50 (D) mm
Weight	450g

The Spectral sensitivity, as specified on the Sony website[2], shows that these cameras share very similar sensitivity, with the EXview having a slightly higher sensitivity in yellow and IR (*Figure 4*).

DS then purchased one Sony LN-300-9H972 for US$56, also of EXview HAD II 960H 700TVL type from AliExpress. The 9H672 is much smaller than the PSCB-100H - closer to the size of the Watec camera (see *Figure 5*). The manufacturer shipped the 9H672 (NTSC), as opposed to the 9H673 (PAL). The 9H672 camera received was missing the adapter that should provide the ability to use CS mount lenses. Another CAMS group member purchased the 9H672 and that did have the adapter ring included. *Figure 2* shows an example of the OSD menu buttons on the back of the camera.

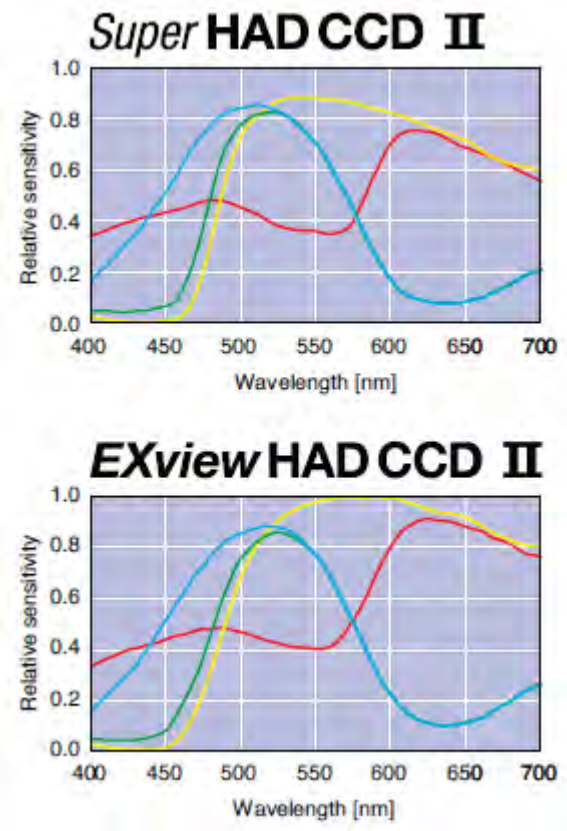

Figure 4 – Spectral Sensitivity Characteristics Comparison between EXview HAD II and Super HAD II. The EXview shows slightly higher response in Yellow and IR.

Figure 5 – LN-300-6H692 based with the Sony EXview HAD II 960H 700TVL sensor.

Table 3 – Vendor's advertised specs for the LN-300-9H672.

Sensor	1/3" EXview HAD II 960H 700TVL High Sensitivity
Resolution	700 TVL
Minimum Illumination	0.003 lux 30 IRE Normal shutter f/1.2/AGC
S/N Ratio	> 50 dB (AGC OFF)
Pixels	976 x 494 NTSC (976 x 582 PAL)
Size	62 (L) x 43 (W) x 42 (H) mm
Weight	150 g

[2] High-Sensitivity, High-Resolution Camera Systems for Security Cameras based on Diagonal 6.0 mm (Type 1/3" 480K/570K-Effective Pixel Color CCD Image Sensors. (CXD4127GG, CXD4816GG, ICX672ADA/ICX673AKA sensor model numbers) This document is the Sony publication that shows the specifications for the sensors: http://www.sony.net/Products/SC-HP/cx_news/vol61/pdf/cxd4127_4816gg.pdf.

Removing the IR-cut Filter

Testing yielded similar results for star sensitivity for all the cameras tested, but the Sony LN camera was slightly more sensitive in the near-IR than the PSCB 100H Super HAD II camera. These cheaper cameras are both delivered, by default, with a near-IR-cut off filter glued over the sensor's environment window. This reduces the sensitivity of the camera and it should be removed. Be sure to order LN-300-9H672 without the IR cut filter. The EQ700 camera is a higher-end model. It has a tiny motor that moves the IR-cut filter out of the way during night mode.

Figure 6 – Experimental removal of IR cut filter from first batch of PSCB-100H cameras by JW improved limiting magnitude by nearly a full magnitude.

The Super HAD II based PSCB 100H cameras had a small IR-Cut filter glued to the sensor. When these were removed (see *Figure 6*), the cameras gain about a magnitude in light gathering. These cameras only reach the 0.0001 lux with this removed. After JW pointed out the need to remove the IR cut filter for meteor observing, the AliExpress vendor made arrangements with the manufacturer such that if the cameras were ordered with the explicit instructions to ship the cameras without the IR-cut filter installed, they would do that. Hence, when DS purchased the Super HAD and the EXview cameras, they were delivered, as per request, without IR cut filters installed.

3 Results for meteor observations

To achieve precise orbital elements, CAMS requires a spatial resolution of about 4 arcminutes/pixel or better and, ideally, with a field of view of around 20 x 30 degrees, for each camera. A good balance between spatial resolution and image scale is achieved by using longer focal lengths and correspondingly smaller field of view for lower elevations (more distant meteors).

Figure 7 – Inexpensive 1/3" CS IR corrected lens set.

We tested various fast lens configurations, including the 8mm f/0.8, 12mm f/0.8, 6mm f/0.8, and 9mm f/0.75. While over 1 magnitude brighter than the f/1.2 lenses used in CAMS, all these fast lenses are difficult to acquire (However, testing showed that the sensitivity of the 1/3" cameras with these brighter lenses matched the sensitivity of the Watec with its f/1.2 lens). We eventually tested with the US$8 near-IR-corrected CS format 6mm f/1.2, 8mm f/1.2, and 12mm f/1.2 lenses (see *Figure 7*). These lenses are all readily available and very inexpensive. As they are IR corrected, they performed very well. There is no coma or pincushion and they provided sharp stars out to the edges of the frame - even in the 1/2" camera.

When a single-CAMS user purchases a camera, it might be a good idea to have at least one full set of these three focal lengths.

The spatial resolution of these lenses is shown in the following table. The lower the elevation angle, the longer the distance to the target. This table shows that these lenses are suitable for CAMS.

Table 4 – Spatial Resolution at distance determined by elevation angle and 90 km height.

Elevation Angle (degrees)	Focal length (mm)	Spatial Resolution per pixel	Coverage Area km^2
29	12	100 meters	9098
46	8	100 meters	5362
75	6	110 meters	4015

For the Sun facing cameras, you might consider purchasing a DC auto-iris lens to protect the sensor. These were not tested. In the 1/3" CS format, they are much cheaper than the 1/2" format and they can generally be obtained for under US$70 online.

Sensitivity Tests Results

We first compared the 1/3" Super HAD camera with the more sensitive 1/2" Watec by capturing for a night with both cameras centered on the same part of the sky using the same focal length and focal ratio lenses. Hence, the field of view for the 1/2" sensor was larger (44 versus 34 degrees). The images in *Figure 8* show the same meteor observed by the Super HAD type camera and the Watec 902H2 Ultimate type camera. Having matched the light gathering settings (8mm f/1.2 for the 1/2" sensor versus 8mm f/1.2 for the 1/3" sensor), the sensitivity of the cameras was close, but the field of view of the Watec 902H2 Ultimate is larger.

The stellar limiting magnitude in the Super HAD II 1/3" cameras (8mm /f1.2) is between magnitude +4.0 and +5.0, while the Watec 902H2U camera has about a +5.0 stellar limiting magnitude with 8mm f/1.2 lens. What's also interesting to note is that the $8 lens appeared to perform adequately, compared to the $90 Pentax lens.

In the CAMS capture software, average frames are used for astrometry. 256 frames are averaged, amounting to 8.542 seconds NTSC or 10.24 seconds of PAL. In the table above, we used the AutoCAMS auto-calibration routine to show the magnitudes of the dimmest stars detected by setting auto-cal to 140 minimum stars and

O-C to a high 2.50 arcmin/pixel. The table lists the faintest star that was matched by the program. Note: Typical auto-calibration results in 0.015 to 0.300 arcmin per pixel for a 12mm lens, around 0.321 for 9mm, and 0.500 for 6mm lenses.

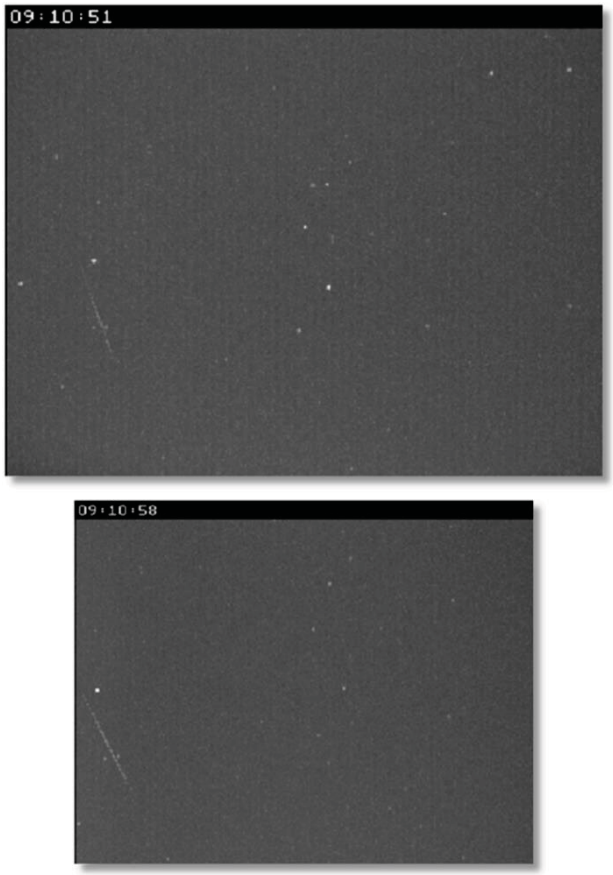

Figure 8 – Same meteor detected (top) by a Watec 902H2 Ultimate with 8mm f/1.2 44 deg FOV(top) and (bottom) by the PSCB-100H 960H camera with 8mm f/1.2 for smaller 34 deg FOV, with MGC set to same levels as AGC. Images are contrast enhanced and brightened to show the differences.

It is difficult to compare one system with another to compare meteor counts unless you have different systems pointing to the target area at the same time with the same focal ratio lens on the camera on the same night. On the night we performed this test, there were 14 meteors in the Watec 1/2" camera and 12 in the 1/3" camera. One interesting result was that the 1/3" camera picked up some meteors that were not detected by the 1/2" camera and vice versa. Hence it is probably safe to say that the 1/3" camera will not detect as many meteors as the Watec, but the percentage difference is quite low. More testing is needed in this area if this is of concern.

During these first few weeks of October, each 1/3" camera was detecting about 20 – 25 meteors per night per camera. The Brentwood and Foresthill stations only ran 2 cameras per station and out of the 40 – 50 meteors per night per site, the average number of orbits calculated was about 26 per night. That is 13 orbits per night per camera in October. This is the same average as we've maintained from the Brentwood station for years, while using the Watec. So overall, we could conclude that the number of orbits per camera per night is about the same as with the Watec 902H2 Ultimate.

We didn't capture the measured stellar limiting magnitudes for all combinations because we later discovered that the camera settings were not ideal. The Foresthill array is currently taking advantage of the set of f/0.8 and f/0.75 lenses available. The 12mm f/0.8 is showing the best-measured stellar limiting magnitude of +8.00 (256 frame average). The 9mm f/0.75 lens is showing +8.10 on a different night. The 6mm f/1.2 is showing +6.41, while the EXview with the 6mm f/1.2 is showing +6.92.

4 An All-sky Array of Cameras

The regular CAMS network deploys 20 cameras for full sky coverage above 30º elevation, using 5 servers. The newer low-cost cameras now make such an array within reach of amateur astronomers. While less sensitive, a larger number of cameras can increase the yield of relatively bright meteors.

Figure 9 – 18-camera amateur array at the Foresthill, CA single-CAM station.

For the purpose of this project, JW designed and built a box housing an array of 18-cameras (His box uses 18 cameras instead of 16 cameras because he has 18. 16 cameras will be run through the dual 8 port Sensoray grabbers while the remaining two will be run from a separate laptop using EZCap grabbers). Inexpensive 1/3-inch PSCB-100H cameras were selected to operate with either a single 16-channel capture card or two 8 channel cards. The lower cost per channel of the Sensoray 8 channel card makes this the most appropriate for cost savings, which was one of the objectives of the design. The cameras are arranged to point through a minimal sized opening to reduce both scattered light within the enclosure and solar flux if left open during daylight hours. It should be noted that camera and lens manufacturers do not recommend direct exposure of the detector to sunlight and the array has always had a secondary cover to block sunlight from entering the aperture.

Cameras are mounted on fixed elevation brackets attached either to the base (for inner ring cameras) or to elevated blocks attached to the base (for the outer ring cameras). Elevations are color-coded and azimuths number-coded so each camera and its cabling is readily identifiable by their unique color/number assignment.

Figure 10 – Inside view of the 18-camera setup, showing cameras, brackets, and 16-port power supply.

The color code can be seen on the mounting blocks and the video cables (*Figure 10*). 500 feet of video cable was purchased, cut into 18 x 27ft lengths, and finished with crimp-on BNC connectors. A 16 channel 12v CCTV power supply was mounted in the lower section of the box with ventilation provided by the cable thru-holes to minimally warm the camera compartment and slow the onset of dewing. Video cables are routed out the bottom of the lower section through an enclosed cable-way to the building interior location for the capture card and computer.

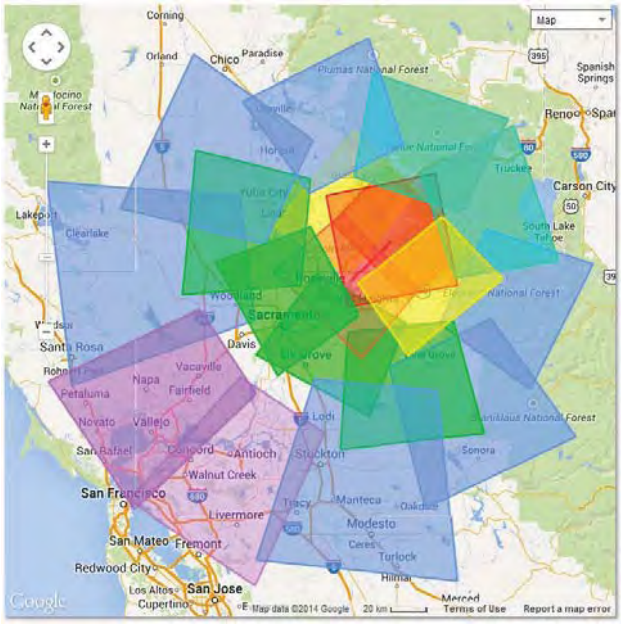

Figure 11 – Eighteen camera layout in current setup based on measured calibrations against the stars.

This 18-camera array provides the same area of coverage as a regular CAMS station (*Figure 11*). Note that the configuration achieves maximum coverage by including some areas at low elevations (*Figure 12*). However, care must be taken to use the appropriate lens to obtain the appropriate spatial resolution.

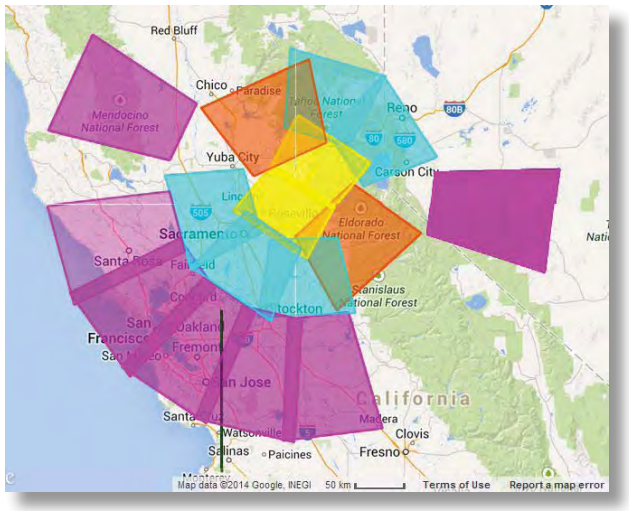

Figure 12 – Sixteen cameras sparsely distributed to reach single-CAMS users.

By varying the focal length of the cameras to match the elevation angle, we achieve the same spatial resolution across the sky (at the 90km target height). We calculated the spatial resolution to be as shown in *table 4*.

Two 16 camera arrays can be tuned for maximum coverage overlap while aiming toward each other. The idea is that a new local CAMS network could optimize two sites to provide overlap between just those two sites. Single-CAMS stations can be used to fill in coverage gaps, if any. Single-CAMS stations can also be used to extend the coverage area.

Based on the lower-cost cameras, a 16 camera site can be established for around US$2600 at current prices, including computer and cabling, so that two 16 camera (32 cameras) sites for triangulation can be established for around US$5200 (approximate prices per October 2014).

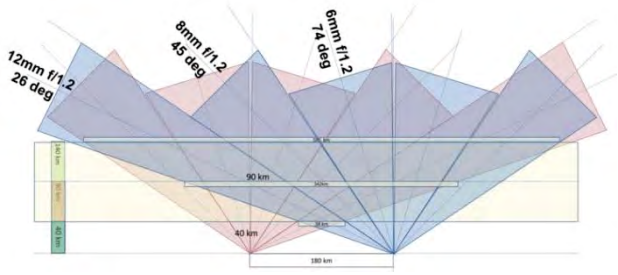

Figure 13 – Elevation angle cross section - Different focal lengths to match the elevation angle. 180 km baseline.

5 Camera Settings

This section describes the camera settings for the EXview camera. The OSD camera settings for the PCSB-100H Effio-E camera are difficult to record currently since the camera is mounted inside its outdoor enclosure.

For some reason, when using the Effio it has proved difficult to keep the camera operating at the 1/60 interlaced setting using the EZCap grabbers. This has not been an issue with the Sensoray 2255S grabber.

EXview OSD Menu Settings

Here are the settings being used for the EXview HAD II 960H 700TVL LN-300-9H692 for CAMS.

EXPOSURE
- LENS = ELC
  - E.SHUTTER = 1/60
  - BRIGHT = 50
- HBLC/D-WDR = OFF
- AGC = MID
- 2D DNR = OFF

WB
- WB MODE = ATW
- R-Y GAIN = 128
- B-Y GAIN – 128

DAY&NIGHT
- D&N MODE = B&W
- C-SUP = 050
- A-SUP = 050

FUNCTION
- MIRROR = OFF
- SHARPNESS = 010
- LSC = OFF
- MONITOR = MODE1
- GAMMA = USER
  - 0.30

MOTION
- MOTION = OFF
- AREA SEL
  - Set all of them to = OFF
- SENSITIVITY = 1
- DISPLAY = ICON
- HOLD TIME = 008
- ALARM = OFF

PRIVACY
- Set all masks = OFF

SETUP
- TITLE = OFF
- MANUAL DPC = MANUAL
- AUTO DPC = AUTOC
  - DPC LEVEL = 150
- OLPF = 850 or 650 (I'm not sure)

- OSD COLOR = GRAY

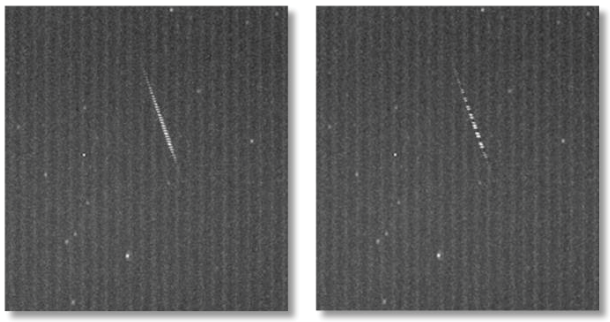

Figure 14 – Watch for strobing caused by various forms of Night Mode.

6 Issues and Workarounds

One issue that we had when using the EZCap video grabber and its delivered software in conjunction with these cameras is that sometimes the settings would revert to a mode in which the camera was imaging at 1/15 or 1/30 sec instead of 1/60. This is very apparent when looking at thumbnails and other samples of the images. These "night-mode" shutter speeds cause a "strobing" effect on meteors (see *Figure 14*). This is also apparent, during coincidence processing, even if you don't have the images or thumbnails available. In such cases, the cameras that are imaging at 1/60 sec will have dots between the dots of the strobing cameras. Hence be careful with this. With the 4 channel Sensoray grabber, this issue was not apparent once the camera settings were established and saved.

With the EZCap and 16 or 18 cameras in position in the box, it becomes somewhat cumbersome for JW to fiddle with the internal OSD menu buttons in order to set all the cameras to their optimal settings. Hence, if you're going to build such a box, be sure that access to the OSD buttons on the back of the camera is available when the cameras are in position and that they can be used without moving the camera.

Another issue that we found was that the cameras produced different levels of brightness and contrast with the same settings. We do not know the source of this inconsistency. Therefore, the cameras were set to mostly use their default settings and, using the EZCap grabber, the ULead driver software was used to make adjustments in the gain, brightness, sharpness and contrast for each camera. Since this could be accomplished on the screen at the computer, it was much easier to do.

Figure 15 – 18-camera box housing. Ventilation maintains internal temperature close to ambient.

Another troublesome issue occurs when the camera settings are set to a level at which there are insufficient stars for a manual star-field calibration. We discovered that, close to sunrise, when there is more sky fog in the background, the cameras seem to show more calibration stars. However, using the EZCap grabber, the settings needed to be manually adjusted to attain a balance between being able to see enough calibration stars (70 is usually the goal) during manual calibration and too high a gain, producing too bright image with excessive noise and quicker saturation for the rest of the normal night's meteor capture.

AutoCAMS also uses an "autocal" routine, which iterates throughout the night's capture session and finds the best calibration from that collection of thousands of files. With the Watec, we typically see over 200 nStars in the calibration field. With the 1/3" cameras, we're seeing around 180 nStars, depending on the focal length.

Hot pixels become a problem after a while. They appear as fixed white spots in the camera's sensor. They don't move with the stars. They become problems when

performing plate-solves and auto-calibration because they are sometimes mistaken for stars. A means of masking these out of calibration will be needed as these cameras encounter more cosmic ray damage as they age. The 1/3" EXview camera has a built-in noise calibration as well as an automatic one (SETUP > MANUAL DPC or AUTO DPC). In the first, the user covers the lens and runs the routine to take a dark. The other method is the automated method whereby the camera can somehow tell from the captured frames how much compensation is required for the hot pixels and variations on the sensor. DPC means "Dead Pixel Compensation". Dead Pixels are black pixels (the opposite issue as hot pixels), which aren't so much of a problem for CAMS. Since the camera that DPC was tested on is not yet showing hot pixels, we could not verify that the DPC feature will remove the hot pixels during capture.

7 AutoCAMS software

AutoCAMS is an open-source Windows scripting language based system for performing most of the daily functions of a single-CAMS site. It consists of almost 40k lines of script code written by Dave Samuels. In many cases, it acts as a wrapper around the executables written by Peter Gural. In some cases, it provides additional functionality. For example, autonomously launching the daily capture procedure, checking on the available disk space, checking on the start/stop times for any date, archiving the sessions into zip files, uploading the daily capture session summaries to the SETI Institute CAMS server, etc.

AutoCAMS has some very specific goals, namely to never send bad data to the SETI Institute server, to consistently and accurately facilitate the capture of meteor data every night, to perform these daily functions autonomously and to perform validation and verification of the data before submitting it to the SETI Institute server. Essentially, it ensures that the network coordinator or the lead scientist never has to ask for reprocessing and/or resubmission of data, and it simplifies the daily tasks into easily workable steps.

8 Conclusions

We have demonstrated the feasibility of applying new low cost 1/3 inch format video cameras and lenses for meteor detection within the parameters specified as suitable for use with the SETI CAMS meteor orbit program. An 18 camera array has been constructed and has been placed in service. These low cost systems are suitable for others to replicate as individual cameras, twin cameras or 16 camera arrays.

The 1/3" cameras averaging about 10 – 15 triangulated orbits per night throughout this period. The accuracy of the calculated orbits falls well within the acceptable tolerances. In fact, the accuracy is the same as with the Watec cameras. The only difference is a slight drop in the count due to the extra sensitivity of the higher priced Watec cameras. This is within about 90% of the rate per camera for the Watec cameras.

The 18-camera array is still waiting for the dual 8 channel Sensoray and a way to work around the changing sensitivity issue.

For camera settings for either Effio or EXview OSD menus, contact dave@davesamuels.com for the settings to start with. For more information about AutoCAMS or to join the single-CAMS user support group, email seticams-subscribe@yahoogroups.com. This is only available to approved members. Hence include a message regarding who you are and what your interest is in joining.

Acknowledgements

Single-CAMS is developed and operated by amateur astronomers and volunteers, using software developed by Peter Gural with input from many CAMS participants and CAMS-lead Peter Jenniskens. The CAMS project is supported by NASA's Near Earth Object Observations Program.

References

Gural P. S. (2011). "The California All-sky Meteor Surveillance (CAMS) System". In, Asher D. J., Christou A. A., Atreya P., and Barentsen G., editors, *Proceedings of the International Meteor Conference*, Armagh, Northern Ireland, 16–19 September 2010. IMO, pages 28–31.

Jenniskens P., Gural P. S., Dynneson L., Grigsby B. J., Newman K. E., Borden M., Koop M., and Holman D. (2011). "CAMS: Cameras for Allsky Meteor Surveillance to establish minor meteor showers". *Icarus*, **216**, 40–61.

Obtaining population indices from video observations of meteors

Sirko Molau[1], **Geert Barentsen**[2], **and Stefano Crivello**[3]

[1] **Abenstalstr. 13b, 84072 Seysdorf, Germany**
sirko@molau.de

[2] **University of Hertfordshire, College Lane, Hatfield, AL10 9AB, U.K.**
geert@barentsen.be

[3] **Via Bobbio 9a/18, 16137 Genova, Italy**
stefano.crivello@libero.it

We present a novel approach for the determination of the population index from meteor showers, which is particularly useful for video camera networks with a large range of limiting magnitudes. Unlike previous approaches in the visual domain, it compares the meteor counts from cameras with different limiting magnitudes to derive the population index. Thus, it is totally independent of the meteor brightness estimate and also resistant to systematic errors in the limiting magnitude calculation or the detection efficiency close to the limiting magnitude of a camera. We derive the new approach step-by-step and present a number or refinements to improve the basic algorithm. Using the Poisson distribution gives the approach a solid probabilistic base and weights each data set according to its contribution to the population index. Finally we present and discuss first preliminary population index profiles obtained from the IMO Video Meteor Network.

1 Introduction

The population index or *r*-value describes the brightness distribution in a meteor shower, or more specifically by what factor the total number of shower meteors increases when the limiting magnitude improves by one magnitude.

As Rendtel (2013) pointed out, the population index plays a vital role in the determination of zenithal hourly rates *ZHRs*, equation (1) and flux densities *FD*, equation (2) from visual and video observations.

$$ZHR = \frac{MC * r^{6.5-LM} * F}{T_{eff} * (\cos ZD)^{\gamma}} \qquad (1)$$

$$FD = \frac{MC * r^{6.5-LM}}{T_{eff} * (\cos ZD)^{\gamma} * CA} \qquad (2)$$

Both equations (1) and (2) look fairly similar, because they are proportional to one another and express the same quantity (meteor shower activity) under different boundary conditions. The *ZHR* is normalized to the "average human field of view", whereas the flux density refers to a standardized collection area in the atmosphere. Identical ingredients are the meteor count *MC*, limiting magnitude *LM*, zenith distance of the radiant *ZD* and the zenith exponent γ. Visual observations are additionally corrected by a factor *F* that describes the obstruction of the field of view, whereas video observations are normalized by the collection area *CA* of the camera.

The impact of the population index *r* is apparent. When *LM* is 6.5, the population index term becomes unity. However, the bigger the difference between the actual limiting magnitude and the reference value of 6.5 mag, the larger becomes the impact of *r*. This is particularly true for video observations. Whereas visual observers often report limiting magnitudes around 6, the *LM* of many video cameras is in the range of magnitude 3 to 4.

To give an example: when the unexpected outburst of the September Perseids (SPE) in 2013 was analyzed first, we used a population index of *r=3.0* as there were no other data available, and obtained a remarkable peak flux density of 70 meteoroids per 1000 km^2 an hour. Later we found that the population index was exceptionally low with *r=1.4*, which reduced the peak flux to 2 (Rendtel et al., 2014).

2 Current state

Until now, all flux densities obtained from data of the IMO Video Meteor Network (Molau and Barentsen, 2014) have been derived with a fixed shower-specific population index taken from the IMO Working List of Meteor Showers. Data originating from earlier analyses of visual observations, and any variation of *r* over time were ignored.

There are two methods to derive population indexes from visual data, and both are based on the meteor brightness distribution. One compares the cumulative meteor counts for different meteor brightness classes well below the limiting magnitude (to account for the fact that the human detection probability for meteors degrades significantly close to the limiting magnitude). The other method relates the average meteor brightness to the limiting magnitude, and gives more robust estimates (Arlt, 2003). In any case, certain prerequisites have to be met for these procedures to work:

- There should be no systematic error in the brightness estimation of meteors.

- The detection probability of meteors should be known as a function of their brightness.
- There should be no systematic error in the limiting magnitude estimation.

Let us compare these prerequisites with the characteristics of video observation obtained by the IMO Video Meteor Network:

- In contrast with other video networks that employ standardized equipment, there is a large variety of cameras with a wide range of fields of view and limiting magnitudes.
- Brightness estimates of meteors obtained by MetRec are unreliable, because the measurement of faint objects in noisy video frames is challenging.
- The effective observing time, field of view and limiting magnitude of each camera are precisely known.
- The detection probability for meteors is independent of where in the field and when a meteor is observed. The only relevant factors are the meteor brightness and angular velocity.

The limited meteor brightness accuracy makes the visual standard procedures for population index calculation unsuitable. Hence why not take advantage of the (supposed) disadvantage that the cameras in the IMO network cover such a wide range of properties?

It is a well-known fact that wide-angle cameras with low limiting magnitude perform best when there are many bright meteors, whereas cameras with smaller fields of view and better limiting magnitude act best when the population index is high and there are many faint meteors. More precisely, there is a direct dependency of the meteor detection ratio between wide and narrow angle cameras and the population index.

3 A new approach for calculating population indices

As described earlier, the flux density of each camera is currently calculated for a typical *r*-value only. The basic idea of the new approach is that the flux density be calculated for each camera and for each possible population index. A population index value is then identified for which the individual flux densities of all cameras agree best with one another. Through this approach we directly get both the optimal population index and flux density.

Since the calculation of the flux density is time-consuming, it would be welcome if the dependency from the population index would be mathematically simple, e.g. linear. Unfortunately that is not the case. Equation (3) is a refinement of equation (2) to cover specific aspects of flux density calculation of meteor showers:

$$FD = \frac{MC}{T_{eff} * (\cos ZD)^{\gamma} * \sum_{pix} \frac{CA}{r^{6.5-MLM}}} \qquad (3)$$

Most notably, the (stellar) limiting magnitude *LM* is replaced here by the meteor limiting magnitude *MLM*. Equation (3) contains terms which are fixed over the field of view (meteor count, effective observing time, radiant zenith distance and zenith exponent) and terms which vary from pixel to pixel. In particular, these are the collection area and the meteor limiting magnitude. The angular velocity of a meteor depends on the radiant distance and altitude. At a pixel which is farther away from the radiant and higher in the sky, the meteor is apparently moving faster, the photons are spread over more pixels and thus the meteor limiting magnitude will become fainter. For this reason, the collection area and limiting magnitude correction are summed over all pixels leading to a complex dependency of *FD* on *r*. In order to reduce the computational overhead we shall find a suitable approximation for this dependency (*Figure 1*).

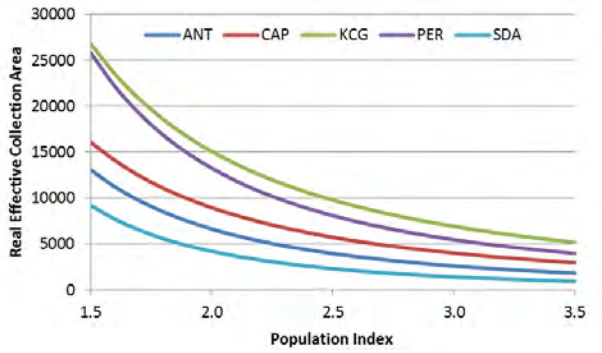

Figure 1 – Dependency of the flux density (which is inversely proportional to the effective collection area) on the population index, calculated for a particular non-intensified video camera in mid-August 2013.

A first approximation is to replace the variable meteor limiting magnitude *MLM* by the average value *AVGMLM*, equation (4), over all pixels. Thus we can pull the term with the population index out of the pixel sum.

$$FD \approx \frac{MC * r^{6.5-AVGMLM}}{T_{eff} * (\cos ZD)^{\gamma} * \sum_{pix} CA} \qquad (4)$$

However, tests with real observational data from August 2013 have shown that this will introduce significant approximation errors of up to 50% relative when a large range of population indexes is covered (*Figure 2*).

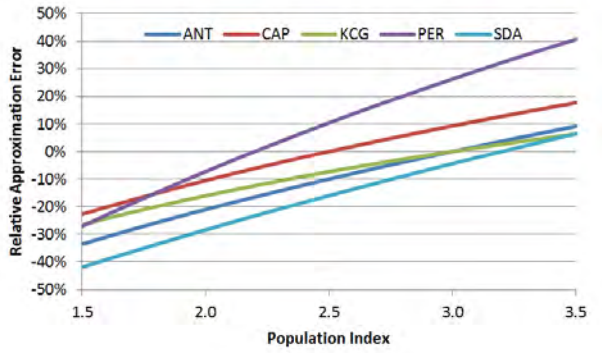

Figure 2 – Approximation error when the limiting meteor magnitude per pixel *MLM* is replaced by the average limiting magnitude *AVGMLM*. If the population index deviates significantly from the shower-specific start value, the relative error may become as big as 50% (same data set as *Figure 1*).

Another, more promising, approach to calculate the flux density for small set of selected *r*-values (e.g. between 1.5 and 3.5 in steps of 0.1) and then fit a parametric function that approximates the dependency of *FD* on *r*. Since in the flux density equations the population index *r* is always taken to the power of some magnitude value it is no surprise that a power function of type $a * r^b$ yields a good approximation. In fact, this approach is a refined version of the first approximation whereby the power exponent is not calculated as the mean meteor limiting magnitude over the full field of view, but estimated from data. Even when a wide range of *r*-values is selected, the relative error is always below 3% (*Figure 3*). When the parameters *a* and *b* of the power function are not calculated once for the full night, but individually for every observing minute, the approximation error is halved once more (*Figure 4*).

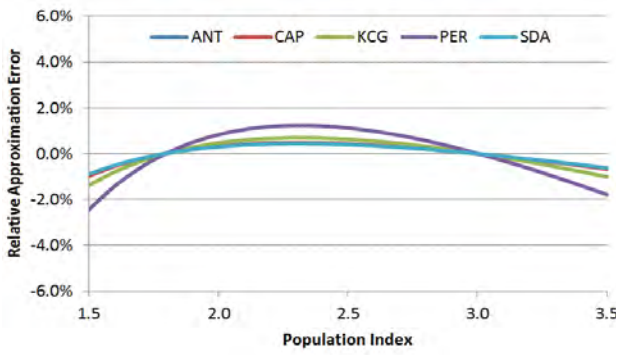

Figure 3 – Approximation error, when a power function of type $a * r^b$ is fitted to the dependency of the flux density on the population index over the full night. The relative error is always lower than 3% (same data set as *Figure 2*).

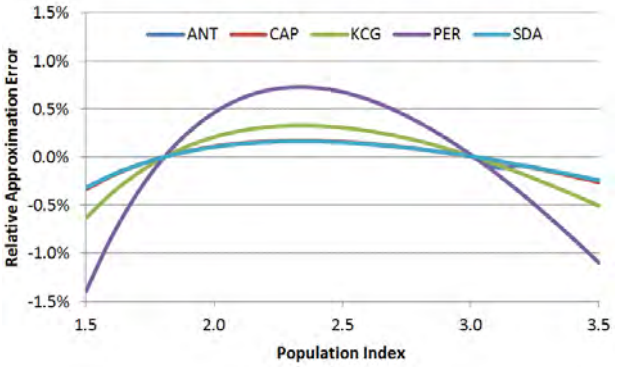

Figure 4 – Same data set as *Figure 3*, but the power function is fitted every minute. The approximation error has once more decreased by a factor of 2 and is now well within the error margins of other assumptions and approximations in the population index calculation.

In summary, we approximate the complex non-linear dependency of *FD* on *r* by a power function of type $a * r^b$ whose parameters are calculated and stored for every observing minute.

Initially we calculate the flux density with some predefined population index r_{start}. When we want to obtain the flux density for another population index, r_{new}, we only have to multiply it with the correction factor $CF = r_{start}^{\ b} / r_{new}^{\ b}$.

Hence the scaling factor *a* is canceled out, and we only have to calculate and store the exponent *b* for every minute. This leads us to the following procedure for the calculation of the population index:

- For each camera and each observing minute, calculate the flux density and the power function exponent *b*, and accumulate the flux density over the full night.
- Try iteratively different *r*-values, correct the flux density for every camera and minute, and accumulate the flux density camera-wise for the full night.
- Select the population index where the flux densities of all cameras agree best.

For testing of the new procedure, we used the video data set from the unexpected September Perseids (SPE) outburst on September 9, 2013. There are no visual observations for this event, but 21 video cameras of the IMO Video Meteor Network contributed observations for that night. It was clear that the outburst must have had a rather unusual population index, because operators of low sensitivity wide-angle cameras reported an unusual number of (bright) meteors that night, whereas more powerful intensified cameras experienced no significant increase in counts.

Figure 5 shows the result of the new procedure. Note the logarithmic presentation of the vertical axis. The closer two lines are, the smaller is the relative deviation in flux density between them.

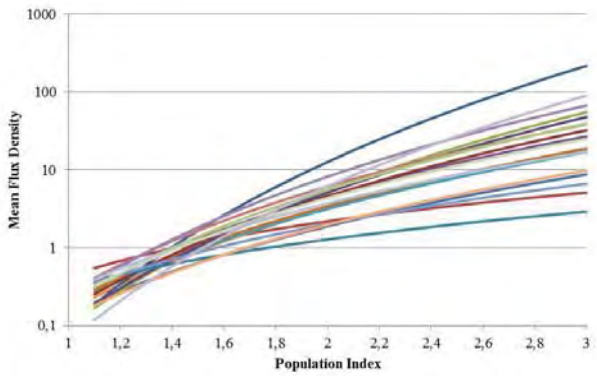

Figure 5 – Dependency of the flux density from the population index, calculated for 21 video cameras that recorded the outburst of the September Perseids on September 9, 2013. The graphs look most compact at a population index below 1.5, but the optimal value is difficult to determine.

It is clear that the procedure is working in principle and that the best population index must be somewhere close to 1.4, but it is hard to determine it more precisely. Cameras with limiting magnitude close to 6.5 create almost horizontal lines, and the lower the limiting magnitude of a camera, the larger is the slope. However, many cameras have similar limiting magnitudes, so their graphs are nearly parallel and will not create a well-defined point of intersection. Furthermore, even cameras with good limiting magnitude may temporarily experience clouded skies or haze, and this will reduce their average *lm*.

In the next chapter we will describe a refinement to the basic approach to overcome these limitations.

4 Refinement to the basic approach

In the first approach, the data set was segmented camera-wise, because each camera has different properties. We learned, however, that the main criterion for the calculation of the population index is the meteor limiting magnitude of the camera, and that is not constant over time. It will vary in the course of a night due to twilight, moon, clouds and variable radiant distance. So a better approach is to bin the data according to this parameter. At the beginning, the limiting magnitude bins are defined, and then it is decided for each observing minute of each camera, to which bin that particular data set contributes. Figure 6 shows the result for the same SPE data set with bins of one magnitude. The result is two-fold: The number of graphs is getting smaller and the intersection angle between the graphs is increasing, which yields a more accurate intersection point.

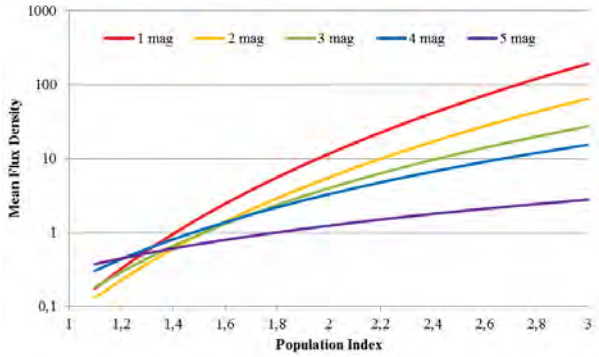

Figure 6 – Same data set as *Figure 5*, but now the data is not binned by camera but by the meteor limiting magnitude of each camera and observing minute.

However, the individual graphs still do not intersect exactly at one point. For this reason we now need to discuss procedures that will derive the best population index under such conditions. A simple approach is to find the point where all graphs are closest to each other in a logarithmic diagram. We can visualize this by blurring the graphs and selecting the point of overall maximum intensity (*Figure 7*).

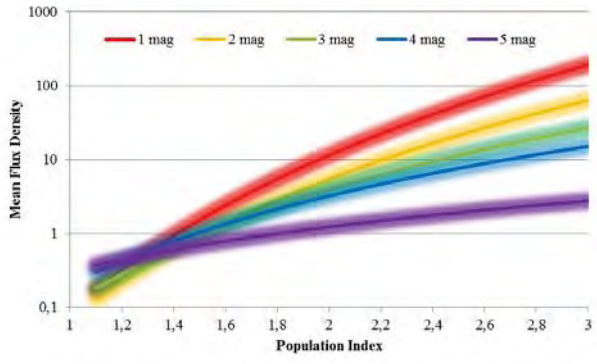

Figure 7 – Schematic plot, how the best intersection point can be determined by blurring the individual graphs and selecting the population index where the accumulated intensity is highest. Note that all graphs have the same weight in this approach.

The drawback for this procedure is that it gives all graphs the same weight, no matter how much data they contain and how discriminant they are for the population index calculation. This can be avoided via a data-driven definition of the limiting magnitude bins. Instead of giving each bin the same size of one mag, the bins are defined such that they contain a defined fraction of the overall data set (for the case depicted in *Figure 8*, we selected four bins with 15/35/35/15% of the collection area). In addition, only those intervals are selected, in which the stellar limiting magnitude was better than magnitude 1.5, as otherwise there would be too few stars for a reliable limiting magnitude estimate. Data-driven binning ensures that all graphs contain a sufficient number of meteors, and in our SPE example, the intersection point becomes significantly more accurate (*Figure 8*).

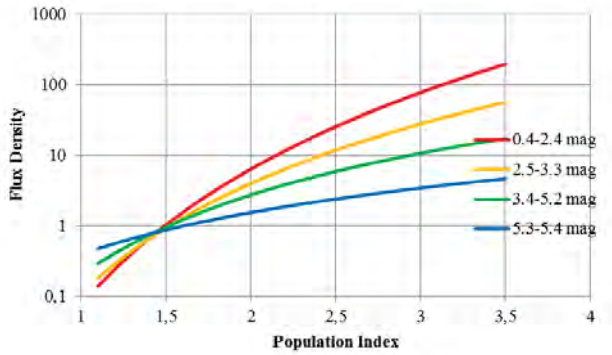

Figure 8 – Same plot as *Figure 7*, but the bins in meteor limiting magnitude are now defined in a data-driven way to ensure that each graph contains a sufficient amount of data.

The problem of the discrimination of the individual *lm* classes is addressed by applying a Poisson distribution.

Short reminder: Given random, independent events with a constant average rate λ per time unit, the (discrete) Poisson distribution $P_\lambda(k)$ provides the probability, that in a particular time unit exactly k events occur.

A practical example: Let's assume that sporadic meteors occur at an average rate λ equal to 5 per hour. The Poisson distribution will tell us the chance that in any particular hour, we observe 0, 1, 2, 3 … sporadic meteors (*Figure 9*). Obviously, the probability to observe 4 or 5 meteors is highest, but the chance that 10 meteors are observed is also not negligible.

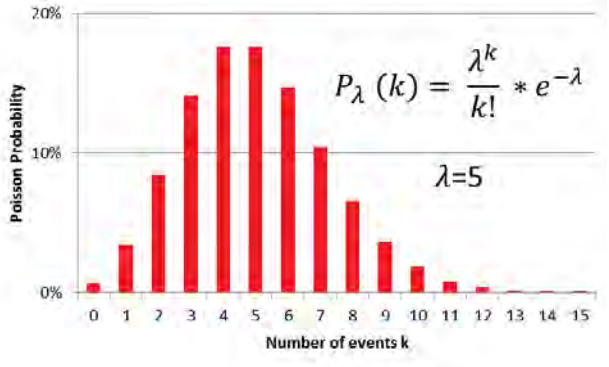

Figure 9 – Example for a Poisson distribution. The bars give the probability that 0 to 15 event are observed per time unit (e.g.

sporadic meteors per hour), when the average rate λ is 5 events per time unit.

Now how is the Poisson distribution applied to our population index calculation? Starting from the overall collection area over all limiting magnitude bins, we can calculate which fraction belongs to which limiting magnitude class. This fraction depends on the population index: For low *r*-values, the contribution of wide-angle cameras with low limiting magnitude will be higher (they are more efficient when many bright meteors are present), whereas for large *r*-values the cameras with smaller field of view and better *lm* become more effective. The meteor count is directly proportional to the collection area, so given the overall number of meteors recorded in a certain time interval we can calculate, how many meteors are expected in which limiting magnitude class (solid lines in *Figure 10*). Note that this figure will vary largely for cameras at the upper and lower end of the limiting magnitude spectrum, but the expected meteor count varies little for the intermediate cameras. They contribute only little information to the population index calculation.

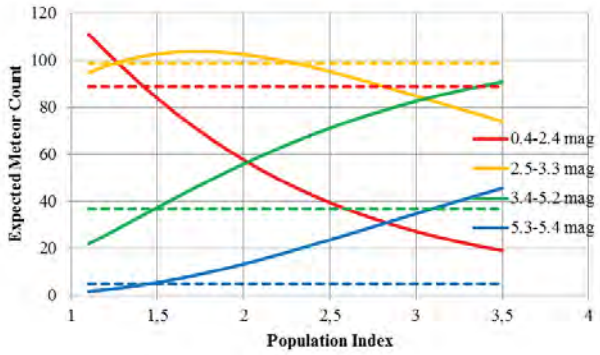

Figure 10 – The same data set as in Figure 8 in a different representation. Solid lines mark the number of expected meteors per limiting magnitude class, dashed horizontal lines the actually observed number of meteors.

Also shown in *Figure 10* is the actually observed number of meteors in each limiting magnitude class (horizontal lines). The best population index is the one where the observation and the expectation values are identical, but again there is not a single *r*-value were all pairs of graphs intersect.

This is where the Poisson distribution is applied: for each graph and each population index, it tells us the probability for the observed number of meteors *k*, given the expected number of meteors λ. In *Figure 11*, we print those Poisson probabilities for the four limiting magnitude classes, and the combined probability. They are represented as log probabilities and normalized by their maximum value, i.e. that the log peak probability of each graph is zero. The maximum of the combined probability graph yields the best population index.

Applying the Poisson distribution has two advantages:

- The number of meteors belonging to each *lm* class is taken into consideration, because the Poisson distribution is different for small and large values of λ and *k*.
- Graphs which are not discriminative for the determination of *r* contribute only marginally to the optimization (the Poisson distribution has a wide peak for these).

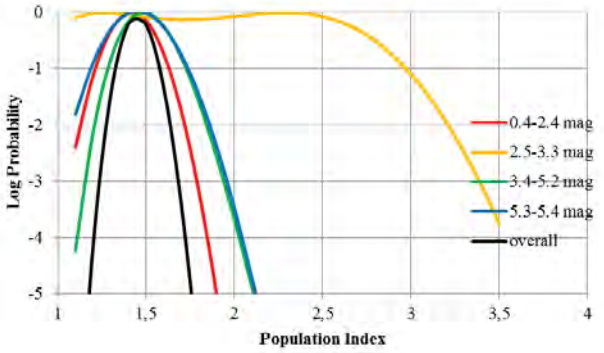

Figure 11 – Poisson (log) probabilities for the individual limiting magnitude classes in the previous figure normalized such that the maximum is always zero. Note that the second *lm* class provides little information about the population index, because the expected meteor count is only slightly dependent on the population index. Hence this graph contributes little to the overall probability.

Looking on a wider scale, the whole new procedure to calculate population indexes has some unique characteristics:

- It is independent of the meteor brightness, which is hard to determine reliably from video observations of meteors.
- It is resistant to possible systematic errors in the stellar limiting magnitude calculation. Since all limiting magnitude classes are affected in the same way, such an error will shift all graphs in *Figure 8* vertically by the same amount, but not horizontally. That is, only the flux density will be affected, but not the *r*-value.
- For the same reason, the procedure is also immune to systematic errors on the meteor detection probability depending on the limiting magnitude. Again, all limiting magnitude bins are affected in the same manner which impacts the flux density, but not the population index.
- Some experiments have shown that the zenith exponent only has a small impact on the calculation of the population index.

In practice, the combined Poisson probability over all limiting magnitude classes is calculated for selected *r*-values, and then a quadratic function $ux^2 + vx + w$ is fitted to the peak *population index* bin and the two neighbors. This five-point-fit closely matches the combined probability distribution. By simple differentiation of the quadratic function, we get a closed form solution for the best population index $r = v/2u$. Furthermore, the absolute value and the width of the combined probability graph give an indication for the error bars of the population index estimate.

5 Preliminary Results

During the development of the new approach in 2013/2014, it was tested on different meteor showers. *Figure 12* gives an overview of *r*-values obtained for the September Perseids and Orionids in 2013, and also for the Quadrantids and Lyrids in 2014. A wide range of population indexes between 1.4 and 2.3 is obtained for the peak times of these meteor showers, and in most cases the intersection point is well-defined. However, that is not always the case for other dates and meteor showers.

For obvious reasons, the ultimate goal is not to obtain single *r*-values just for meteor shower peaks, but also to obtain whole population index profiles over the full activity period of a meteor shower. For this purpose, two programs are currently being developed and will implement the new approach. One is a fat-client application by S. Crivello running on Win XP, and the other an extension of the flux viewer web service by G. Barentsen (Barentsen and Molau, 2013)[1]. Both are still under reconstruction, so we can only present some preliminary graphs here for several major meteor showers between 2011 and 2013 (*Figure 13*). Even though the approach is new, we can still use all IMO Network observations where flux and limiting magnitude data are available (i.e. starting from spring 2011), since the new power function exponent *b* can be calculated afterwards from these data. The recalculation was computationally demanding (1 CPU month), but has now completed. Following an initial phase in which optimal settings for the approach are determined (outlier rejection criteria for cameras with poor *lm* calculation, number of limiting magnitude classes and their share from the overall collection area, etc.) we expect more accurate population index profiles in the near future.

6 Discussion

The first results are promising and yield population indexes similar to those obtained from visual observations. However, our *r*-values are still typically somewhat smaller than the visual results. A detailed comparison between visual and video data revealed the following differences:

- In case of video observations, we use the absolute meteor magnitude *M* (i.e. normalized to 100 km altitude), whereas in visual observations the apparent magnitude *m* is used.
- The observing direction (altitude, radiant distance) is properly accounted for only in case of video observations.
- The effect of meteor motion on the limiting magnitude (fast meteors distribute their photons over more pixels) is only accounted for in case of video observations.

These differences may be the root cause for the observed differences.

[1] http://www.imonet.org/imc13/meteoroids2013_poster.pdf

7 Summary

Having presented why the population index is particularly important for flux density measurements from video meteor observations, we have shown that the traditional procedures for population index calculation do not fit well. For this reason, we derived and refined step by step a new approach that is specifically helpful when a large variety of video cameras with different limiting magnitudes is available. We have shown that the new approach provides certain desirable properties, and first population index profiles obtained from the IMO Network video observations look promising.

Acknowledgements

We are in great debt to all observers of the IMO Video Meteor Network, who collected over years a unique database of video meteors. The Video Meteor Database of IMO is a treasure that allows a wide range of new analysis techniques and results, for which the one presented here is a practical example.

References

Arlt R. (2003). "Bulletin 19 of the International Leonid Watch: Population index study of the 2002 Leonid meteors". *WGN, Journal of the IMO*, **31**, 77–88.

Barentsen G. and Molau S. (2013). "Meteoroid stream flux profiles derived from the IMO Video Meteor Network". Poster at Meteoroids 2013 Conference, A. M. University, Poznań, Poland, 26–30 August 2013. Not published.

Molau S., Barentsen G. (2014). "Status and history of the IMO Video Meteor Network". In Jopek T. J., Rietmeijer F. J. M., Watanabe J., and Williams I. P., editors, *Meteoroids 2013, Proceedings of the Astronomical Conference*, held at A. M. University, Poznań, Poland, 26–30 August 2013. A.M. University Press, 297–305.

Rendtel J. (2013). "From Rates to Fluxes of Meteoroid Streams". In Gyssens M., Roggemans P., and Żołądek P., editors, *Proceedings of the International Meteor Conference*, Poznań, Poland, 22–25 August 2013. IMO, 121–125.

Rendtel J., Lyytinen E., Molau S., Barentsen G. (2014). "Peculiar activity of the September epsilon-Perseids on 2013 September 9". *WGN, Journal of the IMO*, **42**, 40–47.

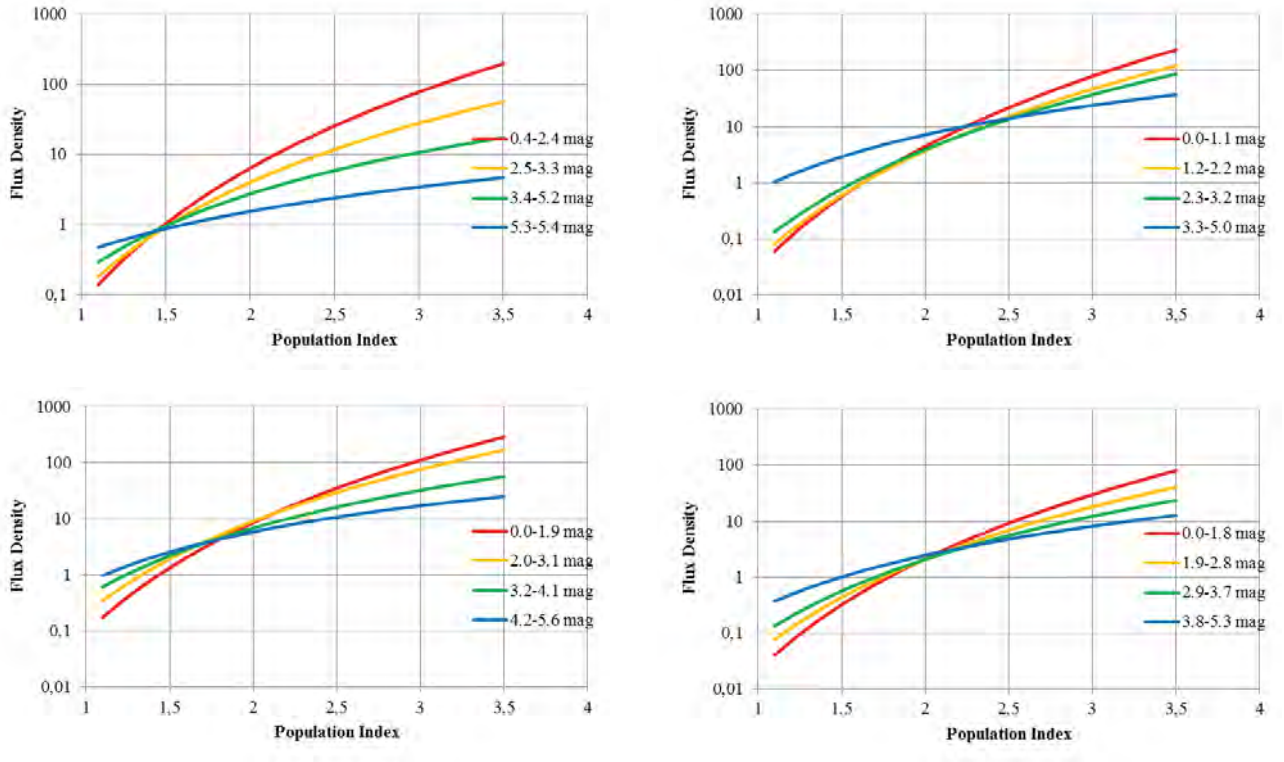

Figure 12 – Population indexes obtained for individual meteor showers near their peak times: *September Perseids* on Sep 9/10, 2013, (top left); *Orionids* on Oct 23/24, 2013, (top right); *Quadrantids* on Jan 3/4,2014, (bottom left); *Lyrids* on Apr 22/23, 2014, (bottom right).

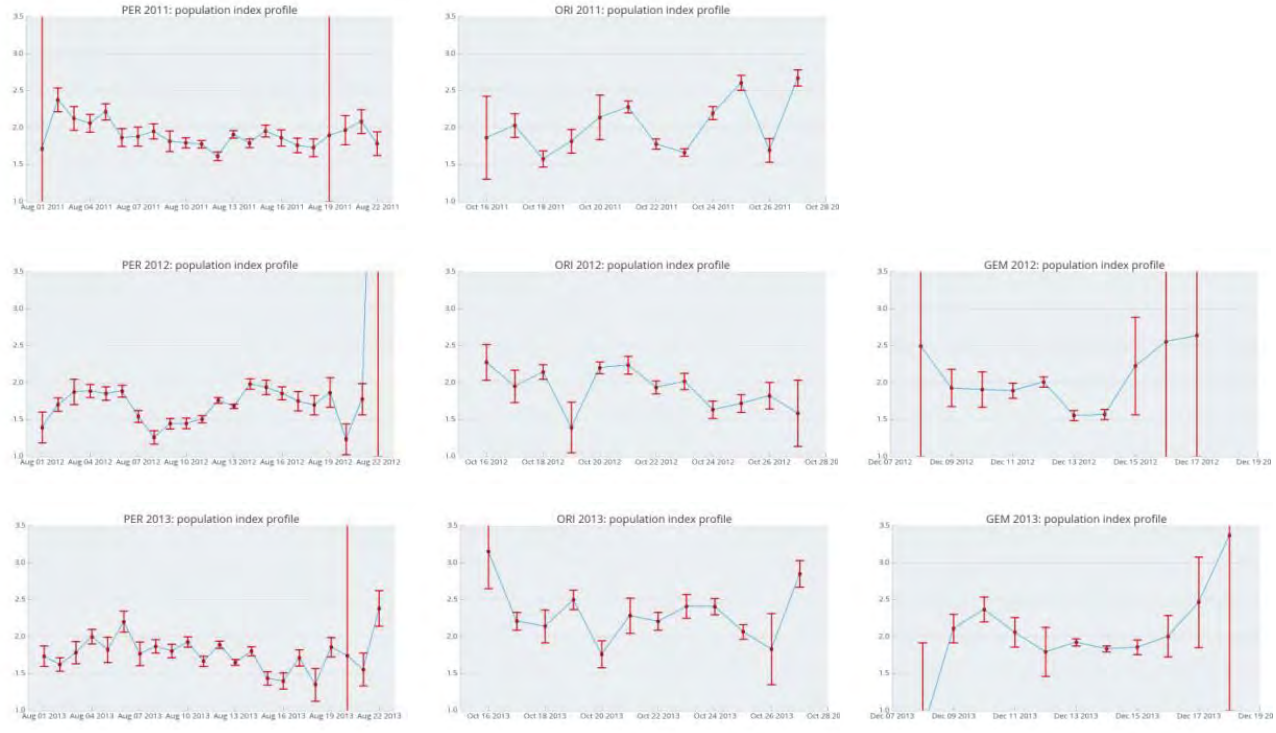

Figure 13 – First preliminary population index profiles for the *Perseids* (left), *Orionids* (center) and *Geminids* (right) in 2011 (top), 2012 (center) and 2013 (bottom).

A possible new shower on Eridanus-Orion border

Damir Šegon[1,2], Peter Gural[3], Željko Andreić[4], Denis Vida[5,6], Ivica Skokić[5], Filip Novoselnik[5,6] and Luciano Gržinić[1]

[1] **Astronomical Society Istra Pula, Park Monte Zaro 2, 52100 Pula, Croatia**
damir.segon@pu.htnet.hr, lgrzinic@inet.hr

[2] **Višnjan Science and Education Center, Istarska 5, 51463 Višnjan, Croatia**
damir.segon@pu.htnet.hr, lgrzinic@inet.hr

[3] **351 Samantha Drive, Sterling, VA 20164-5539, USA**
peter.s.gural@saic.com

[4] **University of Zagreb, Faculty of Mining, Geology and Petroleum Engineering, Pierottijeva 6, 10000 Zagreb, Croatia**
zandreic@rgn.hr

[5] **Astronomical Society "Anonymus", B. Radića 34, 31550 Valpovo, Croatia**
denis.vida@gmail.com, ivica.skokic@gmail.com, filip.novoselnik@gmail.com

[6] **Faculty of Electrical Engineering, University of Osijek, Kneza Trpimira 2B, 31000 Osijek, Croatia**
denis.vida@gmail.com, filip.novoselnik@gmail.com

Three showers on the border between constellations of Eridanus and Orion were found during extensive search for new showers in SonotaCo and CMN video meteor orbit databases. Our results suggest that two of these three showers represent υ Eridanids shower (337 NUE), while third one represents separate possible new shower which has been named π^6 Orionids (552 PSO).

1 Introduction

During the spring of 2013. members of the Croatian Meteor Network did an extensive, automatic D-criterion based search through the SonotaCo and CMN video meteor orbit databases covering years 2009–2011. Briefly, all single meteoroid orbits were compared to all other meteoroid orbits from the database containing more than 133 k of orbits. In cases when there were more than 10 meteoroid orbits satisfying all three D-criteria used, their arithmetic mean orbital parameters were used to start an iterative search through the database, in order to establish if there is a stable, unchanged set of meteoroid orbits. This search yields a high percentage of known showers, but also a quite large number of possible new meteor showers as well. A very interesting case of three, at glance very similar meteor radiant groups was found at the border of the constellations of Eridanus and Orion.

Two of these three showers represent the υ Eridanids shower (337 NUE). This shower has been discovered by SonotaCo. SonotaCo used the clustering method, which proved the existence of a meteor shower with 29 members. Since SonotaCo hasn't published data on orbital parameters for the υ Eridanids, we used the mean solar longitude and α, δ, of the radiant to compare it with our newly found showers. It turned out that two of these three showers represent the υ Eridanids shower (337 NUE), and that the third one is a possible new shower, which was reported to the IAU MDC and got the name π^6 Orionids (552 PSO).

The 552 PSO shower is found to be active from the 29th of August to the 18th of September, having maximal activity on the 10th of September. A search for a possible parent body has been attempted, but none of known NEOs has been found to match either 337 NUE or 552 PSO.

The paper with details on this possible new shower has been submitted to WGN, according to the rules on new showers discoveries (Šegon et al., 2014).

Acknowledgment

Our acknowledgments go to all members of the Croatian Meteor Network. This work was partially supported by the Faculty of Mining, Geology and Petroleum Engineering, University of Zagreb, Višnjan Science and Education Center and by private funds of CMN members.

References

Šegon D., Gural P., Andreić Ž., Vida D., Skokić I., Novoselnik F., Grzinic L. (2014). "A Possible New Shower on Eridanus-Orion Border". *WGN, Journal of the IMO*, **42**, submitted.

Camelopardalids expedition

Mariusz Wiśniewski[1,2], Przemysław Żołądek[1] and Zbigniew Tymiński[1,3]

[1] **Comets and Meteors Workshop, Bartycka 18, 00-716 Warsaw, Poland**
marand.w@gmail.com, brahi@op.pl, zbyszek.tyminski@gmail.com

[2] **Central Office of Measures, Elektoralna 2, 00-139 Warsaw, Poland**

[3] **National Centre for Nuclear Research, RC POLATOM, Sołtana 7, 05-400 Otwock, Poland**

This paper describes preliminary results of the Polish Fireball Network expedition to observe the outburst of the particles stream of comet 209P/LINEAR. According to the theoretical calculations the predicted shower radiated from Camelopardalis constellation and reached its maximum on May 24th 2014. The selection of observation sites and equipment is presented. Eleven analog cameras, digital cameras and DSLR cameras were used in the double station observing system. As a result 174 meteors were recorded, 32 of them were Camelopardalids. Using data from the maximum night the 15 orbits of meteors were calculated – 5 orbits have orbital parameters similar to the expected values for Camelopardalids.

1 Introduction

209P/LINEAR was discovered on February 3rd 2004 by *Lincoln Near-Earth Asteroid Research* (LINEAR). The comet orbit gets close to the Earth's orbit and further analysis showed possibilities for an increased meteor activity from this comet on May 24th 2014. A number of authors presented models according to which the maximum number of meteors could be seen between 6^h00^m and 8^h00^m UT (Table 6j of Jenniskens 2006; Vaubaillon 2012[1]; Jenniskens and Lyytinen 2014; Ye and Wiegert 2014). The radiant of these meteors is located in the constellation of Camelopardalis.

Figure 1 – Logo of Camelopardalids expedition by P. Zaręba.

Because of the possibility to observe meteors from this comet, confirmed by many independent analyzes, we decided to prepare an expedition with three persons (authors of this paper) to observe the Camelopardalids. The logo of the expedition is presented in *Figure 1*.

2 Expedition

The choice of the observation place

The time of the expected maximum activity was unfavorable for European observers. At about 7^h00^m UT on May 24th the Sun is above the horizon and prevents the registration of meteors by the Polish Fireball Network cameras. Analyzing all options for the best place to watch the outburst we took into account:

- the height of the Sun below the horizon at the moment of the maximum;
- the height of radiant at the moment of the maximum;
- moment of Moon rise;
- the length of the night.

These criteria limited the area of potential observations to the vicinity of the border between Canada and the United States. Further factors which were taken into account were:

- the darkness of the sky;
- weather statistics;
- the possibility of tornadoes;
- the probability of the aurora borealis occurrence;
- the cost of transport and accommodation;
- the ability to work with local observers of meteors;
- the necessity to have a visa (USA);
- the easiness to carry the large amounts of equipment across the border.

None of the members of the expedition had a US visa. In order to avoid additional costs and complications we chose for an expedition to Canada.

[1] http://www.imcce.fr/langues/en/ephemerides/phenomenes/meteor/DATABASE/209_LINEAR/2014/index.php

We were able to find a direct cheap flight connection from Poland to Toronto. Thanks to the information obtained from Prof. P. Brown we have selected the area of Tobermory, Bruce Peninsula as the likely darkest place, away from areas of frequent tornadoes. It is also in close proximity to an active fireball network conducted by the University of Western Ontario.

In the neighborhood of Tobermory we were able to rent a house that perfectly suited our purposes (*Figure 2*). The house had two balconies facing south-east, one of them was a spacious terrace with a wide field of view. This place had become our base and the first observing point (A).

Figure 2 – Willow Bank house near Tobermory, base of expedition and location of the first station (A). On the picture: Glenn Aishford (owner of the house), Zbigniew Tymiński, Przemysław Żołądek and Mariusz Wiśniewski, members of the Camelopardalids expedition.

With the help of Prof. P. Brown and Z. Krzeminski we contacted The Fox Observatory. This place was used as a second observation point (B).

Figure 3 – Analog cameras used during the expedition.

Cameras and field of view selection

As a result of the preparation we had selected 12 cameras which we selected for the expedition. Observations were carried out at two stations in order to determine the trajectory and orbit of recorded phenomena. Analog CCTV cameras used during the expedition are displayed in *Figure 3*.

The most sensitive analog cameras were used to create two pairs with similar field of view. The first pair was based on a 6mm lens and the other on a 8 and 9mm lens (see *Figure 4*). These were the very fast lenses.

Watec cameras with wide angle 3.8mm lens worked in pair with a digital camera ZWO ASI 120MM lens 1.8mm.

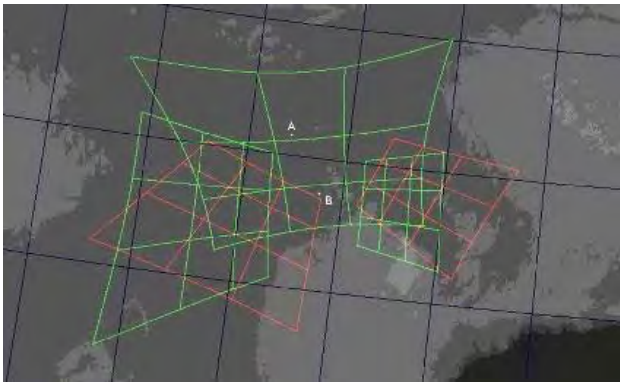

Figure 4 – Field of view of analog cameras used for doublestation observations.

One DSLR has been used for wide-angle observations of the brightest meteors. One analog camera has not been used. The signal from three analog cameras was recorded entirely on DVRs for further analysis. The image of the other three cameras was analyzed in real time.

3 Results

A summary of the number of registered events has been presented in *Table 1*. The number of Camelopardalids remained significantly below the expectations, but no doubt, they were distinguished among other meteors. It has turned out that the most effective instrument were a pair of cameras with 6mm lenses. The ZWO 120MM camera with the Fujinon 1.8mm was most effective in capturing Camelopardalids (see *Figure 5*). Cameras with a smaller field of view were significantly less effective. No meteor spectra have been recorded.

Using the data from the maximum night, 15 meteor orbits were calculated. 5 orbits have orbital parameters similar to the expected values for Camelopardalids.

For spectroscopic observations the PointGrey BlackFly 09 M digital camera, two Canon digital SLR cameras, and one Tayama C3102-01A1 analog camera were used.

4 Conclusion

The maximum of Camelopardalids proved the accuracy of the modeling of meteoroid streams. The Earth crossed the stream of meteoroids at the time it was expected. The number of meteors from this stream was much smaller than expected which greatly reduced the number of registered and calculated meteor trajectories.

The expedition was a very important experience. With well-prepared equipment, all components worked as

Table 1 – Summary of the results.

Camera	Lens	Loc.	Meteors	CAM
MINTRON 12V6	Panasonic 0.75/6mm	A	44	7
MINTRON 12V6	Computar 0.8/6mm	B	36	5
MINTRON 12V6	Tokina 1.3/8mm	B	12	4
WATEC Ultimate	Panasonic 0.75/9mm	A	17	2
WATEC Ultimate	Computar 0.8/3.8mm	B	16	2
ZWO ASI120MM	Fujinon 1.4/1.8mm	A	29	12
PointGrey BlackFly 09 M	Tamron 1.0/3-8mm (Spectra)	A	20	3
Tayama C3102-01A1	Ernitec 1.2/8mm (Spectra)	A	0	0
Canon 550D	Canon 3.5/10-20mm	B	1	0
Canon 1000D	Porst 1.8/35mm (Spectra)	A	0	0
Canon 1000D	Danubia 2.8/35mm (Spectra)	A	0	0
TOTAL			174	32
Orbits			15	5

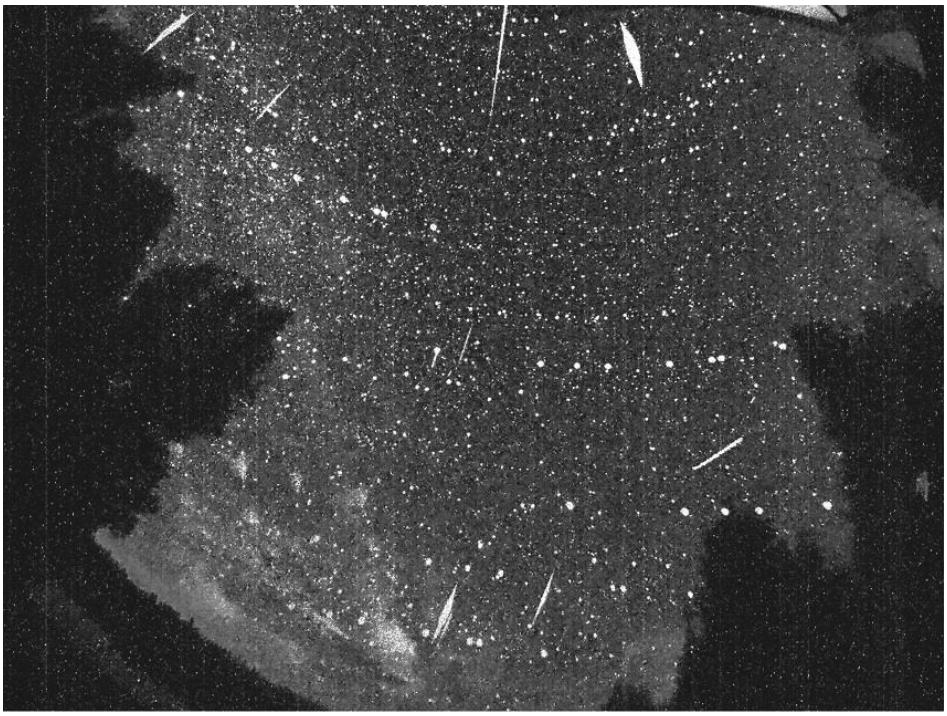

Figure 5 – Camelopardalids captured by the ZWO ASI 120MM camera with a Fujinon 1.4/1.8mm lens.

expected. Luckily the weather was perfect for observing at both locations.

The collected data will be used for more detailed analysis.

Acknowledgment

This work was supported by the National Science Center (decision no. DEC-2013/09/B/ST9/02168).

We would like to thank Roman Piffl for providing us the ZWO ASI 120MM camera and Fujinon 1.4/1.8mm, and Maciej Maciejewski for providing us a number of Mintron cameras and fast lenses. We would like to thank Prof. Peter Brown and Zbyszek Krzeminski for helping to find a suitable place for observations, and many valuable advices. We would like to thank John Hlynialuk for inviting us to the Fox Observatory for our observations. We would like to thank Glenn Aishford for his hospitality in Willow Bank. We would like to thank Paweł Zaręba for the design of the expedition logo.

References

Jenniskens P. (2006). Meteor Showers and their Parent Comets. Cambridge Univ. Press, Cambridge.

Jenniskens P, Lyytinen E. (2014). “Possible new meteor shower from comet 209P/LINEAR”. *Central Bureau Electronic Telegrams*, 3869.

Ye Q, Wiegert P. A. (2014). “Will comet 209P/LINEAR generate the next meteor storm?”. *Monthly Notices of the Royal Astronomical Society*, **437**, 3283–3287.

Camelopardalids 2014, the radio view

Bill Ward

School of Engineering, University of Glasgow, Glasgow, G12 8LT, United Kingdom
william.ward@glasgow.ac.uk

Observations of the predicted encounter with dust tails from comet 209P/LINEAR on 24th May 2014 were made using radio forward scatter.

1 Introduction

Several predictions had been made as to the possibility of the Earth encountering dust trails left by Comet 209P/LINEAR[1,2].

This had also led to claims of a possible "meteor storm". As the timing of the trail crossings were to occur in daylight at the author's location (~56 degrees north) it was decided to monitor the activity using radio forward scatter.

2 Equipment

The radio technique used is well established and described (Rendtel and Arlt, 2009). A 4 element Yagi antenna was mounted at approximately 10m above ground and orientated to an azimuth of 140 degrees. The antenna was connected to a Yaesu FT817 amateur radio receiver. The receiver was tuned to the GRAVES Radar frequency of 143.050 MHz.

3 Operation

The audio output was fed to a PC with soundcard running SPECTRAN audio processing software[3].

The software was configured to take an image of the output screen every 30 seconds in order to build up a time lapse video of any activity. See *Figure 1* taken from the video shown at IMC 2014, Giron, France.

Since there was some doubt as to whether anything may happen at all or if the timings might have been in error, the system was set to run for 10 hours, approximately five hours or so either side of the predicted times.

4 Results

Once the observation period had completed the individual frames were inspected. The number of meteor "pings" detected was counted. The selection was arbitrary based on the noise level indicated by the software. This allowed the level under the cursor to be measured in a relative manner. To try and obtain a reasonable timing precision a bin size of 10 minutes (20 frames) was chosen, again arbitrary based on convenience of counting. This strategy resulted in 60 bins covering 0200UT to 1200UT. The result of the binning is shown in *Figure 2*.

It can be seen that although activity was increasing through the morning hours as normally occurs, the two highest counts were at the predicted times of the trail crossings. It should be noted that there is a slight difference in the corrected time as listed on the website of David Asher[2]. This may be an expression of the particular binning method used here. Another reason for the slight timing discrepancy may be the fact that the meteors being observed were approximately 1000 km+ distant. This would require an additional topocentric correction as the meteors were not directly "over" the observing location at the predicted times.

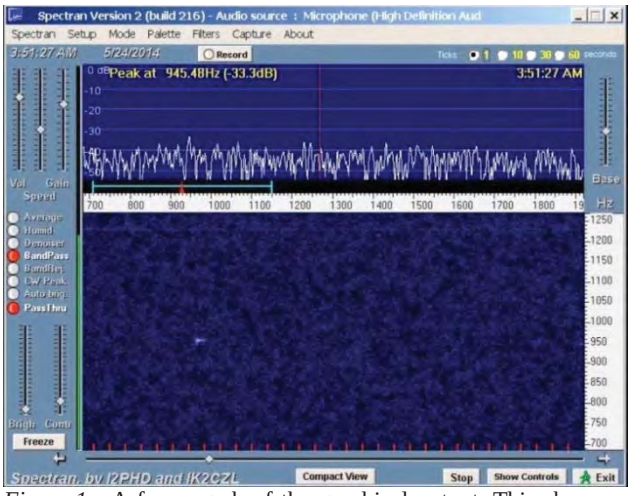

Figure 1 – A frame grab of the graphical output. This shows a strong "ping" in the lower panel.

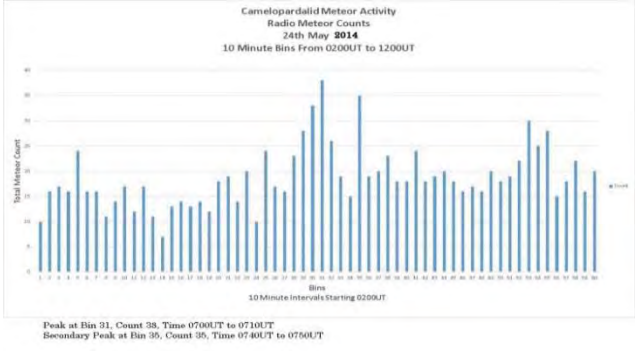

Figure 2 – Graph of count bins.

[1] http://www.imcce.fr/langues/en/ephemerides/phenomenes/meteor/DATABASE/209_LINEAR/2014/
[2] http://star.arm.ac.uk/~dja/209P/
[3] http://www.webring.org/l/rd?ring=homeaudio;id=1;url=http%3A%2F%2Fwww.qsl.net%2Fi2phd%2Fspectran%2Findex.html

5 Conclusion

It can be concluded that the two predicted trail crossings did occur. They were, however, only slightly higher than the normal background activity and not a "storm".

References

Rendtel J. and Arlt R., editors (2009). *Handbook for Meteor Observers*. Third edition. IMO.

During the excursion at CERN, from left to right: Ilija Ivanović, Hillestad Eli Fugelso, Okolic Dragana, Megan Argo, someone hidden,Veljković Kristina, Paul Roggemans, Hillestad Trond Erik, Meister Stefan, Schenker Jonas, Detlef Koschny, Gerhard Drolshagen and Bill Ward. (Credit Axel Haas).

Future plans of the Polish Fireball Network

Przemysław Żołądek

Pracownia Komet i Meteorów, 00-718 Warszawa, ul. Bartycka 18, Poland
brahi@op.pl

The current status and the future plans of the Polish Fireball Network have been presented. A new funding became available and new equipment will be purchased next year. We are testing three megapixel cameras which are sufficiently sensitive for meteor research. We plan to create more than 10 fireball stations equipped with digital megapixel cameras with high quality lenses.

1 Introduction

The Polish Fireball Network has been founded in 2004. The network has been created by polish amateur and professional astronomers, members of the Comet and Meteors Workshop. First video observations were done in 2002 as a test of the new CCTV video equipment. First regular video observations started during the night of 15–16 November 2002 as a part of the Leonid campaign. The activity outburst of the Leonids has been observed by 4 CCTV Tayama cameras with 8mm lenses, the cameras were located in Ostrowik Observatory, 40km south of Warsaw. The collected data were used for accurate radiant determination and for the description of the activity profile (Wiśniewski et al., 2002).

A bright fireball has been observed over the central part of Poland on 20 February 2004. Data from the photographic cameras located in Ostrowik and EN fireball station Lysa Hora have been used for precise trajectory determination (Spurny et al., 2004). This fireball was a milestone for the PFN. The same year the first permanent video stations were created in Ostrowik, Poznań, Kraków and Złotokłos.

Presently the Polish Fireball Network consists of more than 30 video stations with 74 different CCTV cameras (mostly Tayama C3102 but also some with modern Mintron 12V6 and Watec-902H). Most of these cameras have been founded by the Siemens Building Technologies grant between 2004 and 2006. In the last few years new PFN equipment has been purchased by the observers themselves, without any external funding. The Polish Fireball Network currently observes more than 30000 meteors per year. These data are reduced using PyFN software (Zoladek, 2011), UFOAnalyzer and UFO Orbit. Data recorded using MetRec software may be analyzed directly by PyFN or by UFO software, with a video data converter created for this purpose. Since 2010 the Polish Fireball Network is connected with the other neighboring fireball networks as a member of the EDMOND network.

2 Future plans

At the end of 2013 the Polish Fireball Network, cooperating with the Nicolaus Copernicus Astronomical Center, received a large national grant for the years 2014-2017. More than 150000 Euro may be spent on conferences, scientific expeditions and other similar projects. About 30% of all these funding can be used for the purchase completely new observing equipment.

During the last few years new, very sensitive, CMOS and CCD megapixel cameras became available. There are plenty of models with resolutions ranging from 0.9 to 5 Mpix but few of them have also very good quantum efficiency (QE). For example the Sony ICX 692 Mono CCD chip has a peak QE of 72 %, also the latest CMOS detectors have a QE larger than 70%. For meteor science applications these new megapixel cameras have some advantages for video and photographic methods. They are sensitive and they give live video stream with at least 15fps but also provide an image resolution comparable to the first digital DSLRs.

Before the purchase of these new megapixel cameras we decided to test some equipment. As we have a quite large area to cover we need cameras which are not very expensive but with a good sensitivity and frame rate. We found three models with sufficiently good parameters: ZWO ASI120MM (provided by Roman Piffl from the CEMENT network), QHY5-LII Mono and Pointgrey BlackFly 0.9 Mono. The first two cameras are produced with the same Aptina CMOS sensor while the last one has a Sony ICX692 CCD sensor.

Figure 1 – Image taken using PointGrey BlackFly 09 Mono camera with Tokina 3-8mm f/1.0, under a very dark sky.

The PointGrey 0.9 BlackFly Mono is a very small, lightweight CCD camera with a GiGE interface. With native software it is able to take 1s exposures or can be used with higher fps as a typical video camera. The user can separately set the frame rate and the exposure time,

the gain and all other parameters. It is possible to define a region of interest (ROI), images can be saved with 8 and 12 bit depth. This is a high quality CCD megapixel camera but it has some disadvantages too. The first disadvantage is that the sensitivity remains a bit below the expectations (but still sufficient for meteor detection). The second disadvantage is that the video stream format is completely incompatible with UFO Capture and UFO Capture HD.

PointGrey BlackFly 0.9 became the first megapixel camera of the PFN and works continuously at the PFN55 Ursynow station with designation MDC01 (Meteor Digital Camera 1).

Figure 2 – Image from the QHY5-LII Mono camera with Tamron 3-8mm f/1.0 megapixel lens. A meteor is visible in the middle part of the image. Clear weather and a moonless night with significant light pollution.

The second camera tested was the QHY 5-LII Mono, a small unit originally designed as a guiding and planetary camera. This camera uses the Aptina MT9M034 CMOS chip with QE=74%. The resolution of this chip is 1280 x 960 pixels and this is a bit higher than the resolution of the Pointgrey camera. The images taken with this camera look a bit noisy but the limiting magnitude is surprisingly good and comparable to the typical CCTV camera used by PFN. The QHY 5-LII will hopefully work properly with the standard version of UFO Capture. Currently there are some problems with the live image preview. The QHY staff is working on a special version of the driver designed for UFO Capture compatibility. This is the most promising camera and probably will be our best choice. Currently it is mounted at the PFN55 station as a MDC02 camera. The cost of one QHY5-LII is about 300 EUR.

The last megapixel unit tested was the ZWO ASI120 MM camera. It's based on the same CMOS sensor like the QHY and it is also very sensitive. We had the opportunity to test this camera during the Camelopardalids 2014 maximum in Canada. Recently the new version of UFO Capture HD has been developed which is fully compatible with this ZWO camera.

For the test purposes a simple image stacking software has been developed. It uses the images saved by the megapixel cameras on the hard disk and stack it into 1-minute frames.

This way these cameras can be used with exposure times like 100ms, with a low background level. Images processed this way can be easily reviewed after the night and measured with methods used for photographic plates. We are using these cameras as photographic units but we start to work on our own software which will be able to process 14-bit video data in real time.

In the near future we plan to deploy more than ten megapixel fireball stations. Each station will consist of two megapixel cameras pointed into opposite directions. Such station will cover more than half of the sky and will cooperate with another two stations located in other parts of the country. The parts of the atmosphere which are not covered by one pair of the station will be covered by another pair. Additionally, a few spectroscopic stations will be created using megapixel cameras and 1000 groves/mm diffraction gratings. These stations will cover areas observed by other equipment and will provide spectroscopic data of all bright meteors over Poland with good spectral dispersion.

Acknowledgment

This work was supported by the National Science Center (decision no. DEC-2013/09/B/ST9/02168)

We would like to thank Roman Piffl from EDMOND Network who provided us the ZWO ASI-120 MM megapixel camera and the high quality Fujinon fisheye lens.

References

Spurny P., Olech A., Kędzierski P. (2004). "Polish Automated Video Observations (PAVO)". *WGN, Journal of the IMO*, **32**, 48–50.

Wiśniewski M., Kędzierski P., Mularczyk K., Złoczewski K. (2003). "Polish Automated Video Observations (PAVO)". *WGN, Journal of the IMO*, **31**, 33–34.

Żołądek P. (2011). "PyFN – multipurpose meteor software". In Gyssens M., and Roggemans P., editors, *Proceedings of the International Meteor Conference*, Sibiu, 15–18 September 2011. IMO, pages 53–55.

Geminids 2012 – a spectacular show from Oman

Thomas Weiland[1] **and Felix Bettonvil**[2,3]

[1] **Ospelgasse 12-14/6/19, 1200 Wien, Austria**
thomas.weiland@aon.at

[2] **NOVA Optical and Infrared Instrumentation Division at ASTRON, Oude Hoogeveensedijk 4, 7991 PD Dwingeloo, The Netherlands**

[3] **Sterrewacht Leiden, Universiteit Leiden, Niels Bohrweg 2, 2333 CA Leiden, The Netherlands**
bettonvil@strw.leidenuniv.nl

The Geminids are the most reliable prominent meteor shower currently visible. They can be observed from the whole northern hemisphere and even low southern latitudes as well. Nevertheless, as the weather is often unfavourable in Central Europe during December, a six-day-long visual observing campaign was carried out from Oman in 2012. There observing conditions were nearly perfect, especially in the Rub al-Khali desert in the western part of the country. As a consequence, we managed to record more than 1800 Geminids within almost 45 hours of effective observing time. An impression of the campaign together with a summary of the results is given.

1 Why observing the Geminids from Oman?

With a radiant declination of δ = +33°, the Geminid meteor shower is observable from the whole northern hemisphere and even low southern latitudes as well. Unfortunately, humid air often dominates mid-northern December nights, resulting in cloudy skies and high altitude fog respectively. To escape these inferior conditions one has to move south, preferably to the Tropic of Cancer, where dry weather prevails and radiant altitudes are comparable to mid-northern latitudes.

For 2012 the Geminid maximum was expected to fall on December 13th, 23^{h}30^{m} UT (McBeath, 2011), corresponding to night times in Europe, North Africa and Western Asia. Additionally, New Moon on the same day secured perfect astronomical circumstances. Therefore we, Thomas Weiland and Felix Bettonvil, decided in early 2012 to use the moonless spell in the month December for a six-day-long observing campaign from Oman.

Oman, covering the south-eastern tip of the Arabian Peninsula and stretching between 17° and 26° N, offers a 70 to 90 % chance of clear nights in December, with the highest values in its western part. Moreover, these areas, especially the Rub al-Khali desert, are blessed with nearly unspoiled, pristine skies. To add an extra bonus, Oman ranks as one of the safest and friendliest nations in the Arabian world.

2 The 2012 observing campaign

Our campaign started out on December 10th–11th and lasted until December 15th–16th. We concentrated on visual observing; additionally Felix Bettonvil operated one automatic Canon 350D DSLR camera equipped with a 8 mm / f 2.8 Nikkor fisheye lens in order to capture bright Geminids and fireballs.

On the whole, the weather stayed quite cooperative. During the maximum night (December 13th–14th) some cirrus clouds turned up, hampering our observations not much. Only the last observing session (December 15th–16th) fared ill, as fast moving cumulus clouds gave way to clear skies for less than one and a half hour only.

Limiting magnitudes (averaged over each night) were ranging between 6.06 and 6.35 (Felix Bettonvil, BETFE; star counting method) and between 6.10 and 6.50 (Thomas Weiland, WEITH; direct view method, averted vision) respectively.

All in all we managed to record 1811 Geminids within 44.79 hours of effective observing time (see *Table 1*).

3 Results

Magnitude distribution / Population indices

From the total magnitude distribution (see *Table 1*) it can be deduced that 12 % (BETFE) and 15 % (WEITH) of all GEMs respectively reached at least magnitude 0, more or less comparable to other major annual streams.

Fireballs (≥ magnitude -3) were abundant during the maximum night (December 13th–14th; 10 (BETFE); 14 (WEITH)) and, to a much lesser extent, the night before and after. The brightest one of them reached magnitude -7 (December 13th, 22^{h}57^{m}25^{s} UT).

Interestingly, meteor numbers per magnitude class were slightly different for each observer, peaking at +3 (BETFE) and +4 (WEITH) respectively.

In a further step population indices were derived, using the magnitude difference between the meteors and the

Table 1: Observer statistics, magnitude distribution and meteor numbers.

Date	*UT*	T_{eff}	*lm*	*-6*	*-5*	*-4*	*-3*	*-2*	*-1*	*0*	*+1*	*+2*	*+3*	*+4*	*+5*	*+6*	*Σ*	*Observer*
10/11	20:55-00:00	3.17	6.06	0	0	0	0	0	0	0	2	4	8	2	3	0	19	BETFE
	20:30-23:30	2.90	6.10	0	0	0	0	0	0	1	2	4	7	4	1	0	19	WEITH
11/12	21:01-00:00	2.83	6.35	0	0	0	0	0	1	1	7	5	15	19	10	3	61	BETFE
	20:30-23:30	3.19	6.50	0	0	0	0	0	1	2	1	5	8	21	7	0	45	WEITH
12/13	20:55-01:10	3.33	6.25	0	0	0	1	2	0	4	13	14	38	46	21	3	142	BETFE
	21:00-01:00	3.98	6.45	0	0	0	1	2	1	7	22	23	34	91	27	0	208	WEITH
13/14	17:05-01:45	7.77	6.28	1	2	3	4	7	24	45	62	97	142	115	61	2	565	BETFE
	16:45-01:45	8.06	6.48	*3	3	2	6	15	42	51	49	93	117	184	39	0	604	WEITH
14/15	21:08-01:00	3.72	6.13	0	0	1	0	0	1	3	2	7	12	29	14	1	70	BETFE
	21:30-00:30	3.00	6.50	0	0	1	1	0	2	2	2	8	8	31	5	0	60	WEITH
15/16	22:35-23:52	1.87	6.10	0	0	0	0	0	0	1	1	0	3	1	5	0	11	BETFE
	22:15-23:15	0.97	6.35	0	0	0	0	0	0	0	1	0	0	3	3	0	7	WEITH
Σ		22.69		1	2	4	5	9	26	54	87	127	218	212	114	9	868	BETFE
Σ		22.10		*3	3	3	8	17	46	63	77	133	174	334	82	0	943	WEITH
Total		44.79		*4	5	7	13	26	72	117	164	260	392	546	196	9	1811	

** The brightest GEM actually had magnitude -7.*

Figure 1 – Fisheye view, showing the Milky Way and nine bright Geminids. Composite of 15 pictures obtained on December 13th–14th (Canon 350D, Nikkor 8 mm / f 2.8, ISO 1600, 30sec exposures).

limiting stellar magnitudes, based on table 9.2, p. 178 in the HMO, 2nd ed. (Rendtel and Arlt, 2009).

For the time span of December 11th–12th to December 14th–15th this yielded values varying between r = 2,12 and 3.07 (BETFE; average 2.67) and 1.95 and 2.68 (WEITH; average 2.14). Due to the low GEM numbers, no population indices were derived for December 10th–11th and December 15th–16th respectively.

Despite the difference in population indices, which may be caused by the diverging methods of determining the limiting magnitude, the trend, however, is nearly the same: starting out with r-values around 2.7 on December 11th–12th and staying more or less constant during the following night, a distinctive minimum within the order of r = 2.0 was encountered on December 13th–14th. After that r-values were rising again to around 2.7.

Zenithal hourly rates

ZHR calculation followed the procedure given in the HMO, 2nd ed. (Rendtel and Arlt, 2009). Due to the fact that limiting magnitudes were close to, or even matching the standard sky of +6.5, using individual population indices would have a minor impact on ZHR calculation. Nevertheless, we took individual r-values of 2.00

(BETFE; in analogy to the IMO live ZHR profile[1]) and 2.14 (WEITH) respectively and averaged the results. The zenith exponent was assumed to be γ = 1.0. No perception coefficient was applied.

Maximum ZHRs started out with less than 10 on December 10^{th}–11^{th} and were rising more than twice during the following night. During the third session (December 12^{th}–13^{th}) much higher rates were encountered (within the order of 60). The maximum night (December 13^{th}–14^{th}) finally yielded ZHRs hovering around 105 for more than 8 hours. After this period they showed a steep decline, starting with about 35 at the beginning of the fifth run (December 14^{th}–15^{th}) and ending up within the order of 15. During the last session (December 15^{th}–16^{th}) ZHRs were comparable to those at the beginning of the campaign.

Concerning the time of maximum, there is no distinctive trend discernible. In order to smooth the profile and to get the peak out more clearly, ZHR values based on bins of 10 minutes obtained by WEITH were averaged using a sliding mean of 5 bins per step (A5). This puts the time of maximum to $22^h30^m \pm 10^m$ UT (ZHR 127 ± 28), about 1 hour earlier than predicted and quite in agreement with the corresponding IMO live ZHR profile[1].

General Appearance

Geminid meteors can be distinguished from those of other streams by their scarcity of trains. According to that, only 2 % of all GEMs logged by WEITH (n = 943; see *Table 1*) showed a prominent train (-7 to +3 magnitude class) and additional 9 % produced a short one (-6 to +4 magnitude class).

Color estimates by WEITH yielded mainly yellow and fewer white hues, with blue, orange and green tints to a much lesser extent.

Fireballs

The most prominent feature of the 2012 Geminids was a spectacular array of fireballs during the maximum night (December 13^{th}–14^{th}), occurring all within less than 5 hours ($19^h25^m15^s$ to $00^h08^m15^s$ UT). Magnitudes were ranging between -3 and -7 and fireballs ≥ magnitude -5 even showed a stronger concentration in time (3.3 hours; $20^h48^m50^s$ to $00^h08^m15^s$ UT), more or less centred on the time of maximum.

On December 12^{th}–13^{th} the brightest GEM reached magnitude -3 and on December 14^{th}–15^{th} magnitude -4.

Photographic results

Due to the fact that Geminid meteors are of medium speed and often bright, it was not too difficult to get them onto chip. With that in mind, Felix Bettonvil captured a few on the night of December 13^{th}–14^{th} (see *Figure 1*).

[1] http://www.imo.net

4 Conclusion

The 2012 observational results can be summarized as follows:

- Population indices were comparable to previous returns, showing a dip around the time of maximum (Rendtel, 2004; Rendtel et. al., 2009).
- ZHR values were definitely lower than in 2004, the last moonless return within the same time window (Miskotte et. al., 2011).
- The time of maximum was in line with the forecast, about 1 hour earlier than predicted (McBeath, 2011).
- An unusual concentration of fireballs was encountered on December 13^{th}–14^{th} within a relatively short time span (4.7 hours); bright fireballs (≥ magnitude -5) even showed a stronger concentration centred on the time of maximum (3.3 hours). Usually Geminids ≥ magnitude -1 reach their peak after the maximum; Uchiyama, 2010).
- There is probably no correlation between the occurrence of fireballs and the distance of (3200) Phaethon to Earth, with respect to December, 14^{th}, 0^h UT (2012: 1.712 AE; near the maximum value; see Miskotte et. al., 2011).
- Concerning colors, yellow tints were dominating over blue hues; this may be an indication that not all meteoroids are Na-depleted to the same extent (see Jenniskens, 2006).

5 Future Work

In comparison with previous returns, the 2012 observational results may give rise to questions about the evolution of the stream:

- Have the Geminid maximum rates already peaked at the turn of the last century (see Miskotte et. al., 2011) or will they steadily increase until 2050 (Jones and Hawkes, 1986; cit. in Jenniskens, 2006)?
- Is the percentage of bright Geminids still on the rise and will they peak together with the highest rates (Jones and Hawkes, 1986; Williams and Wu, 1993; cit. in Jenniskens, 2006)?

The moonless returns of 2015, 2017 and 2020 offer excellent opportunities to prove this!

References

Jenniskens P. (2006). Meteor Showers and Their Parent Comets, Cambridge Univ. Press, Cambridge.

McBeath A. (2011). Meteor shower calendar 2012. IMO.

Miskotte K., Johannink C., Vandeputte M. and Bus P. (2011). "Geminids: 30 Years of Observations (1980-2009)". *WGN, Journal of the IMO,* **39**, 167–186.

Rendtel J. (2004). "Almost 50 Years of Visual Geminid Observations". *WGN, Journal of the IMO,* **32**, 57–59.

Rendtel J. and Arlt R. (editors) (2009). Handbook for Meteor Observers. IMO.

Uchiyama S. (2010). “Geminids ZHR Activity Profiles as a Function of Magnitude”. *WGN, Journal of the IMO*, **38**, 31–35.

The author, Thomas Weiland, during his lecture. (Credit Axel Haas.)

Daytime meteor showers

Jürgen Rendtel[1,2]

[1] **Leibniz-Institut für Astrophysik Potsdam (AIP), An der Sternwarte 16, 14482 Potsdam, Germany**
jrendtel@aip.de

[2] **International Meteor Organization, Eschenweg 16, Potsdam, Germany**

Radiants of daytime meteor showers are located typically about 20–30° west of the Sun. Radiants and orbits are known from radar observations, but information about the activity and the population index or mass index are missing or incomplete. Two of the daytime showers, the Daytime Arietids (171 ARI) in early June and the Daytime Sextantids (221 DSX) end September to early October are active and are accessible with radio (forward scatter), radar and optical methods. Both the ARI and DSX appear in regular video data analyses. Observations obtained with different methods should allow to calibrate and to combine data to derive a comprehensive meteoroid stream description.

1 Introduction

The Earth crosses numerous meteoroid streams along its orbit around the Sun with radiants in all regions of the sky. Most of the known radiants are located in the nighttime sky. Radiants of a few showers are best observable only during the evening hours such as the π-Puppids, the Draconids and the Puppid-Velids. Studies of radar and radio data show also radiants close to the Sun's position. From radar and radio forward scatter observations we know that there are numerous radiants in the daytime region. Investigation of radar data shows sources linked to the ecliptical objects, such as the Antihelion source (mainly around a region about 10° east of the solar opposition point and the Helion source (about 60° west of the Sun or about 30° east of the Earth's apex). The other two main sources of sporadic meteors, the (northern and southern) Toroidal and the Apex source provide meteors entirely during the night hours (*Figure 1*).

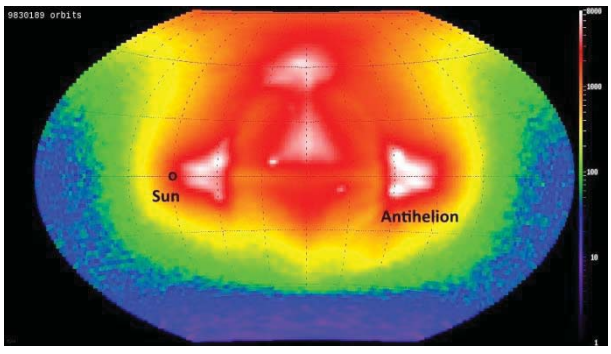

Figure 1 – Sources of sporadic meteors as observed by the Canadian CMOR radar kindly provided by Campbell-Brown.

Radiants of meteor showers within or near the Helion Source of the sporadic background are above the horizon only during daytime. Hence meteors of these showers are generally not observable by optical means from the Earth's surface. The radiants remain very low in the sky even in twilight so that systematic data can only be collected by radio and radar techniques. Our current knowledge of the daytime showers is not as detailed as for most of the nighttime showers.

The motivation for this review and the suggested project came from the preparation of the annual Meteor Shower Calendar of the IMO, edited by Alastair McBeath. It includes a summary of the activity from daytime sources as a basis for forward scatter meteor observers. When compiling the list and completing the full designation including the IAU Meteor Data Center (MDC)[1] codes, a number of inconsistencies was found. Generally, the MDC gives rather few references for most daytime showers. Some showers seem to duplicate other entries. This also led to an additional chapter in the recent Meteor Shower Workbook 2014 (Rendtel, 2014), including information from recent radar meteor studies (Brown et al., 2008; Sanches et al., 2013).

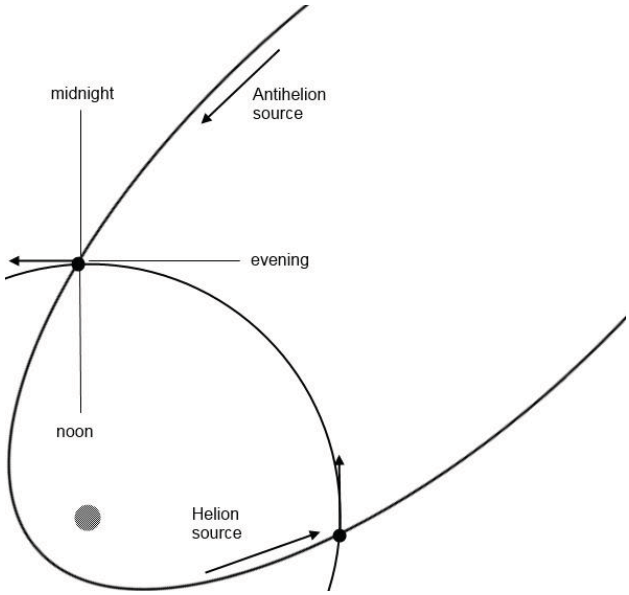

Figure 2 – Typical orbit of a Jupiter family daytime meteoroid and its possible approaches to the Earth's orbit, causing either an antihelion or helion meteor.

[1] http://www.astro.amu.edu.pl/~jopek/MDC2007/index.php

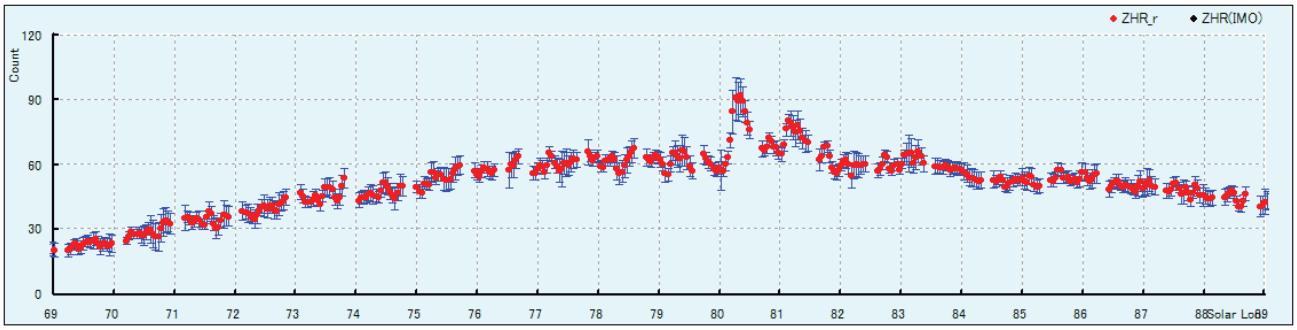

Figure 3 – ZHR profile of the Daytime Arietids in 2011 calculated by Sugimoto (see Sugimoto, 2011).

Table 1 – Current Working List of Daytime Meteor Showers as given in the Workbook (Rendtel,2014). The showers' designations are listed here omitting `Daytime'.

Shower	Activity	Date Max	$\lambda_{\odot(2000)}$	α (°)	δ (°)	Activity
Sgr/Capricornids (115 DSC)	Jan 13–Feb 04	Feb 01	312.5	299	-15	Medium
χ-Capricornids (114 DXC)	Jan 29–Feb 28	Feb 13	324.5	315	-24	Low
April Piscids (144 APS)	Apr 20–Apr 26	Apr 22	32.5	9	+11	Low
ε-Arietids(154 DEA)	Apr 24–May 27	May 09	48.7	44	+21	Low
May Arietids (294 DMA)	May 04–Jun 06	May 16	55.5	37	+18	Low
S. MayArietids (156 SMA)	Apr 20–May 22	May 08	47.5	29	+10	Low
o-Cetids (293 DCE)	May 05–Jun 02	May 20	59.3	28	-4	Low
N. ω-Cetids (152 NOC)	Apr 20–May 20	May 08	47.5	9	+19	Low
S. ω-Cetids (153 OCE)	Apr 24–May 20	May 10	49.5	23	-3	Low
Arietids (171 ARI)	May 14–Jun 24	Jun 07	76.5	42	+25	High
ζ-Perseids (172 ZPE)	May 07–Jun 26	Jun 14	83.5	65	+28	Low
β-Taurids (173 BTA)	Jun 12–Jul 04	Jun 28	96.5	85	+23	Low
γ-Leonids (203 GLE)	Aug 14–Sep 12	Aug 25	152.2	155	+20	Low
κ-Leonids (212 KLE)	Sep 06–Oct 03	Sep 21	178.5	159	+18	Low
Sextantids (221 DSX)	Sep 23–Oct 07	Sep 30	187.5	154	0	Medium

While radiants of the showers and orbits or the streams are well determined and defined, there is little or no information about the activity expressed as a rate or a flux as well as about the population or mass index. Blaauw et al. (2011) provided some data of the mass index of some showers recently, and Campbell-Brown (2004) presented an analysis of the Daytime Arietids with an approach to determine a rate. However, we need to keep in mind that radar `sees' much smaller particles as compared to optical (visual and video) and forward scatter observations.

2 Daytime showers

Daytime shower activity has been observed regularly but a large portion of the recorded data has not yet seen detailed analyses to obtain comparable results to the optical range with rate, flux and population index profiles. A limited attempt was made by McBeath (1998) to perform radio forward scatter data analyses. Sugimoto developed an analyzing method originally for the Japanese International Project for Radio Meteor Observation (IPRMO) project[2]. Sugimoto[3] provided an activity (ZHR) graph for the 2011 return of the Daytime Arietids (*Figure 4*). Sugimoto's method was applied to various meteor shower data, particularly for the Leonids (Ogawa et al., 2002). The idea was continued for a later Quadrantid data analysis by Brower (2006), and a method to determine shower activity was further updated by Steyaert et al. (2006).

Among the currently known sources there are two or three with `moderate' or `high' activity and many others with low activity. *Table 1* gives the list which is currently included in both the 2015 Meteor Shower Calendar (McBeath, 2014) and the Workbook (Rendtel, 2014).

There are close relations between several daytime and nighttime showers. The ζ-Perseids (172 ZPE) and the β-Taurids (173 BTA) both belong to the Taurid complex. The Sextantids (221 DSX) are part of the Phaethon-Geminid complex (Ohtsuka et al., 2006). Another complex is formed by the comet 96P/Machholz and the

[2] International Project for Radio Meteor Observation http://www.amro-net.jp/radio.htm
[3] http://www5f.biglobe.ne.jp/~hro/Flash/2011/ARI/index.html

minor planet (196256) 2003 EH1. The related shower complex includes four well-known meteor showers: Daytime Arietids (171 ARI), Southern δ-Aquariids (005 SDA), Quadrantids (010 QUA), and the Northern δ-Aquariids (026 NDA) as nicely shown by Neslušan et al. (2014). The stream filaments corresponding to the 171 ARI and two Aquariids (005 SDA, 026 NDA) constitute the ecliptical component, and those corresponding to the 010 QUA and their southern counterpart constitute the toroidal component of the complex (Neslušan et al., 2013a; Neslušan et al., 2013b). Further examples are given in Chapter 3 of the Meteor Shower Workbook 2014 (Rendtel 2014).

Table 1 repeats the current compilation of daytime showers as given in the 2015 Meteor Shower Calendar and the recent Meteor Shower Workbook. It is very likely that the list will undergo updates and corrections in the near future.

3 Optical observing possibilities

One attempt to collect data of the above mentioned physical parameters is a combination and thereby calibration of data obtained by different methods. Showers suitable for this attempt should (i) produce a significant activity and (ii) have a radiant with a large elongation from the Sun. The most promising candidates are the Daytime Arietids (171 ARI) and the Daytime Sextantids (221 DSX).

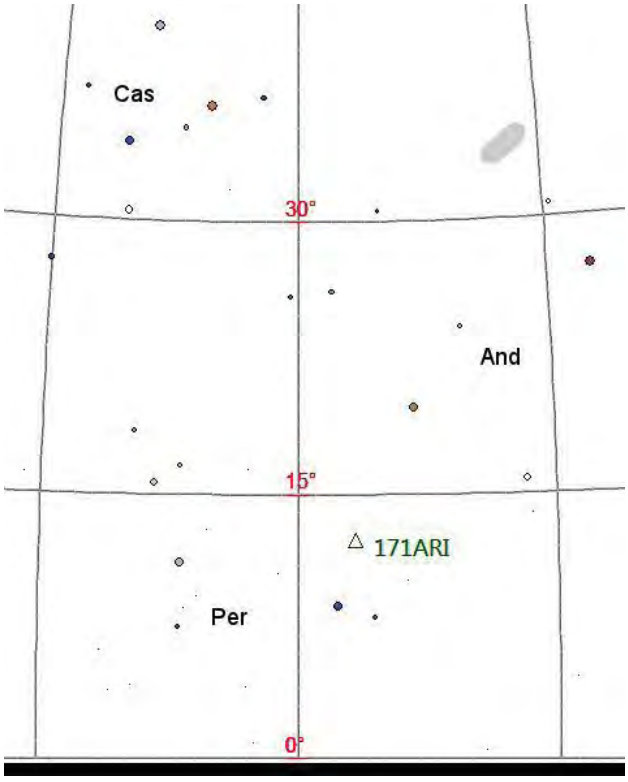

Figure 4 – Radiant position of the 171 ARI close the end of the possible optical observing interval for a location at 30° N.

The general idea that it is possible to collect also optical data of active daytime showers came from the fact that the standard analysis of the EDMOND video data (Rudawska et al., 2014) showed traces of the 171 ARI and the 221 DSX. Data of the IMO Video Meteor Network (Molau et al., 2014) also allowed an analysis of the 171 ARI. So regular observations not expressively extended into the twilight periods captured some of these shower meteors.

The elongation of the radiants from the Sun of the two showers is about 35 degrees. Depending on the geographical latitude, the radiant will rise about two hours before the Sun. Still, this means that the radiant will remain low in the eastern sky and the observing conditions expressed in terms of limiting magnitude. *Figures 4 and 5* show the situation for the Daytime Arietids and the Daytime Sextantids.

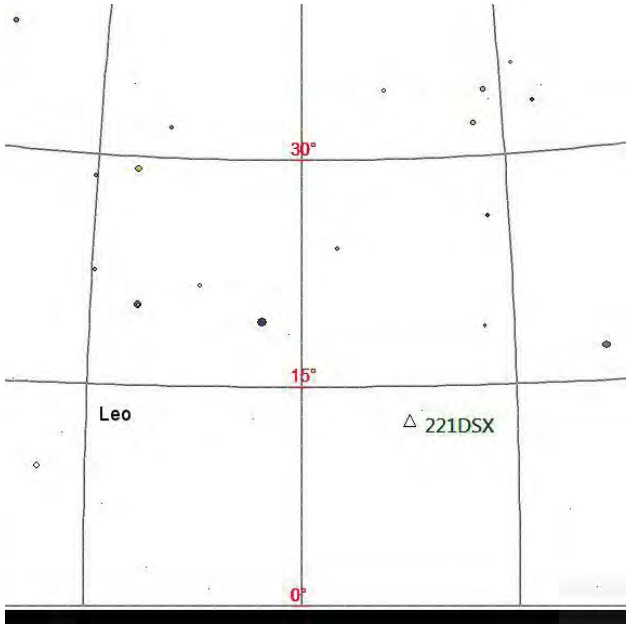

Figure 5 – Radiant position of the 221 DSX close the end of the possible optical observing interval for a location at 30° N.

Daytime Arietids (171 ARI)

The Arietids are one of the showers listed with a high activity level. The original data go back to Clegg et al. (1947), Lovell (1954) and Sekanina (1976). Orbits of stream meteoroids were already published by Almond (1951). Recent CMOR data (Brown et al., 2008) indicate a relatively high flux as the stream is defined by more than 2100 orbits (typical numbers for other streams are of order a few hundred). The shower is also prominent in the SAAMER radar (Janches et al., 2013).

Optical observers roughly between the tropics there have a chance to observe a few shower meteors in early June close to dawn, albeit with low radiant position. Some data of such optical (video) observations have been analysed by Fujiwara et al. (2004), by Jenniskens et al. (2012) and as already mentioned by Rudawska et al. (2014) and Molau et al. (2014). While the radiant and orbital data are well established, there are only estimates of the activity or flux. Campbell-Brown (2004) gives a ZHR of about 200 and compares the shower with the Quadrantids, assuming r=2.75 (s=2.1).

Based on meteoroid orbital data, Jenniskens et al. (2012) suggest an association of the Arietids with the Marsden

group comet C/1999 J6 (= 2004 V9 = 2010 H3) and argue that it seems possible that the meteoroids are debris from a breakup which created the Marsden group comets or are connected with an earlier fragmentation that left comet 96P/Machholz.

Daytime Sextantids (221 DSX)

The activity level of this shower is classified as `medium' and it is detected in essentially all radar data (e.g., Galligan and Baggaley, 2002; Brown et al., 2008). The origin of the `medium' activity level comes from Weiss (1960), giving a numerical level like the Jodrell Bank ones for the o-Cetids and β-Taurids. Forward scatter data could even suggest `high' activity, at least occasionally.

The DSX-maximum is expected around September 30 ($\lambda_\odot$ = 187.5°) with deviations from one return to another. The CMOR radar data confirm rather the late maximum at 187.5°. Janches et al. (2013) detect activity with their radar between 179° and 184°. Several minor maxima in early October may also be due to this radio shower.

4 Conclusions

Radar and radio (forward scatter) data will be the major source regarding daytime meteor showers. The shower identification (radiant and orbits) found from different observational data sets is consistent. Physical parameters, such as the population/mass index and rate/flux, need to be determined. In the case of two showers, the Arietids (171 ARI) and Sextantids (221 DSX), a limited amount of optical data may be used for calibration purposes.

During the following returns of the two showers, observers should report all available data to the author. The combined data sample will become available for a comprehensive study of the activity and physical parameters of the 221 DSX and the 171 ARI. (A first sample has been recorded and reported for the 2014 return of the Daytime Sextantids).

References

Almond M. (1951). "The summer daytime meteor streams of 1949 and 1950. III. Computation of the orbits". *Monthly Notices of the Royal Astronomical Society*, **111**, 37–44.

Blaauw R. C., Campbell-Brown M. D., Weryk R. J. (2011). "A meteoroid stream survey using the Canadian Meteor Orbit Radar - III. Mass distribution indices of six major meteor showers". *Monthly Notices of the Royal Astronomical Society*, **414**, 3322–3329.

Brower J. L. (2006). "Global forward scatter observations of the 2006 Quadrantid maxima". *WGN, Journal of the IMO*, **34**, 25–29.

Brown P., Weryk R. J., Wong D. K., Jones J. (2008). "A meteoroid stream survey using the Canadian Meteor Orbit radar I. Methodology and radiant catalogue". *Icarus*, **195**, 317–339.

Campbell-Brown M. D. (2004). "Radar observations of the Arietids". *Monthly Notices of the Royal Astronomical Society*, **352**, 1421–1425.

Clegg J. A., Hughes V. A., Lovell A. C. B. (1947). "The daylight meteor streams of 1947 May-August". *Monthly Notices of the Royal Astronomical Society*, **107**, 369–378.

Fujiwara Y., Ueda M., Sugimoto M., Sagayama T., Abe S. (2004). "TV observation of the daytime meteor shower; the Arietids". *Earth, Moon and Planets*, **95**, 595–600.

Galligan D. P., Baggaley W. J. (2002). "Wavelet enhancement for detecting shower structure in radar meteoroid data II. Application to the AMOR data". In Green S. F., Williams I. P., McDonnell J. A. M., and McBride N., editors, *Dust in the Solar System and Other Planetary Systems, Proceedings of IAU Coll. 181*, University of Kent, UK, 4–10 April 2000, Oxford, Pergamon (COSPAR colloquia series, Vol. 15), p.48.

Janches D., Hormaechea J. L., Brunini C., Hocking W., Fritts D. C. (2013). "An initial meteoroid stream survey in the southern hemipshere using the Southern Argentina Agile Meteor Radar (SAAMER)". *Icarus*, **223**, 677–683.

Jenniskens P., Duckworth H., Grigsby B. (2012). "Daytime Arietids and Marsden sunskirters (ARI, IAU #171)". *WGN, Journal of the IMO*, **40**, 98–100.

Lovell A. C. B. (1954). Meteor astronomy. Oxford, Clarendon Press.

McBeath A. (1998). "The forward scatter meteor year". In Knöfel A., and McBeath A., editors, *Proceedings of the International Meteor Conference*, Petnica, Yugoslavia, 25–28 September 1997. IMO, pages 39–54.

McBeath A (2014). Meteor Shower Calendar 2015. IMO.

Molau S., Kac J., Crivello S., Stomeo E., Barentsen G., Goncalves R., Igaz A. (2014). "Results of the IMO Video Meteor Network – June 2014". *WGN, Journal of the IMO*, **42**, 201–204.

Neslušan L., Kaňuchová Z., and Tomko D. (2013a). "The meteor-shower complex of 96P/Machholz revisited". *Astronomy & Astrophysics*, **551**, 14 pp. (DOI: 10.1051/0004-6361/201220299.

Neslušan L., Hajduková M., jr., and Jakubík M. (2013b). "Meteor-shower complex of asteroid 2003 EH1 compared with that of comet 96P/Machholz". *Astronomy & Astrophysics*, **560**, id. A47, 10 pp. (DOI:10.1051/0004-6361/201322228).

Neslušan L., Hajduková M., Tomko D., Kaňuchová Z, Jakubík M. (2014). "The prediction of meteor showers from all potential parent comets". In Rault J.-L., and Roggemans P., editors, *Proceedings of the International Meteor Conference*, Giron, France, 18–21 September 2014. IMO, pages 139–145.

Ogawa H., Toyomasu S., Ohnishi K., Amikura S., Maegawa K., Jenniskens P. (2002). "The 2002 Leonids as monitored by the International Project for Radio Meteor Observations". *WGN, Journal of the IMO*, **30**, 225–231.

Ohtsuka K., Sekiguchi T., Kinoshita D., Watanabe J.-I., Ito T., Arakida H., Kasuga T. (2006). "Apollo asteroid 2005 UD: split nucleus of (3200) Phaethon?". *Astronomy & Astrophysics*, **450**, L25–L28.

Rendtel J. (editor). (2014). Meteor Shower Workbook 2014. IMO.

Rudawska R., Matlovic P., Toth J., Kornos L. (2014). "Independent identification of meteor showers in EDMOND database". arXiv:1406.6598.

Sekanina Z. (1976). "Statistical model of meteor streams. IV a study of radio streams from the synoptic year". *Icarus*, **27**, 265–321.

Steyaert C., Brower J., Verbelen F. (2006). "A numerical method to aid in the combined determination of stream activity and observability function". *WGN, Journal of the IMO*, **34**, 87–93.

Weiss A. (1960). "Radio-echo observations of southern hemisphere meteor shower activity from 1956 December to 1958 August". *Monthly Notices of the Royal Astronomical Society*, **120**, 387–403.

The author, Jürgen Rendtel, being offered honorary membership of the IMO for his dedicated efforts as IMO President in the past 25 years. From left to right, Javor Kac, Sirko Molau, Detlef Koschny, Cis Verbeeck, Jürgen Rendtel, Manuela Rendtel, Geert Barentsen, Paul Roggemans and Marc Gyssens. (Credit Ana Žegarac).

Independent identification of meteor showers in EDMOND database

Regina Rudawska, Pavol Matlovič, Juraj Tóth and Leonard Kornoš

Faculty of Mathematics, Physics and Informatics, Comenius University, Mlynska dolina, Bratislava, Slovakia
reginka@amu.edu.pl, juraj.toth@fmph.uniba.sk, leonard.kornos@fmph.uniba.sk

This paper presents the results obtained by a proposed new independent method of meteor showers identification, which is applied to the current version of the database (EDMOND 5.0). In the first step of the survey we used the D_{SH} criterion to find groups around each meteor within the similarity threshold. Mean parameters of the groups were calculated and compared using a new function based on geocentric parameters (λ, α, δ, and V_g). Similar groups were merged into final clusters (representing meteor showers), and compared with the IAU Meteor Data Center list of meteor showers.

1 Introduction

In this paper, we focus on determining an independent method to associate an individual meteor in the EDMOND database with a given meteor shower (Kornos et al., 2013; Kornos et al., 2014a; Kornos et al., 2014b). The outcome of this method is the confirmation of some of the previously reported meteoroid streams listed in the IAU Meteor Data Center (IAU MDC), and leading to the discovery of potential new ones.

2 Methodology

Our cluster identification procedure links two types of meteor parameters: orbital elements (e, q, i, ω, and Ω) and geocentric parameters (λ, α, δ, and V_g). The first set of parameters is applied using the so called D-criteria that determine similarity between orbits of meteoroids. The second set of parameters measures similarity between meteors at the sky in a given meteor shower activity period. In the first step we use the Southworth and Hawkins D_{SH} criterion (1963), while in the second step a new distance function D_x is applied. The D_x criterion, which involves geocentric parameters, is defined as

$$\begin{aligned} D_x^2 &= w_\lambda \left[2 \cdot \sin\left(\frac{\lambda_A - \lambda_B}{2}\right)\right]^2 \\ &+ w_\alpha \left(|V_{g_A} - V_{g_B}| + 1\right) \left[2 \cdot \sin\left(\frac{\alpha_A - \alpha_B}{2} \cdot \cos\delta_A\right)\right]^2 \\ &+ w_\delta \left(|V_{g_A} - V_{g_B}| + 1\right) \left[2 \cdot \sin\left(\frac{|\delta_A - \delta_B|}{2}\right)\right]^2 \\ &+ w_V \left[\frac{|V_{g_A} - V_{g_B}|}{V_{g_A}}\right]^2, \end{aligned}$$

where λ_A and λ_B are the solar longitudes, α_A and α_B are the right ascensions, δ_A and δ_B are the declinations, and V_{gA} and V_{gB} are the geocentric velocities of two meteors. The w_λ , w_α, w_δ , and w_V are suitably defined weighting factors. To normalize the contributions of each term in D_x , we used values: w_λ = 0.17, w_α = 1.20, w_δ = 1.20, and w_v = 0.20.

Our method may be summarized by the following steps:

Step 1: We probe the database using D_{SH} with a low threshold value D_c = 0.05. Around a meteoroid orbit a sphere of orbital parameters and radius D_c is "created". A set of orbits within the sphere creates a group, from which members are excluded following a search around another meteoroid orbit. In this way, we have independent groups around each reference meteoroid orbit. Next, for each group, a weighted mean of parameters is calculated.

Step 2: Using D_x we merge groups into clusters of similar weighted means of geocentric parameters found in Step 1. The groups are associated if $D_x \leq D_{c'}$, where $D_{c'}$ = 0.15. Next, the new weighted mean of the parameters for the cluster found in Step 2 is calculated. We repeat Step 2 using new means till the groups are no longer linked into clusters.

Step 3: We compare parameters of known meteor showers in the IAU MDC with the final mean values of the same parameters of the clusters found. For this purpose, we use D_{SH} criterion with $D_{c''}$ = 0.15.

3 Results

We present here results for selected cases. Figure 1 shows meteor concentrations of the meteor showers at the sky that are the most prominent showers in the EDMOND database, i.e. Geminids, Perseids, and Orionids (top panel). Their activity period lasts about 25-35 days. The Geminids and Orionids are more compact in comparison to the Perseids meteor shower. However, the Perseids are more prominent than the other two showers.

Figure 1 (bottom panel) presents some examples of meteor shower pairs such as: Southern & Northern Taurids, December Monocerotids & November Orionids, and Northern & Southern October δ Arietids. The second listed shower of a given pair is marked in blue. As shown in *Figure 2*, our identification procedure correctly separates those meteor showers. In other words, our method did not fail on separating the branches of the same meteor shower (e.g. Southern & Northern Taurids).

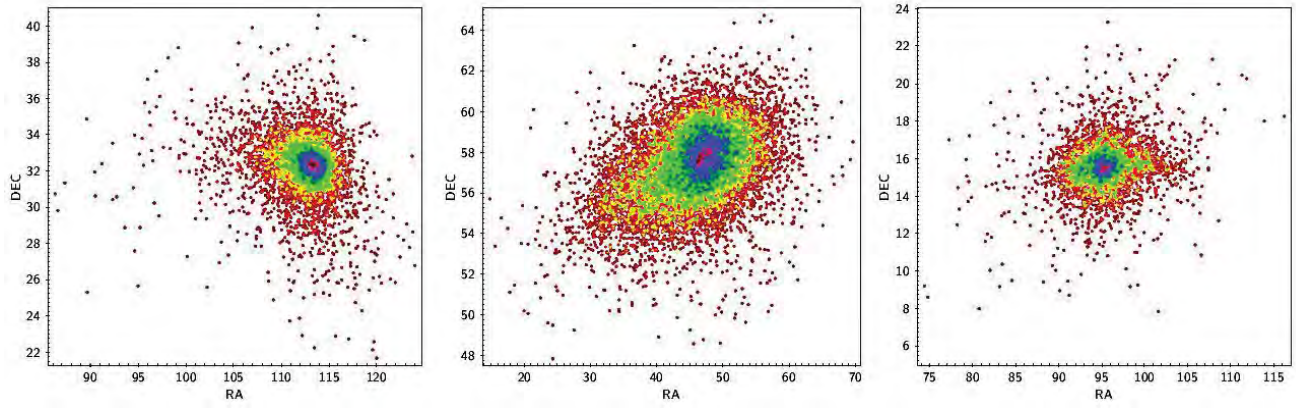

Figure 1 – Identified meteor showers. Geminids (left), Perseids (centre), and Orionids (right). Greyscale represents meteor concentrations at the sky.

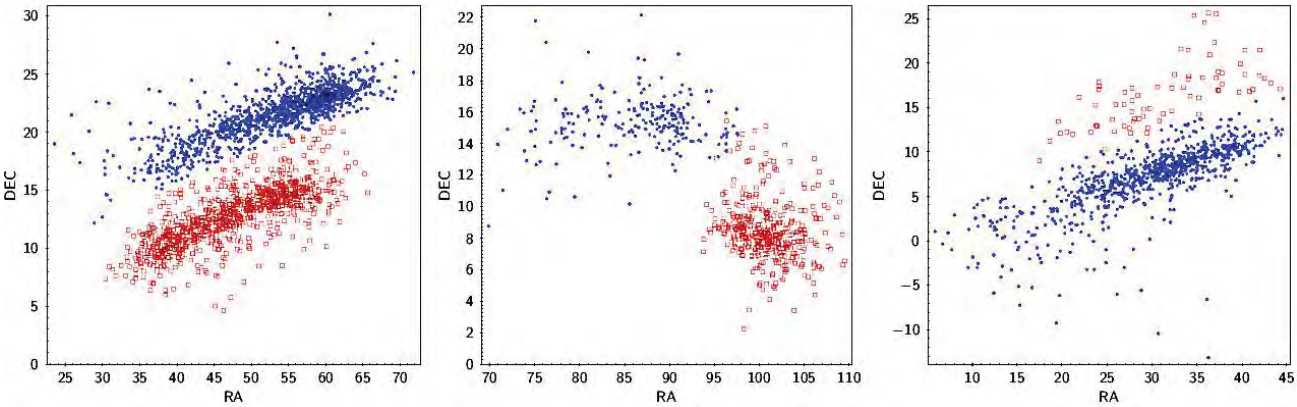

Figure 2 – Southern & Northern Taurids (left), December Monocerotids & November Orionids (centre), and Northern & Southern October δ Arietids (right). Here, shapes indicate different showers of the pair – squares and dots respectively.

Moreover, the identification step based on geocentric parameters is efficient enough to successfully separate two meteor showers located in close distance to each other at the sky (e.g. December Monocerotids & November Orionids).

4 Conclusion

We have identified 257 meteor showers. The list includes 42 already established streams, 152 from the working list and 63 *pro-tempore* meteor showers. For a higher threshold ($D_{c''}$ = 0.20), we found 284 meteor shower in total (44, 173 and 67, respectively). However, with a higher threshold value some of the showers are more contaminated by the sporadic background in comparison to the results obtained with the lower threshold ($D_{c''}$ = 0.15).

This identification was done only for those meteor showers for which their orbital elements are provided by the IAU MDC (as of June 2014). However, there are 174 meteor showers in the IAU MDC with no orbital data (Andreic et al., 2014). Thus, in those cases we could not apply the D_{SH} function to identify these clusters. We identified a few of them, however, using the D_x criterion instead of D_{SH} in Step 3. Their orbital elements were calculated, and they will be subsequently provided to the IAU MDC.

Acknowledgment

The work is supported by the Slovak grant APVV-0517-12, APVV-0516-10 and VEGA 1/0225/14.

References

Andreić Z., Šegon D., Vida D. (2014). "A statistical walk through the IAU MDC database". In Rault J.-L.., and Roggemans P., editors, *Proceedings of the International Meteor Conference*, Giron, France, 18–21 September 2014. IMO, pages 126–133.

Kornos L., Matlovic P., Rudawska R., Toth J., Hajdukova M. Jr., Koukal J., Piffl R. (2014a). "Confirmation and characterization of IAU temporary meteor showers in EDMOND database". In Jopek T. J., Rietmeijer F. J. M., Watanabe J., and Williams I. P., editors, *Meteoroids 2013, Proceedings of the Astronomical Conference*, held at A. M. University, Poznań, Poland, 26–30 August 2013, A.M. University Press, pages 225–233.

Kornos L., Koukal J., Piffl R., Toth J. (2014b). "Edmond Meteor Database". In Gyssens M., Roggemans P., and Żołądek P., editors, *Proceedings of the International Meteor Conference*, Poznań, Poland, 22–25 August 2013. IMO, pages 23–25.

Kornos L., Koukal J., Piffl R., Toth J. (2013). "Database of meteoroid orbits from several European video networks". In Gyssens M., and Roggemans P., editors, *Proceedings of the International Meteor Conference*, La Palma, 20–23 September 2012. IMO, pages 21–25.

Rudawska R., Matlovic P., Toth J., Kornos L. (2014). "Independent identification of meteor showers in EDMOND database". arXiv:1406.6598.

Southworth R. B. and Hawkins G. S. (1963). "Statistics of meteor streams". *Smithsonian Contributions to Astrophysics*, **7**, 261–285.

The author, Regina Rudawska, in front of her poster with Vincent Perlerin. (Credit Dominique Richard.)

Meteor television observations in Russia

Anna Kartashova

Institute of Astronomy of the Russian Academy of Sciences, Moscow, Russia
akartashova@inasan.ru

The meteor television observations are carried out at several Russian observatories. The Institute of Astronomy RAS carries out meteor observations and supports observations by the Geophysical observatory IDG RAS and the Irkutsk State University. Ryazan State University participates in these observations too. Mikhail Maslov takes active part in television meteor observations in Novosibirsk. The results of INASAN observations are presented.

1 Introduction

Meteor observations have as a specific property that we do not know in advance either the area at the celestial sphere, or the time when the event occurs. Besides, a meteor flash in the atmosphere has a duration of few seconds or less. Therefore wide-field view cameras are being used for meteor observations.

2 Meteor TV observations in Russia

The territory of Russia is very extended and the meteor networks are located in different parts of Russia. In *Figure 6* a distribution of the stations is shown on a map of Russia. In the central part of Russia INASAN takes active part in meteor observations (Kartashova, 2013) and supports observations in the East at Irkutsk (Komarova, 2010; Kartashova and Bagrov, 2012). Meteor observations are carried out by Ryazan State University (near Moscow) from two stations (Murtazov, 2011). Meteor observations in Novosibirsk are under supervision of amateur astronomer Mikhail Maslov[1] (IMO code: MASMI). The wide-field of view cameras used for meteor observations in Russia are listed in *Table 1*.

Table 1 – Parameters of the meteor television systems.

Place	Camera	FOV (°)	Lm (mag)
ZO INASAN	WATEC 902H Ultimate (6/0.8)	50x40	+5.0
"ISTRA"	WATEC 902H Ultimate (6/0.8)	50x40	+5.0
IDG RAS	WATEC 902H Ultimate (6/0.8)	50x40	+5.0
RSU-1,2	WATEC 902H Ultimate (6/0.8)	50x40	+5.0
Novosibirsk	WATEC 902H Ultimate (0.8/3.8)	70x93	+3.6
Irkutsk-1,2	WATEC 902HS (6/0.8)	50x40	+5.0

[1] http://feraj.narod.ru/

Figure 1 – Locations of video meteor stations in the central part of Russia.

3 Meteor observations INASAN

The Institute of Astronomy RAS is one of the science institutes of the Russian Federation providing systematic optical meteor observations and supervises several meteor groups in Russia (Kartashova and Bagrov, 2012).

Double-station observations at INASAN with PatrolCa and MobilCa systems started in 2011 at the Zvenigorod observatory and "Istra" station (Kartashova, 2013). The results of the double-station observations are shown in *Figure 2–3*.

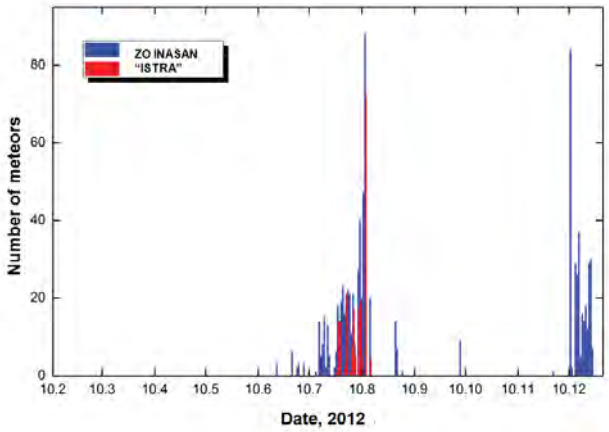

Figure 2 – The distribution of the number of meteors detected at the ZO INASAN and "Istra" in 2012.

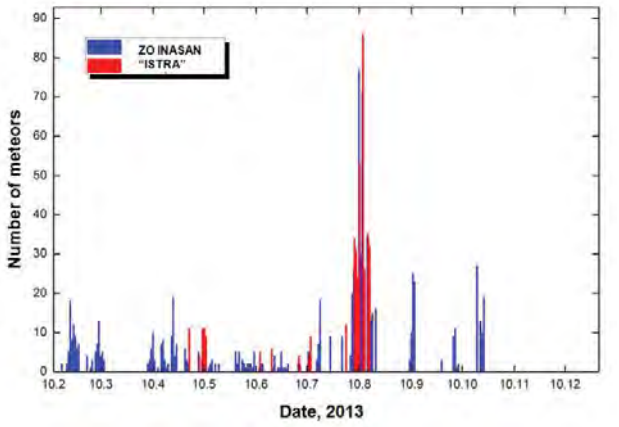

Figure 3 – The distribution of the number of meteors detected at the ZO INASAN and "Istra" in 2013.

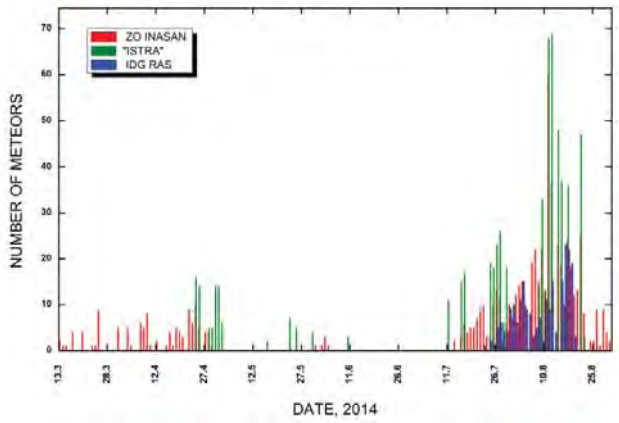

Figure 4 – Results of multi-station observations in 2014 (from three stations).

The weather in the region of Moscow is not very useful for optical observations and we have approximate 120–150 nights (including the nights partly cloudy) per year. The main part of the observations in 2012–2014 was conducted during the summer period (in the period of the Perseid meteor shower activity). The multi-station observations were carried out at 5 stations during this year (*Figure 1*): Zvenigorod observatory (ZO INASAN), "Istra" station, Ryazan State University (RSU) and a station at 18 km from this station (RSU-2) and the Geophysical observatory IDG RAS (GO IDG RAS). The total basis is 240 km. The results of the observations from the ZO INASAN, "Istra" station and GO IDG RAS are presented in *Figure 4*.

The results of the observations at three stations from July 17 until August 30, 2014 are presented in *Figure 5*.

146 double-station meteors were detected for the basis ZO INASAN – "Istra" station and 77 meteors for the basis ZO INASAN – GO IDG RAS. During this year the 22 multi-station meteors (from three stations) were obtained from July 17 until August 20.

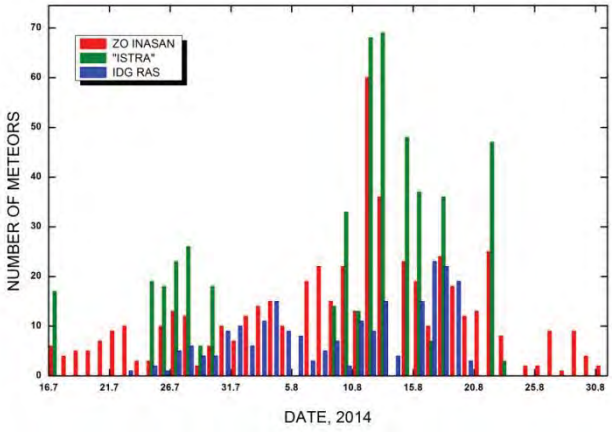

Figure 5 – Results of the multi-station observations of the Perseids activity period 2014 (from three stations).

4 Conclusion

The observations are carried out according to the unified methodology in the region of Ryazan, Irkutsk and Moscow which helps to get objective information about meteoroid streams in the Solar System and the influx of meteoroid matter to the Earth. We are planning to continue our observations and to increase the number of cameras as well as the number of stations.

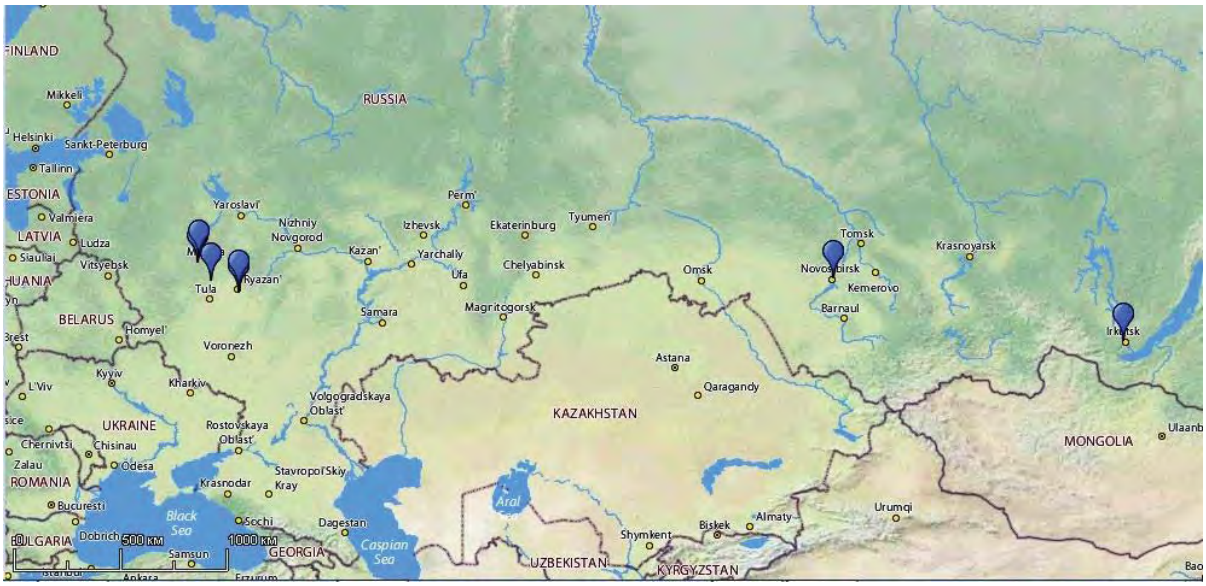

Figure 6 – Locations of television meteor stations in Russia.

Acknowledgment

I would like to thank A. Bagrov, G. Bolgova, A. Murtazov, O. Popova, Yu. Poklad, and Yu. Rybnov for their help with the observations.

References

Kartashova A. (2013). "Television meteor observations in INASAN". In Gyssens M., and Roggemans P., editors, *Proceedings of the International Meteor Conference*, La Palma, Canary Islands, Spain, 20–23 September 2012. IMO, pages 174–177.

Kartashova A. P., Bagrov A. V. (2012). "Meteor observations under the INASAN supervision". *Abstract book European Planetary Science Congress 2012*, Madrid, Spain, 23–28 September 2012. Id. EPSC2012-122.

Komarova Yu. (2010). "The definition of an accessory of separate meteors to meteoritic streams by observations in Irkutsk". *Izvestiya of Irkutsk State University*, **3** , № 2, 97–102.

Murtazov A. (2011). "Arrangement of integrated meteor TV-observations at the Ryazan State University Astronomical Observatory". *Vestnik of the Siberian State Aerospace University*, **39**, 109–113.

The author, Anna Kartashova, during her lecture. (Credit Dominique Richard.)

Software for analysis of visual meteor data

Kristina Veljković and Ilija Ivanović

Petnica Meteor Group, Valjevo, Serbia
mackikac@gmail.com, ilija91ivanovic@gmail.com

In this paper, we will present new software for analysis of IMO data collected from visual observations. The software consists of a package of functions written in the statistical programming language *R*, as well as a *Java* application which uses these functions in a user friendly environment. *R* code contains various filters for selection of data, methods for calculation of Zenithal Hourly Rate (ZHR), solar longitude, population index and graphical representation of ZHR and distribution of observed magnitudes. The Java application allows everyone to use these functions without any knowledge of *R*. Both *R* code and the *Java* application are open source and free with user manuals and examples provided.

1 Introduction

This paper presents results of software development for analysis of IMO visual meteor data. The software consists of a package of functions written in the statistical programming language *R*, as well as a *Java* application. The purpose of *R* functions is to provide basic analysis, and the *Java* application is developed with the aim of making use of these functions in a user friendly environment.

The *R* package *MetFns* contains data frames with visual meteor data (rate or magnitude data), as well as various filters for the selection of the data, methods for calculation of Zenithal Hourly Rate (ZHR), solar longitude, population index and a graphical representation of the ZHRs and the observed magnitude distributions.

The developed *Java* application allows users to call *R* functions without any knowledge about the *R* programming language. Although its purpose is to be a proxy for these functions, the application contains a few extra features which can be useful to users. The application uses a standard graphical interface, and it contains help files from the *R* package.

All the software is open source and free, with manuals and examples provided for both software packages.

The rest of the paper is organized as follows. In Section 2, we provide details about the installation of package *MetFns* and the application *MetRApp*. The description of the *R* package and the *Java* application is given in Sections 3 and 4, respectively. Finally, conclusions are drawn in Section 5.

2 Installation

In order to install the *R MetFns* package, follow these steps:

1. (if not already installed) download and install the latest version of *R*[1];
2. Download the packages *astroFns*[2] and *plotrix*[3];
3. Download the package *MetFns*[4];

In order to install the *MetRApp* application:

1. (if not already installed) download and install latest *JRE*[5];
2. Download and install the *Runiversal* package from *CRAN*[6];
3. Download the application[7].

Please note: In our software we use many components developed by third party organizations. We are not responsible for that content. Also, please note that as new versions of those components are developed, and you use them, they may not be compatible with our software. We will try to keep up with new versions of these components, but if you encounter difficulties, please contact us.

3 R package

The *R* package *MetFns* consists of data frames containing visual meteor data and functions which manipulate these data. Data frames can be divided into three sections, by their type:

a. Yearly rate data named *rateXX*, where XX represents the two last digits of the year;

b. Yearly magnitude data named *magnXX;*

c. Accompanying data includes data frames *radiant* with coordinates of shower radiants throughout the year, *shw_list*, *vmdbpers* and *vmdbsite* with a list of observed meteor showers, observers and observing sites, respectively.

Functions that manipulate visual meteor data can be divided into four types:

[1] cran.r-project.org

[2] cran.r-project.org/web/packages/astroFns/
[3] cran.r-project.org/web/packages/plotrix
[4] cran.r-project.org/web/packages/MetFns/
[5] http://www.oracle.com/technetwork/java/javase/downloads/index.html?ssSourceSiteId=ocomen
[6] http://cran.r-project.org/web/packages/Runiversal/
[7] https://bitbucket.org/ivail/metrapp (alternatively it may be hosted on www.meteori.rs)

- Functions that read rate or magnitude data from the IMO site or file saved on a computer, named *read.rate(data)* and *read.magn (data);*
- Functions that select (filter) data by one or more criteria;
- Functions that perform some calculations over data;
- Functions that draw graphics with the data;

Next, we will cover the last three types of functions in more detail.

Filter functions

The Package *MetFns* contains 13 individual filter functions and a global filter. Some filters can be used only on rate data and it will be specified in the description of the filter.

In the following examples, we suppose that all rate and magnitude data are previously loaded (using *data* function, for example data rate00)

- *filter.shw (data, shw)* selects data for a given visual meteor dataset and specified shower code. For example, if we want to select data for the Perseids from the rate data for the year 2000, we would call the function *filter.shw* in the following way

  ```
  filter.shw (rate00, shw="PER")
  ```

  If we wish to do the same selection for the magnitude data, we would type in the *R* console

  ```
  filter.shw (magn00, shw="PER")
  ```

- *filter.date (data, year, month, day.beg, day.end=day.beg)* selects data for a given visual meteor dataset and specified year, month and day (or days). By default, the argument *day.end* (ending day) is set to be equal to *day.beg* (beginning day). So, if the argument *day.end* is not provided, the function *filter.date* selects data for a given date, otherwise it selects data for a period of days, limited by *day.beg* and *day.end.*

  The day given in meteor datasets corresponds to the beginning of the observing time period. For the selection of the data, the day corresponding to the middle of the observing time period is used. For example, to select rate data for the period from 5–15 August 2007, we would type

  ```
  filter.date (rate07, year=2007,
  month=8, day.beg=5, day.end=15)
  ```

  In a similar way, we would select the magnitude data.

- *filter.time (data, time.low, time.up)* selects data for a given visual meteor dataset and specified time period. Arguments *time.low* and *time.up* are in the format 0–2359 specifying the lower and upper boundary of time respectively in hours and minutes.
- *filter.imocode (data, imocode)* selects data for a given visual meteor dataset and specified IMO observer code.
- *filter.obsname (data, name, name)* selects data for a given visual meteor dataset and specified observer's first and last name. It can be used when one is not certain of the IMO observer code (due to possible non-uniqueness of the five letter combination).
- *filter.gc (data, long.low=0, long.up=180, ew=c ("E","W"), lat.low=0, lat.up=90, ns=c ("N","S"))* selects data for a given visual meteor dataset and specified geographical coordinates of the observing site or interval of geographical coordinates. The arguments *long.low* and *long.up* represent, respectively, the lower and upper boundary of longitude and *lat.low* and *lat.up* are, respectively, the lower and upper boundary of latitude.

  If the values of the arguments *long.low* and *long.up*, as well as *lat.low* and *lat.up*, are the same, *filter.gc* selects data for a particular observing site. This filter enables one to select data only by longitude or latitude, with the geographical coordinates being between given boundaries, less than, greater than or equal to a boundary.

  For example, if we wish to select magnitude data for the year 2004 for a site with longitude 19.7E and latitude 44.2N, we would type into the *R* console.

  ```
  filter.gc (magn04, long.low=19.7,
  long.up =19.7, ew="E", lat.low=44.2,
  lat.up=44.2, ns="N")
  ```

- *filter.site (data, site)* selects data for a given visual meteor dataset and specified observing site. In order to use this filter, the argument *data* has to consist of the column named *"sitecode"*.
- *filter.country (data, country)* selects data for a given visual meteor dataset and specified country. The data selection is performed using *filter.site* which filters data by codes of all sites belonging to the specified country. As for the function *filter.site*, data has to contain the column named *"sitecode"*.
- *filter.sol (data, sol.low=0, sol.up=359.999) s*elects data for a given visual meteor dataset and specified solar longitude or interval of solar longitudes.
- *filter.F (data, F.low=1, F.up=3)* selects data for a given visual meteor rate dataset and specified correction factor or interval of correction factor for clouds. Arguments *F.low* and *F.up* represent, respectively, the lower and the upper boundary for the correction for clouds.
- *filter.mag (data, mag.low=2.0, mag.up=7.5)* selects data for a given visual meteor dataset and specified limiting magnitude or interval of magnitudes. The arguments *mag.low* and *mag.up* are, respectively, the lower and the upper boundary of the limiting magnitude.

- *filter.h (data, shw, Ralpha=NULL, Delta=NULL, h.low=10, h.up=90)* selects data for a given visual meteor dataset, specified shower and its radiant elevation or interval of radiant elevations. The arguments *h.low* and *h.up* specify, respectively, the lower and the upper boundary of the radiant elevation.

- *filter.totcor (data, shw, Ralpha=NULL, Delta=NULL, r, C=5)* selects data for a given visual meteor rate dataset, specified shower, population index and correction factor. The correction factor is equal to (Rendtel and Arlt, 2008)

$$C = \frac{r^{6.5-lmg} F}{\sin(h)},$$

where r is the population index, *lmg* the limiting magnitude, F the correction factor for clouds and h the radiant elevation. One needs to specify the maximum value of the correction factor C (default value of C is 5).

- The function *filter* performs various data selections for a given visual meteor dataset. It is a wrapper function for all previously mentioned filters.

For example, if we want to select rate data for observations of the Perseids in Serbia, time period 5–15th August 2007, limiting magnitude of 5.5 or higher and a total correction factor less than 5, we would use

```
filter (rate07, shw="PER",
year=2007, month=8, day.beg=5,
day.end=15, country= "Serbia",
mag.low =5.5, r=2.2)
```

Calculation functions

In our *R* package, we have three functions that perform different calculations on visual meteor data.

- *solar.long (year, month, day, time)* calculates the solar longitude with respect to the equinox of 2000.0 (Steyeart, 1991) for a given year, month, day and time in hours.

- *zhr (data,year, month, day.beg, day.end, shw, r=NULL, Ralpha=NULL, Delta=NULL, k, c=1)* calculates the average zenithal hourly rate (ZHR) of a meteor shower for a given rate dataset, specified shower, period of days, population index, length of time interval and ZHR correction. The average zenithal hourly rate is given by the formula

$$\overline{ZHR} = \frac{c + \sum_{i=1}^{k} n_i}{\sum_{i=1}^{k} \frac{T_{eff,i}}{C_i}}$$

where k is the number of observing periods, n_i - the number of meteors seen during the observing period i, $T_{eff,i}$ - the effective time or amount of time an observer actually scans the sky for meteors during the observing period i, and C_i – a correction factor.

In the numerator, c is included to correct for the asymmetric high and low end possibilities in a Poisson distribution (Bias, 2011.). By default, it is set to 1.

The standard error of the average zenithal hourly rate is calculated by the formula

$$\sigma = \frac{\overline{ZHR}}{\sqrt{c + \sum_{i=1}^{k} n_i}}$$

The spatial number density of meteoroids producing meteors of magnitude at least 6.5 is (per 10^9 km^3) (Koschack and Rendtel, 1990a)

$$\rho = \frac{(10.65r - 12.15)\overline{ZHR}}{3600 \cdot 178700 r^{-1.82} V},$$

where V is the stream's geocentric velocity.

The standard error of the spatial number density is approximated with

$$\sigma_\rho \cong \frac{\sigma \cdot \rho}{\overline{ZHR}}$$

Day is divided in subintervals of k hours. For example, if $k=12$, subintervals are $[0,12)$ and $[12,24)$. Zenithal hourly rate is calculated for each subinterval in the following manner: If the middle of an observer's time period belongs to the subinterval, his/her data values are used in calculation of ZHR.

For example, if we want to select visual meteor data for observations of the Orionids, period 20-24th October 2006, 12 hour time intervals, and calculate ZHR

```
rateOri <- filter (rate06,
shw="ORI", year =2006, month=10,
day.beg=20, day.end=24)

zhr (rateOri, year=2006, month=10,
day.beg =20, day.end=24, shw="ORI",
r=2.5, k=12)
```

- *pop.index (data, year, month, day.beg, day.end=day.beg, shw, mag=-6:7)* calculates the population index of a meteor shower for a given magnitude dataset, specified period of days and magnitude values.

The cumulative summarized magnitude distribution $\Phi(m)$ is formed by summing cumulative frequencies of all observers for each magnitude class m.

Using the relationship $r = \frac{\Phi(m+1)}{\Phi(m)}$ and substituting 0, 1,...,m magnitudes, equation $\Phi(m) = \Phi(0) \cdot r^m$ (or $\ln \Phi(m) = \ln \Phi(0) + m \ln r$ in logarithmic form) can be written. Then, population index r is calculated by the

method of least squares, for the chosen range of magnitude values.

The standard error of the population index is approximated with

$$\sigma_r \cong r\sqrt{\frac{\sum_{i=1}^{n} e_i^2}{(n-2)\sum_{i=1}^{n} m_i^2}}$$

where n is the number of magnitude values, e_i regression residuals, $i=1,2,\ldots,n$.

The interval for regression is chosen such that: there are at least 3 meteors per magnitude class, the faintest magnitude classes are not included ($m \leq 4$ or in exceptional cases $m \leq 5$) and there are at least 5 magnitude classes available (Koschack and Rendtel, 1990b). All these conditions are fulfilled for the range of magnitude values printed in the results.

To select magnitude data for observations of the Perseids, time period 1-20th August 2007 and calculate the population index using magnitudes -6 to +4, we would type

```
magnPer <-filter (magn07, shw="PER",
year=2007, month=8, day.beg=1,
day.end=20)
pop.index (magnPer, year=2007,
month=8,          day.beg=1,
day.end=20, shw="PER", mag=-6:4)
```

Drawing graphs functions

We have two functions of this type.

- *mag.distr (data, year, month, day.beg, day.end=day.beg, shw)* graphically represents magnitude distribution for a given magnitude dataset, specified meteor shower and period of days. It returns a plot of summarized magnitude distribution consisting of histogram and box-plot.

  For example, to select data for observations of the Perseids, period 12-14th August 2007 and make a graphic of magnitude distribution, we would type into *R* console

  ```
  magnPer <-filter (magn07, shw="PER",
  year =2007, month=8, day.beg=12,
  day.end=14)

  popI.distrib (magnPer, year=2007,
  month=8, day.beg=12, day.end=14,
  shw="PER")
  ```

- *zhr.graph (data, year, month, day. beg, day.end=day.beg, shw, r=NULL, Ralpha=NULL, Delta=NULL, k, c=1, type=c ("UTC", "sol"))* represents graphically the average zenithal hourly rate of a meteor shower with error bars for a given rate dataset, specified shower, period of days, population index, length of time interval, ZHR correction and a type of x-axis display.

  For type="*UTC*", the tick marks on the x-axis represent coordinated universal time (UTC), set *k* distance apart, with labels specifying date (at 00:00 UTC). For type="*sol*", the tick marks and the labels on the x-axis represent the solar longitude, corresponding to the above mentioned time in UTC.

  Function *zhr.graph* returns the *xy* plot of the Zenithal Hourly Rate, with time (UTC) or solar longitude on the *x*-axis and the ZHR on the *y*-axis. The ZHR is represented with black filled circles with 68% confidence intervals/one sigma error bars.

  For example, to select data for observations of the Orionids, period 20–26th October 2006, 6hrs time intervals, and to generate a ZHR graph we would type:

  ```
  rateOri <-filter (rate06, shw="ORI",
  year =2006, month=10, day.beg=20,
  day.end=26)

  zhr.graph (rateOri, year=2006,
  month=10, day.beg=20, day.end=26,
  shw="ORI", r=2.5, k=6, type="UTC")
  ```

4 MetRApp – Java Application

The motivation for this application was to provide a simple user interface to the *R* package and to allow all users to use its functions without any necessary knowledge of *R*. Currently, it is developed only as a desktop application, but with potential to be moved to the web.

User experience

This application uses a standard graphical user interface to communicate with users. The setup needed for runtime is only to provide the paths for the installation of *R* and other resources needed to run the application (datasets, tables etc.).

Software architecture of MetRApp

This application is developed using standard three tier architecture. All compiled versions and the application are available at the link given in section 2 and it can be independently developed by other organizations. The application is developed using *Java* 7 and *Netbeans IDE*. The version control software is *git* and the repository host is *Bitbucket*. A short description of the software architecture of this application is provided too, as a starting point for any potential extensions.

Data tier

MetRApp does not maintain any data in the databases since its function is to be a proxy between the *R* package and the users. However, since the results of the execution of the *R* code are contained in *R* data structures,

appropriate domain classes have to be implemented in *MetRApp*.

In this case, a domain class for the *R data frame* has to be implemented. Three *Java* classes are implemented to provide an appropriate representation of data from the *R data frame* – abstract class *DataFrame*, and two classes which extend the previous one – *StringDataFrame* and *DataFrameFromCSV*. More details about domain classes are provided in the documentation in the project's repository.

In addition to these domain classes, more of them had to be implemented for the IMO data. These new classes are a representation of, for example, persons or sites instances in the corresponding datasets. Also, the *R* code which is used to evaluate data is inserted in the class *InitialRCode.*

Logic tier

The logic part of this system is implemented in several packages. The first part contains filters for the selection of data which correspond to the previously explained *R* filters. These '*Java* filters' had to be implemented to avoid unnecessary parsing of data in the communication between *MetRApp* and *MetFns.* This approach allows very fast filtering of data which is done in *MetRApp* only, without calling *R* code. However, only 11 of the 13 filters could be fully implemented in *Java* because of the dependency on third – party functions available exclusively in *R* for some filters.

The architecture of this package is very basic – there is an abstract class *JavaFilter* which is then extended by concrete filters which implement the logic of the appropriate *R* filter. This abstract class has reference to the current dataset which is used in the application runtime, and also provides the abstract method which accepts *HashMap* of parameters which are needed for a concrete filter to be executed.

As stated before, *MetRApp* calls *R* functions to evaluate data and returns the result to the user. This communication is achieved using *RCaller*[8], a software library for calling *R* functions within *Java* programs. The idea behind *RCaller* is very simple – the *Java* program (in this case *MetRApp*) is the caller and it sends requests (containing *R* code and data) via *XML* and accepts responses, again in *XML* format.

The logic tier of the application also contains a few controllers which are responsible for dispatching calls between objects and for providing an essential backbone for all implemented functionalities. The controllers also have references to all data sources and they provide a control on their correct usage.

Presentation tier

As stated before, this application uses a standard graphical user interface platform. It is based on *Swing* components, without any additional customization (and dependencies). The structure of the presentation tier is not very well optimized, since new efforts were made to move this application to the web.

Future improvements

A very large part of the application is implemented using software patterns which provide a large flexibility and very much simplify the implementation of new functionalities. Six software patterns were implemented in the application, but not all of them are currently used.

Requests for new functionalities are welcome, as well as reviews of the current version of the software. Our group will continue to develop this software, but also support new initiatives by branching this code base.

5 Conclusion

The developed software covers a vast majority of use cases[9] specified by our meteor observation group. Due to its modular architecture, it is possible to expand the application specification and to provide additional features if needed. All resources including source code, test examples, documentation and other files are provided at public repositories, and everyone can develop their specific distribution of this software. We hope that other IMO observers will find our software useful. However, if new features are requested, we shall try to implement them in new releases of our software.

Acknowledgment

We would like to thank Branislav Savić whose suggestions and comments were invaluable in developing our software.

References

Bias P. V. (2011). "A Note on Poisson inference and extrapolations under low raw data and short interval observation conditions". *WGN, Journal of the IMO*, **39**, 14–19.

Koschack R. and Rendtel J. (1990a). "Determination of spatial number density and mass index from visual meteor observations (I)". *WGN, Journal of the IMO*, **18**, 44–58.

Koschack R. and Rendtel J. (1990b). "Determination of spatial number density and mass index from visual meteor observations (II)". *WGN, Journal of the IMO*, **18**, 119–140.

Rendtel J. and Arlt R., editors (2008). IMO Handbook For Meteor Observers. IMO, Potsdam.

Steyaert C. (1991). "Calculating the Solar Longitude 2000.0". *WGN, Journal of the IMO*, **19**, 31–34.

[8] https://code.google.com/p/rcaller/

[9] http://en.wikipedia.org/wiki/Use_case

Atmospheric research and meteoric dust detection by all-sky polarization measurements of the twilight sky

Oleg S. Ugolnikov[1] **and Igor A. Maslov**[1,2]

[1] **Space Research Institute, Russian Academy of Sciences, Moscow, Russia**

[2] **Moscow State University, Sternberg Astronomical Institute, Moscow, Russia**

ougolnikov@gmail.com, imaslov@iki.rssi.ru

The paper describes the results of wide-field polarization measurements of scattered emission in the upper atmosphere during the dark period of twilight. The field of single scattering makes it possible to retrieve the temperature profile of the mesosphere and to estimate the contribution of dust particles. An increase in dust concentration was noticed during the Perseid shower activity period in 2013. The maximum of the dust depolarization effect precedes the visual Perseid maximum but it is in good agreement with the meteor activity index in a nearby location.

1 Introduction

The mesosphere of the Earth is the least-investigated layer of the atmosphere owing to its physical properties and impossibility of long series of *in situ* measurements. Neither planes or balloons nor spacecraft can fly through this layer. The principal means of exploration are optical remote measurements, both from space and from the ground.

The mesosphere is also the place of possibly the fastest climate change on the Earth. Greenhouse gases (like carbon dioxide) which create the "global warming" effect near the ground start the opposite process of radiative cooling above 70 km. The negative temperature trend is not well-known due to absence of long-term measurements, but different estimations listed in (Beig, 2003) give the values up to -1K per year.

The fast cooling of the mesosphere is the most probable reason for noctilucent cloud (NLC) appearances in Europe in the late 19th century. The clouds consist of water ice requiring the temperature to be below 150K at altitudes ~85 km. The condensation nuclei are the tiny meteoric dust particles.

The twilight method of mesospheric remote sensing can be effective for a temperature profile retrieval (if the scattering is Rayleigh-dominated) and for scattering medium investigations including meteoric dust detection and investigations. This can be done if the polarization of the twilight sky is measured together with the intensity. Polarization data also help to separate the multiple scattering which is a basic problem of the twilight analysis.

2 Observations

The method of single and multiple scattering separation and retrieval of scattering matrices depending on the altitude require a rich set of simultaneous intensity and polarization measurements over a large number of sky points during the whole twilight period. This can be successfully performed by an all-sky camera designed for polarization measurements (see *Figure 1*). First; two lenses (1 and 2) create an infinitely remote image of the sky with the zenith angle up to 70°. The visible size of the image is reduced by a factor of 10, and collimated rays cross the polarization filter. Lens 3 creates the secondary sky image on the CCD.

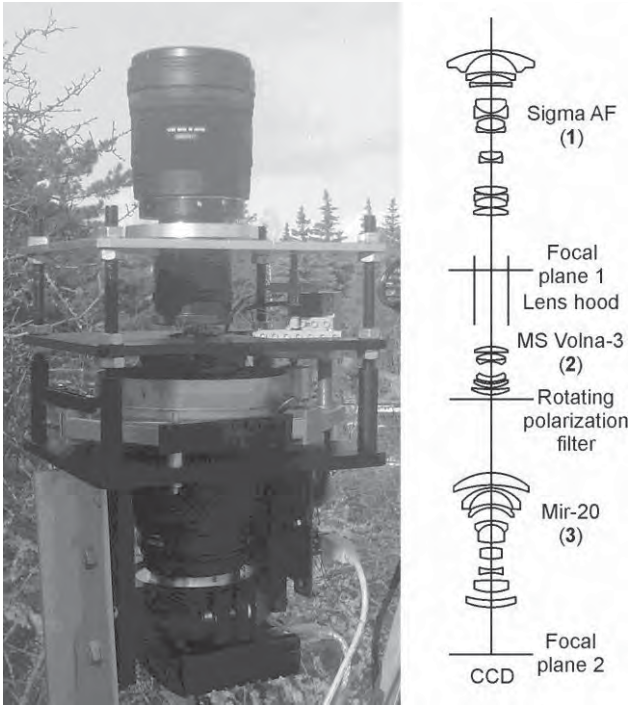

Figure 1 – All-sky polarization CCD-camera and its optical scheme.

Observations started in 2011 at a point (55.2° N, 37.5° E), south of Moscow. The measurements were carried out in a spectral band with effective wavelength equal to 540 nm.

A detailed description of the measurements and of the method of multiple scattering separation are made in

(Ugolnikov and Maslov, 2013). The same paper also contains the results of the temperature analysis. The accuracy of simple measurement is about 5K, the values are in good agreement with space measurements by TIMED/SABER and EOS Aura/MLS instruments.

3 Meteoric dust detection

Most parts of a meteoric mass entering the vicinity of the Earth is burned or moderated in the mesosphere. The meteor products can create the dust layers at different altitudes. Additional twilight sky brightness during the major shower maxima was found in a number of papers starting from (Link and Robley, 1971). But the numerical procedure of dust detection required the multiple scattering separation which was a very difficult problem in the 20th century.

The accuracy of detection of difficult twilight background components can be sufficiently increased using the polarization data. The meteor dust is being detected as the decrease in single scattering polarization. The detailed description of the procedure can be found in (Ugolnikov and Maslov, 2014). The basic parameter calculated from the observational data is the polarization characteristic q:

$$q = p(\theta) / p_R(\theta) \qquad (1)$$

Here p and p_R are measured and the Rayleigh (molecular) polarization of a single light ray-scattered by the angle θ. This parameter is close to unity in a pure gas condition and decreases in the case of dust appearance.

Figure 2a shows the values of q in the atmospheric layer above 80 km for the observations performed in 2011-2013. We see that this value is a little bit less than unity for most of the dates showing the possible effect of the sporadic dust. A remarkable minimum is seen during August 2013. It is probably related to the Perseid shower.

However, a detailed picture for August (*Figure 2b*) shows that the temporal depolarization profile is shifted to earlier dates compared to the traditional Perseid visual maximum, but in very good agreement with television data for the same year and from a nearby location (Kartashova, 2014). We should notice that the visible maximum on the 12th of August is defined by large particles, and the dust layer is formed by a small fraction, whose activity profile is not well-known. Some peaks before and after maximum were noticed in (Bel'kovich and Ishmukhametova, 2006) and they may also coincide with depolarization effects.

The analysis shows that the dust causing the additional scattering and depolarization effect has a maximum concentration at altitudes decreasing from 83 to 81 km during the Perseid activity. It is also close to the NLC typical altitudes, which is not a surprise knowing the physical relation between these phenomena.

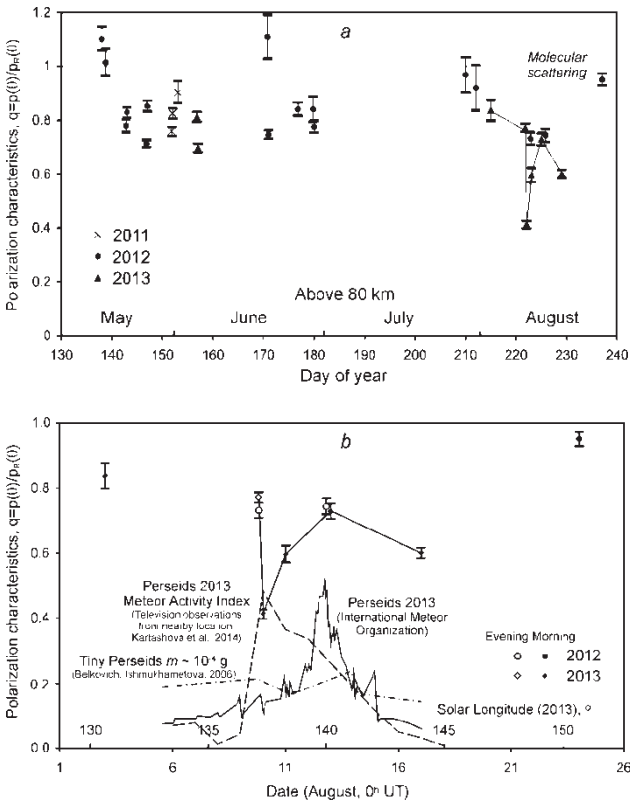

Figure 2 – Single scattering characteristics depending on the date in summer (a) and in August (b) compared to the Perseid activity profiles.

4 Conclusion

Twilight analysis provides an effective tool to solve the different problems of middle and upper atmosphere physics. When multiple scattering is correctly separated, the data can be used for temperature analysis, meteoric dust detection and noctilucent cloud particles investigation.

The effects of the dust inflow can be seen for the major showers like the Perseids. A difference in dust inflow and visual meteor activity profiles is noted. This is related to different profiles for large and small particles, the last one not being too well-known.

All-sky cameras used for scattering analysis during twilight can also be used for meteor registrations during the night. However, the polarization filter and the multi-lensed optics required for correct polarization measurements reduce the sensitivity of the camera.

Acknowledgement

The work is supported by the Russian Foundation for Basic Research: Grant 12-05-00501-a.

References

Beig G., Keckhut P., Lowe R. P., Roble R. G., Mlynczak M. G., Scheer J., Fomichev V. I., Offermann D., French W. J. R., Shepherd M. G., Semenov A. I., Remsberg E. E., She C. Y., Lübken F. J., Bremer J., Clemesha B. R., Stegman J., Sigernes F., and Fadnavis S. (2003). "Review of mesospheric temperature trends". *Reviews of Geophysics*, **41**, 1015–1055.

Bel'kovich O. I., Ishmukhametova M. G. (2006). "Mass distribution of Perseid meteoroids". *Solar System Research*, **40**, 208–213.

Kartashova A. P. (2014), private communication.

Link F., Robley R. (1971). "Meteoritic contamination of the upper atmosphere by the Quadrantid shower". *Planetary and Space Science*, **19**, 1585–1587.

Ugolnikov O. S., Maslov I. A. (2013). "Summer mesosphere temperature distribution from wide-angle polarization measurements of the twilight sky". *Journal of Atmospheric and Solar-Terrestrial Physics*, **105–106**, 8–14.

Ugolnikov O. S., Maslov I. A. (2014). "Mesosphere light scattering depolarization during the Perseids activity epoch by wide-angle polarization camera measurements". *Planetary and Space Science*, **92**, 117–120.

The author, Oleg Ugolnikov, during his lecture. (Credit Axel Haas.)

April ρ Cygnids

Maria Hajdukova Jr.[1], Regina Rudawska[2], Leonard Kornos[2] and Juraj Toth[2]

[1] **Astronomical Institute, Slovak Academy of Sciences, Dubravska cesta 9, Bratislava, SK-84504, Slovakia**
Maria.Hajdukova@savba.sk

[2] **Faculty of Mathematics, Physics and Informatics, Comenius University, Mlynská dolina, Bratislava, SK-84248, Slovakia**
Rudawska@gmail.com
Leonard.Kornos@fmph.uniba.sk
Juraj.Toth@fmph.uniba.sk

We examined the recently-established April ρ Cygnids meteor shower (ARC, IAU#348), discovered by the Canadian Meteor Orbit Radar survey (CMOR; Brown et al., 2010), and later confirmed by video observations made by the Cameras for Allsky Meteor Surveillance project (CAMS; Phillips et al., 2011). As reported by Neslusan and Hajdukova (2014), the ARC is suspected to be a part of a broader meteor shower complex, possibly associated with the long-period comet C/1917 F1 (Mellish). According to their model, one of the filaments of the meteoroid stream originating from the comet corresponds to the April ρ Cygnids. However, the similarity between the mean characteristics of the predicted and the real showers is not clear. Here, we present a dynamical study of the April ρ Cygnids orbits, extracted from several catalogues, using the Rudawska et al. (2014) identification method. The catalogues used include the EDMOND database (Kornos et al., 2014 a, b) and the SonotaCo shower catalogue (SonotaCo, 2009). The results of the orbital evolution of the comet and orbits of the ARC, including published orbits of the ARC from CMOR and CAMS, are presented. The conclusion as to their common origin is also discussed.

1 Summary

In order to check a possible link between the April ρ Cygnids and comet Mellish, the orbital evolution of the comet and the ARC were studied. The behavior of the orbital elements of comet C/1917 F1 (Mellish) reconstructed backwards for 50000 years was compared with the corresponding evolution of the orbital elements of the April ρ Cygnids, determined from the various meteor databases.

We selected April ρ Cygnids from the EDMOND and SonotaCo databases (44 and 21 orbits, respectively) using an independent identification method proposed by Rudawska et al. (2014). The weighted mean values of the orbital elements and geocentric parameters for each sample were determined. Moreover, we used the mean parameters of published orbits of the ARC provided by CMOR and CAMS. The nominal orbit of C/1917 F1 (Mellish) and four mean orbits of the ARC were numerically integrated backwards. In this integration, each ARC orbit is represented by 18 modeled particles distributed equidistantly by 20 degrees in mean anomaly.

The modeled particles of the ARC from all four datasets move in very distinct orbits in comparison to each other, as well as to the relatively stable orbit of comet C/1917 F1 (Mellish). This raises the question of whether the selected particles from the different data correspond to the same meteor shower. However, 11 from 18 particles, modeled along the mean orbit of the ARC determined by Brown et al. (2010), undergo the same orbital evolution ($D_{SH} < 0.1$) as comet Mellish for the time period from about -42000 to -44000 years. This could support the ARC association with the comet. On the other hand, the particles modeled along the mean orbits from the other three datasets do not support their common origin. All 18 particles modeled along the mean orbit determined by Phillips et al. (2011) show similar orbital evolutions to the comet only in the short period from -1600 to -2000 years; after that their orbits split. Theoretical particles along the SonotaCo ARC mean orbit behave similarly to the comet only in the time period about -8000 to -11000 years. In the EDMOND catalogue, none of the particles modeled show a similarity in their evolution to the comet's orbit under $D_{SH} = 0.1$, and only 9 theoretical particles under $D_{SH} = 0.15$, for the time about 11000 years before the present.

The results obtained did not allow us to draw any clear conclusions about the association of the ARC with comet C/1917 F1 (Mellish). The precision of the comet Mellish orbit determination (Asklöf, 1932) is, unfortunately, not very high. The probability of a significant discrepancy with reality increases when integrating this orbit backward in time. Moreover, we know that the geocentric velocity of a meteoroid orbit is usually a poorly determined parameter; similarly, the eccentricity of a meteoroid orbit. This is then reflected in a poor determination of the corresponding semi-major axis and influences the results of the integration.

Acknowledgment

This work was supported by the Slovak Grant Agency for Science VEGA, grant No 1/0225/14, and by the Slovak Research and Development Agency under the contract No. APVV-0517-12.

References

Asklöf S. (1932). *Arkiv for Mat. Astron. och Fys.*, **23A**, 11.

Brown P., Wong D. K., Weryk R. J., Wiegert P. (2010). "A meteoroid stream survey using the Canadian Meteor Orbit Radar II: Identification of minor showers using a 3D wavelet transform". *Icarus*, **207**, 66–81.

Kornos L., Koukal J., Piffl R., Toth J. (2014b). "Edmond Meteor Database". In Gyssens M., Roggemans P., and Żołądek P., editors, *Proceedings of the International Meteor Conference*, Poznań, Poland, 22–25 August 2013. IMO, pages 23–25.

Kornos L., Matlovic P., Rudawska R., Toth J., Hajdukova M. Jr., Koukal J., Piffl R. (2014a). "Confirmation and characterization of IAU temporary meteor showers in EDMOND database". In Jopek T. J., Rietmeijer F. J. M., Watanabe J., and Williams I. P., editors, *Meteoroids 2013, Proceedings of the Astronomical Conference*, held at A. M. University, Poznań, Poland, 26–30 August 2013. A.M. University Press, pages 225–233.

Neslušan L., Hajduková M. Jr., (2014). "The meteor-shower complex of comet C/1917 (Mellish)". *Astronomy & Astrophysics*, **566**, Article A33, 1–9.

Phillips M., Jenniskens P., Grigsby B. (2011). "Confirmation of the April Rho Cygnids (ARC, IAU#348)". *WGN, Journal of the IMO*, **39**, 131–136.

Rudawska R., Matlovic P., Toth J., Kornos L. (2014). "Independent identification of meteor showers in EDMOND database". In Rault J.-L., and Roggemans P., editors, *Proceedings of the International Meteor Conference*, Giron, France, 18–21 September 2014. IMO, pages 98–100.

SonotaCo (2009). "A meteor shower catalog based on video observations in 2007–2008". *WGN, Journal of the IMO*, **37**, 55–62.

The author, Maria Hajdukova, browsing the 2013 Poznan Proceedings, with Pete Gural at right. (Credit Axel Haas.)

Activity and observability of meteor showers throughout the year

Peter Zimnikoval

Observatory Banská Bystrica, Slovakia
zimnikoval@gmail.com

Diagrams on the poster present the activity periods of meteor showers as well as the rising and setting times of meteor shower radiants. Plotted are sunrises, sunsets and the period of twilight. It was constructed according to data from the IMO Meteor Shower Working List. More active showers are displayed in red and less active showers in green. The diagrams are calculated for geographic latitudes of 40° N, 0° and 40° S. The time scale is given as local time at the relevant zonal meridian and supplemented by local daylight saving time. The diagrams contain rounded values of solar longitude J2000.
The star chart shows the radiant positions and drift of IMO meteor showers while the other diagrams display shower activity and date of maximum.

References

McBeath A. (2013). 2014 Meteor Shower Calendar, IMO.

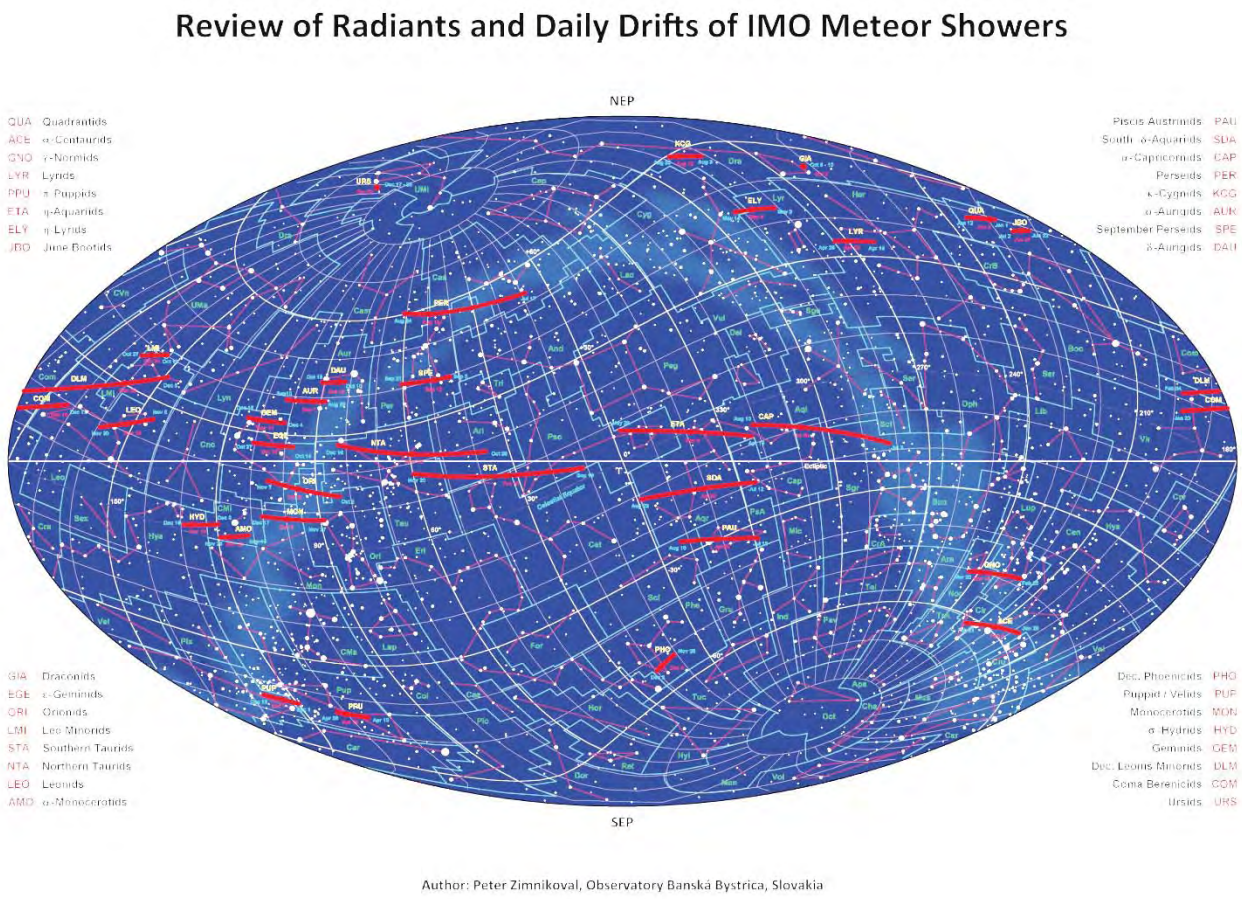

Figure 1 – Radiant positions and drift for all IMO meteor showers.

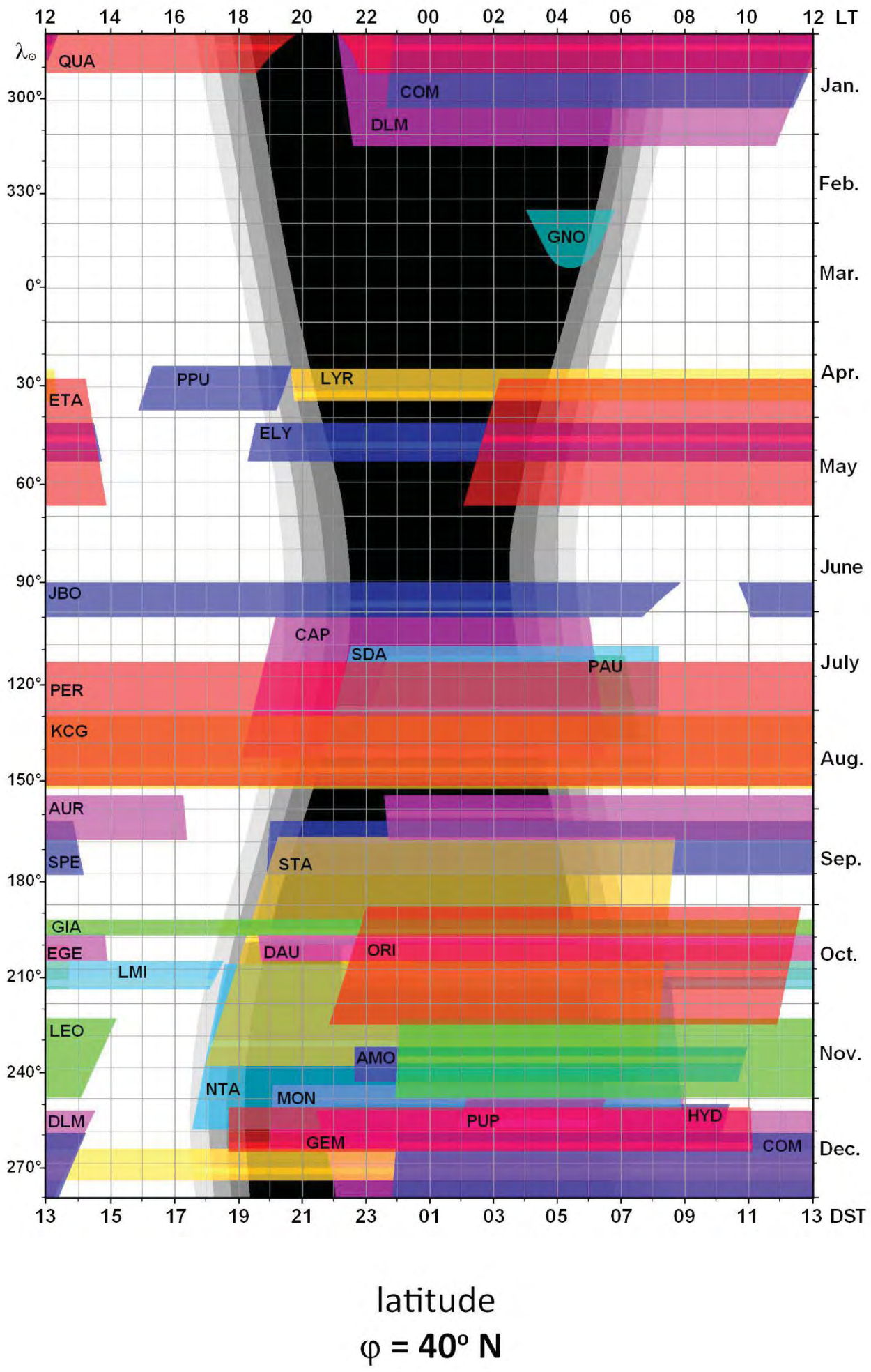

Figure 2 – Meteor shower activity and visibility diagrams for latitude 40°N.

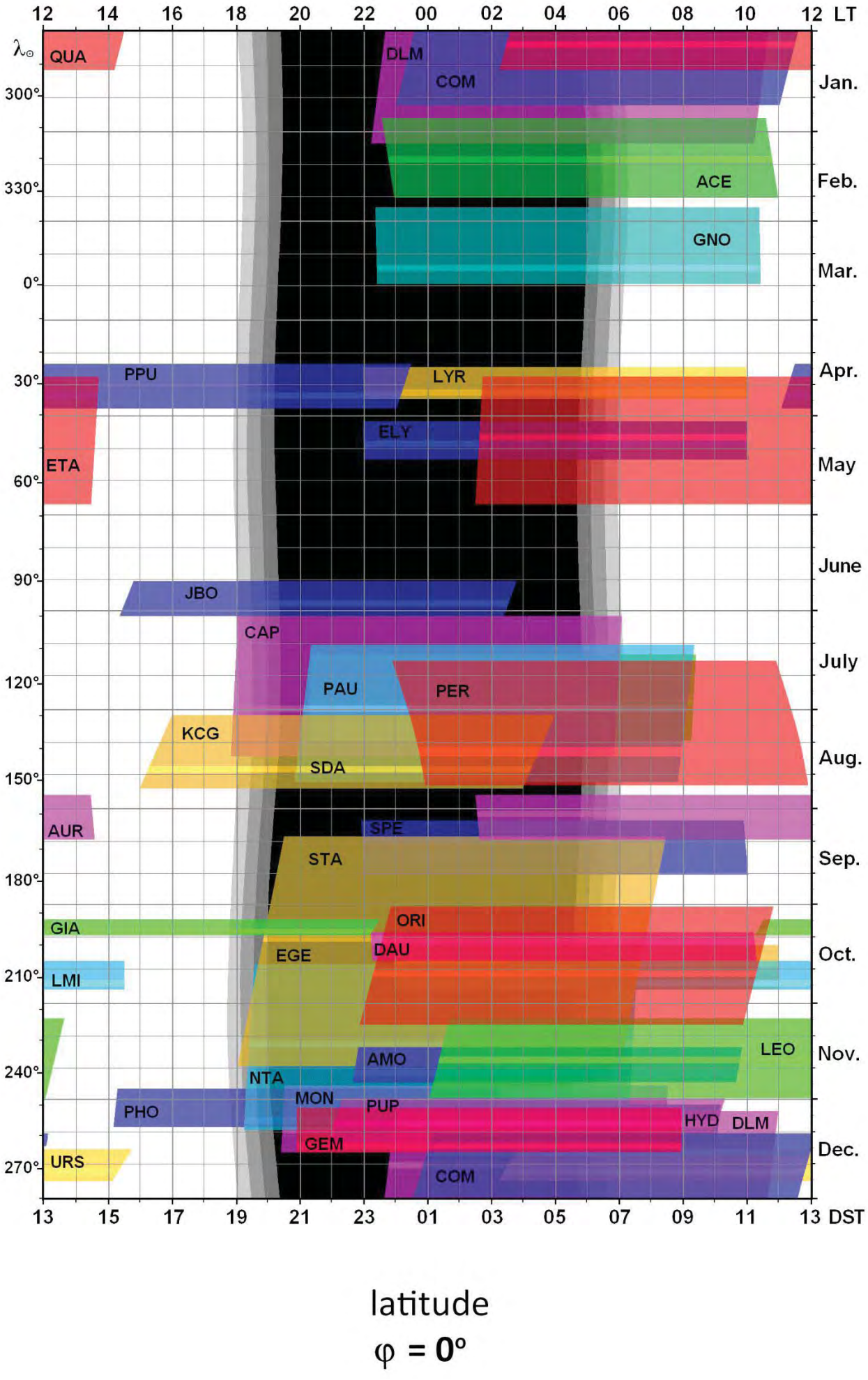

Figure 3 – Meteor shower activity and visibility diagrams for latitude 0° (equator).

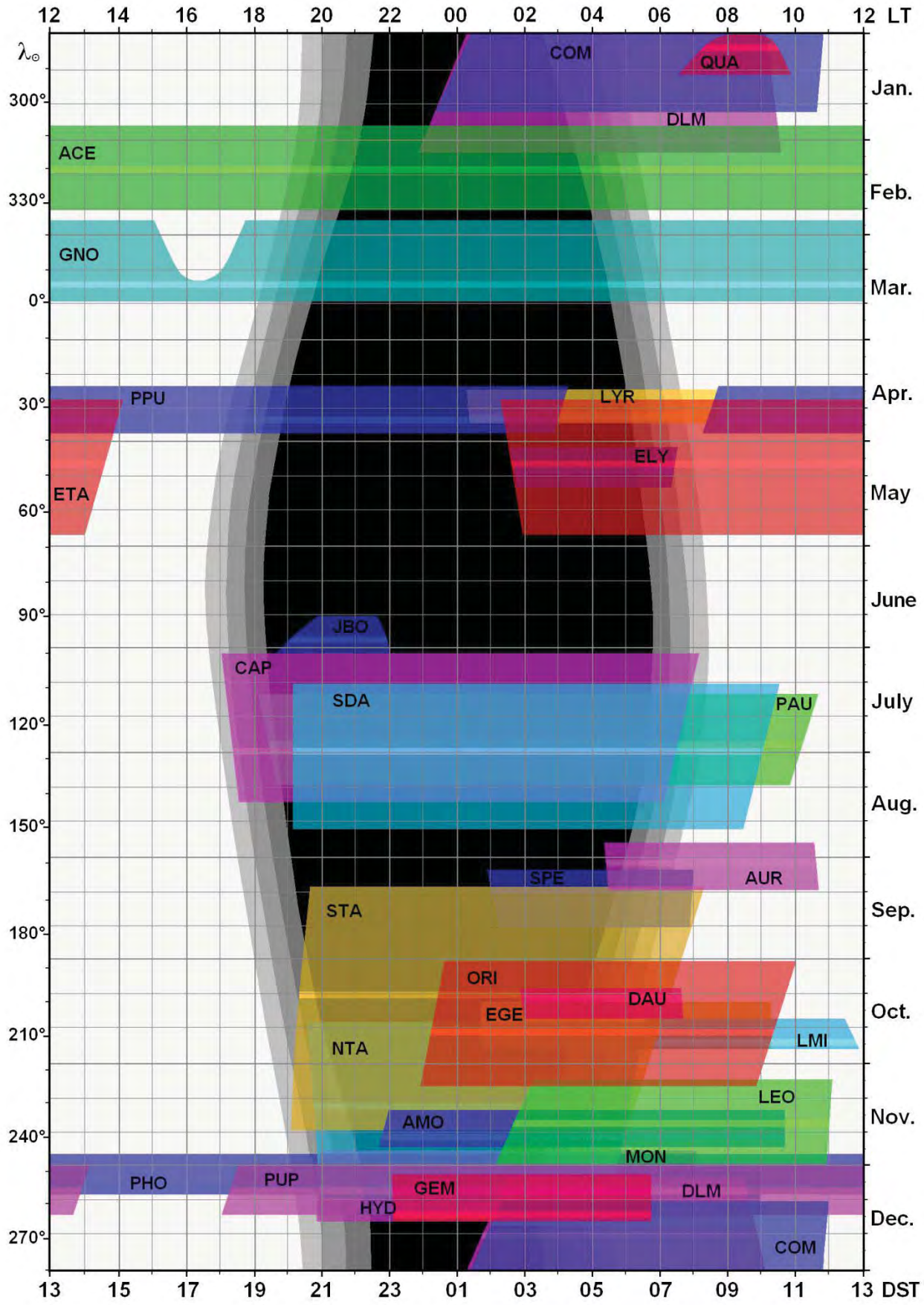

latitude

φ = 40° S

Figure 4 – Meteor shower activity and visibility diagrams for latitude 40°S.

Observations of Leonids, Draconids, α-Monocerotids, ε-Perseids and meteors of comet C/2012 S1 (ISON)

Alexander Golubaev[1], Ivan Bryukhanov[2], Anastasia Tabolich[2], Valentin Tabolich[2], Anastasia Kulakovskaya[2], Dmitry Akulich[2] and Ivan Sergey[3]

[1] **Astronomical Institute of Kharkiv V.N. Karazin National University, Kharkiv, Ukraine**
Alexandr_sky@mail.ru

[2] **Amateur astronomers, the Republican center of technical creativity, team "Astrobloknot", Minsk, Belarus**
betelgeize_astro@mail.ru

[3] **Amateur astronomers, team "Astrobloknot", Molodechno, Belarus**
seriv@rambler.ru

Our group presents new results of the "All-Sky Beobachter" astronomical project which is based on previous experience with different wide-field cameras (All-Sky). In this project we search for meteor phenomena in images obtained with All-Sky cameras. As a result coordinates of radiants of active meteor showers are calculated. In this paper we provide the final result for meteors of comet C/2012 S1 (ISON) found in the period from 05 to 27 January, 2014. Also, we present three possible candidates for the radiant of meteors of comet C/2012 S1 (ISON).

1 Introduction

Our group presents new results of the "All-Sky Beobachter" astronomical project which is based on previous experience of working with different wide-field cameras (All-Sky). In this project we search for meteor phenomena in images obtained with All-Sky cameras. As a result coordinates of radiants of active meteor showers are calculated.

2 Observations of Leonids, Draconids, α-Monocerotids and ε-Perseids

All-Sky cam images were collected in the period 2010 – 2013 and a search for Leonids meteors was conducted on these images. The calculated coordinates of the radiant of the Leonids meteor shower for the mentioned four years are presented in *Figures 1 – 4*. Although the Moon was in the constellation of Leo in 2011, it was possible to detect Leonids activity. Nevertheless only two stationary meteors were found.

In 2012 we detected that the α-Monocerotids meteor shower displayed activity simultaneously with the Leonids, during its maximum activity (*Figure 3*).

In 2011 observing conditions for the Draconids meteor shower were unfavorable due to strong interference of the moonlight. Nonetheless meteors and their coordinates were detected in All-Sky images (*Figures 5 – 6*).

In September 2013 many observers noticed an unexpected increase in activity of the ε-Perseids, a minor meteor shower. Using images of the All-Sky camera at the Liverpool Telescopes we were able to calculate the radiant coordinates of this meteor shower. (*Figure 7*).

An analysis of the results of the search for meteor activity in the All-Sky images shows that it is impossible to detect meteor shower activity during one day if its activity is less than 20 meteors per hour, and when meteors are fainter than +2 – +3 magnitude (for the fast meteors). To detect any activity of a meteor shower with meteors fainter than magnitude +3 and with an average or low angular velocity the meteor activity must be at least 15 meteors per hour. When combining all archived observations for some days from all accessible All-Sky cameras then it's possible to detect the activity of meteor showers with a ZHR value of 10 or more meteors per hour. We got the same results during our work on the data for the Geminids meteor shower for the period 2009 – 2010 (Bryukhanov, et. al., 2012, 2013).

3 Investigation of the possibilities of All-Sky cameras to search for meteors of comet C/2012 S1 (ISON)

In this paper we provide the final results for meteors of comet C/2012 S1 (ISON) found in the period 5 to 27 January, 2014. Also, we present three possible candidates for the radiant position of meteors of comet C/2012 S1 (ISON) (*Figures 8, 9 and 11*).

While analyzing the All-Sky images some fireballs indicated a very uncertain radiant close to the theoretical one. A photo of one of the brightest fireballs is presented in *Figure 10*.

Special research to detect some possible meteoric activity connected to the remains of comet C/2012 S1 (ISON) was conducted in January 2014. This work was based on the observing data obtained at various sites on Earth, by means of 10 CCD cameras, equipped with a "fish-eye" lens (like all-sky cameras) and by means of FM radio observations. Exposure times vary from 60 to 180 seconds for different CCD cameras. The interval between

the images obtained varies from 10 to 120 seconds under Full Moon.

The theoretical research on the possible occurrence of some meteoric activity associated with the close approach of the central point of the orbit of comet C/2012 S1 (ISON) to the Earth has been published (Sekhar and Asher, 2014). The authors drew the conclusion that such meteoric activity is unlikely. However we decided to check the existence or lack of the meteoric activity connected with comet C/2012 S1 (ISON), using the observational data which was at our disposal.

A special technique and the computer program described in (Neslušan et al., 1998) were applied to calculate a theoretical radiant of the meteor shower. Calculations are based on known elements of the heliocentric orbit of comet C/2012 S1 (ISON) published in the Minor Planet Electronic Circular (M.P.E.C. 2012-S63). We present the observing conditions of the possible meteoric activity: α=153°, δ=+16.8°. The maximum of activity was expected on January 16.2, 2014 at $\lambda_{\odot(2000.0)}$=295.7°. On the day of the estimated maximum the Earth passed at a distance of 0.02 a.u. to the closest point of the orbit of the comet where it was 74.7 days prior to its perihelion passage. On 16 January the closest point of the comet's post-perihelion orbit was located at 0.4 a.u. from the Earth. Therefore any meteoric activity connected to the remains of the comet is unlikely after the perihelion passage.

4 Results of CCD and FM radio detection of meteors

43 meteor events were revealed after viewing 54000 images from the period 10 to 17 January 2014. The radiant of the meteors was located in the constellations of UMa, LMi, Leo and Lyn. The position measurements of the images and calculations by means of the program 'RADIANT[1] (1.43) gave the following radiant position: α=156°, δ=+38° (*Figure 11*).

The greatest number of meteors was observed during the period from January 10 to 15, 2014 as a result of the two supervision cameras located at the SAO of the Russian Academy of Sciences (in the Northern Caucasus). The maximum number of meteors was registered on 12 January in observations obtained by means of a camera located at La Palma. Unfortunately, as the sky was strongly lit by the Moon (a Full Moon on 16 January 2014), it failed to get complete observing material for the dates close to the expected maximum of meteoric activity.

Patrol observations of a meteor background with FM broadcast radio on 88.6 MHz by Ivan M. Sergey were carried out in Belarus (*Figure 12a*). An increase in the meteor activity level of the sporadic background was recorded during the period from 8 to 24 January 2014. During this period an increase of the meteor activity above the level of the sporadic background was confirmed by radio observations at 143.05 MHz by Morillas Sanchez (EA7GA)[2] in Spain (*Figure 12b*).

5 Conclusions

All the supervision photographs used in the research weren't suitable. Therefore the orbital elements of the recorded meteoric bodies weren't calculated. The good agreement between the temporary period and the region of the meteor activity with the theoretical prediction gives reasons to assume that the meteors were genetically related to the comet C/2012 S1 (ISON). The meteor activity was very low and was confirmed by the lack of a pronounced active radiant of the meteor shower. Thus, the meteor shower was observed as surge in activity of the sporadic meteors compared to the usual level of the sporadic background. The coordinates of the radiant were found only thanks to the large amount of statistical material collected in various observing posts on the Earth. Possibly some weak meteor activity can be explained by the passage of the Earth through the peripheral part of a swarm of dust particles which have been ejected by comet C/2012 S1 (ISON). The results of the observations are being carefully checked now.

Acknowledgment

We thank William E. Smith, Timofey A. Avilin, Sergei Schmalz and Evgeniya N. Baturina for their help in this work.

References

Bryukhanov I. S., Korotkiy S. A., Lapitsky Z., Molchanov L., Ushakov K., Gain A., Grabovsky R., Starovoytov D., Chernyavsky M., Chernik A., Nazaruk M., Nazaruk I., Poluyanova S., Tumash L., Semenkov-von Zdorrfe A., Prokopovich A., Akulich D., and Zaritskaya E. (2012). "Geminids 2002, 2009, and 2010: a brief report on an experiment with visual and photographic observations and images of all-sky cameras". In Gyssens M., and Roggemans P., editors, *Proceedings of the International Meteor Conference*, Sibiu, Romania, 15–18 September 2011. IMO, pages 102–104.

Bryukhanov I. S, Sergey I. M., Vatutina V., Ivchik A., Pogodina M., Vatolin R., Dovnar S., Osadchaya V., Tabolich A., Tabolich V. (2013). "All-Sky cameras for observation and investigation of variable stars and meteor showers". *Odessa Astron. Publ.*, **26**, 38–42.

Golubaev A. V., Bryukhanov I. S., Tabolich A., Tabolich V., Akulich D., Kulakovskaya A., Mechinsky V. A., Sergey I. M. (2014). "Preliminary Results of the Observations of a Meteor Shower of Comet C/2012 S1 (ISON) in

[1] http://www.imo.net/software/radiant (Rainer Arlt).

[2] http://www.rmob.org/index.php (Lorenzo G. Sanchez).

January 2014". *Astronomicheskii Tsirkulyar*, **1611,** 1–4.

Neslušan L., Svoreň J., Porubčan V. (1998). "A computer program for calculation of a theoretical meteor-stream radiant". *Astronomy & Astrophysics*, **331**, 411–413.

Sekhar A. and Asher D. J. (2014). "Meteor showers on Earth from sungrazing comets". *Monthly Notices of the Royal Astronomical Society*, **437**, L71–L75.

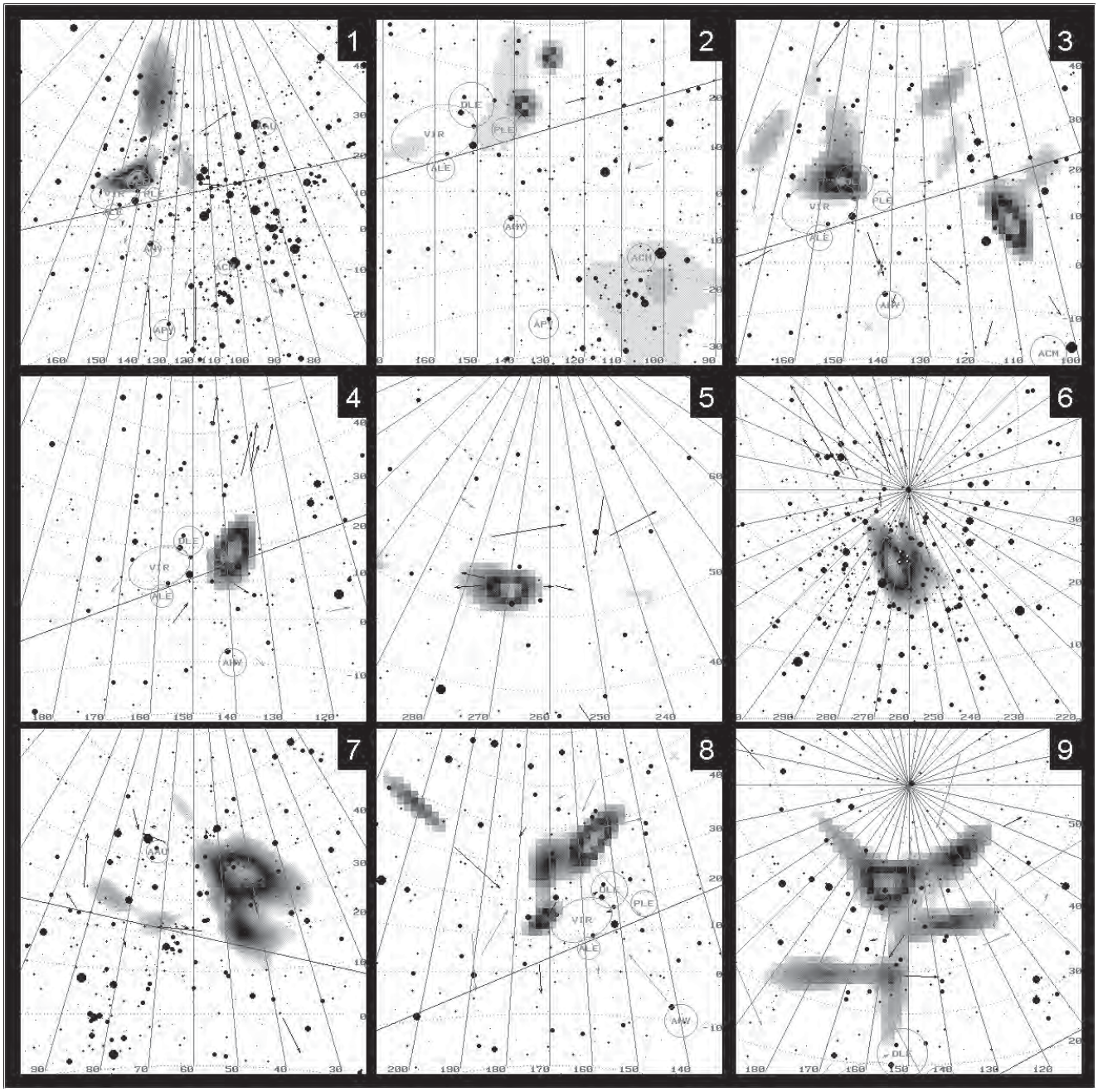

Figures 1 to 9 – meteor shower radiant: **(1)** - Leonids - 2010, RA=152°, Dec=+21°; **(2)** - Leonids - 2011, RA~135°, Dec~+25°; **(3)** - Leonids - 2012, RA=155°, Dec=+21° and α-Monoceratides - 2012, RA=108° , Dec=+09°; **(4)** - Leonids - 2013, RA=138°, Dec=+19°; **(5)** -Draconids - 2011, RA=270°, Dec=+52°, all-sky camera IRF; **(6)** - Draconids - 2011, RA=274°, Dec=+45°, all-sky camera SAO; **(7)** - ε-Perseids - 2013, RA=43°, Dec=+38°; **(8)** - Radiants of meteors of comet C/2012 S1 (ISON) RA~155°, Dec~+45°, all-sky camera The Liverpool Telescope's, January 12, 2014; **(9)** - Radiants of meteors of comet C/2012 S1 (ISON) RA~165°, Dec~+65°, all-sky camera SAO, January 13 - 14, 2014.

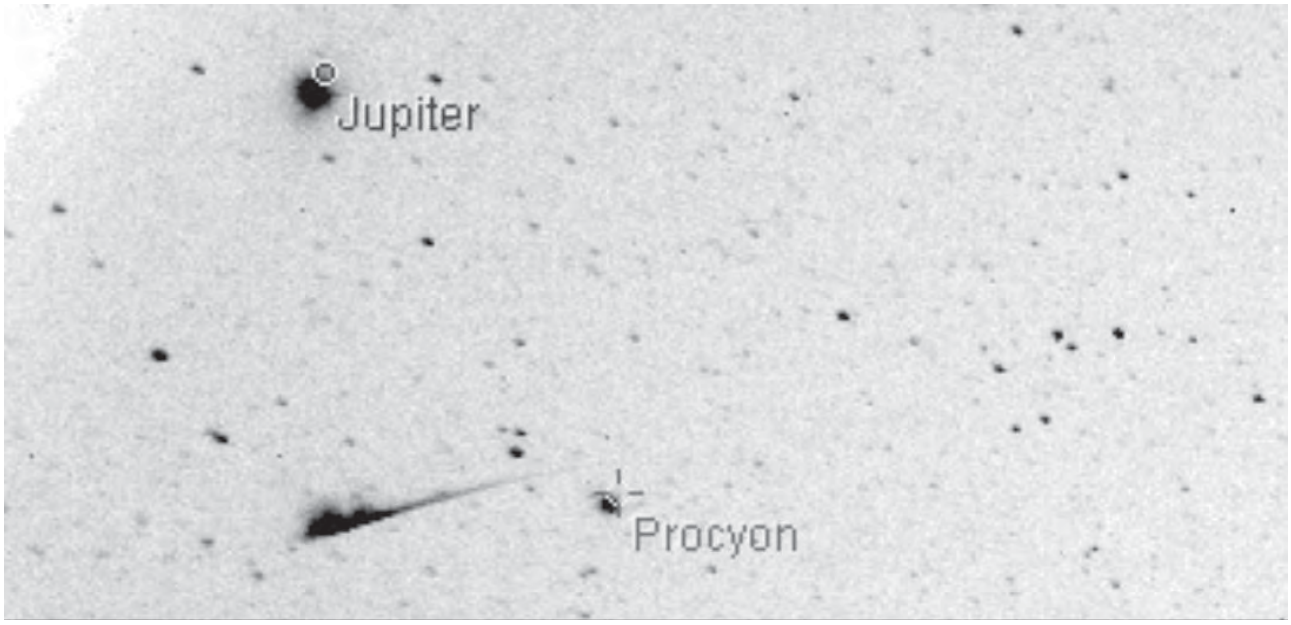

Figure 10 – Fireball (magnitude -3) at the theoretical meteor shower radiant of comet C/2012 S1(ISON): all-sky camera in Australia, January 13, 2014, 18^h03^m UT.

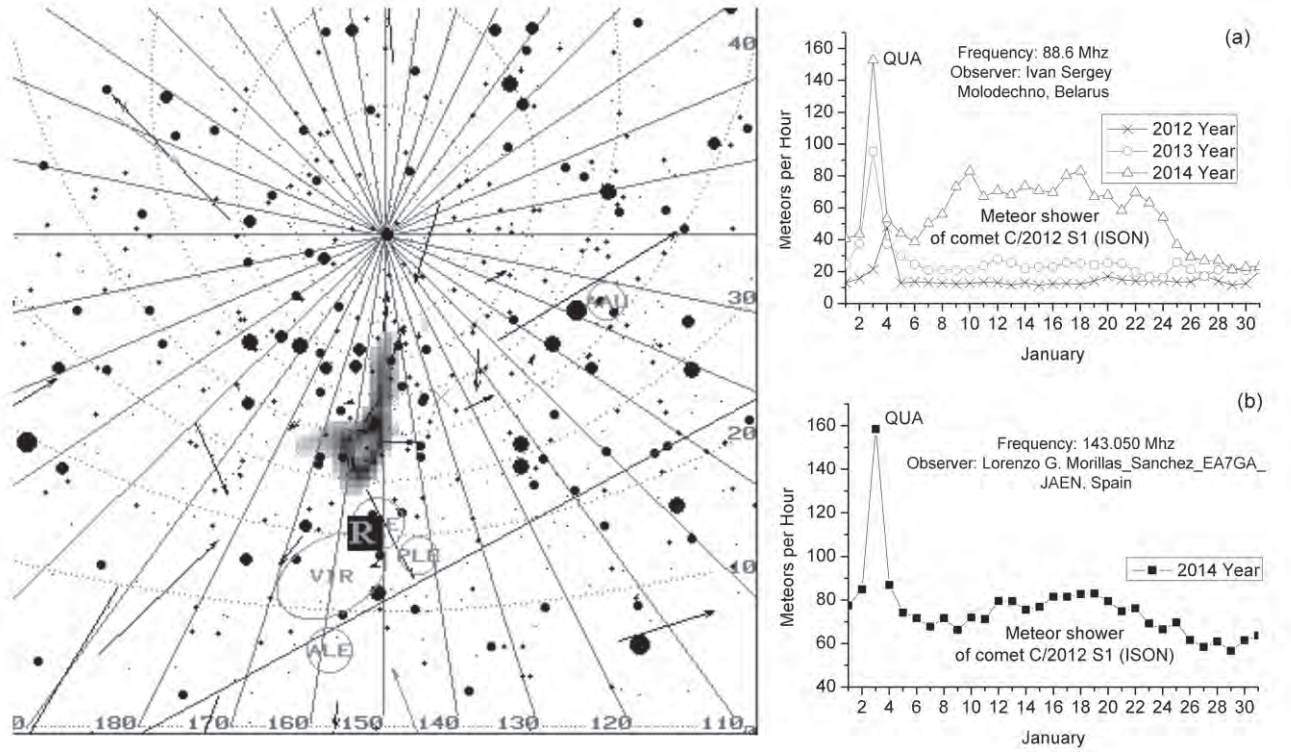

Figure 11 and 12 – Results of CCD observations in January 2014 of a meteor shower of comet C/2012 S1 (ISON). R - theoretical radiant. Observations of meteor background in FM radio frequency range: (a) - (January, 2012, 2013 and 2014, at 88.6 MHz) were carried out in Belarus; (b) - (January 2014, at 143.05 MHz) carried out in Spain; QUA - meteor shower Quadrantids.

Automatic detection of meteors using artificial neural networks

Victor Ştefan Roman[1] **and Cătălin Buiu**

[1] **Dept. of Automatic Control and Systems Engineering, Politehnica University of Bucharest. Bucharest, Romania**
victor.roman@acse.pub.ro

Automatic meteor detection is an important activity in the field of meteor studies. In recent years, various studies have been made on this topic, underlining the interest for the automatic detection of meteors in radio or video recordings of the sky.
In this paper, three novel automatic meteor detection solutions using artificial neural networks are presented. The proposed solutions are trained to analyze radio recordings and extract the meteor samples found within. Two different types of neural networks are tested in this paper, each having its own take on how it detects meteors. Test results report high meteor detection rates on average, of above 70% for all three techniques.

1 Introduction

On its path around the Sun, Earth interacts with a large quantity of small space objects, be it dust grains or small rocks. These spatial objects, called meteoroids, hold useful information about our Solar System and therefore it is useful to study these to better understand our cosmic neighborhood. One important activity in the field of meteor studies is the actual detection of meteors. Although a part of the meteor identification is still done manually, several studies on automatic meteor detection techniques have been made in recent times. There are several advantages with the automatic detection of meteors, ranging from ease of access to meteor data, to a more in depth understanding of meteor showers, all the way to meteor tracking and retrieval.

In the present paper, three automatic meteor detection techniques and their performances are presented. All three techniques employ artificial neural networks (ANNs) to analyze a given set of recordings, and to extract those samples of the input set that they detect as being meteors. Two types of neural networks are used in this study, the classic Multi-Layer Perceptron (MLP) network and the Self-Organizing Map (SOM). These two types of ANNs are used to analyze data coming from two types of radio recordings: raw audio data and spectrograms of the radio recordings.

2 The automatic meteor detection techniques

Detecting meteors in an automatic fashion means extracting a small number of data samples from a much larger input dataset through an algorithm that is able to recognize the meteors from any other type of signals. Furthermore, the detection process has to be fast enough to be considered as a replacement for the manual detection of meteors. These requirements have led us to choose neural networks as the algorithms that will tackle the automatic meteor detection problem.

ANNs are mathematical models of the biological neural networks found in the human nervous system. They emulate most of their biological counterpart's functions and structure. An ANN is a collection of interconnected neurons, which resemble the biological neurons and function in a similar manner. The ANNs need to be trained in order to solve the problem that they are used for, which means they have to be exposed to the object of their work (i.e. in the case of this study, to meteors). In light of the way they are trained, ANNs can be separated in two classes: supervised training ANNs and unsupervised training ANNs. In the present study, a network from each of the two classes was chosen to be used in the automatic detection of meteors.

Self-organizing maps

The first type of neural network trained in this study is the self-organizing map (Kohonen, 1990), (Kohonen, 2001), (Roman and Buiu, 2014). This type of ANN is a competitive learning neural network that clusters data onto a two-dimensional topographic map of neurons. The input data is clustered based on similarity, which leads to the formation of several regions within the self-organizing map where like samples are grouped together. Depending on the problem at hand, the SOM's clustering, and the regions that are formed within the map, are an indication of the number of distinct objects that the neural network has found in the input dataset. A visual representation of a SOM network is presented in *Figure 1*.

The SOM is trained using an unsupervised, competitive algorithm that searches for the neuron in the network which is the most similar (i.e. having the smallest distance) to the input sample, and trains only that neuron and its closest neighbors, with the learning rate and neighborhood distance decaying in time. The end result of a SOM is a 2D map in which data is clustered based on similarity (i.e. similar inputs will be mapped in the same region of the output map), therefore no previous knowledge about the input samples is required, hence the unsupervised nature of the training algorithm.

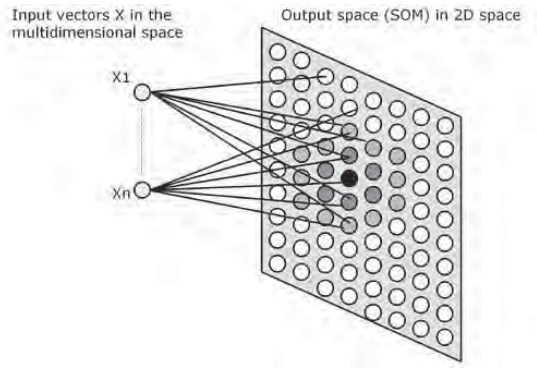

Figure 1 – Simple visual representation of a self-organizing map.

The advantages of using a SOM are the visual end result that this neural network provides, the ability to work with unlabeled data and the training algorithm that the SOM uses, which requires no previous knowledge about the training dataset.

Multi-layer Perceptrons

The second type of neural network used in this study is the MLP (Rumelhart and McClelland, 1986) network, which is one of the oldest types of neural networks. Compared to the SOM network, the MLP uses a different type of training algorithm and a different strategy of analyzing data. A MLP neural network uses supervised training algorithms, which require the network to be taught what types of data it has to be able to recognize. In *Figure 2* a visual representation of a typical MLP neural network is shown.

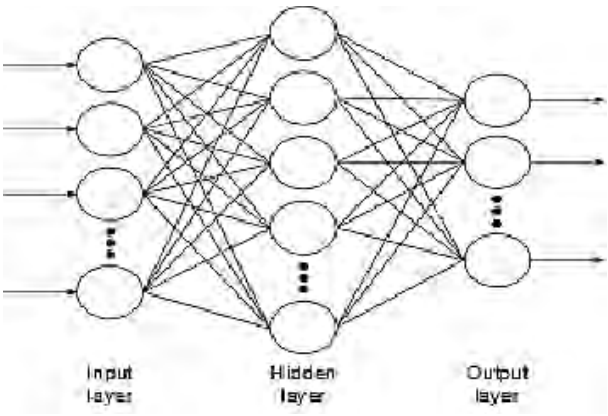

Figure 2 – Typical visual representation of a multi-layer perceptron.

The algorithm used to train the MLP networks in this study is the back-propagation algorithm. This technique implies that a sample is fed to the network and it will pass from layer to layer, going through to the output layer. The output of the network will be compared to the expected output (hence the supervised nature of the training algorithm) and the difference between the two (i.e. the error) will be propagated backwards into the network, modifying the neurons, and thus training the network to know how to respond to that type of input in the future. When the training is finished and an input is given, the MLP network will analyze the input and identify which class of signals (among those used to train the network) the input is part of.

The main advantages of using MLP networks are the speed of training and the simple and easy to read output that the network provides.

3 Results

As previously mentioned, three automatic meteor detection techniques are tested in this study. Using each of these techniques involves going through a three step process: preparing the input data for usage, training the neural network and testing the network's performances in meteor detection.

Two types of input were used in the present study. The first type was the raw audio recordings of radio data. These types of recordings involved two preprocessing steps before they were used to train ANNs. The first process was a filtering process, through which parts of the spectrum were eliminated from the recording (due to the fact that those parts never contained meteor samples), while the second process was a sampling process, after which the recording was broken into 0.1 second long samples, while the sampling process sliding window was 0.05 second long. These sampling process parameters were chosen because it was observed that most meteor samples are at least 0.1 second long. In *Figure 3*, an example of a filtered audio recording is presented.

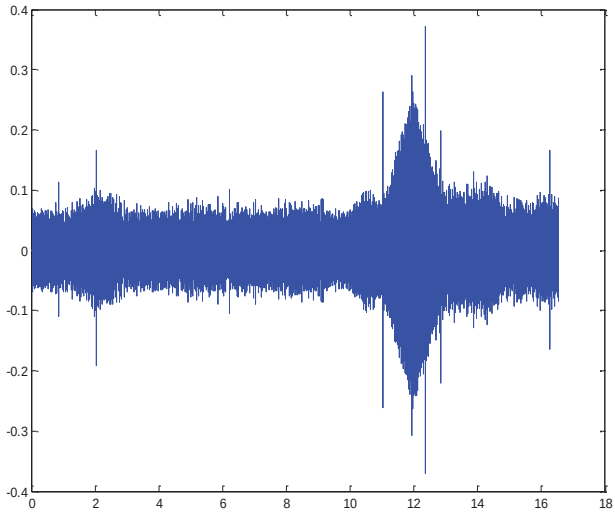

Figure 3 – Example of a filtered audio recording used for training.

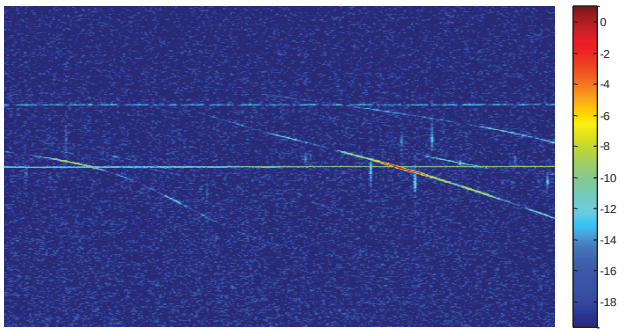

Figure 4 – Example of a spectrogram used for training.

The second type of input is spectrograms of the radio recordings. The advantage of a spectrogram is that it offers a better visual representation of the recordings and a better way to manually detect meteors. As with the

previous type of recording, the spectrograms were filtered and sampled too. The filtering took out the same uninteresting parts of the spectrum, while the spectrogram was sampled on its vertical side, due to the fact that meteor signals have a short duration, therefore they mostly appear as thin, vertical lines in the spectrogram. A spectrogram like the ones used for training is presented in *Figure 4*.

The three proposed automatic meteor detection techniques tested in this study involved training a SOM neural network using raw audio samples, training a MLP network using the raw audio samples and training a MLP neural network using the spectrogram samples.

The first technique to be tested was the SOM trained with raw audio samples. The training dataset for this type of neural network was made of 25 audio recordings, each 5 minutes long, that were processed as mentioned above, after which they were fed to the SOMs for training. This training set contained approximately 140 meteors. The several SOMs that were trained had different sizes, containing between 50 and 200 neurons, but all had been trained for a fixed number of 1000 training epochs. The best results were obtained with an 8x16 network (Roman and Buiu, 2014), which is presented in *Figure 5*. The plot shown there represents the SOM's hits plot, where each hexagon is one of the network's neurons and the numbers inside represent the number of input samples mapped to each neuron.

Once the SOM was trained, a test was made to check its performance. The test dataset was built using 6 audio recordings that contained 14 meteors, which were sampled as previously described. To these inputs, another 58 samples of known meteors were added. The results of this test are presented in *Table 1*. These results show that the proposed solution has promising potential of automatically detecting meteors, although it is not fault free, which is obvious because of the relatively large number of false alarms (i.e. the false positive rate, which represents the number of non-meteor samples that the neural network detected as being meteors).

Table 1 – Results of the test with the proposed SOM network.

Meteor samples		Non-meteor samples	
True Positive Rate	True Negative Rate	False Positive Rate	False Negative Rate
90.28%	9.72%	10.81%	89.19%

The second technique to be tested was the MLP trained with raw audio samples. To train this network, a training set was built with 230 meteor samples and 200 non-meteor samples. The MLPs trained were built with quite similar architectures, the only difference being the number of neurons in each MLP's hidden layer. Thus, the MLP networks were built with 551 neurons in the input layer and 2 neurons in the output layer, while the number of neurons in the hidden layers varied between 50 and 200.

The dataset used to test this technique was built with 161 meteor samples and 11536 non-meteor samples. This dataset was fed to the different MLPs, with the performances of the neural networks being presented in *Table 2*. These results show that the proposed solution has the ability to recognize meteors from a given dataset, but similar to the SOM case, it falsely deemed a good number of non-meteor samples as being meteors. Similar to the SOM solution, even though the percentage of false alarms was not large compared to the percentage of positive non-meteor detection, the number of non-meteor samples falsely detected as being meteors was larger than the number of meteors correctly detected.

Table 2 – Results of testing the MLPs trained with audio samples.

Meteor samples		Non-meteor samples	
True Positive Rate	True Negative Rate	False Positive Rate	False Negative Rate
86-93%	7-14%	10-24%	76-90%

The third technique proposed in this study involves the training of MLP neural networks using spectrogram samples. To test this technique, a new training set was built which contained 600 meteor samples and 500 non-meteor samples. As with the previous proposed technique, various MLP networks were trained using this training dataset. The neural networks were built with 595 neurons in the input layer, 2 neurons in the output layer and a varying number of neurons in the single hidden layer.

Table 3 – Results of testing the MLPs trained with spectrogram samples.

Meteor samples		Non-meteor samples	
True Positive Rate	True Negative Rate	False Positive Rate	False Negative Rate
70-77%	23-30%	46-60%	40-54%

For this technique, the test dataset was built with 245 meteor samples and 200 non-meteor samples. Depending on the size of the trained MLPs, the results obtained after testing are presented in *Table 3*. Compared to the previous two techniques, this one shows lower performance, especially in regards to the false positive rate (i.e. the number of non-meteor samples that are deemed as being meteors by the neural network).

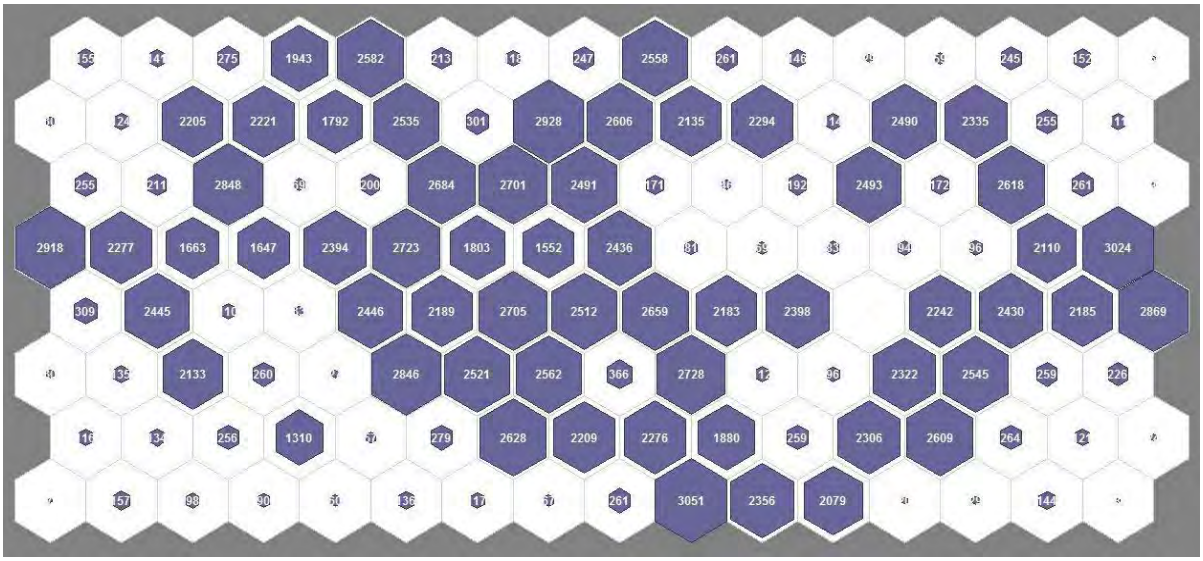

Figure 5 – The resulting self-organizing map.

4 Conclusions and future work

The three techniques presented within this study all show promise in the field of automatic meteor detection. All of them offer high detection rates, which allows for the extraction of the majority of meteors from a given test dataset. The only problem, recurring with all three proposed techniques, is with the quite high (in actual number of samples, not in the overall percentage) false positive rate, especially in the case of the MLPs trained with spectrogram samples. The size of the problem is more obvious when we compare the numbers behind the true positive and false positive rates. As for the reasons behind these high false positive rates, there are several possibilities: the size of the sampling window, size of the window's slide, or the similarity between meteor signals and non-meteor artifacts (e.g. planes).

However, despite the problems with the false positive rates, the three proposed techniques are decent solutions to the problem of automatic detection of meteors. Each technique has its own advantages that make it a good candidate. The SOM networks offer an easy to interpret, visual output. This has the great advantage of being able to work with unknown or unlabeled data because the SOM network gives verdicts based on the similarity of data and not on previous knowledge about it. The MLPs are easier to train than a SOM and offer a very precise output. Furthermore, their supervised training algorithm ensures that the neural networks know what a meteor looks like. Above all, a general attribute that all the techniques have is the high speed of making a decision, each neural network requiring only a brief moment to check a given input and deciding whether it is a meteor or not.

As for future work, the main focus will be on improving detection rates and lowering the false positive rate, thus allowing the three proposed techniques to detect more real meteors and to eliminate fake warnings. To tackle these issues, changes will have to be made in several areas such as: the sampling of the data (changing the sampling window size or slide), size of the neural networks, length of their training or depth of the networks (in the case of MLPs).

Acknowledgments

This work was supported by a grant from the Romanian National Authority for Scientific Research, CNDI-UEFISCDI, project number 205/2012 and by a grant from POSDRU, project number 137390.

V.S. Roman performed part of this work in a research stage at Institut d'Aéronomie Spatiale de Belgique and would like to thank Hervé Lamy for his kind support.

References

Kohonen T. (1990). "The self-organizing map." In *Proc. IEEE*, September 1990, **78**, no. 9, pages 1464–1480.

Kohonen T. (2001). Self-organizing maps. Third Edition. Berlin: Springer Verlag.

Roman V. S. and Buiu C. (2014). "A self-organizing map based solution to the automatic detection of meteor echoes in radio recordings". In *Proceedings of the 6th Edition of the International Conference on Electronics, Computers and Artificial Intelligence*, Bucharest, 23–25 October 2014. Accepted.

Rumelhart D. and McClelland J. (1986). Parallel Distributed Processing: Explorations in the Microstructure of Cognition. Volume 1: Foundations. MIT Press.

A statistical walk through the IAU MDC database

Željko Andreić[1], Damir Šegon[2] and Denis Vida[3]

[1] **University of Zagreb, Faculty of Mining, Geology and Petroleum Engineering, Pierottijeva 6, 10000 Zagreb, Croatia**
zandreic@rgn.hr

[2] **Astronomical Society Istra Pula, Park Monte Zaro 2, 52100 Pula, Croatia**

Višnjan Science and Education Center, Istarska 5, 51463 Višnjan, Croatia
damir.segon@pu.htnet.hr

[3] **Astronomical Society "Anonymus", B. Radića 34, 31550 Valpovo, Croatia**

Faculty of Electrical Engineering, University of Osijek, Kneza Trpimira 2B, 31000 Osijek, Croatia
denis.vida@gmail.com

The IAU MDC database is an important tool for the study of meteor showers. Though the history, the amount of data in the database for particular showers, and also their extent, varied significantly. Thus, a systematic check of the current database (as of 1st of June, 2014) was performed, and the results are reported and discussed in this paper.
The most obvious one is that the database contains showers for which only basic radiant data are available, showers for which a full set of radiant and orbital data is provided, and showers with data span anywhere in between. As a lot of current work on meteor showers involves D-criteria for orbital similarity, this automatically excludes showers without the orbital data from such work. A test run to compare showers only by their radiant data was performed, and was found to be inadequate in testing for shower similarities.
A few inconsistencies and typographic errors were found and are briefly described here.

1 Introduction

As the number of new shower candidates rises rapidly, there is a growing need for a standard database to help with searching for new candidates and to avoid multiple reporting of new shower candidates. Clearly, such a database has to be public and current.

The only database which at the moment fulfills these requirements is the database maintained by the Commission 22 (IAU meteor data center (MDC) homepage)[1] of the IAU. The database can be accessed online (IAU MDC list of all showers)[2]. The user is provided with a list of all showers and shower candidates reported to the IAU MDC. By clicking on a particular shower name a page with all the available data about that particular shower is opened.

The list can be sorted by the shower number in the database, the solar longitude of the shower maximum, RA or DE of the radiant and the geocentric velocity. No search options are offered by the web page.

The most valuable option of the IAU MDC web page is the possibility to download the current shower list in the CSV format, which allows users to use the database with their own software. This option is used, for example, by the search routine provided by the Croatian Meteor Network (CMN search tool for the IAU MDC database)[3] which provides a simple tool for searching the showers with similar parameters (multiple parameter search is supported) across the IAU MDC database.

For the analysis described in this paper, the list of all showers was downloaded on June 1st, 2014. from the IAU MDC page and this version was used in all further work.

2 Overview of the IAU MDC database

The downloaded CSV file contains 728 lines. The first 45 lines are comment lines, including database version (Last update: 2013.12.13) and a short explanation of individual data in the database. Vertical bar (|) is used as the field separator and all data are entered as text, with quotation mark (") used as a text qualifier. Taking this into account, the file can be imported into a spreadsheet program without any problems.

Neglecting the comment lines, the remaining 683 lines contain data about individual showers. According to the on-line statistics from the IAU MDC shower page, the database contains 578 showers, out of which 95 are established (meaning they exist without any doubt) and 95 are pro tempore, meaning that the basic data for them are not published yet. The rest are awaiting a decision of the IAU Commission 22 on their status. Additionally, 24 shower complexes (groups of showers) are listed in the database. The distribution of shower radiants on the celestial sphere is shown on *Figures 1 and 2*.

A nice touch is that the shower data frequently include the link to the reference from which the data originate. Altogether 427 entries have traceable publication data

[1] http://www.astro.amu.edu.pl/~ jopek/MDC2007/index.php.
[2] http://www.astro.amu.edu.pl/~jopek/MDC2007/Roje/roje_lista.php?corobic_roje=0~sort_roje=0.
[3] http://cmn.rgn.hr/in-out/search.html

included. The rest is either missing, or has to be updated so the user of the database can find the reference in question.

For some showers (and complexes) several lines of data are present. Particularly, for 23 showers two different data sets are given, for 30 showers and one complex 3 data sets are given, for 7 showers and one complex 4 data sets and for 2 showers and one complex 5 datasets.

In this analysis, each line of the database is treated as an individual shower (or complex). Thus, for our purpose, the database contains 647 different showers and 36 complexes, and all numerical data quoted below are referring to this set of "shower" and "complex" data.

The data about possible (or confirmed) parent bodies are given in 173 cases, 87 of which are labeled as uncertain with one or two question marks.

It is also interesting to look at the number of known meteors for each shower in the database. The statistics are summarized in *Table 1*. A lot of shower candidates have been reported based on very few meteors, sometimes even only one. Moreover, for 174 showers the number of meteors is not known.

Table 1 – Statistics on the number of known meteors for each reported shower/shower candidate in the IAU MDC database.

number of meteors	number of showers
no data	174
1	9
2	21
3	34
4-5	37
6-9	84
10-19	101
20-49	117
50-99	22
100-199	8
200-499	33
500 and more	43

The only important data which we feel is missing from the database is data about the period of activity of the shower in question. Only the solar longitude of "maximum" activity is given, but from our experience this data alone is quite unreliable for newly discovered minor shower candidates, as the number of the orbits of such candidates is too low to allow the construction of an activity curve. Even the search in much larger single-station meteor databases, for instance on the IMO VDB IMO video meteor database)[4] does not give enough clues about the activity curves of minor showers. Typically the solar longitude of the “maximum activity” is in such a case simply the average of solar longitudes of individual meteors that are suspected to belong to the minor shower in question. The information about the activity period can be quite useful, even if in some cases it usually corresponds to the solar longitudes of the first and the last meteor observed.

3 Minor inconsistencies and typographic errors in the IAU MDC

The CSV file was first checked for obvious errors, inconsistencies and non-standard symbols. A simple parser program was used for this purpose. This program tries to read each entry in the database, taking care of the type of the data and the standard interval in which the data should appear. In other words, integer values are parsed as integers, real numbers as floating point numbers and string values as strings. If the parsing process fails, a warning and the corresponding entry from the database are written to a log file, for later analysis.

A spreadsheet program is not useful for such a test as its parser will import the file without any indication that something is not in order with the data. However, such data will be ignored in calculations performed by the spreadsheet, so the shower in question will effectively be eliminated from the database.

Starting from the first data column, we have identified the following inconsistencies or errors:

- Column 5 (shower name): in 55 cases the name contains stars labeled with number (Flamsteed designations). Those shower names do not conform to the meteor shower naming rules (IAU MDC meteor showers nomenclature rules)[5].
- Column 7 (shower status): in 95 cases the status is "10", a status number that is not explained in the comment lines of the CSV file.
- Column 13 (v_g): in line 93 of the CSV file the missing data is indicated by a "-.-", instead of simply leaving
  the field empty (as in all other cases when no data about geocentric velocity are given).
- Column 14 (a): in 16 cases the value is given between parentheses, probably indicating uncertain values. However, this would cause an error in most cases, excluding the line in question from further analysis. For instance, Microsoft Excel interpreted these numbers as negative, thus changing the orbital parameters significantly.
- Column 17 (peri): in line 114 a value of 1793 is entered as the longitude of perihelion, and in line 277 a range of values is entered as 31-24. In the second case the parser would fail. In two cases the values entered are outside the standard interval of 0-360 degrees.

[4] http://www.imonet.org/database.html.

[5] http://www.astro.amu.edu.pl/~jopek/MDC2007/Dokumenty/shower_ nomenclature.php.

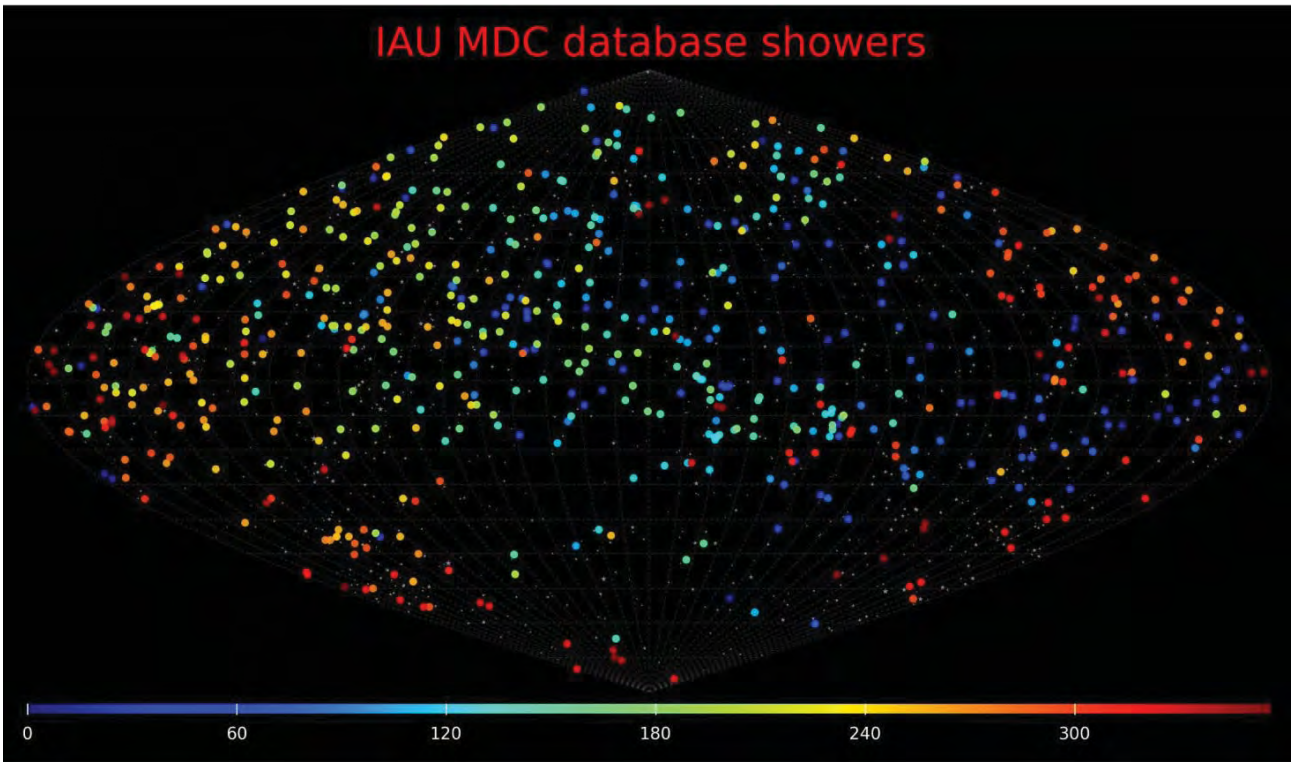

Figure 1 – All radiants from the IAU MDC database. The individual radiants are represented by small circles, with color corresponding to the solar longitude of the maximum activity of the shower in question.

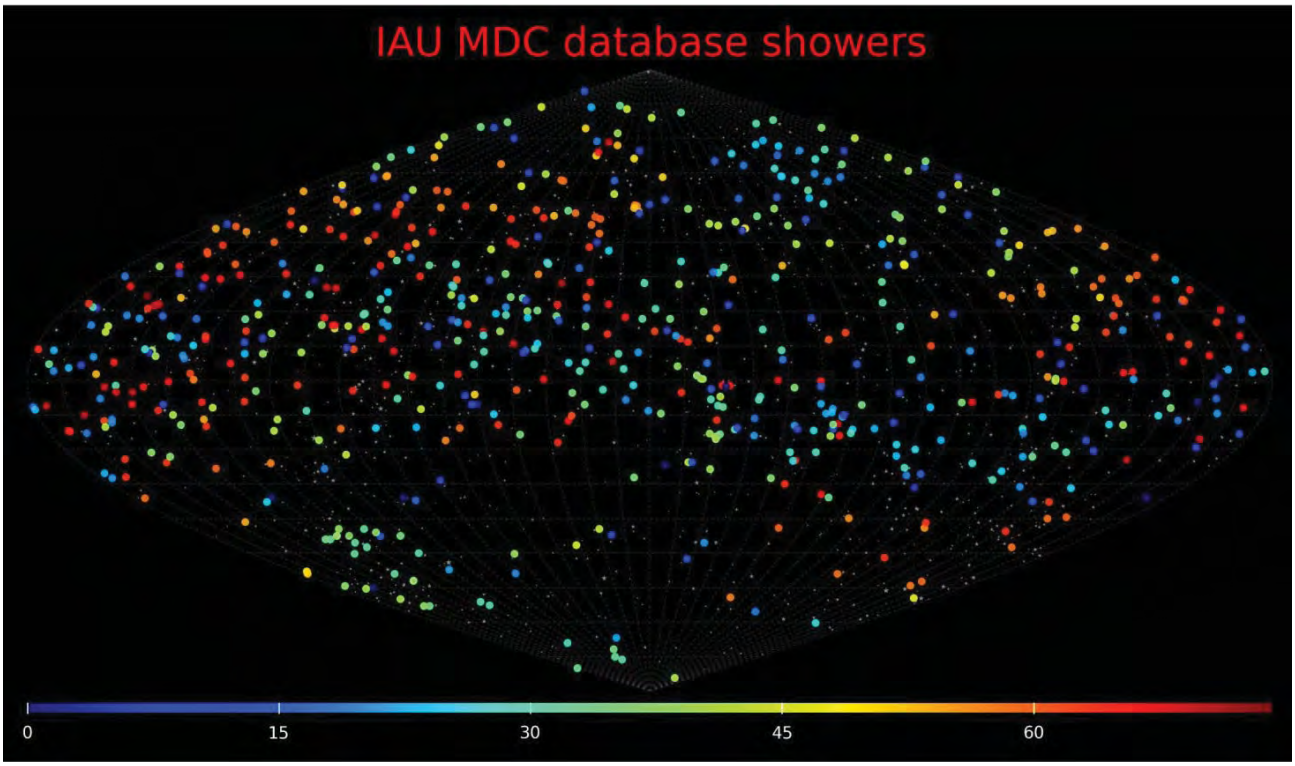

Figure 2 – All radiants from the IAU MDC database. The individual radiants are represented by small circles, with color corresponding to the geocentric velocity of the shower in question.

- Column 18 (node): in 6 cases the given value is outside the standard interval of 0-360 degrees, sometimes being negative, sometimes larger than 360. Also, in line 360 the value is again given between parentheses.
- Column 19 (inclination): in line 277 a range of values is entered as 82-87.
- Column 20 (number of orbits): in 172 cases the missing data is indicated by a "-".

The most serious inconsistency we stumbled upon during our searches through the literature for the individual showers is that for some showers (for example IAU numbers 146, 149, 150, 209 and 409-418) instead of the

geocentric velocity the velocity at infinity is given, thus scrambling any attempts to compare the velocities of these showers with the other ones. Also, if one tries to derive the orbital elements from radiant data and geocentric velocity, they will be seriously wrong.

4 Shower similarities from orbital similarity

Next, the database was searched for showers with similar orbits. For this purpose, the standard D_{SH} criterion was used, and the tolerance was set to 0.15, as we did in all our searches for new shower candidates (see for example Šegon et al., 2013). The search excluded 27 complexes (out of 36) and 120 showers (out of 647) for which orbital data are missing or incomplete. Altogether 42 showers were found to have some orbital similarity to other showers in the database, and often multiple similarities were found. When arranged in pairs, 61 of them have been found. They are listed in *Table 2*.

5 Shower similarities from radiant search

To see what can be done with the showers without the complete orbital data, the database was searched for showers with similar radiant positions and activity periods. As a similarity criterion, we required that the difference in solar longitudes of the maxima of the two showers in question has to be less than 7°, the difference in radiant coordinates (both in RA and in DE) has to be smaller than 7°, after the corrections for the daily motion of the radiant (if data are available) and the arc contraction in RA due to the convergence of the coordinate grid towards the celestial poles have been made. In the case of daily motion, the correction is always done for the radiant of the shower with the lower IAU number, if possible.

Finally, it was required that the geocentric velocities of the two showers do not differ by more than 3 km/s. Under these circumstances, 30 pairs of similar showers were found. Two of them are known to be identical, and are labeled as such in the database, and the remaining 28 pairs are listed in *Table 3*.

The advantage of this search is that all showers in the database are included (apart from complexes, as for most complexes no radiant data are given) so the search is complete. On the other hand, it is very difficult to conclude if two showers are similar on the radiant data and geocentric velocity only.

6 Combined results of both searches

A very interesting result is obtained when one tries to compare the results of the radiant and the orbital similarity searches. Only 4 showers appear on both lists, and we will shortly discuss these 4 cases here.

Southern March Virginids (124 SVI)

Two different orbits are given in the IAU MDC database, but only the second (AdNo=1) was found to be similar to some other shower. The radiant search found that they are similar to the Northern March Virginids (123 NVI, AdNo=1), a fact that seems to be self-explanatory. The pairing was not found by the orbital similarity search as the D_{SH} of the two mean orbits is larger than the pre-set limit, being 0.185 in this case.

The radiant plot of 124 SVI and all other radiants within the window of ±15° around the maximum activity of 124 SVI is shown on the *Figure 3*. The small dots in the background are meteors from the combined CMN and SonotaCo database (CMN 2007-1010, SonotaCo 2007-2011) that we used in our searches (Andreić et al., 2013), with v_g color coded. It can be seen that a lot of possibly active radiants are crowded into this area of the sky (14 altogether). Luckily, most of them are eliminated by the $\Delta v_g \leq 3$ km/s criterion, leaving only the above mentioned 123 NVI radiant as a similar one to the 124 SVI.

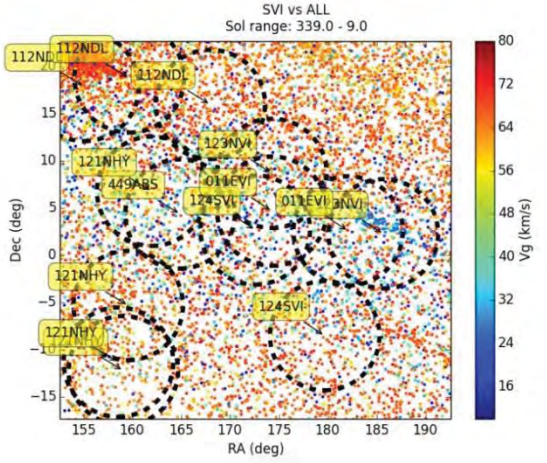

Figure 3 – The radiant plot of 124 SVI and all other radiants within the window of ±15° around the maximum activity of 124 SVI. The small dots in the background are all meteors from the combined CMN and SonotaCo databases in the plotting area and the solar longitude window, regardless of the shower affiliation. The geocentric velocity of individual meteors is color coded.

The orbital similarity search revealed two other pairings, namely with one mean orbit of the α Virginids (21 AVB, AdNo=1, with D_{SH}=0.116) and with one mean orbit of the ν Hydrids (121 NHY, AdNo=2, with D_{SH}=0.138). A quick look into the IAU MDC database reveals why these two pairings were not found by the radiant search: the radiants of the 21 AVB and the 121 NHY are both outside the tolerances we set for the radiant search.

β Equuleids (327 BEQ)

Both searches have found similarities between this shower and the ε Pegasids (326 EPG). The solar longitude differs by only 1°, and radiants are separated by about 6° in both coordinates. The geocentric velocities

are also quite similar, with a difference of 1.7 km/s. The D_{SH} of the mean orbits is 0.124.

The radiant plot is a lot more simple than the previous one (see *Figure 4* and the similarity of the radiant positions is obvious. The radiant of the 548 FAQ is just a little farther, and is eliminated by the search criteria, the most obvious one in this case being a large difference in geocentric velocity of 6.1 km/s.

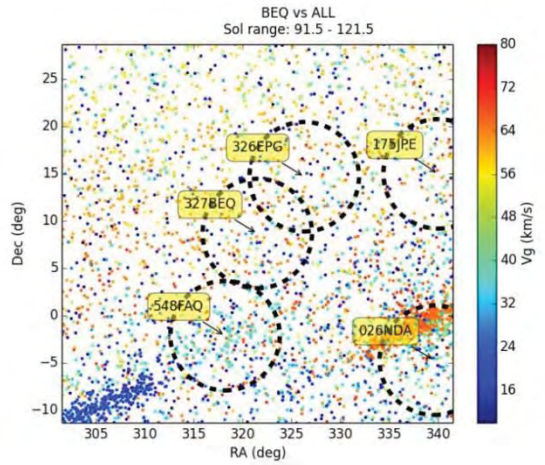

Figure 4 – The radiant plot of 327 BEQ and all other radiants within the window of ±15° around the maximum activity of 327 BEQ. The small dots in background are all meteors from the combined CMN and SonotaCo databases in the plot area and solar longitude window, regardless of the shower affiliation. The geocentric velocity of individual meteors is color coded.

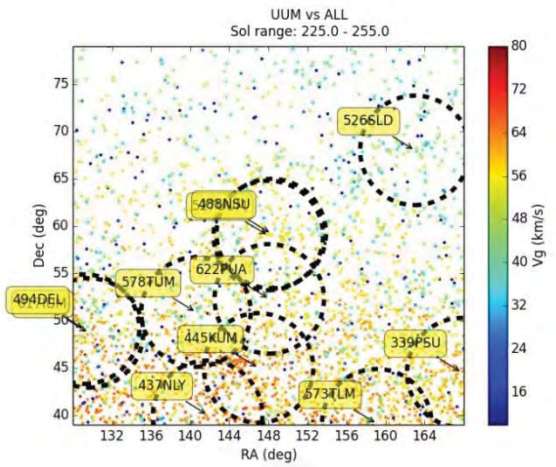

Figure 5 – The radiant plot of the 527 UUM and all other radiants within the window of ±15° around the maximum activity of the 527 UUM. The small dots in the background are all meteors from the combined CMN and SonotaCo databases in the plotting area and the solar longitude window, regardless of the shower affiliation. The geocentric velocity of individual meteors is color coded.

υ Ursae Majorids (527 UUM)

Both searches have found large similarities between this shower and November σ Ursae Majorids (488 NSU). The solar longitudes of both showers differ by 1.6°, and the difference in radiant position is less than one degree. Moreover, the geocentric velocities differ by only 0.2 km/s. The DSH of the mean orbits is 0.036. All this strongly indicates that these showers are identical, and as the 527 UUM is one of the showers found in our previous searches (Andreić et al., 2014), we checked the case thoroughly to see why we missed this fact. We have found that, at the time we reported 527 UUM, the showers 487 to 493 (including 488 NSU) were not entered into the IAU MDC database, so we were not able to check against them. We thus ended with a double detection of the 488 NSU.

The radiant plot of the 527 UUM shows nicely the almost identical radiant position with the 488 NSU (see *Figure 5*).

Sextantids (561 SSX)

The radiant search has found similarities between this shower and the 17 Sextantids (560 SES). The solar longitudes of both showers differ by 0.4°, and the difference in radiant position is about 5° in both coordinates. The geocentric velocities differ by only 0.7 km/s. The pairing was not found by the orbital similarity search as the D_{SH} of the two mean orbits is 0.387 in this case.

The radiant plot of the 561 SSX is again quite crowded, but shows the relative vicinity of the 561 SSX and the 492 DHT clearly (see *Figure 6*). The other two nearby radiants (560 SES and 585 IHY) are eliminated by the Δv_g criterion, as the differences in geocentric velocities between these three showers are very large.

The orbital similarity search has found another shower that has orbital similarity to the 561 SSX: December θ Hydrids (492 DTH). The mean orbits differ by D_{SH}=0.121. However, the difference in solar longitude is very large, 105°, indicating that this may be a case of twin showers.

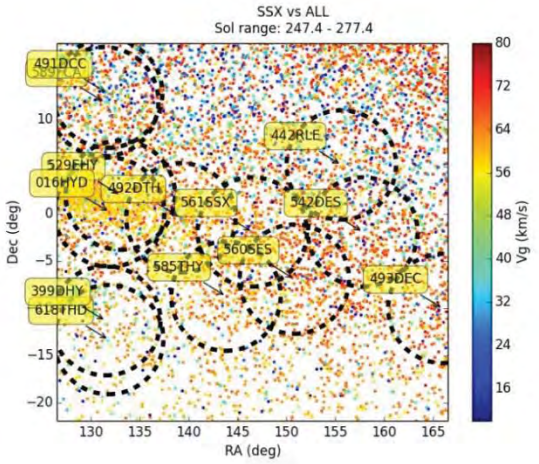

Figure 6 – The radiant plot of the 561 SSX and all other radiants within the window of ±15° around the maximum activity of the 561 SSX. The small dots in the background are all meteors from the combined CMN and SonotaCo databases in the plot area and solar longitude window, regardless of the shower affiliation. The geocentric velocity of individual meteors is color coded.

7 Discussion and conclusions

The IAU MDC database is an important tool in searches for new showers, but also in the study of existing ones.

To be even more useful, we feel the need for the data formats in the database to be fully standardized (for instance, that the missing data are always indicated by an empty data field, and that entries into numerical fields are pure numbers without any other characters that may not be read correctly by a parser program). One has also to understand that the database itself is at the current moment assembled from the data taken from the literature as they are, without any attempt to check or correct them, about which the IAU MDC is highly aware, so we hope an attempt to go one step further to produce a database with the checked/unified data will be done in the future.

Through the extensive use of the database in our work we found that multiple entries for the same shower often complicate the searches, so we would like to have the most accurate data present (or to label the corresponding dataset as such). In the light of modern research techniques and tools, some early data, especially for showers with just a few members, could be labeled with an indication of their accuracy to help in assessing their similarity to newly found shower candidates.

After the database was searched for the obvious inconsistencies, we performed two searches for similar showers in the database. First, the database was searched for orbital similarity between individual showers, which was possible only for showers for which the orbital data are entered into the database (527 of them). To see what can be done about the remaining showers, a search in radiant position, solar longitude of the maximum activity and geocentric velocity was performed. This search encompassed all 647 showers in the database.

Both searches have found several dozens of showers with at least some similarity between their orbital (61 pairs) and radiant (28 pairs) data. The comparison between two sets of "similar" shower pairs resulted in only 4 cases where the same pairs have been found by both searches. However, in two cases, the pairings found were different for the two search methods. If we give more weight to orbital similarity methods, this clearly shows that searching for similar showers by the radiant data only does not produce reliable results.

Finally, we looked a little deeper into the search data to see why there is so little overlap between results of the two search methods described here. We took the results of the orbital similarity search, and looked at the radiant data of the shower pairs detected by this search. After eliminating obvious mismatches in the radiant data, we found out that the tolerances for the radiant search have to be more relaxed, especially the tolerance in the solar longitude of the shower maximum, which turned out to be around 20°. This again stresses the need for entering information about the period of activity of the showers into the database. The more relaxed tolerances for the coordinates of the radiant are 14° in RA and 8° in DE. The effect of the radiant declination on the tolerance for the right ascension (due to convergence of the coordinate grid towards the celestial poles) was found to be minor. Finally, the tolerance for the geocentric velocity is confirmed, being about 3 km/s.

Recently, after this paper was already finished, a nice reference about the IAU MDC database was published in the Meteoroids 2013 conference proceedings (Jopek and Kaňuchová, 2013). It covers the history of the database, its current status and future plans. It explains, for instance, why Flamsteed numbers entered the naming of new showers. More important, the authors are aware of the current problems and needs and they are working on improving the database.

Acknowledgements

The authors wish to thank the Faculty of Mining, Geology and Petroleum engineering, University of Zagreb, Višnjan Science and Education Center, Croatia, and Alexander von Humboldt Stiftung for their support.

References

Andreić Ž., Gural P., Šegon D., Novoselnik F., Vida D., and Skokić I. (2013). "Ten possible new showers from the Croatian Meteor Network and SonotaCo datasets". *WGN, Journal of the IMO*, **41**, 103–108.

Andreić Ž., Gural P., Šegon D., Skokić I., Korlević K., Vida D., Novoselnik F., and Gostinski D. (2014). "The results of CMN 2013 search for new showers across CMN and SonotaCo databases I". *WGN, Journal of the IMO*, **42**, 90–97.

Andreić Ž., Šegon D. (2010). "The first year of Croatian meteor network". In Kaniansky S. and Zimnikoval P., editors, *Proceedings of the International Meteor Conference*, Šachtička, Slovakia, 18 – 21 Septermber 2008. IMO, pages 16–23.

Jopek T. J. and Kaňuchová Z. (2013). "Current status of the IAU MDC meteor showers database". In Jopek T. J., Rietmeijer F. J. M., Watanabe J., and Williams I. P., editors, *Proceedings of the Meteoroids 2013 Conference*, Poznań, Poland, 26-30 August 2013. A.M. University Press, pages 353–364.

Šegon D., Andreić Ž., Korlević K., Novoselnik F., and Vida D. (2012). "Croatian Meteor Network Catalogue of Orbits for 2007.". *WGN, Journal of the IMO*, **40**, 94–97.

Šegon D., Andreić Ž., Korlević K., Novoselnik F., Vida D. and Skokić I. (2013). "8 new showers from Croatian meteor network data". *WGN, Journal of the IMO*, **41**, 70–74.

Table 2 – Pairs of similar showers found by orbital similarity search. The identification of the first shower is given in the first three first columns, followed by identification of the second shower and the D_{SH} of the two mean orbits is in the last column.

IAU No	Ad No	Code	IAU No	Ad No	Code	D_{SH}	IAU No	Ad No	Code	IAU No	Ad No	Code	D_{SH}
527	0	UUM	488	0	NSU	0.036	473	0	LAQ	33	1	NIA	0.130
223	0	GVI	124	1	SVI	0.039	264	0	XCE	263	0	NAN	0.131
478	0	STC	469	0	AUS	0.042	31	1	ETA	8	1	ORI	0.132
452	0	TVI	21	3	AVB	0.051	325	0	DLT	221	0	DSX	0.132
536	0	FSO	535	0	THC	0.064	495	0	DMT	288	0	DSA	0.132
173	0	BTA	17	1	NTA	0.065	532	0	MLD	451	0	CAM	0.132
240	0	DFV	123	0	NVI	0.068	452	0	TVI	21	2	AVB	0.133
31	0	ETA	8	1	ORI	0.078	478	0	STC	218	0	GSA	0.133
173	1	BTA	17	0	NTA	0.084	230	0	ICS	22	0	LMI	0.135
136	0	SLE	123	0	NVI	0.086	475	0	SAQ	467	0	ANA	0.137
286	0	FTA	154	1	DEA	0.096	124	1	SVI	121	2	NHY	0.138
456	0	MPS	261	0	DDC	0.101	167	1	NSS	115	1	DSC	0.138
230	0	ICS	22	1	LMI	0.102	473	0	LAQ	33	0	NIA	0.138
31	2	ETA	8	1	ORI	0.106	286	0	FTA	257	0	ORS	0.139
172	0	ZPE	28	0	SOA	0.107	469	0	AUS	200	0	ESE	0.139
223	0	GVI	21	1	AVB	0.109	367	0	OPG	366	0	JBP	0.140
240	0	DFV	136	0	SLE	0.113	453	0	MML	133	1	PUM	0.140
282	0	DCY	83	0	OCG	0.113	453	0	MML	133	2	PUM	0.140
124	1	SVI	21	1	AVB	0.116	330	0	SSE	320	0	OSE	0.141
218	0	GSA	200	0	ESE	0.116	223	0	GVI	121	2	NHY	0.141
479	0	SOO	226	0	ZTA	0.116	475	0	SAQ	471	0	ABC	0.143
481	0	OML	480	0	TCA	0.117	453	0	MML	125	0	SAL	0.143
476	0	ICE	155	1	NMA	0.118	168	0	SSS	115	3	DSC	0.144
423	0	SLL	161	0	SSC	0.119	449	0	ABS	268	0	BCD	0.145
513	0	EPV	428	0	DSV	0.119	289	0	DNA	288	0	DSA	0.146
167	1	NSS	115	0	DSC	0.120	167	1	NSS	115	2	DSC	0.147
561	0	SSX	492	0	DTH	0.121	469	0	AUS	218	0	GSA	0.147
327	0	BEQ	326	0	EPG	0.124	173	2	BTA	28	0	SOA	0.148
173	0	BTA	2	0	STA	0.125	168	0	SSS	115	4	DSC	0.149
168	0	SSS	115	2	DSC	0.129	123	1	NVI	121	2	NHY	0.150
173	0	BTA	17	0	NTA	0.130							

Table 3 – Pairs of similar showers found by the radiant search. The identification of the first shower is given in the first three columns, followed by identification of the second shower and differences in coordinates of the radiants and geocentric velocity.

IAU No	Ad No	Code	IAU No	Ad No	Code	$\Delta \lambda_\odot$	Δ RA	Δ DE	Δv_g
308	0	PIP	93	0	VEL	-5.3	-6.6	4.3	-0.1
390	0	THA	248	0	IAR	3.4	7.6	0.9	-0.2
527	0	UUM	488	0	NSU	-1.6	0.6	-0.7	-0.2
315	0	OCA	105	1	OCN	-0.7	3.0	-0.9	-0.4
522	0	SAP	175	1	JPE	3.0	-0.2	0.2	-0.6
508	0	TPI	26	3	NDA	7.0	0.4	1.2	0.7
508	0	TPI	342	0	BPI	7.0	0.4	1.2	0.7
561	0	SSX	560	0	SES	0.4	-4.6	5.1	-0.7
582	0	JBC	567	0	XHY	-0.2	-6.8	5.2	-0.8
350	0	MAL	348	0	ARC	5.0	8.1	-2.4	1.2
547	0	KAP	190	0	BPE	2.1	-7.8	4.8	-1.5
585	0	THY	561	0	SSX	-0.5	-2.3	-6.9	-1.5
617	0	IUM	588	0	TTL	6.4	8.8	-0.6	1.6
327	0	BEQ	326	0	EPG	1.0	-6.3	-6.4	1.7
356	0	MVL	151	0	EAU	-5.0	5.6	6.4	1.7
387	0	OKD	385	0	AUM	7.0	0.0	2.7	1.7
577	0	FPI	415	0	AUP	1.7	3.6	-5.1	-1.8
622	0	PUA	488	0	NSU	4.3	-4.5	-4.9	1.9
622	0	PUA	527	0	UUM	5.9	-3.1	-5.0	2.1
585	0	THY	560	0	SES	-0.1	-6.9	-1.8	-2.2
354	0	DDT	351	0	DTR	7.0	-0.6	-0.4	2.2
560	0	SES	542	0	DES	-1.3	-6.1	-5.4	-2.3
589	0	FCA	491	0	DCC	-4.1	3.2	-2.0	2.5
347	0	BPG	143	0	LPE	6.3	3.0	5.8	2.6
17	1	NTA	2	0	STA	0.0	-5.4	5.9	2.7
615	0	TOR	609	0	BOT	2.4	-6.2	-6.4	2.7
616	0	TOB	90	0	JCO	-1.3	5.1	6.2	-2.7
124	1	SVI	123	1	NVI	0.0	-1.7	-6.0	-3.0

Update on recent-past and near-future meteor shower outbursts on Earth and on Mars

Jérémie Vaubaillon[1], Rachel Soja[2], Lucie Maquet[3], Auriane Egal[1], Aswin Sekhar[4], Pavel Koten[5], Regina Rudawska[6], François Colas[1] and Bérénice Reffet[1]

[1] **IMCCE, Paris, Observatoire de Paris, 77 av. Denfert-Rochereau, 75014 Paris, France**
vaubaill@imcce.fr

[2] **University of Stuttgart, Institut für Raumfahrtsysteme, Pfaffenwaldring 29, Germany**
soja@irs.uni-stuttgart.de

[3] **LESIA, Paris Observatory, 5 pl. Jules Janssen, 92190 Meudon, France**
lucie.maquet@imcce.fr

[4] **Armagh Observatory, College Hill, Armagh BT61 9DG, Northern Ireland**
aswinsek@gmail.com

[5] **Astronomical Institute of the Academy of Sciences, Ondřejov Observatory, CZ-25165 Ondřejov, Czech Republic**
pavel.koten@asu.cas.cz

[6] **Comenius University, Mlynská dolina, 842 48 Bratislava, Slovakia**
rudawska@gmail.com

This work presents a brief reflection on the 2014 Camelopardalids and the Mars encounter with comet C/2013 A1 Siding Spring expected in October 2014. These two events were first thought to display an exceptional amount of meteors and later works showed that it would not be the case, at least in optical wavelength. Observation biases and low activity of the comet can explain those differences, but care must be taken when announcing any future meteor shower and close co-operation with other scientists is needed to strengthen the case.

1 Introduction

The year 2014 was rich in meteor shower announcements, with the Camelopardalids shower in May, as well as the encounter between comet C/2013 A1 Siding Spring and Mars in October. However, subsequent work and/or observations revealed significant differences between the expected events and the actual data/observations. Here, we reflect on those two particular events and the way meteor shower forecasting is performed today.

2 The 2014 Camelopardalids

The pioneering work by Jenniskens (2006, pp. 129 and 689), followed by Ye and Wiegert (2014), as well as our own study[1], showed that the dust emitted by comet 209P/LINEAR (2004 CB) during the 17th and the 19th century would intersect with the Earth on 24 May 2014. Because all the particles ejected during several decades would presumably make it to the Earth, the level of the shower was expected to be high, and announcements of ZHR up to 400 per hour were performed. Observation campaigns were organized in North America using optical detection and additionally in Europe using radio detection. However, not much was detected in optical, showing a level up to 15 meteors per hour. Radio detection showed more events (see *Figure 1*). Of course, the question arises as to why the forecasted event did not occur as expected.

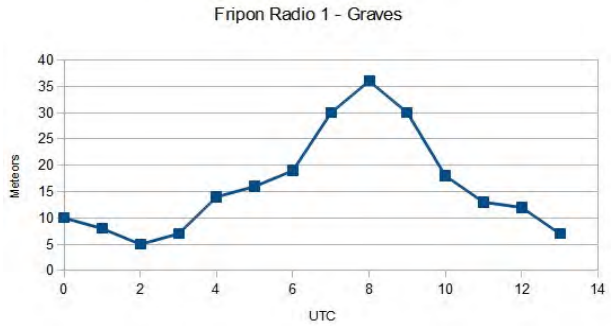

Figure 1 – Radio detection of the 2014 Camelopardalids from the FRIPON radio set-up (F. Colas, IMCCE).

A combination of different factors can be invoked. First of all,the comet is known to be extremely faint, probably not ejecting much dust both at the present as well as in the past centuries. Such low activity is also typical for old comets that have not much dust left. Therefore, the size distribution of the particles for such comets might be shifted towards small sizes. All of this, combined with the fact that the velocity at the Earth is low (16 km/s) might explain why not much was observed in optical wavelength.

[1] http://www.imcce.fr/langues/en/ephemerides/phenomenes/meteor/DATABASE/209_LINEAR/2014/index.php?char=year&body=Earth&year=2014&shower=209_LINEAR

3 Comet C/2013 A1 Siding Spring at Mars

Comet C/2013 A1 Siding Spring was discovered in the early 2013 when it was further than 7 AU from the Sun. It appeared extremely bright for such a large distance, presumably explained by a massive nucleus and activity. Very soon it was realized that its orbit would put it very close to the planet Mars in October 2014. Consequently, a collision with the planet was considered, until further observations showed that it would not be the case. The shortest distance between the comet and the planet will be as short as 138.000 km on the 19th of October with a relative velocity of about 56 km/s. Given the number of spacecraft orbiting the planet, the need for an estimate of the amount of dust arriving into the atmosphere of Mars was urgent.

On the basis of the orbit and photometry measurement of the comet, two studies (Moorhead et al., 2014; Vaubaillon et al., 2014) showed that the cometary dust would enter the Martian atmosphere causing an extremely strong meteor shower, so much that the concept of a meteor hurricane was introduced by us. However, further studies (Farnocchia et al., 2014; Tricarico et al., 2014) showed that the nucleus was not as large as first thought, making the ejection velocity much smaller. As a result, it is today no longer expected that the dust emitted by the comet will actually make it to the Martian atmosphere. As a consequence, no meteor shower is expected at Mars on October 19th, 2014.

4 What have we learned?

From these two events, we can reflect on the way meteor shower forecasting is performed nowadays. After great success during the Leonids in the early 2000, it was shown that the activity of the comet in the past was important to predict the level of the shower. Present cases show that the statement remains true today! Links between the comet science and the meteor science should be tightened even more than ever. Photometry of the comet as well as the size distribution of the dust emitted by the nucleus (which is actually extremely hard to derive with optical observations) is a prior interest.

One of the difficulties is that the predicted level of a meteor shower is extremely sensitive to the value of the size distribution index, particularly from millimeter to centimeter size particles, for which we have usually no observation. The determination of the size distribution index for smaller particles should thus be measured for every comet potentially causing a meteor shower but this might not be enough.

This work has also showed that works considering the photometry information can be misleading when a comet is still at a very high heliocentric distance, where the dust is emitted mainly by CO_2 and the ejection velocity is lower than at smaller distances. As a consequence, dust staying close to the nucleus for a longer period of time makes the overall magnitude of the comet smaller than what it would be at smaller distance. For the same reason, it makes the [Afrho] parameter look higher than what it really is when the ejection is driven by water (Vaubaillon et al., 2005). It is advised that the production of meteor shower forecasting should wait for the comet to enter the zone where the dust is emitted by water mainly. However, this might sometimes conflict with the need for long-term planning of spacecraft operations. Compromise should be defined then.

References

Farnocchia D., Chesley S. R., Chodas P. W., Tricarico P., Kelley M. S. P., Farnham T. L. (2014). "Trajectory Analysis for the Nucleus and Dust of Comet C/2013 A1 (Siding Spring)". *The Astrophysical Journal*, **790**, article id. 114, 7 pp.

Moorhead A. V., Wiegert P. A., Cooke W. J. (2014). "The meteoroid fluence at Mars due to Comet C/2013 A1 (Siding Spring)". *Icarus*, **231**, 13–21.

Jenniskens P. (2006). Meteor Showers and their Parent Comets. Cambridge Univ. Press, Cambridge.

Tricarico P., Samarasinha N. H., Sykes M. V., Li J.-Y., Farnham T. L., Kelley M. S. P., Farnocchia D., Stevenson R., Bauer J. M., Lock R. E. (2014). "Delivery of Dust Grains from Comet C/2013 A1 (Siding Spring) to Mars". *The Astrophysical Journal Letters*, **787**, article id. L35, 5 pp.

Vaubaillon J., Colas F., Jorda L. (2005). "A new method to predict meteor showers. I. Description of the model". *Astronomy & Astrophysics*, **439**, 751–760.

Vaubaillon J., Maquet L., Soja R. (2014). "Meteor hurricane at Mars on 2014 October 19 from comet C/2013 A1, 2014". *Monthly Notices of the Royal Astronomical Society*, **439**, 3294–3299.

Ye Q., Wiegert P. A. (2014). "Will comet 209P/LINEAR generate the next meteor storm?". *Monthly Notices of the Royal Astronomical Society*, **437**, 3283–3287.

A new meteor detection algorithm for shuttered photography

Berénice Reffet, Jérémie Vaubaillon, François Colas

IMCCE, Paris, Observatoire de Paris, 77 av. Denfert-Rochereau, 75014 Paris, France
rberenice@imcce.fr, vaubaill@imcce.fr, colas@imcce.fr

This paper presents a new meteor detection algorithm used on CCD camera images. We detail some methods used on CCD images but also on other types of images. Then we explain the algorithm which applies image difference and then the Hough transform.

1 Introduction

The meteor detection is decisive information to determine the trajectory of an object. Indeed it helps to know where the object comes from and in the case the corresponding meteorite is found, it allows us to determine the composition of solar system objects. Moreover, the trajectory calculation also allows us to estimate the risks of collision with telecommunication satellites or with the Earth.

The new algorithm presented here was created for the CABERNET (**Ca**mera for **BE**tter **R**esolution **NET**work) project. The aim of this project is to determine precise orbits of meteors by using CCD images taken by 3 cameras during a night. The aim of the algorithm is to reduce the number of false detections obtained by the existing algorithm.

2 Related work

Many scientists worked on meteor detection algorithms because there are different ways to capture meteor images. P. Gural (2008) presents different methods to detect meteors, such as the probabilistic methods, the wavelet transform, the mathematical morphology, the Hough transform and the matched filter.

The probabilistic methods put together predictions of near Earth object's orbits (Babadzhanov et al., 2008), which allow us to determine the associated meteor shower and to detect the meteor. We can also use the Latent Dirichlet Allocation with radio astronomy images (Friedlander et al., 2012), to know the pixel distribution in function of the intensity and allow us to detect the source. Another method (Tzannes et al., 2002), applied on infrared images, consists in computing the temporal mean and the standard deviation of each pixel, and then in applying a band-pass filter and some thresholds including one using ROC curves.

Concerning the methods using a CCD image sensor, we can distinguish two techniques. The first one (Mohanty, 1981) uses the maximum-likelihood ratio detection using a simultaneous estimation of the mean and the covariance of the noise, then simulates the target pattern, before correlating the received data with the target patterns and comparing with the corresponding threshold, to finally print out the positions and paths of the targets when present. The second one (Mojzis et al., 2012) uses a statistical test for the Poisson distribution and the False Discovery Rate (FDR) in multiple hypothesis, for analysis on dark frames. Then the method is applied to detect any object.

On CCD images we can also use the wavelet transform (Thenappan, 2008), for example by using the "À trous" algorithm (Anisimova, 2011) to smooth the object.

Another powerful method is the Hough Transform (Kubickova, 2011; Trayner et al., 1999), which detects lines in an image. On videos, we can use the Time Hough Transform algorithm to detect the meteors by computing their velocity.

Finally, the matched filter aim is to make an hypothesis on the movement of an object from a velocity vector and a starting point, and then re-center every frame as a function of the model (Gural et al., 2005; Gural, 2008).

The way to do it is:

- Making a patch which contains one or more segments.
- Correlating with the image to determine whether the template is in the image.

These various articles coming from astronomy and computer reviews allowed to choose which methods of image processing to apply.

3 Our method

The algorithm should respect some constraints like:

- Taking FITS image as entry.
- Working on both Windows XP and Windows 7.
- Processing 60000 images in 3 hours.
- Detecting as many meteors as the previous one.

The detection algorithm begins with the difference between two successive images and then applies the Hough transform on the resulting image.

More precisely, we open the FITS image in C language by using the CIFITSIO library. Then we convert the 16 bit image into an 8 bit image to be able to use the OpenCV functions. Indeed this library includes a Hough transform function which processes 8 bit images.

We apply a threshold to reduce the number of the objects (*Figure 1*).

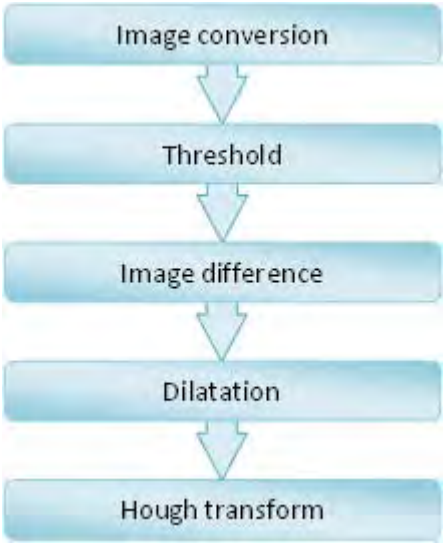

Figure 1 – Diagram of our algorithm.

After these operations we apply an image difference to remove the background. We apply another threshold to keep only our meteor (*Figure 2*). Then we use a mathematical morphology dilatation to be sure that the Hough Transform will detect our meteor. Finally we apply the Hough Transform.

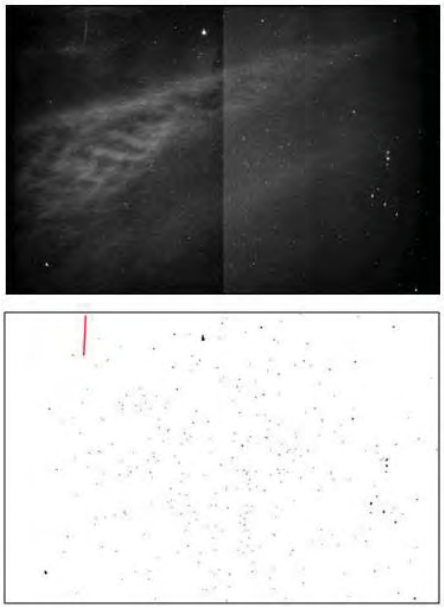

Figure 2 – Upper picture: image with clouds.
Lower picture: image after applying our algorithm.

4 Results

This program gave satisfactory results: all the meteors which had to be detected were detected and we obtained only 2 false detections on the test images database (see also *Figure 3*).

We have in both cases 100% of images containing meteors detected.

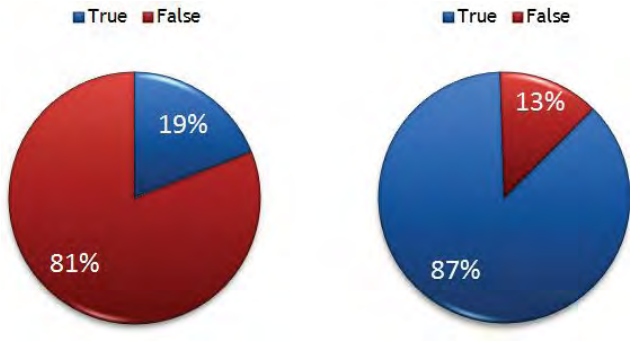

Figure 3 – Left: detections rate with the previous algorithm. Right: detections rate with the new algorithm.

5 Conclusion

The results are more than satisfying, but we could improve the algorithm by using the phase coded disk method or by segregating meteors and satellites in different folders.

Acknowledgment

Many thanks to Pete Gural for his advice, and to IMCCE and Observatoire de Paris for supporting this project.

References

Anisimova E., Páta P., Blazek M., Fliegel K., Vitek S., and Koten P. (2011). "Wavelet transform for processing of video from MAIA system". *Proceedings SPIE* **8306**, 83061Q, 6 pp.

Babadzhanov P. B, Williams I. P., and Kokhirova G. I. (2008). "Near-Earth Objects in the Taurid complex". *Monthly Notices of the Royal Astronomical Society*, **386**, 1436–1442.

Friedlander A., Frean M., Johnston-Hollitt M., and Hollitt C. (2012). "Latent Dirichlet allocation for image segmentation and source finding in radio astronomy images". *Proceedings of the 27th Conference on Image and Vision Computing New Zealand*, pages 429–434.

Gural P. S., Larsen J. A., and Gleason A. E. (2005). "Matched Filter Processing for Asteroid Detection". *Astronomical Journal*, **130**, 1951–1960.

Gural P. S. (2008). "Algorithms and Software for Meteor Detection". *Earth, Moon, and Planets*, **102**, 269–275.

Kubickova E. A. (2011). "Computer Vision in Meteor Research". In Asher D. J., Christou A. A., Atreya P., and Barentsen G., editors, *Proceedings of the International Meteor Conference*, Armagh, Northern Ireland, 16–19 September, 2010. IMO, Pages 41–44.

Mohanty N. C. (1981). "Computer Tracking of Moving Point Targets in Space". *IEEE Trans. Pattern Anal. Mach. Intell.*, **PAMI-3**, n° 5, 606–611.

Mojzis F., Kukal J., and Svihlik J. (2012). "Astronomical systems analysis and object detection". *Radioelektronika 2012 22nd International Conference*, pages 1–4.

Thenappan S., GiriPrasad M. N., Varadajan S. and Reddy T. S. (2008). "Application of Complex Wavelets in radar signal processing". *International Conference on Electronic Design, ICED 2008*, pages 1–8.

Trayner C., Haynes B. R., and Bailey N. J. (1999). "The time-gradient Hough transform, a novel algorithm from meteor science*". IEE Colloquium on Motion Analysis and Tracking*, **103**,16/1–16/6.

Tzannes A. P. and Brooks D. H. (2002). "Detecting small moving objects using temporal hypothesis testing". *IEEE Trans. Aerosp. Electron. Syst.*, **38**, 570–586.

The author, Berénice Reffet, during her lecture. (Credit Dominique Richard).

The prediction of meteor showers from all potential parent comets

Luboš Neslušan, Mária Hajduková,
Dušan Tomko, Zuzana Kaňuchová and Marián Jakubík

Astronomical Institute, Slovak Academy of Sciences, Slovakia
Maria.Hajdukova@savba.sk
ne;kanuchova;dtomko;mjakubik@ta3.sk

The objectives of this project are to predict new meteor showers associated with as many as possible known periodic comets and to find a generic relationship of some already known showers with these comets. For a potential parent comet, we model a theoretical stream at the moment of its perihelion passage in a far past, and follow its dynamical evolution until the present. Subsequently, we analyze the orbital characteristics of the parts of the stream that approach the Earth's orbit. Modelled orbits of the stream particles are compared with the orbits of actual photographic, video, and radar meteors from several catalogues. The whole procedure is repeated for several past perihelion passages of the parent comet. To keep our description compact but detailed, we usually present only either a single or a few parent comets with their associated showers in one paper. Here, an overview of the results from the modelling of the meteor-shower complexes of more than ten parent bodies will be presented. This enables their diversities to be shown. Some parent bodies may associate meteor showers which exhibit a symmetry of their radiant areas with respect to the ecliptic (ecliptical, toroidal, or showers of an ecliptic-toroidal structure), and there are showers which have no counterpart with a similar ecliptical longitude on the opposite hemisphere. However, symmetry of the radiant areas of the pair filaments with respect to the Earth's apex is visible in almost all the complexes which we examined.

1 Introduction

The aim of this project is to reveal alterations in initial orbital corridors of meteoroid streams which were formed due to gravitational action. This enables generic relationships between a meteoroid stream and a parent comet that do not have similar orbits to be found and new meteor showers to be predicted. Stream meteoroids which move each in an orbit similar to the comet's orbit create around the comet's orbit a spatial orbital corridor. If the stream is not significantly perturbed, the orbit of the parent comet will be situated inside the corridor at its center.

If this orbit is situated at a large distance from the orbit of our planet, the particles of the stream do not usually collide with its atmosphere and thus create a meteor shower. However, in some cases, the gravitational perturbations of major planets can deflect a significant number of particles from the corridor around the parent body orbit, being far from the Earth's orbit, into an alternative corridor crossing this orbit. Thus, some cometary or asteroidal objects in distant orbits can still have associated a stream colliding with the Earth's atmosphere.

If the entire orbit of a comet is situated relatively close to the orbit of the Earth, the particles also pass relatively close to the orbit of our planet, and some of them collide with its atmosphere. Here also, the perturbations can change the orbits of a part of a stream. As a consequence, an alternative corridor, or corridors, of orbits are formed. If more than a single corridor of a given stream passes through the Earth's orbit, we observe several meteor showers associated with the same parent body.

All these alterations of the initial orbital corridors can be revealed by our modelling of theoretical streams and studying their dynamical evolutions for a suitably long period. So far, we have modelled meteor-shower complexes of eleven parent bodies, the analyses of which have already been individually published in the following papers: Neslušan (1999), Kaňuchová and Neslušan (2007), Tomko and Neslušan (2012), Neslušan et al. (2013a, b), Tomko (2014), Neslušan and Hajduková (2014), Neslušan et al. (2014), Tomko and Neslušan (2014). Here, we present an overview of these results, comparison of which enables their diversities and/or similarities to be shown. The procedure allows us to map the whole complex of meteoroid particles released from a parent comet. The relationship between a particular comet and known showers can be either confirmed or shown doubtful, or a new relationship can appear. The structure of modeled complexes demonstrates the distribution of the cardinal directions of meteor sources and contributes to the map of the whole meteoroid population in the Solar System.

2 Modeling theoretical streams

Meteoroid streams of several parent bodies and their dynamical evolution were studied with the help of various stream models (e.g., Williams and Wu, 1994; Brown and Jones, 1998; Asher, 1999; Beech, 2001; Asher and Emel'yanenko, 2002; Lyytinen and Jenniskens, 2003; Jenniskens, 2004; Williams et al., 2004; Asher, 2005; Vaubaillon et al., 2005a,b; Wiegert et

al., 2005; Wiegert and Brown, 2005; Porubcan and Kornos, 2005; Vaubaillon and Jenniskens, 2007; Asher, 2008; Babadzhanov et al., 2008; Wiegert et al., 2009; Jenniskens and Vaubaillon, 2010; Babadzhanov et al., 2013; Jopek et al., 2013; Sekhar and Asher, 2014 a,b).

We decided to base our study of the dynamics of meteoroid streams on the gravitational action, exclusively. Since we aim to predict new streams, we do not consider any non-gravitational effects. We assume that including these effects, characterized by the entire ranges of possible free parameters, would only enlarge the dispersion of predicted stream characteristics. Our aim is not to model the stream in all its details corresponding to a realistic scenario (which is never completely known in a specific case), but to cover the orbital phase space of the densest core of an actual stream only. The modelled set of orbits represents the most central part of the stream, not the entire stream.

For a potential parent comet, we model a theoretical stream at the moment of its perihelion passage in a distant past, monitor its orbital evolution up to the present, and select a part of the stream that approaches the Earth's orbit. These particles are used to predict the corresponding meteor showers. The predicted showers are searched for in the databases of actually observed meteors. The whole procedure is repeated for several past perihelion passages of the parent body. The procedure allows us to map the whole complex of meteoroid particles released from a parent comet. A detailed description of the method can be found in the individual papers mentioned in the Introduction.

3 Analyses and results

Our modelling has revealed new relationships among the known meteor showers observed in the Earth's atmosphere that belong to the same complex. New parent bodies associated with known meteor showers have been found, and new meteor showers have been predicted to be observed. The results of our project are summarized and briefly listed in the following paragraphs. All the results contributed significantly to the task of finding parent bodies of minor meteor showers, which is one of the subjects of recent meteor research (Wiegert and Brown, 2004; Brown et al., 2010; Rudawska et al., 2012, Rudawska and Vaubaillon, 2014).

Overlapping meteor-shower complexes of 14P/Wolf and D/1892 T1 (Barnard 3)

The dynamical study of the meteor stream associated with comet 14P/Wolf shows that the planetary gravitational disturbances split the corridor of the stream into several filaments. Meteors of two of them can enter the Earth's atmosphere and become observable. The model corresponds to the orbit of the comet 14P/Wolf before 1922, when the comet was moved to a new orbit by the gravitational disturbance of Jupiter and stopped releasing meteoroid particles into the orbits crossing the orbit of the Earth.

The filament with a higher declination of the mean radiant coincides with the meteor stream associated with comet D/1892 T1 (Barnard 3). The filament of the 14P/Wolf stream with a lower declination of the radiant coincides with the well-known meteor shower α-Capricornids (Neslušan, 1999). We note that Jenniskens and Vaubaillon (2010) found a better parent body for the α-Capricornids shower: the minor planet 2002 EX12 (=169P/NEAT). A possible dynamical relationship of 14P with this asteroid has not been investigated yet.

Nearly identical meteor-shower complexes of the comet 96P/Machholz and asteroid 2003 EH1

Theoretical streams of the comet 96P/Machholz and asteroid 2003 EH1 evolved, after a significant time, into an almost identical structure (Neslušan et al. ,2013a, b, Kaňuchová and Neslušan, 2007). Both streams are highly structured. The 96P approaches the Earth's orbit in six intervals of the ecliptic longitude of Earth. (There are eight approaches in total, but two of these intervals partially overlap.) The particles in three of these intervals hit the Earth from the northern direction and in the other three intervals from the southern direction relative to the ecliptic. As a consequence, we can distinguish six filaments (F1–F6) in the part of the stream that approaches the orbit of the Earth. These filaments correspond to six meteor showers with the radiants distributed on the sky symmetrically with respect to the Earth's apex. Four of them are well known from observations: daytime Arietids (F1), δ-Aquariids S (F5) and N (F2), and Quadrantids (F3). Filament 4, predicted to be the southern branch of the daytime Arietids, could be, with an uncertainty, identified with α-Cetids. Its identification, as well as that of filament 6 (with similar characteristics as the κ-Velids, or the Puppid-Velid Complex, or the Carinid Complex), with corresponding showers in the considered databases were negative. The complex structure of the stream is demonstrated with the predicted radiants of particles expected to collide with the Earth in the present. The positions of the radiants are plotted in *Figure 1* (left).

Similarly, examination of the asteroid 196256 (2003EH1) showed that six well-established and two minor filaments approach the orbit of the Earth, producing the same four well-known meteor showers as the stream 96P (*Figure 1* right). If we followed a longer evolutionary period, then another shower having both northern and southern branches occurred (filaments 7 and 8). If this shower exists, it would be an ecliptical shower related to the Arietids.

Meteor-shower complex of the long-period comet C/1917 F1 (Mellish)

We also focused our attention on the meteor-shower complex of the comet C/1917 F1 Mellish (Neslušan and Hajduková, 2014). The modeled complex is shown in Figure 2. The theoretical stream split into four filaments. We have confirmed the generic relationship between the studied parent comet and the December Monocerotids (F3). The comet is probably also the parent body of the

April ρ-Cygnids (F1). The evolution of the meteoroids to the orbits of this shower is very long, at about 20 millennia. Following even a longer evolutionary period, up to 50 millennia, two other diffuse showers with the radiants situated symmetrically to both the December Monocerotids and April ρ-Cygnids showers with respect to the apex of the Earth's motion occurred (filaments 2 and 4). However, we did not find any corresponding shower in the list of the IAU.

Our simulation did not confirm any relationship between C/1917 F1 and the November Orionids, a shower which is, according to several authors, related to the comet Mellish (Veres et al., 2011).

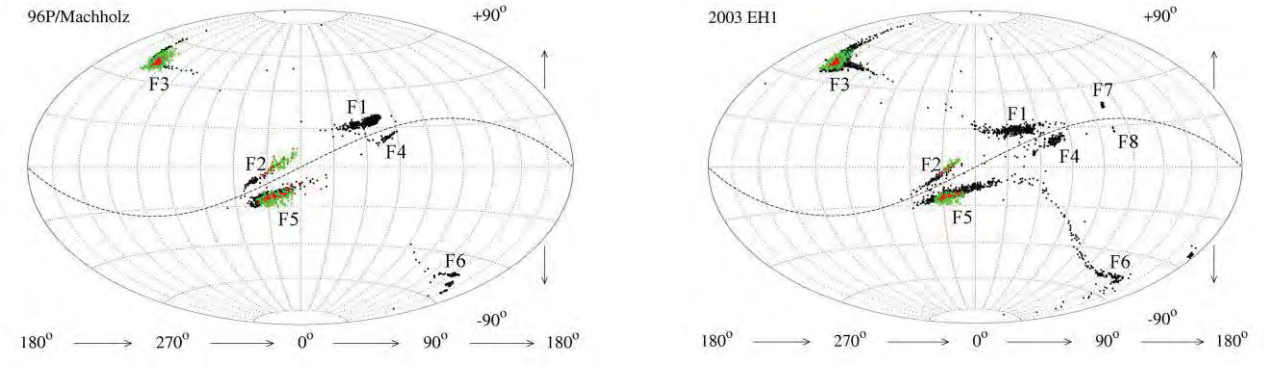

Figure 1 – The nearly identical meteor-shower complexes of the comet 96P/Machholz and the asteroid 2003 EH1. The radiants calculated from the modeled orbits (black dots) are compared with those of the real meteors from the video (pale) and photographic (darker) catalogues (SonotaCo, 2009; Lindblad et al., 2003). The identified associated showers: daytime Arietids (F1), northern (F2) and southern (F5) branch of δ-Aquariids, Quadrantids (F3); possibly associated showers: α-Cetids (F4), κ-Velids, or the Puppid-Velid Complex, or the Carinid Complex (F6). Filaments F7 and F8, which occurred in the model of the asteroid, could not be identified to any showers of the IAU MDC list. Positions of the radiants in right ascension and declination are shown in the Hammer projection of equatorial coordinates. The sinusoid-like curve illustrates the ecliptic.

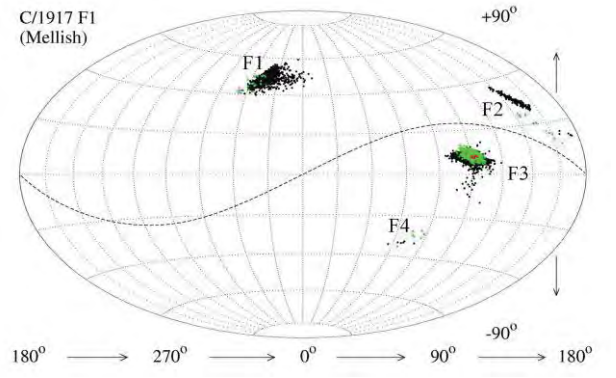

Figure 2 – The radiants of the modeled meteor-shower complex of the comet F1/1917 (Mellish) compared with those of the real meteors. Identified showers: December Monocerotids (F3) and possibly April ρ Cygnids (F1). We did not find any corresponding showers in the IAU MDC list to filaments F2 and F4.

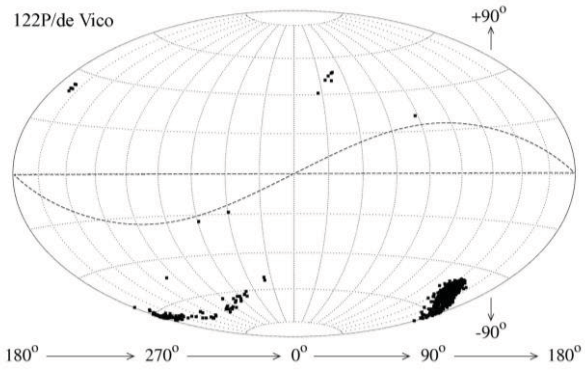

Figure 3 – The radiants of a new meteor-shower, associated with the comet 122P/de Vico, which is predicted in the southern hemisphere. The identification with real meteors was negative, probably because only a low number of real meteors have been detected in the southern sky.

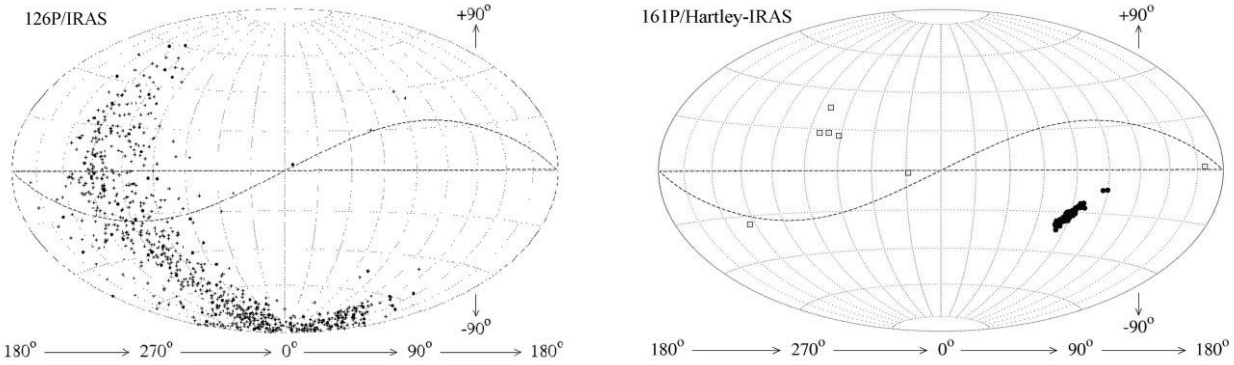

Figure 4 – Parts of the theoretical streams of two comets in orbits situated at a relatively large distance from the orbit of Earth that cross, according to our modeling, the Earth's orbit and, eventually, could be observed as meteors. However, the radiant area of meteors of the 126P/2004 V2 (left) is largely dispersed and, therefore, mixed with the sporadic meteor background. On the other hand, there seems to be a quite high chance of discovering the shower of 161P/2004 V2 (right) with a compact radiant area on the southern sky.

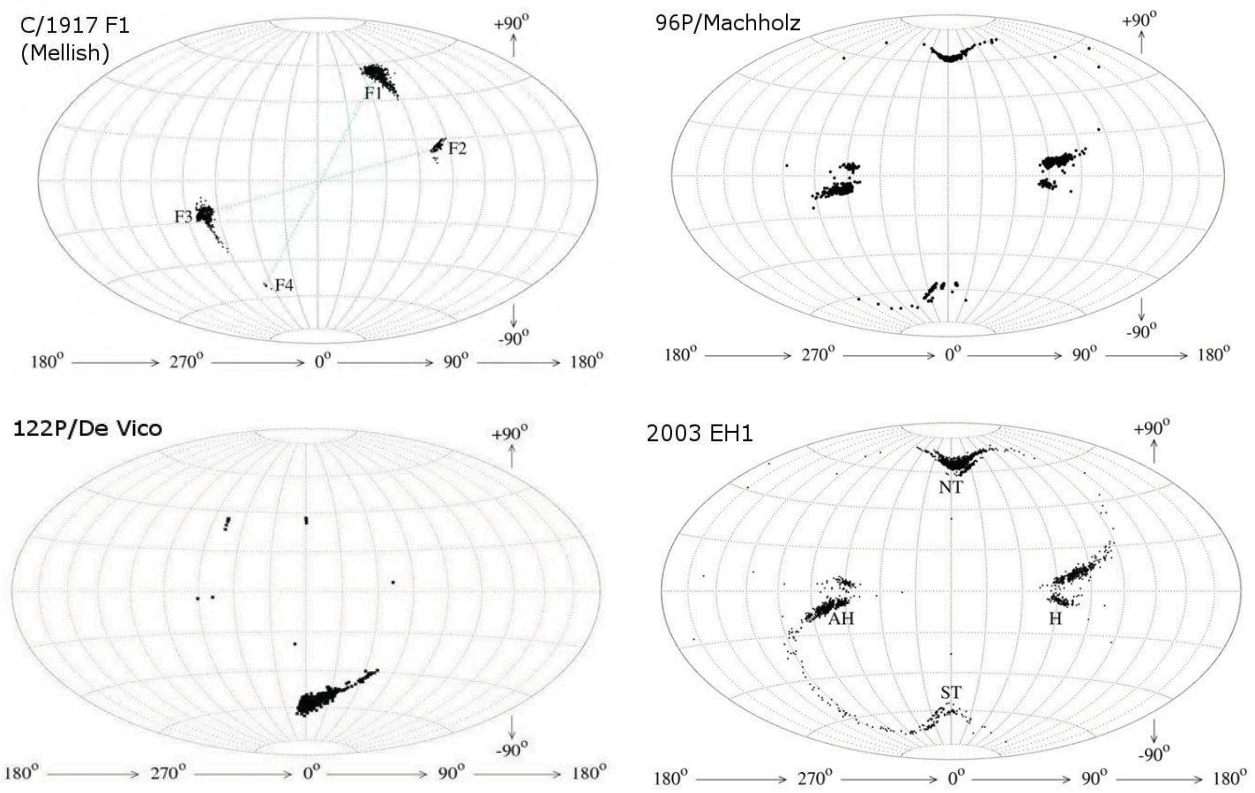

Figure 5 – The radiants of showers are distributed on the sky symmetrically with respect to the Earth's apex. Some of them are symmetrical to the ecliptic (e.g. showers of 96P/Machholz and asteroid 2003 EH1, which create an ecliptic-toroidal structure). Some of them have no counterparts with a similar ecliptical longitude on the opposite hemisphere (C/1917 F1 Mellish). The ecliptical coordinate system is modified to place its origin at the apex of the Earth's motion.

New meteor showers in the southern hemisphere predicted

We modelled theoretical streams of several comets, associated meteor showers of which have predicted radiant areas on the southern sky. The identification with real meteors is, in these cases, difficult because southern sky observations are significantly rarer than observations of the northern sky. Thus, a low number of real meteors of the southern sky has been detected and, therefore, recorded in the databases used.

Two Halley-type comets, 161P/2004 V2 and 122P/de Vico, that were examined, associate meteor showers with compact radiant areas on the southern sky (*Figures 3, 4 right*). We point out that, in spite of a relatively large distance of the orbit of 161P/2004 V2 from the Earth (the minimum distance between the 161P orbit and the Earth's orbit was largest, about 1.8 AU, 4300 years before the present, and it does not, at the present, approach the Earth's orbit closer than 0.4 AU), the comet may associate an Earth-observable meteor shower.

A significant fraction of particles released from another studied comet in a distant orbit, 126P/2004 V2, also cross the Earth's orbit, according to our modelling, and, eventually, could be observed as meteors, prevailingly on the southern sky. However, their radiant area is largely dispersed (declination of radiants spans from about + 60° to the southern pole) and, therefore, mixed with the sporadic meteor background (*Figure 4 left*). Identification with real meteors is practically impossible.

The question of the existence of these showers remains open. However, there seems to be quite a high chance of discovering at least some of them in the future with an expected increase of observations of the southern hemisphere. More detailed description is in the papers of Tomko and Neslušan (2012), Tomko (2014), Tomko and Neslušan (2014).

4 Symmetry on the sky

An interesting issue concerns the symmetry of filaments of the modelled stream. The radiants of showers of all complexes which consist of more than one filament are distributed on the sky symmetrically with respect to the Earth's apex. Some of them are symmetrical to the ecliptic. Some of them have no counterpart with a similar ecliptical longitude on the opposite hemisphere. But, still, they exhibit a symmetry with respect to the Earth's apex.

The cardinal directions of meteor sources, "helion", "antihelion" and "northern and southern toroidal" are more often related to the sporadic meteor background since the ecliptic-toroidal structure appears in the overall distribution of radio-meteor radiants, as published by Campbell-Brown and Brown (2005). According to Jenniskens (2006), many well-known streams, such as Daytime Arietids, δ-Aquariids and others belong to the ecliptical streams in the sense of cardinal meteor directions. Obviously, there are several parent bodies feeding these streams. Our study has showed a relationship between ecliptical streams and toroidal streams. The meteor-shower complexes of comet 96P and

asteroid 2003 EH1 showed that a single parent body can associate showers of both kinds, ecliptical and toroidal (Neslušan et al., 2013a, b, 2014). The ecliptic-toroidal structure is seen transparently in these models (*Figure 5b, 5d*). The predicted radiants of particles that approach the Earth's orbit are plotted in the ecliptical coordinate system modified to place its origin at the apex of the Earth's motion. The filaments corresponding to the Arietids, δ-Aquariids S and N, and possibly α-Cetids constitute the ecliptical component and those corresponding to the Quadrantids, and possibly κ-Velids, constitute the toroidal component of the complex.

Meteor showers of the long-period comet C/1917 F1 Mellish (*Figure 5a*) have no counterpart with a similar ecliptical longitude on the opposite hemisphere, but they show a certain symmetry of their showers' radiant areas with respect to the Earth's apex (Neslušan and Hajduková, 2014).

5 Conclusion

Within the frame of the project "The prediction of meteor showers from all potential parent comets", we have so far investigated 11 parent bodies. Our procedure is based on the modelling of a theoretical stream for several moments of the perihelion passages of a parent body in the distant past, monitoring its orbital evolution up to the present, selecting that part of the stream which approached the Earth's orbit, and comparing the characteristics of this part with the corresponding observed meteor shower. New meteor showers, mainly in the southern hemisphere, were predicted and new parent bodies of meteor showers, resp. new relationships between observed showers were suggested.

A comparison of the theoretical streams of several examined comets enabled their diversities and specific features to be shown. The results are summarized in the following conclusions:

- a single parent body can associate multiple showers
- a shower can be associated to multiple parent bodies
- shower radiants of a complex are distributed on the sky symmetrically with respect to the Earth's apex
- an ecliptic-toroidal structure of complexes was found.

Acknowledgment

The work was supported, by the VEGA – the Slovak Grant Agency for Science, grants No. 2/0031/14 and 1/0225/14 and by the Slovak Research and Development Agency under the contracts No. APVV-0517-12 and APVV-0158-11.

References

Asher D. J. (1999). "The Leonid meteor storms of 1833 and 1966". *Monthly Notices of the Royal Astronomical Society*, **307**, 919–924.

Asher D. J. (2005). "The dynamical structure of meteor streams and meteor shower predictions". In Z. Kneževic Z., and Milani A., editors, Dynamics of Populations of Planetary Systems, *Proceedings of IAU Colloquium #197*, held 31 August – 4 September, 2004 in Belgrade, Serbia and Montenegro. Cambridge: Cambridge Univ. Press, pages 375–382.

Asher D. J. (2008). "Meteor Outburst Profiles and Cometary Ejection Models". *Earth, Moon, and Planets*, **102**, 27–33.

Asher D. J., and Emel'yanenko V. V. (2002). "The origin of the June Bootid outburst in 1998 and determination of cometary ejection velocities". *Monthly Notices of the Royal Astronomical Society*, **331**, 126–132.

Babadzhanov P. B., Williams I. P., and Kokhirova G. I. (2008). "Meteor showers associated with 2003EH1". *Monthly Notices of the Royal Astronomical Society*, **386**, 2271–2277.

Babadzhanov P. B., Williams I. P., and Kokhirova G. I. (2013). "Near-Earth asteroids among the Scorpiids meteoroid complex". *Astronomy & Astrophysics*, **556**, id. A25, 5 pp.

Beech M. (2001). "Comet 72P/Denning-Fujikawa: down but not necessarily out". *Monthly Notices of the Royal Astronomical Society*, **327**, 1201–1207.

Brown P., and Jones J. (1998). "Simulation of the Formation and Evolution of the Perseid Meteoroid Stream". *Icarus*, **133**, 36–68.

Brown P., Wong D. K., Weryk R. J., Wiegert P. (2010). "A meteoroid stream survey using the Canadian Meteor Orbit Radar II: Identification of minor showers using a 3D wavelet transform". *Icarus*, **207**, 66–81.

Campbell-Brown M. D., and Brown P. (2005). "The Meteoroid Environment: Shower and Sporadic Meteors". Dust in Planetary Systems, Proceedings of the conference held September 26-28, 2005 in Kaua'i, Hawaii. *LPI Contribution*, **1280**, 29.

Jenniskens P. (2004). "2003 EH_1 Is the Quadrantid Shower Parent Comet". *Astronomical Journal*, **127**, 3018–3022.

Jenniskens P., Vaubaillon J. (2010). "Minor Planet 2002 EX_{12} (=169P/NEAT) and the Alpha Capricornid Shower". *Astronomical Journal*, **139**, 1822–1830.

Jenniskens P. (2006). Meteor Showers and Their Parent Comets, Cambridge Univ. Press, Cambridge.

Jopek T. J., and Williams I. P. (2013). "Stream and sporadic meteoroids associated with near-Earth

objects". *Monthly Notices of the Royal Astronomical Society*, **430**, 2377–2389.

Kaňuchová Z., and Neslušan L. (2007). "The parent bodies of the Quadrantid meteoroid stream". *Astronomy & Astrophysics*, **470**, 1123–1136.

Lindblad B. A., Neslusan L., Porubcan V., Svoren J. (2003). "IAU Meteor Database of photographic orbits version 2003". *Earth, Moon, and Planets*, **93**, 249–260.

Lyytinen E., and Jenniskens P. (2003). "Meteor outbursts from long-period comet dust trails". *Icarus*, **162**, 443–452.

Neslušan L. (1999). "Comets 14P/Wolf and D/1892 T1 as parent bodies of a common, α-Capricornids related, meteor stream". *Astronomy & Astrophysics*, **351**, 752–758.

Neslušan L., Kaňuchová Z., and Tomko D. (2013a). "The meteor-shower complex of 96P/Machholz revisited". *Astronomy & Astrophysics*, **551**, 14 pp.

Neslušan L., Hajduková M., jr., and Jakubík M. (2013b). "Meteor-shower complex of asteroid 2003 EH1 compared with that of comet 96P/Machholz". *Astronomy & Astrophysics*, **560**, id. A47, 10 pp.

Neslušan L., and Hajduková M., jr. (2014). "The meteor-shower complex of comet C/1917 (Mellish)". *Astronomy & Astrophysics*, **566**, id. A33, 9 pp.

Neslušan L., Kaňuchová Z., and Tomko D. (2014). "The ecliptic-toroidal structure of the meteor complex of comet 96P/Machholz". In Jopek T. J., Rietmeijer F. J. M., Watanabe J., and Williams I. P., editors, *Meteoroids 2013, Proceedings of the Astronomical Conference*, held at A. M. University, Poznań, Poland, 26–30 August 2013, A.M. University Press, pages 235–242.

Porubčan V., Kornoš L. (2005). "The Quadrantid meteor stream and 2003 EH1". *Contrib. Astron. Obs. Skalnaté Pleso*, **35**, no. 1, 5–16.

Rudawska R., Vaubaillon J. and Atreya P. (2012). "Association of individual meteors with their parent bodies". *Astronomy & Astrophysics*, **541**, id. A2, 5 pp.

Rudawska R., Vaubaillon J. (2014). "Don Quixote - a possible parent body of a meteor shower". In Rault J.-L., and Roggemans P., editors, *Proceedings of the International Meteor Conference*, Giron, France, 18–21 September 2014. IMO, pages 152–153.

Sekhar A., and Asher D. J. (2014a). "Resonant behavior of comet Halley and the Orionid stream". *Meteor. Planet. Sci.*, **49**, 52–62.

Sekhar A., and Asher D. J. (2014b). "Meteor showers on Earth from sungrazing comets". *Monthly Notices of the Royal Astronomical Society*, **437**, L71–L75.

SonotaCo (2009). "A meteor shower catalog based on video observations in 2007-2008". *WGN, Journal of the IMO*, **37**, 55–62.

Tomko D., and Neslušan L. (2012). "Search for New Parent Bodies of Meteoroid Streams Among Comets. I. Showers of Comets 126P/1996 P1 and 161P/2004 V2 with Radiants on Southern Sky". *Earth, Moon, and Planets*, **108**, 123–138.

Tomko D., and Neslušan L. (2014). "Prediction of meteor shower of comet 161P/2004 V2". In Jopek T. J., Rietmeijer F. J. M., Watanabe J., and Williams I. P., editors, *Meteoroids 2013, Proceedings of the Astronomical Conference*, held at A. M. University, Poznań, Poland, 26–30 August 2013, A.M. University Press, pages 243–249.

Tomko D. (2014). "Prediction of meteor shower associated with Comet 122P/de Vico". *Contrib. Astron. Obs. Skalnaté Pleso*, **44**, 33–42.

Vaubaillon J., Arlt R., Shanov S., Dubrovski S., and Sato M. (2005a). "The 2004 June Bootid meteor shower". *Monthly Notices of the Royal Astronomical Society*, **362**, 1463–1471.

Vaubaillon J., Colas F., and Jorda L. (2005b). "A new method to predict meteor showers. I. Description of the model". *Astronomy & Astrophysics*, **439**, 751–760.

Vaubaillon J., and Jenniskens P. (2007). "Dust trail evolution applied to long-period comet C/1854 L1 (Klinkerfues) and the ε-Eridanids". *Adv. Space Res.*, **39**, 612–615.

Vereš P., Kornoš L., and Tóth J. (2011). "Meteor showers of comet C/1917 F1 Mellish". *Monthly Notices of the Royal Astronomical Society*, **412**, 511–521.

Wiegert P., and Brown P. (2004). "The problem of linking minor meteor showers to their parent bodies: Initial considerations". *Earth, Moon, and Planets*, **95**,19–26.

Wiegert P., and Brown P. (2005). "The Quadrantid meteoroid complex". *Icarus*, **179**, 139–157.

Wiegert P. A., Brown P. G., Vaubaillon J., and Schijns H. (2005). "The τ Herculid meteor shower and Comet 73P/Schwassmann-Wachmann 3". *Monthly Notices of the Royal Astronomical Society*, **361**, 638–644.

Wiegert P., Vaubaillon J., and Campbell-Brown M. (2009). "A dynamical model of the sporadic meteoroid complex". *Icarus*, **201**, 295–310.

Williams I. P., and Wu Z., (1994). "The Current Perseid Meteor Shower". *Monthly Notices of the Royal Astronomical Society*, **269**, 524–528.

Williams I. P., Ryabova G. O., Baturin A. P., and Chernitsov A. M. (2004). "The parent of the Quadrantid meteoroid stream and asteroid 2003 EH1". *Monthly Notices of the Royal Astronomical Society*, **355**, 1171–1181.

The author, Maria Hajdukova, during her lecture. (Credit Axel Haas).

The Interplanetary Meteoroid Environment for eXploration – (IMEX) project

Rachel H. Soja[1], Maximilian Sommer[1], Julian Herzog[1], Ralf Srama[1], Eberhard Grün[2], Jens Rodmann[3], Peter Strub[1], Jérémie Vaubaillon[4], Andreas Hornig[1], Lars Bausch[5]

[1] **Institute of Space Systems, University of Stuttgart, Stuttgart, Germany**
soja@irs.uni-stuttgart.de

[2] **Max Planck Institute for Nuclear Physics (MPIK), Heidelberg, Germany**

[3] **Institute for Astrophysics, University of Göttingen, Göttingen, Germany**

[4] **IMCEE, Paris, France**

[5] **Aerospaceresearch.net, Stuttgart, Germany**

The 'Interplanetary Meteoroid Environment for eXploration' (IMEX) project, funded by the European Space Agency (ESA), aims to characterize dust trails and streams produced by comets in the inner solar system. We are therefore developing a meteoroid stream model that consists of a large database of cometary streams from all known comets in the inner solar system. This model will be able to predict meteor showers from most known comets, that can be observed anywhere in the inner solar system, at any time 1980-2080. This is relevant for investigating meteor showers on the Earth, on other planets, or at spacecraft locations. Such assessment of the dust impact hazard to spacecraft is particularly important in the context of human exploration of the solar system.

1 Introduction

As they approach the Sun, comets heat up and release dust grains that were previously trapped in surface ices. The heavier dust particles considered here (sizes >100μm) are not strongly affected by radiation pressure or solar wind. Therefore, instead of being blown away by the Sun, they remain near the comet's orbit forming a dust trail. Eventually, however, various effects act to disperse all particles released by comets: planetary perturbations; Poynting-Robertson and solar wind drag; collisions. Eventually these particles lose their dynamical information about their parent bodies and can no longer be associated with individual comets. In this way, comets (and asteroids) populate the interplanetary background dust cloud that we observe from Earth as the zodiacal light, and which is responsible for sporadic meteors that are not associated with any meteor shower.

These cometary trails and meteoroid streams therefore form temporary structures in the solar system, superimposed on top of the interplanetary dust cloud. Cometary trails, visible in infrared images, are more recent structures that are thought to cause meteor storms or outbursts on the Earth; older dust in wider meteoroid streams causes annual meteor showers (Kresak, 1993). Significant modeling work exists for individual streams. In particular, there exists a large body of research on modeling the dust trail of comet 67P/Churyumov-Gerasimenko as a result of ESA's Rosetta mission (Agarwal et al., 2007 , 2010; Kelley et al., 2008; Fulle et al., 2010). Current meteoroid stream modeling is capable of predicting meteor storms (for example, Vaubaillon et al., 2005a,b).

Our approach is to attempt to build a model of meteoroid streams throughout the inner solar system. There are several reasons for building such a model: it can be used to study meteor showers on Earth and on other planets; to develop a map of cometary trails in the sky, which can be used to launch a search for these trails; and to study the timescales on which streams are dispersed by planetary perturbations and other effects.

Our initial motivation for this model, however, is the impact hazard to spacecraft. An understanding of the interplanetary environment, including the dust environment, is crucial for the planning of spacecraft missions in the inner solar system. Particles striking a spacecraft with high velocities can cause damage leading to the impairment or even failure of the spacecraft or its subsystems. Depending on the impactor's size the effects range from degradation of functional surfaces, such as optical systems or solar arrays, to cratering and structural penetration. Additionally, secondary effects such as electromagnetic pulses generated by the plasma release from impacts can interfere or even destroy sensitive electronics. For instance, it is thought that a Perseid meteoroid caused such an event on the Olympus 1 satellite in 1993, which resulted in the loss of the spacecraft (Caswell et al., 1995). Manned space activities are especially vulnerable to any damage caused by meteoroid impacts because of their much lower tolerance level, large cross sections and long exposure times.

ESA and NASA both have meteoroid engineering models to describe the interplanetary meteoroid background, such as ESA's Interplanetary Meteoroid Environment Model (IMEM) (Dikarev et al., 2005). However, no model exists to assess the risk to spacecraft of cometary meteoroid streams. The Interplanetary Meteoroid Environment for

eXploration (IMEX) project attempts to address this problem by asking: can we predict the impact of meteoroid streams at any point in space or time? This extends the application of meteoroid stream modeling at the Earth to ask whether we can determine 'meteor showers' that occur at spacecraft locations. Such a model is also highly valuable as a database of meteor showers at all planets and other locations in the solar system, and can be used to investigate the creation and development of individual trails. The goal is to create a database of dust trails from more than 400 short-period comets in the inner solar system, which can be used for a variety of impact hazard and scientific purposes. Here we introduce our current model, and demonstrate how we use the Leonid meteor shower as a test case to verify the model.

2 The model

The aim of the model is to create a database of meteoroid streams from short period comets. This requires (1) emitting particles from a selection of comets, and (2) following their motion with time by integrating their trajectories. We save their positions and velocities to the database several times per orbit between 1980 and 2080.

We find 422 short-period comets from the JPL Small Body Database (SBDB) that have sufficient information and that have a perihelion within 3AU of the Sun. We include particles between 1700 and 2080 for Halley-type comets, and between 1850 and 2080 for other comets. For each comet apparition, we include particles randomly on the sunlight hemisphere of the comet, at 251 locations while the comet is within 3 AU of the Sun. Hundreds of thousands of particles are ejected for each comet: ~28000 per comet apparition for Halley-type comets; and ~14000 for other comets. Particles have 8 different masses logarithmically distributed, with radii between 100μm and 1cm, and bulk density 1000kgm^{-3}. We use the velocity model developed by Crifo and Rodionov (1997) and the mass distribution from Agarwal et al. (2010). Dust production is estimated using cometary total magnitudes (and total magnitude slopes) as given by the JPL (SBDB), using the result of Jorda et al. (2008). A dust to gas ratio of 1 is assumed. For a small number of major comets we use JPL HORIZONS orbits; for all other comets the orbits have been computed using the MODUST code (Rodmann, 2006), which uses a Hermite individual timestep scheme. This includes all important forces except the non-gravitational cometary forces, which are not well known for most comets.

The orbital integrations for the released particles are performed using a Runge-Kutta-Nyström 7(6) integrator with variable step size (Dormand and Prince, 1978). The emitted particles are individually integrated from their creation time up until 2080. Included are gravity of the Sun and eight planets, as well as radiation pressure and Poynting-Robertson drag (including a factor for solar wind drag). Particle positions and velocities are saved several times per orbit, and more often near perihelion and close planetary encounters. This creates a database from which the full trajectories of each particle from each comet can be reconstructed between 1980 and 2080.

The simulation of dust for many comets is a computationally intensive task, which usually would require the use of a supercomputer. However, supercomputing facilities are expensive and difficult to access, and so instead we share the work with many individual computers, connected through the internet. This approach is called distributed computing. The work (here, our group of dust particles) is split into many work units, which are distributed among participating computers. Once processed, the results are returned and can be stored and analyzed. The distribution and processing of the work units is managed by the BOINC system (Berkeley Open Infrastructure for Network Computing) developed at the University of Berkeley. It was originally designed to enable distributed computing for the SETI@home project, which tries to track down narrow-band signals, potentially sent by extraterrestrial civilizations, by data-mining telescope readouts. Since then, many more scientific projects have added to the BOINC platform. Computers participating in projects are owned by private users who donate their machines' idle computing power.

We utilize the Constellation BOINC platform to perform these meteoroid stream calculations, under the project 'CometTrails' (aerospaceresearch.net). Constellation aims to provide distributed computing capability to aerospace related science and engineering projects. Currently, ~13000 users are donating the idle time on ~70000 PCs. This form of citizen science provides the required computing performance for simulating millions of particles ejected by each of the 422 comets, while developing the relationship between scientists and the general public.

3 Test case: 55P/Tempel-Tuttle and Leonid meteor storms

We verify our model by determining how well it can describe past meteor storms. Here we compare our model for the trail of 55P/Tempel-Tuttle with observations of the 2001 Leonid meteor storm with a peak date of 18 November 18^h16^m UTC. We include particles from the comet between 1690 and 2001, and integrate their trajectories until 2001. Only a subsection of the modeled particles will contribute to the stream at Earth: therefore, we select only those particles that cross the ecliptic plane within 5 days of the date of interest. The locations at which they cross the ecliptic plane (orbital nodes) are plotted in *Figure 1*. The path of the Earth is also plotted, so that we can see that the Earth crosses the meteoroids produced during the comet apparitions with perihelia in 1766, 1866 and 1700. This plot agrees with a similar diagram using the model of McNaught and Asher (1999).

We calculate a zenith hourly rate (ZHR) profile by determining a number density near the Earth as a function of time and estimating the ZHR by calculating a probability of observation based on the meteor

magnitude, which is in turn derived from the meteoroid velocity and mass (*Figure 2*). We use methods described in Koschack and Rendtel (1990). We can see that the peak of both the observed ZHR profile and the modeled profile occurs at similar times: our modeled peak occurs 9 minutes before the observed peak. The width of our modeled profile is slightly too low, which is supposed to be related to differences in ejection mechanisms. The peak ZHR from our model is about 50% higher than the observed peak. This is the most uncertain part of our model, and is related to highly uncertain parameters including the cometary dust production rate and mass distribution. In general, however, the model is able to determine accurately the time at which a meteor shower occurs and to estimate the flux rate to an order of magnitude.

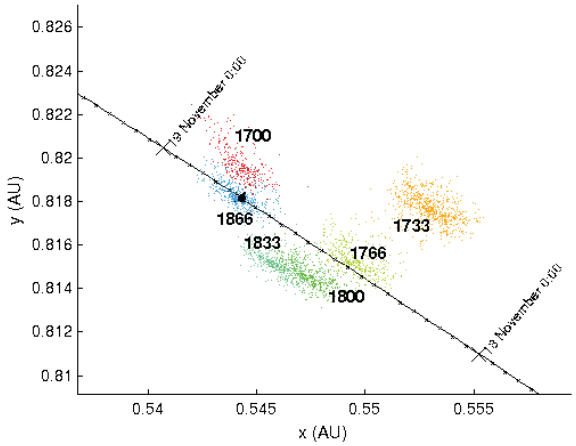

Figure 1 – Node distribution at the Earth of particles released from comet 55P/Tempel-Tuttle between 1690 and 1866, as seen on November 18 2001. Colors represent meteoroids emitted by the comet during different apparitions: the perihelion year of the comet apparition is superimposed. The black line indicates the path of the Earth. The Earth's position is indicated on the 18th and 19th of November and at every full hour.

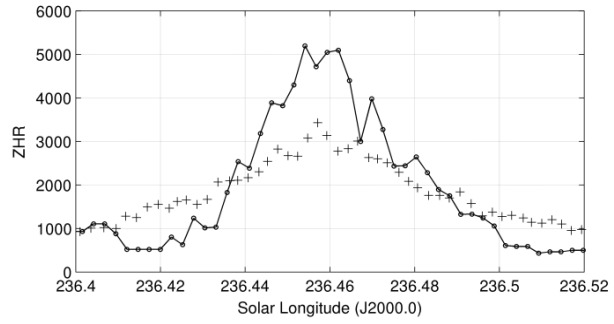

Figure 2 – Modeled (line) and observed (crosses) ZHR profile as a function of solar longitude, for a meteor storm on November 18 18h16m 2001. Observations are taken from Arlt et al. (2001).

Summary

We have developed a model for meteoroid streams in the inner solar system, and demonstrated that it can describe meteor storms at the Earth, as illustrated using the 2001 Leonid storm. We are currently investigating other meteor storms and outburst events. We shortly embark on integrations of emitted particles from all 422 comets using the Constellation distributed computing system. This will provide a database of the trajectories of dust particles that can be accessed to determine meteor storms occurring at any point in the Solar System inwards of Jupiter.

There are several uncertainties in our model that will limit our ability to model the durations and fluxes of these events. Improvement of these requires cometary observations to understand properties and ejection mechanisms for individual comets, including ejection velocities, mass distributions, dust production rates, and the times and comet surface locations at which ejection occurs. It is hoped that the ESA Rosetta mission to 67P/Churyumov-Gerasimenko will dramatically improve our knowledge of comets and of the dust they produce[1].

Acknowledgments

IMEX is an ESA-funded project. Constellation (http://aerospaceresearch.net/) is a young academics group supported by the German Society for Aeronautics and Astronautics DGLR in Stuttgart, Rechenkraft.net e.V. and Selfnet e.V. We thank all individual Constellation users for their computing time.

References

Arlt R., Kac J., Krumov V., Buchmann A., Verbert J. (2001). "Bulletin 17 of the International Leonid Watch: First Global Analysis of the 2001 Leonid Storms". *WGN, Journal of the IMO*, **29**, 187–194.

Agarwal J., Müller M., Grün E. (2007). "Dust Environment Modelling of Comet 67P/Churyumov-Gerasimenko". *Space Science Reviews*, **128**, 79–131.

Agarwal J., Müller M., Reach W. T., Sykes M. V., Boehnhardt H., Grün E. (2010). "The dust trail of Comet 67P/Churyumov-Gerasimenko between 2004 and 2006". *Icarus*, **207**, 992–1012.

Caswell R. D., McBridge N., and Taylor A. (1995). "Olympus end of life anomaly a Perseid meteoroid impact event?". *International Journal of Impact Engineering*, **17**, 139–150.

Crifo J. F., Rodionov A. V. (1997). "The Dependence of the Circumnuclear Coma Structure on the Properties of the Nucleus". *Icarus*, **127**, 319–353.

Dikarev V., Grün E., Baggaley J., Galligan D., Landgraf M. and Jehn R. (2005). "The new ESA meteoroid model". *Advances in Space Research*, **35**, 1282–1289.

Dormand J. R, Prince P. J. (1978). "New Runge-Kutta algorithms for numerical simulation in dynamical astronomy". *Celest. Mech*., **18**, 223–232.

[1] We have also generated a video of the meteoroid stream of comet 67P/Churyumov-Gerasimenko between 1960 and 2100, see: https://www.youtube.com/watch?v=FY0vjbBp4eg

Fulle M., Colangeli L., Agarwal J., Aronica A., Della Corte V., Esposito F., Grün E., Ishiguro M., Ligustri R., Lopez Moreno J. J., Mazzotta Epifani E., Milani G., Moreno F., Palumbo P., Rodríguez Gómez J., Rotundi A. (2010). "Comet 67P/Churyumov-Gerasimenko: the GIADA dust environment model of the Rosetta mission target". *Astronomy & Astrophysics*, **522**, A63, 17 pages.

Jorda L., Crovisier J., Green D. W. E. (2008). "The Correlation Between Visual Magnitudes and Water Production Rates". *Asteroids, Comets, Meteors 2008*, LPI Contributions, 1405, 8046.

Kelley M. S., Reach W. T. and Lien D. J. (2008). "The dust trail of Comet 67P/Churyumov Gerasimenko". *Icarus*, **193**, 572–587.

Koschack R., Rendtel J. (1990). "Determination of spatial number density and mass index from visual meteor observations (I)". *WGN, Journal of the IMO*, **18**, 44–58.

Kresak L. (1993). "Cometary dust trails and meteor storms". *Astronomy & Astrophysics*, **279**, 646–660.

McNaught R. H., Asher D. J. (1999). "Leonid Dust Trails and Meteor Storms". *WGN, Journal of the IMO*, **27**, 85–102.

Rodmann J. (2006). "Dust in circumstellar disks". PhD Thesis, Combined Faculties for the Natural Sciences and for Mathematics of the University of Heidelberg, Germany.

Vaubaillon J., Colas F., Jorda L. (2005a). "A new method to predict meteor showers. I. Description of the Model". *Astronomy & Astrophysics*, **439**, 751–760.

Vaubaillon J., Colas F., Jorda L. (2005b). "A new method to predict meteor showers. II. Application to the Leonids". *Astronomy & Astrophysics*, **439**, 761–770.

The author, Rachel Soja, during her lecture. (Credit Dominique Richard.)

Meteor observations from double station in Morocco

Meryem Guennoun[1], Zouhair Benkhaldoun[1], Jérémie Vaubaillon[2]

[1] **Laboratory for High Energy Physics and Astrophysics, Faculty of science SEMLALIA, University of Cadi Ayad, Marrakech, Maroc**
meryem.guennoun@ced.uca.ma, Zouhair@uca.ma

[2] **IMCCE, Paris, Observatoire de Paris, 77 av. Denfert-Rochereau, 75014 Paris, France**
vaubaill@imcce.fr

We present here a summary description of two first stations dedicated to build the first meteor network in Morocco and the whole African continent. Optimizing the direction of the cameras, in order to conduct permanent meteor observations from double stations, is one of our main goals.

1 Introduction

The monitoring of meteor showers is one of the many aspects of research efforts at the University of Cadi Ayad, Marrakech, Morocco (Rudawska et al. 2011). In this framework, the main purpose of the Oukaïmeden observatory is to monitor the sky and the neighboring environment of the Earth to detect meteors entering the Earth's atmosphere and to determine their trajectories. In Morocco, we have two stations for observations: the first station is installed at Oukaïmeden observatory. The second station is located at AGM observatory (Atlas Golf Marrakech), located 42.38 km south of the observatory (*Figure 1, 2and 3*). For meteor observations, we use 2 cameras Watec 902H2 and 2 lenses 6mm/F1.2 (FOV = 60° * 40°) (*Figure 4*).

Table 1 – Location of the two stations.

	Station 1	Station 2
Latitude	31°12'32" N	31°37'28" N
Longitude	7°52'52" W	7°59'35" W
Altitude	2700m	466m

Figure 1 – Location of the two observation stations.

Figure 2 – AGM observatory.

2 Detections

Direction of the two cameras

At the beginning of the programme, we used random directions for both cameras, but later we started to use the same direction, but slightly shifted. More double detections were obtained.

Now, we are developing a program that computes the exact directions of the cameras. It calculates the coordinates of the center of the region that should be

Figure 3 – Oukaïmeden observatory.

Figure 4 – Watec Camera at AGM observatory.

pointed in the sky by the cameras (angular distance, elevation angle, azimuth, declination and right ascension). The program also determines the intersection of the camera fields at a given height and the region of the sky photographed, it optimizes the camera fields and simulates meteor trails for testing purposes (Rendtel and Arlt, 2011).

Results

In August 2014, we observed more than 170 meteor detections from both stations, including double ones, and we are working at their analysis using UfoAnalyzer software. *Figure 5* shows the number of meteors detected during 6 nights (from 9/10 to 14/15 August 2014). The maximum of detections was obtained during the night of 12/13 August, with 34 meteors for station AGM and 75 meteors for Oukaïmeden observatory.

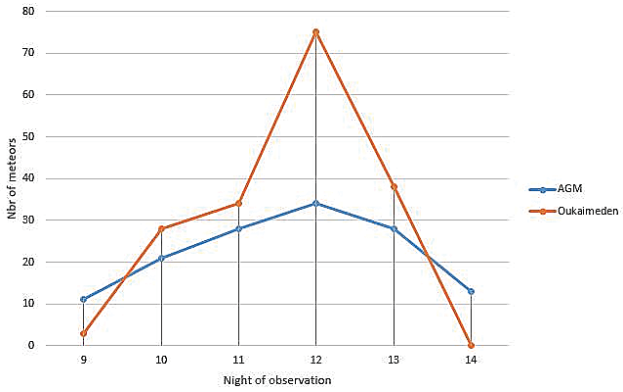

Figure 5 – Number of meteors detected from the night of 9/10 till 14/15 August 2014.

3 Conclusion

Since the detections obtained from the second station are not so clear most of the times, we are considering changing the location and searching for a place located at a higher altitude. If the work goes on very well, we are also talking about having more stations for meteor observations.

The main goal of our future work is to complete the program to calculate the exact direction of the cameras, which also makes the observations, analyzes the captured meteors and determines their trajectories.

Acknowledgment

Special thanks to each member of the LOC of the IMC 2014, for giving us the opportunity to present our work. We also thank Pete Gural for his advice, and Stéphane Jouin and Tioga Gulon for their help with UfoCapture and UfoAnalyze softwares.

References

Rendtel J. and Arlt R., editors (2011). Handbook for Meteor Observers. Third edition. IMO.

Rudawska R., Daassou A., Larbi M. A. M., Benkhaldoun Z., Vaubaillon J., Colas J. F., Baratoux D., Bouley S. (2012). "Birth of meteor network in Morocco – Analysis for the 2012 Geminids". *WGN, Journal of the IMO*, **41**, 121–128.

Don Quixote – a possible parent body of a meteor shower

Regina Rudawska[1] **and Jérémie Vaubaillon**[2]

[1] **Faculty of Mathematics, Physics and Informatics, Comenius University, Bratislava, Slovakia**
reginka@amu.edu.pl

[2] **IMCCE – Observatoire de Paris, Paris, France**
vaubaill@imcce.fr

Here we are interested in whether the meteoroid stream of (3552) Don Quixote can generate some observed meteor showers. We have showed that particles originating from Don Quixote particles produce two meteor showers at Earth: κ Lyrids and August μ Draconids.

1 (3552) Don Quixote

The (3552) Don Quixote asteroid was discovered in 1983 and categorized as Amor asteroid. The Tisserand parameter for the orbit has a value of 2,315 with respect to Jupiter, which indicates a comet-like orbit. The diameter of the object as calculated from the absolute magnitude is in the range of 12,3 – 24,5 km. This all makes Don Quixote a good candidate for a short-period comet among known NEOs, which has been confirmed by recent observations of some cometary activity (Momment et al., 2014).

2 Methodology

We have investigated the orbital evolution of the meteoroid stream originating from Don Quixote. For this purpose, we modelled the generation and evolution of the meteoroid stream in the Solar System. The ejections of meteoroids from the asteroid's surface took place when the asteroid was passing its perihelion between 5000 B.C. and 2013 A.D. Next, the orbits of the ejected meteoroids were integrated to the year 2050. The theoretical radiant of a meteoroid orbit that passed within 0.05 AU from Earth is calculated with the Q method (Hasegawa, 1990). The similarity between the orbits of those particles that reached the Earth and orbits of known meteoroid streams listed at the IAU MDC was established using the Southworth and Hawkins D_{SH} criterion (Southworth and Hawkins, 1963). Additionally, we used the D_V functions proposed by Jopek et al. (2008). The described method pointed to two meteor showers: κ Lyrids (#464, KLY), and August μ Draconids (#470, AMD).

3 Results

We achieved a good matching when comparing the orbits of the κ Lyrids and the August μ Draconids with orbits from our simulation. Calculated values of D_{SH} for KLY and AMD meteor showers (0.11 and 0.12, respectively) are below the conventional threshold value which assumed when establishing orbits similarity, i.e. 0.20 (Babadzhanov et al., 2013). Similarly, the values of D_V are below the usual threshold value of 0.08 (Jopek et al., 2008; Rudawska et al., 2012).

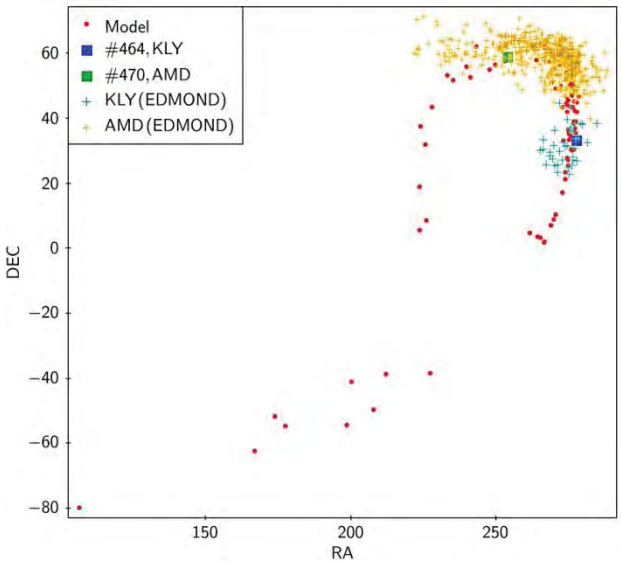

Figure 1 – Radiant positions for the simulated meteor showers, κ Lyrids and August μ Draconids taken from the IAU MDC, and κ Lyrids and August μ Draconids identified in the EDMOND database.

Figure 1 shows the distribution of the theoretical radiants of all the modelled meteors together with the radiant position of KLY and AMD taken from the IAU MDC, as well as KLY and AMD meteors identified by an independent identification method applied to the EDMOND database (Rudawska et al., 2014). The position of both showers taken from the IAU MDC fits nicely to the simulated meteor shower, occupying two parts of the simulated shower. Similarly, the dispersion of the radiants of both meteor showers extracted from the EDMOND database is in excellent agreement with the simulated distribution.

4 Conclusion

Our talk addresses the topic of the meteoroid stream of a parent body in relation to meteor showers observed on Earth. Particularly, we carried out a search to investigate the possibility of meteor shower observations caused by particles ejected from (3552) Don Quixote. With the

methodology applied here and current observational data, we showed that a meteor shower can be created from Don Quixote. Moreover, we found that the particles originating from Don Quixote produce two meteor showers observed on Earth: the κ Lyrids and the August μ Draconids.

References

Hasegawa I. (1990). "Predictions of the meteor radiant point associated with a comet". *Astronomical Society of Japan*, *Publications*, **42**, 175–186.

Jopek T. J., Rudawska R., Bartczak P. (2008). "Meteoroid stream searching: The use of the vectorial elements". *Earth, Moon, and Planets*, **102**, 73–78.

Mommert M., Hora J. L., Harris A. W., Reach W. T., Emery J. P., Thomas C. A., Mueller M., Cruikshank D P., Trilling D. E., Delbo M., and Smith H. A. (2014). "The Discovery of Cometary Activity in Near-Earth Asteroid (3552) Don Quixote". *The Astrophysical Journal* , **781**, 25–35.

Rudawska R., Matlovic P., Toth J., Kornos L. (2014). "Independent identification of meteor showers in EDMOND database". arXiv:1406.6598.

Rudawska R., Vaubaillon J. and Atreya P. (2012). "Association of individual meteors with their parent bodies". *Astronomy & Astrophysics*, **541**, id.A2, 5 pages.

Southworth R. B. and Hawkins G. S. (1963). "Statistics of meteor streams". *Smithsonian Contributions to Astrophysics*, **7**, 261–285.

Vaubaillon J., Colas F., Jorda L. (2005). "A new method to predict meteor showers. I. Description of the Model". *Astronomy & Astrophysics*, **439**, 751–760.

The author, Regina Rudawska, during her lecture. (Credit Axel Haas.)

Meteorite-producing fragment on the orbit of Apophis

Alexandra Terentjeva[1], **Elena Bakanas**[2]

[1] **Institute of Astronomy of the Russian Academy of Sciences, Moscow, Russia**
ater@inasan.ru

[2] **Institute of Astronomy of the Russian Academy of Sciences, Moscow, Russia**
alena@inasan.ru

A meteorite-producing object moving along an orbit almost coinciding with that of the Apophis asteroid (99942) was found. The object may be a fragment of Apophis. It is shown that the orbit of Apophis has approaches to the Earth's orbit (up to the indicated limit of $\rho \leq 0.20$ AU) within a long time interval.

1 Introduction

Apophis (99942) is, as known, a potentially hazardous asteroid for the Earth. Its next approach to the Earth is expected on 13 April 2029 at a geocentric distance[1] of 0.0002561 AU. Apophis diameter is approximately[2] 0.325 km. Apophis is an Sq-class asteroid and most closely resembles *LL* ordinary chondrite meteorites in terms of spectral and mineralogical characteristics (Binzel et al., 2009).

Defining Apophis' place in the system of meteor bodies, one should refer it to the Cyclids' system (Terentjeva and Barabanov, 2011). Meteor bodies of the Cyclids move along orbits almost coinciding with the Earth's orbit ($e \leq 0.14$, $q' \leq 1.2$ AU, $i \leq 15°$). All elements of Apophis' orbit lie within limits of changes in elements of the Cyclids' orbits, differing only for an insignificant value of 0.05 in the eccentricity.

2 Results and conclusions

When studying the interrelation of various populations of minor bodies in the Solar System (asteroids, comets, meteor streams, large meteor bodies – including meteorites, possible genetic relations in the families within the minor bodies complex), Terentjeva (1989) has found a population of 39 meteorite-producing objects. Results of photographic observations of 379 bright fireballs of the Prairie and European networks were analyzed (McCrosky et al., 1976, 1978; Ceplecha, 1978). This population included objects for which the estimated terminal mass was 0.25 kg and more. All 39 objects of this population are essentially meteorites and could be found. The above work provides a Table (and *Figure 1*), containing a total of 39 orbits along which meteorite producing bodies with extra-atmospheric masses M_∞ from several kilograms to about thirty tons moved. Orbit No. 14 of the meteorite producing object, which is almost identical to that of the Apophis asteroid, was found within this population of bodies, the coordinates of the radiants coincide perfectly (*Table 1*). Extra-atmospheric mass of the object $M_\infty = 1.2$ kg.

Concerning the 1950.0 equinox in *Table 1* one should note that the accuracy of the determination of radiant coordinates by means of photographic observations varies on average from several arcseconds to 3°, and in velocity from 0.1 to 3%. For the interval of 75 years (for example from W.F. Denning' Epoch 1875.0 to 1950.0) the difference caused by precession makes about 1°, which is not essential taking into account the accuracy of meteor data (Terentjeva, 1966). In our case for the interval of 50 years (1950.0 – 2000.0) this value will be less than 1°.

We (Terentjeva and Barabanov, 2011) calculated the approaches of Apophis' orbit to the Earth's orbit and the theoretical geocentric radiants in all points of approach (up to the distance of $\rho \leq 0.20$ AU). The study is based on the following system of Apophis' elements (Shor, 2009):

$a = 0.922$ AU	$\omega = 126.41858°$
$e = 0.1911107$	$\Omega = 204.43196°$
$q = 0.746$ AU	$i = 3.33172°$

The orbital elements of Apophis are given for the 2000.0 equinox.

The latest determination of Apophis' orbit[3] is different from the one above in the following way: $\Delta a = 0.00028$ AU, $\Delta e = 0.000037$, $\Delta\omega = 0.023°$, $\Delta\Omega = 0.025°$, $\Delta i = 0.00044°$, which is not essential while comparing it to meteor orbits (considering their low accuracy).

Apophis' orbit turned out to have approaches to the Earth's orbit on the major part of its orbit (except for a perihelion area at 117° in true anomaly) within an 8-month period. There are two points of closest approach of Apophis' orbit with the Earth's (two appulses): in the region of the orbit's ascending node of April 13 ($\lambda_\odot$=24.144°, equinox 2000.0) with $\rho = 0.000307$ AU and in the region of the descending node of December 20 ($\lambda_\odot$=268.736°, equinox 2000.0) with $\rho = 0.0520$ AU.

[1] http:// ssd.jpl.nasa.gov/
[2] http://www.esa.int

[3] http:// ssd.jpl.nasa.gov/

Table 1 – Asteroid (99942) Apophis and meteorite producing fragment. Orbital elements of the asteroid Apophis are given for the 2000.0 equinox; for the meteorite producing fragment they are given for the 1950.0 equinox.

Object	Date	Corr. geocentric radiant		V_∞	a	e	q	i	ω	Ω	π	Sources
		α [°]	δ [°]	km/s	AU		AU	[°]	[°]	[°]	[°]	
Apophis (99942)	Apr 13	214.2	-30.8	12.5	0.922	0.191	0.746	3.3	126.4	204.4	330.9	[1]
Fragment	1969 Apr 7	212.2	-27.2	11.6	0.926	0.13	0.808	1.7	134.5	197	331.5	No 14 [2]

Sources: [1] – Shor (2009), http://ssd.jpl.nasa.gov/, [2] – Terentjeva (1989).

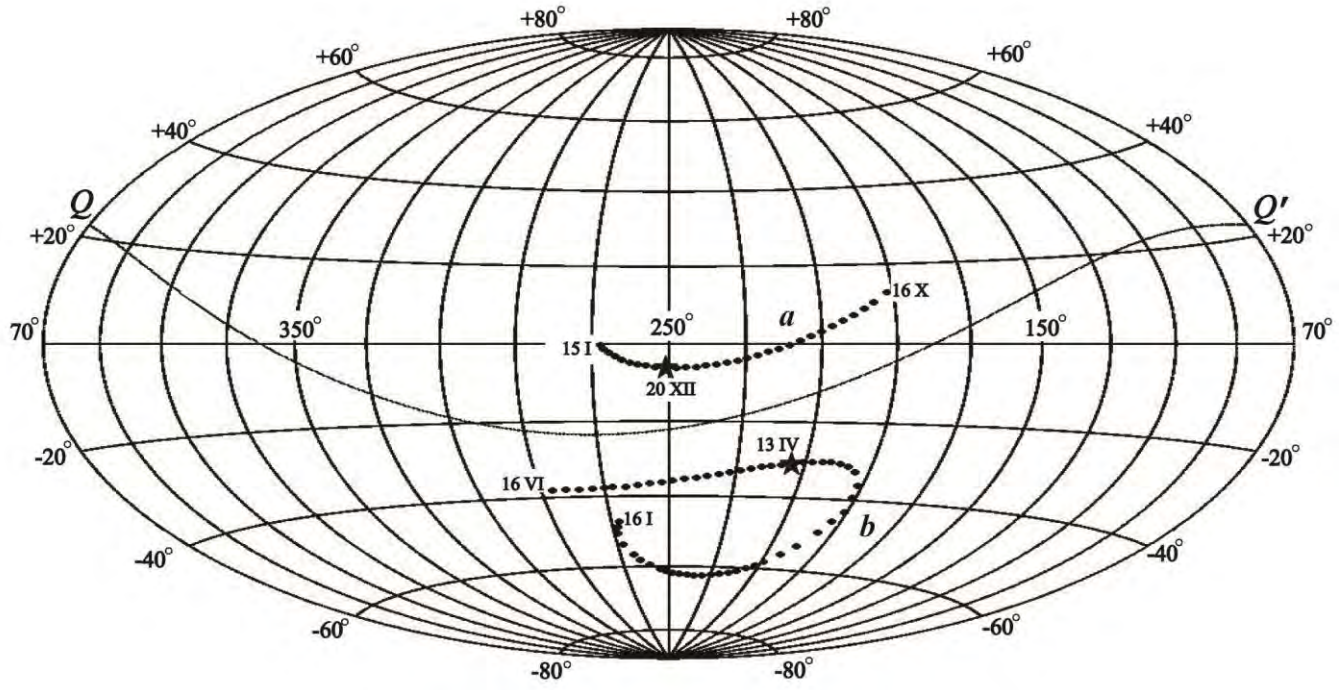

Figure 1 – Ephemerides of the theoretical geocentric radiant of asteroid Apophis (*a* – in the area of the descending node, *b* – in the area of the orbit's ascending node). An asterisk marks radiants for the moment of appulse. *QQ'* – ecliptic.

Over three months, Apophis' geocentric radiant moves along the curve *a* (*Figure 1*), located northward from the ecliptic and corresponding to the appulse area in the region of the orbit's descending node, but further within a short period of time, the radiant is redeployed southward from the ecliptic, and for five months moves along the folded line *b*, corresponding to the appulse area in the region of the orbit's ascending node.

Table 1, provided herein, shows that the meteorite-producing object was observed 6 days before Apophis passed the appulse of April 13 in the region of its orbit's ascending node.

On the basis of the above, it can be concluded:

1) the discovered meteorite producing body could be a fragment of the asteroid Apophis or they both could have a common origin;
2) it is reasonable to observe large meteor bodies (in the appulse area – April 13), which can be found on the Apophis' orbit or nearby.

The more detailed research will be published in the *Journal of the IMO (WGN)*.

Acknowledgment

This work was supported by the Russian Foundation for Basic Research No. 12 02 90444 Ukr_a and Programme 22 of the RAS Presidium "Basic problems of Solar system research and development".

References

Binzel R. P., Rivkin A. S., Thomas C. A., Vernazza P., Burbine T. H., DeMeo F. E., Bus S. J., Tokunaga A. T., Birlan M. (2009). "Spectral properties and composition of potentially hazardous asteroid (99942) Apophis". *Icarus*, **200**, 480–485.

Ceplecha Z. (1978). "Fireballs of European network". *Meteoritika*, **37**, 60–68.

McCrosky R. E., Shao C. Y., Posen A. (1976). Preprint Series No. 665. Cambridge, Center for Astrophysics.

McCrosky R. E., Shao C. Y., Posen A. (1978). “Prairie Network fireball data. I. Summary and orbits”. *Meteoritika*, **37**, 44–59.

Shor V. A. (2009), ed., *Ephemerides of minor planets for 2010*. Institute of Applied Astronomy of RAS, Nauka, St. Petersburg.

Terentjeva A. K. (1966). “Minor meteor streams”. In Result. Issled. MGP, Issled. Meteorov, No. 1, pages 62–132, Moscow.

Terentjeva A. K. (1989). “Minor bodies of the Solar system: meteorite orbits, interrelation, "mirror simmetry" in *C*-distribution”. *Pis'ma v Astron. Zh.*, **15**, 258–269.

Terentjeva A. K., Barabanov S. I. (2011). “Apophis and system of Cyclid meteor bodies”. *Vestnik SibGAU*, 6 (39), 89–90.

The IMC’s have their roots in International Youth Camps in the 1970’s, still now 35 years later this pleasant spirit still keeps people coming to an IMC. In front some of the Croatian guitar players, in the back Jérémie Vaubaillon. (Credit Axel Haas.)

A new approach to meteor orbit determination

Vasily Dmitriev[1], Valery Lupovka[1] and Maria Gritsevich[1,2,3]

[1] **Moscow State University of Geodesy and Cartography (MIIGAiK), Extraterrestrial Laboratory, Moscow, Russian Federation**
vm.dmitriev90@gmail.com
vlupovka@miigaik.ru
maria.gritsevich@fgi.fi

[2] **Finnish Geodetic Institute, Department of Geodesy and Geodynamics & Finnish Fireball Network, Helsinki, Finland**

[3] **Russian Academy of Science, Dorodnitsyn Computing Center, Department of Computational Physics. Moscow, Russian Federation**

It is known that orbits of meteoroids colliding with the Earth are exposed to significant perturbations prior to impact, primarily under the influence of gravity and atmospheric drag at the end of the trajectory. Standard methods of pre-impact meteor orbit computation (Ceplecha, 1987) are traditionally based on a set of static corrections applied to the observed velocity vector, see e.g. (Andreev, 1991). In particular, the popular concept of so-called "zenith attraction" is used to correct the direction of the meteoroid trajectory and its apparent velocity in the Earth's gravitational field. In this work we carry out explicit trajectory integrations of meteoroids with the aim of investigating the magnitude of errors involved by choosing the mentioned simplifications.

1 Theory of the proposed method

We use strict transformations of coordinate and velocity vectors according to the IAU International Earth Rotation and Reference Systems Service (IERS; IERS Conventions, 2010) and backward numerical integration (Plakhov et al., 1989) of equations of motion. A similar approach was applied in Zuluaga et al. (2013) for the Chelyabinsk asteroid orbit reconstruction using the "mercury6" software (Chambers, 1999). In Clark and Wiegert (2011) the authors compared the meteoroid orbit determination method of Ceplecha (1987) with the results of numerical integration, which showed good agreement between the two approaches.

Specifically, the following transformations are in use. Transformation of the velocity vector from topocentric to geocentric coordinate system:

$$\begin{pmatrix} V_x \\ V_y \\ V_z \end{pmatrix} = \mathbf{M}^T \begin{pmatrix} V_n \\ V_e \\ V_u \end{pmatrix}, \quad (1)$$

$$M = Q_1 R_2(90-\varphi) R_3(\lambda), \quad (2)$$

where $(V_n, V_e, V_u)^T$ and $(V_x, V_y, V_z)^T$ are the topocentric and geocentric velocity vectors; R_2, R_3 and Q_1 are appropriate rotation and mirror matrices, accordingly; φ and λ – geodetic latitude and longitude of the beginning point of the atmospheric trajectory.

Diurnal aberration is taken into account as:

$$\begin{pmatrix} \Delta V_x \\ \Delta V_y \\ \Delta V_z \end{pmatrix} = -a_e \omega_\oplus \begin{pmatrix} \cos B \sin L \\ \cos B \cos L \\ 0 \end{pmatrix}, \quad (3)$$

where ω_o is the Earth rotation velocity, and a_e is the equatorial Earth radius. Transformation of the beginning point coordinates and velocity vectors from the Earth-fixed geocentric coordinate system ITRF2000 to Geocentric Celestial Reference System (GCRS) realization ICRF2 (J2000) is conducted according to IERS Conventions (IERS Conventions, 2010):

$$\begin{pmatrix} X_{in} \\ Y_{in} \\ Z_{in} \end{pmatrix} = \mathbf{R}^T \begin{pmatrix} X_{geo} \\ Y_{geo} \\ Z_{geo} \end{pmatrix}, \quad (4)$$

$$\begin{pmatrix} Vx_{in} \\ Vy_{in} \\ Vz_{in} \end{pmatrix} = \mathbf{R}^T \begin{pmatrix} Vx_{geo} \\ Vy_{geo} \\ Vz_{geo} \end{pmatrix}, \quad (5)$$

$$\boldsymbol{R} = P\, N\, \Pi\, S, \quad (6)$$

where P is the precession matrix, N – the nutation matrix, Π – the polar motion matrix, and S – the apparent Greenwich Sidereal Time matrix.

The contributions of the polar motion and high order nutation are negligible in comparison to the observation errors, so these effects can be skipped in this case. The JPL ephemeris DE421 (Folkner et al., 2009) is used for the transformation of the meteoroid position and velocity vectors from the geocentric to the heliocentric coordinate system.

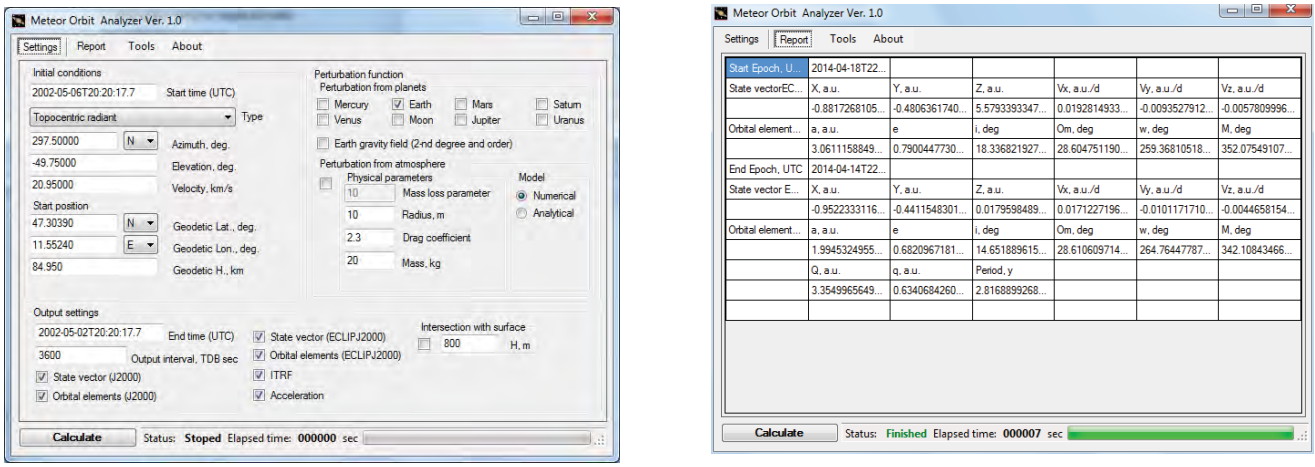

Figure 1 – The interface of the main window of Meteor toolkit.

As a result, the required initial conditions for numerical integration – the meteoroid position and velocity vectors – are obtained in the celestial geocentric coordinate system ICRF2 (J2000). Backward integration of the equations of the perturbed meteoroid motion:

$$\ddot{\vec{r}} = -\frac{GM_{Sun}}{r^3}\vec{r} + \ddot{\vec{r}}_{Earth}(C_{nm}S_{nm},\vec{r},t) + \ddot{\vec{r}}_{Moon}(\vec{r},t) + \\ + \sum \ddot{\vec{r}}_{planets}(\vec{r},t) + \ddot{\vec{r}}_{atm}(\vec{r},t), \quad (7)$$

is performed by an implicit single-sequence numerical method (see equation 6). The equations of the perturbed meteoroid motion include the central body (Sun) attraction, perturbations by the gravitional field of the Earth, Moon, and other planets, as well as atmospheric drag. Backward integration was performed until the meteoroid intersected with the Hill sphere (i.e. about 4 days before the actual event of a meteor) to obtain an undistorted heliocentric orbit. An example of values of the components in the right part of equation 7 is presented in *Figure 2*. The values on the right correspond to the time of entry into the dense layers of the atmosphere.

2 Tools

We have developed a software tool called "Meteor Toolkit" for the determination of the orbit of a meteoroid. This software has a graphical user-friendly interface and uses SPICE routines and kernels for coordinate transformation and computing ephemerides. In addition, it has a module for visualization of computation results. Screenshots of this software are presented in *Figure 1*. Meteor Toolkit makes it possible to perform an analysis of the orbital motion of the meteoroid before the collision with the Earth. Also, we can determine the location of a potential meteorite fall by continuing integration of the equations of motion to the intersection with the surface of the Earth. This could be of great help in finding possible meteorite fragments. Often there is the problem of determining the characteristics of an alleged clash Near-Earth asteroid. With the initial conditions of the asteroid orbital elements, using the Meteor Toolkit it is possible to calculate the estimated collision coordinates and other characteristics such as speed relative to the ground, the angle of entry into the atmosphere, etc. This software can be run on Windows OS, or on a virtual machine emulating Windows. In addition, one would need .Net framework 3.5 or a later version.

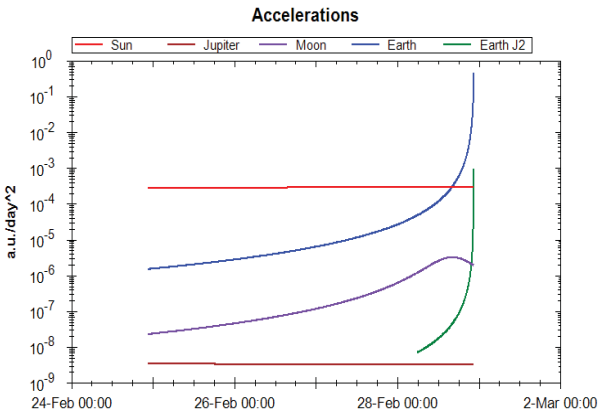

Figure 2 – Absolute values of the components of the right part of the equation 7, calculated for the meteoroid Košice.

3 Summary and discussion

The accuracy of the proposed method does not propagate the observational uncertainties, while obtained results are in good agreement with the traditional orbit-determination method.

Unlike the traditional method, the described approach takes into account the effects of meteoroid attraction by the Moon and planets, Earth's gravitational field, as well as atmospheric drag.

An increase in pre-atmospheric velocity and/or the lowering of the beginning height of a meteor result in bigger differences between the proposed and traditional approaches.

The proposed technique enables analysis of the meteoroid orbital motion before its collision with the Earth. This

only requires further integration (back in time) of the same equations of motion.

Portable software with GUI to determine a heliocentric orbit of a meteoroid and analyze it in time before the impact has been developed in accordance with the here described technique.

Acknowledgements

This work was carried out in MIIGAiK and supported by the Russian Science Foundation, project No. 14-22-00197.

References

Andreev G. (1991). "The Influence of the Meteor Position on the Zenith Attraction". In Heinlein D.; and Koschny D., editors, *Proceedings of the International Meteor Conference*, Violau, Germany, September 6-9, 1990. IMO, pages 25–27.

Chambers J. E. (1999). "A hybrid symplectic integrator that permits close encounters between massive bodies". *Monthly Notices of the Royal Astronomical Society*, **304**, 793–799.

Ceplecha Z. (1987). "Geometric, dynamic, orbital and photometric data on meteoroids from photographic fireball networks". *Bulletin of the Astronomical Institutes of Czechoslovakia*, **38**, 222–234.

Clark D. L., Wiegert P. A. (2011). "A numerical comparison with the Ceplecha analytical meteoroid orbit determination method". *Meteoritics & Planetary Science*, **46**, 1217–1225.

Folkner W. M., Williams J. G., Boggs D. H. (2009). "The Planetary and Lunar Ephemeris DE 421". *The Interplanetary Network Progress Report*, **42-178**, 1–34.

IERS Conventions (2010). Petit G., and Luzum B., editors, IERS Technical Note No. 36, 2010, 179 pp.

Plakhov Y. V., Mytsenko A. V., Shelpov V. A. (1989). "Method for the numerical integration of equations of perturbed satellite motion in problems of space geodesy". *Geodeziia i Aerofotos'emka*, No. 4, 61–67. In Russian.

Zuluaga J., Ferrin I., Geens S. (2013). "The orbit of the Chelyabinsk event impactor as reconstructed from amateur and public footage". Eprint arXiv:1303.1796. Submitted to *Earth and Planetary Science Letters* (EPSL), 10 pp.

Saturday night, the last night of the IMC, when the manager of Fauconière turned up with some percussion instruments, the International Meteor Conference became the International Music Conference, also known as the IMC. (Credit Axel Haas.)

IMO Fireball Reports

Mike Hankey and Vincent Perlerin

American Meteor Society
mike.hankey@gmail.com, vperlerin@gmail.com

In 2013, the American Meteor Society (AMS) offered use of its online fireball report to the International Meteor Organization. The AMS and IMO agreed to extend the capabilities and reach of the application worldwide by enhancing the form to support a multi-lingual user interface.

1 Introduction

The American Meteor Society (AMS), founded in 1911, pioneered the visual study of meteors and has collected data relating to meteor observations and bright fireballs for over 100 years. In December 2010, the online fireball reporting system was upgraded to an interactive application that utilizes Google Maps and other programmatic methods to pinpoint the observer's location, azimuth and elevation values with a high degree of precision (Hankey et al, 2013).

The AMS has collected 10s of 1000s of witness reports relating to 100s of bright fireball events each year since the new application was released. Three dimensional triangulation methods that average the data collected from witnesses have been developed that can determine the start and end points of the meteor with an accuracy of < 50km (when compared to published solutions provided by operators of all sky cameras). Right ascension and declination (RA/dec) radiant estimates can also be computed for all significant events reported to the AMS. Data collected from the AMS fireball application has been used to successfully recover 4 meteorite falls in recent years.

2 IMO version of the Fireball Report form

In 2013 the AMS offered use of the fireball application to the International Meteor Organization. The AMS and IMO agreed to extend the capabilities and reach of the application worldwide by enhancing the form to support a multi-lingual user interface. Volunteers from the IMO worked with the AMS to provide translations for the text and instructions used in the form. The form has been translated in 27 languages thus far (*Figure 1*).

When users reach the form, the application automatically detects the language of the end-user and defaults the form text to that users preferred language. All other languages the form is available in are displayed in a drop down list and the user can override the default display by choosing a different language. In addition to providing the form in multiple languages, a branding option was built into the form so that regional astronomy clubs, observatories or other organizations can link to the form and have the form display that club's logo and color scheme. By providing this branded capability, it is the hope of the AMS and the IMO that regional groups will adopt the form, link to it from their websites and generate a large base of data collection for bright fireball events.

3 Internationalization

Regional groups are also encouraged to develop native language content on their sites to attract witnesses of fireball events from Google and other online searches. Typically a fireball witness will first go to Google and search in their native language for information about what they saw. When searching in English, the AMS has become the authority on Google and this enables witnesses to easily find the fireball form and file a report into the database. Regional clubs should take ownership of this outreach responsibility for their countries and develop native language content that will attract fireball witness to their sites and then route them to the fireball form.

The AMS Fireball FAQ[1] is an excellent content source and the most popular piece of content on the AMS site. The AMS encourages regional groups to translate and host a version of the Fireball FAQ on their own sites. Doing so will attract users to the site and improve the site's ranking in Google. This will in turn generate more reports into the database. Regional groups are also encouraged to write up press releases or blog posts for their sites when significant fireball events occur in their domain. Doing so will attract the attention of the press, create publicity for the group and generate back links to the groups site from the media sources. These back links will generate traffic to the site and in turn fireball reports. The media links will also help the site rank higher in Google and the other search engines. While the forms are now translated into 26 languages and available for regional groups to use, the data will not be gathered if the forms and services are not promoted efficiently in each country. For these reasons the AMS and the IMO encourage regional groups to not only integrate the forms into their sites, but also actively promote them so that end users and fireball witnesses can find them.

[1] http://www.amsmeteors.org/fireballs/faqf/

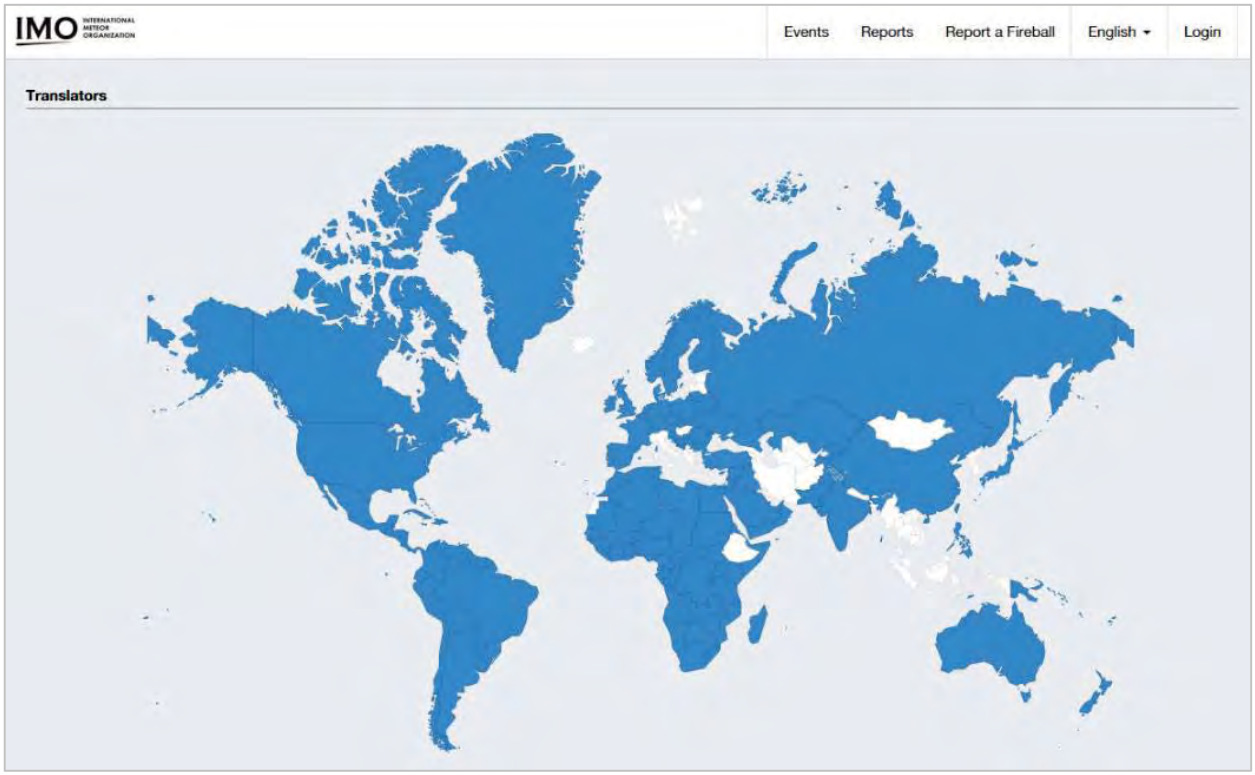

Figure 1 – Screenshot of the IMO version of the Fireball Report: language page.

4 Conclusion

All fireball data collected by the AMS, the IMO and the regional clubs will flow into a single shared worldwide fireball database. Individual fireball sightings will be reviewed by an administrator and then grouped into events based on the time and location of the sightings. These events will be given a sequential number and then trajectories and RA/dec estimates will be calculated for each event. All of the sightings and event data will be publicly accessible by the web and data export APIs. From January to October 2014 the AMS has logged over 512 confirmed fireball events (where a confirmed event is one witnessed by 3 or more witnesses). In 2013 714 confirmed fireball events were logged with the AMS. By expanding the reporting system worldwide with the help of the IMO and regional clubs, we hope to increase the number of events logged in the database at least 3 fold. The AMS and IMO encourage the community to promote this data collection method and to research these events and utilize the data to the full extent possible.

Acknowledgments

The authors would like to thank all the translators of the form: Abderrahmane Ibhi, Valentin Velkov, Ladislav Bálint, Anton Sørensen, Andre Knöfel, Francisco Ocaña González, Arie Blumenzweig, Denis Vida and the Visnjan School of Astronomy, Masahiro Koseki, Audrius Dubietis, Trond Erik Hillestad, Paul and Adriana Roggemans, Przemek Zoladek, Eduardo Placido Santiago, Rui Gonçalves, Marian Stasjuk, Roman Piffl, Javor Kac, Snežana Todorović, Johan Kero, Ferhat Fikri Özeren, Pavel Presnyakov and Wu BingXun.

References

Hankey M., Perlerin V., Lundsford R., and Meisel D. (2013). "*American Meteor Society Online Fireball Report*". In Gyssens M., Roggemans P., and Żołądek P., editors, *Proceedings of the International Meteor Conference*, Poznań, Poland, 22–25 August 2013. IMO, pages 115–119.

First meteorite recovery based on observations by the Finnish Fireball Network

Maria Gritsevich[1, 2, 3, 4], Esko Lyytinen[1], Jarmo Moilanen[1], Tomáš Kohout[1, 5, 6], Vasily Dmitriev[4], Valery Lupovka[4], Steinar Midtskogen[7], Nikolai Kruglikov[3, 8], Alexei Ischenko[3], Grigory Yakovlev[3], Victor Grokhovsky[3], Jakub Haloda[9, 10], Patricie Halodova[9], Jouni Peltoniemi[5, 2], Asko Aikkila[1], Aki Taavitsainen[1], Jani Lauanne[1], Marko Pekkola[1], Pekka Kokko[1], Panu Lahtinen[1, 11], Mikhail Larionov[3]

[1] **Finnish Fireball Network, Finland**

[2] **Finish Geodetic Institute, Department of Geodesy and Geodynamics, Geodeentinrinne 2, P.O, box 15, FI-02431 Masala, Finland**

[3] **Institute of Physics and Technology, Ural Federal University, Mira street 19, 620002 Ekaterinburg, Russia**

[4] **Moscow State University of Geodesy and Cartography (MIIGAiK), Extraterrestrial Laboratory, Moscow, Russia**

[5] **University of Helsinki, Department of Physics, P.O. Box 64, 00014 Helsinki, Finland**

[6] **Institute of Geology, Academy of Sciences of the Czech Republic**

[7] **Norwegian Meteor Network, Norway**

[8] **Institute of Metal Physics Russian Academy of Science, Ekaterinburg, Russia**

[9] **Czech Geological Survey, Prague, Czech Republic**

[10] **Oxford Instruments NanoAnalysis, UK**

[11] **Finnish Meteorological Institute, Helsinki, Finland**

maria.gritsevich@fgi.fi

We present a summary of the trajectory reconstruction, dark flight simulations and pre-impact orbit for a bright fireball that appeared in the night sky over the Kola Peninsula, close to the Finnish border, on April 18 2014, at $22^h14^m13.0^s$ (UTC). The fireball was instrumentally recorded in Finland from Kuusamo, Mikkeli and Muhos observing sites belonging to the Finnish Fireball Network. Additionally, a publicly available video made by Alexandr Nesterov in Snezhnogorsk (Russia), from the opposite side of the fireball track, was carefully calibrated and taken into account in the trajectory reconstruction. Based on a thorough analysis of the fireball, it was concluded that part of the meteoroid survived atmospheric entry and reached the ground. To further specify an impact area for a dedicated expedition, dark flight simulations were done to build a strewn field map showing the most probable distribution of fragments. A 5-day expedition with 4 participants from Russia and Finland took place at the end of May following snow melt and preceding vegetation growth. On May 29, 2014, a first 120.35 g meteorite fragment was found on a local forest road within the predicted impact area. A second 47.54 g meteorite fragment, fully covered with a fusion crust, was recovered nearby on the following day. Both pieces were preserved in very good condition without apparent weathering.

1 Introduction

The Finnish Fireball Network (FFN) was established in 2002 as a result of growing interest for continuous meteor and fireball monitoring using dedicated equipment, initiated by Ilkka Yrjölä in 1998[1]. In its current state, the network consists of 24 permanent active stations (*Figure 1*) with permanent instrumental setup and monitors an area over Finland and neighbouring countries of about 400000 km^2. Most of the active stations are run by amateur astronomers. Most of the interesting events are reduced in the days following their registration, and atmospheric trajectories corresponding to the visual path of any fireballs are reproduced using the fb_entry program (Lyytinen and Gritsevich, 2013). Selected cases are studied more thoroughly, including mass computation, dark flight simulations, and pre-impact orbit estimates.

2 Observational data and preliminary analysis

One recent extremely interesting case was a bright fireball that appeared in the night sky over the Kola Peninsula on April 19, 2014 Finnish time (hereafter FN20140419). The fireball reached a magnitude of at least -18 during its peak brightness, and it was reported by many eye-witnesses in Finland, Russia, and Norway.

[1] http://www.kolumbus.fi/oh5iy/

In Finland, eyewitness fireball reports are collected via a special webpage at Taivaanvahti.fi run by the Tähtitieteellinen yhdistys Ursa (Ursa Astronomical Association). *Figure 2* shows the archived data for April 19, 2014.

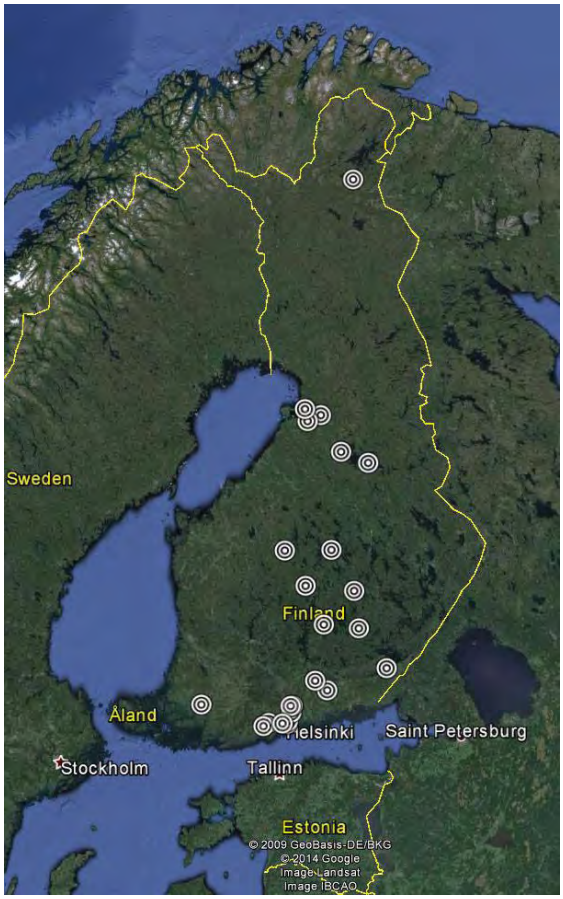

Figure 1 – The locations of the 24 main stations of the Finnish Fireball Network. The map excludes stations with temporary cameras (i.e. not yet operational for sufficient time and/or in continuous mode, such as, for example, the station at Kuusamo).

Figure 2 – Summary of FN20140419 fireball eyewitnesses reports collected in Finland through Taivaanvahti.fi website (image credit: Ursa Astronomical Association).

The fireball was also instrumentally recorded by three FFN stations: Kuusamo, Muhos, and Mikkeli. A spectacular image from Kuusamo is shown in *Figure 3*. Additionally, three video recordings were made from Russia and made publicly available on the internet. From these recordings, a detailed dashcam video made by Alexandr Nesterov in Snezhnogorsk was selected for our analysis.

Figure 3 – FN20140419 fireball image made from one of the FFN stations in eastern Finland (Kuusamo).

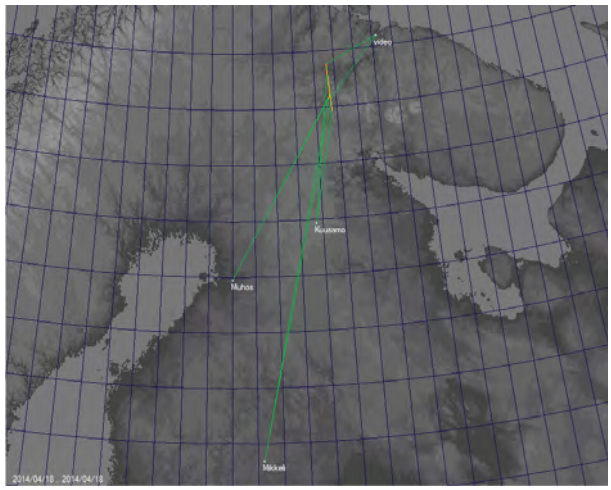

Figure 4 – FN20140419 fireball track reconstructed from the 4 main sites of observation. Map from UFO Analyzer program by SonotaCo.

The analysis of the FFN data, along with the video made from Snezhnogorsk, enabled quite a precise reconstruction of the whole fireball track, as shown in *Figure 4*. Additionally, the determined position of the trajectory matched well with the records of the Norwegian Seismic Array (NORSAR) received from the three infrasound stations - KIR (Kiruna), JAM (Jämtön) and SDK (Sodankylä), *Figure 5a and 5b*.

The pre-impact Solar System orbit of the meteoroid was calculated using several methods. One of the approaches used, described by Dmitriev et al. (2014), uses strict coordinate transformation (IERS Conventions, 2010) and numerical integration of the equation of motion:

$$\ddot{\bar{r}} = -\frac{GM_{sun}}{r^3}\bar{r} + \ddot{\bar{r}}_{Earth}(C_{nm}, S_{nm}, r, t) + \ddot{\bar{r}}_{Moon}(\bar{r}, t) + \sum \ddot{\bar{r}}_{planets}(\bar{r}, t) + \ddot{\bar{r}}_{atm}(\bar{r}, t).$$

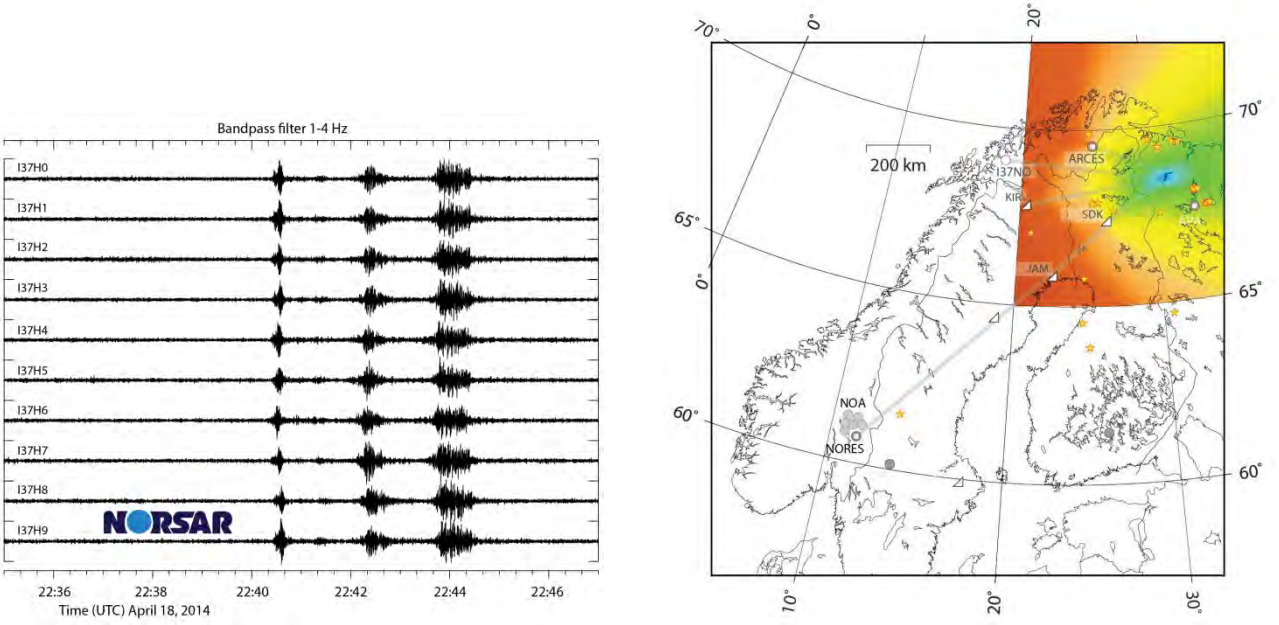

Figure 5 a (left) & b(right) – FN20140419 fireball registration from the three infrasound stations KIR (Kiruna), JAM (Jämtön) and SDK (Sodankylä). Image credit: Norwegian Seismic Array (NORSAR), Swedish Institute of Space Physics, Umeå.

The integration was carried out in an inertial heliocentric coordinate system, taking into account perturbing accelerations by the Earth and Moon as point masses, and Earth flattening. Integration was performed using a strict implicit single-sequence numerical method (Plakhov et al., 1989). For obtaining the undistorted heliocentric orbit, a backward integration was performed until the intersection of the meteoroid trajectory with the Hill sphere (i.e. about 4 days before the actual event of the meteor). The corresponding orbit-determination software is called "Meteor Toolkit" and the orbit derived for the case studied here is plotted in *Figure 6*.

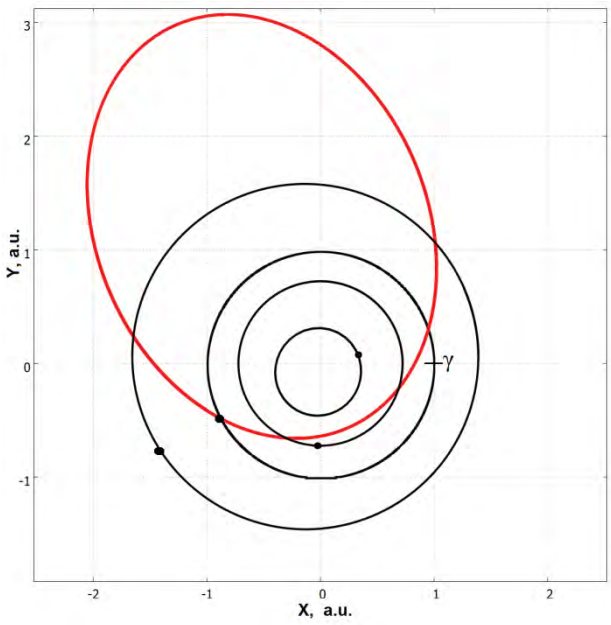

Figure 6 – The derived orbit of the meteoroid (red) projected on the ecliptic plane and its position relative to the orbits of Mercury, Venus, Earth, and Mars (black). The grid corresponds to the ecliptic J2000 coordinate system.

One of the striking features of our analysis was the set of values determined for the scaling parameters (ballistic coefficient α and mass loss parameter β). These values were found to be practically identical to the corresponding values reported earlier by Gritsevich (2008) for the Innisfree meteorite successfully recovered within the MORP program (Halliday et al., 1978). These parameters thus perfectly matched a meteorite-production criterion described in Gritsevich et al. (2012). The deceleration analysis revealed that the pre-atmospheric mass of the meteoroid was about 500 kg, and part of the meteoroid survived the atmospheric entry and reached the ground. It was decided to conduct detailed dark flight simulations of the surviving fragments, taking into account wind effects, and to organize a meteorite recovery expedition to the calculated landing area.

3 Dark flight simulations

In order to narrow down a search area for the predicted meteorite fragments, a dark flight simulation was made using a Monte Carlo (MC) method. Monte Carlo methods use repeated random sampling algorithms to produce a probability distribution of unknown probabilistic processes. The MC dark flight program used for the FN20140419 fireball has been developed for the analysis of data collected by the Finnish Fireball Network and was successfully tested using the data available on the Košice meteorite fall (Borovička et al., 2013). The program was developed by Jarmo Moilanen and is written using Visual Basic 6.0. Simulation results are written in KML-format (=Keyhole Markup Language) and can be viewed in Google Earth.

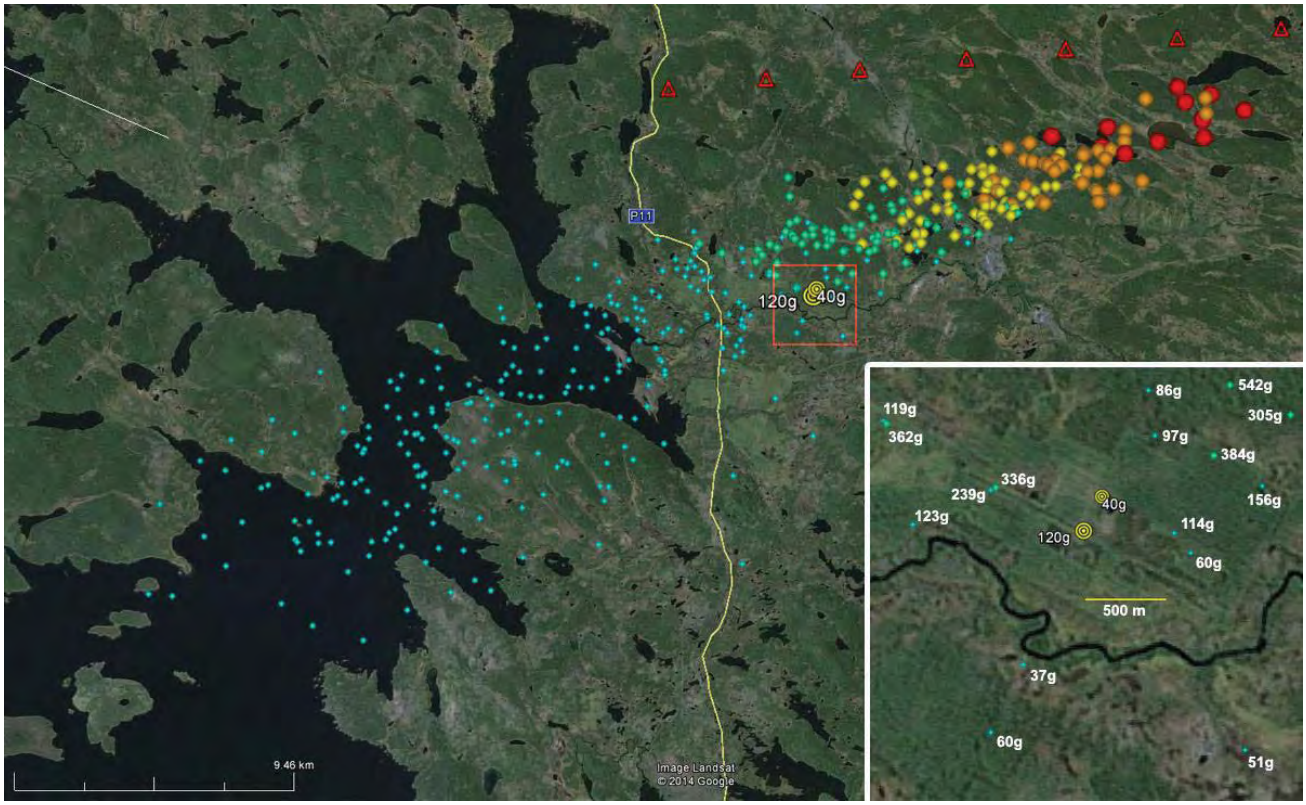

Figure 7 – Color code for the mass of the simulated fragments: blue <0.3 kg, green 0.3 - 1 kg, yellow 1 - 3 kg, orange 3 - 10 kg, red >10 kg. The 2 meteorite fragments later recovered in the expedition are shown inside the red square. The calculated strewn field is located between Verhnetulomsky and Prirechny, Russia. North is to the right.

In our realization, the MC dark flight simulation produces a set of meteorite fragments and a map showing the area where the fragments most probably landed (*Figure 7*). In the present version of the algorithm, random sampling with a normal distribution is applied for most of the trajectory, fragments and atmospheric parameters. Parameter variations are randomly chosen for each simulated fragment, whose trajectory is subsequently followed down to the ground. This simulation is repeated for a large number of fragments. As a result, a probability map showing a probable strewn field of the meteorite fragments is obtained.

Flight-dependent parameters needed for the dark flight simulation are the geographical coordinates, height, velocity, deceleration, direction and entry angle at the starting point of the simulation. In our case, parameters used in the simulation were determined from the observational data of the fireball as described in the previous section. Uncertainties of these for the MC simulation are determined according to a realistic worst-case scenario; they are not actual uncertainties from the observational data. Based on the conducted analysis the starting point for the simulations was defined as

- Longitude 30.642°E
- Latitude 68.581°N
- Height 34.6 km (±0.2 km)
- Velocity 22.7 km/s (±0.3 km/s)
- Entry angle 33.6° (±1.8°) to horizon
- Flight direction 355.8° (±1.8°) 0°=N, 90°=E
- Deceleration 2.7 km/s^2 (-10% - +30%)
- Drag coefficient multiplied by the shape parameter 1.5 (±0.5)

Fragment-specific parameters are mass, bulk density, drag and shape coefficients. A bulk density of 3.5 g/cm^3 is used as a default value. Both fragmentation and ablation have an effect on the fragment masses. Ablation is applied only if the velocity of the fragment is still relatively high. In our case ablation was set to cease when velocity drops below 3 km/s. This seems to be quite a good approximation for most meteorites. The current implementation of the MC program has a simplified fragmentation algorithm which allows one fragmentation event per fragment. After fragmentation, the flight path of the fragment changes slightly. A power-law relationship is used to choose mass of the produced fragment, and we foresee implementation of more elaborate fragment distributions in the future (Gritsevich et al., 2014a). In the FN20140419 simulation, the possibility of fragmentation was considered only during the first 2 seconds, approximately the time from the start of simulation to the end of luminous flight.

Correct atmospheric data are the most critical input in the dark flight simulation. Atmospheric parameters are wind velocity, wind direction and air pressure at different altitudes. MC alteration of these parameters produces a spread in the simulated strewn field. In our case the actual atmospheric data were kindly provided by the Finnish

Meteorological Institute and were used in the following configuration:

- Atmospheric data from Global Forecast System (GFS)
- Date and location: 18 April 2014 at 21:00UT for location 70°N, 31°E
- Wind direction (±20°)
- Wind velocity (±20%)
- Air pressure (±3%)

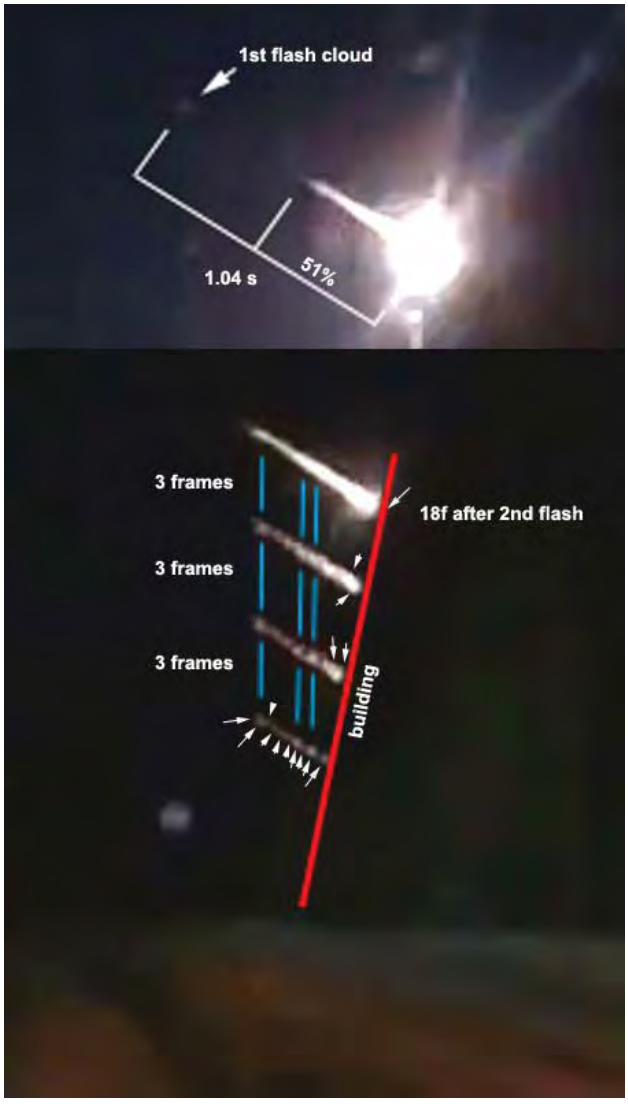

Figure 8 – Early stage fragmentation as seen in the dashboard video of the fireball.

The MC simulation was applied from the first bright flash of the fireball at a height of 34.6 km. This starting point was chosen because it was the main fragmentation event and the idea was to further follow the fragments formed at this stage. A simulation starts by choosing MC alternated parameters for every fragment. A fragment is then tested with a deceleration filter. The deceleration filter algorithm excludes fragments which produce decelerations too small when compared to the actual observations, and prevents unrealistically big fragments from showing up in the results. The MC program simulates the first fragment without MC alterations, which gives an estimation of the main fragment mass if it survives the atmospheric flight and impacts the ground. In our case the main fragment mass was estimated to be 17.1 kg.

The MC dark flight simulation for the FN20140419 fireball gave a strewn field approximately 40 km long and 6 km wide. Due to wind effects, fragments drifted several kilometers eastwards from the nominal flight trajectory (*Figure 7*). Since a meteorite-recovery expedition was planned, alternative scenarios were thoroughly considered in order to develop the best search strategy. Thus, the simulations were also performed for three fragments resulting from the earlier-stage fragmentation. These fragments are seen trailing the main mass in the car dashboard video from Snezhnogorsk (*Figure 8*). Parameters for the MC program were resolved for each of these early fragments and additional simulations were made. These trailing fragments also landed inside the simulated strewn field shown in *Figure 7,* as meteorites with a total mass of up to 4.7 kg. The first two meteorites recovered later (as described in the following section) were found inside the simulated strewn field of the last trailing fragment. This scenario indicates that, according to our simulations, larger meteorite fragments may still be found inside the calculated area.

Figure 9 – Nikolai Kruglikov with the first recovered meteorite fragment found on a local forest road.

4 Meteorite-recovery expedition to the predicted impact area

The calculated impact area is located roughly 100 km west of Murmansk, Russia. It was decided to organize an international meteorite-recovery expedition in the calculated landing area, in collaboration with the meteorite recovery group from Ural Federal

Figure 10 – The first 120,35 g (left) and the second 47,54 g (right) recovered fragments of the meteorite.

University, Ekaterinburg. The 5-day expedition took place at the end of May, following snow melt but preceding vegetation growth. The participants of the expedition were Alexei Ischenko, Tomas Kohout, Nikolai Kruglikov, and Grigory Yakovlev, and they were logistically supported by Maria Gritsevich and Victor Grokhovsky. On May 29, 2014, a first 120.35 g meteorite fragment was found by Nikolai Kruglikov on a local forest road within the predicted impact area (*Figure 9 and 10*). A second 47.54 g meteorite fragment fully covered with fusion crust (*Figure 10*) was recovered nearby on the following day by Alexei Ischenko. The coordinates of the finds in the World Geodetic System 84 (WGS 84) are:

NK1: 68°46'49.4" N, 30°47'42.5" E

AI1: 68°46'55.8" N, 30°47'09.9" E

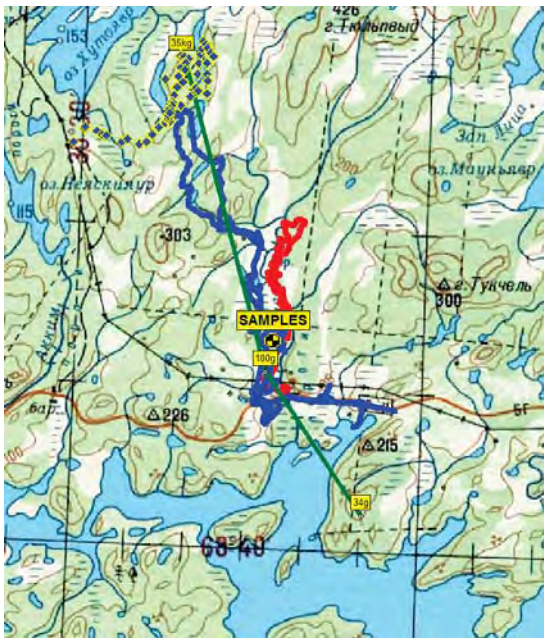

Figure 11 – A summary of the search campaigns known to the authors at the time of writing. The blue line and the points correspond to the 1st and 2nd campaigns. The red line shows the amateur astronomer's campaign. The green line is the initial nominal landing prediction for the fragments ranging from 34 g to 35 kg.

Figure 11 provides an up-to-date summary of the searched meteorite areas known to the authors. Although more fragments are expected to be found in the target area, the terrain consists of numerous wetlands and dense bush making recovery of further meteorite fragments difficult (*Figure 12*). Another problem is an abundance of discharged metallic ammunition cartridges left behind by hunters in the grass; these disturb visual object identification as well as searches using metal detectors. Another feature of the region is the absence of regular residents. Most people in the area are tourists, hunters or fishermen coming from Murmansk and other big cities of Russia, as well as from Finland and Norway, meaning that the probability of meeting eyewitnesses is substantially lower than in well-settled territories.

The next recovery expedition lasted 7 days and was organized by Ural Federal University two weeks after the first meteorite recovery, but yielded only eyewitness reports and no samples. Two shorter expeditions were organized by amateur astronomers from Finland and Russia in July and September 2014. Unfortunately neither expedition resulted in any new meteorite finds.

Figure 12 – Picture taken during the second expedition: Nikolai Kruglikov in the very head of the fireball track with account for dark flight (calculated landing point for a fragment 35 kg).

5 Eyewitness reports

In addition to instrumental registration by FFN and the dashboard cameras, as well as distant eyewitness observations from Finland, Norway and Russia, the fireball was observed by casual eye-witnesses residing near the impact area. Despite the event occurring during the night in the Murmansk region, some local residents were outdoors and observed the event. Particularly valuable reports were collected during the recovery expedition by Nikolai Kruglikov, from several observers who were close to the Verhnetulomsky water reservoir at the time of the event.

Residents in apartments in Verhnetulomsky saw the flash of the fireball coming from outside. A security guard at the camp next to the lake was almost under the track (approximately five kilometers east), he was watching TV inside the building and interpreted the fireball as a storm. In Prirechny, residents did not see or hear the fireball.

There were three more detailed eyewitnesses' reports of the event from the search area (*Figure 13*). All of them agree with our derived theoretical direction of the trajectory. One of the witnesses (No.2 in Figure 13) reported facing to the North along the Akkim river was driving on a snowmobile, from Vekhnetulomsky to Prirechny, and he sensed a bright flare behind him. He described an associated sound like the rumble of a landing military interceptor. A second witness was located south of the Verhnetulomsky water reservoir and saw the bright fireball moving along a straight line from South to North. A third witness stopped his car on the road near the western entry of Verkhnetulomsky. He saw the fireball, but no specific sound was reported from his position.

6 Details of the recovered meteorite fragments

Mineralogical and physical analyses of the main piece were done at the Czech Geological Survey and at the University of Helsinki respectively, using methods and instruments described in Kohout et al. (2014). The meteorite was classified as an H5 ordinary chondrite, of S2 shock level and W0 weathering grade. The bulk density (measured with the modified Archimedean method using glass beads) and grain density (measured with gas pycnometry) are 3.5 g/cm^3 and 3.8 g/cm^3 respectively. The resulting porosity is 5%, and the magnetic susceptibility (in log units of 10^{-9} m^3/kg) is 5.4 (Gritsevich et al., 2014b).

At the time of discovery, the 120.35 g meteorite was approximately 70% covered by a black fusion crust with apparent stream lines on one side (*Figure 10*). The fresh surface was bright with abundant thin dark impact melt veins. The second 47.54 g meteorite fragment was fully covered with a fusion crust. With the aim of scientific research, the 120.35 g main meteorite mass was divided into 98.40 g specimen (stored in the Ural Federal University collection in Ekaterinburg, Russia), a 6.24 g cut-off (GEOKHI RAS, Moscow, Russia), two thin sections (GEOKHI RAS and Finnish Museum of Natural History, Helsinki, Finland) and several smaller (less than 1 g) fragments (University of Helsinki, Finland and Ural Federal University collection in Ekaterinburg, Russia). The other 47.54 g meteorite was divided into 40.045 g and 6.580 g fragments, both located in Helsinki, Finland (Finnish Museum of Natural History and University of Helsinki).

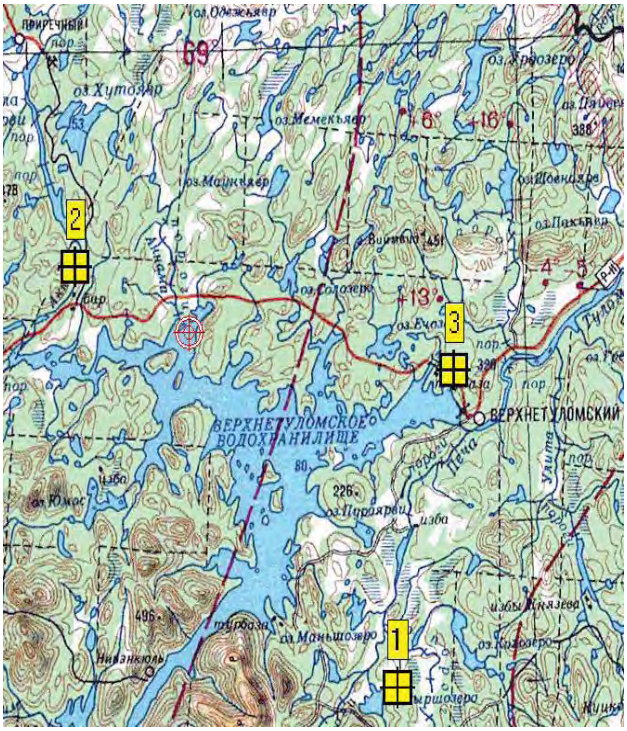

Figure 13 – Positions of the interviewed eyewitnesses close to the impact area.

The submission of the data to the Meteorite Bulletin was done in July 2014 by Victor Grokhovsky with Annama as the suggested name for the recovered meteorites (after the nearby river running parallel to the fireball track). In fact, the first meteorites were found between the Annama river and Annama hill.

7 Conclusions

This magnificent discovery was possible due to several factors: (1) the continuous organized observational efforts made by the Finnish Fireball Network; (2) the detailed fireball analysis and applied fb_entry program developed by Esko Lyytinen; (3) the MC dark flight simulation done by Jarmo Moilanen; (4) the enthusiastic international expedition (Alexei Ischenko, Tomas Kohout, Nikolai Kruglikov, and Grigory Yakovlev, all with previous meteorite recovery experience). As a result, two meteorites were found inside the area of the simulated strewn field. The recovery expedition was organized quickly within a relatively short time after the fall, resulting in a collection of unaltered meteorites. This meteorite fall is also among only 22 historical cases where it was possible to determine the pre-impact Solar

System orbit from reliable atmospheric entry data. Such meteorites are key to our understanding of how the Solar System formed and evolved (Trigo-Rodríguez et al., 2015).

Given the fact that the location of the finds and significant amount of data regarding this discovery were released for the public in July 2014, the authors kindly ask to be informed by members of other expeditions about any search activities or Annama meteorite finds. In return, the authors will, upon request, support any new meteorite recovery efforts and can provide additional data and information, including detailed maps of the searched area and practical advice.

Acknowledgments

This work is joint research between scientists and meteor observers from Finland, Russia, Czech Republic and Norway. The development of the "Meteor Toolkit" software and the corresponding orbital studies were carried out by Vasily Dmitriev, Valery Lupovka and Maria Gritsevich at MIIGAiK under the support of the Russian Science Foundation, project No. 14-22-00197 "Studies of Fundamental Geodetic Parameters and Topography of Planets and Satellites". The expeditions and the related laboratory research were partly supported by the Academy of Finland projects No. 257487 and No. 260027, Ministry of Education, Youth and Sports of the Czech Republic grant No. LH12079, and by the Ural Federal University. We thank Ursa Astronomical Association for continuous support and help with coordination of FFN activities.

References

Borovička J., Tóth J., Igaz A., Spurný P., Kalenda P., Haloda J., Svoreň J., Kornoš L., Silber E., Brown P., Husárik M. (2013). "The Košice meteorite fall: Atmospheric trajectory, fragmentation, and orbit". *Meteoritics and Planetary Science*, **48**, 1757–1779.

Dmitriev V., Lupovka V., Gritsevich M. (2014). "A new approach to meteor orbit determination". In Rault J.-L., and Roggemans P., editors, *Proceedings of the International Meteor Conference*, Giron, France, 18–21 September 2014. IMO. pages 157–159.

Gritsevich M., Lyytinen E., Kohout T., Moilanen J., Midtskogen S., Kruglikov N., Ischenko A., Yakovlev G., Grokhovsky V., Haloda J., Halodova P., Lupovka V., Dmitriev V., Peltoniemi J., Aikkila A., Taavitsainen A., Lauanne J., Pekkola M., Kokko P., Lahtinen P. (2014b). "Analysis of the bright fireball over Kola peninsula on April 19, 2014 followed by successful meteorite recovery campaign". *Meteoritics and Planetary Science*, **49**, A143.

Gritsevich M., Vinnikov V., Kohout T., Tóth J., Peltoniemi J., Turchak L., Virtanen J. (2014a). "A comprehensive study of distribution laws for the fragments of Košice meteorite". *Meteoritics and Planetary Science*, **49**, 328–345.

Gritsevich M. I. (2008). "The Pribram, Lost City, Innisfree, and Neuschwanstein Falls: An analysis of the Atmospheric Trajectories". *Solar System Research*, **42**, 372–390.

Gritsevich M. I., Stulov V. P., Turchak L. I. (2012). "Consequences for Collisions of Natural Cosmic Bodies with the Earth Atmosphere and Surface". *Cosmic Research*, **50**, 56–64.

Halliday I., Blackwell A. T., Griffin A. A. (1978). "The Innisfree meteorite and the Canadian camera network". *Journal of the Royal Astronomical Society of Canada*, **72**, 15–39.

IERS Conventions (2010). Petit G., and Luzum B., editors, IERS Technical Note No. 36, 179 pp.

Kohout T., Gritsevich M., Grokhovsky V., Yakovlev G., Haloda J., Halodova P., Michallik R., Penttilä A., Muinonen K. (2014). "Mineralogy, reflectance spectra, and physical properties of the Chelyabinsk LL5 chondrite - Insight into shock-induced changes in asteroid regoliths". *Icarus*, **228**, 78–85.

Lyytinen E., Gritsevich M. (2013). "A flexible fireball entry track calculation program". In Gyssens M., and Roggemans P., editors, *Proceedings of the International Meteor Conference*, La Palma, Canary Islands, Spain, 20–23 September 2012. IMO, pages 155–167.

Plakhov Y. V., Mytsenko A. V., Shelpov V. A. (1989). "Method for the numerical integration of equations of perturbed satellite motion in problems of space geodesy". *Geodeziya i Aerofotos'emka* (ISSN 0536-101X), **4**, 61–67. (In Russian).

Trigo-Rodríguez J. M. et al., (2015). "Orbit and dynamic origin of the recently recovered Annama meteorite". Forthcoming.

Early education opportunities in metoritics

Chris Peterson[1,2]

[1] **Denver Museum of Nature and Science, Denver, Colorado, USA**
clp@alumni.caltech.edu

[2] **Cloudbait Observatory, Guffey, Colorado USA**

Cloudbait Observatory and the Denver Museum of Nature and Science have been operating an allsky camera network in Colorado since 2001. Most of the cameras are hosted at middle schools (ages 12-14) and high schools (ages 15-18), with some notable exceptions targeting even younger students. In addition to generating a rich collection of scientific data, this program has been very successful at introducing students to "real science", where relevant data is collected and analyzed, and the opportunity for new discovery and even publication is present. I will discuss our experience with exploring meteoritics with pre-college age students and the value to both our science program and to early science education.

1 Introduction

The Colorado Allsky Camera Network was established in 2001 by the Denver Museum of Nature and Science (Peterson, 2010). The Museum has a long history of investigating fireball reports and searching for Colorado meteorites. The availability of low-cost video cameras motivated a shift from visual to instrumental analysis, and was also recognized as an educational opportunity, in line with the primary charter of the Museum. Nearly all of the network cameras were installed in schools, and curriculum was developed around their use.

2 Focus

In recent years, STEM (**S**cience, **T**echnology, **E**ngineering, **M**athematics) has become a central focus of educational systems in most developed countries. Experiential learning, inquiry-based instruction, and problem-based learning are all techniques that have been shown especially effective for STEM subjects (Kolb, 1984; Gilmore, 2013). These methods all involve presenting the student with real-world problems which are solved by hands-on approaches, often student designed as well.

Meteoritics represents a powerful educational tool for STEM education. It is inherently interesting to nearly all young people, and can have all the STEM disciplines applied to its understanding.

Here I discuss different curricular ideas we have developed over more than ten years for teaching science and other STEM subjects using a meteor camera network and meteor science as primary tools.

Most cameras in the Colorado Allsky Network are located at high schools, with students ages 15-18. Several are also located in middle schools (ages 12-14) and primary schools (ages 5-11).

3 Curriculum Examples

Triangulation

Because the primary principle in analyzing meteors involves triangulation, this is a good place to start, and a practical introduction to a topic that is either left untreated by conventional math programs, or is only treated abstractly. With younger students, we place a group in a circle with two or more blindfolded, and place a coin on the ground somewhere inside the circle. The teacher then utilizes a mechanical clicker at the coin, and the blindfolded students all point to the sound. The teacher exits the circle, the students have their blindfolds removed, and then identify the intersection of their pointing, allowing them to quickly find the coin.

Figure 1 – Triangulation exercise.

Maps and Directions

Because the primary output from each camera for a meteor event is a pair of altitudes and azimuths representing the beginning and end points, it is natural for students to plot lines on maps (reinforcing triangulation for multiple station events). With primary school students, this may not only represent one of their first practical exposures to maps, but also an opportunity to introduce the idea of angles and using tools such as

protractors. Middle school curriculum is similar, but is more likely to utilize technology in the form of mapping software. High school curriculum extends the mapping to three dimensions- using tools such as Google Earth to determine the 3D meteor path and not simply the ground track.

Where potential local falls are identified, ground searches utilizing topographical maps also prove educational.

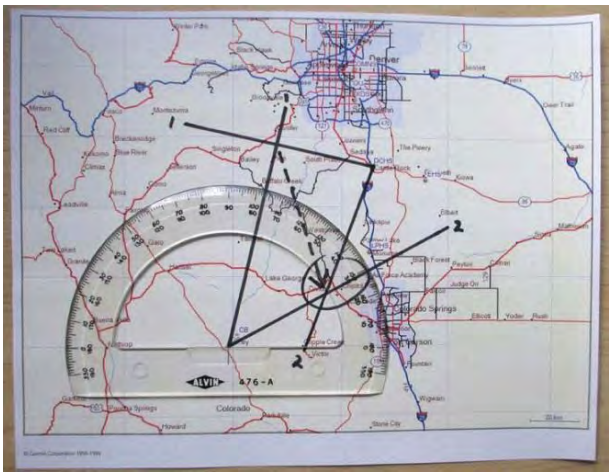

Figure 2 – Mapping exercise.

Statistics

Statistics is usually not addressed seriously until high school. We've found that meteoritics offers an opportunity to introduce statistical concepts much earlier. Students as early as primary school are offered multiple years of meteor data, working in groups to bin events by date. They then plot large histograms on fan-fold paper. This is a labor intensive process, typically requiring several hours. The result is a chart that immediately allows them to identify major periodic showers (periodicity being an important concept itself). We then demonstrate how a spreadsheet program can be used to import data and plot a similar histogram in just a few minutes. In many cases, this is the first time students have ever used this technological tool for any non-trivial purpose. The difference in effort between manual and automated data analysis is apparent to even the youngest students.

Other important statistical analyses are possible with just the basic data from a single station. What is the average speed of a meteor? How does the frequency change with time of night? In a shower, what is the brightness distribution? Students are encouraged to develop questions that can be addressed using statistical techniques applied to a rich dataset.

Light Production

Meteoroids are introduced as bodies that produce light because of material heating. The mechanisms of heating are readily explored with simple experiments such as generating heat by inflating tires with hand pumps. Both black body radiation and narrowband emission are explored in the lab. These concepts, not usually introduced before high school, are readily accessible to much younger students when presented in the context of meteors- exciting events that most of the students have personally witnessed. Of course, all students have a degree of fascination with the idea of heating something until it glows, or of burning chemicals and producing different colors.

Comets and Asteroids

The subject of comets, asteroids, and space dust is generally not presented to pre-university students except in the most cursory way, typically just identifying the terms. These concepts become highly relevant to students working with meteor cameras and live data, however. Recording meteors inspires a natural curiosity about the bodies responsible for these streaks on their cameras. We have developed curriculum around the formation and evolution of asteroids (such as an egg model of differentiation), comets (comet modeling with water, dry ice, dirt, and gravel), comet observation from SOHO data, and visible dust by field observations of zodiacal light (for schools in or near dark locations).

Meteorites

Closely related to understanding asteroids is the study of meteorites. The Denver Museum of Nature and Science is fortunate to curate an extensive meteorite collection, which it has opened up to students who participate in the Allsky program. Working with meteor data adds context to actually handling and analyzing meteorite samples. In addition, discussion of meteorite mineralogy provides an excellent entry into geology.

We also explore impacts–structures such as Meteor Crater in Arizona, and documented events such as Tunguska and Chelyabinsk. Activities for younger students include using topographical maps to create scale models of Meteor Crater; older students explore impact science by dropping or launching small bodies into various media and seeking to explain the nature of the pits created.

Technology

The engineering component of STEM is often the most neglected, as it can be difficult to integrate with conventional curricula. Operating a meteor camera necessarily involves working with an assortment of hardware (cameras, digitizers, computers), solving engineering problems (keeping domes clean, repelling birds, minimizing issues with dew), and working with a variety of software tools (meteor capture and analysis, spreadsheets, GIS).

We have chosen to provide the cameras to participating schools in kit form, requiring the students to understand the design and assemble it on their own. In many cases, especially with younger classes, this is the first time students have ever built anything themselves.

Most recently, we have begun exploring improved camera designs using CAD software and 3D printing. This allows students to develop skills with tools which are frequently not encountered until university or later,

and realize their designs with actual components which can be empirically tested.

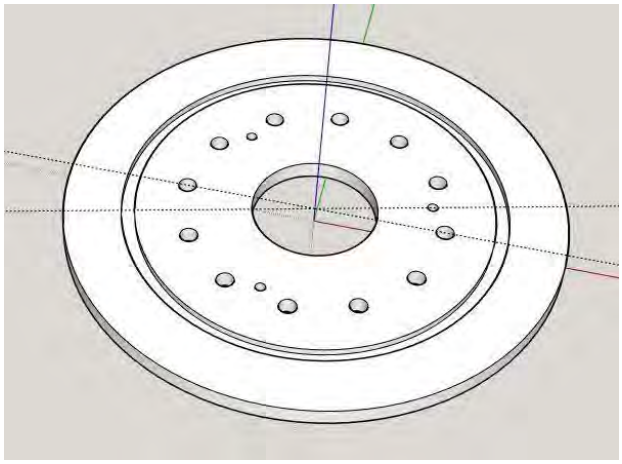

Figure 3 – CAD model of camera component.

Figure 4 – Presenting results.

Context in Learning

Direct experience with meteor data provides context when students visit collections at museums or academic institutions. While it is common to educate students about the facts of a subject before they encounter it in a setting such as a museum, those facts are typically quite abstract. For students operating cameras, analyzing data, and inferring results, concepts useful in interpreting paleontological, geological, and meteoritic collections are much more immediate. Curators and docents frequently observe that the students that are part of this program ask significantly better and more directed questions.

Presentation Skills

Students are commonly taught non-technical presentation skills (drama, book reports, show-and-tell). Technical presentations are seldom seen or made, however. We include curriculum that involves reading actual scientific papers (a complex skill seldom encountered before university), writing analysis results in the format of a scientific paper, and making oral presentations of those results in the style typically found at scientific conferences.

Collaboration

Students have the opportunity to participate in two types of collaboration: working with students at other schools operating cameras, and working with professional and amateur meteor scientists. Collaboration is a vital part of modern science, but is seldom taught or experienced even at STEM intensive schools. Collaboration is natural and essential for operators of meteor cameras, as the most valuable analyses require input from more than one station. Students may work together in person or by telephone, but most commonly utilize email. I am aware of no other science curriculum programs that offer this degree of student-to-student collaboration.

Because meteoritics is also a professional field, the students have opportunities to work with career scientists. This is particularly well suited to meteoritics given that it is naturally a field where professional and amateur scientists work together regularly. Our students have collaborated with scientists at the Museum and at various universities, as well as sharing data with NASA and other institutions. This is very exciting for young students, and builds enthusiasm for science and STEM subjects in general. It also allows students to understand that scientists are “ordinary” people- something that is especially important in a world where they are frequently portrayed by popular media in a very distorted way.

4 Conclusion

We have over ten years of experience incorporating experimental and theoretical meteoritics into early education settings, with students ranging in age from 5 to 18. This has supported an experiential approach to all the STEM components- science, technology, engineering, and mathematics. It has not only made these subjects more accessible than more traditional curricula, but has allowed for the natural introduction of complex concepts at a much earlier age than is common, and has fostered an early excitement about science and science related disciplines. Modern tools make the creation and operation of a small meteor camera network relatively simple and inexpensive.

References

Peterson C. (2010). “Report on the operation of the Colorado Allsky Camera Network”. In Asher D. J., Christou A. A., Atreya P. and Barentsen G., editors, *Proceedings of the International Meteor Conference*, Armagh, Northern Ireland, 16–19 September, 2010. IMO, pages 87–89.

Kolb D. (1984). Experiential Learning. Prentice-Hall.

Gilmore M. (2013). “Improvement of STEM Education: Experiential Learning is the Key”. *Mod Chem.& Appl.*, **1**, 1–3.

Tighert: A new eucrite meteorite fall from Morocco

Abderrahmane Ibhi

Laboratory of Geo-heritage and Geo-materials Science, Ibn Zohr University, Agadir, Morocco
a.ibhi@uiz.ac.ma

The fall of the Tighert meteorite took place in the night of 9 July 2014 at 22^h30^m. The bolide traveled from North-West to South-East and experienced several fragmentation events along its atmospheric trajectory. Eyewitnesses in several localities of the Guelmim-Es-Semara (Tata, Tirhert, Foum El Hisn, Douar Imougadir, Taghjijt, Assa, etc.) saw the bolide and heard audible detonations a few minutes later. Immediately after the fireball event the authorities of the area organized a field search to check for possible security problems. Detailed mineralogical and petrological examination of the meteorite have revealed that it is comparable to an eucrite "magmatic" meteorite that comes from the asteroid belt, exactly Vesta-4.

1 Introduction

Observed meteorite falls are interesting for several reasons. Material from observed falls has not been subjected to terrestrial weathering, making the find a better candidate for scientific studies. Historically, observed falls were the most compelling evidence supporting the extraterrestrial origin of meteorites. Furthermore, observed fall discoveries are a better representative sample of the meteorites' types which fall to Earth.

During the last eighty years, thirteen meteorite falls were recorded in Morocco, of which ten are well documented, named Douar Mghila, Oued el Hadjar, Itqiy, Zag, Bensour, Oum Dreyga, Benguerir, Tamdakht, Tissint and Aoussred. It represents only 0.011 % of the Moroccan declared meteorites (or equivalently, 0.1 fall per year per 71085 km^2) (Ibhi, 2013a and 2013b). All those objects have been watched by eyewitnesses and all last Moroccan falls have been recovered by hunters that spend much time searching for meteorites especially in the desert.

On Wednesday, July 9, 2014 at 22^h30^m, a stone meteorite shower occurred in the region of Foum Lhisen. This was the second wide-area meteorite shower in the Tata province following the martian Tissint meteorite shower in 2011. The first meteorites were recovered the following day close to the road between Foum El Hisn and Assa city. Thousands of people moved to the site from surrounding cities and villages to search. The fall area is ~20 km^2 and is elliptical in shape. The major axis of the ellipse is ~7 km from North-West to South-East.

In this article, the first observations and field data will be presented as preliminary mineralogical and chemical characteristics of this new meteorite.

2 Collecting observations

Eyewitnesses reported that they saw a brilliant light that shot across the night sky. It seemed to be brighter than an electric welding light. The nomads reported that it was at first yellow, and then turned red-green before it split into many parts. Then, they saw innumerable falling sparks. After 10 s, the fireball exploded, producing a sharp peal of thunder, which resonated about 5 s. A few moments later, the sound disappeared, fragments of the meteorite fell accompanied by whistling noises. The fireball was seen by people from cities and villages more than 300 km around the fall site. No deaths or injuries happened by the fall.

Figure 1 – Many of the nomadic people in the region converged to assist in recovering the fresh samples before valuable information was lost to weathering. Initial searches by nomads, converging in the direction of the bolide, produced the first few fragments (photo, Meteor center).

Figure 2 – The Tighert village (Photo, Meteor center).

Thousands of people moved to the site from surrounding cities and villages to search (*Figure 1*), the first meteorites were recovered the following day close to the

road between Foum El Hisn and Assa Near the Tighert village (*Figure 2*). Most of the specimens found were quickly identified as meteorites because they exhibited a prominent fusion crust covering part of their surface. The largest recorded mass was about 1100 g, with an estimated total mass of 15 kg. Most pieces are covered by a very shiny, glassy black fusion crust with translucent patches.

3 The Tighert meteorite

The fragment provided to researchers at the University of Agadir (UIZ) was approximately 25 mm in diameter and about 10 mm thick. The measurement of the magnetic susceptibility on this fragment, showed that Log χ (10^{-9} m^3/kg) is about 2.7 and the density of 2.77. This value corresponds well to the confidence interval of the eucrite meteorites in the alignment chart given by Folco et al. (2006), revealing in this way, that it is a "magmatic" meteorite that comes from the asteroid belt, exactly asteroid Vesta-4. The isotopic analysis of oxygen of acid-washed subsamples by laser fluorination done by Ziegler K. of the Institute of Meteoritics, New Mexico University (Meteoritical Bulletin, 2014, no. 103, in preparation) confirmed that this meteorite is an unbrecciated eucrite and the name “Tighert” has been approved by the Meteorite Nomenclature Committee of the Meteoritical Society.

Eucrites consist of basaltic rock from the crust of Vesta-4 or a similar parent body. They are mostly composed of Ca-poor pyroxene, augite or pigeonite, and Ca-rich plagioclase. Based on differences in chemical composition and features of the component crystals, they

Figure 3 – Tighert meteorite fragments (a complete piece of the Tighert meteorite showing intact, black fusion crust).

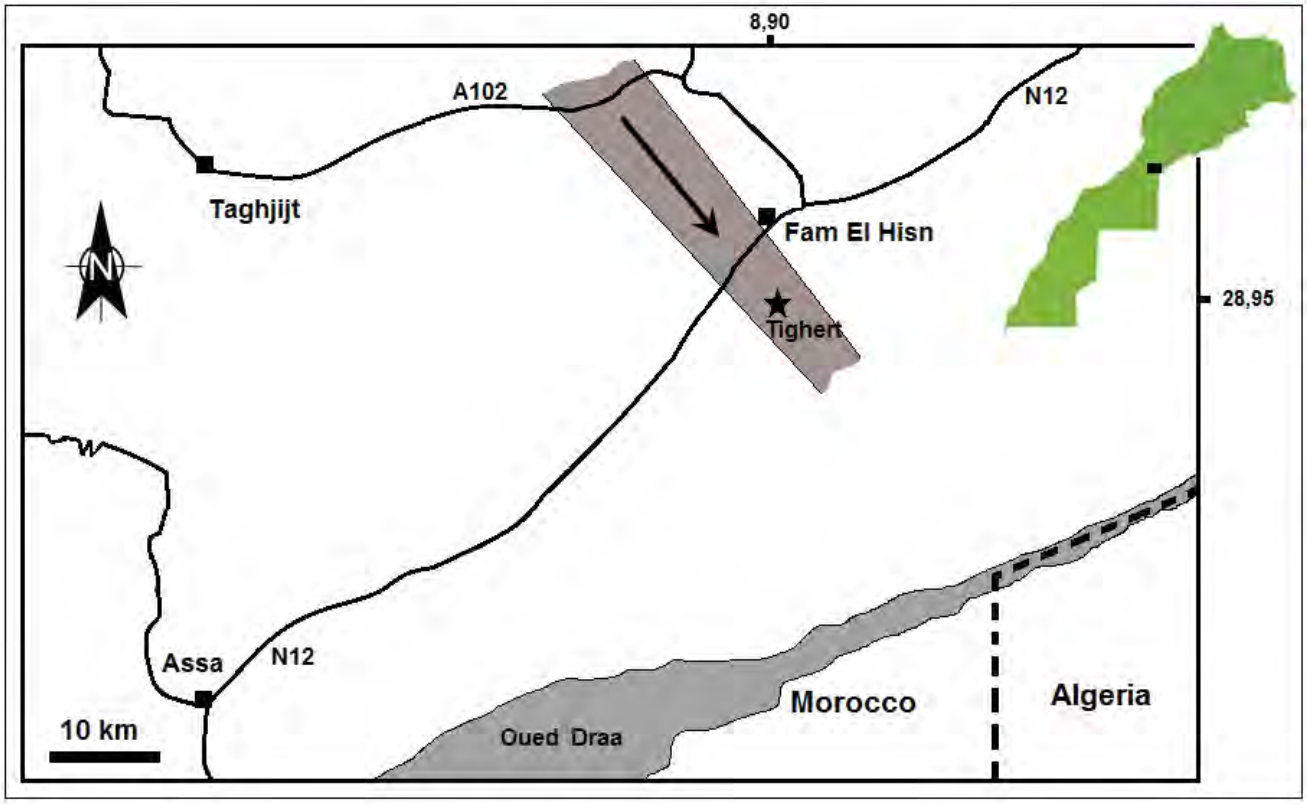

Figure 4 – Estimated flight path of the fireball which resulted in the Tighert meteorite.

are subdivided into several groups (Mittlefehldt et al., 1998). The unbrecciated eucrites (Tighret meteorite type, *Figure 3*) are important to understand the lithological diversity on their parent body, which is especially relevant with the ongoing DAWN mission to Vesta (Mayne et al., 2009). Unbrecciated eucrites are also important to understand the early planet differentiation mechanisms, where unbrecciated eucrites may be free from the influence of post crystallization impact additions (Jasmeet et al., 2013).

4 Discussion and conclusion

The meteor entered the atmosphere at a very acute angle and disintegrated into a large number of fragments after more than 10 s of flight, throwing numerous fragments into similar tracks ending in an extended zone called the ellipse of the fall (*Figure 4*). It is estimated that the intense fireball moved horizontally from North-West to South-East, shortly followed by multiple sonic booms. The largest explosion was recorded at a height of approximately 5 km in the West of Tighert. An accurate speed has not been obtained; however, on average, meteors and fireballs move through the atmosphere at speeds up to or greater than 15 km/s.

The strewnfield of Tighert is not yet well studied; it is situated at about 10 km of linear distance to the south of Foum El Hisn city in the region of Guelmim-Es Smara. The mapping of the locations, where the fragments of the meteorite were found, showed us that the fireball exploded into hundreds of fragments that are scattered on a field with a North-West to South-East direction about 7 km long, which is also the flight direction of the meteorite according to the observations of the nomads and which would be the direction of the strewn field. The width of the ellipsoid is not yet well defined due to the lack of data, especially in the very steep northern part.

Acknowledgments

We want to thank Ait Ouzrou Mohamed (Agadir), Bachikh Mouloud (Es Smara), Lhcen Iydda (Tighert) and Aziz Amslouh (Foum Lhisn) for their assistance in the collection of information.

References

Folco L., Rochette P., Gattacceca J. and Perchiazzi N. (2006). “In situ identification, pairing, and classification of meteorites from Antarctica through magnetic susceptibility measurements”. *Meteoritics and Planetary Science*, **41-3**, 343–353.

Ibhi A. (2013a). “Meteors and meteorite falls in Morocco”. *International Letters of Chemistry, Physics and Astronomy*, **12**, 28–35.

Ibhi A. (2013b). “Moroccan Meteorites Falls and Finds”. *Meteorite*, **19-4**, 30–33.

Jasmeet K., Dhaliwa J. K., Corder C. A., Day J. M. D., Patchen A. D., Taylor L. A. (2013). “Petrology of the unbrecciated eucrite, cumulus Hills 04049”. 44th Lunar and Planetary Science Conference, # 2434.

Mayne R. G., McSween H. Y, McCoy T. J. and Gale A. (2009). “Petrology of the unbrecciated eucrites”. *Geochimica et Cosmochimica Acta*, **73-3**, 794–819.

Mittlefehldt D. W., McCoy T. J., Goodrich C. A. and Kracher A. (1998). “Non-chondritic Meteorites from Asteroidal Bodies”. *Reviews in Mineralogy and Geochemistry*, **36**, p. 4.1–4.195.

Meteor Terminology poster translated into different languages

Vincent Perlerin and Mike Hankey

American Meteor Society
vperlerin@gmail.com, mike.hankey@gmail.com

The American Meteor Society (AMS) has created an educational poster that defines the major terms of the meteor terminology. This poster is an educational tool made available for free on the AMS website. We offer this poster to be translated and shared among the IMO members.

1 Introduction

In a constant effort to create excitement about Science and to increase the level of the general population's knowledge about Meteor Astronomy, the American Meteor Society (AMS) has created an educational poster about Meteor Terminology (*Figure 1*). This poster illustrates and defines the following terms and concepts:

- Comet
- Asteroid
- Meteoroid
- Meteor
- Bolide
- Fireball
- Meteor Showers
- Meteorite

2 Definitions

Some terms of Meteor Science suffer from having different definitions depending on the scientists who are using them. There is a lack of consensus in our community about the definition of *meteoroid* (Rubin and Jeffery, 2010) or *bolide*[1] (Belton, 2014) for instance.

In an educational perspective, we decided to use the most commonly used and the most comprehensible and consensual definitions:

Comet: A solid body made of ice, rock, dust and frozen gases. As they fracture and disintegrate, some comets leave a trail of solid debris. *Nucleus (solid part): tens of kilometers, Tail: millions of kilometers.*

Asteroid: Small rocky, iron or icy debris flying in space. *From 1 meter to hundreds of kilometers.*

Meteoroid: A small asteroid. *From microns to 1 meter.*

Meteor: The light emitted from a meteoroid or an asteroid as it enters the atmosphere.

Fireball: A meteor brighter than the planet Venus.

Bolide: The light emitted by a large meteoroid that explodes in the atmosphere.

Meteorite: A fragment of a meteoroid or an asteroid that survives passage through the atmosphere and hits the ground. *From few grams to several dozen of tonnes.*

Meteor shower: An annual event, when the Earth passes through a region having a great concentration of debris, such as particles left by a comet. From Earth, it looks like meteors radiate from the same point in the night sky.

We understand these definitions can be discussed and we encourage all IMO members and all scientists of the field to share their opinion about these definitions with us.

3 Translation

The AMS Meteor Terminology poster has already been translated in Croatian by Vanesa Ujčić Ožbolt and in French by Vincent Perlerin. The translated versions of the poster are available from www.amsmeteors.org[2]. All the versions of the poster will be soon available for free on the new IMO website and on each IMO organization members' website.

Sometimes, a literal translation is impossible. For instance, the term *Fireball* cannot be directly translated in French as the difference between a *Fireball* and a *Bolide* doesn't exist in French. For the French version of the poster, we decided to define the explosion of a fireball – "Explosion de bolide".

We encourage all the IMO members to send us the translation of the terms defined in the poster in their own language. Once approved, we will send them a PDF of the poster that they will be able to print and share among the community and beyond.

4 Design

The poster has been designed to dramatize and illuminate scientific principles. The graphical representation of each phenomenon doesn't necessarily reflect the reality. Once again, we would be very happy to receive feedback and

[1] *"Introduction: What is a Bolide?*". (1998). woodshole.er.usgs.gov/epubs/bolide/introduction.html.

[2] www.amsmeteors.org/resources/posters/

suggestions from the members of the Meteor Science community.

Acknowledgments

The authors would like to thank Vanesa Ujčić Ožbolt, Jonas Schenker and all the IMO members who expressed their interest in translating and sharing the poster.

References

Belton M. J. S. (2004). Mitigation of hazardous comets and asteroids. Cambridge University Press. ISBN 0521827647.:156.

Rubin A., and Jeffrey N. (2010). "Meteorite and meteoroid: New comprehensive definitions.". *Meteoritics & Planetary Science*, **45**, 114–122.

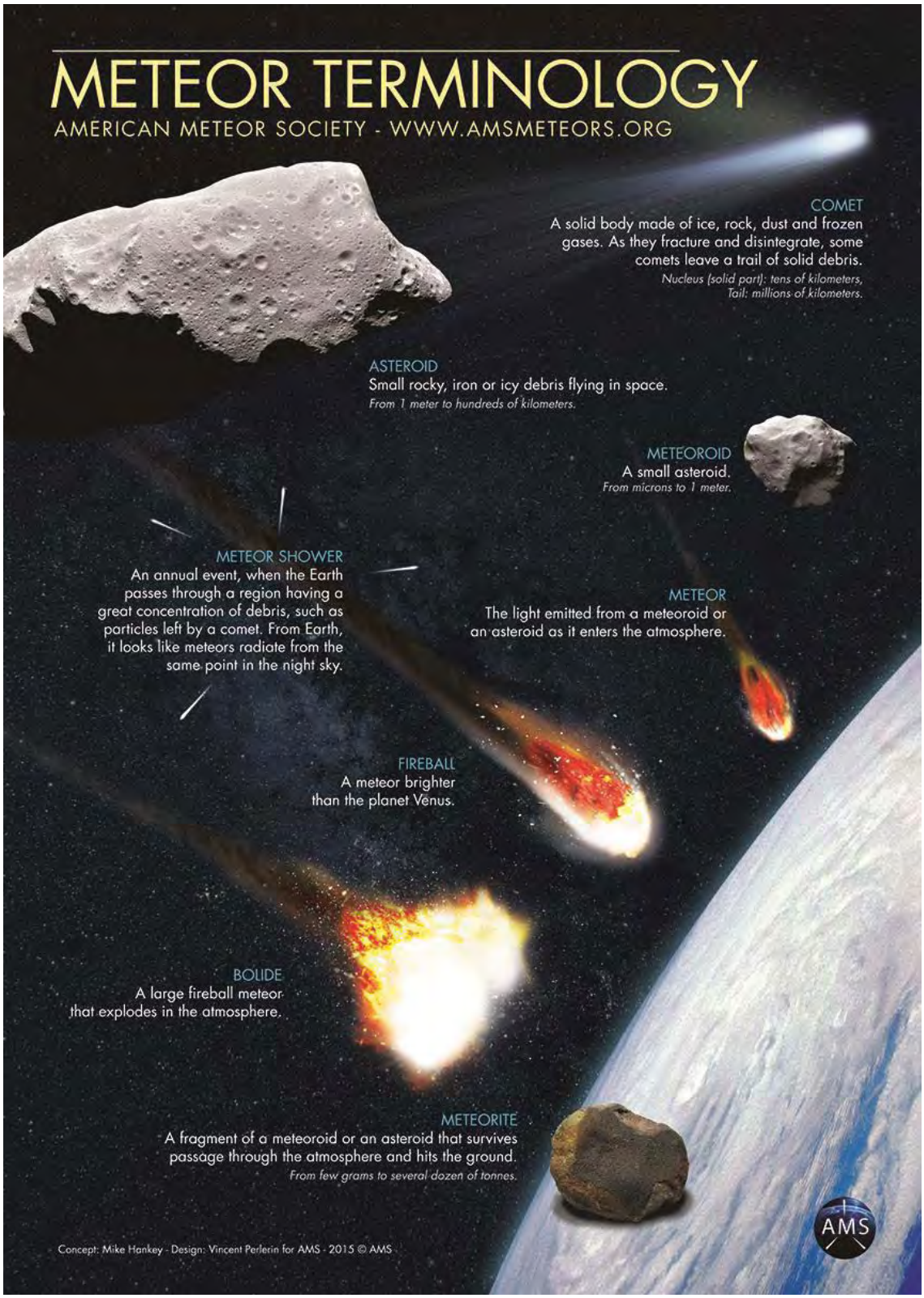

Figure 1 – English version of the AMS poster "Meteor Terminology".

The Košice meteoroid investigation: from trajectory data to analytic model

Daria Kuznetsova[1,2], **Maria Gritsevich**[3,1,2,4], **Vladimir Vinnikov**[1]

[1] **Dorodnicyn Computing Centre RAS, Moscow, Russia**
morven9@yandex.ru, maria.gritsevich@fgi.fi,
vvinnikov@list.ru

[2] **Moscow State University of Geodesy and Cartography (MIIGAiK), Moscow, Russia**

[3] **Finnish Geodetic Institute, Masala, Finland**

[4] **Ural Federal University, Ekaterinburg, Russia**

Impact rate estimates for the upper atmosphere are significantly higher than for the Earth's surface due to the presence of the atmosphere. Thus to account for this properly, one needs to model drag and ablation processes along the atmospheric trajectory (e.g. Bland and Artemieva, 2003). The best way to validate the resulting model is to apply it to meteorite-producing fireballs with a complete observational record. We consider the recent meteorite fall – Košice (2010). In this investigation, we propose a special model based on the analytical solution of the drag and mass-loss equations (Gritsevich, 2009; Gritsevich et al., 2012). Using the available trajectory data (Borovička et al., 2013), two key dimensionless parameters (the ballistic coefficient and mass loss parameter) are obtained which allow us to describe the mass and velocity changes of the main fragment of the meteoroid entering the atmosphere, as well as to estimate the pre-atmospheric meteoroid mass. Good agreement between the calculated functions and real trajectory characteristics is shown. We also apply statistical methods to describe the fragmentation process and provide insights into the pre-atmospheric meteoroid shape (Vinnikov et al., 2014). Furthermore, the most probable scenario suggests that the Košice meteoroid, prior to further extensive fragmentation in the lower atmosphere, consisted of two independent pieces with cumulative residual masses of approximately 2 kg and 9 kg respectively (Gritsevich et al., 2014a). The conducted analysis leads to the conclusion that two to three larger Košice fragments of 500-1000 g each should exist in addition to the already reported meteorite finds.

1 Introduction

This study is focused on the development of a theoretical model which can describe the trajectory of a meteoroid after the entry in the atmosphere and predict the consequences of the impact. The existing data on meteoroid entry in the atmosphere should be used to show its validity once the model is constructed. In order to show the application of our model to real data, a recent fireball event was chosen.

The Košice meteorite fall is the result of the fireball event over central-eastern Slovakia which occurred on February 28, 2010. The landing area was successfully computed using the data from the surveillance cameras operating in Hungary (Borovička et al., 2013), and a meteorite recovery became possible (Tóth et al., 2010). 218 fragments of the Košice meteorite, with a total mass of 11.285 kg, have been documented (Gritsevich et al., 2014a). Laboratory analysis showed that the Košice meteorite (*Figure 1*) is an ordinary H5 chondrite with average bulk and grain densities of 3.43 and 3.79 g/cm^3 respectively (Kohout et al., 2014).

2 Mathematical model

The main equations for the motion of a body entering the terrestrial atmosphere are:

$$M\frac{dV}{dt} = -\frac{1}{2}c_d\rho_a V^2 S$$

$$\frac{dh}{dt} = -V\sin\gamma$$

$$H^*\frac{dM}{dt} = -\frac{1}{2}c_h\rho_a V^3 S$$

where M is the body mass, V is the body velocity, t is the time, h is the height above the planetary surface, H^* is the effective destruction enthalpy, S is the cross-section area of the body, ρ_a is the atmospheric density, c_d is the drag coefficient, and c_h is the coefficient of heat exchange.

We introduce the dimensionless quantities as follows:

$$M = M_e\, m; \quad V = V_e\, v;$$

$$h = h_0\, y$$

$$\rho_a = \rho_0\, \rho; \quad S = S_e\, s \qquad (1)$$

where M_e is the pre-entry mass, V_e is the pre-entry velocity, h_0 is the height of the homogeneous atmosphere, and ρ_0 is the atmospheric density near the planetary surface.

Figure 1 – Four fragments of Košice meteorite. Photo credit: T. Kohout, University of Helsinki, Finland.

Then from the initial equations one can obtain the equations for dimensionless mass and height as functions of velocity:

$$m\frac{dv}{dy} = \frac{1}{2}c_d \frac{\rho_0 h_0 S_e}{M_e}\frac{\rho v s}{\sin\gamma}$$

$$\frac{dm}{dy} = \frac{1}{2}c_h \frac{\rho_0 h_0 S_e}{M_e}\frac{V_e^2 \rho v^2 s}{H^* \sin\gamma}$$

We consider the isothermal atmosphere:

$$\rho = \exp(-y)$$

and we use the following relation between the cross-section area and the body mass:

$$s = m^{\mu}$$

where μ=const is a parameter characterizing the possible rotation role during the flight.

Then mass and height above the surface for a meteoroid entering the terrestrial atmosphere can be represented by the following functions of velocity:

$$m = \exp\left(-\frac{\beta}{1-\mu}\left(1-v^2\right)\right) \qquad (2)$$

$$y = \ln\alpha + \beta - \ln\frac{\Delta}{2} \qquad (3)$$

where

$$\Delta = Ei(\beta) - Ei(\beta v^2), Ei(x) = \int_{-\infty}^{x}\frac{e^z dz}{z}$$

and two dimensionless parameters are introduced:

the ballistic coefficient:

$$\alpha = \frac{1}{2}c_d \frac{\rho_0 h_0 S_e}{M_e \sin\gamma} = \frac{1}{2}c_d \frac{\rho_0 h_0 A_e}{M_e^{1/3}\rho_b^{2/3}\sin\gamma}$$

(where A_e is the pre-atmospheric shape factor and ρ_b is the meteoroid density), and the mass loss parameter:

$$\beta = \frac{1}{2}(1-\mu)\frac{c_h V_e^2}{c_d H^*} \ .$$

For every meteor event one can find corresponding α and β values from the observational data (observed at certain points along the trajectory with corresponding heights h_i and velocities V_i, i = 1, 2, ..., n) according to the method described in Gritsevich (2007). Application of this method to the case of Košice is explained in Gritsevich et al. (2014b). Thus, after obtaining the values of α and β from the observational data, it is possible to calculate the

trajectory and follow the change in meteoroid mass based on equations 2 and 3. In *Figure 2* the obtained height-velocity relation is shown, and in *Figure 3* the corresponding height-time dependence is shown, where symbols denote the observational data and the line is the calculated trajectory. A good agreement can be seen between observational and calculated data, as well as in the cases of Přibram, Lost City, Innisfree, and Neuschwanstein falls (Gritsevich, 2008).

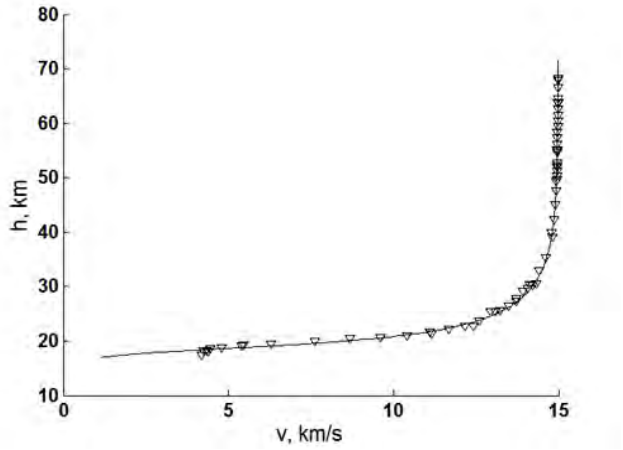

Figure 2 – Height vs velocity (in dimensional form) for the Košice meteorite case. Symbols – observational data (Borovička et al, 2013) (for the main fragment), full line – calculated trajectory according to equations 3 and 1.

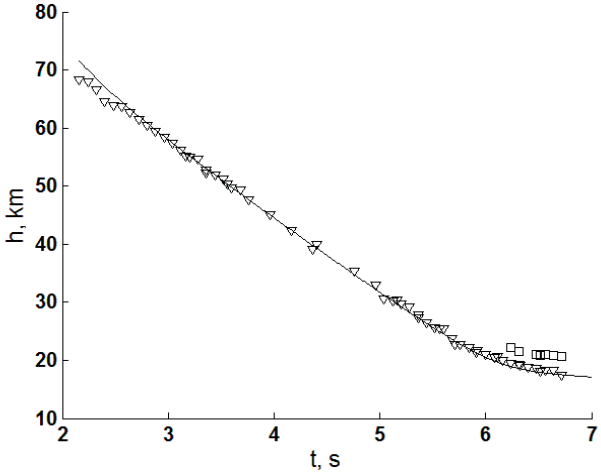

Figure 3 – Height change with time (in dimensional form) for the Košice case. Symbols – observational data (Borovička et al, 2013) (triangles – for the main fragment, squares – for the second fragment), full line – calculated trajectory.

3 Mass estimation and fragment distribution

The value of the ballistic coefficient α found using the observational data can be used to estimate the dynamic mass of the main fragment of the Košice meteoroid:

$$M_e = \left(\frac{1}{2} c_d \frac{\rho_0 h_0}{\alpha \sin\gamma} \frac{A_e}{\rho_m^{2/3}} \right)^3$$

According to the fragment mass data (Gritsevich et al., 2014a), we can also use statistical methods for additional analysis to describe the Košice fragmentation process. In particular, it was found that bimodal Weibull, bimodal Grady and bimodal lognormal distributions are the most appropriate (Gritsevich et al., 2014b). As an example of fragment distribution the approximation by the bimodal Weibull distribution is shown in *Figure 4*:

$$F_W(m,\omega,\gamma_1,\mu_1,\gamma_2,\mu_2) =$$

$$= \omega\left[1-\exp\left(-\left(m/\mu_1\right)^{\gamma_1}\right)\right] +$$

$$+ (1-\omega)\left[1-\exp\left(-\left(m/\mu_2\right)^{\gamma_2}\right)\right]$$

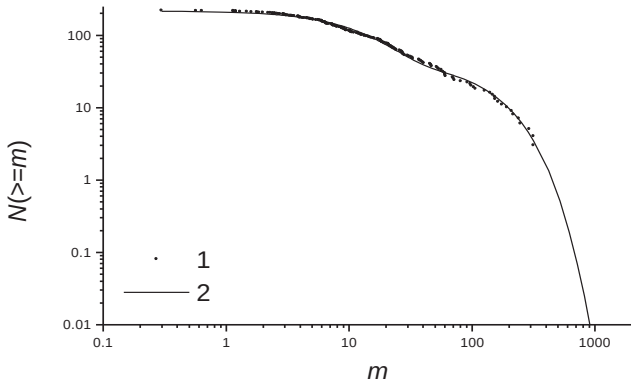

Figure 4 – Complementary cumulative number of fragments $N(\geq m)$ vs m (decimal logarithm scale) for the sample. 1 – Observed data, 2 – Bimodal Weibull distribution with the weighting factor ω=0.8, $\gamma_1=\gamma_2$=1.14 and μ_1=13.1, μ_2=140.

Also, for different types of approximating distributions the probabilities for missing fragments are calculated. Based on these results, we conclude that at least two missing fragments of mass 500-1000 g should exist (e.g. for the here referred Weibull distribution, this probability is around 0.839).

Acknowledgments

The numerical simulations and development of the analytical model were carried out by Maria Gritsevich and Daria Kuznetsova at MIIGAiK and supported by the Russian Science Foundation, project No. 14-22-00197. The fragment distribution was studied by Maria Gritsevich and Vladimir Vinnikov under support of the Academy of Finland No. 260027 (Maria Gritsevich) and Russian Foundation for Basic Research, projects No. 13-07-00276 (Vladimir Vinnikov) and 14-08-00204 (Maria Gritsevich).

References

Bland P. A., Artemieva N. A. (2003). "Efficient disruption of small asteroids by Earth's atmosphere". *Nature*, **424**, 288–291.

Borovička J., Tóth J., Igaz A., Spurný P., Kalenda P., Haloda J., Svoreň J., Kornoš L., Silber E., Brown P., Husárik M. (2013). "The Kosice meteorite fall: Atmospheric trajectory, fragmentation, and orbit". *Meteoritics and Planetary Science*, **48**, 1757–1779.

Gritsevich M. I. (2007). "Approximation of the observed motion of bolides by the analytical solution of the equations of meteor physics". *Solar System Research*, **41**, 509–514.

Gritsevich M. I. (2008). "The Pribram, Lost City, Innisfree, and Neuschwanstein Falls: An analysis of the Atmospheric Trajectories". *Solar System Research*, **42**, 372–390.

Gritsevich M. I. (2009). "Determination of Parameters of Meteor Bodies Based on Flight Observational Data". *Advances in Space Research*, **44**, 323–334.

Gritsevich M. I., Stulov V. P., Turchak L. I. (2012). "Consequences for Collisions of Natural Cosmic Bodies with the Earth Atmosphere and Surface". *Cosmic Research*, **50**, 56–64.

Gritsevich M., Vinnikov V., Kohout T., Tóth J., Peltoniemi J., Turchak L., Virtanen J. (2014a). "A comprehensive study of distribution laws for the fragments of Košice meteorite". *Meteoritics and Planetary Science*, **49**, 328–345.

Gritsevich M., Kuznetsova D., Vinnikov V., Pupyrev Yu., Peltoniemi J., Lupovka V., Dmitriev V., Oberst J. (2014b). "Constraining preatmospheric parameters of large meteoroids: A case study for Košice", in preparation.

Kohout T., Havrila K., Tóth J., Husárik M., Gritsevich M., Britt D., Borovička J., Spurný P., Igaz A., Svoreň J., Kornoš L., Vereš P., Koza J., Zigo P., Gajdoš Š., Világi J., Čapek D., Krišandová Z., Tomko D., Šilha J., Schunová E., Bodnárová M., Búzová D., Krejčová T. (2014). "Density, porosity and magnetic susceptibility of the Košice meteorite shower and homogeneity of its parent meteoroid". *Planetary and Space Science*, **93–94**, 96–100.

Stulov V. P. (1997). "Interactions of space bodies with atmospheres of planets". *Appl. Mech. Rev.*, **50**, 671–688.

Tóth J., Svoreň J., Borovička J., Spurný P., Igaz A., Porubčan V., Kornoš L., Husárik M., Krišandová Z., Vereš P., Kaniansky S. (2010). "Meteorite Košice – The Fall in Slovakia". International Meteor Conference, IMC 2010, Sep. 16-19, 2010, Armagh, UK. Not published. http://www.imo.net/imc2010/talks/Kaniansky.pdf

Vinnikov V., Gritsevich M., Kuznetsova D., Turchak L. (2014). "Empirical fragment distributions in meteorites". *45th LPSC Abstracts*, Abstract # 1439.

A conference without socializing? One of the important aspects for a successful IMC is a good bar and the very best is when this can be managed by IMC participants. Our French friends did their very best at the IMC bar. From left to right: Lucie Maquet, Sylvain Bouley, François Colas, Brigitte Zanda, Karl Antier and Arnaud Leroy. (Credit Axel Haas.)

Detection of spectral UV from meteors by a nanosatellite

Nicolas Rambaux[1,2], Dimitri Galayko[1,3], Jean-François Mariscal[4], Michel-Andres Breton[1,2], Jérémie Vaubaillon[2], Mirel Birlan[2], François Colas[2] and Thierry Fouchet[1,5]

[1] **Sorbonne Universités, UPMC Univ Paris 06, 4 Place Jussieu, 75005 Paris, France**
Nicolas.Rambaux@imcce.fr

[2] **Institut de Mécanique Céleste et Calcul des Ephémérides, Observatory of Paris, CNRS UMR8028, 77 Avenue Denfert-Rocherau, 75014 Paris**
Breton@obspm.fr, Vaubaillon@imcce.fr, Birlan@imcce.fr, Colas@imcce.fr

[3] **Lip6, 4, place Jussieu, 75252 Paris Cedex France**
dimitri.galayko@lip6.fr

[4] **LATMOS, Quartier des Garennes, 11 boulevard d'Alembert 78280, Guyancourt, France**
jean-francois.mariscal@latmos.ipsl.fr

[5] **LESIA, Observatoire de Paris, CNRS, UPMC, Université Paris-Diderot, 5 place Jules Janssen, 92195 Meudon, France**
Thierry.Fouchet@obspm.fr

Here, we present a cubesat space mission concept devoted to the UV detection of meteors from space. Space observations have the advantages of being able to continuously observe meteors independently of weather conditions on large portions of the atmosphere and, specifically, to perform ultra-violet light measurement as it is above the ozone layer. The UV spectrum is interesting for the detection of chemicals such as iron, carbon and hydroxide that can yield a signature of elements present during the solar system's formation.

1 Introduction

The atmosphere is constantly colliding with extraterrestrial particles that give rise to the luminous phenomenon of meteors. Such an event is very short (0.2-5 seconds), it results from the heating of a particle called a meteoroid (see Ceplecha et al., 1998). The meteoroids come from comets or asteroids and each year the flux of meteoroids is estimated with a great uncertainty between 30 and 200 ktons (Bland et al., 1996). Consequently, the Earth's atmosphere can be seen as a giant detector of these primordial objects.

At present, meteors are mainly observed ground based from the Earth by imagery, spectroscopy, and radar detection. The two first methods are limited in space coverage, depend on the weather conditions, and on the absorption band of the atmosphere. A space mission offers a unique possibility to measure meteors continuously and to assess the flux of meteoroids that collide with the Earth. In addition, the vantage point of a space mission allows exploring the UV spectrum to characterize the meteor. Until now only two space detections of meteors in the UV spectrum have been reported in literature (e.g. Jenniskens et al., 2002). That paper highlights the signature of carbon and hydroxide, two prebiotic constituents.

Here we present the development of a nanosatellite that could reach the objective to characterize meteors. Such a mission will consist of two instruments, namely a visible camera and a UV spectrometer. The main objectives of this mission are: (1) to measure the luminous spectrum of a meteor and to determine the composition of the meteoroid, (2) to analyze the light curve and to quantify the physical process acting during the entry in the atmosphere, and (3) to contribute to the determination of the meteoroid's trajectory by combining these observations with ground-based data on Earth. Secondary objectives are to enable the study of transient luminous phenomenon, the study of Earth's UV spectrum, and the detection of artificial debris during the mission.

2 Why a nanosatellite?

A nanosatellite is a small satellite with a mass of between 1 and 10 kg. Here, we use the cubesat norm developed by California Polytechnic State University at San Luis Obispo and by the University of Stanford. The cubesat is a cube of 10 cm edge, a volume of 1 liter, a mass of 1 kilogram and a power of 1 Watt (on average). Such a satellite offers all the vital functions of a normal satellite plus either a technological package to test a Technology Merit Level, to test the resistance for radiation, or a small sensor or a camera to perform science investigation.

We schedule to develop a three units cubesat (3 cubes, 3U), which will contain a scientific payload composed by a visible camera and a UV spectrometer. In addition to the scientific objectives the nanosatellite offers hands-on experience to aerospace engineering for students in all the development of the project (design, development, test, and qualification of a real spacecraft).

3 Science investigation

The main objective of the mission is to detect and record the UV spectrum of a meteor. The UV spectrum is useful to detect chemicals such as iron, carbon, and hydroxide (Jenniskens et al., 2002; Carbary et al., 2004). In particular, carbon and hydroxide radicals are tracers of physical and chemical conditions in the primordial solar nebula, and their study gives information on the solar system's formation and the contribution of prebiotic materials on the Earth. The main knowledge of meteoroids comes from the short time of their interaction with the Earth's atmosphere (Ceplecha et al., 1998). Several methods, on the Earth or airborne, have been used over the years in order to accurately measure meteors such as imagery, spectroscopy, and radar detection to determine the flux and origin of primitive material brought by meteoroids (see e.g. Ceplecha et al., 1998). The collection of meteorites and micro-meteorites on the ground is crucial to bring back samples into the laboratory and to perform thorough studies.

However, very few space missions have been dedicated to the detection of meteors. Only two missions, ARGOS and MSX, have detected meteors from space. The first one (ARGOS) is the observation of an American military satellite in far-UV while the second one, MSX, explored a large spectrum band with the instrument UVISI (Jenniskens et al., 2002). The UVISI instrument has recorded the presence of carbon and hydroxide in the UV spectrum illustrating the strong potential of detection from space in UV. *Figure 1* presents a meteor synthetic spectrum reconstruction using as input the observations of Jenniskens et al. (2002) and the database of laboratory spectra for a given number of chemical elements and compounds. This synthetic spectrum is used to determine the technical specification of the nanosatellite. The objective of the nanosatellite is to reach a range of detection in the 200-400 nm spectral window with a spatial resolution below 1.5 nm in order to distinguish between the carbon and iron bands.

In addition, the recording of meteors with the camera brings information on the physical interaction of meteoroids with the atmosphere. Notably, it will significantly improve the statistics for global studies. Indeed, the position of the nanosatellite (scheduled at an altitude of 500-600 km) allows observing a broad surface on the Earth and is independent of the meteorological conditions. The increase of statistics on these data is crucial to improve the ablation models of meteoroids (Gritsevich and Koschny, 2011; Campbell-Brown and Koschny, 2004).

At an altitude of 500 km and pointing at the nadir, a meteor with a magnitude between 0 and -5 should be detected with an irradiance of 78-7800 photons/s/cm^2/Å. If the measurement is done at the limb, a meteor at 2400 km, with a magnitude between 0 and -5, produces an irradiance of 1.3-130 photons/s/cm^2/Å. During a meteor shower, the number of meteors can reach 50-100 per hour (detected from the ground) while the rate of sporadic detections can reach 12 meteors per hour for a high-quality camera such as SPOSH (Oberst et al., 2011; Bouquet et al., 2014).

The determination of the trajectory is crucial to track the origin of the parent body (Rudawska et al., 2012). Here the objective is to combine space observations with ground-based observations obtained by survey networks such as FRIPON (Colas et al., 2012). This requires an accurate follow-up of the nanosatellite and attitude determination of the spacecraft.

4 Scientific instruments and cubesats

The project is at the beginning and we schedule 3U cubesat in order to include a UV spectrometer, a visible camera, and an altitude control system that are the three

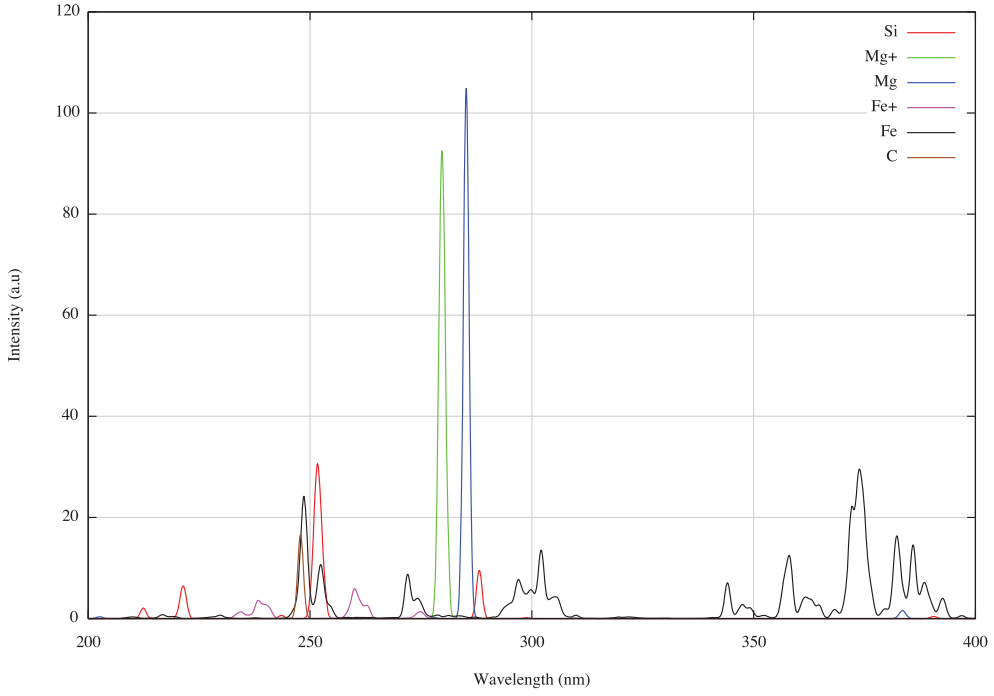

Figure 1 – Synthetic spectrum of a meteor. This example is build from detection of a Lenoids by Jenniskens et. al (2002).

larger parts of the payload. The orbit will be heliosynchronous with an ascending node at 10^h30^m to allow recharging the battery of the nanosatellite. In addition, the meteors are observed during the night. In order to detect faint magnitude meteors and to stay in orbit at least one year, the cubesat will stay at an altitude of 500–600 km and will respect the LOS (re-entry in the atmosphere in less than 25 years).

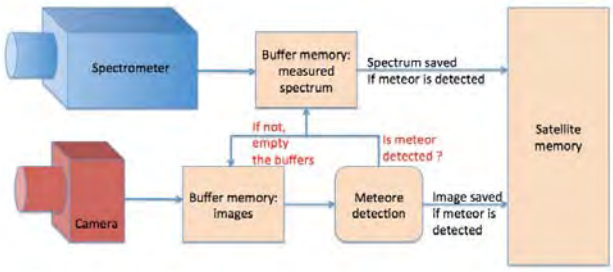

Figure 2 – Diagram illustrating the meteor detection and spectrum measurement.

The most important challenge related to meteor spectrometry is the transient character of the light emission by meteors (<0.5 s duration), coupled to the ambiguous location of the upcoming phenomenon in the field of view of the instrument. Obviously, the nanosatellite should be a fully autonomous meteor observatory. This challenge will be addressed in the following way (*Figure 2*): both camera and spectrometer have the same orientation and capture the image of the same area. They permanently register the visible data (images and spectra) in the buffer memory, so that the buffer memory always has the full data of last N seconds (the exact duration is to be defined). In parallel, the buffer memory of the camera is processed by an onboard computing unit, and if a meteor is detected, the last data registered from the spectrometer is archived as the data about the phenomenon of interest. Otherwise, both the camera and spectrometer buffers are erased.

The meteor detection software package is challenging and it should inspect a video data stream in real time and determine the time of appearance of meteors.

Technical key challenges are:

- the altitude control system (the camera should be stabilized at a known, predictable altitude)
- The telemetry of a large amount of data: the estimated required rate is 3.8 Mbits/second during the communication with the ground station; S-band and X-band telemetry solutions are being explored.
- The camera and spectrometer raw video data output, this should be pre-processed, in order to reduce the quantity of data to be transmitted toward the ground station.

Acknowledgment

We thank the support of the UPMC/SU, JANUS/CNES and ESEP.

References

Bland P. A., Smith T. B., Jull A. J. T., Berry F. J., Bevan A. W. R., Cloudt S., Pillinger C. T. (1996). "The flux of meteorites to the Earth over the last 50,000 years". *Monthly Notices of the Royal Astronomical Society*, **283**, 551–565.

Bouquet A., Baratoux D., Vaubaillon J., Gritsevich M. I., Mimoun D., Mousis O., Bouley S. (2014). "Simulation of the capabilities of an orbiter for monitoring the entry of interplanetary matter into the terrestrial atmosphere". *Planetary and Space Science*, **103**, 238–249.

Campbell-Brown M. D., Koschny D. (2004). "Model of the ablation of faint meteors". *Astronomy & Astrophysics*, **418**, 751–758.

Carbary J. F., Morrison D., Romick G. J., Yee J. H. (2004). "Spectrum of a Leonid meteor from 110 to 860 nm". *Advances in Space Research*, **33**, 1455–1458.

Ceplecha Z., Borovička J., Elford W. G., Revelle D. O., Hawkes R. L., Porubčan V., Šimek M. (1998). "Meteor Phenomena and Bodies". *Space Science Reviews*, **84**, 327–471.

Colas F., Zanda B., Vernazza P., Vaubaillon J., Bouley S., Gattaccecca J., Baratoux D., Birlan M., Cournede C., Fieni C., Hutzler A., Jambon A., Maquet L., Mousis O., Rochette P., Strajnic J., Vachier F. (2012). "(FRIPON) Fireball Recovery and Interplanetary Matter Observation Network". *Asteroids, Comets, Meteors 2012*, Proceedings of the conference held May 16-20, 2012 in Niigata, Japan. LPI Contribution No. 1667, id.6426.

Gritsevich M., Koschny D. (2011). "Constraining the luminous efficiency of meteors , Model of the ablation of faint meteors". *Icarus*, **212**, 877–884.

Jenniskens P., Tedesco E., Murthy J., Laux C. O., Price S. (2002). "Spaceborne ultraviolet 251-384 nm spectroscopy of a meteor during the 1997 Leonid shower". *Meteoritics & Planetary Science*, **37**, 1071–1078.

Oberst J., Flohrer J., Elgner S., Maue T., Margonis A., Schrödter R., Tost W., Buhl M., Ehrich J., Christou A., Koschny D. (2011). "The Smart Panoramic Optical Sensor Head (SPOSH)—A camera for observations of transient luminous events on planetary night sides". *Planetary and Space Science*, **59**, 1–9.

Rudawska R., Vaubaillon J., Atreya P. (2012). "Association of individual meteors with their parent bodies". *Astronomy & Astrophysics*, **541**, id. A2, 5pp.

Radio set-up design for the FRIPON project

Jean-Louis Rault[1], François Colas[2] and Jérémie Vaubaillon[2]

[1] **IMO Radio Commission, 16, rue de la Vallée, Épinay sur Orge, France**
f6agr@orange.fr

[2] **IMCCE, Paris, Observatoire de Paris, 77 av. Denfert-Rochereau, 75014 Paris, France**
colas@imcce.fr,vaubaill@imcce.fr

The French FRIPON (Fireball Recovery and InterPlanetary Observation Network) project consists of about 100 allsky cameras which are currently being installed at various locations in France. The purpose of FRIPON is to detect large meteors thanks to optical systems, to compute the orbits of their parent bodies, and to predict as precisely as possible the impact locations of the related meteorites, if any. Video cameras deliver accurate target positions but lack the precision required for accurate meteor velocity measurements, a precision which is mandatory for good meteoroid orbits and meteorite location assessments. Therefore 25 radio systems, which are in charge to deliver accurate meteor velocities data, are being installed to complement the FRIPON video network.

1 Introduction

The French FRIPON project is using about 100 allsky video cameras (Colas, 2014) for observing large meteors. The video data are processed to obtain the orbit parameters of the related parent bodies, and also to determine the impact locations of the potential meteorites. Video systems are supposed to deliver good precision positional data, but due to the refreshment rate of the video frames, the computed meteor velocity would not be precise enough to obtain accurate parent body orbital parameters. Radio meteor observations should allow more accurate meteor velocity measurements, therefore about 25 radio systems are going to be added to the FRIPON video cameras network.

2 Radio observations principle

Due to its very high geocentric speed (~11 km/s up to ~72 km/s), a meteoroid creates a long column of free electrons when hitting the air molecules of the Earth atmosphere. During the first part of its travel in the upper atmosphere, the meteor body itself is surrounded by a plasma envelope. The ionized trail and the free electrons surrounding the moving body are able to reflect radio waves, as long as the frequency of these radio waves used to observe the meteors is lower than the critical frequency f_c.

$$f_c = \sqrt{\frac{e^2 \times N_e}{\Pi \times m}} = 9 \times \sqrt{N_e} \quad [1]$$

with m and e, representing the electrical charge and the mass of the electron, N_e the number of free electrons per cm^3 and f_c the critical frequency expressed in megahertz. The echoes of radio waves radiated by a distant transmitter which are scattered on the plasma surrounding a meteor are called head echoes. Head echoes are detectable as long as the frequency used to observe them is lower than f_c. (Close et al., 2002). It is desirable to use the shortest wavelength possible to observe the meteor head echoes, because the ERS (Equivalent Radar Surface) of the small sized plasma envelopes are not large. Knowing that the amplitudes of the meteor echoes decrease according to a $1/f^3$ law, powerful radio transmitters have to be used for detecting the head echoes.

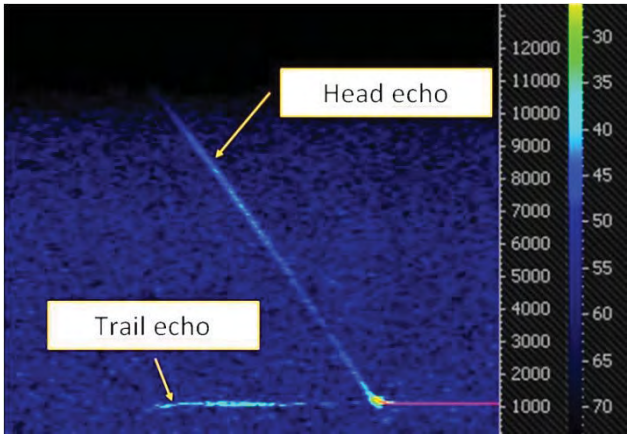

Figure 1 – Example of spectral analysis of a meteor head echo received from GRAVES transmitter at Pic du Midi observatory.

If the observer and the transmitter are considered as motionless, a head echo at the observation location is affected by a variable frequency shift due to the Doppler-Fizeau effect. The moving target is illuminated by an incident radio wave which frequency is shifted according to the radial velocity between the meteor and the transmitter location. This radio wave is scattered by the meteor plasma. At the observation location, the frequency received from this scattered wave is shifted again in frequency according to the radial speed between the meteor and the observation location (Steyaert et al., 2010). So the resulting double Doppler frequency shift is directly linked to the 3D-geometry of the transmitter, the receiver and the moving target (see *Figure 1*). Therefore, using several time-synchronized radio receivers and a single transmitter, the reduction of the Doppler-Fizeau shifted head echoes recorded at separate locations should offer good precision velocity information.

3 Radio set-up

Radio system configuration

At least two radio transmitters will be used for the FRIPON project: the military GRAVES radar located near Dijon (143.050 MHz) in the South part of France, and the BISA BRAMS transmitter located near Dourbes, Belgium (49,980 MHz) for the Northern part of the country.

Figure 2 – Locations of BRAMS and GRAVES transmitters. The yellow pins show the various receiving places which have already successfully been tested with low gain receiving antennae.

Figure 3 – FRIPON radio antennas installed on a roof at IMCCE, Observatoire de Paris.

Set-up design

The highest geocentric velocity of a solar system meteoroid being around 72 km/s, the expected theoretical maximum Doppler-Fizeau frequency shift will be about 23 kHz for a 49 MHz transmitter such as the BRAMS set-up, and 67 kHz for the VHF GRAVES radar. Therefore, a large bandwidth receiver compatible with such values must be used. The cheap but efficient SDR (Software Defined radio) FUNcube Dongle Pro + developped by the AMSAT-UK association[1] has been selected for FRIPON. Technical details about this receiver are described in (Rault, 2013). 4 element 143 MHz and 5 element 49 MHz Yagi beam antennae are completing the radio set-up (see *Figure 3*).

[1] http://www.funcubedongle.com/

4 Conclusion

A small size, light-weight, low cost but efficient radio set-up has been designed for the FRIPON project. First operational results are expected at the end of 2015.

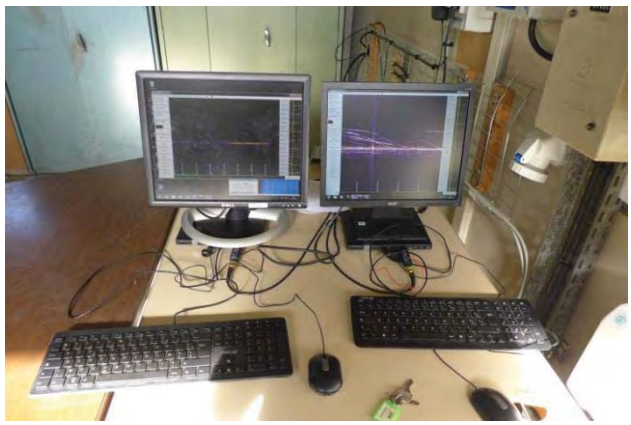

Figure 4 – First lights of the 49 and 143 MHz FRIPON radio receivers running at IMCCE, Observatoire de Paris.

References

Colas F., Zanda B., Bouley S., Vaubaillon J., Vernazza P., Gattacceca J., Marmo C., Audureau Y., Kyung Kwon M., Maquet L., Rault J.-L., Birlan M., Egal A., Rotaru M., Birnbaum C., Cochard F., Thizy O. (2014). "The FRIPON and Vigiel-Ciel networks". In Rault J.-L., and Roggemans P., editors, *Proceedings of the International Meteor Conference*, Giron, France, 18–21 September 2014. IMO, pages 34–38.

Rault J.-L. (2013). "New trends in meteor radio receivers". In Gyssens M. and Roggemans P., editors, *Proceedings of the International Meteor Conference*, Poznań, Poland, 22–25 August 2013. IMO, pages 70–72.

Steyaert C., Verbelen F. (2010). "Meteor trajectory from multiple station head echo Doppler observations". *WGN, Journal of the IMO*, **38**, 123–129.

Close S., Oppenheim M., Hunt S., Dyrud L. (2002). "Scattering characteristics of high-resolution meteor head echoes detected at multiple frequencies". *Journal of Geophysical Research*, **107,** SIA9-1 – SIA9-12.

EARS, MARS combined radio observations - 2014

Giancarlo Tomezzoli

European Patent Office, Bayerstrasse 152, 80335 Munich – Germany
gtomezzoli@epo.org

The Lyrid meteor shower was generated on 21-22 April 2014 by the passage of the Earth through the path of the debris of the comet C/1861 G1 (Thatcher). The Camelopardalids meteor shower was generated on 23-24 May 2014 by the passage of the Earth through the path of the debris of the comet 209P/Linear. The EurAstro Radio Station (EARS) and the Malta Astro Radio Station (MARS) were operated in parallel for two combined radio observation campaigns. The campaigns revealed that further combined radio observation campaigns are necessary to solve the problem of estimating the number of lost radio meteor echoes.

1 Introduction

The Lyrid meteor shower was generated on 21–22 April 2014 by the passage of Earth through the path of the debris of the comet C/1861 G1 (Thatcher).

The EurAstro Radio Station (EARS), based on the forward scattering principle and operated by myself, adopted the following configuration: a radio beacon from radar Graves (emitter at Broyes-les-Pesmaes, 47°20'51.72" N, 5°30'58.68" W, about 500 Km from Munich)[1], a vertical antenna J-Pole 144[2], a receiver ICOM 1500 (USB mode, 143,049 MHz), a computer Pavillion dv6 (processor Intel Core Duo T2500) and a SpecLab V26 b10 (Tomezzoli, 2014).

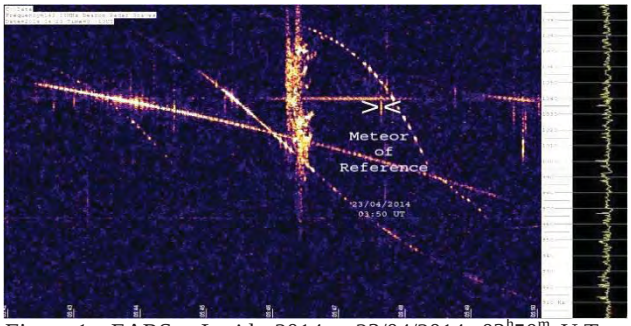

Figure 1 – EARS - Lyrids 2014 – 23/04/2014, 03^h50^m U.T. - airplane radio echoes (arcuate traces), overdense radio echo in the middle, underdense radio echoes and underdense reference meteor echo.

In order to catch the maximum of the Lyrids 2014, the EARS radio recording was started on 21 April 2014 at 15^h00^m UT and stopped on 24 April 2014 at 03^h50^m UT. For the first time, EARS and the Malta Astro Radio Station (MARS) operated by Alexei Pace worked in parallel for a combined radio observation campaign, in order to provide a cross check of the results. The presence in the past EARS JPG images of conspicuous airplanes radio echoes (*Figures 1 and 2*, arcuate traces) advised me against the use of an automatic meteor counting program because it is generally known that such programs are "confused" by airplane radio-reflections.

[1] http://fr.wikipedia.org/wiki/Radar_GRAVES
[2] http://www.antennepkw.com/1/j_pole_326922.html

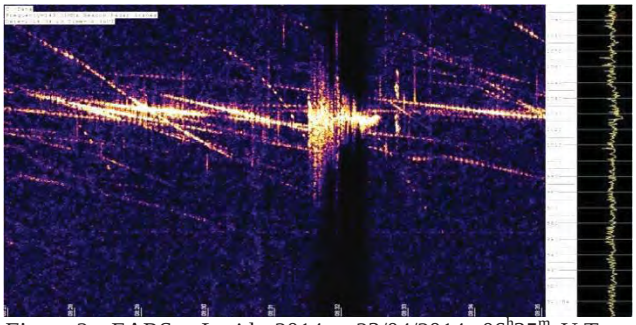

Figure 2 – EARS - Lyrids 2014 – 23/04/2014, 06^h35^m U.T. - airplane radio echoes (arcuate traces), overdense radio echo in the middle and underdense radio echoes.

2 Lyrids 2014

MARS Results

MARS, because of its distance (about 1500 km) from the Graves radar emitter, is not influenced by airplane radio reflections (*Figures 3 and 4*). Therefore, an automatic meteor counting program was used. The configuration of MARS and the results of the MARS radio observations of the Lyrids 2014 are summarised in *Figures 5 and 6*.

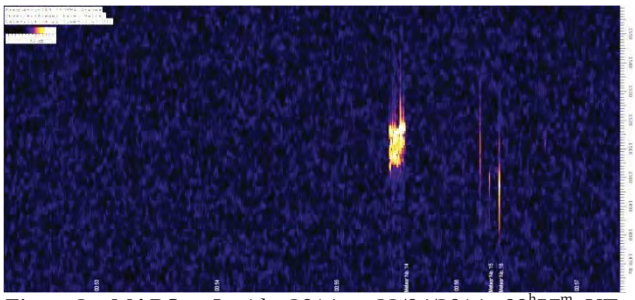

Figure 3 – MARS - Lyrids 2014 – 22/04/2014, 00^h57^m UT, overdense radio echo in middle right and three underdense radio echoes on the right.

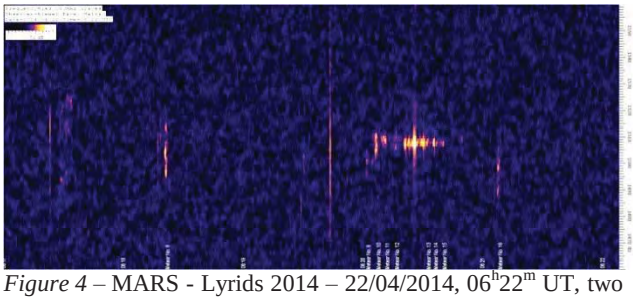

Figure 4 – MARS - Lyrids 2014 – 22/04/2014, 06^h22^m UT, two overdenses radio echoes in the middle right and underdense radio echoes on the left and on the right.

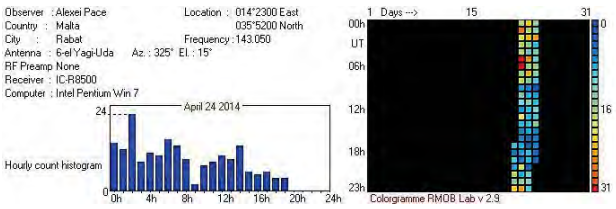

Figure 5 – MARS position, configuration and radio observation colorgramme.

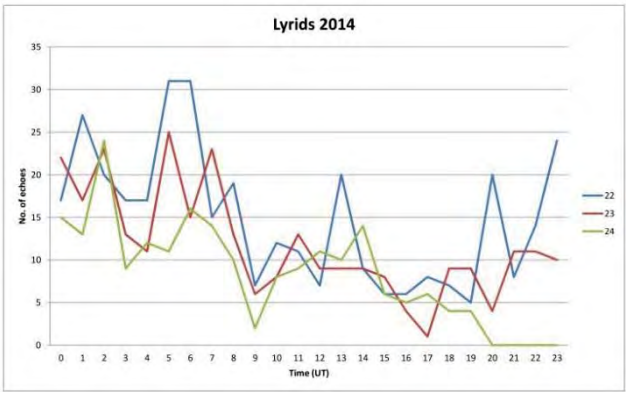

Figure 6 – MARS – Lyrids 2014 counting details.

EARS Results

The EARS results are summarized in *Figure 7*. I rely on the visual counting of the meteor radio echoes on the JPG images produced by SpecLab V 2.76 b10, distinguishing underdense radio echoes and overdense radio echoes.

Discussion

EARS (*Figure 7*) recorded a double maximum for the Lyrids 2014 superimposed on the background of the sporadic meteors. A first maximum (*Figure 7*, better indicated by the overdense radio echoes) on 22/04/2014 between 03^h00^m – 10^h00^m UT and a second maximum (*Figure 7*, better indicated by the overdense radio echoes) on 23/04/2014 between 00^h00^m – 08^h00^m UT. The MARS counts, although not distinguishing between underdense and overdense radio echoes, are in agreement (*Figure 6*), although with different numbers of radio echoes compared to the EARS counts (*Figure 7*). EARS detections of spectacular overdense radio echoes like those in *Figures 1 and 2* were not confirmed by MARS.

EARS visual counts on the JPG images were surely contaminated by missing faint underdense and overdense radio echoes, and by missing meteor radio echoes hidden by the airplane radio echoes. But, apparently, the MARS automatic meteor counting program overlooked part of the underdense and overdense radio echoes. For example, as can be seen in *Figure 3*, one of the three underdense radio echoes on the left side was overlooked, and, as can be seen in *Figure 4*, one underdense radio echo on the left side was overlooked and two overdense radio echoes on the right were counted as seven radio echoes. The different counting methods (visual counting on the JPG images for EARS, automatic counting for MARS), the contamination on the visual counting of EARS, the "behaviour" of the MARS automatic meteor counting program and the weaker meteor radio reflections received by MARS due to its longer distance from the Graves radar emitter, explain the EARS – MARS meteor radio echo counting differences.

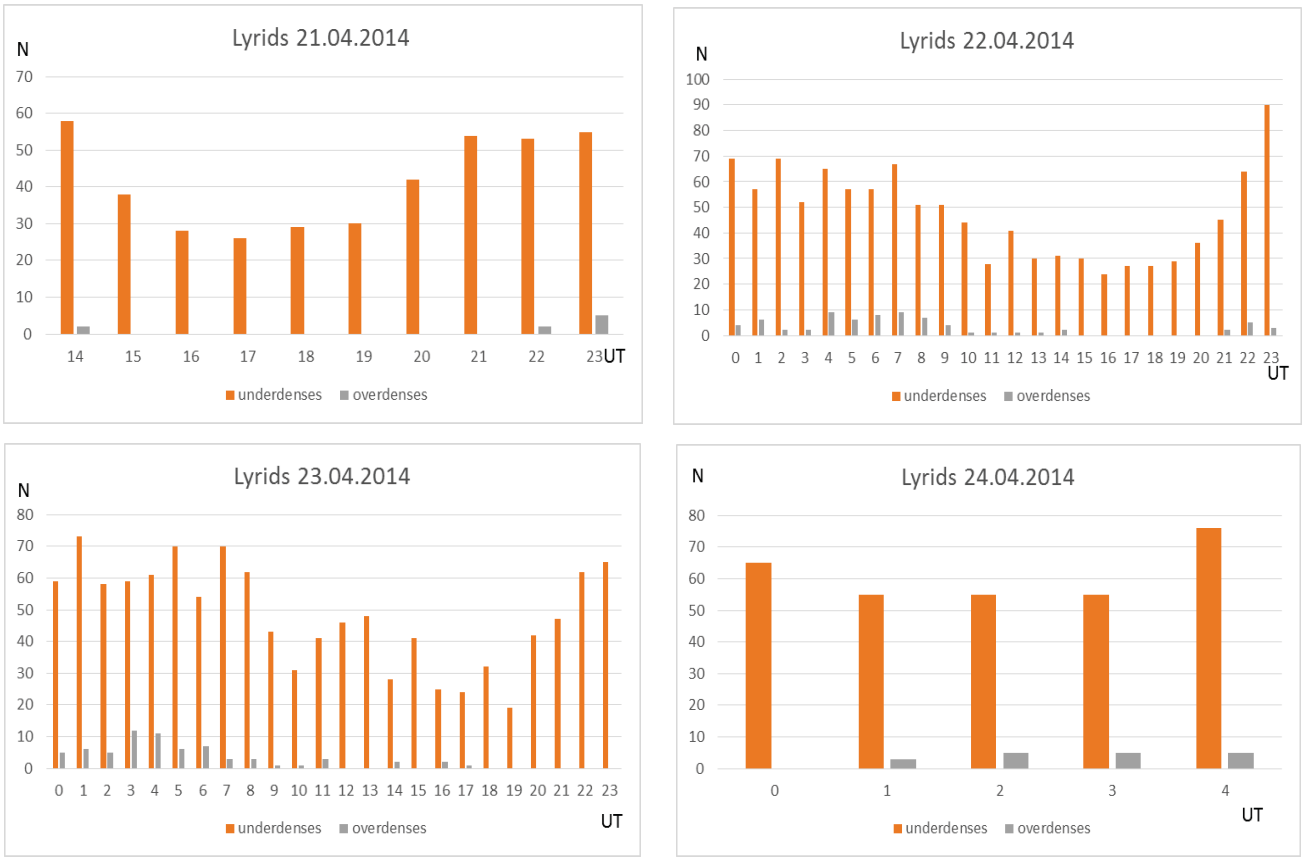

Figure 7 – EARS – Lyrids 2014 counting details (N number of echoes).

3 Camelopardalids 2014

The Camelopardalid meteor shower was generated on 23-24/05/2014 by the passage of Earth through the path of the debris of comet 209P/Linear. EARS and MARS worked again in parallel on 23-25/04/2014 for a new combined observation campaign.

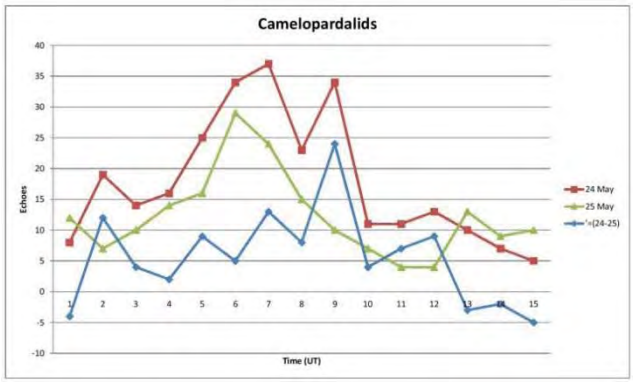

Figure 8 – MARS – Camelopardalids 2014 counting details.

MARS Results

The results of the MARS radio observations of the Camelopardalids 2014 are summarised in *Figure 8*.

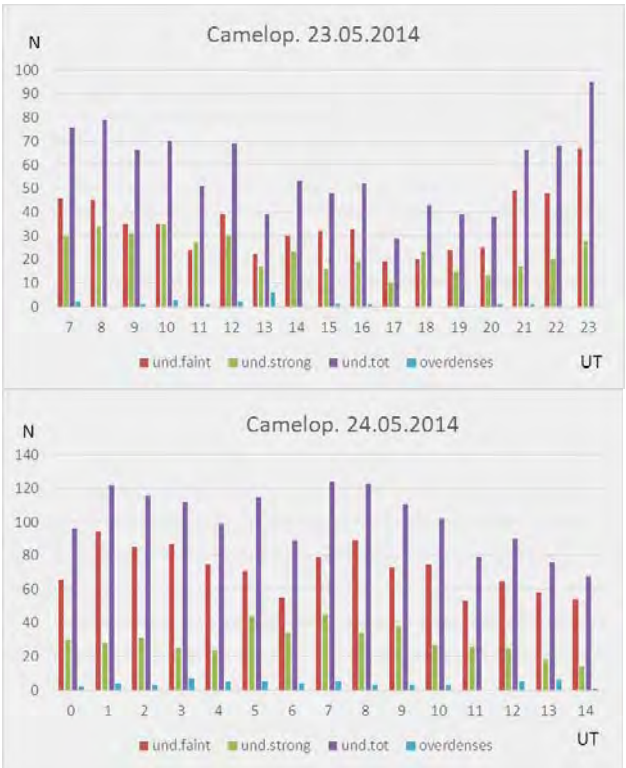

Figure 9 – EARS – Camelopardalids 2014 counting details.

EARS Results

The results of the EARS radio observations of the Camelopardalids 2014, by distinguishing between strong and faint radio echoes on the basis of the adopted underdense reference meteor echo (*Figure 1*), are summarised in *Figure 9*.

Discussion

EARS (*Figure 9*) recorded a double maximum for the Camelopardalids 2014 superimposed on the background of the sporadic meteors. A first maximum (*Figure 9*, better indicated by the overdense radio echoes) on 23/05/2014 between 09^h00^m – 16^h00^m UT and a second maximum (*Figure 9*, better indicated by the overdense radio echoes) on 24/05/2014 between 00^h00^m – 09^h00^m. The MARS counts, although not distinguishing between underdense and overdense radio echoes, are in agreement (*Figure 8*), although with different numbers of radio echoes compared to the EARS counts (*Figure 9*).

4 Conclusion

As expected, the radio observing results of EARS and MARS are in agreement to each other. However, further observations are necessary, as usual in science, to estimate the missing faint underdense and overdense radio echoes and the missing meteor radio echoes hidden by the airplane radio echoes in the EARS radio observations, and to estimate the underdense and overdense radio echoes missing because of the "behaviour" of the MARS automatic meteor counting program in the MARS radio observations.

Acknowledgement

I am grateful to Alexei Pace for having given me the permission of inserting the MARS results concerning the Lyrids and Camelopardalidis 2014 in the present article.

References

Tomezzoli G. T. (2014). "Progress on radio astronomy in Munich, Germany". In Gyssens M., Roggemans P., and Żołądek P., editors, *Proceedings of the International Meteor Conference*, Poznań, Poland, 22–25 August 2013. IMO, pages 78–80.

The Global Radio Camelopardalids 2014

Christian Steyaert

VVS, Vereniging voor Sterrenkunde, Belgium
steyaert@vvs.be

The on-line hourly radio counts are analyzed for the presence of the predicted May 24 Camelopardalids. Selection criteria are developed and an averaging method is proposed. Meteor activity is indeed detected during the predicted period. The method works for short duration outbursts and almost stationary radiants.

1 Introduction

Several authors (Ye and Wiegert, 2014) alerted about a possible meteor activity associated with Comet 209P/LINEAR. Dust trails would intersect with the Earth path on May 24, 2014, centered around 7^h UT, with radiant position $\alpha = 122^o$, $\delta = +79^o$.

Thanks to its high declination, the radiant has a small daily movement. This means that the Observability Function is not varying a lot during the timeframe under study, and that the whole day is covered by observers in the Northern hemisphere. The meteors are very slow (20 km/s with zenith attraction), like the Draconids which got an outburst in 2011 (Steyaert, 2012).

2 The observations

The initial screen (*Figure 1*) of Radio Meteor Observatories On-Line (RMOB) includes now the name of the observers for easy positioning[1]. During May 2014, 45 submissions were made, most of them counting automatically.

Figure 1 – Participating stations in Radio Meteor Observatories On-line.

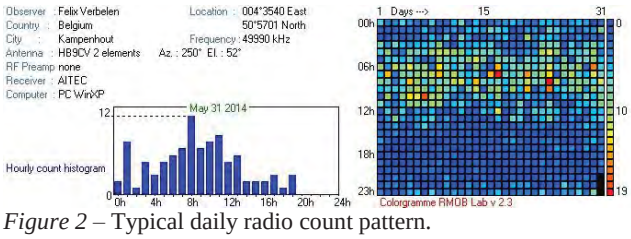

Figure 2 – Typical daily radio count pattern.

[1] http://www.rmob.org/livedata/main.php

A typical monthly graph (*Figure 2*) shows the daily pattern with a maximum in the morning hours local time, and a minimum in the evening, with superimposed stream activity, like the η-Aquariids around May 8.

3 The selection technique

Unfortunately not all observations can be used. A first category comprises observations:

- having erratic counts / system setup or sensitivity change during the month,
- not observed on May 24.

Ten submissions are removed applying thess criteria.

In a second pass, also removed are observations:

- having no data adjacent to May 24,
- not using UT.

Another 15 observations are removed applying these criteria. Please note that having increased counts in the predicted CAMs activity period was *not* a selection criterion. Eventually we are left with 11 observations in Europe, 6 in North America, and 3 in Japan. Six of the European observations are using the GRAVES transmitter.

Figure 3 – The GRAVES transmitter and the six retained observing stations for May 2014.

4 The GRAVES observations

GRAVES stands for ***G**rand **R**éseau **A**dapté à la **Ve**ille **S**patiale*, a space debris tracking radar, capable of detecting objects of size 10 cm in low orbit (Federation of

American Scientists, 2013)[2]. The transmitter is located near Dijon, France. Its EIRP (Equivalent Isotropically Radiated Power) is several megawatts at 143.050 MHz, and it applies beam switching. Due to its enormous radiated power, the signal can be observed up to more than 1000km from the transmitter.

5 An averaging technique

Multiple observations can be combined in several ways. We are trying out the geometric mean of m counts n_1, n_2,..., n_m defined as:

$$(n_1\, n_2\, \cdots\, n_m)^{\frac{1}{m}}$$

The geometric mean smooths out the higher values, which is the more conservative approach to avoid spurious values.

If one or more of the counts equal zero, the geometric mean is zero too. This is a convenient way to deal with missing counts, which are represented by a zero count. Hence the geometric mean is always based on the total number m of observations.

We tried this technique with just two observations, those labeled *_AAV__052014* and *TERRIER_052014*. In the resulting graph (*Figure 4*) the η Aquariids early May, as well as activity on May 24 is clearly seen.

Adding *SVAKOV-R4_052014* (*Figure 5*) makes the May 24 activity even standing out better. If on the other hand the observations would be uncorrelated or random, the signals would cancel each other out.

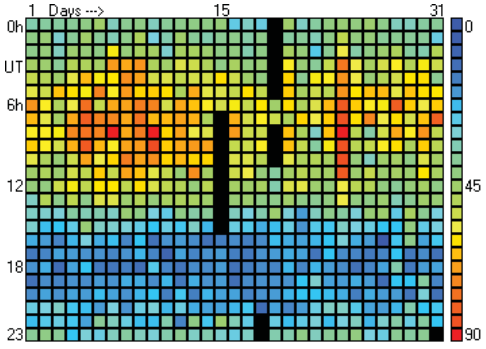

Figure 4 – Combining two.

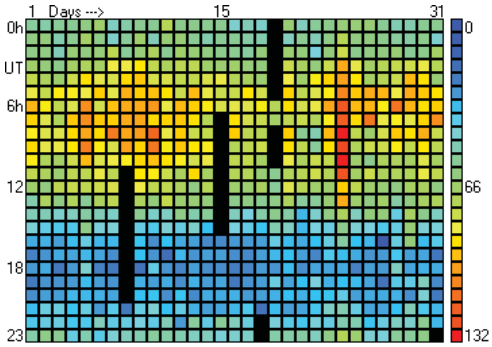

Figure 5 – Combining three.

[2] http://fas.org/spp/military/program/track/graves.pdf "A GRAVES Sourcebook"

Adding the three remaining observations, *Jones_052014 ZVPP_052014* and *Observatory_Vyskov_052014*, yields *Figure 6*.

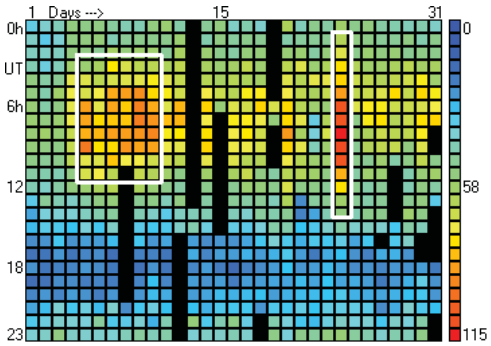

Figure 6 – The GRAVES transmitter and the six retained observing stations for May 2014.

The combined result of these heterogeneous observations exceeds the expectations. There is an extended activity period on May 24, from 1^h UT to 13^h UT. There is a shallow maximum from 7^h to 9^h UT, in line with the 209P/LINEAR stream forecasts. *Figure 7* is the periodogram of the May 23-25 geometric means.

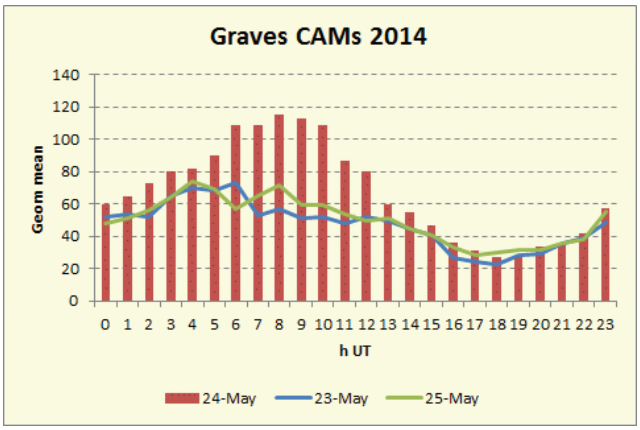

Figure 7 – Showing the excess averaged counts during May 24, 0^h to 14^h UT interval.

On *Figure 6* the CAMs activity of May 24 is higher than that of the η Aquariids. However the Observability Function of the η Aquariids is varying strongly during the day and is very different for the various observers. Hence the averaging technique reduces the signature of this stream. No conclusions about absolute strength of a stream can be made.

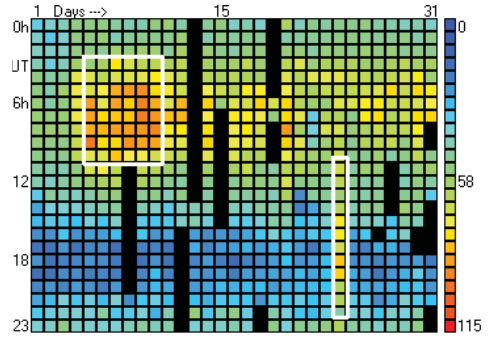

Figure 8 – Simulation of the CAMs activity would have happened 10 hours later.

Assuming that the CAMs activity would have happened 10 hours later, the combined GRAVES observations would have looked like *Figure 8*. As the CAMs are superimposed on the lower activity in the local afternoon/evening, the total counts would be lower too. However, the signature would even be clearer.

6 Other observations

The only other reported multiple observations of the same transmitter are by *De_Wilde_052014*, *Dubois_052014*, *Steyaert_052014*, *Verbelen_052014* of the VVS beacon (49.99 MHz, 50 W output power). There is activity detected on May 24, but so there is e.g. on May 30. The probable reason for the less efficient detection is the relatively low counts of Verbelen.

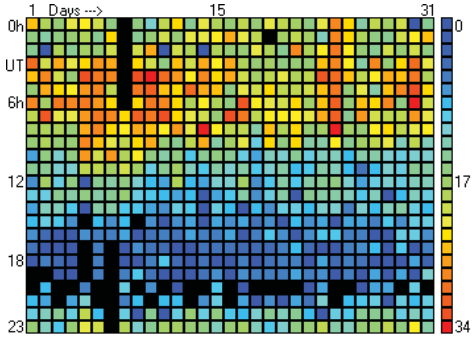

Figure 9 – VVS beacon four observations.

Single Japanese observations do not show well increased activity, although the timing (during the low of the daily cycle) was favorable. Antenna geometry and the low counts might be the reason.

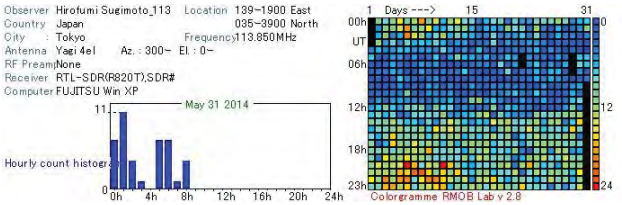

Figure 10 – Representative Japanese observation.

An observer located 550 km to the southwest of the 250 W ouput power BRAMS beacon (49.97 MHz) did record activity, but only around the maximum.

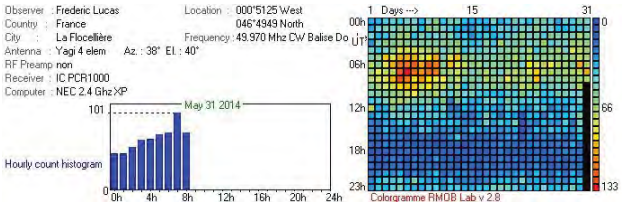

Figure 11 – BRAMS beacon observation.

The author used the Draconids 2011 (Steyaert, 2013) and η Aquariids 2012 (Steyaert, 2014) observations of Michael Svoiski. This time, hardly any activity can be noted. Unfavorable geometry (which doesn't change a lot) must be the cause, although it was not investigated in detail.

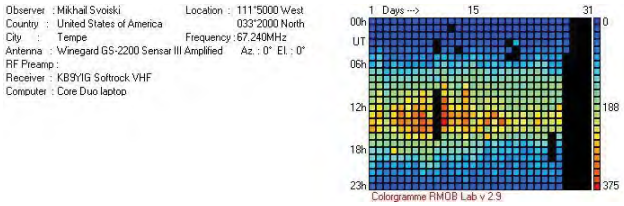

Figure 12 – Michael Svoiski – United States.

Conditions were apparently more favorable for Jeff Brower in Canada.

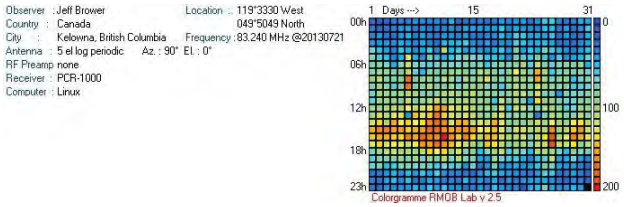

Figure 13 – Jeff Brower - Canada.

7 Detailed observations and spatial correlation

We looked in detail at the spectrograms and found out that many overdense meteors, characterized by the 'ε' shaped reflections appeared in the period May 24, 08^h15^m – 08^h40^m, while there are mainly underdense reflections outside that interval. This is both the case for European and North American observers (*Figures 14 and 15*).

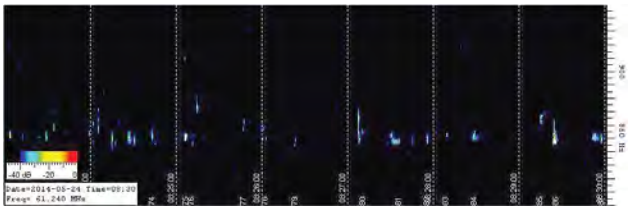

Figure 14 – Seven minute activity period Brower Canada.

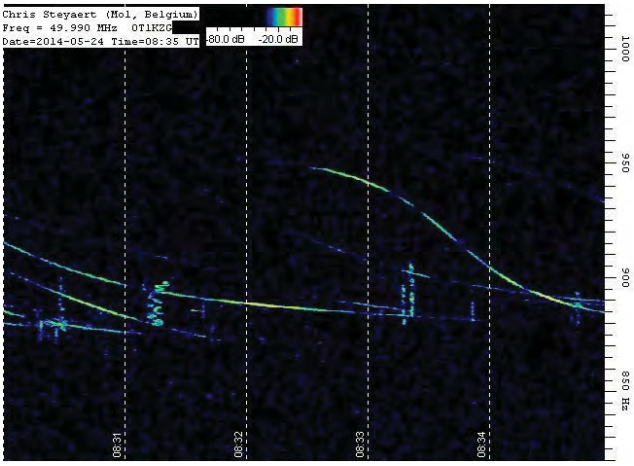

Figure 15 – Five minute activity period at Steyaert, Belgium.

The distance between the two observers orthogonal to the direction in which the meteoroids move is approx. 8000km (*Figure 16*). The difference along the travelling direction is much smaller. A difference of 1000km corresponds to approx. 1 minute in arrival time. This is small compared to the dimension of the stream, which

confirms that the longer lasting reflections take place at almost the same time.

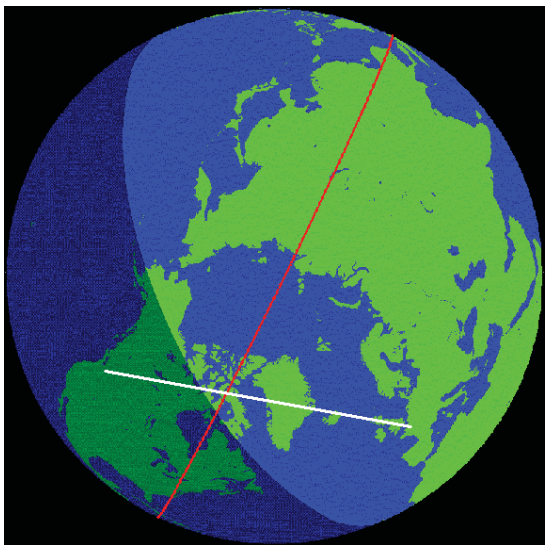

Figure 16 – Encounter geometry according to (Maslov, 2014)[3].

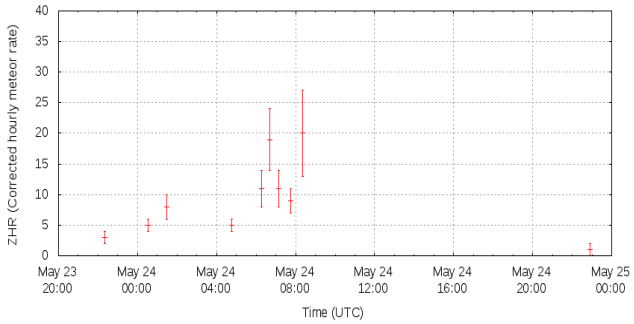

Figure 17 – Visual observations collected by IMO.

The visual observations collected by IMO[4] (Figure 17) situation on July 9, 2014 stop around 8^h UT, perhaps due to daylight or other adverse visual conditions. Maybe the maximum of brighter meteors wasn't seen by anybody.

8 Analysis opportunity

Readers interested in making their own analysis of the CAMs 2014 or of any other stream can find the basic data in the Visual RMOB Archives[5,6]. The number of monthly submissions and their quality is steadily increasing since the start in 2000.

9 Conclusion

The CAMs were detected beyond doubt in most radio forward scatter observations. Most successful were the observations of the GRAVES transmitter. Not only was it observed from many places, also its strong power favored the registration of smaller particles during the long interval of May 24, 1^h – 13^h UT. A maximum of larger particles occurred on May 24, 8^h – 9^h UT.

Acknowledgment

The author wishes to thank the `rmob.org` contributors, Pierre Terrier for his hosting and continuous improvements of `rmob.org`, and Jeff Brower for his detailed observations. We learned about the 209P/LINEAR promise at the IMC 2013 meeting. The (meteorobs) mailing list kept the world in real time informed about the progress of the 209P/LINEAR stream.

References

Steyaert C. (2013). "Global radio Draconids". In Gyssens M., and Roggemans P., editors, *Proceedings of the International Meteor Conference*, La Palma, Canary Islands, Spain, 20–23 September 2012. IMO, pages 88–92.

Steyaert C. (2014). "Global radio η Aquariids". In Gyssens M., Roggemans P., and Żołądek P., editors, *Proceedings of the International Meteor Conference*, Poznań, Poland, 22–25 August 2013. IMO, pages 73–77.

Ye Q., and Wiegert P. A. (2014). "Will Comet 209P/LINEAR Generate the Next Meteor Storm?". *Monthly Notices of the Royal Astronomical Society*, **437**, 3283–3287.

[3] http://feraj.narod.ru/Radiants/Predictions/209p-ids2014eng.html "209P-ids 2014: prediction of activity"
[4] http://www.imo.net/live/cameleopardalids2014/
[5] http://www.rmob.org/articles.php?lng=en&pg=28
[6] http://rmob.org/visual/2014/

Automatic detection of meteors in the BRAMS data

Stijn Calders and Hervé Lamy

Belgian Institute for Space Aeronomy, Brussels, Belgium
Stijn.Calders@aeronomie.be, Herve.Lamy@aeronomie.be

BRAMS is a Belgian network consisting of one beacon and 26 receiving stations to detect radio meteors by forward scattering. Because of the large amount of data generated by these stations, a good automatic detection algorithm is needed. In this paper, four algorithms currently under test are briefly described. Application of three of them to an example of BRAMS data is shown with a comparison to manual count in order to emphasize the advantages and disadvantages of each method.

1 Introduction

The BRAMS (Belgian RAdio Meteor Stations) network consists of one beacon located in Dourbes and 26 receiving stations spread over Belgium. Each station records continuously a bandwidth of 2.5 kHz more or less centered on 49.97 MHz, the beacon frequency. The data are stored in WAV (sound) files of 5 minutes each. In total about 7500 files (288 files per station) are generated per day. Checking all those files manually for meteors is too much time-consuming, so an automatic detection algorithm is mandatory. In this article, a quick overview of four different automatic detection methods of radio meteors in BRAMS data files is provided. Each method works either on the raw data obtained in the time domain or on a spectrogram.

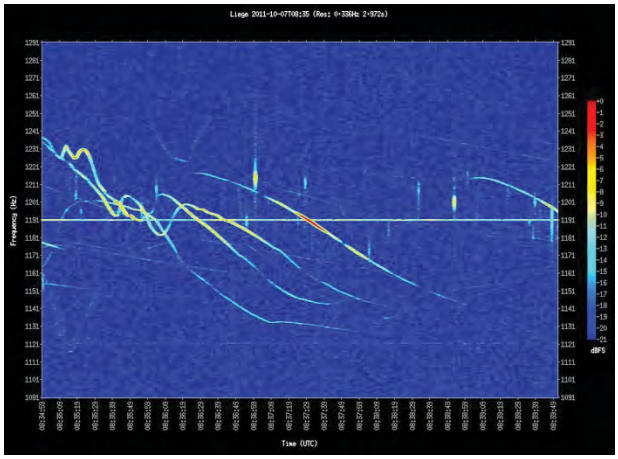

Figure 1 – A typical spectrogram from a BRAMS receiving station. Frequency range is 200 Hz centered on the beacon frequency. Duration is 5 minutes. Power is color coded. The horizontal line in the middle of the spectrogram is the direct reception of the BRAMS beacon, the inverse S-shaped lines are reflections on airplanes moving on a straight line and the short vertical lines are meteor echoes. The complex shapes on the left hand side of the spectrogram are also produced by airplanes which change directions. Manual count gives 17 underdense meteors.

A spectrogram is a visual representation of the spectrum of frequencies in a signal as it varies with time. It is obtained from the time signal using a FFT (Fast Fourier Transformation).

The result is a two-dimensional representation of the signal, where the horizontal axis represents time, the vertical axis is frequency and the color indicates the power of the signal. *Figure 1* shows a typical BRAMS spectrogram.

Three of the four methods are currently under evaluation by the BRAMS team by comparing their results to manual counts. An example is provided below for each method. So far the comparison is made only for short-lived underdense meteor echoes with a typical duration of a few tenths of seconds at most. These meteor echoes constitute the majority of meteor echoes detected in BRAMS data.

2 Image recognition on spectrograms (I)

The first method, developed by Pierre Ernotte, uses image recognition on spectrograms. The first step in the algorithm is the binarization of the spectrogram. Only pixels above a certain threshold are kept to filter out noise and their values are set to 1. It means that the information about the variations in the signal power is lost. Then the algorithm applies a vertical erosion (Gonzalez and Woods, 2007) using the fact that underdense meteor echoes appear mostly vertical in spectrograms while the beacon frequency and the plane echoes have a dominant horizontal component. The erosion operator superimposes a mask to each pixel with a value of 1 and keeps its value if all pixels underneath the mask are equal to 1, otherwise it is set to 0. In our case, the mask is a vertical line whose length is chosen to be larger than the typical frequency width of plane echoes or of the beacon frequency. This vertical erosion may divide some meteor echoes in different parts. Dilation (Gonzalez and Woods, 2007) along columns and adjacent lines is then performed to reconnect them.

Since this technique is performed on spectrograms, it is easy to compare the results with manual counts which are also made on spectrograms (Calders et al., 2014). Planes are removed decently well, and the method provides good results for short meteors which appear mostly vertical (see *Figure 2*). However, some faint meteor echoes can be missed, when their vertical/frequency signature is discontinuous and hence they may not survive the erosion. The method does not work for long lasting

meteors (not present in the example in *Figure 1*) which have a large horizontal component and/or a complex structure. Also the creation of the spectrogram as well as the erosion/dilation are very time consuming operations. Finally, the method contains several empirical parameters which may have to be adapted for different BRAMS stations.

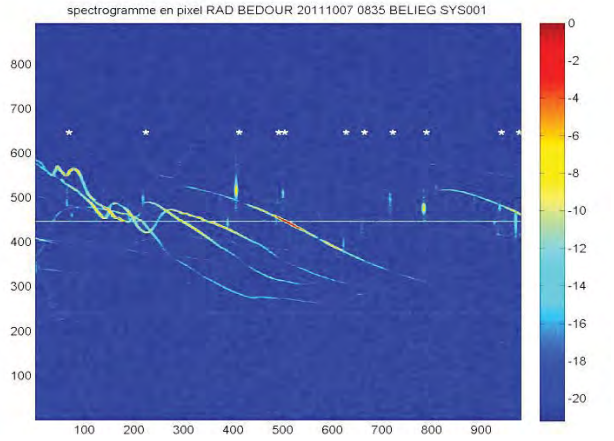

Figure 2 – Application of Ernotte's method to the example spectrogram of *Figure 1*. Units for the axes are here given in pixels. The method detects 11 meteors (white dots) but six faint meteors do not survive the erosion and are missed.

3 Image recognition on spectrograms (II)

Another method using spectrograms has been developed by Emil Kraaikamp. First, an horizontal median filter is applied to the spectrogram to remove the direct reception of the beacon signal (and possibly other local transmitters). Then a set of oblique median filters is used to remove the airplane echoes, because those signals can be approximated by a set of straight lines with different inclinations and lengths. Finally a detection threshold using the median and the MAD (median absolute deviation) is used to distinguish between meteors and noise.

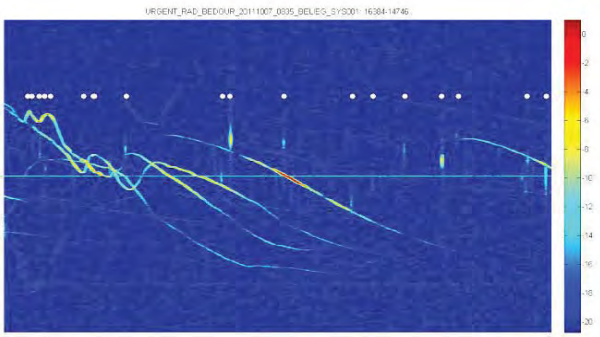

Figure 3 – Application of Kraaikamp's method to the same example in *Figure 1*. The method detects 18 meteors. Some parts of the complex airplane echoes (on the left side of the picture) are not fully removed and incorrectly detected as meteors (3 cases). 1 faint meteor is not detected.

Like for Ernotte's method, comparison with manual counts is easy. The method does not use binarization, which gives the possibility to use the signal power in the final detection step. It removes quite well the plane echoes as long as the shape is simple (i.e inverse S-shaped lines). But it can produce false meteor detections when complex airplane echoes are present in the spectrogram (see *Figure 3*). Another drawback is again that the method is CPU intensive.

4 Meteor detection using only the time signal

Tom Roelandts is developing a method based only on the signal in the time domain. First, an adequate filtering is applied to keep only frequencies within 200 Hz below or above the beacon frequency (where all meteor echoes appear). This strongly reduces the noise in the data. Then the method computes running averages on a short and a long timescale (typical of the duration of an underdense meteor resp. plane echo) and divides them to obtain an indicator signal. The basic idea is that an underdense meteor echo will contribute strongly to the short running average but not to the long one, hence creating a peak in the indicator signal. An appropriate threshold is used to detect these peaks. More information about this method can be found in Roelandts (2014). Here we only provide in *Figure 4* the results of the application of this method to the raw data used to compute the spectrogram in *Figure 1*. The method may miss faint meteor echoes appearing at the same time as the brightest part of an airplane echo. In this case the resulting peak of the indicator signal can be lower than the threshold and the meteor is missed.

Since this method does not compute spectrograms, its main advantage is that it is much faster than the previous ones. Also the duration of a meteor can be measured more accurately in the time domain than in a spectrogram. It also has only three parameters. The choice of the threshold is however currently empirical and varies from station to station.

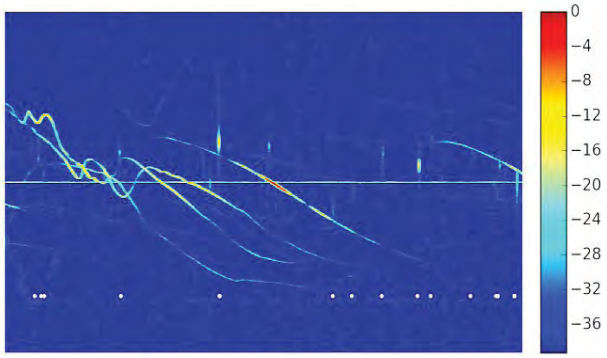

Figure 4 – Application of Roelandts 'method to the raw data used to compute the spectrogram in *Figure 1*. The method detects 14 meteors whose locations have been added to the spectrogram a posteriori for comparison with the previous methods. Three meteors are missed as they appear at the same time as the brightest (red) part of airplane echoes (see text).

5 Meteor detection using neural networks

This method is developed by Victor Roman and is based on two different types of artificial neural networks. Firstly, the Self-Organizing Map, SOM, (Kohonen, 1998) is a type of neural network that produces a low-dimension (typically two) representation (map) of the input signals (in our case, a vector containing the power or amplitude recorded in WAV files). A SOM consists of components called neurons whose spatial location in the map corresponds to a particular domain of the input signal patterns. SOM operates in two successive modes: training builds the map using input examples while the mapping automatically classifies a new input vector. The idea behind using this method is that meteor echoes will be mapped on specific meteor neurons, while plane echoes or noise will be mapped to different locations of the map. The SOM is trained using unsupervised learning (meaning, in our case, that the user does not tell the network that a meteor is given as input).

Another type of artificial neural network considered is the Multi-Layer Perceptron, MLP (Gardner and Dorling, 1998) which consists of multiple layers of interconnected neurons, representing a non-linear mapping from an input vector to an output vector. Each neuron in a given layer is connected to all neurons from the previous and subsequent layers with weights that are calculated using a non-linear transfer/activation function. For this study, a feed forward architecture was chosen, meaning that the data is only propagated from the input to the output layer. Training such a neural network requires a supervised algorithm, the one used here being the back propagation algorithm. In both methods input data can be taken either from the (filtered) raw data (e.g. a vector with power samples taken during 0.1 sec) or from spectrograms (e.g. a vector with pixel intensities taken as one of the spectrogram's vertical lines).

More information about these methods and preliminary results can be found in (Roman, 2014). The results are not discussed here as they cannot easily be compared to the other methods.

6 Conclusion and further work

We have briefly presented four different algorithms considered for the automatic detection of radio meteors in the BRAMS data. Two of the methods are based on image recognition on spectrograms, one uses neural networks and one detects the meteors using only the time signal.

These methods have been applied to one test case for comparison only and to illustrate the strengths and weaknesses of each method. No firm conclusion can be reached from this test case only. Statistical studies on a large set of data are necessary and currently carried out by the BRAMS team. All methods work relatively fine for short-lived (underdense) meteors except when many plane echoes with complicated shapes are superimposed on them (e.g. in the left part of *Figure 1*). The longer (overdense) meteor echoes (not present in *Figure 1*) pose another real challenge. Their automatic detection will be considered in a later phase of the project.

Results from the various automatic detection methods must be assessed by comparing with manual counts. At the moment, there is only a single day of manually detected meteors for one receiving station. We plan to extend our manual count dataset to more stations, several days, with and without high meteor stream activity, in order to better assess the different automatic detection algorithms.

Acknowledgments

BRAMS is a project of the Belgian Institute for Space Aeronomy which is funded by the Belgian Solar Terrestrial Centre of Excellence. This project is carried out in collaboration with many radio amateurs. We would like to thank them for their participation in this project. Last but not least: special thanks to Pierre Ernotte, Emil Kraaikamp, Victor Roman and Tom Roelandts for the development of the automatic detection algorithms and Antonio Martinez for proofreading this paper.

References

Calders S., Lamy H., Gamby E. and Ranvier S. (2014). "Recent developments in the BRAMS project". In Gyssens M. and Roggemans P., editors, *Proceedings of the International Meteor Conference*, Poznan, Poland, 22-25 August 2013. IMO, pages 170–172.

Gardner W. M. and Dorling S. R. (1998). "Artificial Neural Networks (the MultiLayer Perceptron) – a review of applications in the atmospheric sciences". *Atmospheric Environment*, **32**, 2627–2636.

Gonzalez R. C. and Woods R. E. (2007). Digital Image Processing (3rd edition). Prentice-Hall, ISBN 978-0131687288. 976 pages.

Kohonen T. (1998). "The Self-Organizing Map". *Neurocomputing*, **21**, 1–6. doi: 10.1016/S0925-2312(98)00030-7.

Roelandts T. (2014). "Meteor Detection for BRAMS Using Only the Time Signal". In Rault J.-L., and Roggemans P., editors, *Proceedings of the International Meteor Conference*, Giron, France, 18–21 September 2014. IMO, pages 197–200.

Roman V. S., Buiu C. (2014). "Automatic detection of meteors using artificial neural networks". In Rault J.-L., and Roggemans P., editors, *Proceedings of the International Meteor Conference*, Giron, France, 18–21 September 2014. IMO, pages 122–125.

Meteor detection for BRAMS using only the time signal

Tom Roelandts

Impulse Response, Beerse, Belgium
tom@impulseresponse.eu

Approaches for meteor detection in the BRAMS project often start from a spectrogram, since that is the default view of the received signal. In this paper, we argue that it is better to use the original time signal for detection. We define an indicator signal that consists of the ratio of received energy in a short time interval that is the length of a typical underdense meteor, and a longer time interval that represents the background signal. A simple threshold can then be used to detect underdense meteors, also in the presence of the carrier and reflections on planes.

1 Introduction

The default way to view the recorded data from the *BRAMS* (*Belgian RAdio Meteor Stations*) network (Calders and Lamy, 2012) is through a spectrogram that shows a 200 Hz range around the carrier frequency, using the *BRAMS Viewer* (Lamy et al., 2013). In this spectrogram, time is on the horizontal axis and frequency is on the vertical axis. *Figure 1* shows an example of such a spectrogram, in which several reflections are visible. The short signals with a relatively broad frequency range are *underdense* meteors, the "s-shaped" structures are *planes*, and the complicated structure near the end is an *overdense* meteor. The sampling rate is 5512 Hz, and the complete spectrogram spans a period of five minutes.

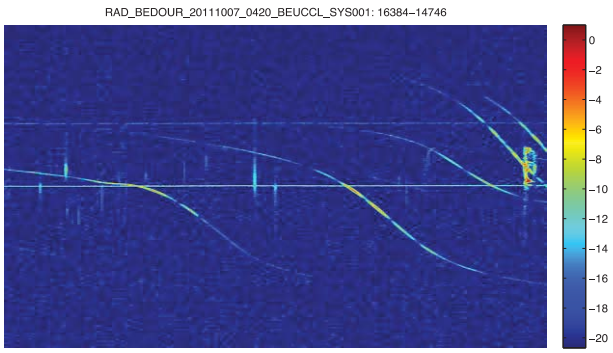

Figure 1 – Typical BRAMS spectrogram.

Since the data of the BRAMS network are viewed almost exclusively through these kinds of spectrograms, it might seem natural to attempt automatic detection of meteors on these spectrograms, using an *image processing* approach. However, in this paper we propose a technique in which the original time signal is used directly for detection of underdense meteors. Advantages of this approach are that it is potentially faster, and that the detection parameters may have a more straightforward physical meaning as compared to an image processing approach.

The proposed method computes an *indicator signal* that has the same number of samples as the original time signal. The value of each sample of the indicator signal is the ratio of the energy in a short interval that is the length of a typical underdense meteor, and a longer interval that represents the background signal. Underdense meteors can then be detected using a simple threshold.

The remainder of this paper is structured as follows. In Section 2, the method is introduced. Section 3 describes the experiments that were performed on data of the BRAMS network. In Section 4, the results are discussed and a conclusion is reached.

2 Method

In this section, we first describe the preliminary *band-pass filter* that we apply to the time signal. We then show a straightforward, but unsuccessful, approach for detection. Finally, the indicator signal itself is introduced.

Notation

We define a discrete-time signal as a sequence of numbers $x[n]$, with $n \in \mathbb{Z}$.

Preliminary filtering

The frequencies at which the meteor reflections appear are spread around the frequency at which the carrier is received. This frequency spread is due to the Doppler effect that is caused by the intrinsic movement of the plasma trail. Since there is a physical limit to the speed of the plasma trail, there is also a certain frequency range in which the meteor reflections can be expected to appear. However, the *noise* is typically broadband, so a large part of it can be removed with a band-pass filter around the frequency of the carrier. In the experiments that follow in Section 3, we have applied a *windowed sinc* filter to implement this.

Straightforward approach

A basic observation is that underdense meteors are very short in comparison with planes and overdense meteors (see *Figure 1* for examples). If no assumptions are made on the shape of the meteor reflections, i.e., if they are considered to be short transient signals in white Gaussian noise, then *Nuttall's Maximum Detector* (Nuttall, 1997), defined as

$$x[n]_{\mathrm{NMD}} \equiv \max_{m} \left\{ \sum_{i=m}^{m+M-1} (x[i])^2 \right\}, \quad (1)$$

where M is the expected length of the transient, would be a very efficient way to detect them. Despite being extremely simple, this was the best performing algorithm in the review by Wang and Willett (Wang and Willett, 2000). However, it assumes that a single transient signal appears in white Gaussian noise, which is not the case here due to the reflections on planes and the fact that there are multiple meteor reflections present.

To enable detection of multiple reflections, we replace Nuttall's Maximum Detector with the running average of the signal power $(x[i])^2$, defined as

$$p_s[n] \equiv \left(\sum_{i=n-\lfloor S/2 \rfloor}^{n+\lfloor S/2 \rfloor} (x[i])^2 \right) / S, \quad (2)$$

where S (odd) is the length of the running average. This length should be chosen to be close to the typical length of an underdense meteor. In the absence of planes, a threshold could then be used to detect the meteors.

To counteract the effect of the planes, we might create a second (and much longer) running average $p_L[n]$ (defined as in (2) with L substituted for S), which could then be used to create a detection threshold that tracks the average signal power. However, practical tests have shown that the short-term fluctuations during a plane reflection are too important to allow this, and result in many false detections. This is briefly illustrated in Section 3.

The indicator signal

To define the indicator signal, we first observe that a running average of the signal power provides the mean power at every sample point. Multiplying the mean power with the length of each averaging interval provides the energy that was received over each of the intervals, i.e., $E_S[n] = Sp_S[n]$ and $E_L[n] = Lp_L[n]$.

We recall that $p_S[n]$ (and, hence, $E_S[n]$, since that is simply a multiple of $p_S[n]$) would be expected to be a very good detector if the meteors were embedded in white noise, due to its similarity to Nuttall's Maximum Detector, as detailed in the previous section. However, they are not expected to work for the BRAMS data, due to the disturbances that are caused by the planes.

The indicator signal compensates for the plane reflections by comparing the received energy in a short time interval with the energy in a much larger surrounding interval. It is defined as

$$I[n] \equiv \frac{E_S[n]}{E_L[n]}. \quad (3)$$

Since each sample of $I[n]$ has $E_L[n]$ in the denominator, a very small value $E_L[n]$ might cause relatively high values for $I[n]$, even though $E_S[n] \leq E_L[n]$ always. Hence, to avoid false detections, we limit the value of $E_L[n]$ to some small value in the experiments of Section 3.

Meteor detection

The detection of the meteors is then trivial. A fixed threshold is chosen, and a meteor starts when the indicator signal rises above the threshold and stops when it drops under the threshold again.

3 Experiments and results

The experiments were based on data from the BRAMS project. For all datasets, a band-pass filter of width 60 Hz centered on the carrier was applied, and the values $S = 101$ and $L = 30001$ were used. Note that these values depend on the sampling rate and cannot be used directly for other systems.

The first experiment, for which we provide detailed results, was recorded with the Uccle receiving station. This is the data set of which the example spectrogram in Section 1 was made (*Figure 1*).

We now illustrate that the preliminary filtering that was introduced in Section 2 clearly improves the detectability of the meteor reflections. The reflections are not visible as clear peaks in the original time signal (*Figure 2*) or in the signal power (*Figure 3*). After band-pass filtering (*Figure 4*), the detectability of the meteors has clearly improved. The corresponding spectrogram of the filtered signal is shown in *Figure 5*. However, the signal strength that is generated by the reflections on some of the planes is of the same magnitude as those of the smaller meteors, making it impossible to discriminate between them using a simple threshold.

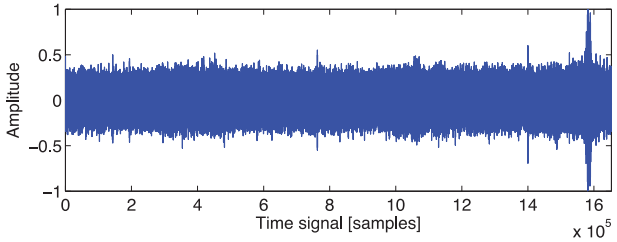

Figure 2 – Amplitude of original signal.

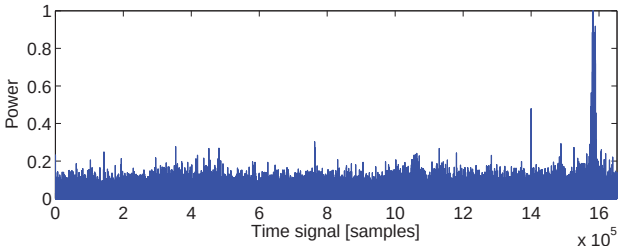

Figure 3 – Power of original signal.

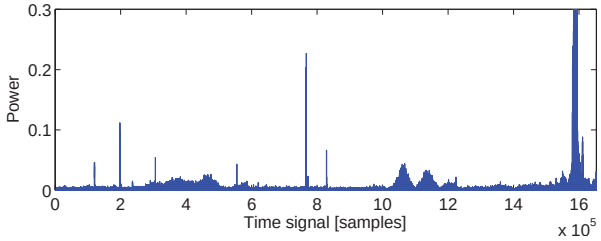

Figure 4 – Power of band-pass-filtered signal.

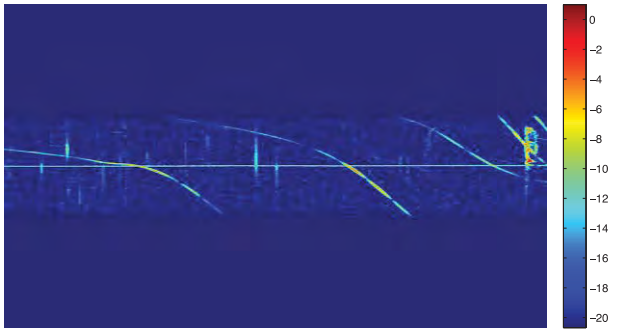

Figure 5 – Band-pass-filtered spectrogram.

The straightforward approach with running averages of Section 2 is illustrated in *Figure 6*. The blue curve is a running average of length S. The red curve is a running average of length L that has been offset by a certain amount, i.e., a constant has been added, to form a threshold. Even when, in this example, the threshold is too high to detect the smaller meteor reflections, it already touches the plane reflections, which would result in false detections. This shows that the approach with simple running averages cannot be expected to work in practice.

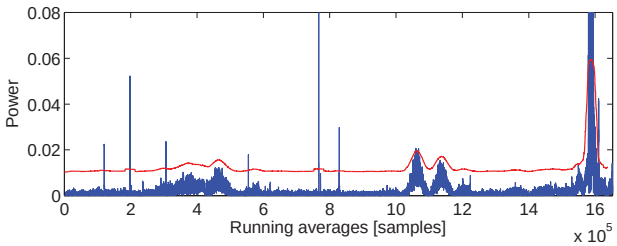

Figure 6 – Running averages of (blue) 101 samples and (red) 30001 samples.

The indicator signal for this data set is shown in *Figure 7*. The "bulges" that were caused by the plane reflections in *Figure 4* have disappeared. This allows using a simple constant threshold, as indicated by the red line in *Figure 7*. The spectrogram of *Figure 1* is shown again in *Figure 8*, with added red dots that indicate where meteors were detected.

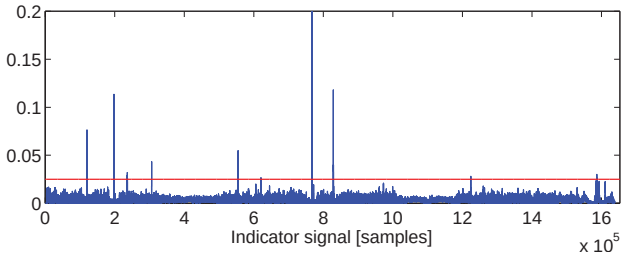

Figure 7 – Indicator signal (blue) and detection threshold (red).

We now show, for three other datasets, the indicator signal and the corresponding spectrogram with added red dots that indicate where meteors were detected. We reiterate that these experiments were run using the exact same set of parameters. This does not imply that these parameters should never be adapted to the data at hand, but it does imply that the parameters do not have to be tuned for each specific data set.

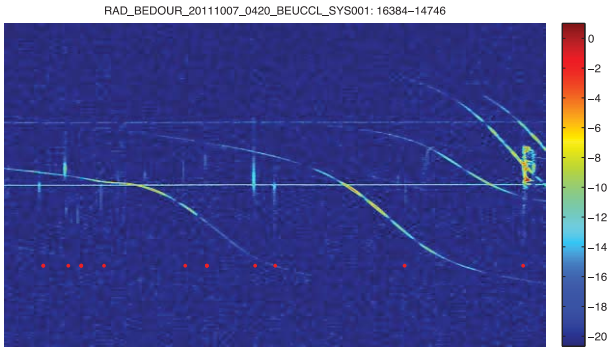

Figure 8 – Spectrogram with detected meteors.

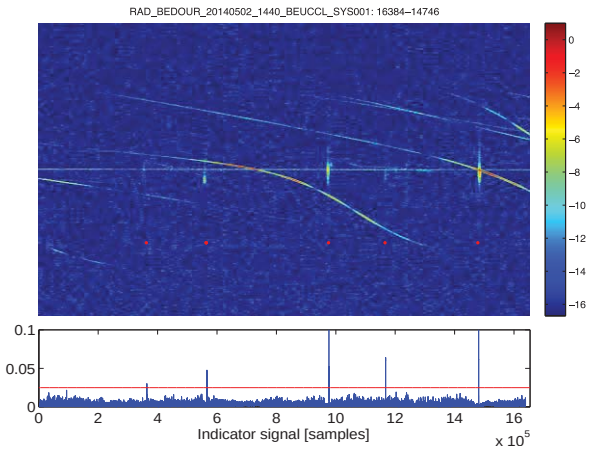

Figure 9 – Detected meteors and indicator signal.

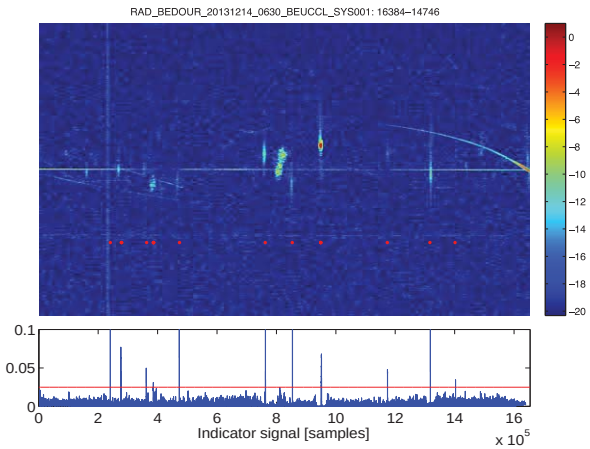

Figure 10 – Detected meteors and indicator signal for a spectrogram containing a wideband pulse.

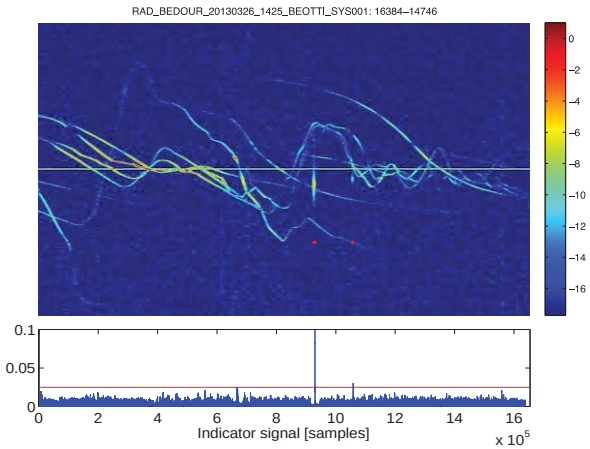

Figure 11 – Detected meteors and indicator signal for a spectrogram with many planes.

Figure 9 is a clean example with some planes and some underdense meteors that are all detected correctly. The

spectrogram of *Figure 10* contains a wideband pulse. Since the pulse is short, it is detected as a meteor. This means that it is necessary to check for these kinds of pulses separately and reject them. One way to do this is check (for each potential meteor) whether it can also be detected outside of the normal frequency range. This would indicate that it is too wideband to be a meteor. In *Figure 11*, many planes are present, and they seem to be performing more complicated maneuvers than usual. However, this does not hamper the detection of the meteors.

4 Discussion and conclusion

Much of the research that is done towards detection of meteors in systems such as the BRAMS network is concentrated on image processing techniques that operate on the spectrogram. With this paper, we have tried to present an alternative method that uses the time signal directly. And, even though the presented indicator signal should be considered a preliminary result, it does show that this is possible.

For future work, we intend to study a *matched filter* approach, where the expected shape of the meteor reflection, i.e., a sudden rise followed by an exponential decay, is matched directly through correlation. The current solution amounts to correlation with a rectangular pulse, which is not the at all like the true shape of the reflection. Another possibility is that the indicator signal can possibly also provide a confidence level for each meteor detection, since it indicates exactly which fraction of the energy is concentrated in the central peak. It might also be beneficial to repeat the detection process several times with different lengths for the long and short intervals, to detect shorter and longer meteors separately.

In conclusion, we have introduced an indicator signal based on the time signal, which can be used to detect underdense meteors using a simple threshold, for systems such as the BRAMS network.

A Python implementation of the indicator signal is available on the website of the author[1].

References

Calders S. and Lamy H. (2012). “Brams : status of the network and preliminary results”. In Gyssens M. and Roggemans P., editors, *Proceedings of the International Meteor Conference*, Sibiu, Romania, 15–18 September 2011. IMO, pages 73–76.

Lamy H., Gamby E., Ranvier S., Geunes Y., Calders S., and De Keyser J. (2013). “The BRAMS Viewer: an on-line tool to access the BRAMS data”. In Gyssens M. and Roggemans P., editors, *Proceedings of the International Meteor Conference*, La Palma, Canary Islands, Spain, 20–23 September 2012. IMO, pages 48–50.

Nuttall A. H. (1997). Detection capability of linear-and-power processor for random burst signals of unknown location. Naval Undersea Warfare Center Division.

Wang Z. and Willett P. (2000). “A performance study of some transient detectors”. *IEEE Trans. Image Process.*, **48**, 2682–2685.

[1] http://tomroelandts.com/articles/meteor-detection-for-brams-using-only-the-time-signal.

Modeling and calibration of BRAMS antenna systems

Antonio Martínez Picar[1], **Sylvain Ranvier**[2]
Michel Anciaux[2] **and Hervé Lamy**[2]

[1] **Solar–Terrestrial Centre of Excellence – Royal Observatory of Belgium, Brussels, Belgium**
antonio.martinez@observatory.be

[2] **Belgian Institute for Space Aeronomy, Brussels, Belgium**
herve.lamy@aeronomy.be

Because of the geometry associated with the forward-scatter method for observing meteors via radio, knowing the radiation pattern of the involved antennas is essential to obtain parameters of scientific interest such as the meteoroid flux density. In this paper results of simulations of the antennas belonging to the Belgian RAdio Meteor Stations network (BRAMS) that are directly managed by the Belgian Institute for Space Aeronomy (BISA) are presented, as well as plans for verifying their patterns using an Unmanned Aerial Vehicle (UAV).

1 Introduction

BRAMS is a project coordinated by BISA under the frame of the Solar–Terrestrial Centre of Excellence (STCE) that, based on *forward-scattering* techniques, aims to study the meteoroid population. Currently BRAMS comprises a network of 26 radio receiver stations mostly hosted by Belgian radio amateurs or groups of amateur astronomers, and a dedicated beacon located at Dourbes Geophysical Centre (Southern Belgium) acting as a transmitter radiating on 49.97 MHz (Calders and Lamy, 2012).

One of the main goals of BRAMS is calculating meteoroid flux densities for meteor showers and mass indexes for meteor showers and sporadic meteors. The meteoroid flux density $Q(m_0)$ is a parameter which measures meteoroid abundance in the vicinity of the Earth's orbit and it can be calculated from the statistics of a set of observed meteors, without requiring detailed information on the occurrence of an individual meteor. It is important to obtain precise meteoroid flux density values in order to compare results of different radio systems.

However, due to the geometry involved in the *forward-scatter* method, this calculation requires knowledge of specific technical characteristics of each transmitter-receiver pair or *set-up* (Suleymanova et al., 2007). Among other figures, the antenna gain value for both transmitter and receiver systems in the direction of the reflection point are required. Because the reflection point's spatial location is virtually random in the sky, full antenna directional patterns need to be known.

Antenna systems can be modeled to obtain their theoretical directional patterns. In Section 2, the approach and results of modeling the directional antenna patterns for the BRAMS beacon and the stations directly managed by BISA are presented.

Nevertheless, a real antenna directional pattern is actually influenced by many factors, from its own building features (geometry, connections, materials, etc.) to the environmental characteristics of the location (conductivity of the ground, nearby buildings, humidity, etc.) In Section 3, a strategy for verifying the obtained antenna patterns based on the usage of an UAV is introduced, as well as a report on the status of this development.

2 Modeling of BRAMS antenna systems

Numerical Simulation Approach

Many applications in science and technology rely increasingly on electromagnetic (EM) field computations, meaning solving Maxwell's equations. Nevertheless, in complex systems, complicated differential equations cannot be solved by analytical methods. Antenna engineering is among the major electrical engineering areas of complex EM problems where numerical simulation approaches are increasingly being used.

An antenna is a device that provides a transition from a *guided wave* on a transmission line to a *free-space wave* (or vice versa). Most antennas are reciprocal devices and behave the same while transmitting and receiving.

One of the most powerful techniques, which has been in use for more than three decades in frequency domain, is the Method of Moments (MoM). A MoM code synthesizes the far field of an antenna by integrating the Green's functions of individual metallic surface patches. The technique is based on solving complex integral equations by reducing them to a system of linear equations and by applying the *method of weighted residuals* (Weiland et al., 2008).

The Numerical Electromagnetic Code (NEC) is a software package which uses a MoM technique for analyzing the electromagnetic response of an arbitrary structure consisting of wires and surfaces in free space or over a ground plane. The code was initially written in FORTRAN and developed in the 1970s by the Lawrence Livermore National Laboratory, under the sponsorship of the Naval Ocean Systems Center and of the Air Force

Table 1 – Features of the modeled BRAMS antenna systems
(ε and σ are the relative permittivity and conductivity of the ground, respectively).

Location	ε	σ [mS/m]	Antenna systems	Azimuth [º]	Elevation [º]	Height (driven el.) [m]
Uccle	3	0.6	Yagi 3-el X-Yagi 3-el	165	35	3.75
Humain	15	9.0	Yagi 3-el ×4 X-Yagi 3-el	N/A	90	2.62
Dourbes	15	2.0	Turnstile	N/A	2.0	1.41

Table 2 – Parameters used in modeling the BRAMS antenna systems.

Type	No. Wires	No. Segments	Loads
Yagi 3-elements	8	584	Al
X-Yagi 3-elements	16	1168	Al
Turnstile & Reflector Plane	44	1028	Al & SS

Weapons Laboratory (Burke and Poggio, 1981). For the simulation of BRAMS antenna systems, the latest version of the code within the public domain without license (officially called NEC-2) has been selected in its C compiled version from Neoklis Kyriazis[1] named NEC2C.

BRAMS Antennas and NEC Models

The radiating system of the Dourbes beacon consists of a turnstile antenna arranged in normal mode, with an 8 m × 8 m grid acting as reflector plane disposed between the antenna elements and the ground. The size of each aluminum element of the turnstile is 2.82 m, with 14 mm in diameter. The grid is made of stainless steel (SS).

The antenna used in every standard receiving station is a 3-element Yagi with a director of 2.67 m, a driven element of 2.81 m, and a reflector of 2.97 m in size. Additionally, the receiving stations directly managed by BISA have a 3-element crossed Yagi (X-Yagi) antenna, built with two standard Yagis in which main axes overlap but elements are arranged perpendicularly. The diameter of each aluminum element is 15 mm.

Figure 1 – Locations of the modeled BRAMS antenna system.

Additional relevant features of these antenna systems and the environment of their location are shown in *Table 1*.

To improve the quality of the results of the simulations, the gamma matches were included in the models and adjusted to obtain an input impedance of Z_{in} = 50 Ω.

The map of *Figure 1* shows the locations of the analyzed antenna systems in Belgium, and Figure 2 shows some pictures of them.

NEC-2 assumes any metallic object to be a superposition of small segments on which the current distributions are of interest, therefore the software works with individual straight *wires*, although complex geometric shapes can be formed joining those wires at their ends. Then each wire in an element should be segmented. Since MoM is based on the calculation of currents on small segments and since it is formulated as a matrix system, the memory and computation time requirements drastically increase as the number of segments increases. The number of segments depends on the size of the structure and the frequency. *Table 2* shows the definite segmentation values applied as well as the material (characteristic impedance) of the antenna structures.

The convergence of the simulations' results and the Average Gain Test (Miron, 2006) over free space were applied to verify the reliability of the numerical simulations.

Simulation Results

The original results of a NEC-2 simulation is a structured text file with details of the model, including partial EM field calculation results and the antenna gain values in different directions for the far field centered on the antenna location. From this information, visualizations can be built to graphically show the shape of the antenna pattern in a convenient and more intuitive way.

[1] "Readme file for nec2c", http://www.qsl.net/5b4az/pkg/nec2/nec2c/README, Ham Radio Station 5B4AZ webpage.

Figure 2 – Images of BRAMS antenna systems directly managed by BISA (*Top left:* Yagi at Humain Radio Astronomy Station. *Top right:* Crossed Yagi at BISA facilities, Uccle. *Bottom:* Turnstile at Dourbes Geophysical Center).

MayaVi is a general-purpose 3D scientific visualization package (Ramachandran and Varoquaux, 2008) which uses the Visualization Toolkit (Schroeder, Martin and Lorensen, 2002) and it is entirely written in Python. *Figures 3 – 5* show still images of the visualizations obtained after processing the simulation results with MayaVi.

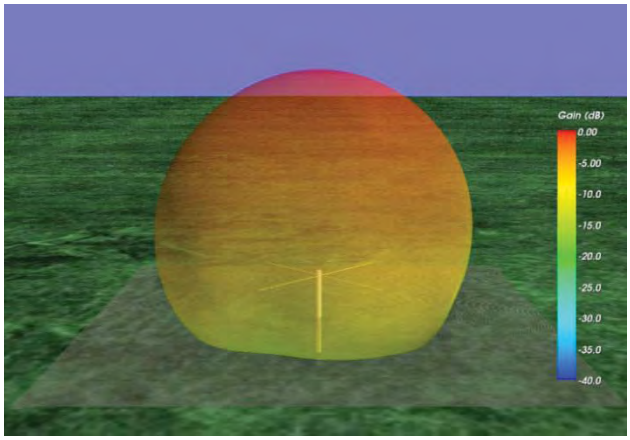

Figure 3 – Antenna pattern of the BRAMS beacon antenna obtained from numerical simulation (turnstile antenna and reflective plane).

3 Approach for verification of the antenna patterns

Measurement system

The next step in increasing the knowledge of the BRAMS antenna patterns is characterizing them in their real environment. In this regard, a low-cost antenna pattern verification method based on an Unmanned Aerial Vehicle (UAV) device was devised.

The chosen aircraft – an OktoXL ARF-Mikrokopter (HiSystems, 2013) – is shown in *Figure 6*. Its electronic boards (FlightCtrl V2.1, NaviCtrl V2.0, and MKGPS V2.1) and a software interface allow for loading arbitrary GPS-controlled autonomous flight with a stable orientation of the aircraft during the overall flight. A fully charged LiPo (Lithium Polymer) battery offers a maximum autonomy of 15 minutes. For the takeoff and landing operations, a remote pilot is needed instead. The position and orientation angles (bearing, pitch, and roll) of the aircraft during the flight are available for post-processing.

A continuous-wave RF generator, designed and built at BISA[2], has been adapted below the battery holder on the bottom of the UAV aluminum frame set. The RF generator, which is tuned at the BRAMS beacon frequency with a maximum output power of -6 dBm, is powered by an independent battery bank through a USB standard connector. A shortened monopole antenna (Z_{in} = 50 Ω) is connected to the RF generator, disposed vertically downward the UAV. A metallic mesh has been inserted between the UAV battery holder and the RF signal generator in order to reduce the EM influence of the UAV frame set over the radiation pattern of the RF

[2] "Calibrator for BRAMS", http://brams.aeronomie.be/files/BRAMS_annualmeeting_2014_MichelAnciaux_calibrator.pdf, BRAMS webpage.

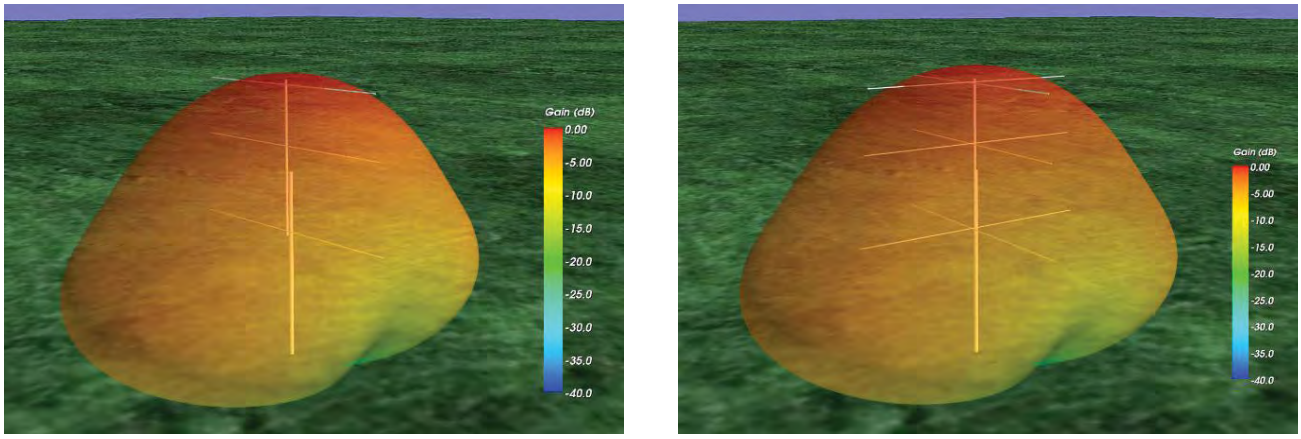

Figure 4 – Antenna patterns of the BRAMS Humain station obtainedfrom numerical simulation (*left:*Yagi antenna, *right:* X-Yagi antenna).

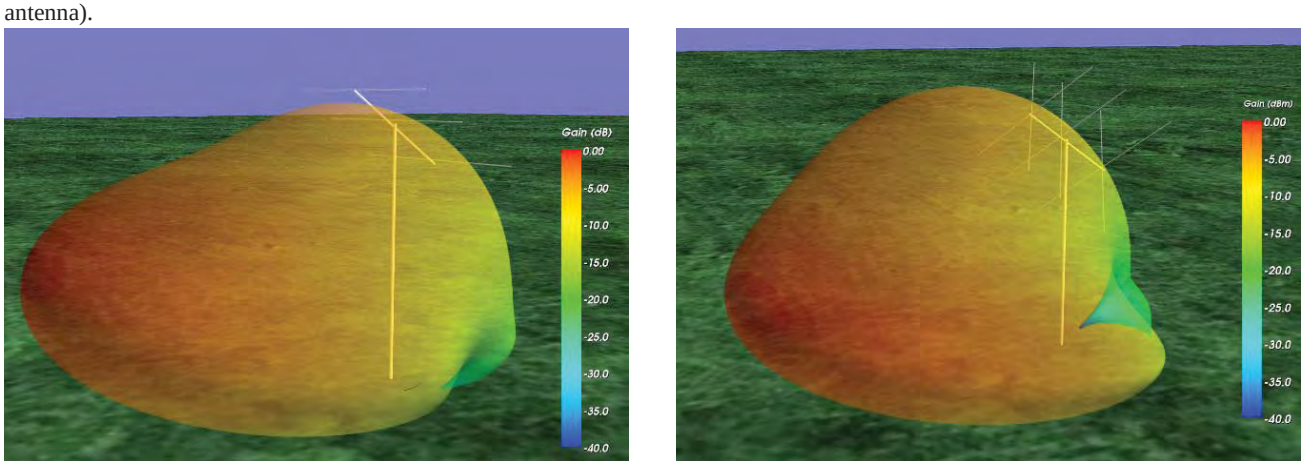

Figure 5 – Antenna patterns of the BRAMS Uccle station obtained from numerical simulation (*left:*Yagi antenna, *right:* X-Yagi antenna).

generator antenna. Land gear extensions were necessary to guarantee room enough for the antenna when the aircraft is grounded (see *Figure 6*).

The signal from the RF generator must be recorded with accurate timestamps to allow matching the position of the UAV and the total received power. Although during the first testing flights the receivers employed were a spectrum analyzer and a software defined radio (SDR) based receiver, the current BRAMS receiving hardware and software configuration (Calders and Lamy, 2012) is suitable to accomplish this task.

Measurement strategy

In order to guarantee that the measured values of the received signal power are suitable for determining the antenna pattern, it is necessary to locate the RF generator in the far–field range of the corresponding antenna under test (AUT). The basic idea is to fly around each AUT outside the minimum far–field distance boundary (Balanis, 2005), following successive circular paths at different altitudes until completing a semi-spherical shape centered on the AUT.

The far field distance for the Yagi and X-Yagi antennas is 2.94 m, and for the beacon's turnstile is 42.67 m, way less than the maximum remote control distance for the aircraft. Test flights have been performed to verify the accuracy of the GPS-controlled positioning of the UAV. The preliminary results show a typical drift of 3–5 m off the desired stable way-point of the flight path. These results show that the variation depends mainly on weather conditions, specifically on the wind strength.

It is worth mentioning that, taking into account that some UAVs are capable of performing flights over 1000 m in altitude, the Belgian government (as well as many other countries) is currently discussing a legal framework to regulate the Remote Pilot Aircraft Systems (RPAS) activities. Because the final instrument is not ready yet, the STCE obtained a special permission from national air navigation authority (BELGOCONTROL) for flying the UAV up to 150 m above ground, only for research purposes.

4 Future work

Simulated antenna patterns of the BRAMS stations directly managed by BISA are already available for processing of observations of radio meteors. In the next months, the received power pattern of the antennas in their real environment will be derived from a series of measurements to be performed by the system previously described.

The reliability of the results will rely on a statistical analysis over a relatively large set of measurements. This implies carrying out intense measurements campaigns to

Figure 6 – Measurement system (*Top*: UAV OktoXL in flight equipped with RF signal generator, battery bank, transmitting antenna and isolating metallic mesh; *bottom-left*: screenshot of the control software with the flight plan and the tracking of the actual flight; *bottom-right*: RF signal generator).

collect enough information which allows reconstructing the antenna patterns and comparing them to the simulated ones. Measurements taken under high and low environmental humidity conditions will be classified and analyzed separately. On the other hand, the ongoing acquisition of extra resources (batteries and a multiple battery charger) to extend the effective flight time per day aims to increase the performance of the measurement campaign day.

Currently the characterization effort is focused only on stations directly managed by BISA. However, to be able to characterize the whole BRAMS network, a similar procedure must be performed at the rest of the stations. Numerical simulations for every station antenna can be carried out as long as the critical information is available for modeling, but the power measurement through the UAV is constrained by the permission from BELGOCONTROL which currently allows flying only at the locations of the stations included in this work.

Acknowledgments

The authors would like to thank Urška Pajer and Cis Verbeeck for having proofread the manuscript. This work is funded by the Solar–Terrestrial Centre of Excellence of the Federal Science Policy (BELSPO) of Belgium.

References

Balanis C. A. (2005). Antenna Theory – Analysis and Design. John Wiley & Sons, New Jersey.

Burke G. J., and Poggio A. J. (1981). Numerical Electromagnetics Code (NEC) – Method of Moments, Part I: Program Description – Theory, Lawrence Livermore National Laboratory.

Calders S. and Lamy H. (2012). "BRAMS: status of the network and preliminary results". In Gyssens M. and Roggemans P., editors, *Proceedings of the International Meteor Conference*, Sibiu, 15–18 September 2011. IMO, pages 73–76.

HiSystems GmbH (2013). ARF-Mikrokopter – OktoXL – Instruction Manual. HiSystems GmbH, Moormerland.

Miron D. (2006). Small Antenna Design. Newnes.

Ramachandran P. and Varoquaux G. (2008). "Mayavi: Making 3D data visualization reusable". In Varoquaux G., Vaught T. and Millman J., editors, *Proceedings of the 7th Python in Science Conference*, pages 51–57.

Schroeder W., Martin K., and Lorensen B. (2002). The Visualization Toolkit – An object-oriented approach to 3D graphics. Third edition. Kitware Inc.

Suleymanova S., Verbeeck C. and Wislez J.-M. (2007). "Calculating the meteoroid flux density of a meteor shower from radio forward scatter observations". In Bettonvil F. and Kac J., editors, *Proceedings of the International Meteor Conference*, Roden, the Netherlands, 14–17 September 2006. IMO, pages 162–174.

Weiland T., Timm M., and Munteanu I. (2008). "A practical guide to 3-D simulation". *IEEE microwave magazine*, **9(6)**, 63–75.

The author, Antonio Martinez Picar, during his lecture. (Credit Dominique Richard.)

Report on radio observation of meteors (Iža, Slovakia)

Peter Dolinský, Ivan Dorotovič and Marian Vidovenec

Slovak Central Observatory, Hurbanovo, Slovakia
peter.dolinsky@suh.sk, ivan.dorotovic@suh.sk, marian.vidovenec@suh.sk

During the period from 1 to 17 August 2014 meteors were experimentally registered using radio waves. This experiment was conducted in the village of Iža, Slovakia. Its main objective was to test the technical equipment intended for continuous registration of meteor echoes, which will be located in the Slovak Central Observatory in Hurbanovo. These tests are an indirect continuation of previous experiments of observation of meteor showers using the technology available in Hurbanovo at the end of the 20th and the beginning of the 21st century. The device consists of two independent receiver systems. One recorded echoes of the transmitter Graves 143.050 MHz (N47.3480° E5.5151°, France) and the second one recorded echoes of the TV transmitter Lviv 49.739583 MHz (N49.8480° E24.0369°, Ukraine). The apparatus for tracking radio echoes of the transmitter Graves consists of a 9-element Yagi antenna with vertical polarization (oriented with an elevation of 0° at azimuth 270°), the receiver Yaesu VR-5000 in CW mode, and a computer with registration using the program HROFFT v1.0.0f. The second apparatus recording the echoes of the transmitter Lviv consists of a LP (log-periodic) antenna with horizontal polarization (elevation of 0° and azimuth of 90°), the receiver ICOM R-75 in the CW mode, and also a computer with registration using HROFFT v1.0.0f. A total of about 78000 echoes have been registered during around 700 hours of registration. Probably not all of them are caused by meteors. These data were statistically processed and compared with visual observations in the IMO database. Planned own visual observations could not be performed due to unfavourable weather conditions lasting from 4 to 13 August 2014. The registered data suggest that observations were performed in the back-scatter mode in this configuration and not in the planned forward-scatter mode. Deeper analysis and longer data sets are, however, necessary to calibrate the observation system and this will be subject of our future work. A realization of a custom radio system similar to the BRAMS system is also being considered.

1 Introduction

Reflections of radio waves from meteor trails were experimentally recorded and registered during the Perseid meteor shower activity in the period from 1 to 17 August 2014 in Iža, near (~15 km) Hurbanovo Observatory. A number of meteor showers occurred during this period, but they cannot be distinguished when using this equipment. All meteors except of the sporadic meteor background are therefore attributed to the Perseids. The distinction of the sporadic background is also difficult due to the short record length and the long activity period of the Perseids. The main objective of the experiment was, besides obtaining data on the Perseids, testing of instruments and software to build a continuous registration of meteors in our observatory. Originally, these observations should be supplemented by the visual and photographic observations, but these observations could not be done because of the bad weather.

2 Description of the Equipment

We used two very similar equipment which registered meteor reflections in two directions, one oriented towards the east and the other towards the west.

Description of the eastward station (referred hereafter as the 50 MHz station)

A horizontally polarized log-periodic antenna with an operating range from 40 MHz to 1300 MHz with a gain of about 6 dB_d and a width of the main lobe (at - 3 dB) of 60° in the horizontal and vertical plane was used. The antenna was oriented towards azimuth = 90° (east) with an elevation of 0°. Given the relatively small height of the antenna, the conductive ground effect cannot be neglected and the beam peak of the antenna has an elevation of about 15°. The analog television transmitter Lviv at 49.739583 MHz (N49.8480° E24.0369°, Ukraine) was used as a source of electromagnetic waves. Of course, it is impossible to exclude the interference of other television broadcasters at this frequency. Since it is a television transmitter, one can assume omnidirectional transmission characteristics of the transmitter in the horizontal plane. The communication receiver ICOM-R75 was used to detect radio waves. It was tuned to a frequency of 49.73970 MHz with CW modulation. The difference in frequencies between the transmitter and the receiver ensured a low-frequency output in the range between 880 Hz and 940 Hz. A notebook with Windows XP as operating system and the program HROFFT v1.0.0f was used to record echoes.

Description of the westward station (referred hereafter as the 144 MHz station)

A vertically polarized 9-element Yagi antenna with a gain of about 10dB_d and with an operating range of 143 - 148 MHz was used. The width of the main lobe of the antenna (at - 3 dB) is approximately 40° in both the vertical and the horizontal plane. The azimuth of the antenna was 270° (west) with an elevation of 0°. Due to the proximity of a conductive ground a shift of reception maximum to the elevation from 12° to 15° can be assumed. The transmitter of the GRAVES radar at 143.050 MHz (N47.3480° E5.5151°, France) was used as a source of electromagnetic waves. The communication receiver

Yaesu VR-5000 was used to detect radio waves. It was tuned to a frequency of 143.05062 MHz with CW modulation. The difference in frequencies between the transmitter and the receiver ensured a low-frequency output in the range between 880 Hz and 940 Hz. A notebook with Windows XP as operational system and the program HROFFT in 1.0.0f was used to register echoes.

A separate notebook was used for each equipment to prevent disruptions of registration at the same time on both stations and to avoid interference of the low-frequency signal and a mutual interference of the registration software. Both antennas were placed under the roof of the house covered by tiles. Walls of the roof are made of lightweight bricks, so that the thickness of material in front of the antenna is only about one third of the wall thickness. Reasons for this solution were difficulties with the installation of antennas above the roof. Considering their size and the fact that it was only a short registration and testing of the equipment, we accepted this solution as sufficient. This placement of antennas caused, however, a decrease in the sensitivity of the whole equipment, the possibility of signal reflections, and worsening of reception characteristics of both antennas.

3 Data Processing

The areas of the atmosphere in which meteors trajectories can be observed were identified by the conversion of the reception characteristics of the antennas. *Figure 1* shows the boundaries of the observed areas by the antennas for the lower and the upper height in which it is assumed that a sufficient ionization of the meteor trails would cause a reflection of electromagnetic waves. We used 80 km and 120 km as height, respectively, to calculate the boundaries. This model does not consider the impact of conductive ground to the reception characteristics of the antennas. Small circles mark areas of the highest antenna sensitivity by assuming the conductivity of the ground. Positions of the transmitters and receivers are indicated in this figure too.

A total of about 78000 records was obtained during the experiment. However, probably not all the echoes came from meteors. It can be seen from the hourly values plotted in *Figure 3* that a relatively high number of echoes is recorded while there are only small changes in the frequency of the records during a day and during the period of observation. Here, it would be necessary to analyze the shapes and the lengths of the echoes and their frequencies to separate the interferences and sporadic meteor background from the shower meteors. This would enable us to perform corrections on the non-meteoric component and sporadic meteors. Observations in periods without significant meteor showers are also needed to determine the background in a more reliable way. This was impossible due to the short time frame. A period with saturation of the receiver occurred fairly regularly in the 50 MHz record which can be attributed to the effect of the ionosphere, namely to the sporadic Es layer. A graph of hourly moving averages is shown in *Figure 2*.

During the registration process several gaps occurred, caused by either an equipment failure or its deliberate switching off during a thunderstorm. The most serious equipment failure occurred on 12 August 2014 at the 144 MHz station for 5 hours due to an operating system failure of the computer. This outage occurred at the time of the daily maximum in meteor rates.

We used the program HROFFT to RMOB v3.0 for further processing, to analyze the distribution of the numbers of meteors according to the level of low-frequency signal. From these hourly data, we selected a part from 4 to 10 August 2014 at levels of 10 and 20 dB, i.e. the range of data without any interruption and without major changes in the daily amplitude in both records. Using the method of cross-correlation, we found the highest correlation between the evolution of the detection at the 50 MHz and the 144 MHz with a mutual shift of about 2 hours. The dependence of the correlation coefficient for the mutual shift of the records is shown in *Figure 3*. The correlation coefficient at 20 dB is not significant and it reaches very low levels. The correlation coefficient reaches a maximum value of 0.73788 at the level of 10 dB. By analyzing the plot of the correlation and by comparing it with the field of view of both antennas, we can conclude that the time difference of 2 hours in local time reaches the outermost observing periods. It can be calculated that the maxima occur at the time when the radiant is near the upper culmination in the given area. It is therefore possible to conclude that our experiment used mainly the backscatter method and not the forward scatter method which we originally anticipated.

Activity of the Perseids

The activity of the Perseid meteor shower is evident on the plots of hourly counts of meteors (*Figure 2*), but it is not seen clearly as in the plot of visual observations (*Figure 4*)[1]. This is caused by various factors that have been mentioned above. More consistency between visual and radio observations can be seen in the plots with one hour values for the total lengths of the echoes in seconds (*Figure 5*) for both stations, especially at levels 10 and 20 dB. Similar consistency can also be found in the hourly numbers of meteors for both stations at levels of 20 and 30 dB (no plots are presented). Outages of registrations on 3rd, 4th and 12th August 2014 can be also seen in *Figure 5*.

4 Conclusion

It was experimentally found that the described equipment is applicable to record the evolution of meteor showers. To ensure continuity of registrations it is recommendable to use either a more stable operating system, or double the measuring device. Both receivers need about an hour to stabilize the frequency, but a slight variation of the

[1] http://www.imo.net/live/perseids2014/

received frequency is not a defect and can be compensated by changing the frequency ranges of registration. The signal from existing transmitters turned out to be not fully suitable for meteor registration. We are currently working on an opportunity to build our own transmitter in Slovakia that would be suitable. Since the tested equipment is able to provide at least some basic information about meteoric activity and does not require high costs, we began with the work needed for its installation for continuous registration of meteors in the SCO in Hurbanovo. An extension of this basic assembly is planned, which would allow registration of spectrograms of meteor records and registration of the amplitude of received RF signals.

Acknowledgment

The authors are grateful to R. Jekkel and D. Tóth for the help with the experiment and to P. Zigo and J. Tóth from the AGO Modra (CU Bratislava) for their helpful advice.

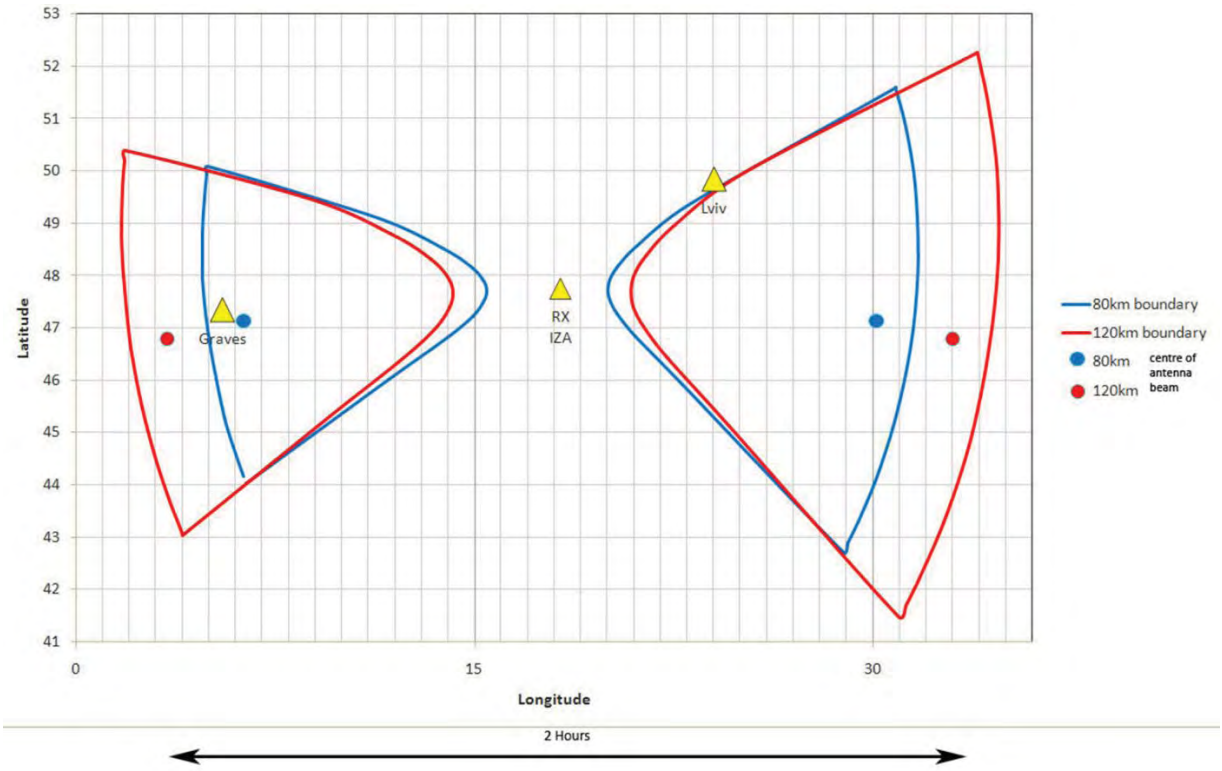

Figure 1 – Theoretical field of view of both antennas calculated for the upper (120 km AGL) and the lower (80 km AGL) boundary of detectability of radiometeors.

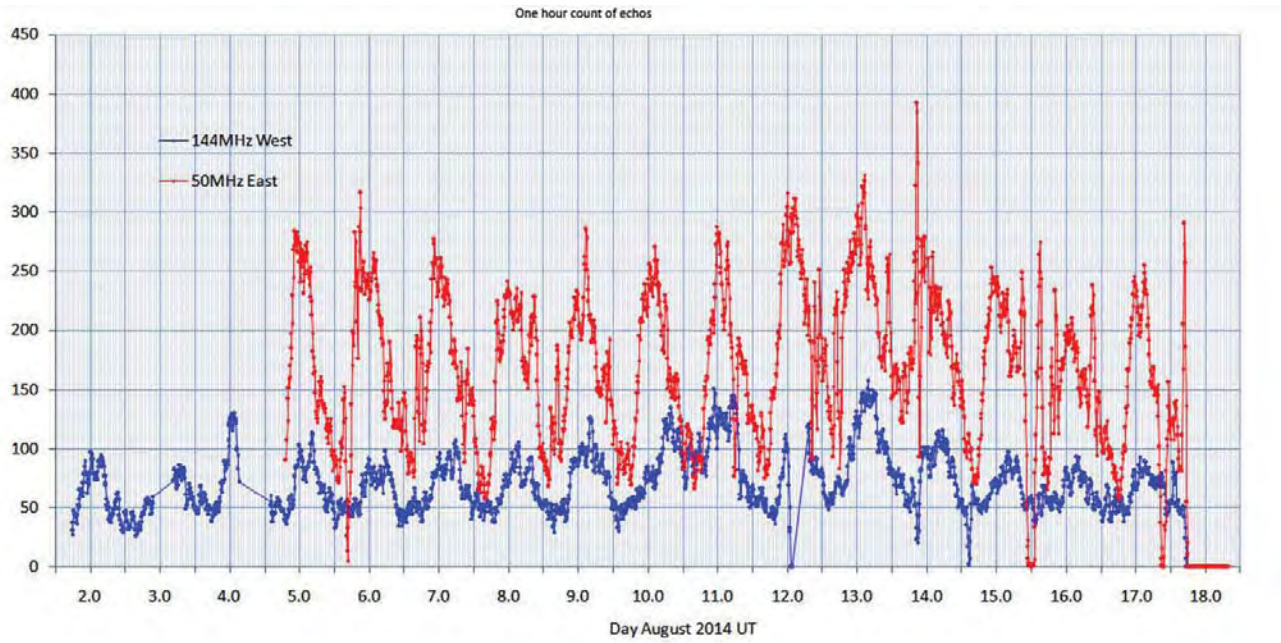

Figure 2 – Hourly counts of echoes from both stations.

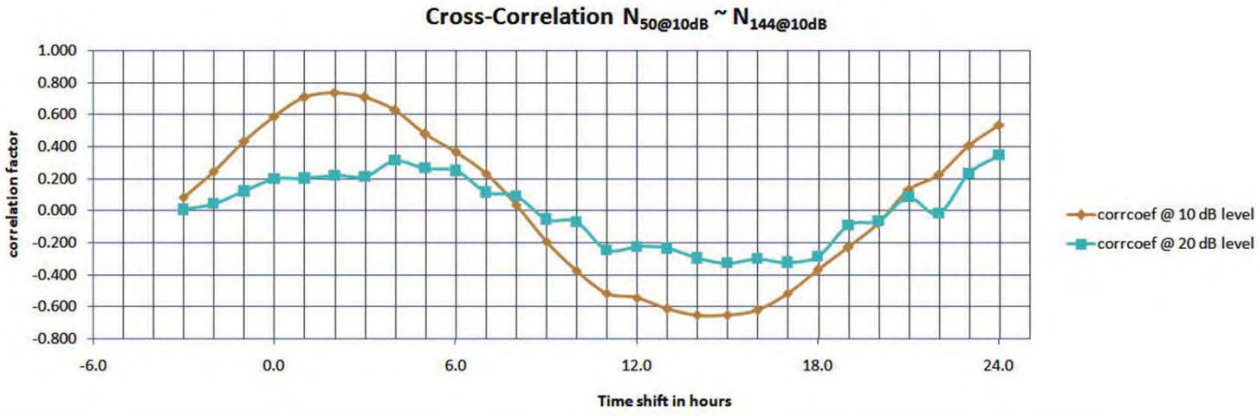

Figure 3 – Cross-correlation coefficient between the number of echoes for both the 50 MHz and the 144 MHz registrations at levels of 10 dB and 20 dB.

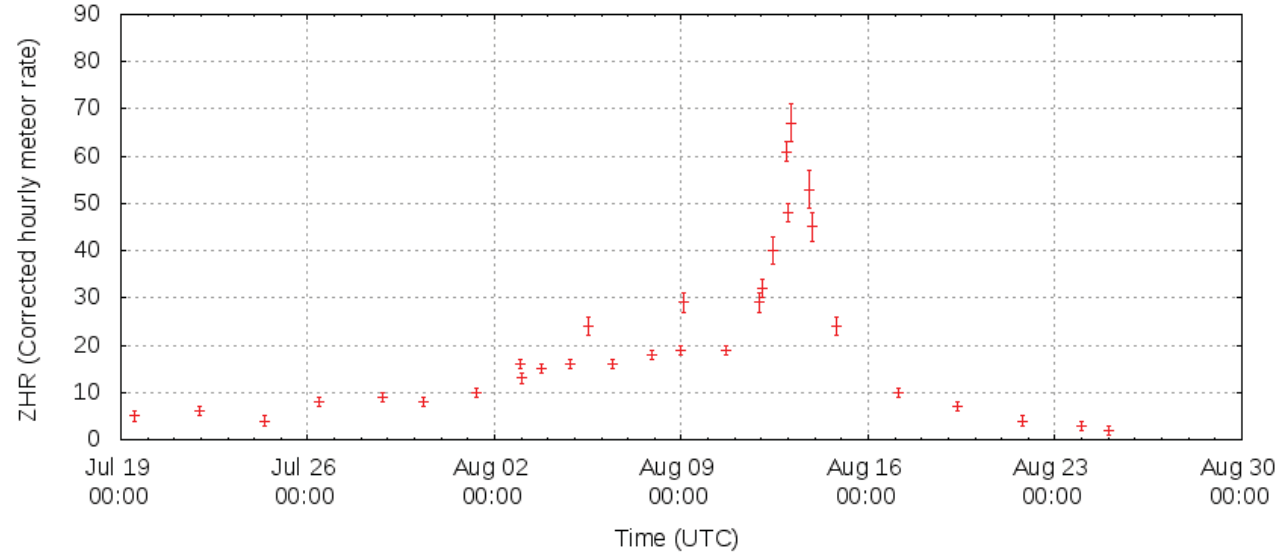

Figure 4 – Reduced hourly counts of visual meteors (http://www.imo.net/live/perseids2014/).

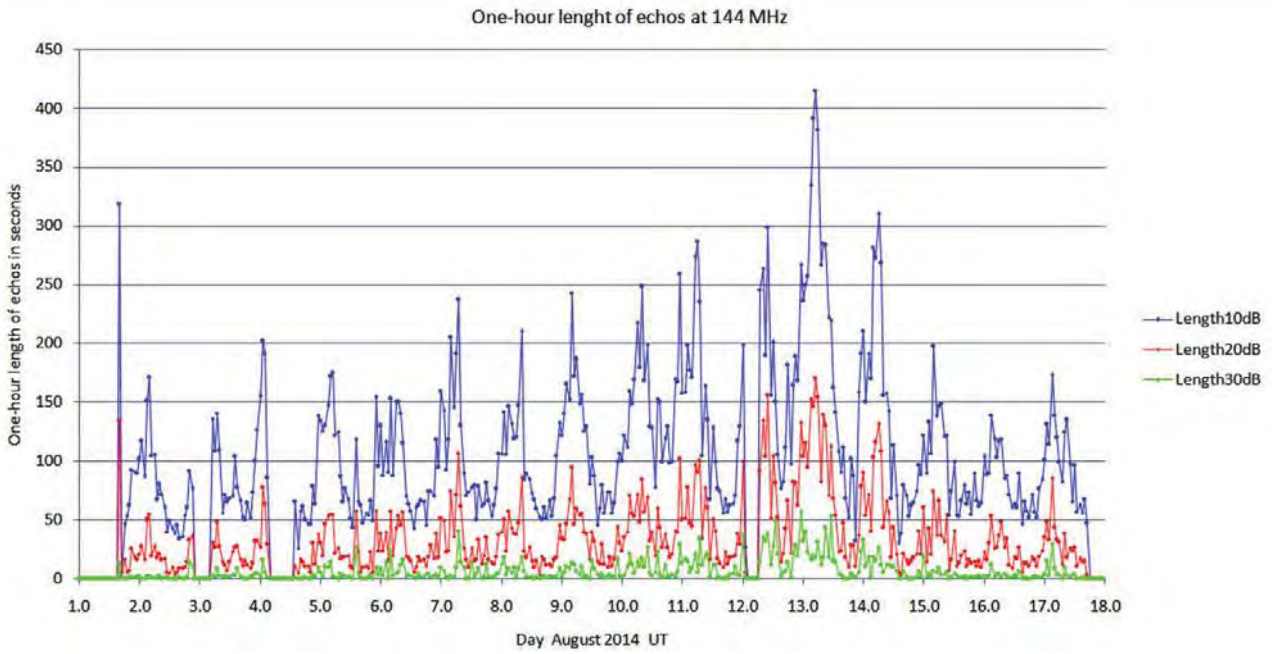

Figure 5 – One-hour values of echo length totals for the 144 MHz registration at the levels of 10 dB, 20 dB, and 30 dB.

RETRAM: recognition and trajectories of meteors

Jean-Jacques Maintoux, Sylvain Azarian, Jérémy Maintoux, Frédéric Rible

ARRL / RETRAM, Velizy-Villacoublay, France
contact@retram.org

Meteor detection and tracking is the main activity of the RETRAM group, part of the French ARRL organization. Our project uses passive radar techniques and real-time processing to detect and recognize falling objects and tries to estimate their trajectory to help in fireball recovery. The experiment started in the vicinity of Paris, France. This paper shows our observations and analyses, then it describes our technical approach, our first passive radar station and first meteor 3D localization. Finally, we describe the evolution of the system and subsequently its extension in the form of a network of stations grouping radio and optical detectors.

1 Introduction

RETRAM (as **RE**cognition and **TRA**jectories of **M**eteors) is a group of amateurs working together to make experiments around meteors detection and their trajectories, using radio signals through passive radar techniques. Goals for the RETRAM project – our wishes – are:

- to experiment with new methods for detecting and recognizing meteors using radio signals;
- to design and to test new algorithms and processing to obtain automatic detections;
- to design and to test new techniques to reconstruct a meteor path and to help in meteorite recovery;
- to use optical detection if possible to enhance results;
- to cooperate with the scientific community to share the outcome of the project.

RETRAM is built around the use of radio signals because they allow a constant survey in all weather conditions (therefore not limited by the visibility conditions) and at any time (not limited by lighting conditions).

2 Observations and principle of RETRAM

To avoid electromagnetic hazard and electromagnetic compatibility risks, RETRAM started with classic passive radar techniques using transmitters of opportunity. Starting in 2012, a survey was dedicated to the observation of meteors using the well-known Graves transmitter and some aeronautical VHF VOR beacons. (Some measurement reports are available on our WEB site (RETRAM - Recognition & trajectory, 2014)[1]. These transmitters allowed to confirm:

- the minimum "radar" budget necessary to observe the meteors;
- the various signals we have to measure (signals level, speed, spectrums…).

[1] http://www.retram.org/wpcontent/uploads/2014/06/3D_FM_Results.pdf.

We were able to confirm previous observations done by amateurs and other works like (Close et al., 2002; Close et al., 2011) and to define the criteria we have to measure to develop our project.

Optical and radio observations

Optical observations performed simultaneously by radio measurements and Doppler analysis both revealed the optical trail is correlated (in time) with the radio head echo of the meteor. This head echo is characterized by a huge Doppler slope (or fast Doppler shifting). The head echo was observed using different transmitters and the *Figure 1* shows such a correlation. The phenomenon of head echo and its radio detection were also detected using VOR beacon as shown in *Figure 2*. *Figure 3* shows a head echo and non-specular train signals collected at VHF frequencies (Close et al., 2011). The head echo, characterized by a fast Doppler shift (or high penetrating speed in atmosphere) is red circled. The head echo is followed by a long train (depending on the object and environment) presenting a very low Doppler shift (or very low speed) depending also of the environment in high atmosphere.

Principle of RETRAM

Previous observations and measurements were performed with signals (waveforms in radar wording) having no or poor temporal information (named narrow band signals). These waveforms allow integration of the signal over a relatively long time and made Doppler slope measurement possible with good accuracy. But it was impossible to find the location of meteors at any time.

To enhance the meteor path reconstruction, the RETRAM project is based on a larger waveform bandwidth, with a good Range/Doppler ambiguity, permitting to measure temporal information with an enhanced accuracy (better than 1km). The Doppler accuracy is still limited by the integration time. As shown by numerous papers and measurements, the VHF band offers the best results for the detection of meteors. With a large transmitted power, the FM band (88/108 MHz) seems to be a good candidate (RETRAM – Recognition & trajectory, 2014). This paper gives a list of criteria for the choice of the transmitters. The principle of RETRAM is the following and is shown below in *Figure 4 and 5*.

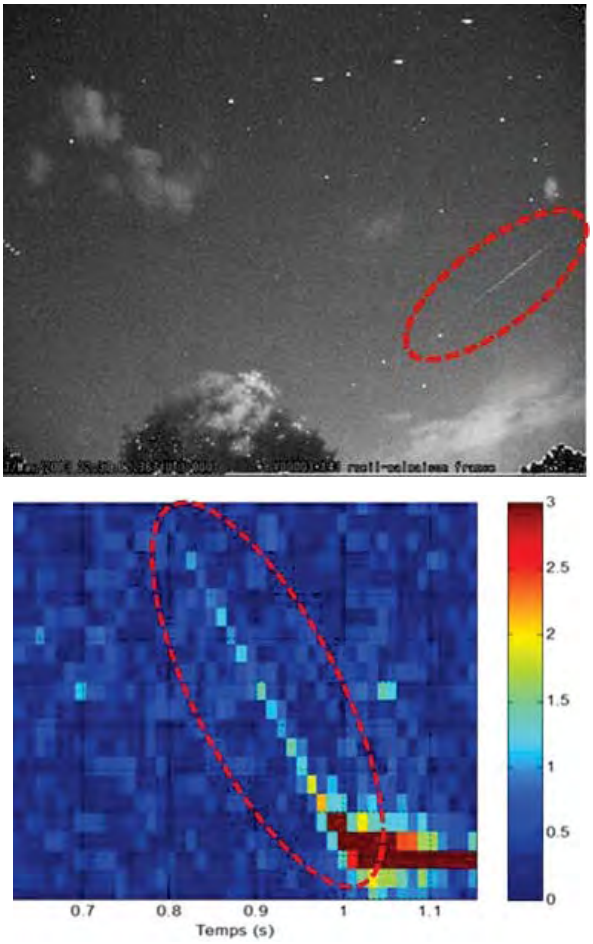

Figure 1 – Optical observation and the radio Doppler slope – both red circled (observation done by Dominique André – Rueil/France).

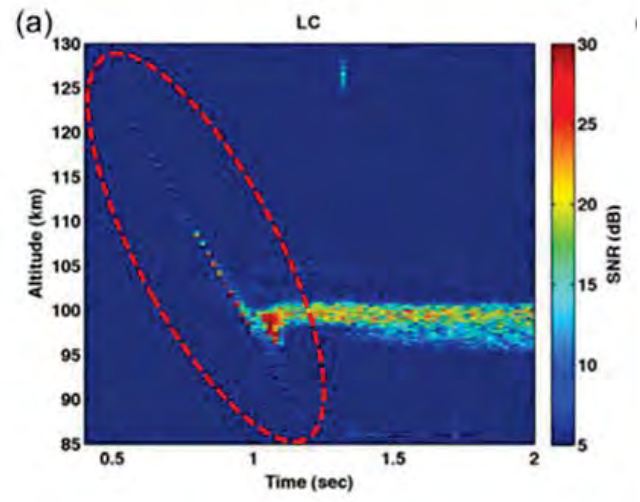

Figure 2 – Head echo and non-specular train.

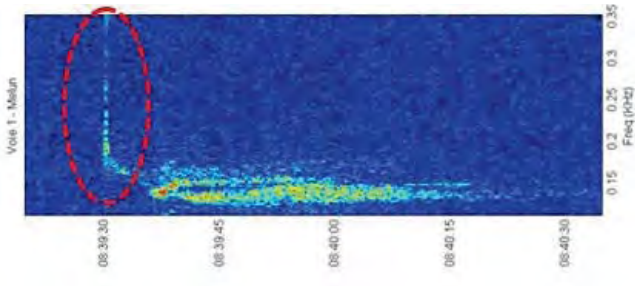

Figure 3 – VOR detection (60s measurement during Leonids 2012) by RETRAM.

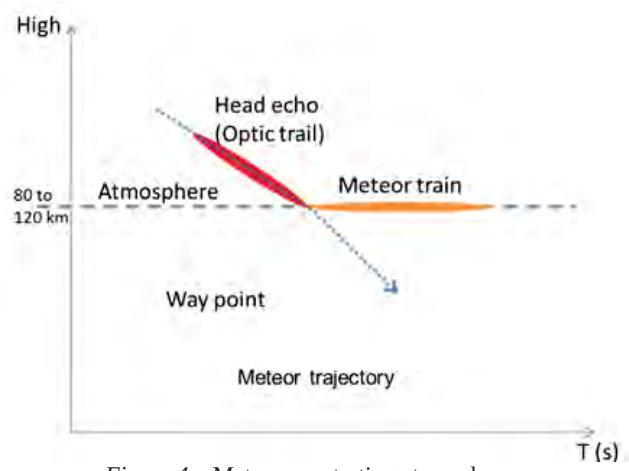

Figure 4 – Meteor penetrating atmosphere.

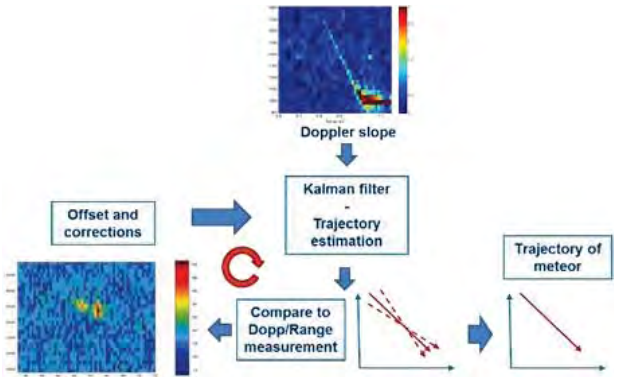

Figure 5 – Processing to align the Doppler slope of head echo on the way point of meteor.

The first step consists in:

- detecting the beginning of the meteor train, to localize a reference point of the meteor trajectory;
- measuring the Doppler slope of the head echo.

Then the process is completed by the projection of the Doppler slope in the 3D bistatic domain and by the comparison to the Doppler / Range measurement of the reference point to find the right trajectory of the meteor during its atmospheric penetration.

3 FM passive radar

For this project, RETRAM has developed a FM passive radar at the beginning of 2014. As said before, this radar uses the transmitters of the FM broadcasting band (88/108 MHz). The description of the radar is done in a dedicated paper (Azarian et al., 2014). This system delivers bistatic information for each detection. The bistatic distance sets the possible position for the detected meteor to be an ellipsoid whose foci are the transmitter and the receiver locations, as illustrated by *Figure 6*. This curve is also called the iso-range contour.

To find the right position of a meteor, more than one transmitter/receiver couple must be used to remove any localization ambiguity. By using 3 or more transmitter/receiver couples, the intersections of these ellipsoids give the possible target position as shown by *Figure 7*.

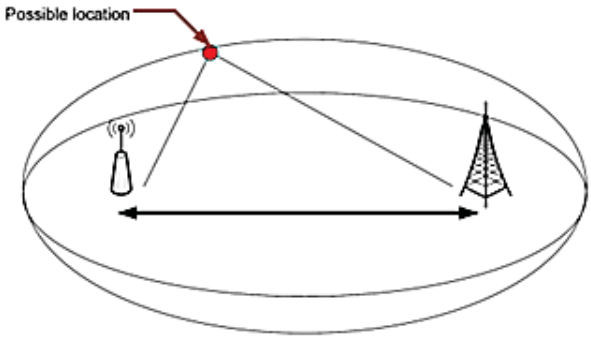

Figure 6 – Bistatic ellipsoid – iso-range contour.

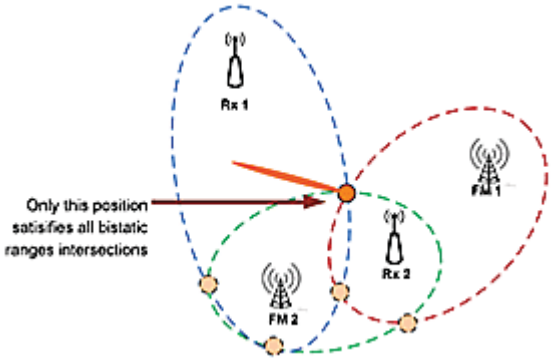

Figure 7 – Multistatic setup for meteor localization (2D cut in altitude).

4 First RETRAM station

To assess the performance of meteor detection using FM broadcast transmitters, RETRAM installed its first station near Paris. To survey the sky of the Paris area (Ile de France), an experimental mockup was made of:

- two FM Yagi antennas placed on the top of a shelter (see *Figure 8*). They are directed towards the sky and oriented so that , by combining the collected signal, they present an omnidirectional pattern in the horizontal plan;
- a two RF ways front-end followed by a 2 ways SDR (software defined radio) receiver. The SDR digitizes four frequency channels corresponding to four FM transmitters located around Paris.
- A real time processing to detect the beginning of the meteor train. In case of detection, the processor saves the last FIFO (First In First Out) batch of data. It permits to reduce the amount of data by using dedicated criteria of meteor train recognition, such as:
    - range > 70 km corresponding to the frequent altitude of meteors penetrating the atmosphere;
    - Doppler near 0 m/s. Meteor train begins with a very low speed;
    - detection length > 1s to avoid parasitic and very weak detection;
    - SNR (Signal to Noise ratio) > 11 dB to reduce any false detections.
- a hard disk to store raw data and detection plots;
- a dedicated post processing software calculating the Doppler slope of the meteor head echo (currently worked out).

Figure 8 – Two FM Yagi antennas on the top of the shelter.

Figure 9 – RF Front End, digital receiver and real time processing.

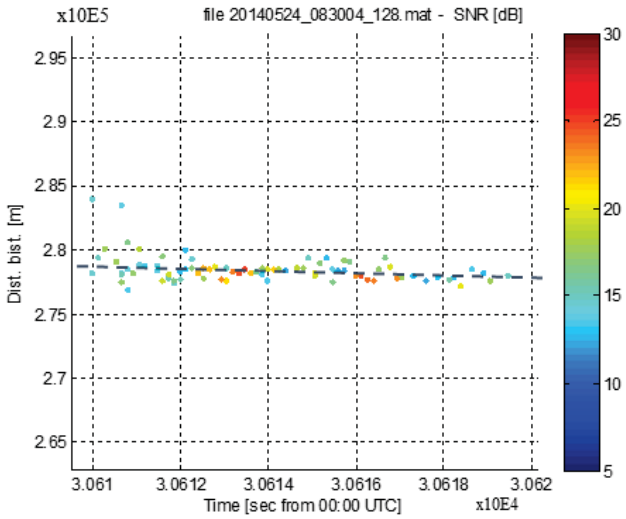

Figure 10 – The processing reveals the bistatic distance evolution (raw data) of the meteor train during a 10s duration (here very low, about only 1 km).

5 First results

The first detections were performed rapidly. First of all, the processing is able to deliver the range change (but also the Doppler change) during the "life" of the meteor train as shown on *Figure 10*. These measurements could help to assess the meteor dispersion in the atmosphere and moreover to reveal speed and direction of wind and probably even more data of interest to scientists. Secondly, since May 2014 we collect numerous detections using three or four FM transmitters. We were able to deliver 3D localization and to reveal the waypoint

for these meteors, mainly during the path of the dust trails released by comet 209P/LINEAR. Recently, we have started performance assessment. Thanks to BOAM[2], we did a first comparison between an optical detection and a radio 3D localization.

Figure 11 shows this result. To help reading and understanding the ellipsoids interception, *Figure 11* shows a cut of 3 ellipsoids at the altitude of 95km (measured altitude of the meteor train). More details are available in the report "RETRAM – 3D results" (2014)[3].

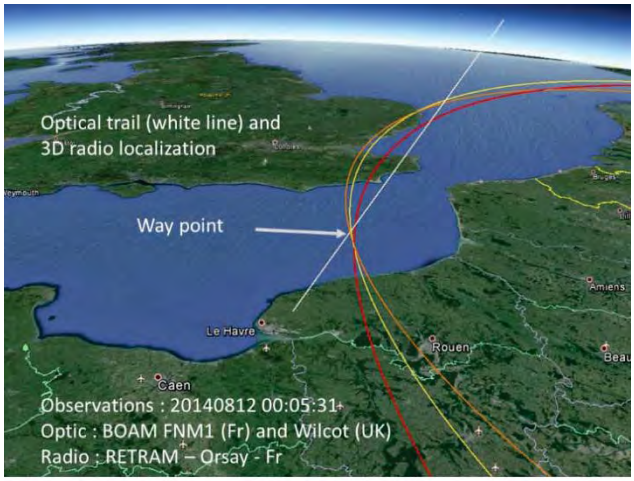

Figure 11 – 3D Interception of 3 ellipsoids (cut @ altitude 95 km) and optical trail calculated by BOAM (white line).

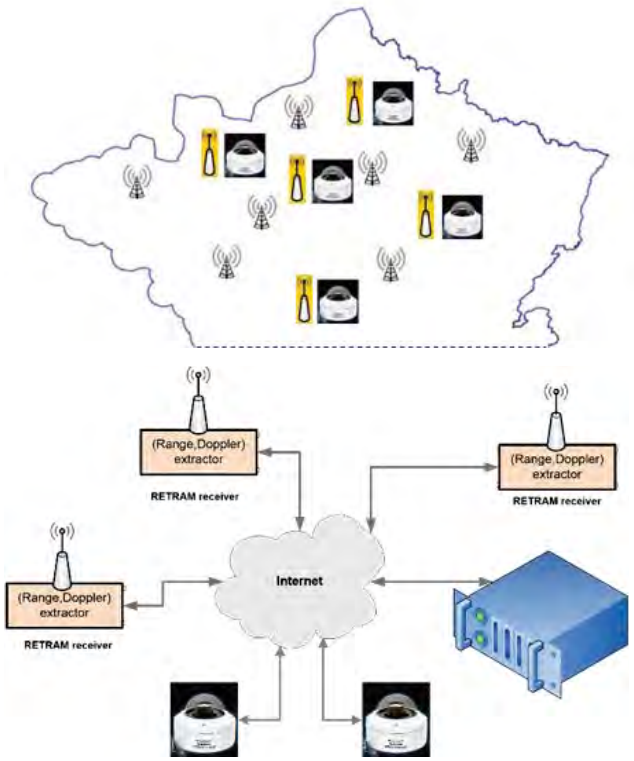

Figure 12 – RETRAM Network.

6 RETRAM : to be continued…

We have to continue to assess performance in sensitivity and 3D localization accuracy. The Doppler slope was observed on numerous detections and we are working on the dedicated processing to replace visual estimations by automatic measurements. Then we will work on the complete processing loop to deliver the meteor trajectory (see section 2). As discussed previously and depicted in *Figure 7*, the best solution for an accurate estimation of the meteor position is to extend the number of receivers and transmitters involved in the signal processing. So RETRAM has planned to build, in the coming months, a first node of a network based on optimized receivers and processors. This node will be used as a mockup for a possibly wider system to cover a much larger area as illustrated by *Figure 12*. Moreover, radio and optical methods are very complementary and the network should be extended by adding optical devices with the help of the BOAM[2] network.

7 Conclusion

In this paper, we have presented the first results of our meteor detections using FM broadcast signals. The type of processing involved in this paper is very similar to the techniques generally used with success in passive radar.

To enhance the localization capabilities of the system, RETRAM and BOAM groups respectively plan to setup new receivers and sky cameras, interconnected using the Internet. This network should open promising results with continuous and accurate detections.

References

Close S., Oppenheim M., Hunt S., Dyrud L. (2002). "Scattering characteristics of high-resolution meteor head echoes detected at multiple frequencies". *Journal of Geophysical Research*, **107-A10**, SIA 9.1-SIA 9.12.

Close S., Kelley M., Vertatschitsch L., Colestock P., Oppenheim M., Yee J. (2011). "Polarization and scattering of a long-duration meteor trail*"*. *Journal of Geophysical Research*, **116-A1**, A01309.1-A01309.12.

Azarian S., Maintoux J.-J., Rible F., Maintoux J. (2014). "A network of passive radars to detect and track meteors*"*. *IEEE Radar Conference – Lille.*

[2] BOAM: French meteor observers database. See: http://www.boam.fr/?lang=en

[3] "Meteors detection & localization using FM transmitters - First 3D localization results". http://www.retram.org/wp-content/uploads/2014/06/3D_FM_Results.pdf.

25 years since IMO's Founding General Assembly

Paul Roggemans

Pijnboomstraat 25, 2800 Mechelen, Belgium
paul.roggemans@gmail.com

In 2014 we remembered the Founding General Assembly of the International Meteor Organization which took place 25 years ago, on Saturday 7 October 1989 at Balatonföldvár in Hungary.

1 Introduction

The creation of the IMO was the result of an evolution in amateur meteor observing during more than a decade. Although the benefits of global cooperation were evident for everybody involved, the making of the IMO proved to be a difficult happening. While the author started to prepare the creation of the IMO in 1987, it took until begin of 1988 before a representative group of founding members got involved in the preparations of the IMO constitution. While the official birthday of the IMO has been set as 1st of May 1988, the preparation of the IMO Constitution and the Founding General Assembly took more than one year. All negotiations happened via written letters involving 97 physical persons from 21 different nations, this hectic task was managed by the author who kept very good contacts worldwide with many meteor workers. Once everybody agreed on the draft for an IMO constitution, it still took a remarkable long time before the official version got published. The rather difficult 'birth' of the IMO has been remembered at the IMC in Poznan, Poland, last year (Roggemans, 2014).

2 The break in the wall

On Saturday 7 October 1989, after more than two years of preparations, the IMO was ready to become a constitutional society. The timing and the place of the Founding General Assembly could not be more symbolic: in Hungary, close to where the post WWII Iron Curtain had just started to collapse, about a month before the fall of the Berlin Wall.

While all attempts to get Slovak meteor astronomers to the IMC in 1985 had still failed, a first single Hungarian meteor observer managed to 'escape' and attended the 1986 IMC in Belgium. In March 1988, more participants from Eastern Europe could participate at the IMC in the Netherlands, among them Jürgen Rendtel from the German Democratic Republic, together with a few Hungarian and a few Slovak participants. Although this was a clear indication that something had changed, nobody dare to hope what would happen 18 months later.

Hungarian amateurs had organized an international conference for astrophotography in 1988 and they were recommended to contact the author to propose a meteor conference via some contacts in France. One of the Hungarian amateurs was a student at the Sorbonne University in Paris, France and this way the preparations for the 1989 IMC in Hungary were discussed in a residence for Hungarian students in Paris, most of these students were being prepared for diplomatic careers. The talks about how and where to organize the 1989 IMC did not only concern the Foundation of the IMO. Never before, the Western IMC participants had to travel so far for an IMC, which required more time, more expenses and the bureaucracy to obtain visa. In order to make this challenge more worthwhile, the author decided to extend the IMC with one day and to include an excursion. Until 1988 an IMC started Friday late afternoon, had its main lecture day on Saturday and ended Sunday noon after lunch. The abilities of the amateurs in that time did not allow to fill an entire IMC program. In the early years, invited lectures were required to offer a worthwhile lecture program. While the travelling constraints inspired to extend the IMC by one day, the input of lectures would be insufficient to extend the IMC lecture program with an extra day. To fill the expected dead time, another novelty was introduced in 1989: the IMC excursion. An excursion during the IMC would make the travelling worthwhile, to see something of the region of the IMC.

Figure 1 – In order to prepare the IMO Founding General Assembly the provisional board of IMO stayed at a farm house that served as observatory in Kötcse (credit Casper ter Kuile).

The founding of the IMO made the IMC in Hungary even more historical. The Hungarian hosts offered a free stay at a barn that was used as observing place. When the first participants arrived, the barn had to be installed to overnight. It was very comparable to an adventurous youth camp. Beds had to be carried from some Hungarian army deposit. This way people were surprised to see a long queue of iron beds being carried along the road in twilight through their village by British, Belgian, French, Dutch and German visitors. The next day lunchtime was

in a kindergarten, with a kind of food that people from the West hadn't ever seen in lifetime.

Figure 2 – Meals were provided in a local school in Kötcse, from left to right first table Evelyne Blomme, Rainer Arlt, Marc Gyssens, Jürgen Rendtel, André Knöfel and in front at right Malcolm Currie (credit Casper ter Kuile).

The IMC itself took place in a huge impressive hotel at Lake Balaton. Although the hotel was well aware we all came for a conference, they had no conference room and nothing had been prepared for a conference at all. The first IMC that was managed by the IMO turned out to be a real test for the skills of all involved in solving unforeseen problems. The huge entrance hall of the Hotel turned out to be the only possible place for a lecture room. In no time all chairs from all over the hotel were collected, curtains fixed to cover the big windows, combined with sheets from beds to darken the improvised lecture room. Luckily we had anticipated on any possible occurrence of the Laws of Murphy and some had brought a slide projector and someone had an overhead projector. This was the only IMC ever all presentations were projected on some bed sheet.

Figure 3 – From left to right Alexandra Terentjeva, Jürgen Rendtel and Malcolm Currie (credit Casper ter Kuile).

The 1989 IMC welcomed the first participants from Bulgaria, the former Soviet Union and Yugoslavia while many Western amateurs for various reasons did not travel to Hungary for the IMC. The founding General Assembly would take place with a majority of amateurs who had not been involved in the making of the IMO. Many participants didn't even know very well the meaning of the first IMO General Assembly.

Figure 4 – Marc Gyssens and the IMO Founding General Assembly, on the first row André Knöfel, Ralf Koschack, Rainer Arlt, second row Jeroen Van Wassenhove, Mark Vints and Jan Hollan (credit Casper ter Kuile).

3 The Founding General Assembly

More than two years had passed since the author had started to prepare the IMO. At the very beginning the idea of the IMO was strongly supported by several of the most active meteor observers, many of who were already many years active. At the beginning the chances to succeed looked very poor, the idea to create the IMO met great skepticism and for some it became a challenge to prevent the IMO from being founded. In these difficult circumstances the biggest support for the IMO came from a number of enthusiast meteor workers, some of who are still active, others meanwhile disappeared from the meteor scene. One of the most difficult moments in the starting period was beyond doubt the workshop about IMO at the IMC in March 1988, where it came to a real clash between an international group of pro-IMO amateurs and some local Dutch anti-IMO amateurs. In the end the pro-IMO group managed to organize its plans by simply closing the official workshop to get rid of the anti IMO protesters, in order to resume the workshop a little bit later.

When candidates for the first IMO Council were solicited, the opponents of the IMO concept saw some of their skepticism confirmed. Most of those who had frank and firmly defended the ideas pro-IMO, often the most active amateurs were not the first to apply for any official function. Instead about half of the first IMO Council were people who had preferred to keep distance in the most difficult times of the struggle to create IMO. WGN, which became the IMO Journal, struggled with chronic delays, which was seen as a sign of weakness for the newly founded IMO. Many meteor observers, among who several very active amateurs decided to just wait and see if the IMO was going to last much longer than just one or two years. The IMO got finally founded but did not get very much credit or support. The new organization was challenged to prove it could survive and this with rather few people who could really do the real work for it.

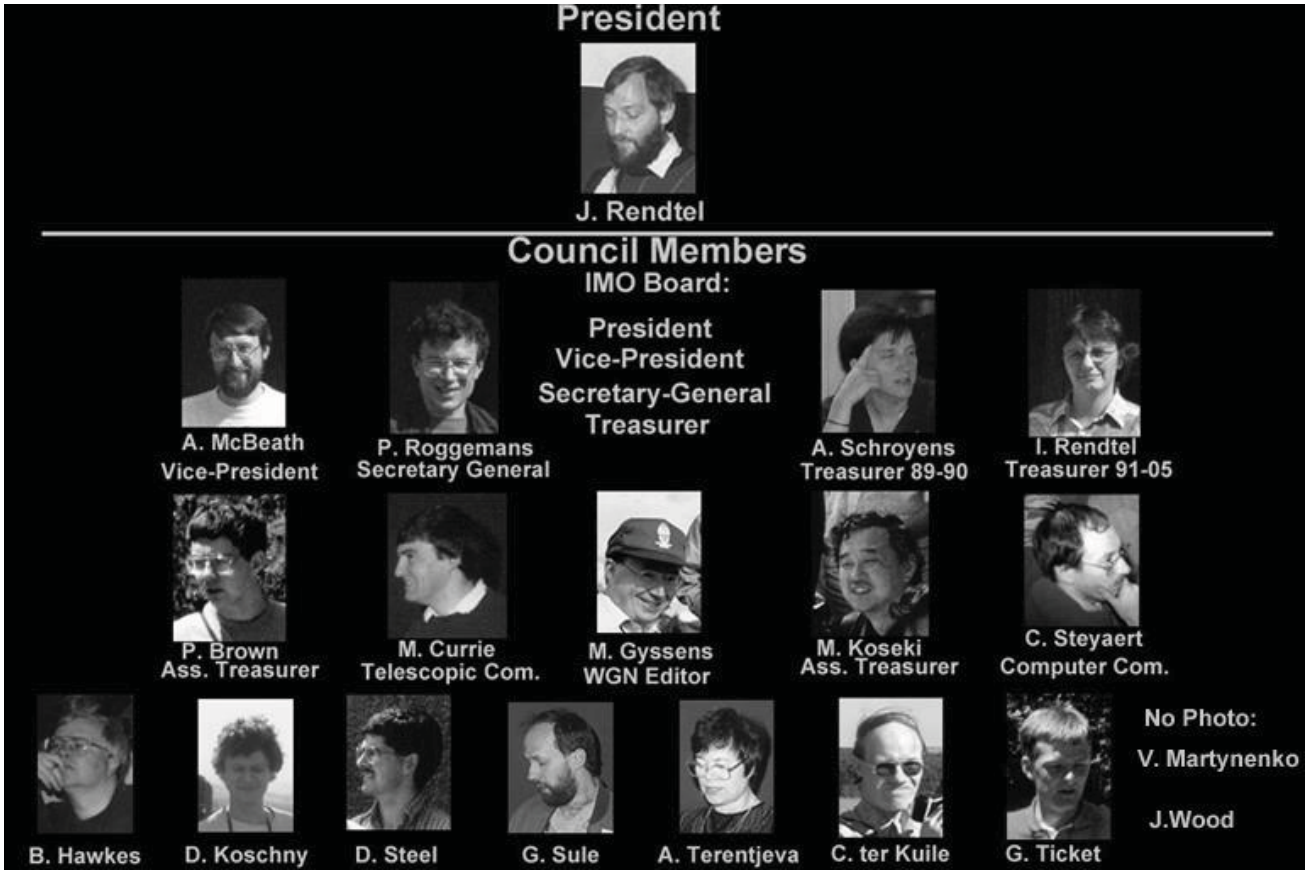

Figure 5 – The first IMC Council as proposed to the Founding General Assembly after a voting by letter some months before by all voting IMO members 1989.

If the Berlin Wall hadn't collapsed just around the time of the creation of IMO, the whole project would have definitely failed. The difference was made by Jürgen Rendtel and his team from the German Democratic Republic. Being one of the most active amateur meteor observers with a lot of dedication for meteor work, it was no surprise that Jürgen was invited to become the first IMO President, a task he would continue until end of 2013. Jürgen became the only IMO officer to take care so long of his function with many achievements for the IMO thanks to his efforts.

Figure 6 – The first IMO President, Jürgen Rendtel at the IMO Founding General Assembly on Saturday 7 October 1989.

The IMO Council decided to propose Honorary Membership for Jürgen for his meanwhile 25 years of work for the IMO and celebrated this moment with a meteorite as a gift as well as a reception for all participants offered by the other Council Members.

Figure 7 – The IMO President, Jürgen Rendtel at the IMO General Assembly on Friday 19 September 2014.

As the IMO is an amateur organization, interest and passion are the main drive for the motivation of people. Nobody can be forced to do anything and everything is being done on voluntary bases. For these reasons it is really exceptional if somebody as a volunteer remains motivated for such a long time like Jürgen did.

One of the first tasks of Jürgen was to thank the provisional IMO board on his behalf as President of the first elected IMO Council. This first Council was elected by the Founding Members of IMO by a written voting bulletin sent out in April 1989 with a voting deadline of June 16, 1989. All candidates were elected; most key functions were assigned to invited candidates. The first IMO Council involved many people from different origin in order to make the IMO more widely accepted.

4 How did the IMO evolve?

The IMO met a lot of skepticism and got rather very little credibility, mainly because all previous failures with attempts to set up international meteor work, but also because of chronic delays with its publications. One of the very first achievements of the IMO was the VMDB and its highly efficient tools to store large amounts of data and its global analyzing tools. The advantages of worldwide observing efforts became well illustrated as the 1988 Perseids activity profile surprised with a detailed profile showing a double peak. Later this new peak could be associated with Perseid outbursts all related with the return of the parent comet. The VMDB allowed also to generate impressive volumes of annual reports containing all visual observations in a single (heavy) annual volume. Soon other meteor shower activity profiles as well as variations in the population indices across meteoroid streams followed and all these results impressed many people. A real break-through occurred in 1992 with a first IMC being combined with a professional Meteoroids Meeting in Smolenice, Slovakia. Time had proven that the IMO was not just another caprice of not too reliable amateurs. When also a most successful video network got started along with a steady input of good quality visual meteor observing, the organization definitely marked meteor astronomy.

5 Future concerns for the IMO

Being an amateur organization all activities are the work of volunteers driven by enthusiasm and personal motivation. In the past 25 years 35 Council members from 17 different nations shared the workload: *Rainer Arlt (1998-2013), David Asher (2002-2009,2012- ...), Godfrey Baldacchino (1996-1999), Geert Barentsen (2010- ...), Peter Brown (1989-1997), Malcolm Currie (1989-1993), Marc Gyssens (1989- ...), Robert Hawkes (1989-1993), Javor Kac (2012- ...), André Knöfel (1998-2001), Ralf Koschack (1994-1997), Detlef Koschny (1989-1993, 2010- ...), Masahiro Koseki (1989-1993), Robert Lunsford (1997- ...), Vasili Martynenko (1989-1993), Alastair McBeath (1989-2010, 5 terms), Huan Meng (2006-2009), Sirko Molau (1998- ...), Jean-Louis Rault (2012- ...), Ina Rendtel (1991-2005, 4 terms), Jürgen Rendtel (1989- ..., 6 terms), Paul Roggemans (1989-1997, 2012- ...), Ann Schroyens (1989-1990), Duncan Steel (1989-1993), Chris Steyaert (1989-1993), Gabor Süle (1989-1993), Alexandra Terentjeva (1989-1993), Casper ter Kuile (1989-1993), Glenn Ticket (1989-1993), Chris Trayner (2004-2009), Mihaela Triglav (2002-2009), Josep Trigo (2006-2009), Cis Verbeeck (2006- ...), Jeff wood (1989-1997), Graham Wolf (1994-1997).*

At the very beginning rather few really bothered to stand up to join IMO. Promising competent meteor workers were actively solicited to consider joining the Council, especially for the vital key functions in the IMO board. The future stands or falls with the qualities and commitment of these few IMO officers. As the IMO became a notion with some prestige, there is a serious threat that functions attract the kind of people who hunt for personal prestige while IMO only needs officers who effectively do the work related to a function.

Selecting future IMO officers requires some talent in human resource management. For each task a typical profile of qualities and talent is required. The worst scenario for the future would be that key functions get taken by individuals who don't have much time and expect the membership to be understanding for their lack of commitment. This was the scenario predicted by those who opposed the IMO more than 25 years ago. The best protection for such scenario is to actively search for suitable follow up for the IMO officers. This requires a lot of time for communication, sense for initiative and common sense for a practical approach. We need a kind of head hunter to find suitable future IMO officers. There are two important points to be observed: IMO needs officers with enough free time and practical talent.

What the future will bring for IMO may depend on you. If you have a lot of free time, a strong commitment in meteor work and some talent for practical management, you may perhaps be the one who will assure a great future for the next 25 years of the IMO.

References

Roggemans P. (2014). "Twenty five years of IMO (1988–2013)". In Gyssens M., Roggemans P., and Żołądek P., editors, *Proceedings of the International Meteor Conference*, Poznań, Poland, 22–25 August 2013. IMO, pages 9–12.

List of participants

The alphabetical list below contains all participants of the 33rd International Meteor Conference. Numbers serve to identify positions in the group photographs, if applicable. People marked with "∗" were visitors who posed together with the participants in the group photograph on p. 223.

Ali Dib Mohamad, France (43)
André Dominique, France (Not in group picture)
Andreic Zeljko, Croatia (9)
Antier Karl, France (17)
Argo Megan, United Kingdom (11)
Audureau Yoan, France (95)
Barentsen Geert, United Kingdom (14)
Bek Nataša, Croatia (4)
Bettonvil Dusan, Netherlands (2)
Bettonvil Felix, Netherlands (Not in group picture)
Bettonvil Uros, Netherlands (1)
Biondic Damir, Croatia (5)
Birlan Mirel, France (106)
Bouley Sylvain, France (90)
Bozhurova Eva, Bulgaria (85)
Braconnier Robert, France (Not in group picture)
Brower Jeffrey, Canada (122)
Brower Annette, Canada (82)
Buchmann Andreas, Switzerland (118)
Butusova Sofy, Russia (76)
Calders Stijn, Belgium (79)
Ćiković Ivica, Croatia (3)
Colas Francois, France (Not in group picture)
Čotar Klemen, Slovenia (55)
Çubuk Kerem, Turkey (86)
Dmitriev Vasily, Russian Federation (78)
Dolinsky Peter, Slovakia (68)
Dorotovic Ivan, Slovakia (65)
Drolshagen Gerhard, Netherlands (117)
Drolshagen Esther, Germany (124)
Dubs Martin, Switzerland (120)
Egal Auriane, France (59)
Fleet Richard, United Kingdom (77)
García Vega Pilar, Spain (116)
Georgescu Tudor, Romania (103)
Georgescu Ana, Romania (104)
Gherase Radu, Romania (96)
Guennoun Meryem, Morocco (45)
Gulon Tioga, France (84)
Gural Peter, United States (98)
Gyssens Marc, Belgium (87)
Haas Axel, Germany (Not in group picture)
Hajdukova Maria, Slovakia (34)
Hankey Michael, United States (101)
Hillestad Trond Erik, Norway (49)
Hillestad Eli Fugelso, Norway (50)
Ivanović Ilija, Serbia (113)
Jouin Stéphane, France (69)
Kac Javor, Slovenia (63)
Kanianska Paulina, Slovakia (13)
Kaniansky Stanislav, Slovakia (15)
Kartashova Anna, Russian Federation (81)
Kieffer Bernard, France (Not in group picture)
Klemt Bernd, Germany (56)
Koschny Detlef, Netherlands (73)
Kuczuro Aleksandra, Poland (97)
Kurtovic Goran, Croatia (27)
Kwon Min-Kyung, France (57)
Leroy Arnaud, France (61)
Maciejewski Maciej, Poland (107)
Malaric Mirjana, Croatia (6)
Maquet Lucie, France (8)
Martinez Picar Antonio, Belgium (70)
Matković Filip, Croatia (28)
Meister Stefan, Switzerland (111)
Molau Sirko, Germany (40)
Molnar Klaudija, Croatia (7)
Morillas Sánchez Lorenzo G., Spain (115)
Neijts Marc, Netherlands (29)
Nijland Jos, Netherlands (31)
Nogami Nagatoshi, Japan (Not in group picture)
Novoselnik Filip, Croatia (Not in group picture)
Okolic Dragana, Netherlands (Not in group picture)
Ott Theresa, Germany (123)
Özeren Ferhat Fikri, Turkey (108)
Paillart Christian, France (127)
Pavletić Lovro, Croatia (102)
Perkov Anton, Croatia (48)
Perlerin Vincent, France (92)
Peterson Chris, United States (36)
Piffl Roman, Slovakia (18)
Polakowski Krzysztof, Poland (112)
Polard Jean Marie, France (66)
Rault Jean-Louis, France (119)
Reffet Bérénice, France (58)
Rendtel Manuela, Germany (44)
Rendtel Juergen, Germany (42)
Richard Dominique, France (72)
Roelandts Tom, Belgium (75)
Roggemans Paul, Belgium (91)
Roggemans Adriana, Belgium (89)
Roman Victor Stefan, Romania (74)
Rudawska Regina, Slovakia (35)
Sandor Adina, Romania (93)

Schenker Jonas, Switzerland (125)
Schmidt Hans-Georg, Germany (64)
Schneider Alexander, Slovakia (38)
Šegon Damir, Croatia (99)
Šegon Marko, Croatia (53)
Šegota Sandi, Croatia (51)
Shuttleworth Alan, United Kingdom (121)
Silađi Emil, Croatia (24)
Skokić Ivica, Croatia (26)
Skunca Gordan, Croatia (25)
Slavec Stane, Slovenia (67)
Smith Andy, United Kingdom (83)
Soja Rachel, Germany (33)
Stewart Peter, Northern Ireland (126)
Steyaert Chris, Belgium (80)
Sutherland Paul, United Kingdom (71)
ter Kuile Casper, Netherlands (100)
Theiler Carina, Germany (41)
Theiler Laura, Germany (40)
Todorović Snežana, Serbia (Not in group picture)
Tomezzoli Giancarlo, Germany (110)
Toth Juraj, Slovakia (37)
Tukkers Arnold, Netherlands (16)
Ugolnikov Oleg, Russia (Not in group picture)
Ujcic Ozbolt Vanesa, Croatia (30)
Vaubaillon Jeremie, France (10)
Veljković Kristina, Serbia (Not in group picture)
Verbeeck Cis, Belgium (94)
Vida Denis, Croatia (21)
Vidovenec Marian, Slovakia (62)
Vješnica Stella, Croatia (128)
Vrban Fran Ivan, Croatia (32)
Ward Bill, United Kingdom (114)
Weiland Thomas, Austria (12)
Winkler Roland, Germany (47)
Winkler Dagmar, Germany (46)
Wiśniewski Mariusz, Poland (105)
Yancheva Yulia, Bulgaria (88)
Zanda Brigitte, France (54)
Žegarac Ana, Serbia (Not in group picture)
Zigo Pavel, Slovakia (60)
Żołądek Przemysław, Poland (109)
Zubović Dario, Croatia (52)

If you wish to locate a particular person on the group photo on the adjacent page, search for his or her name in the alphabetical list above, and find the face corresponding to the number mentioned using the key under the group photo.

Conversely, if you wish to identify a face on the group photo, find the corresponding number in the key, and find his or her name in the numerically ordered list below:

(1) Uros Bettonvil; (2) Dusan Bettonvil; (3) Ćiković Ivica, Croatia; (4) Bek Nataša, Croatia; (5) Biondic Damir, Croatia; (6) Malaric Mirjana, Croatia; (7) Molnar Klaudija, Croatia; (8) Maquet Lucie, France; (9) Andreic Zeljko, Croatia; (10) Vaubaillon Jeremie, France; (11) Argo Megan, United Kingdom; (12) Weiland Thomas, Austria; (13) Kanianska Paulina, Slovakia; (14) Barentsen Geert, United Kingdom; (15) Kaniansky Stanislav, Slovakia; (16) Tukkers Arnold, Netherlands; (17) Antier Karl, France; (18) Piffl Roman, Slovakia; (19) Eloise Mousis; France; (20) Olivier Mousis; France; (21) Vida Denis, Croatia; (22) Eglantine Mousis; France; (23) Pauline Mousis; France; (24) Silađi Emil, Croatia; (25) Skunca Gordan, Croatia; (26) Skokić Ivica, Croatia; (27) Kurtovic Goran, Croatia; (28) Matković Filip, Croatia; (29) Neijts Marc, Netherlands; (30) Ujcic Ozbolt Vanesa, Croatia; (31) Nijland Jos, Netherlands; (32) Vrban Fran Ivan, Croatia; (33) Soja Rachel, Germany; (34) Hajdukova Maria, Slovakia; (35) Rudawska Regina, Slovakia; (36) Peterson Chris, United States; (37) Toth Juraj, Slovakia; (38) Schneider Alexander, Slovakia; (39) Theiler Laura, Germany; (40) Molau Sirko, Germany; (41) Theiler Carina, Germany; (42) Rendtel Juergen, Germany; (43) Ali Dib Mohamad, France; (44) Rendtel Manuela, Germany; (45) Guennoun Meryem, Morocco; (46) Winkler Dagmar, Germany; (47) Winkler Roland, Germany; (48) Perkov Anton, Croatia; (49) Hillestad Trond Erik, Norway; (50) Hillestad Eli Fugelso, Norway; (51) Šegota Sandi, Croatia; (52) Zubović Dario, Croatia; (53) Šegon Marko, Croatia; (54) Zanda Brigitte, France; (55) Čotar Klemen, Slovenia; (56) Klemt Bernd, Germany; (57) Kwon Min-Kyung, France; (58) Reffet Bérénice, France; (59) Egal Auriane, France; (60) Zigo Pavel, Slovakia; (61) Leroy Arnaud, France; (62) Vidovenec Marian, Slovakia; (63) Kac Javor, Slovenia; (64) Schmidt Hans-Georg, Germany; (65) Dorotovic Ivan, Slovakia; (66) Polard Jean Marie, France; (67) Slavec Stane, Slovenia; (68) Dolinsky Peter, Slovakia; (69) Jouin Stéphane, France; (70) Martinez Picar Antonio, Belgium; (71) Sutherland Paul, United Kingdom; (72) Richard Dominique, France; (73) Koschny Detlef, Netherlands; (74) Roman Victor Stefan, Romania; (75) Roelandts Tom, Belgium; (76) Butusova Sofy, Russia; (77) Fleet Richard, United Kingdom; (78) Dmitriev Vasily, Russian Federation; (79) Calders Stijn, Belgium; (80) Steyaert Chris, Belgium; (81) Kartashova Anna, Russian Federation; (82) Brower Annette, Canada; (83) Smith Andy, United Kingdom; (84) Gulon Tioga, France; (85) Bozhurova Eva, Bulgaria; (86) Çubuk Kerem, Turkey; (87) Gyssens Marc, Belgium; (88) Yancheva Yulia, Bulgaria; (89) Roggemans Adriana, Belgium; (90) Bouley Sylvain, France; (91) Roggemans Paul, Belgium; (92) Perlerin Vincent, France; (93) Sandor Adina, Romania; (94) Verbeeck Cis, Belgium; (95) Audureau Yoan, France; (96) Gherase Radu, Romania; (97) Kuczuro Aleksandra, Poland; (98) Gural Peter, United States; (99) Šegon Damir, Croatia; (100) ter Kuile Casper, Netherlands; (101) Hankey Michael, United States; (102) Pavletić Lovro, Croatia; (103) Georgescu Tudor, Romania; (104) Georgescu Ana, Romania; (105) Wiśniewski Mariusz, Poland; (106)

Birlan Mirel, France; (107) Maciejewski Maciej, Poland; (108) Özeren Ferhat Fikri, Turkey; (109) Żołądek Przemysław, Poland; (110) Tomezzoli Giancarlo, Germany; (111) Meister Stefan, Switzerland; (112) Polakowski Krzysztof, Poland; (113) Ivanović Ilija, Serbia; (114) Ward Bill, United Kingdom; (115) Morillas Sánchez Lorenzo G., Spain; (116) García Vega Pilar, Spain; (117) Drolshagen Gerhard, Netherlands; (118) Buchmann Andreas, Switzerland; (119) Rault Jean-Louis, France; (120) Dubs Martin, Switzerland; (121) Shuttleworth Alan, United Kingdom; (122) Brower Jeffrey, Canada; (123) Ott Theresa, Germany; (124) Drolshagen Esther, Germany; (125) Schenker Jonas, Switzerland; (126) Stewart Peter, Northern Ireland; (127) Paillart Christian, France; (128) Vješnica Stella, Croatia.

Missing from the group photo: André Dominique, France; Bettonvil Felix, Netherlands; Braconnier Robert, France; Colas Francois, France; Haas Axel, Germany; Kieffer Bernard, France; Nogami Nagatoshi, Japan; Novoselnik Filip, Croatia; Okolic Dragana, Netherlands; Todorović Snežana, Serbia; Ugolnikov Oleg, Russia; Veljković Kristina, Serbia; Žegarac Ana, Serbia.

During the celebration of Jürgen Rendtel at the 26th IMO General Assembly, from left to right: Oleg, Ugolnikov, Arnold Tukkers, Dusan Bettonvil, Dragana Okolic, Kerem Çubuk, Uros Bettonvil, Fikri Özeren Ferhat, Gerhard Drolshagen, Tom Roelandts, Hans-Georg Schmidt, Bernd Klemt, Giancarlo Tomezzoli, Nagatoshi Nogami, Adriana Roggemans, Trond Erik Hillestad, Jonas Schenker, Thomas Weiland and Bill Ward (Credit Axel Haas.)

Time for socializing: From left to right, Ilija Ivanovic, Javor Kac, Snežana Todorović, Ana Žegarac, Kristina Veljković, Min-Kyung Kwon and Dragana Okolic. (Credit Axel Haas.)

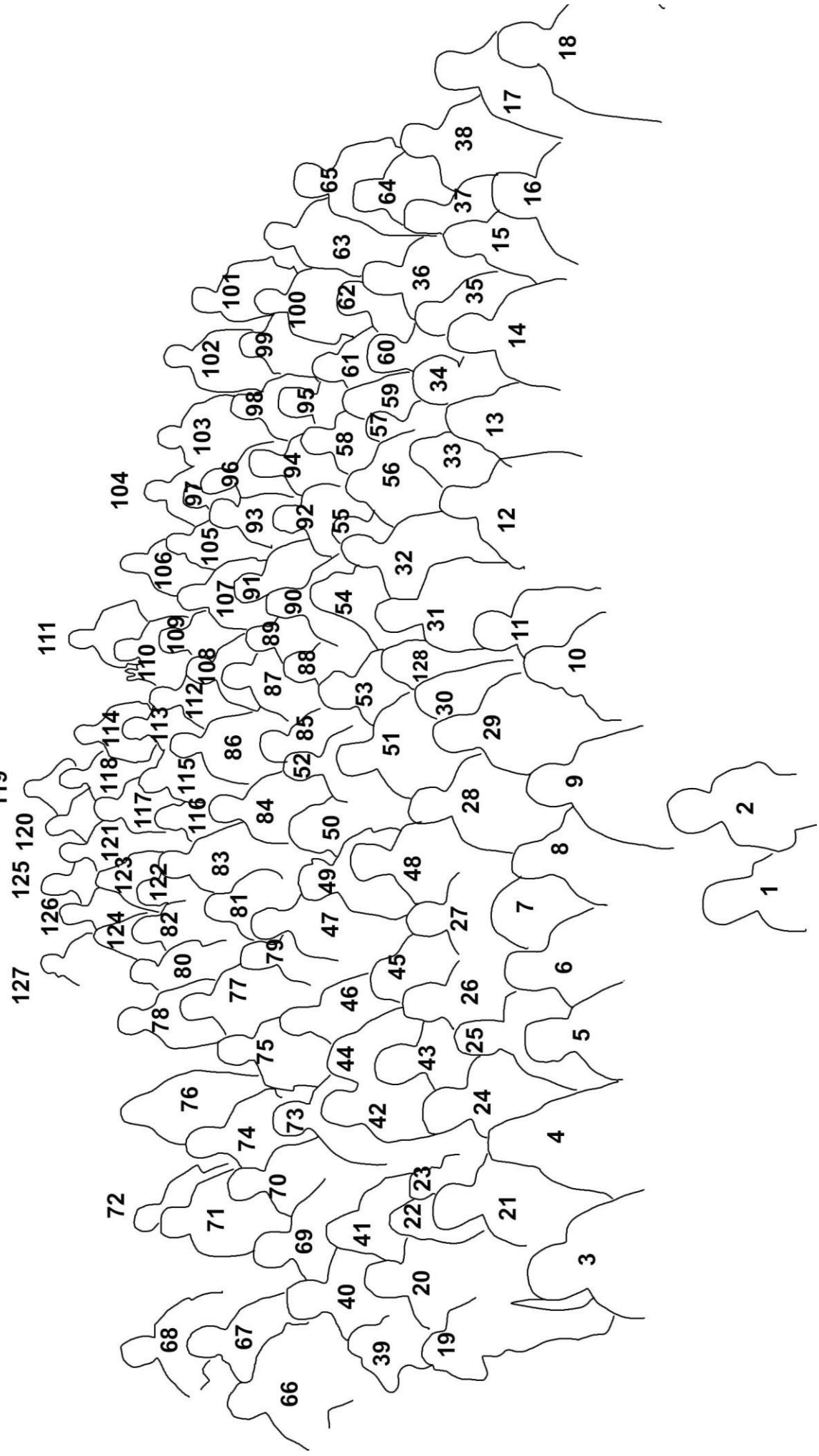
1
2
3
4
5
6
7
8
9
10
11
12
13
14
15
16
17
18
19
20
21
22
23
24
25
26
27
28
29
30
31
32
33
34
35
36
37
38
39
40
41
42
43
44
45
46
47
48
49
50
51
52
53
54
55
56
57
58
59
60
61
62
63
64
65
66
67
68
69
70
71
72
73
74
75
76
77
78
79
80
81
82
83
84
85
86
87
88
89
90
91
92
93
94
95
96
97
98
99
100
101
102
103
104
105
106
107
108
109
110
111
112
113
114
115
116
117
118
119
120
121
122
123
124
125
126
127
128

Author index

134 participants at the IMC, 145 authors and co-authors involved in all the papers in these Proceedings, many more who will read and consult these papers via different channels. How would meteor astronomy have been today without IMO and without the IMC? (Credit Axel Haas.)